

F. Gerson, W. Huber
**Electron Spin Resonance
Spectroscopy of Organic
Radicals**

Related Titles from WILEY-VCH

E. Pretsch, G. Toth, M. E. Munk, M. Badertscher

Computer-Aided Structure Elucidation Spectra Interpretation and Structure Generation

2002. Ca. 270 pages.

Hardcover. ISBN 3-527-30640-4

H.-G. Schmalz, T. Wirth

Organic Synthesis Highlights V

2003. Ca. 320 pages.

Hardcover. ISBN 3-527-30611-0

P. Bigler

NMR Spectroscopy: Processing Strategies includes CD-ROM

2003. 271 pages.

Hardcover. ISBN 3-527-29990-4

P. Renaud, M. P. Sibi

Radicals in Organic Synthesis 2 Volumes

2001. 1158 pages.

Hardcover. ISBN 3-527-30160-7

Fabian Gerson, Walter Huber

Electron Spin Resonance Spectroscopy of Organic Radicals

 **WILEY-VCH**

Prof. Dr. Fabian Gerson
Department of Chemistry
University of Basel
Klingelbergstraße 80
4056 Basel
Switzerland

P. D. Dr. Walter Huber
Hoffmann-La Roche & Cie AG
Grenzacherstraße 124
4070 Basel
Switzerland

This book was carefully produced. Nevertheless, editors, authors and publisher do not warrant the information contained therein to be free of errors. Readers are advised to keep in mind that statements, data, illustrations, procedural details or other items may inadvertently be inaccurate.

Library of Congress Card No.: applied for

A catalogue record for this book is available from the British Library.

Bibliographic information published by Die Deutsche Bibliothek

Die Deutsche Bibliothek lists this publication in the Deutsche Nationalbibliografie; detailed bibliographic data is available in the Internet at <http://dnb.ddb.de>

© 2003 WILEY-VCH Verlag GmbH & Co. KGaA, Weinheim

All rights reserved (including those of translation in other languages). No part of this book may be reproduced in any form – by photoprinting, microfilm, or any other means – nor transmitted or translated into machine language without written permission from the publishers. Registered names, trademarks, etc. used in this book, even when not specifically marked as such, are not to be considered unprotected by law.

Printed in the Federal Republic of Germany.

Printed on acid-free paper.

Typesetting Asco Typesetters, Hong Kong

Printing betz-druck gmbh, Darmstadt

Bookbinding Litges & Dopf Buchbinderei GmbH, Heppenheim

ISBN 3-527-30275-1

Contents

Preface *ix*

Abbreviations and Symbols *xi*

A General Part 1

1 Physical Fundamentals of Electron Spin Resonance 3

- 1.1 Spin and Magnetic Moment of Electron 3
- 1.2 Zeeman Splitting and Resonance Condition 4
- 1.3 Spin-lattice Relaxation 6
- 1.4 Line-width and Line-form 8

2 Paramagnetic Organic Species and Their Generation 10

- 2.1 Spin Multiplicity 10
- 2.2 Neutral Radicals 13
- 2.3 Radical Ions 19
- 2.4 Triplets: Electron–Electron Magnetic Interaction 27

3 Electron–Nuclear Magnetic Interaction 37

- 3.1 Nuclear Magnetism 37
- 3.2 Hyperfine Splitting of ESR Signal 39

4 Spin Density, Spin Population, Spin Polarization, and Spin Delocalization 49

- 4.1 Concepts 49
- 4.2 π Radicals 56
- 4.3 σ Radicals 75
- 4.4 Triplet States 79
- 4.5 Calculations of Spin Populations 80

5 Multiresonance 83

- 5.1 Historical Note 83
- 5.2 ENDOR 84

5.3	TRIPLE Resonance	94
5.4	ELDOR	96
6	Taking and Analyzing ESR Spectra	97
6.1	Instrumentation	97
6.2	g_e Factor	99
6.3	Optimal Conditions	102
6.4	Unravelling Hyperfine Pattern	109
6.5	Assignment and Sign of Coupling Constants	127
6.6	Ion Pairing	141
6.7	Intramolecular Dynamic Processes	153
B	Special Part	167
7	Organic Radicals Centered on One, Two, or Three Atoms	169
7.1	C-, N-, and O-centered Radicals	169
7.2	Si-, P-, and S-centered Radicals	186
7.3	CC-, NN-, and OO-centered Radicals	189
7.4	NO- and NO ₂ -centered Radicals	200
7.5	PO-, PP-, SO-, SS-, and SO ₂ -centered Radicals	208
8	Conjugated Hydrocarbon Radicals	210
8.1	Theoretical Introduction	210
8.2	Odd Alternant Radicals	217
8.3	Odd Nonalternant Radicals and Radical Dianions	224
8.4	Even Alternant Radical Ions	229
8.5	Even Nonalternant Radical Ions	254
8.6	Radicals and Radical Ions with a Perturbed π Perimeter	261
8.7	Radical Ions of Phanes	278
8.8	Radical Ions of Radialenes	287
9	Conjugated Radicals with Heteroatoms	290
9.1	Neutral Radicals	290
9.2	Radical Anions of Electron Acceptors	302
9.3	Radical Cations of Electron Donors	346
9.4	Radical Cations with Special Structures	366
9.5	Radical Ions of Multi-redox Systems	372
10	Saturated Hydrocarbon Radicals	375
10.1	Radical Cations of Alkanes	375
10.2	Structurally Modified Radical Cations	380
11	Biradicals and Triplet-state Molecules	386
11.1	Biradicals	386

11.2	Molecules in Photoexcited Triplet State	389
11.3	Molecules in Ground or Thermally Accessible Triplet State	393
	Appendices	405
A.1	Nitroxyls as Spin Labels and Spin Adducts	405
A.2	Hyperfine Splitting by Alkali-Metal Nuclei in Counterions of Radical Anions	409
	References	415
	Index	447

Preface

Several years ago, electron spin resonance (ESR) spectroscopy celebrated the 50th anniversary of its discovery in 1944. Its application to organic radicals [1] underwent rapid expansion in the following three decades, with many monographs being published between 1965 and 1978 [2–15]. Among them, a booklet by one of us, entitled *High-Resolution ESR Spectroscopy* [6], concerned the multiline hyperfine patterns of organic radicals in solution. The radicals discussed were mostly ions readily generated by reduction or oxidation of aromatic compounds. This limitation permitted the number of pages to be kept low, and the comprehensible treatment made the booklet attractive to researchers with a background in organic chemistry. Suggestions for writing a second, updated version have been made repeatedly since then, but for various reasons, they were not implemented. Only recently, after the author's retirement in 1997, was such a project envisaged and, two years later, also tackled. It soon became obvious that supplementing the booklet with a few paragraphs would not suffice to account for the important developments in the field and, particularly, for the enormous amount of data accumulated in the literature during the last third of the 20th century. Thus, an almost completely new and more comprehensive volume had to be written, but we have tried to preserve the lucidity of its modest forerunner.

The term ESR has been retained throughout, even though the more extensive term electron paramagnetic resonance (EPR) has been recommended. As argued in Chapt. 2.1, this is because the magnetism of organic radicals is predominantly due to the electron spin. Also retained has been a division of the contents into a General Part A, serving as an introduction to the field, and a Special Part B, in which organic radicals are classified and characterized by their hyperfine data.

The most important topics added to the first version are as follows.

(1) Organic π radicals, both charged and neutral, as well as σ radicals, have been fully dealt with. (2) Biradicals and triplet molecules have also received consideration. (3) More attention has been given to g_e factors of radicals. (4) The origin and consequences of g_e and hyperfine anisotropies have been described (thus the epithet "high-resolution" is no longer appropriate). (5) New methods for generation of radicals have been introduced, in particular those producing radical cations from compounds with higher ionization energy, either by more efficient reagents in solution or by X- or γ -irradiation in solid matrices. (6) Multiresonance methods

have been described, especially electron-nuclear double resonance (ENDOR) spectroscopy [12, 15, 16] and its physical fundamentals. (7) Modern quantum-chemical procedures for calculation of spin distribution in radicals, going beyond the π -electron models, have been briefly presented and their results for particular radicals are quoted. However, the theories underlying these procedures are outside the scope of this monograph; the pertinent computer programs are readily available and can easily be handled by experimentalists.

Several areas in the field, which are less relevant to ESR spectroscopy of organic radicals and thus have not been dealt with, are listed below.

(1) Paramagnetic species in physics and biology, like color centers in crystals and radicals produced by high-energy irradiation of biological material. (2) Chemistry of radicals as such, although we have indicated throughout how radicals are generated and, in many cases, into which secondary paramagnetic species they convert. (3) Complexes of organic ligands with transition metals, because their structure strongly differs from that of organic radicals and their hyperfine interactions are dominated by those with the nuclei of heavy atoms. (4) Instrument conditions other than those at constant waves (CW), namely the pulsed ESR and ENDOR techniques.

A book illuminating the achievements in the ESR field appeared in 1997 [17]. Data relevant to radicals (g_e factors and hyperfine-coupling constants) have been compiled in the Landolt-Börnstein Tables since 1965 [18], and publications on ESR spectroscopy have been reviewed in Chemical Society Special Reports since 1973 [19].

We thank our colleagues, Professors Alwyn G. Davies, London, Harry Kurreck, Berlin, and Ffrancon Williams, Knoxville (Tennessee), and Ms. Marj Tiefert, San Ramon (California), for critical reading the manuscript and suggesting improvements. A constructive collaboration with Drs. Gudrun Walter, Karen Kriese, and Romy Kirsten, and Mr. Hans-Jörg Maier of Wiley-VCH, Weinheim, is gratefully acknowledged. Our special thanks are also due to Ms. Ruth Pfalzberger for the skilful drawings of the Figures.

Abbreviations and Symbols

ESR	electron spin resonance
EPR	electron paramagnetic resonance
ENDOR	electron-nuclear double resonance
ELDOR	electron-electron double resonance
TRIPLE	electron-nuclear-nuclear triple resonance
NMR	nuclear magnetic resonance
MW	microwaves
RF	radio frequency
SLR	spin-lattice relaxation
SSR	spin-spin relaxation
ZFS	zero-field splitting
AO	atomic orbital
LCAO	linear combination of AOs
MO	molecular orbital
SOMO	singly occupied MO
HOMO	highest occupied MO
LUMO	lowest occupied MO
NHOMO	next highest occupied MO
NLUMO	next lowest occupied MO
NBMO	nonbonding MO
IE	ionization energy
EA	electron affinity
UHF	unrestricted Hartree-Fock
DODS	different orbitals for different spins
INDO	intermediate neglect of differential overlap
MNDO	modified neglect of differential overlap
AM1	Austin model 1 (reparametrized version of MNDO)
DFT	density functional theory
ACN	acetonitrile
DME	1,2-dimethoxyethane

DEE	diethylether
DMF	<i>N,N</i> -dimethylformamide
DMSO	dimethylsulfoxide
MTHF	2-methyltetrahydrofuran
TFA	trifluoroacetic acid
THF	tetrahydrofuran
Alk	alkali-metal atom
COT	cyclooctatetraene
DABCO	1,4-diazabicyclo[2.2.2]octane
DDQ	2,3-dichloro-5,6-dicyano- <i>p</i> -benzoquinone
DPPH	2,2-diphenyl-1-picrylhydrazyl
TCNE	tetracyanoethene
TCNQ	7,7,8,8-tetracyanobenzo-1,4-quinodimethane
TEMPO	2,2,6,6-tetramethyl-4-oxopiperidin-1-oxyl
TME	tetramethyleneethane
TMM	trimethylenemethane
TTF	1,4,5,8-tetrahydro-1,4,5,8-tetrathiafulvalene
<i>e</i>	elementary charge
m_e	(rest) mass of electron
m_p	(rest) mass of proton
<i>A</i>	absorption intensity of ESR line
\vec{B}	external magnetic field
<i>B</i>	strength of magnetic field \vec{B}
ΔB	line-width in mT
$\Delta B_{1/2}$	line-width at half-height
dA/dB	first derivative of <i>A</i> with respect to <i>B</i>
ΔB_{pp}	peak-to-peak-distance in dA/dB
ν	frequency
$\omega = 2\pi\nu$	circular frequency
ν_e	resonance frequency of electron
ν_n	resonance frequency of nucleus
$\Delta\nu$	line-width in MHz
<i>T</i>	absolute temperature in K
<i>t</i>	time
Δt	lifetime of spin state
T_{1e}	SLR time of electron
T_{2e}	SSR time of electron
T_{1n}	SLR time of nucleus
T_x	SLR cross-relaxation time
τ	lifetime of an individual form of radical

τ_r	rotational correlation time
P	transition probability
η	viscosity of the solvent
h	Planck constant
\hbar	$h/2\pi$
k	Boltzmann constant
μ_0	permeability of vacuum
\vec{S}	electron-spin vector
S_x, S_y, S_z	components of \vec{S}
S	electron-spin quantum number
M_S	magnetic electron-spin quantum number
α	spin function for $M_S = +1/2$ (spin up)
β	spin function for $M_S = -1/2$ (spin down)
$\vec{\mu}_e$	magnetic moment of electron
$\mu_{e,x}, \mu_{e,y}, \mu_{e,z}$	components of $\vec{\mu}_e$
g_e	g factor of electron
μ_B	Bohr magneton
γ_e	gyromagnetic ratio of electron
\vec{I}	nuclear spin vector
I	nuclear spin quantum number
M_I	magnetic nuclear spin quantum number
I_s	spin quantum number of a subset of equivalent nuclei
$\vec{\mu}_n$	magnetic moment of nucleus
$\mu_{n,x}, \mu_{n,y}, \mu_{n,z}$	components of $\vec{\mu}_n$
g_n	g factor of nucleus
μ_N	nuclear magneton
γ_n	gyromagnetic ratio of nucleus
T_x, T_y, T_z	components of triplet spin state
T_{+1}, T_0, T_{-1}	components of triplet spin state in a relatively strong field \vec{B}
D	ZFS tensor
D_x, D_y, D_z	principal values of D
D and E	ZFS parameters in cm^{-1}
D' and E'	ZFS parameters in mT
\vec{r}	vector joining $\vec{\mu}_e$ and $\vec{\mu}_n$ or \vec{S} and \vec{I}
r	length of \vec{r}
φ	angle between \vec{r} and \vec{B} in a relatively strong field \vec{B}
J	exchange integral over two SOMOs

E_{hf}	energy of hyperfine interaction
E_{dip}	energy of dipolar hyperfine interaction
E_{Fc}	energy of Fermi-contact term
δ_{Fc}	NMR shift due to Fermi-contact term
$\rho(x, y, z)$	electron density
$\rho_{\text{S}}(x, y, z)$	spin density
ρ_{X}^{ψ}	spin population in an orbital ψ (AO or MO) centered at the nucleus X
ρ_{μ}^{π}	π -spin population at π -center μ
ψ_j	π -MO
ϕ_{μ}	p_z -AO at π -center μ
$c_{j,\mu}$	LCAO coefficient at center μ for ψ_j
X	nucleus or the atom pertinent it
$X(\alpha), X(\beta), X(\gamma), X(\delta), X(\varepsilon), \dots$	X separated from the spin-bearing center (usually π -center) by 1, 2, 3, 4, 5, \dots sp^3 -hybridized atoms
a_{X}	isotropic hyperfine-coupling constant of X in mT
a'_{X}	isotropic hyperfine-coupling constant of X in MHz
$a_{\text{X},\mu}$	isotropic hyperfine-coupling constant of X in or at π -center μ in mT
$a'_{\text{X},\mu}$	isotropic hyperfine-coupling constant of X in or at π -center μ in MHz
\mathbf{A}_{X}	hyperfine tensor of X
$A_{\text{X},x}, A_{\text{X},y}, A_{\text{X},z}$	principal values of \mathbf{A}_{X} in mT
$A'_{\text{X},x}, A'_{\text{X},y}, A'_{\text{X},z}$	principal values of \mathbf{A}_{X} in MHz
$A_{\text{H}\parallel}, A_{\text{H}\perp}$	principal values of an axial tensor \mathbf{A}_{X} in mT
$A'_{\text{H}\parallel}, A'_{\text{H}\perp}$	principal values of an axial tensor \mathbf{A}_{X} in MHz
$\mathbf{A}_{\text{X,dip}}$	(traceless) hyperfine-anisotropy tensor of X
$2B_{\text{X,dip}}, -B_{\text{X,dip}}$	principal values of an axial tensor $\mathbf{A}_{\text{X,dip}}$ in mT
$2B'_{\text{X,dip}}, -B'_{\text{X,dip}}$	principal values of an axial tensor $\mathbf{A}_{\text{X,dip}}$ in MHz
\mathbf{G}_{e}	tensor of the g_{e} factor
$g_{\text{e},x}, g_{\text{e},y}, g_{\text{e},z}$	principal values of \mathbf{G}_{e}
$g_{\text{e}\parallel}, g_{\text{e}\perp}$	principal values of an axial \mathbf{G}_{e} tensor
Δg_{e}	$g_{\text{e}\parallel} - g_{\text{e}\perp} = g_{\text{e},z} - 1/2(g_{\text{e},x} + g_{\text{e},y})$
$\mathbf{G}_{\text{e,aniso}}$	(traceless) tensor with anisotropic contributions to g_{e} as principal values
$Q_{\text{H}}^{\text{X},\text{H}_{\mu}}$	π,σ -spin polarization parameter for α -protons
$B_{\text{H}}^{\text{X},\text{H}_{\mu}'}$	π,σ -spin delocalization parameter for β -protons
$Q_{\text{X}}, Q_{\text{X}}^{\text{X}_{\mu}\text{X}_{\nu}}, Q_{\text{X}}^{\text{X}_{\nu}\text{X}_{\mu}}$	π,σ -spin polarization parameters for nuclei X other than protons
S_{C}	π -1s spin polarization parameter for C

θ	dihedral angle between p_z -axis at the spin-bearing center and direction of C-H(β) bond of an alkyl substituent, in particular, and of X(α)-X(β), in general.
U, V, W	parameters for anisotropy contributions to ΔB in solution

A General Part

Part A, comprising Chapters 1.1 through 6.7, is an introduction to electron spin resonance (ESR) spectroscopy of organic radicals. It is amply garnished with examples illustrating how ESR spectra are obtained and what information they provide on the structure of these paramagnetic species. A large number of cited references and most of the illustrating examples have been taken from our work, because we are best familiar with them. This selection has been made by convenience and it does not claim to be guided by criteria of quality.

1

Physical Fundamentals of Electron Spin Resonance

1.1

Spin and Magnetic Moment of Electron

Spin is an intrinsic, nonclassical, orbital angular momentum. If one considers electron spin to be a kind of motion about an axis of the electron, an analogy may be drawn between an atom (microcosmos) and the solar system (macrocosmos), as illustrated in Figure 1.1.

The concept of spin was suggested by Uhlenbeck and Goudsmit in 1925 [17a, 20] to account for the splitting of lines in the electronic spectra of alkali-metal atoms in a magnetic field. Such splitting, known as the *Zeeman effect*, could not arise from an orbital angular momentum, which is zero for electrons in the s orbitals of an alkali-metal atom. Spin functions were introduced theoretically in 1926 by Pauli, as a complement of spatial functions [21]. Later, Dirac [22] showed that spin emerges without additional postulates from a relativistic treatment of quantum mechanics.

Pauli's procedure is generally followed, according to which a spin quantum number $S = 1/2$ is assigned to an electron. In the presence of a strong external magnetic field \vec{B} , a second (magnetic) quantum number $M_S = +1/2$ or $-1/2$ becomes effective, and the functions associated with M_S are denoted α and β , respectively. The spin can then be represented by a vector \vec{S} precessing about \vec{B} in the z direction (Figure 1.2). The length of this vector is $|\vec{S}| = \hbar\sqrt{S(S+1)} = \hbar\sqrt{3}/2$, where $\hbar = h/2\pi$ and $h = 6.6262 \cdot 10^{-34}$ J·s is Planck's constant. The component S_z in the z direction is $\hbar M_S = +\hbar/2$ or $-\hbar/2$, with the former

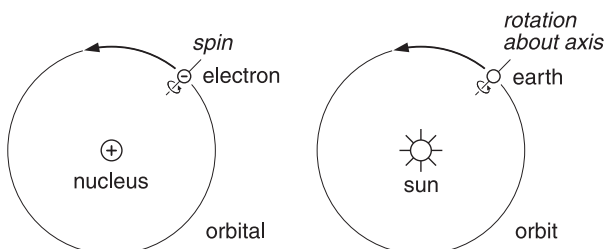


Fig. 1.1. Analogy between an atom and the solar system.

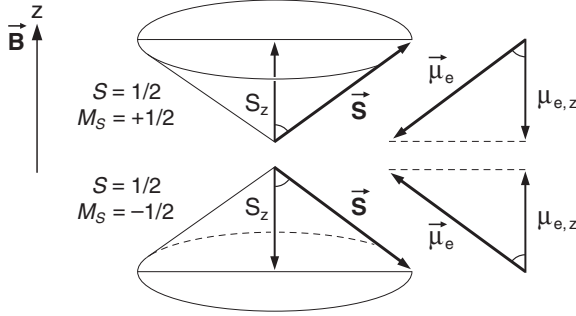


Fig. 1.2. Precession of the spin vector \vec{S} about the magnetic field \vec{B} in the z direction.

being parallel and the latter antiparallel to the z direction. The spin with $M_S = +1/2$ is also denoted spin up (\uparrow) and α , and its counterpart with $M_S = -1/2$ is named spin down (\downarrow) and β . While precessing about \vec{B} , the vector \vec{S} traces a conic area with a half-opening angle of $\arccos(1/\sqrt{3}) = 54.73^\circ$. The components S_x and S_y , perpendicular to the z direction of \vec{B} , cannot be determined individually; however, the sum of their squares, $S_x^2 + S_y^2 = |\vec{S}|^2 - S_z^2 = \hbar[S(S+1) - M_S^2] = \hbar[3/4 - 1/4] = \hbar/2$ is an observable quantity.

Due to its spin (classically, a rotating charge), an electron possesses a *magnetic moment* $\vec{\mu}_e$ which is proportional to \vec{S} (Figure 1.2).

$$\vec{\mu}_e = [g_e(-e)/(2m_e)]\vec{S} \quad (1.1)$$

with $|\vec{\mu}_e| = [g_e e/(2m_e)]\hbar\sqrt{S(S+1)}$ and $\mu_{e,z} = [g_e(-e)/(2m_e)]\hbar M_S$. Here, g_e is the (dimensionless) *g factor* of the electron, which is 2.0023 for a free electron (0.0023 is the relativistic correction), $e = 1.6022 \cdot 10^{-19}$ C is the elementary charge, and $m_e = 9.1096 \cdot 10^{-31}$ kg is the rest mass of the electron. Setting $\hbar e/(2m_e) = \mu_B = 9.2741 \cdot 10^{-24}$ A·m² or J·T⁻¹, where μ_B is the *Bohr magneton*, and T = Tesla = V·s·m⁻² is the unit of magnetic field \vec{B} , Eq. 1.1 becomes

$$\vec{\mu}_e = -[g_e\mu_B/\hbar]\vec{S} \quad (1.2)$$

with $|\vec{\mu}_e| = g_e\mu_B\sqrt{S(S+1)} = g_e\mu_B\sqrt{3}/2$ and $\mu_{e,z} = -g_e\mu_B M_S = -g_e\mu_B(\pm 1/2)$. As $g_e \approx 2$, $|\vec{\mu}_e| \approx \mu_B\sqrt{3}$ and $\mu_{e,z} \approx \mp\mu_B$. Due to the negative charge of the electron, the direction of $\vec{\mu}_e$ is opposite to that of \vec{S} (Figure 1.2).

1.2

Zeeman Splitting and Resonance Condition

By virtue of its magnetic moment $\vec{\mu}_e$, the electron interacts with the external magnetic field \vec{B} , the interaction energy E being equal to the negative value of the scalar

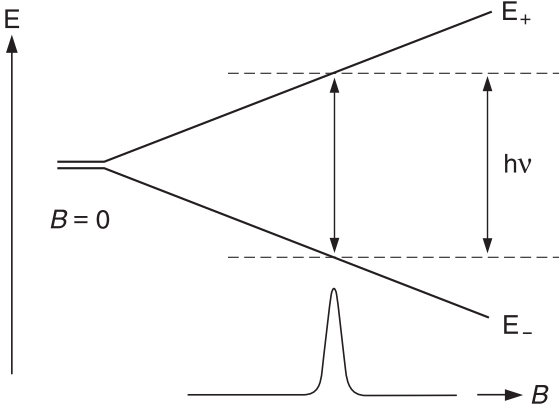


Fig. 1.3. Electron-Zeeman splitting as a function of the strength, B , of the magnetic field and the resonance condition.

product of $\vec{\mu}_e$ and \vec{B} . Accordingly, this energy is

$$E = -\vec{\mu}_e \cdot \vec{B} = -\mu_{e,z}B = -(-g_e\mu_B M_S)B = +g_e\mu_B M_S B \quad (1.3)$$

where $|\vec{B}| = B$ the field strength, and $\mu_{e,z} = -g_e\mu_B M_S$. Therefore, E is different for the two sorts of spin (Figure 1.3), namely:

$$\begin{aligned} E_+ &= (+1/2)g_e\mu_B B \quad \text{for } M_S = +1/2 \quad (\text{spin up; } \alpha) \\ E_- &= (-1/2)g_e\mu_B B \quad \text{for } M_S = -1/2 \quad (\text{spin down; } \beta) \end{aligned} \quad (1.4)$$

The difference $E_+ - E_- = g_e\mu_B B$ is the electron-Zeeman splitting, which is proportional to the strength, B , of the applied external magnetic field \vec{B} (Figure 1.3). Transitions $E_+ \leftrightarrow E_-$ between the two levels, i.e., spin inversions $\alpha \leftrightarrow \beta$, comply with the selection rule $\Delta M_S = \pm 1$. These transitions can be induced by electromagnetic radiation $h\nu$, provided that

- (i) the direction of the magnetic field associated with this radiation is perpendicular to that (z) of the external magnetic field \vec{B} , i.e., it lies in the xy plane (Figure 1.2), and
- (ii) the energy of the radiation is equal to that of the *Zeeman splitting*

$$h\nu = E_+ - E_- = g_e\mu_B B \quad (1.5)$$

a relation known as the *resonance condition* (Figure 1.3). This condition can be expressed as

$$\nu = g_e(\mu_B/h)B = \gamma_e B \quad \text{or} \quad \omega = g_e(\mu_B/\hbar)B = 2\pi\gamma_e B \quad (1.6)$$

where ν (in $\text{Hz} = \text{s}^{-1}$) is the frequency of the electromagnetic radiation, and $\omega = 2\pi\nu$ is the circular frequency, which is also the frequency of the spin \vec{S} precessing about \vec{B} (the *Larmor frequency*) at resonance. The conversion factor of the frequency ν into the field strength B , $\gamma_e = \nu/B = g_e\mu_B/h$, is called the *gyromagnetic ratio* of the electron. For $g_e = 2.0023$, $\gamma_e = 2.8024 \cdot 10^{10} \text{ Hz/T} = 28.024 \text{ MHz/mT}$.

To satisfy the resonance condition, one can vary ν or B or both. For technical reasons, the frequency ν is kept constant and the field strength B is varied to bring it to the value at which the resonance condition is fulfilled. One generally uses the microwave (MW) X band with a frequency ν of ca. 9500 MHz, which requires a field strength B of ca 340 mT.

1.3

Spin-lattice Relaxation

Besides the resonance condition, other prerequisites must be met for a successful electron spin resonance experiment. To observe an ESR signal, a single electron is not sufficient, but many of them (an *ensemble*) are needed. Also, the electrons should not be isolated but must be embedded in a suitable environment (a *lattice*), which is usually provided by atoms and molecules.

The numbers of electrons in the two Zeeman levels, E_+ and E_- , are their *populations* n_+ and n_- , respectively. According to the Boltzmann distribution law, the ratio of these populations is

$$n_+/n_- = \exp[-(E_+ - E_-)/(kT)] = \exp[-(g_e\mu_B B)/(kT)] \quad (1.7)$$

where $k = 1.3806 \cdot 10^{-23} \text{ J}\cdot\text{K}^{-1}$ is the Boltzmann constant, and T is the absolute temperature in K. In the absence of an external magnetic field ($B = 0$), n_+ is equal to n_- , but for $B > 0$, n_- is larger than n_+ , i.e., there is an excess, $\Delta n = n_- - n_+$, of spins in the lower level E_- relative to the higher level E_+ . To bring about this excess, some “hot” spins in E_+ ($M_S = +1/2$; spin up; α) must be converted into spins in E_- ($M_S = -1/2$; spin down; β). Such a “cooling” process, leading to magnetization, requires energy transfer from the spin ensemble to the lattice and is effected by *spin-lattice relaxation* (SLR). The excess Δn_m , at full magnetization at B , is

$$\Delta n_m \approx (n/2)(g_e\mu_B B)/(kT) \quad (1.8)$$

where $n = n_+ + n_-$ is the total number of spins in the ensemble. This excess is only slight: for $g_e = 2$, $B = 340 \text{ mT}$, and $T = 298 \text{ K}$, it amounts to merely 0.00077n. However, because the probability for an $E_+ \rightarrow E_-$ and an $E_- \rightarrow E_+$ transition is the same, it is due to an excess of this size that the radiation $h\nu$ gives rise to net ESR absorption.

When the magnetic field is switched on, Δn should increase from 0 to Δn_m as a function of time t (Curve ①, Figure 1.4):

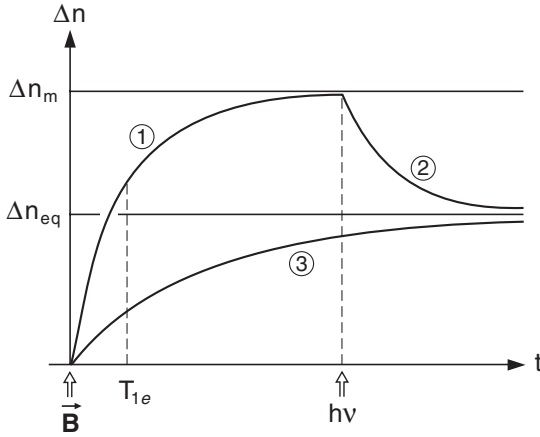


Fig. 1.4. Population excess, $\Delta n = n_- - n_+$ as a function of time t . Curve ①, magnetization upon switching on \vec{B} ; curve ②, partial decay of magnetization as a consequence of starting $h\nu$; curve ③, magnetization upon simultaneous application of \vec{B} and $h\nu$.

$$\Delta n = \Delta n_m (1 - \exp[-t/T_{1e}]) \quad (1.9)$$

At $t = 0$ (switching on of \vec{B}), $\Delta n = 0$, for $t \rightarrow \infty$, $\Delta n \rightarrow \Delta n_m$, and for $t = T_{1e}$, $\Delta n = \Delta n_m (1 - \exp[-1]) \approx \Delta n_m (2/3)$. T_{1e} is called the *SLR time* of an electron, in which the number of hot spins drops to $1/e$ or to ca $1/3$. A short (or long) T_{1e} means an efficient (or inefficient) SLR. This relaxation provides not only the means for magnetization in the field \vec{B} but it also takes care that Δn does not vanish upon continuous radiation $h\nu$. When $h\nu$ is applied, and if SLR was ineffective, the populations n_+ and n_- would equalize, with Δn decreasing from Δn_m to 0. This is because the number of transitions $E_- \rightarrow E_+$ exceeds that of $E_+ \rightarrow E_-$. The decrease of Δn , known as *saturation*, follows the equation

$$\Delta n = \Delta n_m \exp(-2Pt) \quad (1.10)$$

where P is the transition probability, common to $E_- \rightarrow E_+$ and $E_+ \rightarrow E_-$. At $t = 0$ (start of $h\nu$ in \vec{B}), $\Delta n = \Delta n_m$, and for $t \rightarrow \infty$, $\Delta n \rightarrow 0$.

Fortunately, SLR counteracts this effect and, consequently, equilibrium is achieved at $0 < \Delta n_{eq} < \Delta n_m$ (Curves ② and ③, Figure 1.4):

$$\Delta n_{eq} = \Delta n_m / (1 + 2PT_{1e}) \quad (1.11)$$

The denominator $1 + 2PT_{1e}$, referred to as the saturation term, is large when P is high and/or T_{1e} is long and small when P is low and/or T_{1e} is short.

The most important mechanism of SLR is *spin-orbit coupling*, which is substantial for heavy atoms. For organic radicals lacking such atoms, SLR is not very effi-

cient and T_{1e} is rather long. Therefore, to keep the saturation term PT_{1e} as small as possible, P must be relatively low, which is achieved by attenuating the intensity of $h\nu$. However because the ESR absorption is proportional to both P and Δn_{eq} , i.e. to $P/(1 + 2PT_{1e})$, the attenuation should be carried on until the P value is optimal for observing a strong signal. Such P value is not the same for different samples investigated: the shorter (or longer) T_{1e} is, the larger (or smaller) it is and the higher (or lower) is the allowed intensity of $h\nu$. T_{1e} can be determined by saturation experiments, in which the term PT_{1e} is measured as a function of the applied intensity of $h\nu$.

1.4

Line-width and Line-form

The Heisenberg uncertainty relation, $\Delta E \cdot \Delta t \approx \hbar$, can be expressed by an equivalent formula:

$$\Delta\nu \cdot \Delta t = \gamma_e \Delta B \cdot \Delta t \approx 1/(2\pi) \quad (1.12)$$

where $\Delta\nu (= \gamma_e \Delta B)$ (in Hz) or ΔB (in mT) stands for the width of the ESR signal, and Δt (in s) is the lifetime of a spin state. A long- (or short-) lived state thus gives thus rise to a narrow (or broad) ESR signal.

The lifetime, Δt , of the spin state α ($M_S = +1/2$; spin up) or β ($M_S = -1/2$; spin down) is determined by the relaxation times T_{1e} and T_{2e} :

$$1/\Delta t \approx (1/T_{1e}) + (1/T_{2e}) \quad (1.13)$$

where T_{1e} is the spin-lattice relaxation (SLR) time, introduced in Chapt. 1.3, and T_{2e} is the *spin-spin-relaxation* (SSR) time of electron. Whereas SLR governs energy exchange between the spin ensemble and the environment (lattice), SSR comprises interactions within the ensemble itself without such an exchange. For instance, two radicals, 1 and 2, may interchange the different states of their electron spins ("flip-flop"), so that their total energy is not changed, but, nevertheless, the lifetime of an individual spin is reduced:

$$\begin{array}{l} \text{Radical} \\ \text{Spin} \end{array} \quad \begin{pmatrix} 1 & 2 \\ \alpha & \beta \end{pmatrix} \rightarrow \begin{pmatrix} 1 & 2 \\ \beta & \alpha \end{pmatrix}$$

Such a phenomenon, referred to as *Heisenberg exchange*, is particularly effective when the spin-bearing orbitals of the radicals overlap, which occurs with high radical concentrations. As mentioned above, T_{1e} is long for organic radicals without heavy atoms (10^{-3} to 10^{-1} s). Because T_{2e} is much shorter (10^{-5} to 10^{-7} s), the relations $T_{1e} \gg T_{2e}$ and $1/T_{1e} \ll 1/T_{2e}$ generally hold, leading to

$$1/\Delta t \approx 1/T_{2e} \quad (1.14)$$

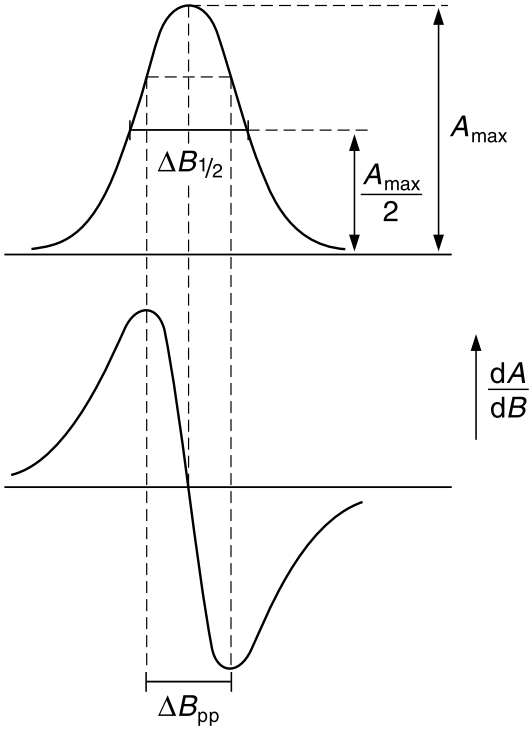


Fig. 1.5. ESR absorption A and its first derivative, dA/dB , as a function of the strength, B , of the magnetic field.

Hence, according to the uncertainty principle, the line-width becomes

$$\Delta\nu = \gamma_e \Delta B \propto 1/\Delta t \approx 1/T_{2e} \quad (1.15)$$

with $\Delta\nu \approx 10^5$ to 10^7 Hz and ΔB lies roughly in the range between 0.001 and 0.1 mT. Thus, T_{2e} can be determined from the measurements of the line-width ΔB .

The ESR signal is usually recorded as the first derivative, dA/dB , of the absorption A with respect to B as a function of B (Figure 1.5). The form of A can be approximated by a *Gaussian* or a *Lorentzian* curve or by an appropriate mixture of both, in which T_{2e} is multiplied by a function of T_{1e}^2 , with T_{2e}^2 either in the exponent (Gaussian) or in the denominator (Lorentzian). The characteristic values are A_{\max} , the maximum of A , and $\Delta B_{1/2}$, the peak width at its half-height ($A_{\max}/2$), and ΔB_{pp} , the peak-to-peak distance of the derivative curve dA/dB (Figure 1.5). For the Gaussian, $A_{\max} = \gamma_e 2T_{2e}$, with $\Delta B_{1/2} \approx 0.47/(\gamma_e T_{2e})$ and $\Delta B_{pp} \approx 0.85\Delta B_{1/2} \approx 0.40/(\gamma_e T_{2e})$, and for the Lorentzian, $A_{\max} = \gamma_e 2T_{2e}$, with $\Delta B_{1/2} \approx 0.32/(\gamma_e T_{2e})$ and $\Delta B_{pp} \approx 0.58\Delta B_{1/2} \approx 0.18(\gamma_e T_{2e})$. The bell-like form of the Gaussian curve thus has a broader waist and shorter tails than its Lorentzian counterpart.

2 Paramagnetic Organic Species and Their Generation

2.1 Spin Multiplicity

Radicals are a special class of *paramagnetic* molecules [17b], i.e., those which are amenable to ESR spectroscopy. Although *diamagnetism* is a general property of matter, *paramagnetism* is diagnostic of molecules with an overall nonzero magnetic moment of their electrons. In such molecules, the paramagnetism masks the diamagnetism, because the contribution of the former is two orders of magnitude larger than that of the latter. In atoms, magnetic moments are due to the electron spins described in Chapt. 1.1, as well as to nonzero orbital angular momenta characteristic of electrons in other than the spherically shaped s orbitals. However, in molecules generally, and in organic molecules particularly, the orbital angular momenta are essentially ineffective (“quenched”), although they can slightly alter the g_e factor via spin-orbit coupling. The paramagnetism of organic molecules thus arises almost entirely from the electron spins.

When speaking about magnetic resonance of such molecules, one is, therefore, justified in using the name *electron spin resonance* (ESR) instead of more general expression *electron paramagnetic resonance* (EPR). Because organic molecules contain many electrons, the total spin function is derived from contributions by all electrons. These contributions cancel for most electrons (which occupy orbitals pairwise and have opposite spins). Thus, only electrons with unpaired spins in the singly occupied, usually uppermost, orbitals are relevant to the total spin function. The spin-quantum number S then becomes a positive algebraic sum of the corresponding numbers, $1/2$, of the unpaired electrons; and the spin multiplicity, $2S + 1$, which is even (or odd) for an odd (or even) number of electrons, represents the multitude of the magnetic spin-quantum numbers, $M_S = S, S - 1, \dots - S$, associated with S . A single unpaired electron thus gives rise to a *doublet*, because $2S + 1 = 2$ for $S = 1/2$ and $M_S = +1/2$ or $-1/2$. Two unpaired electrons have either $S = (1/2) - (1/2) = 0$ or $S = (1/2) + (1/2) = 1$, i.e., they lead to a *singlet* with $2S + 1 = 1$ and $M_S = 0$ or to a *triplet* with $2S + 1 = 3$ and $M_S = +1, 0$, or -1 .

The pertinent singlet-spin function is

$$(1/\sqrt{2})(\alpha\beta - \beta\alpha) \quad \text{for } S = 0 \text{ and } M_S = 0 \quad (2.1)$$

and the analogous triplet functions are

$$\begin{aligned}
 \alpha\alpha & \quad \text{for } S = 1 \text{ and } M_S = +1 \\
 (1/\sqrt{2})(\alpha\beta + \beta\alpha) & \quad \text{for } S = 1 \text{ and } M_S = 0 \\
 \beta\beta & \quad \text{for } S = 1 \text{ and } M_S = -1
 \end{aligned} \tag{2.2}$$

where the first and the second letters in $\alpha\alpha$, $\alpha\beta$, $\beta\alpha$, and $\beta\beta$ refer to the first and the second unpaired electron. The singlet function is *antisymmetric*, whereas the three components of the triplet are *symmetric* with respect to the exchange of the two electrons. Because the spin orbital, which is the product of the spin and the space (orbital) functions of electron, must be antisymmetric in this respect, the total function must be symmetric for the singlet and antisymmetric for the triplet.

The formalism introduced in Chapt. 1.1 and 1.2 holds for the spin vectors \vec{S} and magnetic moments $\vec{\mu}_e$ and their interaction with \vec{B} for any multiplicity $2S + 1$. Thus, for a doublet with $S = 1/2$ and $M_S = +1/2$ or $-1/2$, the resulting values are essentially the same as those given in this chapters, and the illustration of \vec{S} precessing about \vec{B} (Figure 1.2) is also valid. For a singlet, with $S = M_S = 0$, the vectors \vec{S} and $\vec{\mu}_e$ vanish, and so does the interaction of $\vec{\mu}_e$ with \vec{B} . On the other hand, for a triplet, with $S = 1$ and $M_S = +1, 0$, or -1 , one obtains

$$\begin{aligned}
 |\vec{S}| = \hbar\sqrt{2}, \quad S_z = +\hbar, 0, \text{ or } -\hbar; \quad |\vec{\mu}_e| = g_e\mu_B\sqrt{2}; \quad \text{and} \\
 \mu_{e,z} = g_e\mu_B M_S = +g_e\mu_B, 0, \text{ or } -g_e\mu_B
 \end{aligned} \tag{2.3}$$

As $g_e \approx 2$, $|\vec{\mu}_e| \approx 2\mu_B\sqrt{2}$ and $\mu_{e,z} \approx +2\mu_B, 0$, or $-2\mu_B$. The interaction of $\vec{\mu}_e$ with \vec{B} is

$$E = -\mu_{e,z}B = +g_e\mu_B M_S B = +g_e\mu_B B, 0, \text{ or } -g_e\mu_B B \tag{2.4}$$

for $M_S = +1, 0$, or -1 , respectively.

The precessions of the spin vectors \vec{S} of the singlet and the three components of the triplet in the magnetic field \vec{B} are shown in Figure 2.1.

According to the ESR-selection rule, $\Delta M_S = \pm 1$, transitions should be allowed between the energy levels with $M_S = +1$ and 0 , as well as between those with $M_S = 0$ and -1 when the resonance condition, $h\nu = g_e\mu_B B$, is fulfilled for both kinds of transition. In fact, the transition scheme is more complicated, because of interaction between the spin vectors \vec{S}_1 and \vec{S}_2 of the unpaired electrons (Chapt. 2.4).

The spin multiplicities for any number of unpaired electrons in a molecule can be derived from a branching diagram (Figure 2.2). For example, three electrons yield one quartet and two doublets, and four electrons give rise to one quintet, three triplets, and one singlet. Clearly, singlets with $|\vec{\mu}_e| = 0$ are, diamagnetic,

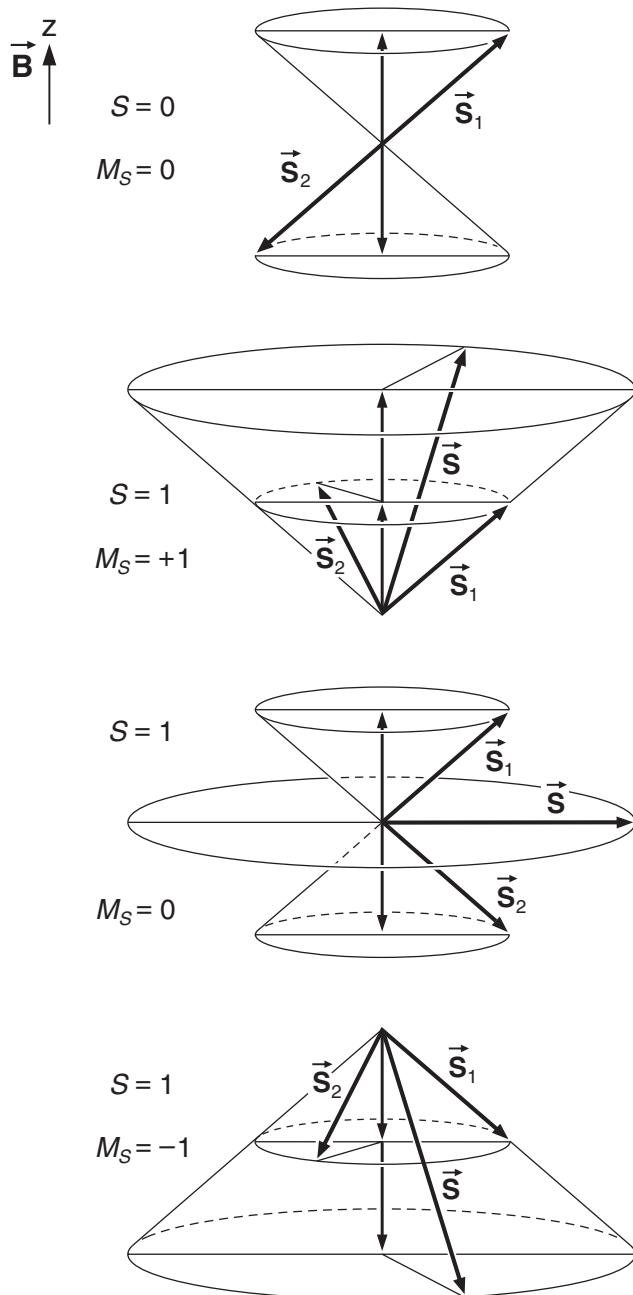


Fig. 2.1. Precession of the spin vector \vec{S} about the magnetic field \vec{B} in the z direction for the singlet (top) and the three components of the triplet.

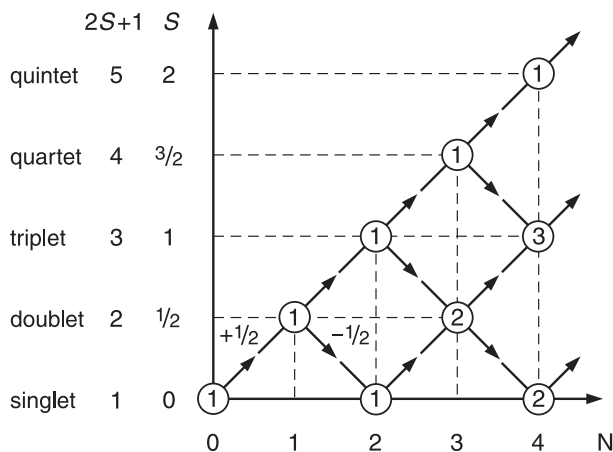


Fig. 2.2. Branching diagram. Spin multiplicity $2S + 1$ as a function of the number, N , of unpaired electrons. The number of states of a given multiplicity is indicated in the circles.

whereas molecules with higher spin multiplicities should exhibit paramagnetic properties.

In this book, only triplets will be considered in addition to radicals in the doublet state. Organic molecules with a spin multiplicity higher than triplet rarely occur in ordinary chemistry, but such species have been synthesized in the past decade as models of organic magnets [23–27]. They generally duplicate molecules in the triplet state such as *m*-xylene (Chapt. 2.4).

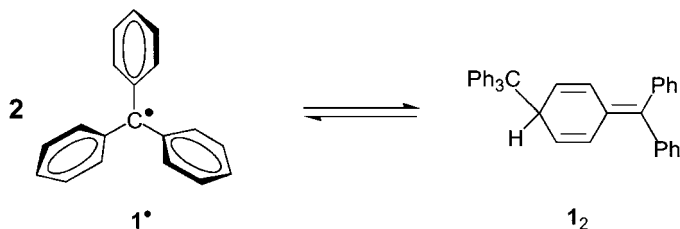
2.2

Neutral Radicals

Radicals are paramagnetic molecules with one unpaired electron, i.e., molecules in the doublet spin state. The term “free” radicals originated because, for chemists in the 19th century, radicals were defined as groups of atoms with an unpaired electron, such as methyl and allyl groups, which can be transferred from one molecule to another. Such “radicals” were not considered to have an independent existence. Therefore, upon the discovery that radicals may be separate molecules by themselves, the term “free” radicals was required to distinguish them from the conventional “nonfree” radicals. The adjective “free” has by now become superfluous and is not used in this book.

The existence of a radical, in the modern sense, was first proved in 1900 by Gomberg [28, 29], whose seminal papers on triphenylmethyl (trityl; 1') marked the birth of organic radical chemistry. In his attempt to prepare the sterically hindered

hexaphenylethane, he identified trityl in equilibrium with its dimer (1_2), which 60 years later was shown to be a derivative of cyclohexa-1,4-diene [30].



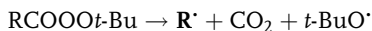
Radicals can be classified as π or σ , according to whether the spin-bearing orbital is of the π or σ type (Chapts 4.2 and 4.3). π Radicals, in particular those with an extended π system, are thermodynamically more stable than their σ counterparts, and so most radicals studied by ESR spectroscopy are of the π type. More relevant to the lifetime of radicals than their thermodynamic stability, however, is their kinetic stability (or *persistence*). Persistent radicals [31] are often sterically protected, so that dimerization and other reactions with paramagnetic or diamagnetic molecules are impeded. Another classification of radicals is based on their charge. Thus, one speaks of neutral radicals, radical ions, and radical polyions. They differ not only in their charge but also in the methods of their generation.

This chapter deals with neutral radicals. The formation of neutral radicals involves, in principle, homolytic cleavage of a covalent bond. To produce a hydrocarbon radical, a C–H or C–C bond must be broken, which requires a dissociation energy of 300 to 400 $\text{kJ}\cdot\text{mol}^{-1}$, unless the bond is weakened by steric strain [32], as in the extreme case of the nonexistent hexaphenylethane. Clearly, such a large amount of energy is not readily provided by conventional reactions. Moreover, as the radicals thus formed are, in general, highly reactive and short-lived, they must be immobilized in inert matrices or produced so efficiently that a steady concentration is achieved. In a classical work, Fessenden and Schuler [17], 33, 34] irradiated liquid hydrocarbons in situ with 2.8 MeV electrons and succeeded in observing ESR spectra of a large number of basic transient alkyl radicals in fluid solution, both aliphatic and cyclic, nonconjugated and conjugated. Among others, simple and important radicals such as methyl, ethyl, and allyl were produced in substantial concentrations from methane, ethane, and propene, respectively.

This highly efficient method is, however, not available in most laboratories, which do not have access to a van de Graaf accelerator. Thus, alternative, less involved, less expensive procedures were developed for generating neutral hydrocarbon radicals. These procedures circumvent the need to cleave the strong C–H or C–C bond by photolyzing in situ precursors with a weaker C–halogen bond, preferably iodides [35, 36] or diacylperoxides, in which the labile O–O bond is readily broken by photolysis and two CO_2 molecules are expelled, leaving two alkyl radicals R^\bullet [37–39]:

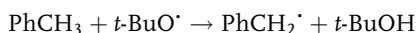
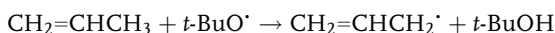
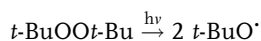


Alkyl radicals are also easily prepared by photolysis of *tert*-butyl peresters, yielding alkyl \mathbf{R}^{\bullet} and *tert*-butoxyl radicals [40, 41]:

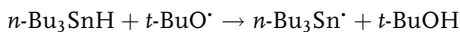
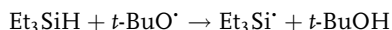


In this way, high concentrations of methyl radical are obtained. The spectrum of *t*-BuO \bullet is not observed because of extreme line broadening caused by a large g_e anisotropy.

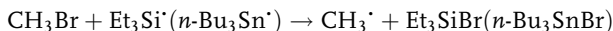
An efficient and relatively simple method, also involving *t*-BuO \bullet , has some obvious advantages over that of Fessenden and Schuler was introduced by Krusic and Kochi [42–46]. It makes use of a solution of di-*tert*-butyl peroxide in the hydrocarbon precursor, neat or diluted with cyclopropane. Photolysis of the peroxide at low temperature yields two *tert*-butoxyl radicals, which abstract an H atom from the precursor to form a radical. This method is particularly appropriate for generation of conjugated radicals, such as allyl and benzyl:



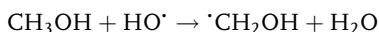
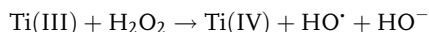
A frequently used modification of this method involves radical formation from a halide by a trialkylsilyl or trialkylstannyl radical [47–53], for example:



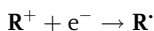
This intermediate radical then abstracts a halogen from a halide, for example:



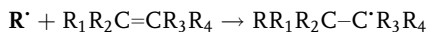
Instead of peroxides, HO \bullet radicals, formed by cleavage of the O–O bond in H₂O₂, can be used to abstract H atoms from alcohols and water-soluble esters. The cleavage is effected photolytically in a rigid matrix at low temperature [54–58] or, preferably, in a flow system consisting of an acidified aqueous solution of the alcohol or ester in question, along with H₂O₂ and Ti(III) [59–63], Fe(II) [64], or Ce(III) ions [65].



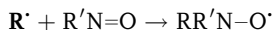
In some cases, the neutral radical can be generated from an organic cation (\mathbf{R}^+) salt by reaction with zinc powder [66, 67] or by electrolytic reduction [68]:



Secondary radicals are often obtained by addition of primary radicals (R') to the double bond of alkenes [69–71]:

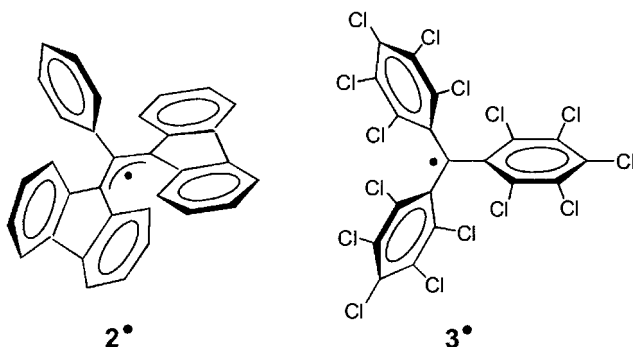


Such an addition can also be carried out when the formal double bond is part of an aromatic compound [72–74] or a fullerene [75, 76]. This type of addition is particularly useful when R' is transient but the secondary radical is persistent, as occurs if the latter is nitroxyl:

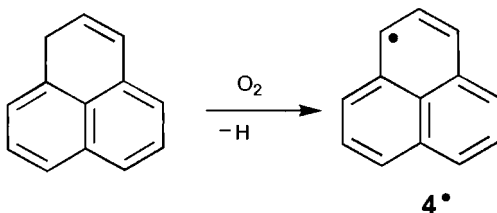


$R'N=O$ and $RR'N-O\cdot$ are called the spin trap and spin adduct, respectively [77, 79] (Appendix A.1).

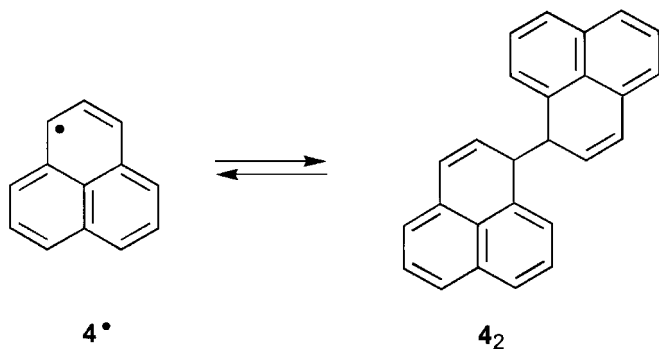
Short-lived radicals, such as aminyl and oxyl radicals, can be generated from an appropriate precursor by X-irradiation in an adamantane matrix at room temperature [80–83]. This matrix functions as an isotropic medium, and the observed ESR spectra resemble those in fluid solution. In most persistent hydrocarbon radicals, the spin-bearing segment of the molecule is sterically protected by bulky substituents. Two radicals of this type are 1,3-bis(diphenylene)-2-phenylallyl (2^\cdot) [84] and perchlorotriphenylmethyl (3^\cdot) [85].



Examples of highly persistent neutral hydrocarbon radicals (Chapt. 8.2) without protecting groups are phenalenyl (4^\cdot) and its derivatives [86–91]. The phenalenyl radical, which can be detected in pyrolysis products of petrol fractions [87], can be formed merely by exposing a solution of phenalene in tetrachloromethane to air, whereby a H atom is abstracted by dioxygen [86, 88].

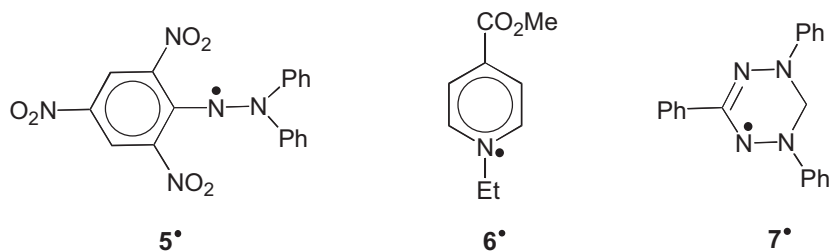


The phenalenyl radical is in equilibrium with its dimer (4_2) and can be readily regenerated by heat.



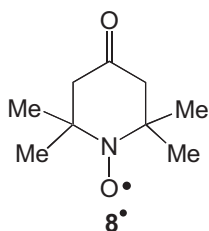
Persistent neutral radicals with the unpaired electron largely located on heteroatoms (Chapt. 9.1) are much more common than C-centered ones. This statement holds also, in particular, for radicals with N as the heteroatom, such as some picrylhydrazyls, pyridinyls, and verdazyls and many nitroxyls. Representative examples are given below.

Solid 2,2-diphenyl-1-picrylhydrazyl (DPPH; 5^\bullet) [2, 3, 92, 93] is commercially available and was one of the first radicals most intensively studied by ESR spectroscopy. Reduction of the corresponding pyridinium iodide with zinc powder yields 1-ethyl-4-carbomethoxypyridinyl (6^\bullet) which can be purified by distillation [66]. Alkylation of the formazan precursor and subsequent oxidation with O_2 produces the stable 1,3,5-triphenylverdazyl (1,3,5-tetraphenyl-1,2,5,6-tetrahydro-1,2,4,5-tetrazyl; 7^\bullet) [94, 95]:

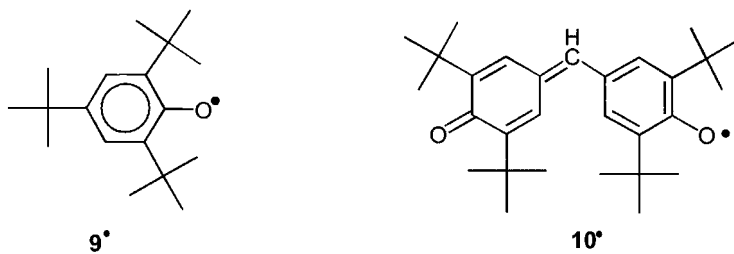


A large class of persistent radicals, the nitroxyls [96], derive from nitric oxide (NO^\bullet), one of the simplest inorganic radicals and a biologically important “messenger”. The general formula of nitroxyls is $RR'NO^\bullet$, where R or R' is an alkyl or an aryl group. Nitroxyls are readily prepared by oxidation of the corresponding secondary amine or oxime with H_2O_2 [96–99], peroxides [100–102], $Ag(I)$ [103], or H_2O_2 with $Ti(III)$ [104] in various solvents. In particular, nitroxyls have become known as spin adducts of transient radicals to nitroso compounds and nitrones as spin traps and also as spin probes inserted in biological systems (Appendix A.1).

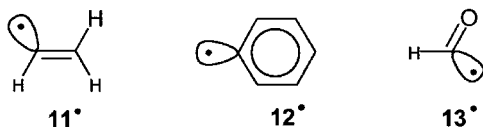
The most well-known nitroxyl is probably 2,2,6,6-tetramethyl-4-oxopiperidinyl-1-oxyl (TEMPO; **8[•]**) [97, 105]:



Some radicals with the unpaired electron largely located on O atom, such as aroxyls [106–109], are also persistent when these centers are protected by bulky substituents. They are generated by oxidation of the corresponding phenol in an organic solvent admixed with an alkaline aqueous solution of potassium hexacyanoferrate. Prominent representatives are 2,4,6-tri-*tert*-butylphenoxyl (**9[•]**) [108] and the galvinoxyl **10[•]** (Coppinger's radical) [109].

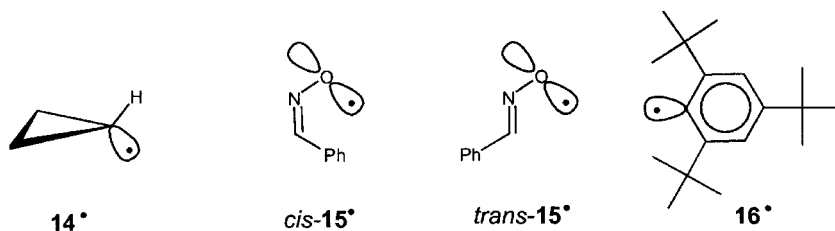


All radicals considered up to now are of the π type. Because of their low stability and high reactivity, σ radicals are less easy to detect; however, a few simple, important species have to be mentioned. These are vinyl (**11[•]**), generated from liquid ethane by 2.8 MeV electrons [17j, 34] or by photolysis of HI in acetylene [110]; phenyl (**12[•]**), obtained from solid iodide in a matrix by reaction with sodium [111] or photolysis [36] or from bromide by 2.8 MeV electrons in aqueous solution [112]; and formyl (**13[•]**), first produced by photolysis of HI in solid CO [113] or by photolysis of solid formaldehyde [114].



Cyclopropyl (**14[•]**), first generated by irradiation of liquid cyclopropane with 2.8 MeV electrons [34], can be classified as intermediate between a π and an σ radical (Chapts. 4.3 and 7.1).

Among heteroatom-centered radicals of the σ type, we should mention iminoxyls (Chapt. 7.4), such as (**15**[•]), which is formed from the corresponding aldoxime with Ce(IV) in methanol by the use of a flow system [115].

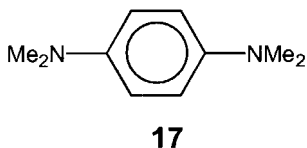


Even a σ radical can be made persistent by steric protection, as is true for 2,4,6-tri-*tert*-butylphenyl (**16**[•]) generated in solution from the 1-bromo precursor by reaction with $\text{Me}_3\text{Sn}^\bullet$ [49].

2.3

Radical Ions

The 19th-century chemists repeatedly came across organic radical ions, such as Wurster's blue, the cation of *N,N,N',N'*-tetramethyl-*p*-phenylenediamine (**17**), but they could not recognize the nature of these colored species [17e].



The existence of organic radical ions, e.g., the anions of ketones [116–119], quinones [120, 121], and naphthalene [122, 123] was postulated as early as 1920–1940. However, it was not until the advent of ESR spectroscopy that their structure could be established beyond a doubt.

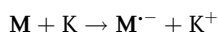
Generation of a radical ion requires a redox reaction, i.e., electron transfer from or to a neutral diamagnetic molecule. Electron abstraction from such a molecule, yielding a radical cation, is *oxidation* (also called *ionization* in the gas phase and in solids); whereas electron uptake, leading to a radical anion, is *reduction*. Thus, in the formation of its radical cation and anion, a molecule functions as an electron donor and acceptor, respectively. In the gas phase, the propensity of a molecule to release an electron is characterized by its *ionization energy* (IE), and its *electron affinity* (EA) is a measure of its readiness to admit an additional electron. Both quantities strongly depend on the molecular structure [9d]. For organic molecules, IE is +5 to +15 eV (+500 to +1500 $\text{kJ}\cdot\text{mol}^{-1}$), which is the amount of energy that has to be invested in ionization. The value of EA for organic molecules is +4 to

-2 eV ($+400$ to -200 $\text{kJ}\cdot\text{mol}^{-1}$). Actually, because EA is equal to IE of the resulting radical anion, positive values signify an energy decrease upon uptake of an electron and negative values signify an energy increase. Thus, from the energetic point of view, formation of radical anions should occur at less expense than formation of radical cations. In fact, up to 1980, many more radical anions than cations were investigated by ESR spectroscopy [18], although this imbalance has been somewhat redressed in the past two decades due to new methods of ionization.

The large amounts of energy required for formation of radical cations and some radical anions in the gas phase, as indicated by the IE and EA values, seem discouraging at first sight. Fortunately, in solution, the energy balance between neutral molecules and their radical ions is often shifted in favor of the latter, because the radical ions benefit from interactions with the surrounding species, such as solvation by solvent molecules or the Coulombic attraction of counterions. In principle, if appropriate conditions are found, every molecule can be oxidized to its radical cation and reduced to its radical anion. Thus, on the whole, generation of radical ions appears to be a more straightforward procedure than generation of neutral radicals. Because of their charge, dimerization is less common for radical ions than for their neutral counterparts, and many of the former persist in solution when air and moisture are excluded. The methods for generation of radical ions are chemical (frequently combined with photolysis), electrolytic, and radiolytic.

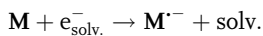
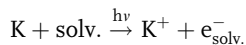
Radical Anions

The oldest and still the standard procedure for reducing an organic compound to its radical anion is reaction with potassium or another alkali metal in an ethereal solvent, usually 1,2-dimethoxyethane (DME) and tetrahydrofuran (THF) [124–142], or, less often, 2-methyltetrahydrofuran (MTHF) [140–142]. The more polar N,N,N',N',N'',N'' -hexamethylphosphoric triamide (HMPT) can also be used as a solvent [143, 144], although it is less easily dried and purified. In the reduction, the organic molecule accepts an electron from Li, Na, K, Cs, or Rb:

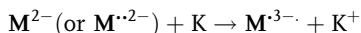
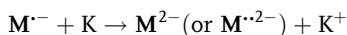


The reducing power of the alkali metal increases with its decreasing ionization energy, i.e., on going from Li via Na, K, and Rb to Cs. The reaction is carried out in a vacuum by bringing a carefully dried ethereal solution of the compound into contact with a freshly cut piece of Li metal or a sublimed metallic mirror of Na, K, Rb, or Cs, whereby for the highly reactive Rb and Cs, the thermally dissociable azide is preferred as the starting material. Formation of radical ions is generally accompanied by the appearance of a bright color. In a modification of the procedure, direct contact of the compound with the metallic mirror can be avoided by first dissolving the alkali metal, preferably K or a Na/K alloy, in DME or HMPT at low temperature and subsequently carrying out the reaction with the blue solution of solvated electrons thus formed [145]. The reducing power of such a solution is enhanced by simultaneous irradiation with visible light, so that even benzene

derivatives with very low electron affinity can be converted to their radical anions [146]:

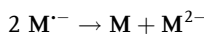


Reaction with an alkali metal was used to generate the radical anions of almost all aromatic hydrocarbons [6, 18, 124–139, 145, 146], annulenes [147–150], cyclophanes [151–156], heterocyclic compounds [157–167], ketones [168–172] and fullerenes [173, 174]. Upon prolonged contact with an alkali-metal mirror, easily reducible neutral compounds or those containing more than one electron-accepting group may take up more than one electron to yield diamagnetic dianions M^{2-} or dianionic triplet states $\text{M}^{\cdot\cdot 2-}$ [175, 176] (Chapt. 2.4) and even radical trianions M^{3-} :

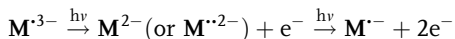
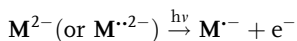


Radical trianions have been obtained from tetracyanoarenoquinodimethanes with high electron affinity [177, 178]; from several nonalternant aromatic hydrocarbons, annulenes, and 1,8-diphenylnaphthalene [178]; and from phenyl-substituted dibenzo[2.2]paracyclophane-1,9-dienes [156], corrannulene [179], 2,4,6-triphenylphosphabenzene [180, 181] and diphosphapolyphenylenes [181], and fullerenes [174].

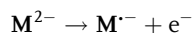
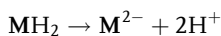
In some cases, disproportionation of radical anions to neutral molecules and dianions [182] impairs observation of the former [183]:



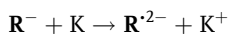
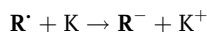
Because of ion pairing with positively charged counterions (Chapt. 6.6), this disproportionation is favored by ethereal solvents of low solvation power, such as MTHF. Radical anions can be regenerated from the dianions or trianions by photolytically induced loss of an electron:



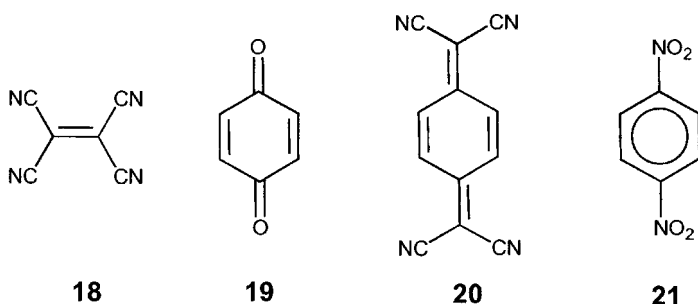
This method is particularly useful when dianion salts are available as starting materials [184, 185]. Dihydroprecursors can be deprotonated to a dianion and subsequently converted by mild oxidation into radical anions [177]:



Neutral radicals \mathbf{R}^{\cdot} with an odd number of π centers are often reduced to diamagnetic anions \mathbf{R}^{-} and even to radical dianions $\mathbf{R}^{\cdot 2-}$ [67, 147, 186–189]:



Good electron acceptors, such as diones, quinones, and compounds substituted with many cyano or nitro groups, are converted to their radical anions by mild reagents like glucose [148, 190], sodium dithionite [191], zinc powder [190, 192], or mercury metal [193]. Typical acceptors are tetracyanoethene (TCNE; **18**), benzo-1,4-quinone (**19**), 7,7,8,8-tetracyanobenzo-1,4-quinodimethane (TCNQ; **20**), and 1,4-dinitrobenzene (**21**) (Chapt. 9.2):



An important alternative to the chemical methods discussed above is electrolytic reduction in situ, which was initially applied to nitro derivatives of benzene [194–197] and to azulene [198]. Acetonitrile (ACN), dimethylsulfoxide (DMSO), or *N,N*-dimethylformamide (DMF), all containing 0.1 M tetraalkylammonium perchlorate, served as the solvent with a mercury pool as the working electrode. Later, this method was used for polyenes in liquid ammonia [199–201] or in THF [202], with platinum wire replacing the mercury pool, and for aromatic hydrocarbons in DMF, THF, or DME, with a helical cathode of amalgamated gold [203, 204]. On the whole, electrolytic reduction in all its facets has been extensively applied to many classes of organic compounds, such as nitroalkanes [205], cyano-substituted compounds [206, 207], heterocycles [167, 208, 209], annulenes [210, 211], ketones [212–215], and quinones [216–219].

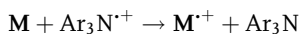
Radical Cations

In contrast to radical anions, for which alkali-metal reduction is the standard chemical method of generating them, no analogous single procedure exists for oxidation of neutral compounds to their radical cations. Dissolving aromatic hydrocarbons in concentrated sulfuric acid was the first conventional method to generate the radical cations of aromatic compounds; the acid served as both solvent

and oxidizing agent [127, 129, 136, 159, 220–224]. In a few cases, the efficiency of the method was enhanced by UV irradiation [225]. Use of sulfuric acid is a rather crude procedure, and its exact mechanism is not fully understood; thus, it has been superseded by more refined methods [226, 227]. Instead of H_2SO_4 , oxidation can be carried out in other protic acids such as CF_3COOH (TFA) or $\text{FSO}_3\text{H}/\text{SO}_2$ [228] or in mixtures of TFA with nitromethane or dichlorobenzene [229, 230]. The protic acids are often replaced by Lewis acids, AlCl_3 [150, 230, 231–235], SbF_5 [236, 237], molten SbCl_3 [238–241], or SbCl_5 [242], in nitromethane or dichloromethane. In particular, aluminum trichloride in dichloromethane proved to be the system of choice for hydrocarbons [233–235], thia-heterocycles [230], and organosilicons [232], and antimony pentafluoride was appropriate for many trialkylamines [236, 237]. The nature of some negative counterions in these reactions is still uncertain.

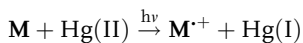


Oxidation by electron transfer occurs in the reaction of many compounds, both hydrocarbons and nitrogen-containing compounds, with commercially available tris(4-bromophenyl)ammoniumyl hexachloroantimonate [243–246] or its tris(2,4-dibromophenyl) analogue [245, 247] in dichloromethane. These reagents, which are paramagnetic, are called “magic blue” and “magic green”, respectively, with the latter being the more powerful oxidant.



where Ar is 4-bromo- or 2,4-dibromophenyl. More recently, for compounds that are not too hard to oxidize, 1,1,1,3,3,3-hexafluoropropan-2-ol has been found to be a suitable solvent for generation of highly persistent radical cations with various electron acceptors [248–250].

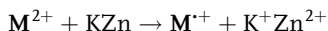
In addition, salts of Ag(I) in a protic solvent [164] and salts of Hg(II) [251–254], Tl(III) [255, 256], Ce(IV) [257], and Co(III) [258–260] in trifluoroacetic acid, dichloromethane, or their mixtures have been efficiently applied to generation of radical cations, especially when their oxidizing power is enhanced by UV irradiation [251–253]:



In this way, derivatives of azulene [261, 262] and cyclooctatetraene [263] can be converted to their radical cations. Oxidation of the parent azulene [259] and cyclooctatetraene [260] required the use of a rapid-flow system, and unsubstituted benzene and polyenes had to undergo the more rigorous treatments indicated below. When quinones [264, 265] and diazoaromatics [265–267] are reduced electrolytically in acid solution or “chemically” with zinc or sodium dithionite, the corresponding persistent radical cations, which represent radical anions diprotonated at the two O or N atoms, are formed:



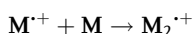
In some cases, radical cations have been obtained by reduction of diamagnetic dications by a potassium mirror in DME or by zinc powder in DMF or methanol [267, 268]:



Electrolytic oxidation was introduced as a method of generating radical cations almost simultaneously with the analogous reduction method for producing radical anions [17h]. The first radical cation obtained by this method was that of *p*-phenylenediamine in ACN, containing 0.1 M sodium perchlorate, with platinum wire as the working electrode [269]. A helical gold anode in a 10:1:1 mixture of dichloromethane with trifluoroacetic acid and its anhydride [204, 270] proved to be more efficient, particularly for oxidation of aromatic hydrocarbons. For the cations, as for the anions, electrolysis turned out to be a match for the chemical methods of generating radical ions. Electrolysis has been widely used to oxidize derivatives of some hydrocarbons [204, 270–273] and many amines and hydrazines [274–281].

In contrast to their negatively charged counterparts, paramagnetic species bearing more than one positive charge were rather rarely observed by ESR spectroscopy. The tris(dimethylamino)cyclopropenium radical dication has been produced with sulfuric acid or by electrolytic oxidation from the corresponding diamagnetic cation [282]. The radical trication was reported to be formed from a hexaazaoctadecahydrocoronene [283], and strong evidence for formation of radical trications and radical pentacations was recently obtained upon oxidation of phosphines containing two and three tetrathiafulvalene moieties, respectively [284]. Formation of triplet dications was also observed in a few studies [277, 283, 285] (Chapt. 2.4).

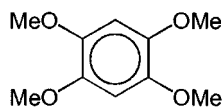
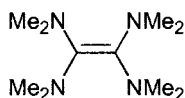
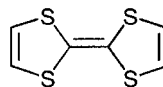
A frequently-occurring reaction is the formation of a dimeric radical cation by π complexation of the radical cation with its neutral precursor [204, 242, 270, 287, 288]. This reaction is favored by mild oxidizing agents, a high concentration of the precursor, and low temperature [204].



Such dimeric radical cations will be considered in more detail in Chapt. 8.4.

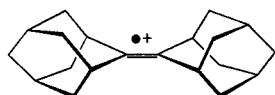
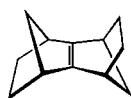
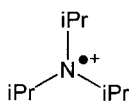
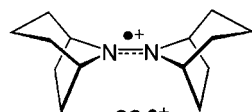
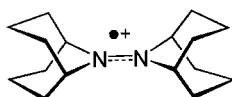
Good electron donors, as counterparts of good acceptors, are π systems substituted with electron-repelling alkoxy and amino groups, such as 1,2,4,5-tetramethoxybenzene (22), *N,N,N',N'*-tetramethyl-*p*-phenylenediamine (17), and tetrakis(dimethylamino)ethene (23), or those containing electron-rich heteroatoms, mostly sulfur, such as 1,4,5,8-tetrahydro-1,4,5,8-tetrathiafulvalene (TTF; 24) (Chapt. 9.3). These compounds are readily converted to their radical cations by a variety of chemical and electrolytic methods. Since a crystalline charge-transfer complex of 7,7,8,8-tetracyanobenzo-1,4-quinodimethane (TCNQ; 20) and TTF (24) was discovered as the first organic material exhibiting high electrical conductivity (an “organic metal”) [289], good electron acceptors and donors have aroused much

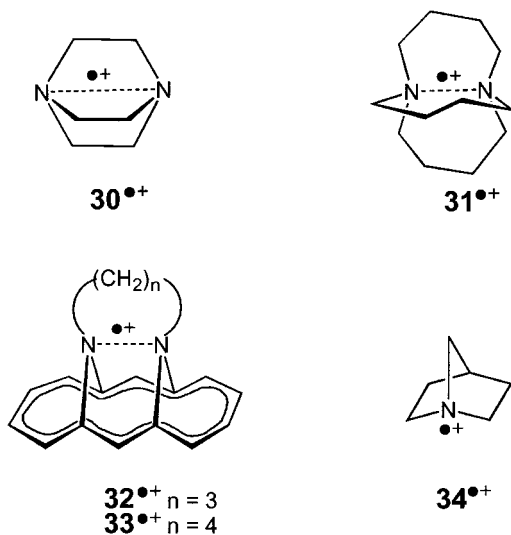
attention. Subsequently, the radical cations of many derivatives of TTF were studied [230], and the conducting properties of their salts or of the complexes of these derivatives with acceptors were examined [290–294].

**22****23****24**

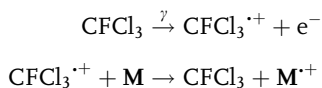
Some hydrocarbons and N-containing compounds are moderate electron donors, although they do not comprise conjugated π systems. Their radical cations, which were studied by EPR spectroscopy and by chemical and electrolytic methods, owe their thermodynamic and kinetic stability to their special structural features. In this regard, alkyl-substituted derivatives of ethene, ammonia, and hydrazine, as well as some diazabicycloalkanes, deserve particular attention. Representatives of such compounds are adamantylideneadamantane (**25**) [272], *syn*- and *anti*-sesquiterpenes (*syn*-**26** and *anti*-**26**) [273], triisopropylamine (**27**) [236, 237], 8,8'-bis(8-azabicyclo[3.2.1]octane) (**28**) [295], 9,9'-bis(9-azabicyclo[3.3.1]nonane) (**29**) [272, 296], 1,4-diazabicyclo[2.2.2]octane (DABCO; **30**) [297], and 1,6-diazabicyclo[4.4.4]tetradecane (**31**) [298–300].

The radical cations of hydrazines owe their higher stability to the formation of a three-electron N–N π bond. On the other hand, a three-electron N–N σ bond is formed in the radical cations of several diazabicycloalkanes, like **30** and **31**, and of polymethylene-*syn*-1,6:8,13-diimino[14]annulenes, such as **32** and **33** [244]. The radical cations of **28** [295], **29** [296], **31** [301], **32** [302], and **33** [303] have been isolated as salts and studied by X-ray crystallography.

**25**^{•+}*syn*-**26**^{•+}*anti*-**26**^{•+}**27**^{•+}**28**^{•+}**29**^{•+}



In general, only radical cations of compounds having an ionization potential below 8 eV can be studied in fluid solution. Those, like unsubstituted polyenes and saturated hydrocarbons, that are harder to oxidize and which yield highly reactive radical cations became amenable to ESR spectroscopy in the early 1980s by ionization in rigid matrices [304–308]. In this procedure, which has led in the past two decades to intense research activity in the field of radical cations, the organic compounds are subjected to high-energy irradiation or other rigorous methods in halocarbons (Freons) [304, 305–330], sulfur hexafluoride [313, 331–332], or inert-gas matrices at cryogenic temperatures [333–336]. The host molecules are initially ionized, and the electron holes thus created migrate across the matrix until they are trapped by the dissolved guest compound, which has a lower ionization potential than the host (ca 11.5 for Freons, 15.7 for SF₆, and 21.6 eV for Ne). In particular, γ radiolysis by a ⁶⁰Co probe in Freons, like CFCl₃, CF₃CCl₃, or CF₂ClCFCl₂, at 77 K was frequently used for generating radical cations of many hydrocarbons [309–319, 327–330], ethers [320–323], amines [237, 324–326], and other organic compounds. The ESR spectra of the resulting radical cations can often be observed up to the softening point of the matrix.

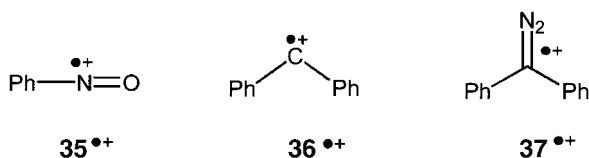


Because of the high energy provided for ionization, rearrangements of the primary formed radical cation are frequently encountered [318, 321, 323, 325–330, 340]. In the more “mobile” CF₂ClCFCl₂ matrix, loss of a proton in a bimolecular reaction can yield a neutral radical **R**[•], usually of the allyl or dienyl type [307, 328, 337–340]:



Radical cations are also formed from some hydrocarbons in zeolites at room temperature [341–346]. Again, apart from radical cations generated from alkanes and other saturated hydrocarbons in solid matrices by high-energy irradiation [309–313, 331–336, 347] and some nonplanar radical cations of polycyclic amines, such as 1-azabicyclo[2.2.1]heptane (azanorbornane; **34**) [348], all radical ions studied have been the π type. A further notable exception is the relatively long-lived radical cations with three-electron N–N σ bonds like those in **30** \cdot^+ –**33** \cdot^+ (see above), as well as radical cations with analogous N–N [349], P–P [350–353], S–S [354–357], Se–Se [358], and As–As [350, 359] bonds formed both intra- and intermolecularly.

Nitrosobenzene (**35**) [360] and diphenylcarbene (**36** \cdot^+) [361] also give σ radical cations, while the radical cation of the precursor of **36** \cdot^+ , diphenyldiazomethane (**37**), has either π or σ structure (it's a “chemical chameleon”), depending on the conditions of its generation [245].



Theoretical calculations predict the existence of radical cations $\text{M}^{\bullet+}$, in which spin and charge are located in separate sites of the molecule **M**. The name *distonic* has been suggested for such species, which are expected to occur especially in the gas phase [362–365]. For example, a radical cation $\text{CH}_3\text{X}^{\bullet+}$ ($\text{X} = \text{F}, \text{OH}, \text{or } \text{NH}_2$) should be in equilibrium with a distonic cation $\cdot\text{CH}_2\text{X}^+\text{H}$, which is formally obtained from the former by transfer of a proton from C to X [365]. ESR evidence in favor of distonic radical cations is rather meager; since they have been proposed only in a few studies as transient intermediates formed upon γ irradiation in Freon matrices at low temperature [363].

2.4

Triplets: Electron–Electron Magnetic Interaction

Organic molecules with two unpaired electrons in singly occupied orbitals (open shells) are often called biradicals. This notation is justified when the interaction between the two electrons is weak, because of their separation by an “isolating” segment of the molecule. In an extreme case, when such interaction is negligible, a biradical may be considered to be the sum of two radicals in the doublet spin state. If the two spin-bearing parts are interchangeable, the ESR spectrum will be that of a monoradical with a twofold intensity. However, when there is significant interaction between the two electrons, the two doublets yield a singlet, in which these electrons are paired, and a triplet spin state, in which they remain unpaired. Hund rule for atoms usually applies also to molecules with two electrons in singly

occupied orbitals, i.e., the triplet is generally lower in energy than the corresponding singlet. Exceptions exist when the two spin states have strongly different geometry, and the distorted singlet may then be more stable than the triplet. The singlet–triplet energy difference is determined by the so-called exchange integral J over the functions of the two spin-bearing orbitals.

ESR spectra of the organic triplet states differ from those of their doublet counterparts by the appearance of *fine splitting* which is due to the classical *dipolar interaction*, E_{dip} , of the magnetic moments of the two unpaired electrons:

$$\begin{aligned} E_{\text{dip}} &= (\mu_0/4\pi)[(\vec{\mu}_{e,1} \cdot \vec{\mu}_{e,2})r^{-3} - 3(\vec{\mu}_{e,1} \cdot \vec{r})(\vec{\mu}_{e,2} \cdot \vec{r})r^{-5}] \\ &\propto (\vec{S}_1 \cdot \vec{S}_2)r^{-3} - 3(\vec{S}_1 \cdot \vec{r})(\vec{S}_2 \cdot \vec{r})r^{-5} \end{aligned} \quad (2.5)$$

where μ_0 is the permeability of vacuum, with $\mu_0/4\pi = 10^{-7} \text{ V}\cdot\text{s}\cdot\text{A}^{-1}\cdot\text{m}^{-1}$; $\vec{\mu}_{e,1}$ and $\vec{\mu}_{e,2}$ are the magnetic moments of the two unpaired electrons associated with their spin vectors \vec{S}_1 and \vec{S}_2 ; and \vec{r} is the vector joining \vec{S}_1 and \vec{S}_2 ($|\vec{r}| = r$). The vector pairs in parentheses represent their scalar products. Clearly, E_{dip} as a function of \vec{r} , is strongly *anisotropic*, i.e., orientation-dependent.

The expression (Eq. 2.5) is conveniently transformed into a product of the type

$$\vec{S}_1 \cdot \mathbf{D} \cdot \vec{S}_2 \quad (2.6)$$

where \mathbf{D} , a function of \vec{r} , denotes a symmetric, traceless tensor called the *zero-field splitting* (ZFS) tensor. This is because ZFS, responsible for the *fine splitting* in the ESR spectra of triplet states, is effective even in the absence of an external magnetic field \vec{B} ($B = 0$). Because the sum, $D_x + D_y + D_z$, of the principal values of \mathbf{D} is zero (a tensor is formally a matrix), the three values are usually replaced by two ZFS parameters D and E .

The $|E|$ value is generally much smaller than $|D|$, and $|E|$ vanishes for molecules of axial symmetry, in which $D_x = D_y$. Both energy parameters, D and E , are generally expressed in wavenumbers (cm^{-1}). In ESR spectra, they are measured as $D' = D/g_e\mu_B$ and $E' = E/g_e\mu_B$ in T, the unit of the field strength B . Here, 1 T corresponds to 0.93 cm^{-1} or to $0.011 \text{ kJ}\cdot\text{mol}^{-1}$ for $g_e \approx 2$. Because D depends on r^{-3} , it is a very sensitive function of the molecular structure. The value of $|D|$ ranges from 0.001 to 2 cm^{-1} , i.e., $|D'|$ is of the order 1 mT to 2 T. Using the point-dipole approximation, $|D'|$ can be estimated from r , the average distance between the two unpaired electrons, and vice versa:

$$|D'| = 2.78 \cdot 10^9 r^{-3} \quad \text{or} \quad r = \sqrt[3]{2.78 \cdot 10^9 / |D'|} \quad (2.7)$$

where D' is in mT and r in pm [366].

Clearly, when $|D'|$ is comparable to or even larger than B , quantization of the spin in terms of $M_S = 1, 0, -1$ is meaningless, and specification by the space

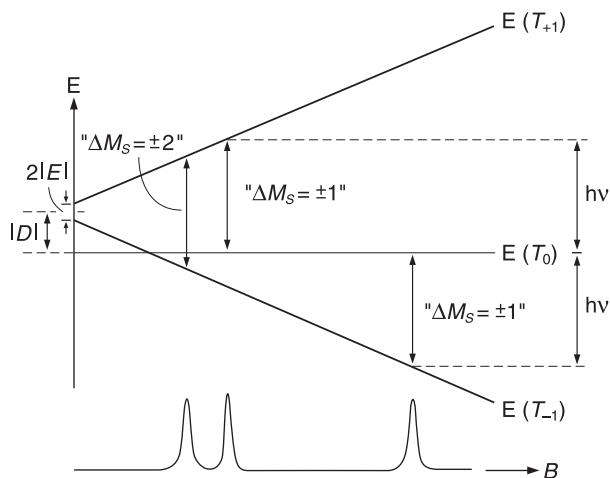


Fig. 2.3. Zero-field (D and E) and Zeeman splittings for an organic molecule in the triplet state as a function of the strength, B , of the magnetic field and ESR signals at resonance.

coordinates, x , y , z , is indicated. While the triplet function T_z (z is the direction of \vec{B}) can be identified with $T_0 = (1/\sqrt{2})(\alpha\beta + \beta\alpha)$, T_x and T_y are expressed as linear combinations of $T_{+1} = \alpha\alpha$ and $T_{-1} = \beta\beta$. Figure 2.3 shows the Zeeman splitting of an organic molecule in the triplet state with a positive D value of the order of 0.1 cm^{-1} and an orientation of \vec{B} perpendicular to the molecular π plane (z -direction). For large field-strength B (right side), the notation T_1 , T_0 , and T_{-1} and the ESR selection rule, $\Delta M_S = \pm 1$, are still valid; however, for low B values (left side), the notation T_x , T_y , and T_z is required, and this rule need not be strictly followed. With a constant energy, $h\nu$, of electromagnetic irradiation, two transitions, $E(T_{+1}) \leftrightarrow E(T_0)$ and $E(T_0) \leftrightarrow E(T_{-1})$ are allowed for $B \gg |D|$. Due to ZFS, they are strongly anisotropic and appear at different field strengths B ; both are labelled “ $\Delta M_S = \pm 1$ ” in Figure 2.3, although the lower-field component occurs at a rather small B value. In addition, for substantial ZFS, a third transition is usually observed at low B , where the ESR-selection rule is no longer effective. This “forbidden” transition is called “half-field” or “ $\Delta M_S = \pm 2$ ” and, in contrast to its “ ± 1 ” counterparts, it is essentially isotropic.

Because the $|D|$ value is relatively large, the dipolar interaction, E_{dip} , between the two unpaired electrons in the triplet state is, in general, not averaged out in solution by Brownian motion. The ESR absorption is spread over a wide field range and escapes observation [367, 368]. Therefore, except for species resembling biradicals with a long distance, r , between the two electrons (and thus a negligible $|D|$ value), ESR spectra of triplet-state molecules cannot be observed in fluid solution. That is why such spectra were first reported 10 years later than those of radicals and radical ions in the doublet state.

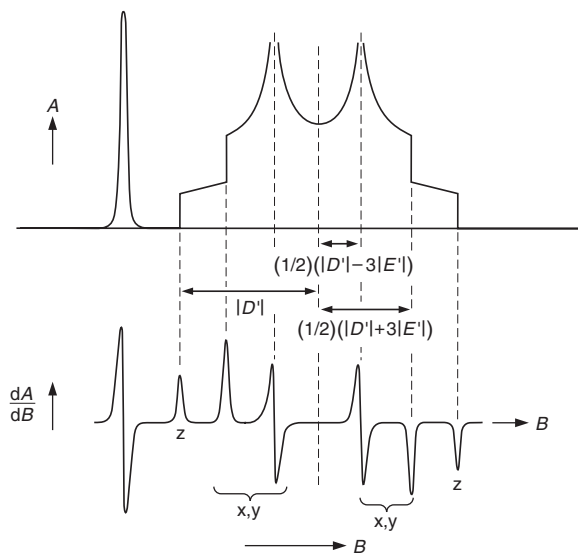


Fig. 2.4. Calculated ESR absorption, A , and its derivative, dA/dB , for an organic molecule in a randomly oriented triplet state as a function of the strength, B , of the magnetic field. Reproduced by permission from [368a].

To observe an ESR spectrum for a triplet molecule in a fixed orientation, a single crystal is required. Furthermore, because intermolecular interaction between the unpaired spins must be avoided, the paramagnetic species has to be diluted by embedding it within diamagnetic host molecules of similar shape. ESR spectra are then registered by rotating the crystal in the magnetic field. The first report on a successful ESR experiment of this kind was that of Hutchison and Mangum [369–371] for a triplet state generated by in-situ electronic excitation of naphthalene molecules in a single crystal of durene at 77 K. Use of diluted material instead of single crystals of pure naphthalene in this procedure prevented rapid exchange of the excitation and thus lengthened the lifetime of the triplet state. Similar studies on excited guest molecules in a crystal of a diamagnetic host followed (see below).

However, the single-crystal procedure, which can yield not only the parameters $|D|$ and $|E|$ for different orientations but also their relative signs, is very laborious, because a crystal of mixed compounds must be grown. Therefore, an alternative procedure is generally used. In a rigid glassy solution, summing of the individual contributions of randomly oriented, yet temporally immobilized, molecules in the triplet state does not lead to a broad, undifferentiated, ESR absorption A , and the derivative curve dA/dB exhibits marked turning points corresponding to the principal molecular axes x , y , and z (Figure 2.4) [372–374]. Six resonance lines then appear for the anisotropic “ $\Delta M_S = \pm 1$ ” transitions, in addition to the line at the half-field for the nearly isotropic “ $\Delta M_S = \pm 2$ ” transition. When $E = 0$, the x - and y -lines collapse, and only four lines are observed for the “ $\Delta M_S = \pm 1$ ” transitions.

The distance between the two outermost z lines yields twice the parameter $|D'|$, and $|E'|$ is derived from the positions of the x and y lines (Figure 2.4). For rigid glassy solutions in which randomly oriented triplets are photolytically produced, it is advantageous to use MTHF or mixtures of solvents that freeze to form an amorphous solid, namely decalin/cyclohexane and diethylether/pentane/ethanol (EPA), although other matrices are also applicable to this purpose.

It has been shown [17n, 375] that the “half-field $\Delta M_S = \pm 2$ ” transition gives rise to relatively strong ESR signals for triplet state with a short inter-spin distance r (large D values), because the intensity of this signal is proportional to r^{-6} .

Organic molecules in the triplet state can be classified into those generated by photoexcitation from their singlet ground state and those for which the triplet either is the ground state or is thermally accessible. Molecules with such a low-lying triplet state are rather exceptional, but, not uncommon, as follows from the examples given below.

Photoexcited Triplet States

Nearly all stable molecules are in a singlet ground state, with all their electrons paired in doubly occupied orbitals (*closed shells*), and this state is separated by several eV from electronically excited states. For systems, in which paired electrons are in bonding π orbitals or in nonbonding n orbitals of heteroatoms, promotion of an electron from these orbitals to an antibonding π^* orbital ($\pi \rightarrow \pi^*$ and $n \rightarrow \pi^*$) leads to a π, π^* or a n, π^* state having two singly occupied orbitals (*open shells*). Such an excited state is singlet or triplet; the latter lies below the former, and the singlet–triplet energy gap is markedly larger for a π, π^* than for a n, π^* state.

Excitation of molecules in the singlet ground state by irradiation in the UV or visible region leads to singlet states, because only electronic transitions with no change in spin multiplicity ($\Delta S = 0$) are allowed. The sequence of events following this excitation is illustrated by the so-called Jablonski diagram [376] (Figure 2.5). The excited states are energetically rather close, so that the upper singlets decay rapidly in a nonradiative way to the lowest excited state (*internal conversion*). The latter, referred to as the first excited singlet state, is also relatively short-lived (ca 10^{-8} s), because a radiative return to the singlet ground state is allowed; the emission is known as *fluorescence*. Nevertheless, some molecules in the first excited state may “prefer” to undergo nonradiative transition to the corresponding lower-lying triplet state (*intersystem crossing*). Because this transition is favored by a small singlet–triplet energy gap and by spin-orbit coupling, it is more frequent for molecules with n orbitals (e.g., ketones) and for those containing heavy atoms; the presence of heavy atoms in the solvent is also helpful. Radiative return from the triplet state to the singlet ground state is not allowed, so that the lifetime of this excited triplet is relatively long (10^{-3} to 10^2 s). Still, such a return can occur by *phosphorescence*, an emission which, compared to fluorescence, is at longer wavelength and delayed.

The phosphorescent state was recognized as a triplet state shortly before the advent of ESR spectroscopy [377], which provided definitive confirmation of this

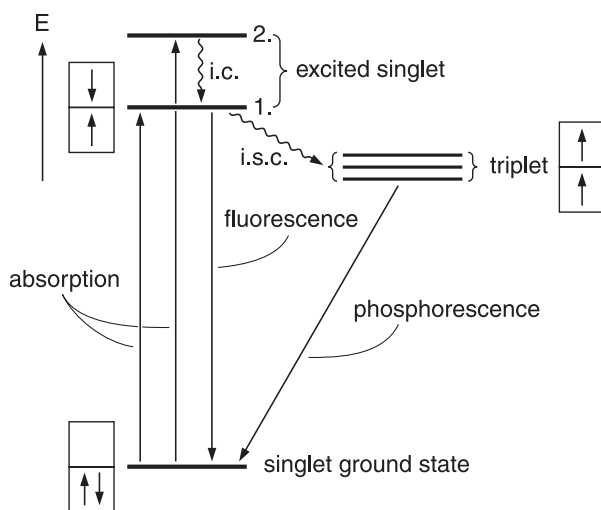


Fig. 2.5. Jablonski diagram. Nonradiative transitions, such as internal conversion (i.c.) and intersystem crossing (i.s.c.) are indicated by wavy lines.

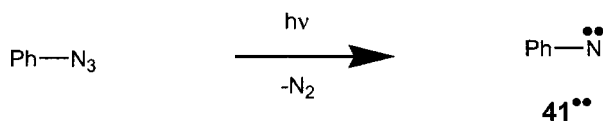
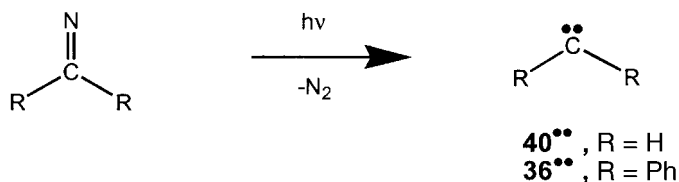
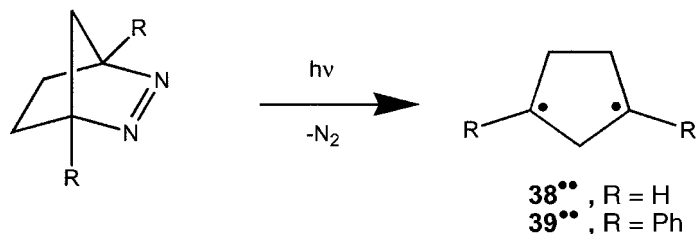
perception [17m]. ESR spectra of photoexcited triplet molecules in mixed single crystals were observed not only for naphthalene in durene [369–371] but also for other π -electron systems, e.g., toluene in benzene [378]; anthracene in phenazine [379]; phenanthrene [380] and acridine in biphenyl [381]; perdeuteriopyrene in fluorenone [382]; biphenyl in dibenzofuran [383]; quinoxaline, quinoline, and isoquinoline in durene [384, 385]; chrysene in *p*-terphenyl [386]; tolane (diphenylacetylene) in benzophenone [387]; and indene, indole, indazole, and cumarin in 1,4-dibromobenzene [388, 389].

UV irradiation of many benzenoid hydrocarbons and their derivatives in glasses led first to observation of the “ $\Delta M_S = \pm 2$ ” transition [390–392] and later also to that of the “ $\Delta M_S = \pm 1$ ” transitions. Among the compounds for which “ $\Delta M_S = \pm 1$ ” transitions were investigated by ESR spectroscopy in glasses are naphthalene, anthracene, and triphenylene [373]; phenanthrene and coronene [393]; chrysene [394]; and derivatives of pyrazine [395] and *sym*-triazine [396]. Analogous studies of excited triplet states have also been reported for paracyclophanes [397] and fullerenes [398].

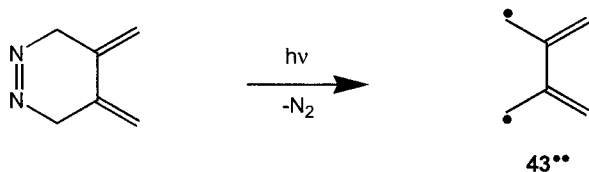
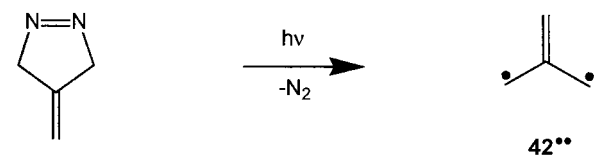
Ground or Thermally Accessible Triplet States

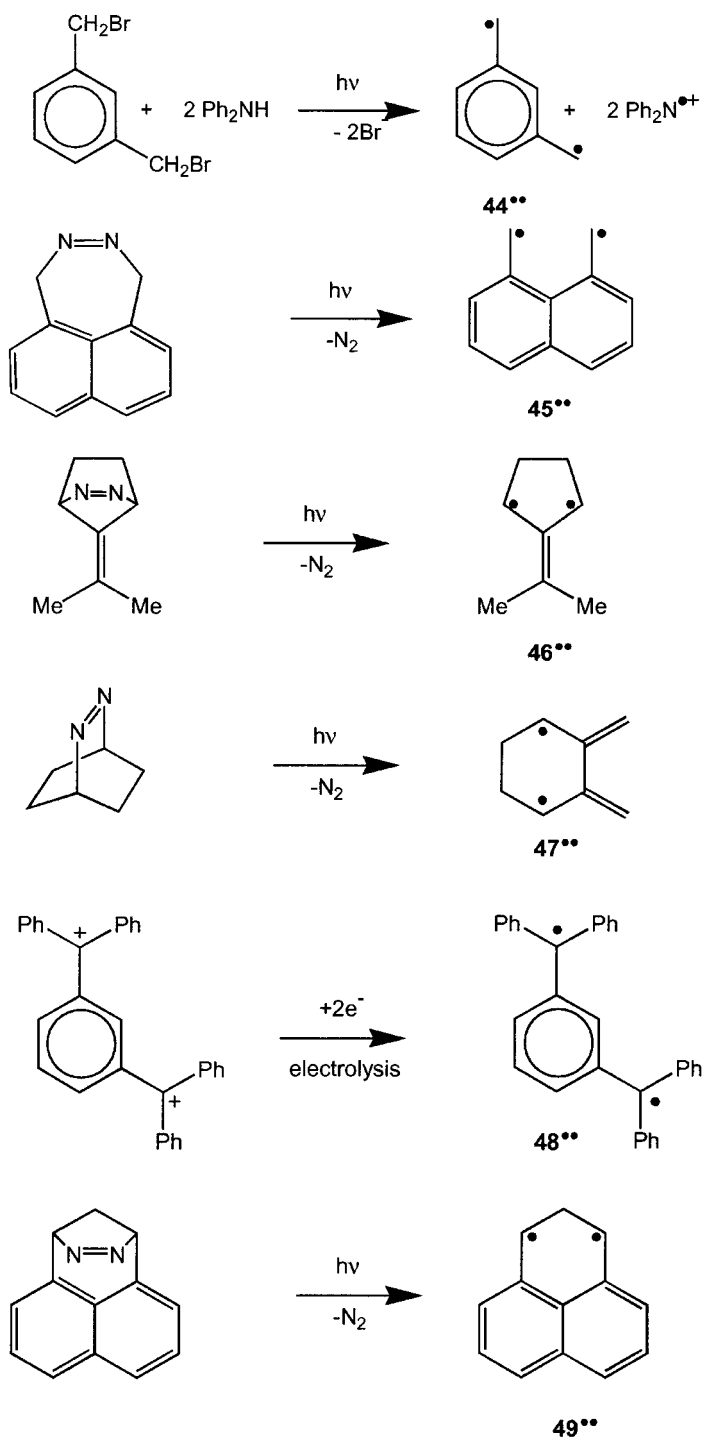
Neutral organic molecules in which the triplet is the ground state or is thermally accessible comprise alkanediyls, carbenes, and nitrenes, as well as non-Kekulé hydrocarbons. Unless stabilized by heavy substitution or by incorporation in a protecting molecular framework, they are short-lived. The usual method for generating them is photolysis of the corresponding diazo compound or other precursor in a glass. The two unpaired electrons in carbenes and nitrenes are primarily

accommodated by a single C and N atom, respectively, although one or two of these electrons can be delocalized over the π system of a substituent. Examples of alkanediyls are cyclopentane-1,3-diyl (**38 $\cdot\cdot$**) [399, 400] and its diphenyl derivative (**39 $\cdot\cdot$**) [401], while representatives of carbenes and nitrenes are the simplest carbene itself (**40 $\cdot\cdot$**) [402–404], diphenylcarbene (**36 $\cdot\cdot$**) [405, 406], and phenylnitrene (**41 $\cdot\cdot$**) [407, 408].



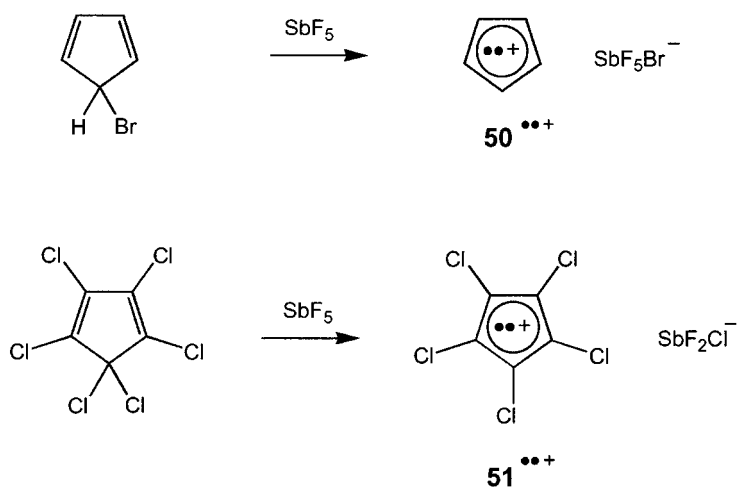
Non-Kekulé hydrocarbons [409] are π systems, like trimethylenemethane (TMM; **42 $\cdot\cdot$**) [410, 411], tetramethyleneethane (TME; **43 $\cdot\cdot$**) [412, 413], *m*-xylylene (*m*-benzoquinodimethane, **44 $\cdot\cdot$**) [414], and 1,8-naphthoquinodimethane (**45 $\cdot\cdot$**) [415], for which a Kekulé formula with fewer than two non- π -bonded carbon atoms cannot be written. They have been studied by ESR spectroscopy, as well as their derivatives such as **46 $\cdot\cdot$** [416], **47 $\cdot\cdot$** [417, 418], and **48 $\cdot\cdot$** [419] and **49 $\cdot\cdot$** [420].

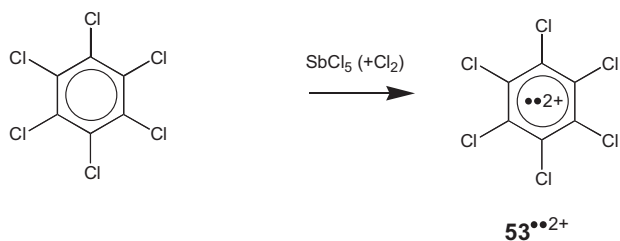
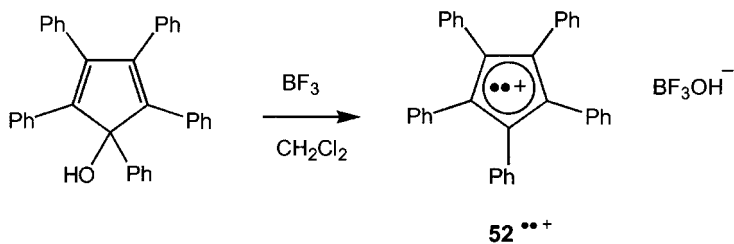




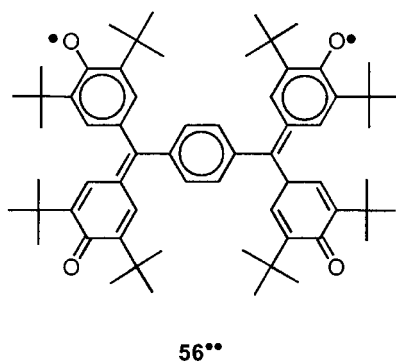
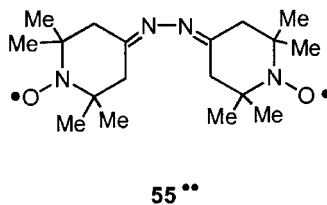
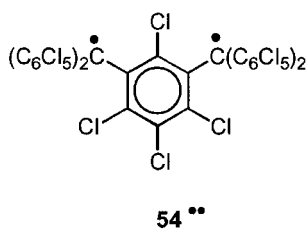
Dianions also can exist as ground-state or thermally accessible triplets. As stated in the Chapt. 2.3, dianions M^{2-} are generated via the radical anions $M^{\cdot-}$ by a prolonged reaction of the molecule M with an alkali-metal in a ethereal solution, preferably MTHF. These dianions, M^{2-} , are mostly diamagnetic, because the two additional electrons pairwise occupy the same lowest antibonding π orbital. However, for some molecules having axial symmetry (rotation axis C_n with $n \geq 3$), such orbitals are degenerate and their single occupancy, each by one unpaired electron, is allowed. ESR spectra of the pertinent triplet molecules can be observed in frozen solution. Such triplet dianions, $M^{\cdot\cdot 2-}$, of triphenylene [176], 1,3,5-triphenylbenzene, and decacyclene [175] are in the ground state, but that of coronene is a thermally accessible excited state [421]. Triplet dianions were also observed for [60]fullerene [422] and for molecules having two well-separated π systems, after prolonged contact with a potassium mirror [146, 156, 423, 424]. A ground-state triplet can often be distinguished from a thermally accessible triplet by the temperature dependence of the ESR spectrum. When a triplet is in the ground state, lowering the temperature, T , leads to enhancement of the absorption intensity, A , of the ESR signals, because magnetization is roughly proportional to $1/T$ (Eq. 1.8). On the other hand, for a thermally accessible triplet state, such an enhancement is counteracted by the Boltzmann distribution of the populations in this triplet and in the ground-state singlet. A plot of A vs. $1/T$ can thus exhibit a maximum at a certain value of T .

Positively charged organic triplet molecules are rare. ESR spectra of a ground state or a thermally accessible triplet have been reported for rigid solutions of the cations of cyclopentadienyl ($50^{\cdot\cdot+}$) [425] and its pentachloro- ($51^{\cdot\cdot+}$) [426, 427] and pentaphenyl ($52^{\cdot\cdot+}$) [427, 428] derivatives (see also [429–431]), as well as for the dications of hexachlorobenzene ($53^{\cdot\cdot 2+}$) [285], a hexaazaoctadecahydrocoronene [283] and a derivative of triaminobenzene [277].





Persistent biradicals, like **54** $\bullet\bullet$ [432], **55** $\bullet\bullet$ [433, 434], and **56** $\bullet\bullet$ [435, 436], contain persistent radical moieties, namely perchlorotriptyl (**3** \bullet), a nitroxyl related to TEMPO (**8** \bullet), and galvinoxyl (**10** \bullet), respectively (Chapt. 11.1).



The recently isolated stable carbenes, which are derivatives of imidazol, have a singlet ground state [437]. Like radicals in the doublet state, most triplet molecules are of the π type.

3

Electron–Nuclear Magnetic Interaction

3.1

Nuclear Magnetism

The spin and magnetic properties of a nucleus can be described by formulas that are fully analogous to those for an electron (Chapter 1.1). One merely has to replace the spin-quantum numbers S and $M_S = S, S - 1, \dots -S$, the multiplicity $2S + 1$, and the spin vector \vec{S} by the corresponding numbers I and $M_I = I, I - 1, \dots -I$, the multiplicity $2I + 1$, and the vector \vec{I} . In addition, the magnetic moment of an electron $\vec{\mu}_e = -[g_e\mu_B/\hbar]\vec{S}$ and its z component $\mu_{e,z} = -g_e\mu_B M_S$ are replaced by

$$\vec{\mu}_n = +[g_n\mu_N/\hbar]\vec{I} \quad \text{and} \quad \mu_{n,z} = +g_n\mu_N M_I \quad (3.1)$$

where g_n and $\vec{\mu}_n$ are the g factor and magnetic moment of the nucleus, and $\mu_N = 5.0508 \cdot 10^{-27} \text{ A}\cdot\text{m}^2$ or $\text{J}\cdot\text{T}^{-1}$ is the nuclear magneton. The essential differences between the spin and magnetic properties of an electron and those of a nucleus are as follows:

- (1) Whereas S is $1/2$ for a single electron and the g_e factor is ca 2 for an organic radical, the spin-quantum number I is a multiple of $1/2$, ranging from $1/2$ to $9/2$, and the g_n factor can assume values between -4 and $+6$, with both I and g_n depending on the individual nucleus X .
- (2) The nuclear magneton μ_N stands for $\hbar/(2m_p)$, where $m_p = 1.6726 \cdot 10^{-27} \text{ kg}$ is the rest mass of the proton. Thus, μ_N is smaller, by a factor $m_p/m_e = 1836$, than the Bohr magneton μ_B and, correspondingly, the nuclear magnetic moments $|\vec{\mu}_n|$ are about three orders of magnitude less than $|\vec{\mu}_e|$.
- (3) Because nuclei are positively charged throughout, the direction of $\vec{\mu}_n$ relative to \vec{I} is determined by the sign of g_n . For the great majority of nuclei, which have $g_n > 0$, the vector $\vec{\mu}_n$ is in the same direction as \vec{I} . Only for nuclei with $g_n < 0$ are the vectors $\vec{\mu}_n$ and \vec{I} opposed, like $\vec{\mu}_e$ and \vec{S} for the negatively charged electron.

The spin-quantum number I is closely related to the composition of the nucleus X . In this respect, the latter can be characterized as (even,even), (even,odd),

(odd,even), or (odd,odd), where the first notation refers to the number of protons and the second to the number of neutrons.

The (even,even) nuclei have $I = 0$ and include many stable, abundant nuclei such as ${}^4\text{He}(2,2)$, ${}^{12}\text{C}(6,6)$, ${}^{16}\text{O}(8,8)$, ${}^{24}\text{Mg}(12,12)$, ${}^{28}\text{Si}(14,14)$, ${}^{32}\text{S}(16,16)$, and ${}^{40}\text{Ca}(20,20)$. For the (even,odd) nuclei, like the less-abundant isotopes ${}^{13}\text{C}(6,7)$, ${}^{17}\text{O}(8,9)$, ${}^{25}\text{Mg}(12,13)$, ${}^{29}\text{Si}(14,15)$, and ${}^{33}\text{S}(16,17)$, the number I is an odd multiple of $1/2$, as it also is for the (odd,even) nuclei like ${}^1\text{H}(1,0)$, ${}^7\text{Li}(3,4)$, ${}^{11}\text{B}(5,6)$, ${}^{15}\text{N}(7,8)$, ${}^{19}\text{F}(9,10)$, ${}^{23}\text{Na}(11,12)$, ${}^{27}\text{Al}(13,14)$, ${}^{31}\text{P}(15,16)$, ${}^{35}\text{Cl}(17,18)$, ${}^{37}\text{Cl}(17,20)$, and ${}^{39}\text{K}(19,20)$. Lastly, I is an even multiple of $1/2$, i.e., an integer, for the (odd,odd) nuclei such as ${}^2\text{H}(1,1)$, ${}^6\text{Li}(3,3)$, ${}^{10}\text{B}(5,5)$, and ${}^{14}\text{N}(7,7)$.

The (even,even) nuclei, having $I = 0$, are clearly nonmagnetic, and their spins do not interact with those of electrons nor with an external field \vec{B} ; in contrast, the (even,odd), (odd,even), and (odd,odd) nuclei, by virtue of the fact that $I \neq 0$, are magnetic and amenable to such interactions. Table 3.1 lists the spin-quantum numbers I and M_I , the factors g_n , and the natural abundance of those magnetic

Tab. 3.1. Characteristic data of some magnetic nuclei.

<i>Isotope</i>	I	M_I	g_n	<i>Natural abundance (%)</i>
${}^1\text{H}$	$1/2$	$\pm 1/2$	5.5854	99.985
${}^2\text{H} \equiv \text{D}$	1	$\pm 1, 0$	0.8574	0.0148
${}^6\text{Li}$	1	$\pm 1, 0$	0.8221	7.5
${}^7\text{Li}$	$3/2$	$\pm 3/2, \pm 1/2$	2.1710	92.5
${}^9\text{Be}$	$3/2$	$\pm 3/2, \pm 1/2$	-0.7850	100
${}^{10}\text{B}$	3	$\pm 3, \pm 2, \pm 1, \pm 0$	0.6002	19.8
${}^{11}\text{B}$	$3/2$	$\pm 3/2, \pm 1/2$	1.7924	80.2
${}^{13}\text{C}$	$1/2$	$\pm 1/2$	1.4048	1.11
${}^{14}\text{N}$	1	$\pm 1, 0$	0.4038	99.63
${}^{15}\text{N}$	$1/2$	$\pm 1/2$	-0.5664	0.366
${}^{17}\text{O}$	$5/2$	$\pm 5/2, \pm 3/2, \pm 1/2$	-0.7575	0.038
${}^{19}\text{F}$	$1/2$	$\pm 1/2$	5.2577	100
${}^{23}\text{Na}$	$3/2$	$\pm 3/2, \pm 1/2$	1.4784	100
${}^{25}\text{Mg}$	$5/2$	$\pm 5/2, \pm 3/2, \pm 1/2$	-0.3422	10.00
${}^{27}\text{Al}$	$5/2$	$\pm 5/2, \pm 3/2, \pm 1/2$	1.4566	100
${}^{29}\text{Si}$	$1/2$	$\pm 1/2$	-1.1106	4.67
${}^{31}\text{P}$	$1/2$	$\pm 1/2$	2.2632	100
${}^{33}\text{S}$	$3/2$	$\pm 3/2, \pm 1/2$	0.4291	0.75
${}^{35}\text{Cl}$	$3/2$	$\pm 3/2, \pm 1/2$	0.5479	75.77
${}^{37}\text{Cl}$	$3/2$	$\pm 3/2, \pm 1/2$	0.4561	24.23
${}^{39}\text{K}$	$3/2$	$\pm 3/2, \pm 1/2$	0.2610	93.26
${}^{41}\text{K}$	$3/2$	$\pm 3/2, \pm 1/2$	0.1433	6.73
${}^{79}\text{Br}$	$3/2$	$\pm 3/2, \pm 1/2$	1.4043	50.69
${}^{81}\text{Br}$	$3/2$	$\pm 3/2, \pm 1/2$	1.5137	49.31
${}^{85}\text{Rb}$	$5/2$	$\pm 5/2, \pm 3/2, \pm 1/2$	0.5413	72.17
${}^{87}\text{Rb}$	$3/2$	$\pm 3/2, \pm 1/2$	1.8343	27.83
${}^{127}\text{I}$	$5/2$	$\pm 5/2, \pm 3/2, 1/2$	1.1253	100
${}^{133}\text{Cs}$	$7/2$	$\pm 7/2, \pm 5/2, \pm 3/2, \pm 1/2$	0.7378	100

nuclei X that are relevant to the ESR spectra of organic radicals dealt with in this book.

The behavior of a magnetic nucleus X in a field \vec{B} upon irradiation $h\nu$ is also described by formulas analogous to those for an electron. Thus, the interaction energy is

$$E = -\vec{\mu}_n \cdot \vec{B} = -\mu_{n,z}B = -g_n\mu_N M_I B \quad (3.2)$$

where $\vec{\mu}_n$ and g_n are characteristic of X. The resonance condition for observing a signal in nuclear magnetic resonance (NMR) spectra is

$$h\nu = g_n\mu_N B \quad (3.3)$$

in account of the selection rule $\Delta M_I = \pm 1$. Because the magneton μ_N is so much smaller than μ_B , the frequency ν is substantially lower for NMR ($\nu = \nu_n$) than for ESR ($\nu = \nu_e$) spectroscopy, even with a higher field strength B ; it usually lies in the region of radio waves.

Analogous to the gyromagnetic ratio, γ_e , of the electron, its nuclear counterpart, γ_n , is defined by

$$\nu_n = \gamma_n B \quad (3.4)$$

where $\gamma_n = g_n\mu_N/h = g_n \cdot 7.6226 \cdot 10^{-3}$ MHz/mT. For a proton with $g_n = 5.5854$, γ_n is $4.2575 \cdot 10^{-2}$ MHz/mT.

In the context of ESR spectroscopy, the enormous importance of the nuclei consists in their magnetic interaction with unpaired electrons. This interaction gives rise to the *hyperfine splitting* of ESR spectra, which provides the *most* important structural information for organic radicals. It justifies the expensive and complicated apparatus of ESR, as compared to the magnetic balance previously used for probing the paramagnetism of matter.

3.2

Hyperfine Splitting of ESR Signal

For a paramagnetic organic molecule in a magnetic field \vec{B} , the interactions due to the spins of unpaired electrons and magnetic nuclei can be symbolically represented by five terms:

$$“\vec{S} \cdot \vec{B}” + “\vec{I} \cdot \vec{B}” + “\vec{S} \cdot \vec{S}” + “\vec{S} \cdot \vec{I}” + “\vec{I} \cdot \vec{I}” \quad (3.5)$$

The first two terms, “ $\vec{S} \cdot \vec{B}$ ” and “ $\vec{I} \cdot \vec{B}$ ”, represent the electron- and nuclear-Zeeman interactions, respectively. The third term, “ $\vec{S} \cdot \vec{S}$ ”, is relevant to paramagnetic species with more than one unpaired electron, e.g., to triplets with \vec{S}_1 and \vec{S}_2 (fine splitting). The fourth term “ $\vec{S} \cdot \vec{I}$ ” stands for electron–nuclear inter-

action (hyperfine splitting), and the fifth, “ $\vec{\mathbf{I}} \cdot \vec{\mathbf{I}}$ ”, symbolizes nuclear–nuclear interaction (spin–spin coupling).

By virtue of $|\vec{\mu}_n|$ being about three orders of magnitude less than $|\vec{\mu}_e|$, terms in which $\vec{\mathbf{I}}$ replaces $\vec{\mathbf{S}}$ become smaller by the same magnitude. In a field strength B of 0.34 T, generally used in ESR spectroscopy, the relative sizes of the five terms are as follows:

$$“\vec{\mathbf{S}} \cdot \vec{\mathbf{B}}” \approx “\vec{\mathbf{S}} \cdot \vec{\mathbf{S}}” \gg “\vec{\mathbf{I}} \cdot \vec{\mathbf{B}}” \approx “\vec{\mathbf{S}} \cdot \vec{\mathbf{I}}” \gg “\vec{\mathbf{I}} \cdot \vec{\mathbf{I}}”$$

Together with the selection rules $\Delta M_S = \pm 1$ and $\Delta M_I = 0$, the three terms “ $\vec{\mathbf{S}} \cdot \vec{\mathbf{B}}$ ”, “ $\vec{\mathbf{S}} \cdot \vec{\mathbf{S}}$ ”, and “ $\vec{\mathbf{S}} \cdot \vec{\mathbf{I}}$ ” have to be considered in the ESR spectra of species with more than one unpaired electron, but “ $\vec{\mathbf{S}} \cdot \vec{\mathbf{B}}$ ” and “ $\vec{\mathbf{S}} \cdot \vec{\mathbf{I}}$ ” are sufficient for treating radicals. In NMR spectra, the selection rules $\Delta M_S = 0$ and $\Delta M_I = \pm 1$ and the terms “ $\vec{\mathbf{I}} \cdot \vec{\mathbf{B}}$ ”, “ $\vec{\mathbf{S}} \cdot \vec{\mathbf{I}}$ ”, and “ $\vec{\mathbf{I}} \cdot \vec{\mathbf{I}}$ ” are relevant in studies of paramagnetic species, although only “ $\vec{\mathbf{I}} \cdot \vec{\mathbf{B}}$ ” and “ $\vec{\mathbf{I}} \cdot \vec{\mathbf{I}}$ ” are involved in the usual investigations of diamagnetic molecules. The two terms “ $\vec{\mathbf{I}} \cdot \vec{\mathbf{B}}$ ” and “ $\vec{\mathbf{S}} \cdot \vec{\mathbf{I}}$ ” are important in *electron-nuclear double resonance* (ENDOR) spectroscopy, which is dealt with in Chapt. 5.2.

Because the magnetic electron–nuclear or hyperfine interaction “ $\vec{\mathbf{S}} \cdot \vec{\mathbf{I}}$ ” is usually much weaker than the electron–Zeeman energy “ $\vec{\mathbf{S}} \cdot \vec{\mathbf{B}}$ ”, the former can be treated as a perturbation of the latter. This treatment functions the better, the higher B and is, therefore, called the *strong-field approximation*. The perturbation by hyperfine interaction, which does not depend on B , splits every electron–Zeeman energy level, E_+ and E_- for radicals and $E(T_0)$, $E(T_{+1})$, and $E(T_{-1})$ for triplets, into several sublevels.

This hyperfine interaction, E_{hf} , is the sum of the classical *dipolar* term, E_{dip} , and the “quantum mechanical” term called the *Fermi-contact term* E_{Fc} :

$$E_{\text{hf}} = E_{\text{dip}} + E_{\text{Fc}} \quad (3.6)$$

Dipolar Interaction

This electron–nuclear interaction, E_{dip} , is fully analogous to its electron–electron counterpart, described by Eq. 2.5 for a triplet state. One has merely to replace the spin $\vec{\mathbf{S}}$ and the magnetic moment $\vec{\mu}_e$ of one unpaired electron by the corresponding vectors $\vec{\mathbf{I}}$ and $\vec{\mu}_n$ of the nucleus X.

$$E_{\text{dip}} = (\mu_o/4\pi)[(\vec{\mu}_e \cdot \vec{\mu}_n)r^{-3} - 3(\vec{\mu}_e \cdot \vec{\mathbf{r}})(\vec{\mu}_n \cdot \vec{\mathbf{r}})r^{-5}] \\ \propto (\vec{\mathbf{S}} \cdot \vec{\mathbf{I}})r^{-3} - 3(\vec{\mathbf{S}} \cdot \vec{\mathbf{r}})(\vec{\mathbf{I}} \cdot \vec{\mathbf{r}})r^{-5} \quad (3.7)$$

Being a function of $\vec{\mathbf{r}}$, which is here the vector joining $\vec{\mu}_e$ and $\vec{\mu}_n$ or $\vec{\mathbf{S}}$ and $\vec{\mathbf{I}}$, E_{dip} is strongly anisotropic. Analogous to its electron–electron counterpart (Eq. 2.6), it can be expressed as a product of the type

$$\vec{\mathbf{S}} \cdot \mathbf{A}_{\text{X,dip}} \cdot \vec{\mathbf{I}} \quad (3.8)$$

where $A_{X,\text{dip}}$ denotes a symmetric traceless tensor that depends on \vec{r} ; it is called the dipolar hyperfine tensor and is, like $\vec{\mu}_n$, characteristic of the nucleus X. In a strong field \vec{B} , the magnetic dipole moments can be considered to be aligned with the field (z-direction), so that $(\vec{\mu}_e \cdot \vec{\mu}_n) = \mu_{e,z} \cdot \mu_{n,z} = -g_e g_n \mu_B \mu_N M_S M_I$, $(\vec{\mu}_e \cdot \vec{r}) = \mu_{e,z} r \cos \varphi = -g_e \mu_B M_S r \cos \varphi$, and $(\vec{\mu}_n \cdot \vec{r}) = \mu_{n,z} r \cos \varphi = g_n \mu_N M_I r \cos \varphi$, where φ is the angle formed by \vec{r} with \vec{B} . By substitution into Eq. 3.7, one obtains

$$E_{\text{dip}} = (\mu_o/4\pi) g_e g_n \mu_B \mu_N M_S M_I r^{-3} (3 \cos^2 \varphi - 1) \quad (3.9)$$

The orientation dependence of E_{dip} is thus expressed by $(3 \cos^2 \varphi - 1)$. For a magnetic nucleus in an atom with nucleus X, E_{dip} has its maximum at $\varphi = 0^\circ$ or 180° with $3 \cos^2 \varphi - 1 = 2$, and its minimum at $\varphi = 90^\circ$ or 270° with $3 \cos^2 \varphi - 1 = -1$; it vanishes at $\varphi = 54.7^\circ$ (the *magic angle*). For example, when an unpaired electron is accommodated by a $2p_z$ orbital of a C atom, the maximum and minimum of E_{dip} are found for the orbital axis in a parallel (z) and perpendicular (x, y) orientation, respectively, relative to the direction of the field \vec{B} . The anisotropic interaction E_{dip} is ineffective when the unpaired electron occupies a “spherical” orbital of a “pure” s character. This interaction is preferably studied in single crystals, but can also be observed in glasses and powders for which the ESR absorption A and its derivative dA/dB exhibit a shape similar to that occurring with randomly oriented triplet molecules (Figure 2.4).

As stated above, electron–nuclear interactions are about three orders of magnitude weaker than their electron–electron counterparts, a statement that holds, in particular, for the dipolar interactions E_{dip} . Thus, in contrast to the analogous electron–electron interaction, the electron–nuclear interaction is generally averaged out to zero by the Brownian motion of molecules in fluid solution, although in a viscous medium an incomplete averaging out merely broadens the ESR lines. Thus, even though ESR studies of radicals in solid media, where E_{dip} is resolved and adds to E_{Fc} , can provide valuable structural information, most studies have been performed in fluid solution, in contrast to studies of triplet molecules.

Fermi-contact Term

Analysis of hyperfine splitting in the ESR spectra of radicals in fluid solution is more straightforward than in solid and viscous media, because it is exclusively due to the isotropic Fermi-contact term E_{Fc} . This term is expressed as

$$E_{\text{Fc}} = -(2/3) \mu_o (\vec{\mu}_e \cdot \vec{\mu}_n) \rho_S(0) \quad (3.10)$$

in which $\rho_S(0)$ is the spin density $\rho_S(x, y, z)$ at the nucleus ($x = y = z = 0$), where it is “contacted” by the unpaired electron. (Spin density is defined in Chapt. 4.1.) With the magnetic moments aligned in a strong field B , the formula in Eq. 3.10 transforms into

$$E_{\text{Fc}} = (2/3) \mu_o g_e g_n \mu_B \mu_N M_S M_I \rho_S(0) = [(2/3) \mu_o g_e g_n \mu_B \mu_N \rho_S(0)] M_S M_I \quad (3.11)$$

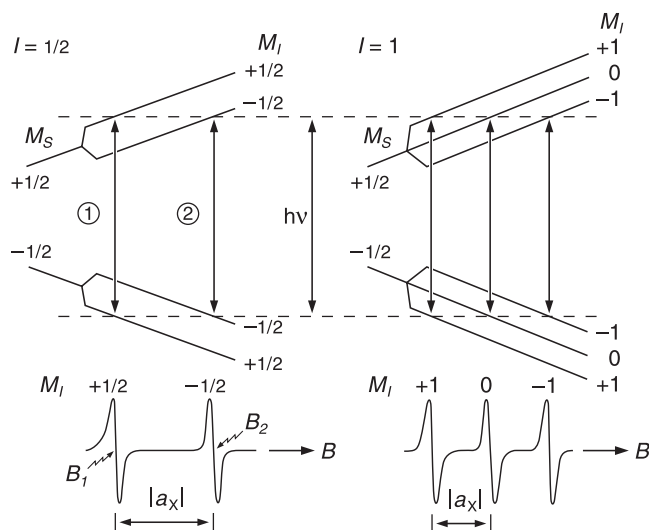


Fig. 3.1. Hyperfine splitting of the electron-Zeeman levels for one nucleus with $I = 1/2$ (left) and 1 (right). ESR signals as observed upon meeting the resonance condition. The signs of the quantum numbers M_I (positive in

the low- and negative in the high-field halves of the spectrum) hold for a positive coupling constant a_x . They are opposite for a negative a_x value.

The term in brackets is constant for a nucleus X and a given radical, and its sign depends on those of g_n of X and $\rho_S(0)$. Assuming that both are positive, the sign of E_{FC} is determined by that of $M_S M_I$, i.e., it is positive when M_S and M_I have the same sign but negative when they have opposite signs. Thus, the hyperfine interaction leads to a destabilization of the electron-Zeeman level in the former and to its stabilization in the latter case.

Figure 3.1 shows the hyperfine splitting by one nucleus X with $I = 1/2$ and $I = 1$ for a radical in a magnetic field \vec{B} when both g_n of X and $\rho_S(0)$ are positive. According to the ESR-selection rules $\Delta M_S = \pm 1$ and $\Delta M_I = 0$, two transitions are allowed for $I = 1/2$ and three for $I = 1$. The hyperfine components (lines) have practically the same intensity, because the nuclear magnetization and the differences in populations of the nuclear-Zeeman levels are about three orders of magnitude smaller than their electron counterparts (Eq. 1.8) and can be neglected here. The distance between the lines is the absolute value of the hyperfine coupling constant a_x of the nucleus X. Because $|a_x|$ is independent of the field strength B , it is usually measured in the unit of this field.

The resonance condition for the two transitions when $I = 1/2$ (Figure 3.1, left) is

$$\begin{aligned} h\nu &= g_e \mu_B B_1 + 2|E_{FC}| \quad \text{for transition ①, and} \\ h\nu &= g_e \mu_B B_2 - 2|E_{FC}| \quad \text{for transition ②} \end{aligned} \quad (3.12)$$

Equating the right-hand sides and setting $|E_{Fc}| = (2/3)\mu_o g_e \mu_B \mu_N |g_n \rho_S(0)|(1/4)$, where $1/4$ stands for $|M_S M_I|$, one obtains

$$|a_X| = B_2 - B_1 = 4|E_{Fc}|/(g_e \mu_B) = (2/3)\mu_o \mu_N g_n \rho_S(0) \quad (3.13)$$

in units of B . Although only the absolute value of a_X is directly derived from an ESR spectrum of a radical in fluid solution, its sign can be determined by several methods, described in Chapt. 6.5. Like the sign of the term in brackets in Eq. 3.11, that of a_X depends on the signs of g_n of X and of $\rho_S(0)$, i.e., it is positive when g_n and $\rho_S(0)$ have the same sign and negative when they have opposite signs. For the great majority of nuclei, which have positive g_n factors (Table 3.1), the sign of $\rho_S(0)$ is thus reflected by that of a_X .

Both the absolute value and the sign of the coupling constant a_X are given by

$$a_X = (2/3)\mu_o \mu_N g_n \rho_S(0) = K_X \rho_S(0) \quad (3.14)$$

The same formula for a_X can be deduced from the resonance conditions for a nucleus X with $I = 1$ (Figure 3.1, right), and it holds for *any* nucleus X and *any* spin-quantum number I . $K_X = (2/3)\mu_o \mu_N g_n$, which has the same sign as g_n of X, is characteristic of the nucleus X, and a_X is diagnostic of the interaction between X and the unpaired electron in a given radical, where it depends on $\rho_S(0)$.

The number of hyperfine lines grows multiplicatively with the number n of magnetic nuclei, because each additional nucleus X splits every line into equidistant $2I + 1$ lines of the same intensity; n nonequivalent nuclei thus give rise to $(2I + 1)^n$ lines. However, when n nuclei X are equivalent, some of the lines coincide and their number is reduced to $2nI + 1$. The hyperfine pattern then exhibits a characteristic distribution of intensities that is binomial for $I = 1/2$. Figure 3.2 shows the hyperfine splitting by two equivalent nuclei X with $I = 1/2$ and 1, and the scheme below presents the distribution of intensities for n equivalent nuclei with $n = 1$ through 6 for $I = 1/2$ (Pascal's triangle), with $n = 1$ through 4 for $I = 1$, and with $n = 1$ and 2 for $I = 3/2$.

$n = 0$	$I = 1/2$	1		$I = 1$		1
1		1	1		1	1
2		1	2	1	1	2
3		1	3	3	1	1
4	1	4	6	4	1	1
5	1	5	10	10	5	1
6	1	6	15	20	15	6

$n = 0$	$I = 3/2$	1
1		1
2	1	2

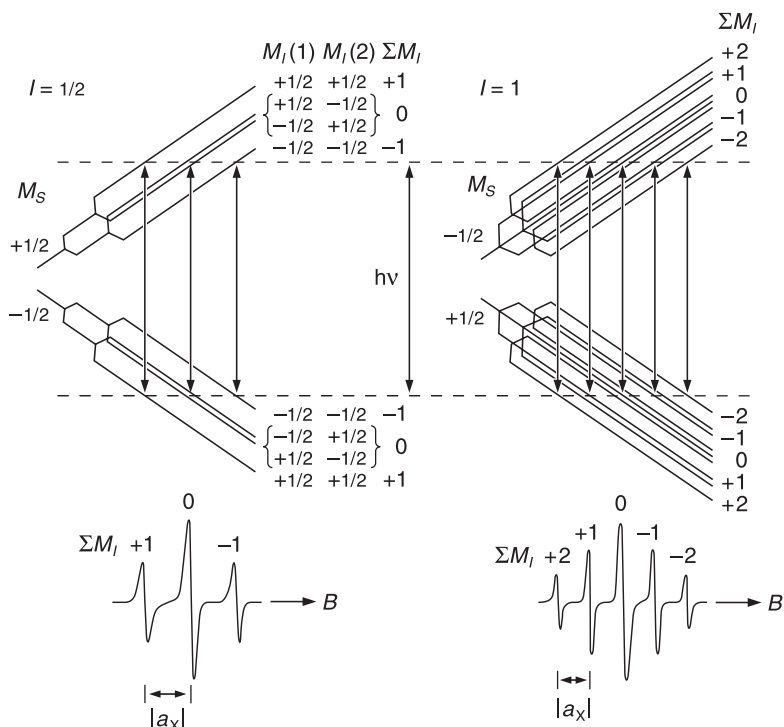


Fig. 3.2. Hyperfine splitting of the electron-Zeeman levels for two equivalent nuclei with $l = 1/2$ (left) and $l = 1$ (right). ESR signals as observed upon meeting the resonance condition. The signs of the quantum numbers M_I

(positive in the low- and negative in the high-field halves of the spectrum) hold for a positive coupling constant a_x . They are opposite for a negative a_x value.

When a radical contains 1, 2, 3, ... k sets, each consisting of $n_1, n_2, n_3, \dots, n_k$ equivalent nuclei X with $I_1, I_2, I_3, \dots, I_k$, the total number of lines is

$$(2n_1 I_1 + 1)(2n_2 I_2 + 1)(2n_3 I_3 + 1) \dots (2n_k I_k + 1) \quad (3.15)$$

With the coupling constants $a_{X1}, a_{X2}, a_{X3}, \dots, a_{Xk}$ pertinent to these sets, the total extent of the ESR spectrum, i.e., the distance between the outermost lines, is

$$(2n_1 I_1 |a_{X1}|) + (2n_2 I_2 |a_{X2}|) + (2n_3 I_3 |a_{X3}|) + \dots + (2n_k I_k |a_{Xk}|) \quad (3.16)$$

For example, the radical anion of 1,4,5,8-tetraazanaphthalene (57), which is associated with one sodium cation (ion pairing) [162], contains four ^{14}N nuclei with $I = 1$ and four protons with $I = 1/2$ and exhibits an interaction with one ^{23}Na nucleus ($I = 3/2$) of the counterion Na^+ . The total number of lines is $(2 \cdot 4 \cdot 1 + 1)(2 \cdot 4 \cdot 1/2 + 1)(2 \cdot 1 \cdot 3/2 + 1) = 9 \cdot 5 \cdot 4 = 180$, and the ESR spectrum extends over $8|a_{\text{N}}| + 4|a_{\text{H}}| + 3|a_{\text{Na}}|$.

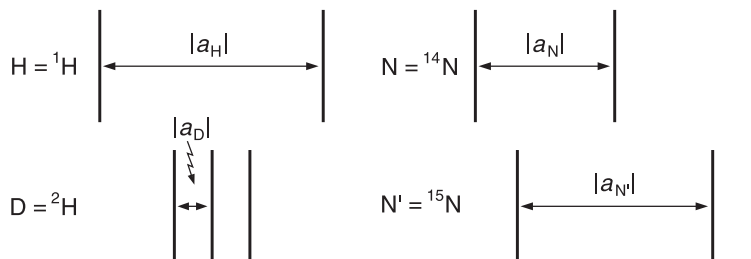
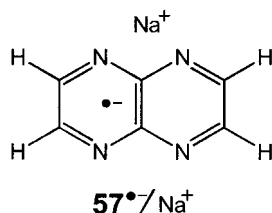


Fig. 3.3. Hyperfine patterns on replacing a proton (H) by a deuteron (D) and a ^{14}N nucleus (N) by its ^{15}N isotope (N').



Substitution of one nucleus X, having the spin quantum number I and the factor g_n , by its isotope X' with I' and g_n' changes the number of lines from $2I + 1$ to $2I' + 1$ and the coupling constant from a_X to $a_{X'} = a_X g_n' / g_n$. Thus, replacing a proton ($X = {}^1\text{H}=\text{H}$; $I = 1/2$; $g_n = 5.5854$) by a deuteron ($X = {}^2\text{H}=\text{D}$; $I = 1$; $g_n' = 0.8574$) increases the number of lines from $2 \cdot 1/2 + 1 = 2$ to $2 \cdot 1 + 1 = 3$ and decreases the coupling constant from a_H to $a_D = a_H 5.5854 / 0.8574 = 0.1535 a_H$. On the other hand, substituting a ^{14}N nucleus ($^{14}\text{N}=\text{N}$; $I = 1$; $g_n = 0.4038$) by its ^{15}N isotope ($^{15}\text{N}=\text{N}'$; $I = 1/2$; $g_n' = -0.5664$) decreases the number of lines from $2 \cdot 1 + 1 = 3$ to $2 \cdot 1/2 + 1 = 2$ and converts the coupling constant a_N into $a_{N'} = a_N (-0.5664) / 0.4038 = -1.4027 a_N$. However, as stated above, the sign of the coupling constant cannot be directly derived from the ESR spectrum, so that only an increase of $|a_N|$ to $|a_{N'}| = 1.4027 |a_N|$ is observed. The changes of $|a_H|$ into $|a_D|$ and of $|a_N|$ into $|a_{N'}|$ are illustrated in Figure 3.3. One can readily verify that, if in the ion pair $57^{\bullet-}/\text{Na}^+$ all four ^{14}N nuclei were replaced by the ^{15}N isotopes and all four protons by deuterons, the total number of lines would (exceptionally) remain the same, although their positions and relative intensities would change. The total extent of the ESR spectrum would decrease to $4|a_{N'}| + 8|a_D| + 3|a_{\text{Na}}| = 5.6108|a_N| + 1.2280|a_H| + 3|a_{\text{Na}}|$.

Second-order Splitting

So far, we have treated the hyperfine interaction as a first-order perturbation, which is sufficient for most organic radicals. In such a treatment, the values $|a_X|$ of the coupling constants are equal to the observed splittings, and the positions of the $2nI + 1$ lines arising from n equivalent nuclei X can be expressed by the first-order term

$$-a_X \sum M_I \quad (3.17)$$

which specifies these positions relative to the center of the ESR spectrum. The sum $\sum M_I$ is the magnetic spin quantum number of the total set of n equivalent nuclei X ; it can assume $2nI + 1$ values, namely $nI, nI - 1, \dots, -nI$. However, for some small radicals with large $|a_X|$ values, a second-order perturbation treatment may be required, so that a second-order term allowing for this perturbation must be added to that in Eq. 3.17, giving

$$-a_X \sum M_I - (a_X^2/2B)[I_s(I_s + 1) - (\sum M_I)^2] \quad (3.18)$$

In the calculation of this second-order term, each set of equivalent nuclei is divided into subsets with different spin multiplicities. For nuclei with $I = 1/2$, such as protons, in analogy to N electrons with $S = 1/2$ (branching diagram in Figure 2.2), these multiplicities are: singlet with $I_s = \sum M_I = 0$; doublet with $I_s = 1/2$ and $\sum M_I = +1/2, -1/2$; triplet with $I_s = 1$ and $\sum M_I = +1, 0, -1$; quartet with $I_s = 3/2$ and $\sum M_I = +3/2, +1/2, -1/2, -3/2$; quintet with $I_s = 2$ and $\sum M_I = +2, +1, 0, -1, -2$; and so on. One proton gives one doublet, two protons lead to one triplet and one singlet, three yield one quartet and two doublets, and four result in one quintet, three triplets and two singlets. The values of I_s , $\sum M_I$, and $I_s(I_s + 1) - (\sum M_I)^2$ required for the calculation of the second order term for $n = 1-4$ equivalent nuclei with $I = 1/2$, as well as the intensities of the resulting hyperfine lines, are given in Table 3.2. Figure 3.4 depicts the pertinent hyperfine patterns. Thus, in general, observation of the second-order splitting increases the number of hyperfine lines. Their relative intensity is determined by their statistical weight, i.e. by the number of subsets associated with these lines and having the same multiplicity. Taking three protons as an example, the lines due to the *two* doublets are thus twice as intense as those arising from the *sole* quartet (Table 3.2 and Figure 3.4).

On passing from the first-order pattern to the second-order splitting pattern, there is a slight shift of the center of gravity of the spectrum to lower field, so that the g_e factor seems to be increased and must be corrected for this shift. When $n = 1$ and $I = 1/2$, for which the two-line pattern remains unchanged, the shift of the center to lower field and the apparent increase in g_e are the only effects of the

Tab. 3.2. Numbers for calculating second-order splitting for $n = 1-4$ equivalent nuclei with $I = 1/2$. A = singlet, d = doublet, tr = triplet, qr = quartet, qn = quintet.

n	1	2			3			4					
I_s	1/2	1	1	0	3/2	3/2	1/2	2	2	2	1	1	0
$\sum M_I$	$\pm 1/2$	± 1	0	0	$\pm 3/2$	$\pm 1/2$	$\pm 1/2$	± 2	± 1	0	± 1	0	0
	(d)	(tr)	(tr)	(s)	(qr)	(qr)	(d)	(qn)	(qn)	(qn)	(tr)	(tr)	(s)
$I_s(I_s + 1) - (\sum M_I)^2$	1/2	1	2	0	3/2	7/2	1/2	2	5	6	1	2	0
relative intensity	1	1	1	1	1	1	2	1	1	1	3	3	2

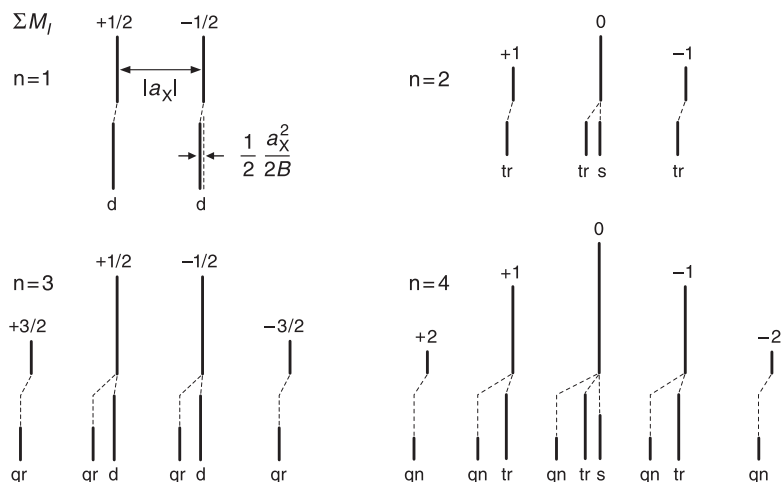


Fig. 3.4. Changes in the hyperfine pattern of n equivalent nuclei with $l = 1/2$ ($n = 1, 2, 3$, and 4) by allowing for second-order splitting. The signs of the quantum numbers ΣM_l (positive in the low- and negative in the high-field halves

of the spectrum) hold for a positive coupling constant a_X . They are opposite for a negative a_X value. s = singlet, d = doublet, tr = triplet, qr = quartet, qn = quintet.

second-order perturbation. It is obvious that, for $B = 340$ mT, the second-order splitting can be resolved only if $a_X^2/2B$ is comparable to the line-width of ca 0.01 mT, which holds for $|a_X|$ larger than ca 1.5 mT.

Complementary Remarks

When the dipolar interaction E_{dip} is effective and the corresponding hyperfine splitting is resolved, the contribution of this interaction adds to the isotropic value a_X , so that the observed coupling constant becomes orientation-dependent. In general, the coupling constant is represented by the hyperfine tensor A_X , of which the principal values, $A_{X,z}$, $A_{X,y}$, and $A_{X,x}$, are the anisotropic coupling constant in the directions z , y , and x (z is the direction parallel to the magnetic field \vec{B} , and x and y are perpendicular to it). Averaging of these values yields $a_X = (1/3)(A_{X,z} + A_{X,y} + A_{X,x})$. The anisotropic contributions to the coupling constant, $A_{X,z} - a_X$, $A_{X,y} - a_X$, and $A_{X,x} - a_X$, are the principal values of the dipolar hyperfine tensor $A_{X,\text{dip}}$ introduced in Eq. 3.8. Evidently, the sum of these values is zero, i.e., $A_{X,\text{dip}}$ is traceless. In the simplest case, for an unpaired electron in a $2p_z$ orbital of a single atom (AO) with nucleus X , the tensors A_X and $A_{X,\text{dip}}$ are axial. The principal values of an axial tensor A_X can then be denoted as $A_{X\parallel} (= A_{X,z})$ and $A_{X\perp} (= A_{X,y} = A_{X,x})$, and those of the also-axial tensor $A_{X,\text{dip}}$, which are proportional to $(3 \cos^2 \varphi - 1)$ (Eq. 3.9), can be represented by $+2B_{X,\text{dip}} (= A_{X\parallel} - a_X)$, $-B_{X,\text{dip}} (= A_{X\perp} - a_X)$, and $-B_{X,\text{dip}} (= A_{X\perp} - a_X)$. For an unpaired electron in a molecular orbital (MO) delocalized over several atoms and nuclei, as is usual, the situation is more compli-

cated, because the entire spin distribution must be considered. Examples are presented in Chapt. 4.1 and 4.2.

The treatment of the hyperfine splitting, presented above for radicals with one unpaired electron, is also valid for molecules in the triplet state with two unpaired electrons. However, with the exception of molecules in which the dipolar interaction between the two unpaired electrons is very weak, triplet molecules have to be studied in solid or viscous media, and the hyperfine splitting is only rarely resolved.

4 Spin Density, Spin Population, Spin Polarization, and Spin Delocalization

4.1 Concepts

Electron density $\rho(x, y, z)$ is the number of electrons per unit volume at a given site in a molecule, defined by the space coordinates x, y, z . It can be determined experimentally by X-ray diffraction or theoretically by quantum mechanical calculations, and it can be considered as the *sum* of contributions due to electrons having either spin up (\uparrow ; $M_S = +1/2$; α) or down (\downarrow ; $M_S = -1/2$; β):

$$\rho(x, y, z) = \rho^\uparrow(x, y, z) + \rho^\downarrow(x, y, z) \quad (4.1)$$

Analogously, spin density $\rho_S(x, y, z)$ introduced in Chapt. 3.2, denotes the *difference* between the contributions due to electrons having spin up (\uparrow ; $M_S = +1/2$; α) and down (\downarrow ; $M_S = -1/2$; β):

$$\rho_S(x, y, z) = \rho^\uparrow(x, y, z) - \rho^\downarrow(x, y, z) \quad (4.2)$$

In diamagnetic molecules in which all electrons are paired, $\rho^\uparrow(x, y, z) = \rho^\downarrow(x, y, z)$, and thus $\rho(x, y, z) = 2\rho^\uparrow(x, y, z) = 2\rho^\downarrow(x, y, z)$ and $\rho_S(x, y, z) = 0$ throughout the molecule. On the other hand, in paramagnetic molecules with at least one unpaired electron, the spin density $\rho_S(x, y, z)$, on the whole, is nonzero. Because, by convention, the spin up is assigned to the unpaired electrons, $\rho^\uparrow(x, y, z)$ should be larger than or, at most, equal to $\rho^\downarrow(x, y, z)$, i.e., the spin density $\rho_S(x, y, z)$ should generally be positive and rarely zero at some sites in the molecule. However, the occurrence of small negative spin densities at particular sites in a paramagnetic molecule is often predicted by theory and confirmed by experiment.

Hydrogen Atom

The simplest chemical paramagnetic system is the hydrogen atom H^\cdot that has a single proton in the nucleus and one unpaired electron in an *atomic 1s orbital* (1s-AO). Hence, $\rho(x, y, z) = \rho_S(x, y, z) = \rho^\uparrow(x, y, z) = \psi_{1s}^2(r) = [1/(\pi r_0^3)] \exp(-2r/r_0)$, where $\psi_{1s}(r)$ is a function of the 1s-AO, $r = \sqrt{x^2 + y^2 + z^2}$, and $r_0 = 0.5292 \cdot 10^{-10}$ m is the Bohr radius.

The term $K_H = (2/3)\mu_o g_n \mu_N$ in Eq. 3.14 amounts to $2.363 \cdot 10^{-32}$ V·s·m for a proton with $g_n = 5.5854$, and the spin density at the proton in H^\cdot is $\rho_S(0) = \psi_{1s}^2(0) = 1/(\pi r_o^3) = 2.148 \cdot 10^{30} \text{ m}^{-3}$. Therefore, the coupling constant is $a_H(H^\cdot) = K_H \rho_S(0) = 2.363 \cdot 10^{-32} \text{ V·s·m} \cdot 2.148 \cdot 10^{30} \text{ m}^{-3} = +5.076 \cdot 10^{-2} \text{ V·s·m}^{-2} = +50.76 \text{ mT}$. Isotropic substitution of the proton by deuteron reduces this value to $a_D(D^\cdot) = +50.76 \text{ mT} \cdot 0.1535 = +7.79 \text{ mT}$.

These purely theoretical values are in agreement with the experimental data, which depend somewhat on the conditions under which atomic H^\cdot or D^\cdot is generated (gas phase, liquid, solid) [18]. As stated above, because of the spherical shape of the 1s-AO, there is no dipolar magnetic hyperfine interaction in H^\cdot , so that the ESR spectra are purely isotropic in all media.

Unfortunately, such an exact calculation of $\rho_S(0)$ as for H^\cdot are computationally too hard for more complex paramagnetic systems like organic radicals. A convenient, albeit theoretically less strictly defined, quantum mechanical concept is the ψ -spin population ρ_X^ψ , where X is the nucleus of the atom in question, and ψ stands for the orbital. This spin population may be interpreted as an integrated spin density $\rho_S(x, y, z)$ in the orbital ψ centered on the nucleus X and is the difference in the populations of unpaired electrons with spin up and spin down:

$$\rho_X^\psi = \rho_X^{\psi\uparrow} - \rho_X^{\psi\downarrow} \quad (4.3)$$

Like $\rho_S(x, y, z)$, the spin population ρ_X^ψ is generally positive but can be zero or even negative in some sites of a paramagnetic molecule. A positive value of ρ_X^ψ signifies that the probability of finding the unpaired electron with the conventional spin up in the orbital ψ is larger than that for the spin down, and a negative value indicates the opposite situation. In contrast to the spin density $\rho_S(x, y, z)$, which is in units of m^{-3} , the spin population ρ_X^ψ is dimensionless. Unfortunately, most authors do not sufficiently differentiate between the two quantities and use the notation spin density also for the spin population. For H^\cdot , the unique spin population ρ_H^{1s} is obviously +1, because there is only a single unpaired electron, with spin up, in the 1s-AO.

In the following, the concept of a ψ -spin population will be applied to interpretation of the hyperfine splitting in the ESR spectra of some representative organic radicals. The two mechanisms of electron-spin transfer, *spin polarization* and *spin delocalization*, are introduced by considering the spin distribution in the methyl and ethyl radicals.

Methyl Radical

This simplest organic radical, H_3C^\cdot (**58** $^\cdot$), is planar (symmetry D_{3h}) and contains nine electrons, of which the unpaired one is accommodated in a nonbonding carbon $2p_z$ -AO with its axis perpendicular to the molecular x, y plane. Besides this uppermost, singly-occupied AO with a spin population $\rho_C^{2p} = +1$, there are four doubly-occupied orbitals, namely the nonbonding 1s-AO in the carbon inner shell and the three *molecular σ -orbitals* (σ -MOs) which are responsible for the C–H bonds

and are equivalent by symmetry. Each of these σ -MOs is formed by a hydrogen 1s-AO and a carbon sp^2 -hybrid orbital (h) that is constructed from one third of the 2s- and two thirds of $2p_x$ - and $2p_y$ -AOs. If electron–electron interaction is neglected, as for an independent-electron model, the spin density in 58^\bullet is determined solely by the squared function, $\psi_{2p_z}^2$, of the singly-occupied $2p_z$ -AO, which vanishes at the carbon nucleus and at the three protons lying in the nodal x, y plane of this orbital. Accordingly, the coupling constants a_C of a ^{13}C isotope and a_H of the three protons should be zero, and no hyperfine splitting should be observed in the ESR spectrum of 58^\bullet . This prediction is, however, in sharp contrast with experiment, because a value $|a_H| = 2.30$ mT [34] was found for the three protons, and, in addition $|a_C| = 3.83$ mT was determined for the ^{13}C isotope in 58^\bullet [438]. Remarkably, although a positive sign is required for a_C [439], that of a_H should be negative [440]. Admittedly, the size of $|a_H|$ is rather small compared with the corresponding value for H^\bullet , but, nevertheless, it clearly differs from zero. The σ -spin population, $\rho_H^{\sigma(1s)}$, in each hydrogen 1s-AO of the methyl radical (58^\bullet) can be deduced by comparison of the ^1H -coupling constants for the two species. Thus, $\rho_H^{\sigma(1s)}(58^\bullet) = \rho_H^{1s}(\text{H}^\bullet) \cdot a_H(58^\bullet)/a_H(\text{H}^\bullet) = +1(-2.30 \text{ mT})/50.76 \text{ mT} = -0.045$, where $\rho_H^{1s} = +1$ is the 1s-spin population of H^\bullet .

To account for this value of -0.045 , one has to realize that, in a many-electron system, the spin density and the spin population are not determined solely by the contribution of the singly-occupied orbital that formally accommodates the unpaired electron. This is because the unpaired electron spin polarizes the spins of the two formally paired electron spins in the doubly occupied orbitals, so that the latter are no longer perfectly paired. The spin polarization must be traced back to the theoretically and experimentally well-known fact that two electrons having the same spin interact differently from those with opposite spins. Whereas two electrons with the same spin cannot approach each other closely, such an approach is tolerated for those with opposite spins. Electrons with the same spin thus move, on average, farther apart than those with opposite spins. Consequently, an electron correlation by spin decreases the electrostatic repulsion of two negative charges for electrons with the same spin relative to that for electrons with opposite spins, and it lowers the energy for the former relative to the latter. On the same grounds, a triplet is more stable than a singlet for an equal electron configuration (Hund rule).

In the methyl radical (58^\bullet), it is the unpaired electron spin in the $2p_z$ -AO that polarizes the paired electron spins in the inner-shell carbon 1s-AO ($2p_z$, 1s-spin polarization) and in each of the three C–H σ bonds ($2p_z$, σ -spin polarization). The correlation by spin makes the spin arrangement labeled I in Figure 4.1 to be energetically slightly more favorable than that labeled II. Arrangement I shows that the electron in the carbon sp^2 -hybrid (h) orbital, forming the C–H σ bond, has the spin up, and its partner in the hydrogen 1s-AO is left with the spin down. In arrangement II, the spins of the two electrons in the C–H σ bond are reversed. Considering the C atom by itself, the two electrons in the sp^2 -hybrid orbital and in the $2p_z$ -AO can be regarded as a triplet when they have the spins shown in arrangement I but as a singlet when their spins are opposite, as in arrangement II. If one could take momentary snapshots of the spins in a C–H σ bond of 58^\bullet , the chance of

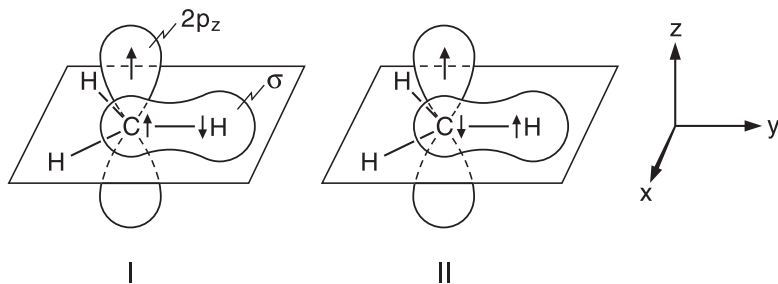


Fig. 4.1. Two alternative spin arrangements (I and II) of the formally paired electrons in a C–H σ bond of the methyl radical (58^{\bullet}).

seeing the spins in arrangement I would be 4.5% larger than in arrangement II. The spin population $\rho_{\text{H}}^{\sigma(1s)}$ (58^{\bullet}) of -0.045 corresponds to this percentage, and its negative sign accounts for the spin down of the electron in the hydrogen $1s$ -AO.

Spin polarization can be introduced into MO theory by using *different orbitals for different spins* (DODS). In the methyl radical, the σ -MO of a C–H bond is generally represented by a *linear combination of atomic orbitals* (LCAO), $c_{\text{h}}\psi_{\text{h}} + c_{1s}\psi_{1s}$, where ψ_{h} and ψ_{1s} are the AOs forming the bond, i.e., the sp^2 -hybrid, h , of C and the $1s$ of H. In the “restricted” MO version, which does not account for spin polarization, this MO is occupied by two paired electrons, so that it does not contribute to the spin population. However, in the “unrestricted” version, different MOs are assigned to different spins. In the slightly more stable σ -MO occupied by the electron with the spin up, this electron has some preference for the sp^2 -hybrid, h , of C, whereas its MO counterpart accommodating the electron with the spin down favors the $1s$ -AO of H. Consequently, $c_{\text{h}}^{\uparrow 2} > c_{\text{h}}^{\downarrow 2}$ and $c_{1s}^{\uparrow 2} < c_{1s}^{\downarrow 2}$, which leads to a small positive spin population $\rho_{\text{C}}^{\sigma(h)} = c_{\text{h}}^{\uparrow 2} - c_{\text{h}}^{\downarrow 2} = +0.045$ and a corresponding negative spin population $\rho_{\text{H}}^{\sigma(1s)} = c_{1s}^{\downarrow 2} - c_{1s}^{\uparrow 2} = -0.045$.

The coupling constant a_{C} is less easily interpreted than a_{H} , because it is due to several contributions by spin polarization. First, there are three contributions by $2p_z, \sigma$ -spin polarization, $\rho_{\text{C}}^{\sigma(h)} = 3(+0.045) = +0.135$ in the sp^2 -hybrid orbitals of the C atom. In addition, the unpaired electron spin in the $2p_z$ -AO interacts with the two formally paired electrons in the carbon inner-shell $1s$ -AO ($2p_z, 1s$ -polarization). As a result, the spins of the two electrons in this spherical AO correlate with unpaired electron spin in such way that the electron having the same spin up moves slightly closer to the unpaired electron than its partner with the spin down. Because an electron in the outer-shell $2p_z$ -AO is on average more remote from the C nucleus than those in the inner-shell $1s$ -AO, this displacement means that the electron with the spin up in the $1s$ -AO traces an orbit with a slightly larger radius than its partner with the spin down. The spin population ρ_{C}^{1s} is thus negative, because it is determined by the electron with the spin down, which is closer to the nucleus. The contributions by $2p_z, \sigma$ - and $2p_z, 1s$ -spin polarization were calculated as $3(+1.95 \text{ mT}) = +5.85 \text{ mT}$ and -1.27 mT , respectively, the sum of which gives $+4.58 \text{ mT}$ as a predicted value of a_{C} [439].

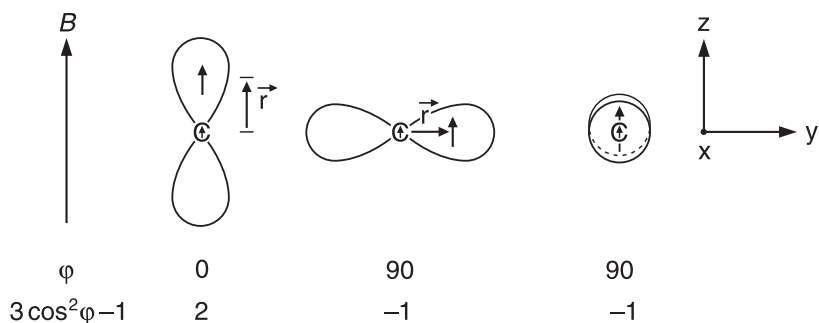


Fig. 4.2. Orientation-dependent magnetic dipolar interaction of a ^{13}C -nuclear spin with the unpaired electron spin in a carbon p-AO.

Both observed values, $a_{\text{H}} = -2.30$ mT and $a_{\text{C}} = +3.83$ mT, are isotropic coupling constants. The anisotropic contributions to the ^{13}C -coupling constant are due to the dipolar interaction between the magnetic moment of the unpaired electron in carbon p-AO and that of the ^{13}C nucleus of this atom. The orientation dependence of this interaction is expressed by Eq. 3.7, where \vec{r} is the vector joining two moments. Figure 4.2 shows the orientations of \vec{r} relative to \vec{B} . The principal values of the axial dipolar tensor $\mathbf{A}_{\text{C,dip}}$ are proportional to $3 \cos^2 \varphi - 1$, where φ is the angle formed by \vec{r} and \vec{B} (Eq. 3.9). This function of φ is +2, -1, and -1, when the axis of the spin-bearing p-AO is parallel to the z, y, and x directions, respectively (Chapt. 3.2). The anisotropy contributions to the ^{13}C -coupling constants, as the principal values of the tensor $\mathbf{A}_{\text{C,dip}}$, are $+2B_{\text{C,dip}}$, $-B_{\text{C,dip}}$, and $-B_{\text{C,dip}}$, in the directions z, y, and x, respectively. With $B_{\text{C,dip}}$ calculated as +3.25 mT [440], these values are +6.5 (z), -3.25 (y), and -3.25 mT (x). After adding to them the observed isotropic a_{C} value of +3.83 mT, the anisotropic ^{13}C -coupling constants, as the principal values of an axial tensor \mathbf{A}_{C} , should thus be $A_{\text{C}\parallel} (= A_{\text{C,z}}) = +10.4$ and $A_{\text{C}\perp} (= A_{\text{C,y}} = A_{\text{C,x}}) = +0.6$ mT. Experimentally available values for H_3C^\cdot formed in a MeV-irradiated single crystal of sodium acetate trihydrate are +8.7 (z), +1.55 (y), and +1.50 mT (x) [441] which yield a_{C} of +3.77 mT as the isotropic coupling constant.

The anisotropic contributions to the ^1H -coupling constant are due to the dipolar interaction between the magnetic moment of the unpaired electron in the carbon $2p_z$ -AO and a proton in the C-H bond. Because this interaction inversely depends on the 3rd power of the distance, r , between the unpaired electron and the nucleus, and because the proton is more remote from this electron than the ^{13}C nucleus, the hyperfine anisotropy is less pronounced for the proton than for ^{13}C nucleus. Figure 4.3 shows the orientations of the vector \vec{r} joining the magnetic moments of the electron and the proton. Their dependence on $3 \cos^2 \varphi - 1$ requires that the principal values of the (nonaxial) dipolar tensor $\mathbf{A}_{\text{H,dip}}$ should be in the ratio of to ca -0.25, +1.25, and -1 when the axis of the spin-bearing p-AO is parallel to the z, y, and x directions, respectively. They are calculated for the three orientations as -0.18 (z), +1.54 (y), and -1.36 mT (x) [442], and adding to them the observed

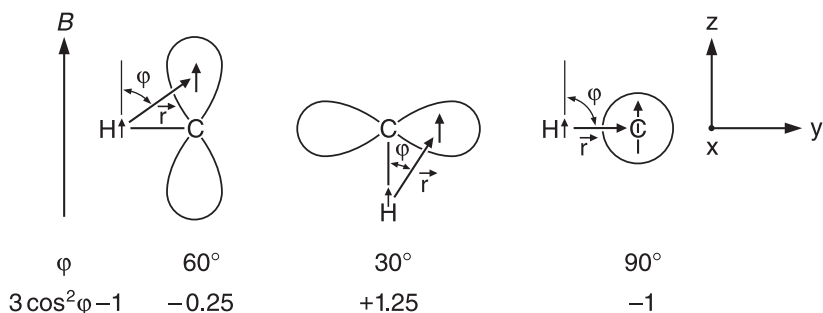


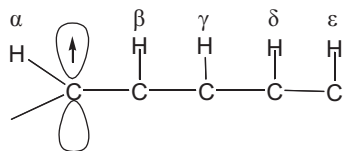
Fig. 4.3. Orientation-dependent magnetic dipolar interaction of a proton spin in a C–H σ bond with the unpaired electron spin in a carbon p-AO.

isotropic a_H value of -2.30 mT yields $A_{H,z} = -2.5$, $A_{H,y} = -0.8$, and $A_{H,x} = -3.8$ mT as the anisotropic ^1H -coupling constants and principal values of the (nonaxial) tensor \mathbf{A}_H in an oriented radical. Experimentally, similar values of -2.28 (z), -1.0 (y), and -3.3 mT (x) were found for the radical $\text{HC}^\bullet(\text{COOH})_2$ in a single crystal of an irradiated malonic acid [443].

Ethyl Radical

Substituting an H atom in $\text{H}_3\text{C}^\bullet$ by a methyl group yields the ethyl radical $\text{H}_2\text{C}^\bullet\text{--CH}_3$ (**59** $^\bullet$), in which the unpaired electron is still primarily accommodated in a carbon $2p_z$ -AO with its nodal x, y plane passing through the two C nuclei and the two methylene protons. The structure of **59** $^\bullet$ should thus be closely related to that of the methyl radical (**58** $^\bullet$), an expectation that is supported by similar coupling constants for the nuclei in the methylene group of **59** $^\bullet$, namely by $|a_H| = 2.24$ mT for the two protons [33, 34] and by $|a_C| = 3.91$ mT for the ^{13}C isotope [438]. Also, the sign of a_H and a_C ought to be negative and positive, respectively. Surprisingly, the value $|a_H| = 2.69$ mT, observed for the three equivalent protons in the freely rotating methyl group of the ethyl radical is larger than 2.24 mT, although the three protons are separated from the spin-bearing $2p_z$ -AO by an sp^3 -hybridized C atom. This value and the positive sign required for it cannot be accounted for by $2p_z$ - σ -spin polarization over two σ bonds and they point to a different mechanism of spin transfer.

Here, it is advisable to introduce the ESR nomenclature that denotes protons separated from the radical center by 0, 1, 2, 3, 4, or more sp^3 -hybridized C atoms as α , β , γ , δ , ϵ , etc.



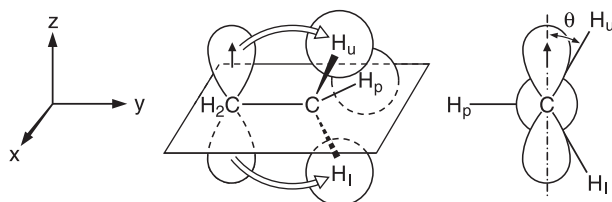


Fig. 4.4. Middle: Spin delocalization from the $2p_z$ -AO of the C atom to the $1s$ -AOs of methyl-H atoms in the ethyl radical (59^\bullet). Right: Newman projection in the direction of the C–C bond, showing the dihedral angle θ between the $2p_z$ -axis at the C atom and the methyl C–H bond.

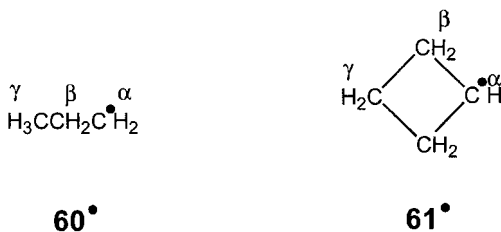
In alkyl radicals, such a center is the C atom with the spin-bearing $2p_z$ -AO; it is the only C atom in the methyl radical (58^\bullet) and the one in the methylene group of the ethyl radical (59^\bullet). The protons in H atoms linked to this C atom are labeled α , i.e., the three protons in 58^\bullet and the two methylene protons in 59^\bullet . The three methyl protons in 59^\bullet are labeled β , whereas there are no such protons in 58^\bullet . In π radicals, which are discussed in Chapt. 4.2, the same nomenclature is used with respect to each of the n π centers.

It is essential to note that, in contrast to the two protons directly linked to the C atom having the spin-bearing $2p_z$ -AO, the three β protons of 59^\bullet do not generally lie in the nodal plane of this orbital, so that spin population can delocalize from it into the $1s$ -AOs of the methyl-H atoms. The pertinent mechanism of spin transfer is $2p_z, 1s$ -spin delocalization which, in this particular case, is tantamount to the hyperconjugation familiar to organic chemists. In the conformation of the methyl group of 59^\bullet shown in Figure 4.4, the atoms H_u (upper) and H_l (lower) are situated above and below the nodal x, y plane of the $2p_z$ -AO, and H_p lies in this plane. A combination, $(1/\sqrt{2})(\psi_{H_u}^{1s} - \psi_{H_l}^{1s})$, of the $1s$ -AOs of H_u and H_l , represents a pseudo p_z -orbital that has the proper nodal properties for conjugation with the spin bearing $2p_z$ -AO and for a direct transfer of some spin population from this AO to the pseudo p_z -orbital. Although, in the conformation shown in Figure 4.4, the $1s$ -AO of H_p does not participate in this transfer, rotation of the methyl group assures that this AO has an equal share in the spin delocalization.

Clearly, the extent of hyperconjugation, and thus the size of the coupling constant, a_H , of a β proton, depends on the dihedral angle θ formed by the directions of the $2p_z$ axis and the C–H(β) σ bond (Figure 4.4); a_H should be proportional to $\cos^2 \theta$. The maximum of a_H should occur when the C–H bond eclipses the $2p_z$ -AO ($\theta = 0^\circ$ or 180° ; $\cos^2 \theta = 1$; optimal hyperconjugation), whereas a_H should vanish when this bond lies in the nodal plane of the AO ($\theta = 90^\circ$ or 270° ; $\cos^2 \theta = 0$; no hyperconjugation). For a freely rotating methyl group like that in 59^\bullet , the effective value $\langle \cos^2 \theta \rangle = 0.5$ corresponds to $\theta = 45^\circ$. This value is obtained by considering the conformation shown in Figure 4.4, in which the angle θ is 30° , 150° , and 270° for C– H_u , C– H_l , and C– H_p , respectively, and θ is averaged by rotation of the methyl groups to $\langle \cos^2 \theta \rangle = (1/3)(0.75 + 0.75 + 0) = 0.5$.

The $\cos^2 \theta$ dependence holds generally for coupling constants of β protons. It is used to derive the dihedral angle θ , which is diagnostic of the conformation, from the observed $|a_{\text{H}}|$ values of these protons when free rotation of the pertinent group is restricted.

The coupling constants of γ protons in acyclic and monocyclic alkyl radicals are, as expected, at least one order of magnitude smaller than those of their α and β counterparts. For example, the $|a_{\text{H}}(\gamma)|$ values for the freely rotating methyl group of the *n*-propyl radical (**60** \cdot) and for the less mobile methylene group of the cyclobutyl radical (**61** \cdot) were found to be 0.038 and 0.112 mT, respectively [34].



Such coupling constants can arise by both spin polarization and spin delocalization and may have either sign. The coupling constants, $a_{\text{H}}(\delta)$, of δ protons are still smaller, and the corresponding hyperfine splittings are usually unresolved. Only in more rigid polycyclic radicals can the γ and δ protons assume relatively large $|a_{\text{H}}(\gamma)|$ and $|a_{\text{H}}(\delta)|$ values, due to a special mechanism of spin delocalization (*long-range coupling*; see below).

Anisotropic contributions to the ^1H -coupling constants by dipolar interactions are much smaller for β than for α protons, because β protons are farther than α protons from the unpaired electron in the $2p_z$ -AO at the radical center. Except at very low temperatures, the methyl groups rotate freely even in solids, so that the tensors, \mathbf{A}_{H} and $\mathbf{A}_{\text{H,dip}}$, of the β protons in **59** \cdot are axial with the local symmetry axis C_3 in the z direction and x and y perpendicular to this axis. Because a value of +0.1 mT was found for $B_{\text{H,dip}}$ [444], the anisotropic contributions, representing the principal values of the tensor $\mathbf{A}_{\text{H,dip}}$, are +0.2 (z), -0.1 (y), and -0.1 mT (x). Such contributions decrease even more for the γ and δ protons and can often be neglected.

4.2

π Radicals

Coupling to α Protons

The methyl radical (**58** \cdot) can be considered as a prototype of a π system, because the sp^2 -hybridized C atom is the “unique π center”. In a π system with an unpaired electron, called a π radical, the electrons are delocalized over n sp^2 -hybridized C atoms, so that the spin population is distributed over all these n π

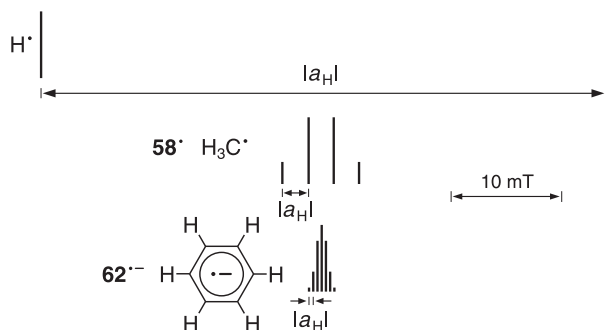


Fig. 4.5. Schematic hyperfine patterns of the hydrogen atom (H^\bullet), methyl radical (58^\bullet), and benzene radical anion ($62^{\bullet-}$).


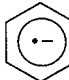
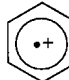

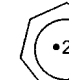
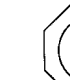
centers μ . Thus, the $2p_z$ -spin population, $\rho_C^{2p} = +1$, at the C atom of the methyl radical is distributed among n centers μ to yield π -spin populations ρ_μ^π as fractions of 1. Their sum over the n centers in the π radical must be unity:

$$\sum_{\mu=1}^n \rho_\mu^\pi = +1 \quad (4.4)$$

Notwithstanding the decreased spin population ρ_μ^π relative to ρ_C^{2p} , the same mechanism of spin polarization as that introduced for the α protons in the methyl radical is effective for such protons in the H atoms directly linked to the centers μ in the π radicals. One has merely to replace the C–H segment in the methyl radical (Figure 4.1) by a corresponding C–H segment of the π radical, which comprises a center μ with the spin population ρ_μ^π and the pertinent C_μ – H_μ σ bond. Strictly, the spin polarization, which is responsible for the spin transfer from the π -MO at this center μ to the $1s$ -AO of the H_μ atom linked to it, must now be regarded as a π, σ - rather than a $2p_z, \sigma$ -polarization. An illustrative example is the radical anion of benzene ($62^{\bullet-}$), which has six equivalent π centers μ . Hence, by symmetry, the spin population ρ_μ^π at each center μ must be $+1/6$. The observed $|a_{H_\mu}|$ value of the coupling constant of the six equivalent α protons is 0.375 mT [132]. It is instructive to compare the ESR spectra of the H^\bullet , the methyl radical (58^\bullet), and the benzene radical anion ($62^{\bullet-}$), as is done schematically in Figure 4.5. The spectrum of $62^{\bullet-}$ extends over $6|a_{H_\mu}| = 6 \cdot 0.375 \text{ mT} = 2.25 \text{ mT}$, which is almost equal to the $|a_H|$ value (2.30 mT) for each of the three α protons in 58^\bullet . This equality suggests a simple and important relation between the coupling constant, a_{H_μ} , of an α proton in a π radical and the spin population ρ_μ^π at the adjacent center μ :

$$a_{H_\mu}(\alpha) = Q_H^{C_\mu H_\mu} \rho_\mu^\pi \quad (4.5)$$

Tab. 4.1. Coupling constants a_{H_μ} and parameters $Q_H^{C_\mu H_\mu}$ in mT for some monocyclic π radicals.

						
n	5	6	6	7	7	18
a_{H_μ}	-0.602	-0.375	-0.444	-0.392	-0.348	-0.321
$Q_H^{C_\mu H_\mu}$	-3.01	-2.25	-2.66	-2.74	-2.44	-2.57
	[446]	[132]	[447]	[448]	[188]	[449]

In this relation, known as the McConnell equation [17f, 445], the proportionality factor $Q_H^{C_\mu H_\mu}$, in which the subscript H stands for the proton and the superscript $C_\mu H_\mu$ for the polarized σ bond, is usually referred to as the π, σ -spin-polarization parameter Q. Its sign is negative, in accord with the mechanism of spin polarization. Because 58^\bullet has a “single π center”, and the spin population ρ_μ^π in Eq. 4.5 is equal to $\rho_C^{2p} = +1$, the Q value must be comparable to $a_H = -2.30$ mT. This parameter is not a constant but depends, to some extent, on the structure of the π radical. Table 4.1 lists the values $|a_{H_\mu}|$ of the n equivalent α protons in a series of monocyclic π radicals of D_{nh} symmetry [132, 188, 446–449]. The spin population ρ_μ^π at each center μ of such a radical is $+1/n$, and a negative sign is required for the coupling constants a_{H_μ} .

Also shown are the corresponding values $Q = na_{H_\mu}$. As indicated by comparing monocycles of the same structure but different charge, such as the anion (62^{-}) and cation (62^{+}) of benzene and the neutral tropylium (cycloheptatrienyl; 63^\bullet) and its dianion (63^{2-}), $|Q|$ increases with a positive and decreases with a negative charge. In general, a Q value of -2.0 to -2.6 mT is appropriate for radical anions and dianions, -2.4 to -3.0 mT for neutral radicals, and -2.6 to -3.2 for radical cations. This variation of Q is traced back to a contraction of the orbitals by a positive charge. A relation using two parameters, Q_1 (corresponding to Q) and $Q_2 > 0$ ($|Q_2| < |Q|$), together with an excess π -charge population, ε_μ , at the center μ , $a_{H_\mu} = (Q_1 + \varepsilon_\mu Q_2)\rho_\mu^\pi$, was proposed to account for the charge dependence of a_{H_μ} [450], but it has rarely been applied in practice.

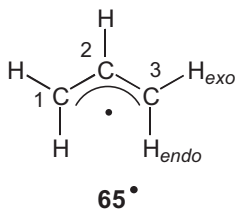
The π -spin populations, ρ_μ^π , at the centers μ and the coupling constants, a_{H_μ} , of the α protons map the distribution of the unpaired electron in the singly-occupied π -MO (SOMO). Because the unpaired electron has, by convention, the spin up, and because the ρ_μ^π values can be considered the probabilities of finding such an electron at the center μ , the ρ_μ^π values should generally be positive and only exceptionally zero when the π -SOMO happens to have an additional node at the pertinent center μ . Accordingly, the coupling constants a_{H_μ} , which for the α protons have a sign opposite to that of ρ_μ^π , are expected to be mostly negative and rarely zero. Such a view agrees with an MO model in which the π -SOMO ψ_j is represented by a linear combination of $2p_z$ -AOs ϕ_μ (LCAO) centered at the n sp^2 -hybridized C atoms (centers μ):

$$\psi_j = \sum_{\mu=1}^n c_{j,\mu} \phi_{\mu} \quad (4.6)$$

The π -spin population, ρ_{μ}^{π} , at the center μ is then given by the square of the LCAO coefficient $c_{j,\mu}$, whereby the normalization of these coefficients takes care of the requirement that they sum to one (Eq. 4.4):

$$\rho_{\mu}^{\pi} \approx c_{j,\mu}^2 \quad \text{and} \quad \sum_{\mu=1}^n \rho_{\mu}^{\pi} \approx \sum_{\mu=1}^n c_{j,\mu}^2 = 1 \quad (4.7)$$

The identification of ρ_{μ}^{π} with $c_{j,\mu}^2$ was, however, challenged by experiment, as exemplified by the ESR data for the allyl radical (**65** \cdot). The nonbonding SOMO ψ_2 of this radical with three π centers and three electrons in the π -MOs (π electrons) is expressed by $\psi_2 = 0.707\phi_1 - 0.707\phi_3$, so that $\rho_1^{\pi} = \rho_3^{\pi} \approx c_{2,1}^2 = c_{2,3}^2 = 0.5$ and $\rho_2^{\pi} \approx c_{2,2}^2 = 0$. The probability of finding the unpaired electron should thus be 50% at each of the two terminal π centers 1 and 3 but zero at center 2, where the SOMO has a nodal plane perpendicular to that of the π system. This prediction is in line with the description of **65** \cdot by the two mesomeric formulae $\text{CH}_2=\text{CH}-\text{CH}_2\cdot \leftrightarrow \cdot\text{CH}_2-\text{CH}=\text{CH}_2$.



Actually, a substantial value $|a_{\text{H}2}| = 0.406$ mT was observed for the α proton at center 2 of **65** \cdot , in addition to the values $|a_{\text{H}1,3\text{endo}}| = 1.393$ and $|a_{\text{H}1,3\text{exo}}| = 1.483$ mT, for the two equivalent α protons in the *endo* and *exo* positions at centers 1 and 3 [34]. Moreover, as shown below, although $a_{\text{H}1,3\text{endo}}$ and $a_{\text{H}1,3\text{exo}}$ should be negative, $a_{\text{H}2}$ is expected to have a positive sign.

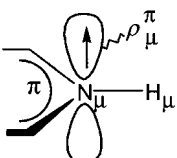
To account for the discrepancy between the simple MO model and the experimental data, π,π -spin polarization must be invoked. The unpaired electron with the conventional spin up in the π -SOMO polarizes not only the formally-paired electron spins in the σ bonds (π,σ -spin polarization) but also those in any doubly occupied orbital. This statement holds in particular for electron pairs in π -MOs (π,π -spin polarization). In a spin-polarized doubly occupied π -MO, the electron with the spin up favors the centers μ at which the probability of finding the unpaired electron is high and avoids the centers where such probability is low. Its partner with the opposite spin down behaves in the opposite way. The two electrons with different spins thus occupy somewhat different orbitals (DODS). Due to electron correlation by spin, the MO occupied by the electron with the spin up is energetically slightly favored relative to that in which the electron has the spin down.

For the allyl radical, the π,π -spin polarization involves the bonding π -MO, $\psi_1 = 0.500\phi_1 + 0.707\phi_2 + 0.500\phi_3$, which accommodates two out of three π electrons. The electron with the spin up occupies a slightly more stable MO ψ_1^\uparrow , for which the squared LCAO coefficients, $c_{1,1}^{12} = c_{1,3}^{12}$, at centers 1 and 3 are increased and the coefficient, $c_{1,2}^{12}$, at center 2 is decreased. The effect of the π,π -spin polarization on the MO ψ_1^\downarrow occupied by the electron with the spin down is opposite. As a result, $c_{1,1}^{12} = c_{1,3}^{12} > c_{1,1}^{12} = c_{1,3}^{12}$, and $c_{1,2}^{12} < c_{1,2}^{12}$. The differences are calculated as $c_{1,1}^{12} - c_{1,1}^{12} = c_{1,3}^{12} - c_{1,3}^{12} = +0.0885$ and $c_{1,2}^{12} - c_{1,2}^{12} = -0.177$ (Chapt. 4.5). They have to be added to the values, $c_{2,1}^2 = c_{2,3}^2 = 0.5$ and $c_{2,2}^2 = 0$, for the SOMO ψ_2 to yield the spin populations $\rho_1^\pi = \rho_3^\pi = +0.500 + 0.09 = 0.59$ and $\rho_2^\pi = 0 - 0.18 = -0.18$. According to the McConnell equation (Eq. 4.5), with the parameter $Q_H^{C_\mu H_\mu}$ of ca -2.4 mT, these $\rho_{1,3}^\pi$ and ρ_2^π values comply with the observed coupling constants $|\bar{a}_{H1,3}| = (1/2)(|a_{H1,3endo} + a_{H1,3exo}|) = 1.438$ and $|a_{H2}| = 0.406$ mT, if $a_{H1,3endo}$ and $a_{H1,3exo}$ are negative and a_{H2} is positive.

It is noteworthy that the sum of ρ_μ^π in 65° , $2(+0.59) - 0.18$, is $+1$, in accord with Eq. 4.4, but the sum of $|\rho_\mu^\pi|$, $2 \cdot 0.59 + 0.18$ is 1.36 . In general, as a consequence of the occurrence of negative π -spin populations and of the compensating increase in the positive π -spin populations, the sum $\sum |\rho_\mu^\pi|$ exceeds unity. Concomitantly, the total extent of the ESR spectrum, which depends on $|a_{H_\mu}|$ and, therefore, on $|\rho_\mu^\pi|$, is wider.

In summary, due to spin polarization, negative spin populations occur in the nodal planes of the π -SOMO. First, this statement holds for α protons situated in the molecular plane of the π radical that is the nodal plane of the π system. Because the π -spin population, ρ_μ^π , at a center μ is generally positive, π,σ -spin polarization leads to a negative $1s$ -spin population at the pertinent H_μ atom and likewise to a negative coupling constant a_{H_μ} . However, when the SOMO has an additional nodal plane perpendicular to that of the π system and passing through the π -center μ , π,π -spin polarization causes the π -spin population ρ_μ^π itself to be negative, so that the effects of both polarization mechanisms are superimposed to yield a positive spin population ρ_H^{1s} at the H_μ atom and a positive a_{H_μ} value for the α proton. Actually, a negative π -spin population ρ_μ^π and a positive coupling constant a_{H_μ} appear even when the center μ does not lie exactly in the additional nodal plane of the SOMO ψ_j but when the node passes close to it. Such a situation implies that the squared coefficient, $c_{j,\mu}^2$, is very small, and thus the negative contribution to ρ_μ^π by the π,π -spin polarization dominates this π -spin population.

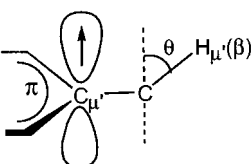
A relation corresponding to the McConnell equation (Eq. 4.5) can be also applied to radicals with hetero- π -centers μ . For example, when an α proton linked to an N atom as the π center μ , such a relation is

$$a_{H_\mu}(\alpha) = Q_H^{N_\mu H_\mu} \rho_\mu^\pi \quad (4.8)$$


with the parameter $Q_H^{N_\mu H_\mu}$ having negative values, similar to those of $Q_H^{C_\mu H_\mu}$ [451].

Coupling to β Protons

While the methyl radical (58 \cdot) may be regarded as a prototype of an unsubstituted π radical, the ethyl radical (59 \cdot) can be considered a prototype of an alkyl-substituted π radical. $2p_z, \sigma$ -Spin delocalization (hyperconjugation), which is responsible for the spin transfer from the $2p_z$ -AO at the methylene-C atom to the $1s$ -AOs at the methyl-H atoms in the ethyl radical (59 \cdot), is also the main mechanism of spin transfer in alkyl-substituted π radicals [452, 453]. Because the $2p_z$ -AO at a substituted center μ' takes part in the π -SOMO extended over n sp^2 -hybridized C atoms, such a mechanism must be renamed π, σ -spin delocalization, and the spin population, $\rho_C^{2p} = +1$, also has to be scaled down to the π -spin population, $\rho_{\mu'}^{\pi}$. The coupling constant, $a_{H_{\mu'}(\beta)}$, of a β proton separated from the center μ' by a sp^3 -hybridized C atom likewise depends on $\langle \cos^2 \theta \rangle$, where θ is the dihedral angle formed by the direction of the $2p_z$ -axis at center μ' and the direction of the pertinent C–H(β) σ bond of the alkyl group (Figure 4.6, right). The relation between the coupling constant, $a_{H_{\mu'}(\beta)}$, of a β proton in an alkyl substituent, the π -spin population, $\rho_{\mu'}^{\pi}$, at the substituted center μ' , and $\langle \cos^2 \theta \rangle$ is expressed by [454, 455]

$$a_{H_{\mu'}(\beta)} = B_{\text{H}}^{C_{\mu'}\text{CH}_{\mu'}} \rho_{\mu'}^{\pi} \langle \cos^2 \theta \rangle \quad (4.9)$$


which is analogous to Eq. 4.5 for the α protons. The proportionality factor $B_{\text{H}}^{C_{\mu'}\text{CH}_{\mu'}}$, in which the subscript H stands for the β proton and the superscript $C_{\mu'}\text{CH}_{\mu'}$ for the two σ bonds between this proton and the substituted center μ' is the π, σ -spin-delocalization parameter, usually denoted B. The parameter B has a positive sign, consistent with this mechanism of spin transfer, and its value is comparable to $2(+2.69 \text{ mT}) = +5.38 \text{ mT}$, which is twice the coupling constant of the three β

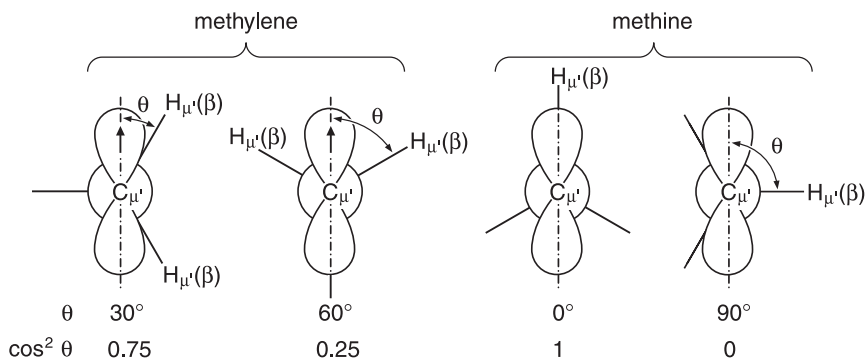
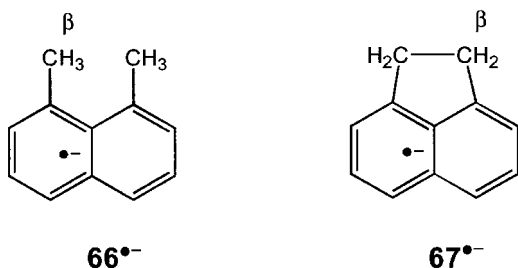
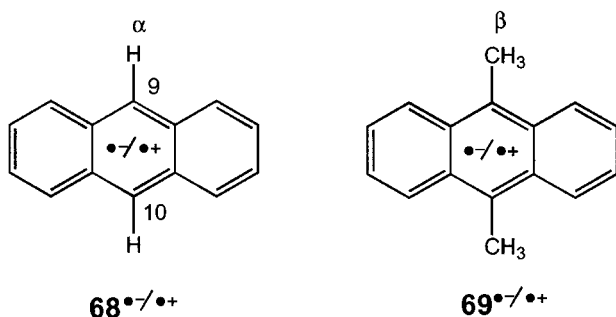


Fig. 4.6. Newman projections in the direction of the $C_{\mu'}\text{--C(alkyl)}$ bond for some characteristic conformations of methylene and methine groups.

protons in 59^{\cdot} . This is because, for 59^{\cdot} , $a_{H_{\mu'}}$ can be set to +2.69 mT and the spin population $\rho_{\mu'}^{\pi}$ to +1, and $\langle \cos^2 \theta \rangle$ is 0.5 for the freely rotating methyl group (Chapt. 4.1). Characteristic conformations of two equivalent methylene β protons and a single methine β proton are shown in Figure 4.6. The dependence of the coupling constants, $a_{H_{\mu'}}$, of β protons on the angle θ is illustrated by the data for the radical anions of 1,8-dimethylnaphthalene (**66**) (Table 8.9) [135] and acenaphthylene (**67**) (Table 8.9) [453], which have a similar π -spin distribution. Whereas in $66^{\cdot-}$ the methyl groups are freely rotating and $\langle \cos^2 \theta \rangle$ is 0.5, for the methylene groups in $67^{\cdot-}$, $\theta \approx 25^{\circ}$ and $\langle \cos^2 \theta \rangle \approx 0.82$. The ratio of the coupling constant of the six methyl β protons in $66^{\cdot-}$ to that of the four methylene β protons in $67^{\cdot-}$ is $+0.451 \text{ mT}/+0.753 \text{ mT} = 0.6$, which is close to $0.50/0.82$, as expected.



The parameter B depends even more strongly on the π charge at the relevant substituted center μ' than the Q value (Eq. 4.5) on such charge at a center μ , a finding which is in line with the experience that hyperconjugation is enhanced in positively charged molecules. Appropriate values of B are +4 to +5 mT for radical anions, +5 to +6 mT for neutral radicals, and +6 to +9 mT for radical cations. The stronger charge dependence of the coupling constants of β protons relative to those of α protons is demonstrated by the data for the radical ions of anthracene (**68**) (Table 8.8) [134] and its 9,10-dimethyl derivative (**69**) [223]. Such a comparison is justified by the fact that the π -spin distribution in the radical anion and radical cation of the same alternant π system, like **68**, is almost equal (Chapt. 8.1). The coupling constant, $a_{H_{9,10}}$, of the two α protons in the 9,10 positions increases by a factor $-0.653 \text{ mT}/-0.534 \text{ mT} = 1.22$ on going from $68^{\cdot-}$ to $68^{\cdot+}$; however, on passing from $69^{\cdot-}$ to $69^{\cdot+}$, the analogous factor for the six β protons of the methyl substituents in these positions is $+0.800 \text{ mT}/+0.388 \text{ mT} = 2.06$.



Because the parameter $B_{\text{H}}^{C_{\mu'}\text{CH}_{\mu'}}$ is positive, the coupling constants, $a_{\text{H}_{\mu'}}$, of the β protons have the same sign as has the π -spin population, $\rho_{\mu'}^{\pi}$, at the substituted center μ' , i.e., this sign is usually positive and less frequently negative.

In general, Eq. 4.9, in which the coupling to β protons is considered as being solely due to π, σ -spin delocalization (hyperconjugation), satisfactorily accounts for the $a_{\text{H}_{\mu'}}$ values of these protons, because the contribution by π, σ -spin polarization over two σ bonds can be neglected. Only when the β proton lies in the molecular π plane, which is the nodal plane of the π -SOMO, the dihedral angle θ is 90° and the hyperconjugation is ineffective, so that the observed, usually very small, coupling constant, $a_{\text{H}_{\mu'}}$, of this proton arises from π, σ -spin polarization.

Eq. 4.9 has to be modified when a methylene or a methine group bridges two π centers μ' and μ'' , which means that it is linked to both centers [456]. The coupling constant of the β protons in this group is

$$a_{\text{H}_{\mu', \mu''}}(\beta) = B_{\text{H}}^{C_{\mu'}\text{CH}_{\mu'}} (\sqrt{\rho_{\mu'}^{\pi}} \pm \sqrt{\rho_{\mu''}^{\pi}})^2 \langle \cos^2 \theta \rangle \approx B_{\text{H}}^{C_{\mu'}\text{CH}_{\mu'}} (c_{j, \mu'} + c_{j, \mu''})^2 \langle \cos^2 \theta \rangle \quad (4.10)$$

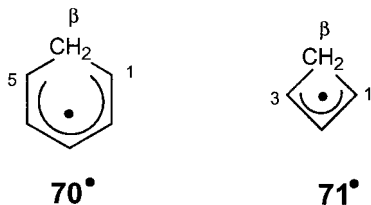
instead of $a_{\text{H}_{\mu', \mu''}}(\beta) = B_{\text{H}}^{C_{\mu'}\text{CH}_{\mu'}} (\rho_{\mu'}^{\pi} + \rho_{\mu''}^{\pi}) \langle \cos^2 \theta \rangle \approx B_{\text{H}}^{C_{\mu'}\text{CH}_{\mu'}} (c_{j, \mu'}^2 + c_{j, \mu''}^2) \langle \cos^2 \theta \rangle$. The π -spin populations, $\rho_{\mu'}^{\pi} \approx c_{j, \mu'}^2$ and $\rho_{\mu''}^{\pi} \approx c_{j, \mu''}^2$, at the centers μ' and μ'' are both positive, but the pertinent LCAO coefficients $c_{j, \mu'}$ and $c_{j, \mu''}$ in the π -SOMO ψ_j can have the same or opposite signs. In the algebraic sum $\sqrt{\rho_{\mu'}^{\pi}} \pm \sqrt{\rho_{\mu''}^{\pi}}$ of Eq. 4.10, “plus” has to be used when the signs of these coefficients are the same and “minus” when they are opposite. In most cases, the bridged centers μ' and μ'' are equivalent by symmetry, so that $\rho_{\mu'}^{\pi} = \rho_{\mu''}^{\pi}$ and $c_{j, \mu'}^2 = c_{j, \mu''}^2$. With $c_{j, \mu''}$ and $c_{j, \mu'}$ having the same sign, Eq. 4.10 then simplifies to

$$a_{\text{H}_{\mu', \mu''}}(\beta) = 4B_{\text{H}}^{C_{\mu'}\text{CH}_{\mu'}} \rho_{\mu'}^{\pi} \langle \cos^2 \theta \rangle \approx 4B_{\text{H}}^{C_{\mu'}\text{CH}_{\mu'}} c_{j, \mu'}^2 \langle \cos^2 \theta \rangle \quad (4.11)$$

a relation that holds instead of $a_{\text{H}_{\mu', \mu''}} = 2B_{\text{H}}^{C_{\mu'}\text{CH}_{\mu'}} \rho_{\mu'}^{\pi} \langle \cos^2 \theta \rangle \approx 2B_{\text{H}}^{C_{\mu'}\text{CH}_{\mu'}} c_{j, \mu'}^2 \langle \cos^2 \theta \rangle$.

The striking twofold increase in the coupling constant of β protons, sometimes referred to as the “Whiffen effect” [456], has been confirmed often by experiment [233, 317, 457]. Less spectacular is the situation when $c_{j, \mu''} = -c_{j, \mu'}$, i.e., when the bridging methylene group lies in the additional nodal plane of the SOMO (perpendicular to the molecular plane), because then a coupling constant $a_{\text{H}_{\mu', \mu''}} = 0$ is predicted. Illustrative examples are the cyclohexadienyl (70^\bullet) (Table 8.3) [34] and the cyclobutenyl (71^\bullet) (Table 8.2) [458] radicals. The SOMO ψ_3 of the pentadienyl π system in 70^\bullet has $c_{3,1}^2 = c_{3,5}^2 = 0.33$ and $\rho_1^{\pi} = \rho_5^{\pi} = +0.43$ at the bridged centers $\mu' = 1$ and $\mu'' = 5$, and the SOMO ψ_2 of the allyl π system in 71^\bullet has $c_{2,1}^2 = c_{2,3}^2 = 0.50$ and $\rho_1^{\pi} = \rho_3^{\pi} = +0.59$ at the corresponding centers 1 and 3. The angle θ and the $\langle \cos^2 \theta \rangle$ values are estimated as 30° and 0.75 for 70^\bullet and as 20° and 0.88 for 71^\bullet . Thus, both the π -spin populations $\rho_{\mu'}^{\pi} = \rho_{\mu''}^{\pi}$ and the $\langle \cos^2 \theta \rangle$ values are even larger for 71^\bullet than for 70^\bullet . However, the coupling constant of the two methylene β protons in 70^\bullet is unusually large, +4.77 mT, whereas the analogous value

of the protons in **71** \cdot , 0.445 mT (sign undetermined), is ten times smaller. These findings are clear evidence for the validity of Eq. 4.10, because the relevant LCAO coefficients at the centers μ' and μ'' have the same sign in **70** \cdot ($c_{3,5} = c_{3,1}$) but opposite signs in **71** \cdot ($c_{2,3} = -c_{2,1}$).



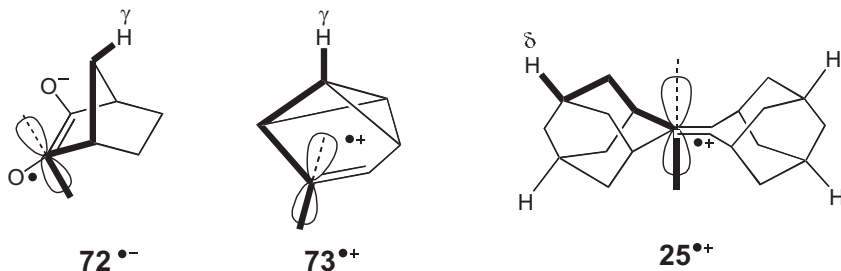
As for α protons, a relation analogous to that for the C centers can also be used for hetero- π centers. Thus, when such a substituted center μ' is replaced by an N center, the relation

$$a_{H_{\mu'}}(\beta) = B_H^{N_{\mu'}CH_{\mu'}} \rho_{\mu}^{\pi} \langle \cos^2 \theta \rangle \quad (4.12)$$

in which the parameter $B_H^{N_{\mu'}CH_{\mu'}}$ has a positive value comparable to $B_H^{C_{\mu'}CH_{\mu'}}$ [237], is valid (as are equations analogous to Eqs. 4.10 and 4.11) with $B_H^{N_{\mu'}CH_{\mu'}}$ replacing $B_H^{C_{\mu'}CH_{\mu'}}$.

Long-range Coupling

It was stated in Chapt. 4.1 that the size of the ^1H -coupling constants in acyclic and monocyclic alkyl radicals decreases rapidly with the number of σ bonds separating the protons from the radical center with the spin-bearing $2p_z$ -AO, so that the coupling constants of the γ protons are generally at least ten times less than those of the α and β protons, and the hyperfine splittings by the δ protons are usually too small to be resolved. Only in some rigid polycyclic radicals can the coupling constants of γ and δ protons assume relatively large values. The mechanism of spin transfer in such a long-range coupling is π, σ -spin delocalization which, like hyperconjugation in the case of β protons, is enhanced by a positive charge at the substituted or bridged π center μ' . The spin delocalization occurs mostly through σ bonds and generally leads to positive ^1H -coupling constants. The through-bond interaction is effective particularly when the $2p_z$ axis at the center μ' and the σ bonds linking it with the γ or δ proton lie almost in a plane and are arranged in a zigzag line which, for the γ proton, is also called a W arrangement (homo-hyperconjugation). Illustrative examples are these coupling constants: +0.648 mT for the methylene *anti*- γ proton in the radical anion of bicyclo[2.2.1]heptane-2,3-dione (**72**) (Table 9.15) [7c, 459], +2.79 mT for the two methine γ protons in the radical cation of tricyclo[3.1.0.0^{2,6}]hex-3-ene (benzvalene; **73**) (Table 7.15) [460], and +0.605 mT for the four equatorial methine δ protons in the radical cation of adamantylideneadamantane (**25**) (Table 7.15) [272].



Long-range coupling can also occur through space as in some *syn*-aryliminoxyl radicals (Chapt. 7.4), but it is rather rarely observed, because such an interaction requires close proximity between the proton and the π center μ' , which leads to a substantial overlap between the π -MO at this center and the 1s-MO of the pertinent H atom.

Coupling to Nuclei Other than Protons

The coupling constant, a_{X_μ} , of a magnetic nucleus X in a π center μ is related to the π -spin populations, ρ_μ^π and ρ_ν^π , at the center μ and the adjacent centers ν , by

$$a_{X_\mu} = Q_X \rho_\mu^\pi + \sum_\nu Q_X^{X_\nu X_\mu} \rho_\nu^\pi \quad (4.13)$$

where Q_X and $Q_X^{X_\nu X_\mu}$ are spin-polarization parameters [439]. Q_X accounts for polarization of electron spins in the AOs of X_μ and in the X_μ - X_ν σ bonds by the unpaired π electron at the center μ itself (π -spin population ρ_μ^π), and $Q_X^{X_\nu X_\mu}$ is responsible for the polarization of the electron spins in the X_ν - X_μ σ bonds by the unpaired π electron at the adjacent centers ν (π -spin populations ρ_ν^π). The two parameters are discussed in more detail for the particular case of nucleus X being ^{13}C and the centers μ and ν being C atoms ($X_\mu = \text{C}_\mu$; $X_\nu = \text{C}_\nu$). Here, Eq. 4.13 is expressed by

$$a_{\text{C}_\mu} = Q_{\text{C}} \rho_\mu^\pi + \sum_\nu Q_{\text{C}}^{\text{C}_\nu \text{C}_\mu} \rho_\nu^\pi \quad (4.14)$$

In Eq. 4.14, Q_{C} represents a sum of several parameters, namely:

$$Q_{\text{C}} = S_{\text{C}} + n_{\text{H}} Q_{\text{C}}^{\text{C}_\mu \text{H}_\mu} + (3 - n_{\text{H}}) Q_{\text{C}}^{\text{C}_\mu \text{C}_\nu} \quad (4.15)$$

where n_{H} is the number of H atoms at the C center μ . The parameter S_{C} and $Q_{\text{C}}^{\text{C}_\mu \text{H}_\mu}$, calculated as -1.27 and $+1.95$ mT [439], respectively, were considered, without being denoted as such, for interpretation of the ^{13}C -coupling constant of the methyl radical (**58'**) (Chapt. 4.1). S_{C} accounts for polarization of electron spins in the nonbonding inner-shell 1s-AO by ρ_μ^π . This π ,1s-spin polarization gives rise to

a negative 1s-spin population at the ^{13}C isotope, because the electron with the spin down moves preferably in an orbit closer to the nucleus. The parameters $Q_C^{C_\mu H_\mu}$ and $Q_C^{C_\mu C_\nu}$ are responsible for polarization of electron spins in the $C_\mu\text{-H}_\mu$ and $C_\mu\text{-C}_\nu$ σ bonds. These polarization parameters lead to positive spin populations in the sp^2 -hybrid orbitals of C_μ , because arrangements in which the electron closer to the nucleus in C_μ has the spin up are favored. Such spin arrangements are like those labeled I in Figure 4.1 for a C-H σ bond in **58**. Because $\rho_\mu^\pi = +1$, and $n_H = 3$, $Q_C = S_C + 3Q_C^{C_\mu H_\mu} = +4.58$ mT for this radical. However, in π radicals with a delocalized unpaired electron, the center μ is generally linked to two ($n_H = 1$) or three centers ν ($n_H = 0$). The third parameter $Q_C^{C_\mu C_\nu}$ in Eq. 4.15 is then relevant. It has been calculated as +1.44 mT [439] and, therefore, $Q_C = S_C + Q_C^{C_\mu H_\mu} + 2Q_C^{C_\mu C_\nu} = +3.56$ mT for a proton-bearing center μ , or $Q_C = S_C + 3Q_C^{C_\mu C_\nu} = +3.05$ mT for a center that is devoid of protons (a *blind* center).

Polarization of electron spins in the $C_\nu\text{-C}_\mu$ σ bonds by the π -spin population, ρ_ν^π , at the adjacent centers ν is taken into account by the parameter $Q_C^{C_\nu C_\mu}$ in Eq. 4.14. This π, σ -spin polarization yields negative spin populations in the sp^2 -hybrid orbitals of C_μ , because now an arrangement is preferred in which the electron with the spin up is closer to the nucleus in C_ν , so that its partner with the spin down is nearer to the nucleus in C_μ . With $Q_C = +3.56$ or $+3.05$ mT and $Q_C^{C_\nu C_\mu}$ calculated as -1.39 mT [439], Eq. 4.14, is expressed in mT by

$$a_{C_\mu} = +35.6\rho_\mu^\pi - 1.39(\rho_\nu^\pi + \rho_{\nu'}^\pi) \quad (4.16)$$

for a center μ bearing one proton, and by

$$a_{C_\mu} = +3.05\rho_\mu^\pi - 1.39(\rho_{\nu'}^\pi + \rho_{\nu''}^\pi) \quad (4.17)$$

for a blind center μ [439].

The spin arrangements pertinent to the parameters S_C , $Q_C^{C_\mu H_\mu}$, $Q_C^{C_\mu C_\nu}$, and $Q_C^{C_\nu C_\mu}$ are shown in Figure 4.7.

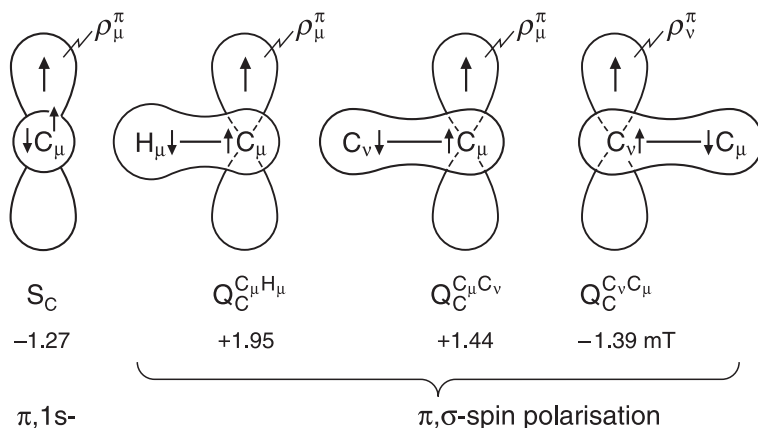
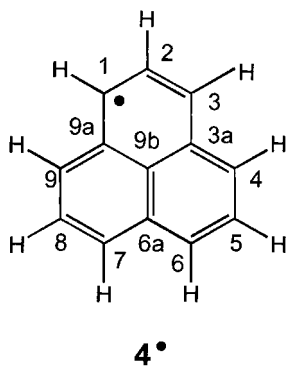


Fig. 4.7. Spin arrangements pertinent to the parameters S_C , $Q_C^{C_\mu H_\mu}$, $Q_C^{C_\mu C_\nu}$, and $Q_C^{C_\nu C_\mu}$ for a_{C_μ} .

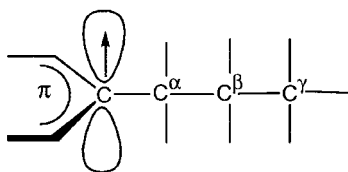
A relation analogous to Eq 4.16 was also derived empirically with somewhat modified values of Q^C and $Q_{C_i}^{C_i, C_\mu}$ in mT [461]:

$$a_{C_\mu} = +38.6\rho_\mu^\pi - 1.16(\rho_v^\pi + \rho_{v'}^\pi) \quad (4.18)$$

A simple example for application of these relations is the coupling constant of a ^{13}C isotope in a π center μ of the radical anion of benzene (**62**), for which a value $|a_{C_\mu}| = 0.28$ mT was determined [132]; its sign should be positive. Because, in this radical anion, the π -spin population $\rho_{v'}^\pi = \rho_v^\pi = \rho_\mu^\pi = +1/6$, the coupling constant a_{C_μ} is calculated as +0.13 and +0.26 mT with the use of Eqs. 4.16 and 4.18, respectively. A further, more illustrative, example is provided by the ^{13}C -coupling constants for the phenalenyl radical (**4'**), with the observed values $a_{C1,3,4,6,7,9} = +0.966$ and $a_{C2,5,8} \approx a_{C3a,6a,9a} = -0.784$ mT [88]. The π -spin populations, ρ_μ^π , at the proton-bearing centers μ in **4'** are preferably derived from the observed ^1H -coupling constants $a_{H1,3,4,6,7,9} = -0.629$ and $a_{H2,5,8} = +0.181$ mT. (The signs of all these a_{C_μ} and a_{H_μ} values were determined experimentally [90, 462].) Using the McConnell equation, $a_{H_\mu}(\alpha) = Q_{H_i}^{C_\mu, H_\mu} \rho_\mu^\pi$, with $Q_{H_i}^{C_\mu, H_\mu} = -2.8$ mT, values of $\rho_{1,3,4,6,7,9}^\pi = +0.225$ and $\rho_{2,5,8}^\pi = -0.065$ are obtained. The π -spin populations at the remaining blind centers can be derived by combining these values with the results of theoretical calculations, taking care that the condition that the sum of ρ_μ^π over all μ must be +1 (Eq. 4.4) is met. This procedure yields $\rho_{3a,6a,9a}^\pi = -0.049$ and $\rho_{9b}^\pi = +0.008$. The coupling constants a_{C_μ} can now be calculated with Eq. 4.16 or 4.18 for the proton-bearing centers μ and Eq. 4.17 for the blind ones. The values thus obtained are $a_{C1,3,4,6,7,9} = +0.959$ or +1.001 mT, $a_{C2,5,6} = -0.857$ or -0.773 mT, and $a_{C3a,6a,9a} = -0.786$ mT, in good agreement with the experimental data.



The C nuclei outside the centers μ in π radicals can be labeled analogously to protons. Thus, those separated from the π center by 0, 1, 2, ... sp^2 -hybridized C atoms are specified as α , β , γ , ...

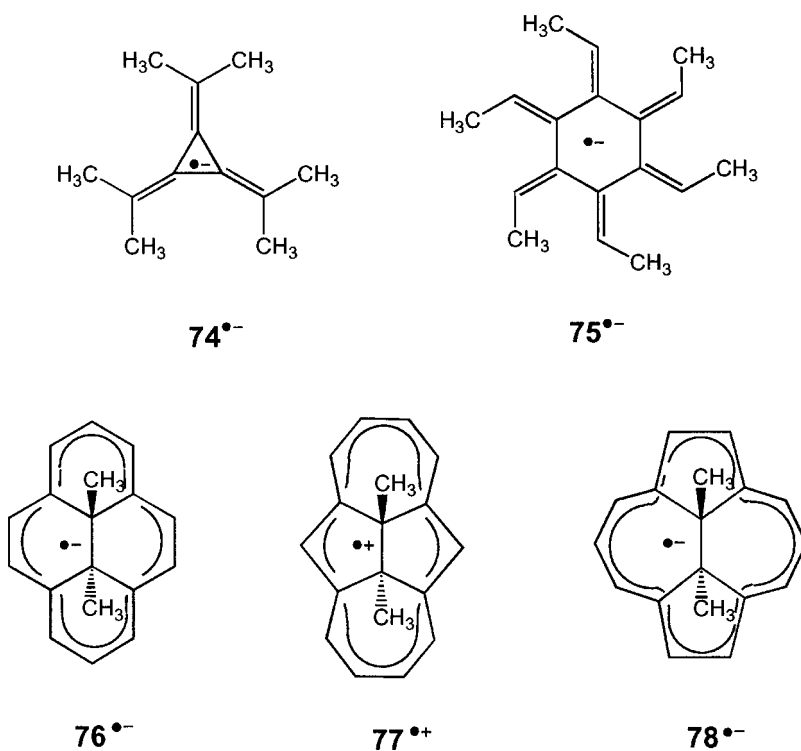


For a $^{13}\text{C}(\alpha)$ nucleus, the coupling constant $a_{\text{C}_{\mu'}}(\alpha)$ is due to π,σ -spin polarization by the π -spin population, $\rho_{\mu'}^{\pi}$, at the substituted center μ' , and it depends on this spin population with a proportionality factor of $Q_{\text{C}}^{\text{C}_{\mu'}} = -1.39$ (Eqs. 4.16 and 4.17) or -1.16 mT (Eq. 4.18).

$$a_{\text{C}_{\mu'}}(\alpha) = -1.39\rho_{\mu'}^{\pi} \text{ or } -1.16\rho_{\mu'}^{\pi} \quad (4.19)$$

On the other hand, for a β - $^{13}\text{C}(\beta)$ nucleus separated from the substituted center μ' by an sp^2 -hybridized C atom, the coupling constant $a_{\text{C}_{\mu'}}(\beta)$, like $a_{\text{H}_{\mu'}}(\beta)$, is due to π,σ -spin delocalization (hyperconjugation) [463]. The pertinent relation is analogous to Eq. 4.9 for β protons. The parameter B for $a_{\text{C}_{\mu'}}(\beta)$ in this relation, has positive values (+4 to +9 mT) similar to its counterpart B for $a_{\text{H}_{\mu'}}(\beta)$, and θ stands for the dihedral angle formed between the direction of the 2p_z axis at the substituted center μ' and the direction of the $\text{C}_{\mu'}-\text{C}(\beta)$ σ bond.

Applications of Eqs. 4.16 and 4.17 are further illustrated by the ^{13}C -hyperfine data for $\text{C}(\alpha)$ nuclei in the radical anions of hexamethyl derivatives of [3]radialene (74) [464] and [6]radialene (75) (Table 8.24) [465]. For $\text{C}(\beta)$ nuclei, the pertinent ^{13}C -coupling constants in radical ions of several bridged [14]annulenes such as 76 (Table 8.20)–78 can serve as an example [463]. It is interesting that, in these radical ions, the $\text{C}(\beta)$ nuclei are located in the bridging alkylidene group, and their ^{13}C -coupling constants require the use of a relation analogous to Eq. 4.11 to account for the enhancement by the “Whiffen effect”.



When, in Eq. 4.13, nucleus X is ^{14}N and the hetero- π center N_μ is linked to C atoms as the centers ν , the relation between the ^{14}N -coupling constant a_{N_μ} and the π -spin populations ρ_μ^π and ρ_ν^π is

$$a_{N_\mu} = Q_N \rho_\mu^\pi + \sum_\nu Q_N^{C_\nu N_\mu} \rho_\nu^\pi \quad (4.20)$$

No quantum mechanical calculation for the parameters Q_N and $Q_N^{C_\nu N_\mu}$, analogous to those for Q_C and $Q_C^{C_\nu C_\mu}$, have been made, and the empirical estimates made by different authors vary widely. However, it is generally accepted that Q_N , like Q_C , is positive with its value lying between +2 and +3 mT, and also that $|Q_N^{C_\nu N_\mu}|$ is much smaller than $|Q_N|$. For an aza-N atom as the center μ and two adjacent C atoms as the centers ν , values of $Q_N = +2.75$ and $Q_N^{C_\nu N_\mu} = -0.15$ mT were suggested, so that Eq. 4.16, in mT, is expressed by [163]

$$a_{N_\mu} = +2.75\rho_\mu^\pi - 0.15(\rho_\nu^\pi + \rho_{\nu'}^\pi) \quad (4.21)$$

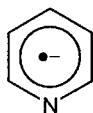
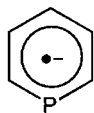
Clearly, because of $|Q_N^{C_\nu N_\mu}| \ll |Q_N|$, the second term can be neglected in the first approximation, and the coupling constant a_{N_μ} is then considered to be proportional to the π -spin population, ρ_μ^π at the pertinent center μ . Eqs. 4.20 and 4.21 are thus reduced to

$$a_{N_\mu} \approx Q_N \rho_\mu^\pi \quad (4.22)$$

the simplicity of which is reminiscent of Eq. 4.5 for α protons. Moreover, because the $|Q_N|$ value is similar to $|Q_H^{C_\mu H_\mu}|$, the coupling constants $|a_{N_\mu}|$ are comparable to $|a_{H_\mu}|$, provided that the π -spin populations, ρ_μ^π , at the relevant centers μ are similar. However, one should keep in mind that, in contrast to $Q_H^{C_\mu H_\mu}$, the parameter Q_N is positive, and that the values of a_{N_μ} therefore have the same sign as ρ_μ^π , whereas those of a_{H_μ} and ρ_μ^π are of opposite sign.

For X = ^{13}C or ^{14}N , respectively, in C_μ or N_μ , with the π center μ linked to hetero- π centers ν such as N_ν or O_ν , relations analogous to Eq. 4.13 were proposed for the coupling constant a_{C_μ} and a_{N_μ} , e.g., for radical anions containing cyano [466] and nitro [196] groups.

When an aza-N atom is replaced in the center μ by P as the element of the next period, and if the π -spin distribution does not markedly change on such a replacement, the observed ^{31}P -coupling constant a_{P_μ} is 4 to 5 times larger than its ^{14}N counterpart a_{N_μ} (in general, the sign should not change). This finding is demonstrated by the hyperfine data for the radical anions of pyridine (**79**) (Table 9.8) [467] and phosphabenzene (**80**) (Table 9.11) [165].

**79**^{•-}**80**^{•-}

On going from $79^{\cdot-}$ to $80^{\cdot-}$, the coupling constants of the α protons are modified by, at most, 25%, but $a_N = +0.623$ mT is much smaller than $a_P = +3.56$ mT. The more than fivefold increase is due mainly to the g_n factor of ^{31}P (+2.261) being larger than that of ^{14}N (+0.404). From the data for the radical anions of several phenyl-substituted phospho derivatives of benzene, biphenyl, terphenyl, and quarterphenyl (Table 9.11), a relation was derived between the coupling constant a_{P_μ} , in mT, and the π -spin population, ρ_μ^π , at the center μ with the parameter $Q_P = +9.2$ mT as the proportionality factor [181]:

$$a_{P_\mu} \approx Q_P \rho_\mu^\pi = +9.2 \rho_\mu^\pi \quad (4.23)$$

The atoms corresponding to N and P in the next group of elements are O and S, which can also function as hetero- π centers μ and give rise to coupling constants a_{O_μ} and a_{S_μ} of their magnetic isotopes ^{17}O and ^{33}S . According to Eq. 4.13, relations between the a_{O_μ} and a_{S_μ} values and the π -spin populations, ρ_μ^π and ρ_ν^π at the hetero- π center μ and the adjacent C centers ν are

$$a_{O_\mu} = Q_O \rho_\mu^\pi + \sum_\nu Q_O^{C, O_\mu} \rho_\nu^\pi \quad (4.24)$$

and

$$a_{S_\mu} = Q_S \rho_\mu^\pi + \sum_\nu Q_S^{C, S_\mu} \rho_\nu^\pi \quad (4.25)$$

Most π radicals having an O atom as the center μ are ketyl anions with a carbonyl group. For the coupling constant, a_{O_μ} , of the ^{17}O isotope in this center, parameters $Q_O = -4.1$ and $Q_O^{C, O_\mu} = +0.6$ mT were suggested [468], so that Eq. 4.24, in mT, is expressed by

$$a_{O_\mu} = -4.1 \rho_\mu^\pi + 0.6 \rho_\nu^\pi \quad (4.26)$$

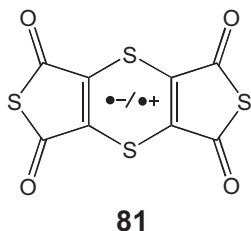
where the ρ_μ^π and ρ_ν^π are the π -spin populations at the O center μ and the C center ν of the ketyl group. Note that Q_O and Q_O^{C, O_μ} have signs opposite to those of the analogous parameters Q_X and Q_X^{X, X_μ} with $X = ^{13}\text{C}$, ^{14}N , ^{31}P , and ^{33}S . This is because the g_n factor of ^{17}O is negative, whereas the g_n factors of the other nuclei are all positive. As $|Q_O^{C, O_\mu}| \ll |Q_O|$, Eqs. 4.24 and 4.26 can be approximated by

$$a_{O_\mu} \approx Q_O \rho_\mu^\pi = -4.1 \rho_\mu^\pi \quad (4.27)$$

For the coupling constant, a_{S_μ} , of a ^{33}S isotope in the center μ , a parameter $Q_S = +3.3$ mT was proposed, with $|Q_S^{C, S_\mu}|$ being small enough to be neglected [469]. Eq. 4.25 in mT, is thus simplified to

$$a_{S_\mu} \approx Q_S \rho_\mu^\pi = +3.3 \rho_\mu^\pi \quad (4.28)$$

where ρ_μ^π is the π -spin population at the S center μ . An example of the application of Eq. 4.13 to the coupling constants a_{C_μ} , a_{O_μ} , and a_{S_μ} , of ^{13}C , ^{17}O , and ^{33}S nuclei in the center μ with various atoms X_ν as the adjacent centers ν , is provided by the radical ions of dithieno[3,4-*b*;3',4'-*e*]paradithiin-1,3,5,7-tetraone (**81**) [172], a π system that does not bear protons (Chapt. 6.4).



Among the remaining magnetic nuclei X, which give rise to substantial hyperfine splitting in the ESR spectra of π radicals, we should mention ^{19}F and ^{29}Si . The F atoms usually replace H atoms linked to π centers μ or H atoms in alkyl groups separated by a sp^3 -hybridized C atom from the substituted π centers μ' , and, accordingly, the ^{19}F nuclei may be specified $F_\mu(\alpha)$ or $F_{\mu'}(\beta)$.

The mechanism of spin transfer from the π system to the orbitals of an F atom is much more complex than it is for an H atom with only 1s-AOs. In the relation [470, 471]:

$$a_{F_\mu}(\alpha) = Q_F^{C_\mu F_\mu} \rho_\mu^\pi + Q_F \rho_F^{2p} \quad (4.29)$$

for the coupling constants of $F_\mu(\alpha)$ nuclei, the first parameter $Q_F^{C_\mu F_\mu}$, involves the π - σ -spin polarization of the C_μ - F_μ σ bond by the spin population, ρ_μ^π , at the adjacent C center μ . The second parameter Q_F takes into account the slight π character of the C_μ - F_μ bond and the delocalization of some π -spin population into the $2p_z$ -AO of the F atom; this spin population ρ_F^{2p} polarizes, on its part, the electron spins in the remaining doubly occupied 1s-, 2s-, and 2p-AO's of the F atom. Attempts to empirically produce consistent values for the two parameters have failed, and theoretical estimates vary widely according to the method of calculation. However, because the ratio of the spin populations $\rho_F^{2p}/\rho_\mu^\pi = r$ is often constant, ρ_F^{2p} can be set equal to $r\rho_\mu^\pi$, and Eq. 4.29 is then simplified to a relation analogous to the McConnell equation (Eq. 4.5) for α protons:

$$a_{F_\mu}(\alpha) \approx (Q_F^{C_\mu F_\mu})_{\text{eff}} \rho_\mu^\pi \quad (4.30)$$

where $(Q_F^{C_\mu F_\mu})_{\text{eff}}$ is identified with $Q_F^{C_\mu F_\mu} + rQ_F$.

The observed coupling constants $|a_{F_\mu}(\alpha)|$ are, in general, 2 to 3 times larger than $|a_{H_\mu}(\alpha)|$ at π centers μ with a similar π -spin population ρ_μ^π , and so also must $|(Q_F^{C_\mu F_\mu})_{\text{eff}}|$ be relative to $|Q_H^{C_\mu H_\mu}|$. A parameter $(Q_F^{C_\mu F_\mu})_{\text{eff}}$ of +5.5 mT seems appropriate for neutral π radicals and radical anions, but a value up to +9 mT is suitable for radical cations [471]. It is essential to note that a positive sign is required for

this parameter [472], in sharp contrast to the negative sign of its counterpart $Q_{\text{H}}^{C_{\mu}\text{H}_{\mu}}$ in the McConnell equation.

Upon replacement of a β proton in an alkyl substituent at a π center μ' by a $^{19}\text{F}(\beta)$ nucleus, the observed coupling constant $|a_{\text{F}_{\mu'}}|$ also seems to increase relative to $|a_{\text{H}_{\mu'}}|$. The reported data are rather scarce, most of them concerning the $^{19}\text{F}(\beta)$ nuclei in trifluoromethyl substituents. The pertinent ^{19}F -coupling constants should also depend on the spin populations both at the substituted π center μ' and at an F atom. The parameters relating $|a_{\text{F}_{\mu'}}|$ to these spin populations are expected to be positive, and their values were found to be sensitive to the position of substitution [471, 473]. Even less is known about the coupling constants of $^{19}\text{F}(\beta)$ nuclei in substituents other than trifluoromethyl groups (Chapt. 9.2) [193].

The hyperfine splitting due to the magnetic nuclei, ^{35}Cl and ^{37}Cl , of the next larger halogen atom, are mostly unresolved in the ESR spectra of π radicals. This is because the ^{35}Cl - and ^{37}Cl -coupling constants are small, and the hyperfine components involved are broadened by nuclear quadrupole interaction [471].

^{29}Si isotopes in π radicals are located in Si atoms either directly attached to a π center μ , $^{29}\text{Si}(\alpha)$, or separated from such a center μ' by an sp^3 -hybridized C atom of a substituent, $^{29}\text{Si}(\beta)$. For $^{29}\text{Si}(\alpha)$, hyperfine interaction was mostly studied in radical anions, like those of trimethylsilyl-substituted buta-1,3-diene, benzene, naphthalene (Table 9.27) [474], whereas for $^{29}\text{Si}(\beta)$, such interactions were investigated in radical cations such as those of bis-, tetrakis-, and hexakis-trimethylsilylmethyl derivatives of but-2-ene, *p*-xylene, durene, and hexamethylbenzene (Table 9.38) [232], in which 1, 2, or 3 H atoms of the methyl substituent were replaced by trimethylsilyl groups. For radical anions, this relation between the coupling constants, $a_{\text{Si}_{\mu}}(\alpha)$, of the $^{29}\text{Si}(\alpha)$ isotope in a trimethylsilyl group at a center μ and the spin populations, ρ_{μ}^{π} , at the π center μ and $\rho_{\text{Si}}^{3\text{p}}$ in the 2p_z -AO (eventually with a 3d admixture) of the Si atom, can be formulated as

$$a_{\text{Si}_{\mu}}(\alpha) = Q_{\text{Si}}^{C_{\mu}\text{Si}_{\mu}} \rho_{\mu}^{\pi} + Q_{\text{Si}} \rho_{\text{Si}}^{3\text{p}} \quad (4.31)$$

an expression analogous to Eq. 4.29 for an $^{19}\text{F}(\alpha)$ nucleus. The second parameter Q_{Si} has a value that is not significantly different from zero, so that Eq. 4.31 can be simplified to

$$a_{\text{Si}_{\mu}}(\alpha) \approx (Q_{\text{Si}}^{C_{\mu}\text{Si}_{\mu}})_{\text{eff}} \rho_{\mu}^{\pi} \quad (4.32)$$

where the parameter $|(Q_{\text{Si}}^{C_{\mu}\text{Si}_{\mu}})_{\text{eff}}|$ has a value of ca 2 mT with presumably a negative sign (Chapt. 9.2) [474]. Here too, as with ^{17}O , we should keep in mind that the g_{n} factor of the ^{29}Si isotope is negative.

For radical cations, the coupling constants, $a_{\text{Si}_{\mu'}}(\beta)$, of a $^{29}\text{Si}(\beta)$ isotope that replaces a β proton in a substituent at a π center μ' can be related to the π -spin population $\rho_{\mu'}^{\pi}$ at the center μ' by an expression corresponding to Eq. 4.9 for the β protons. In this expression, θ is the dihedral angle between the direction of the 3p_z axis at the substituted π center μ' and that of the C–Si(β) bond. The value of the pertinent parameter $|B|$ was estimated as 3.2 mT [232]. Its sign should be negative, because of the negative g_{n} factor of the ^{29}Si isotope.

Hyperfine Anisotropy

ESR studies on π radicals are generally carried out in fluid solutions, in which the anisotropic magnetic electron–nuclear interaction is averaged out by molecular motion. Among radicals that have been investigated in glasses, radical cations generated by γ -rays in Freon matrices are particularly important. Also notable are viscous or solid biological samples with radical centers created by high-energy irradiation or by introduction of a spin label, usually a nitroxyl. In most studies, contributions due to hyperfine anisotropy remained unresolved and contributed solely to a specific line broadening that (e.g., for spin labels) provided valuable information about the viscosity of the medium (Appendix A.1). Resolved splittings of this kind could be observed usually for magnetic nuclei other than protons when such nuclei were situated in π centers μ with a high “local” spin population ρ_μ^π and exhibited large hyperfine anisotropy. This is because, as stated in Chapt. 4.1, the dipolar interaction is proportional to r^{-3} , where r is the electron–nucleus distance.

Here, it is appropriate to recall the notation $A_{X,z}$, $A_{X,y}$, and $A_{X,x}$ for the anisotropic coupling constants of nucleus X in the z , y , and x directions, as the principal values of the tensor \mathbf{A}_X (z is the direction perpendicular to the x, y plane of the π system). For an axial tensor \mathbf{A}_X , these values can be expressed by $A_{X\parallel} = A_{X,z}$ and $A_{X\perp} = A_{X,x} = A_{X,y}$ (Chapt. 3.2), and a similar formulation is also used for many other, not-strictly-axial π radicals for which $A_{X\perp} = (1/2)(A_{X,x} + A_{X,y})$.

An example of a large resolved hyperfine anisotropy for $X = {}^{31}\text{P}$ with a nearly axial tensor \mathbf{A}_P is shown in Figure 4.8, which reproduces the ESR spectra of the radical anion of 2,4,6-tri-*tert*-butylphosphabenzene (**82**) (Table 9.11) in fluid and glassy MTHF solutions [165]. Because the smaller hyperfine splittings due to the protons are hidden in the line-width of ca 0.2 mT, only the ${}^{31}\text{P}$ -coupling constants are observed. The anisotropic coupling constants amount to $A_{P\parallel} = A_{P,z} = +11.76$ mT, and $A_{P\perp} = (1/2)(A_{P,y} + A_{P,x}) = (1/2)[-1.42 + (-1.52)]$ mT = -1.47 mT (the z , y , and x directions are defined in Figure 4.8, and the small difference between $A_{P,y}$ and $A_{P,x}$ is unresolved but indicated by computer simulation of the spectrum). Hence, $a_P = (1/3)(A_{P\parallel} + 2A_{P\perp}) = +2.94$ mT and $B_{P,\text{dip}} = (1/2)(A_{P\parallel} - a_P) = a_P - A_{P\perp} = +4.41$ mT, so that the principal values of the quasi-axial tensor $\mathbf{A}_{P,\text{dip}}$ are $+8.82$, -4.41 , and -4.41 mT. The isotropic coupling constant a_P is due to the spin population in the s-AOs of the P atom, where it arises from spin polarization by the π -spin population, ρ_μ^π , at the P center. In contrast, the $B_{P,\text{dip}}$ value is a direct measure of the ρ_μ^π value, which is ca $+0.4$ in the $3p_z$ -AO of the P atom (a ${}^{31}\text{P}$ -coupling constant of $+1.0$ [475] to $+1.3$ mT [476] was calculated for a spin population of $+1$ in the $3p_z$ -AO). Because both the spin population ρ_μ^π at the P atom and the g_n factor of ${}^{31}\text{P}$ are positive, the finding that, in the isotropic spectrum of **82**⁻ in fluid solution, the high-field line is broader than the low-field line agrees with the positive sign of a_P (Chapt. 6.5).

The ESR spectra of radical cations with an extended π system generated in solid matrices usually exhibit insufficiently resolved ${}^1\text{H}$ -hyperfine anisotropy, so that they are difficult to analyze. An example is the ESR spectrum of the radical cation of naphthalene (**83**). In rigid media the monomeric radical cation, **83**⁺, is obtained, whereas in fluid solution the dimeric radical cation, **83**₂⁺, is formed

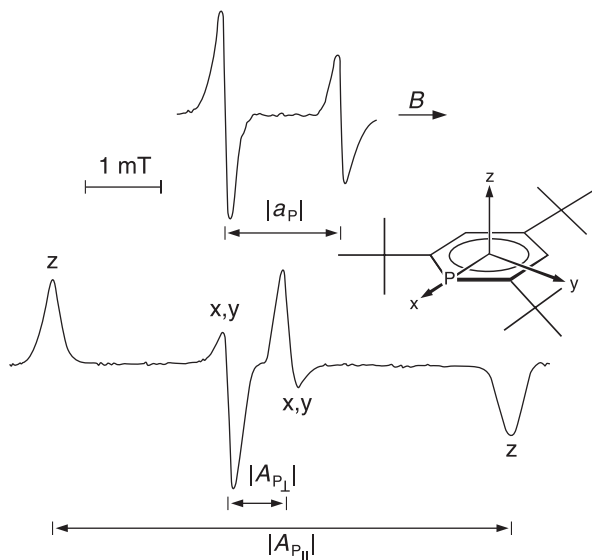
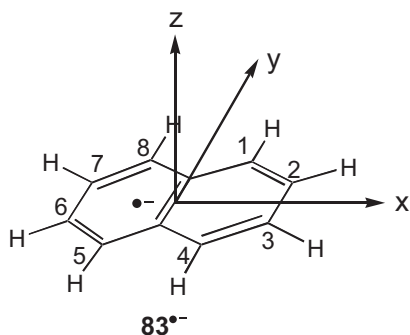


Fig. 4.8. ESR spectra of the radical anion of 2,4,6-tri-*tert*-butylphosphabenzene (**82**) in a fluid (top) and glassy (bottom) MTHF solution. Counterion K^+ ; temperature 213 (top), and 123 K (bottom). Deviation from symmetry near the center of the spectrum

taken with glassy MTHF is caused by the anisotropy of the g_e factor, which is considered in the Chapt 6.2. Hyperfine data in the text and Table 9.11. Reproduced by permission from [165].

[242, 286, 287, 477]. The first, partly-resolved, ESR spectrum of $83^{+\cdot}$ was reported for UV-irradiated naphthalene in boric acid glass [478]. Better resolution, along with the corresponding ENDOR spectrum, was obtained for $83^{+\cdot}$ upon γ -irradiation of this compound in a $CFCl_3$ matrix [479]. Later, similar ESR and ENDOR spectra were obtained from X-irradiated samples in the same matrix. These spectra were reanalyzed (with greater experimental and theoretical expenditure) in terms of the 1H -coupling constants in the three principal directions indicated below [480].



The tensors A_H and $A_{H,dip}$ are distinctly nonaxial and different for the two sets of protons in $83^{+\cdot}$: For the 4 α protons at the centers $\mu = 1, 4, 5, 8$, the z , y , and x

directions coincide with those of the 3 twofold-rotational axes C_2 in the symmetry group D_{2h} , whereas for the second set of α protons at the centers $\mu = 2, 3, 6, 7$, the analogous directions are $z' = z$, $y' = 0.297x + 0.955y$, and $x' = 0.955x - 0.297y$. The reported principal values of A_H are, in mT, $A_{H,z} = -0.620$, $A_{H,y} = -0.282$, and $A_{H,x} = -0.859$ for $\mu = 1, 4, 5, 8$ and $A_{H,z'} = -0.239$, $A_{H,y'} = -0.271$, and $A_{H,x'} = +0.011$ for $\mu = 2, 3, 6, 7$ [480]. Averaging yields the isotropic coupling constants $a_{H1,4,5,8} = -0.587$ and $a_{H2,3,5,6} = -0.166$ mT. The principal values of the hyperfine anisotropy tensors $A_{H,dip}$, as the orientation-dependent contributions to these isotropic coupling constants in mT, are thus -0.033 (z), $+0.305$ (y), and -0.272 mT (x) for $\mu = 1, 4, 5, 8$ and -0.073 (z'), -0.105 (y'), and $+0.177$ mT (x') for $\mu = 2, 3, 6, 7$.

The anisotropic contributions for $\mu = 1, 4, 5, 8$ are proportional to those calculated for a proton attached to a C atom bearing a spin population of $+1$ in a $2p_z$ -AO [-0.18 (z), $+1.54$ (y), and -1.36 mT (x) (Chapt. 4.1)]. The proportionality factor, ca 0.2, represents the spin population $\rho_{1,4,5,8}^{\pi}$ in $83^{+\cdot}$. This investigation of $83^{+\cdot}$ in glassy CF_3Cl is an example of an application of the ENDOR technique to radical cations in a Freon matrix; this technique is an important tool for resolving residual hyperfine anisotropy (see Chapt. 5.2).

4.3

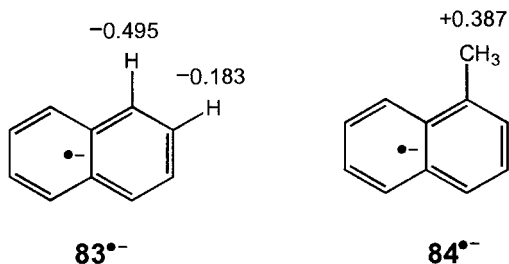
σ Radicals

Chapt. 2.2 mentioned that organic radicals can be classified as π or σ , according to whether the spin-bearing orbital is the π or σ type; σ orbitals are defined as *symmetric* and π orbitals as *antisymmetric* with respect to the molecular plane that is also the nodal plane of the π system. Clearly, radicals such as vinyl (11^{\cdot}) (Table 7.9), phenyl (12^{\cdot}) (Table 7.11), formyl (13^{\cdot}) (Table 7.9), and iminoxyl (15^{\cdot}) (Table 7.23), presented in Chapt. 2.2, are σ . These radicals essentially retain the geometry of the corresponding diamagnetic compound, ethene, benzene, formaldehyde, and aldoxime, respectively, despite abstraction of a H atom and breaking of the C–H bond. Less obvious is the classification of radicals lacking a molecular plane, in which the specification is determined merely by the “character” of the spin-bearing orbital. For example, formation of the cyclopropyl radical (14^{\cdot}) from cyclopropane leaves the spin-bearing orbital intermediate between a $2p_z$ -AO and a sp^3 hybrid. The geometry at the spin bearing C atom is thus pyramidal (in contrast to the planar π radicals), although not as pyramidal as might be expected if the radical would fully retain the geometry of cyclopropane (Chapt. 7.1). Therefore, as mentioned in Chapt. 2.2, 14^{\cdot} can be classified as intermediate between π and σ . According to the character of their SOMOs responsible for the N–N three-electron bond, the radical cations of hydrazines are π , but those of diamines, like 1,4-diazabicyclo[2.2.2]octane (DABCO; **30**), 1,6-diazabicyclo[4.4.4]tetradecane (**31**) (Table 7.18), and the polymethylene-*syn*-1,6:8,13-dimino[14]annulenes **32** and **33** (Table 9.40), introduced in Chapt. 2.3, are σ .

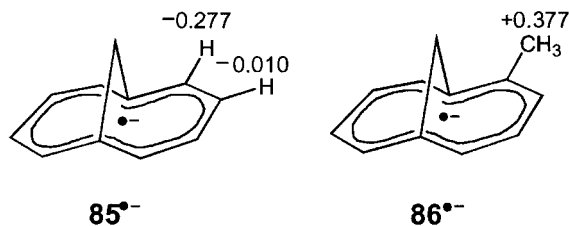
A feature of ESR spectra that is often diagnostic of σ radicals is the large size of the hyperfine coupling constants, which are generally of positive sign [17i]. These large values are due to a substantial “s-character” of the spin-bearing orbitals, so

that the hyperfine interaction does not depend on the indirect mechanism of π, σ -spin polarization, but arises by the much more efficient direct mechanism, as expressed by the Fermi-contact term.

Transition from a π to a σ radical occurs with substantial deviations of the radical center from planarity, because such deviations bestow some s-character upon the spin-bearing p_z or π orbital and lead to positive contributions to the coupling constants. For nuclei in the radical centers, such as ^{13}C and ^{14}N , which have a positive coupling constant a_{C} and a_{N} , these s-contributions cause an *increase* in the observed values. However, for α protons with a negative coupling constant a_{H} , the positive s-contributions first compensate partly or wholly for the $|a_{\text{H}}|$ values of these protons, so that, if the deviations from planarity are not too excessive, a *decrease* in $|a_{\text{H}}|$ is observed. An example is provided by the ^1H -hyperfine data for the radical anion of 1,6-methano[10]annulene (**85**) (Table 8.20) [149], in which marked deviations of the cyclic π system (π perimeter) from planarity do not impair the π conjugation, but do substantially reduce the $|a_{\text{H}}|$ values of the α protons. This decrease becomes evident on comparing the ^1H -hyperfine data for **85** $^{\cdot-}$ with those for the radical anion of naphthalene (**83**) (Table 8.8) [135], which has a π -SOMO of closely similar shape (Figure 8.11). Because the coupling constants of the two sets of four equivalent α protons in both radical anions are negative, the s-contributions, on going from **83** $^{\cdot-}$ to **85** $^{\cdot-}$, amount to $-0.271 \text{ mT} - (-0.495 \text{ mT}) = +0.224 \text{ mT}$ and $-0.010 \text{ mT} - (-0.183 \text{ mT}) = +0.173 \text{ mT}$.



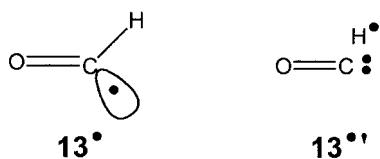
A definite proof that these changes are due to deviations of the π perimeter in **85** $^{\cdot-}$ from planarity and not to a π distribution being different from that in **83** $^{\cdot-}$ is given by the coupling constants of the methyl β protons in the radical anions of 1-methylnaphthalene (**84**) and 2-methyl-1,6-methano[10]annulene (**86**) [481]. These values, $+0.387 \text{ mT}$ for **84** $^{\cdot-}$ and $+0.377 \text{ mT}$ for **86** $^{\cdot-}$ mT, are similar, because coupling constants of β protons are rather insensitive to moderate deviations from planarity at the π centers.



Marked reduction in the observed $|a_{\text{H}}|$ values of α protons relative to the expected values for a corresponding planar π radical can be used as an estimate of the extent of deviation from planarity of the π system in the radical under study [150, 210].

With enhanced “pyramidalization” at a radical center, the originally negative a_{H} values of α protons first tend to zero and then become positive while steadily growing to the large values diagnostic of σ radicals. A simple example is provided by the cyclopropyl radical (**14'**) (Table 7.2) as intermediate between π and σ . The C–H(α) bond in **14'** does not lie in the plane of the three-membered ring, and the coupling constant of the single methine α proton is -0.651 mT (Table 7.2) [34], compared with the corresponding a_{H} value of -2.120 mT for the essentially planar cyclobutyl radical (**61'**) (Table 7.2) [34].

More impressive is the very large ^1H -coupling constant of $+13.7$ mT for the “bent” formyl radical $\text{O}=\text{C}^{\bullet}-\text{H}$ (**13'**) (Table 7.9) [113]. This value is one of the largest observed for a proton and corresponds to a spin population $\rho_{\text{H}}^{1\text{s}}$ of $+13.7$ mT/ $+50.7$ mT = $+0.27$, where $+50.7$ mT is the ^1H -coupling constant for H^{\bullet} . Such a high 1s-spin population may be identified with the weight of a “valence bond structure” (**13''**), in which the formyl radical is represented by the stable CO molecule and a H^{\bullet} atom.

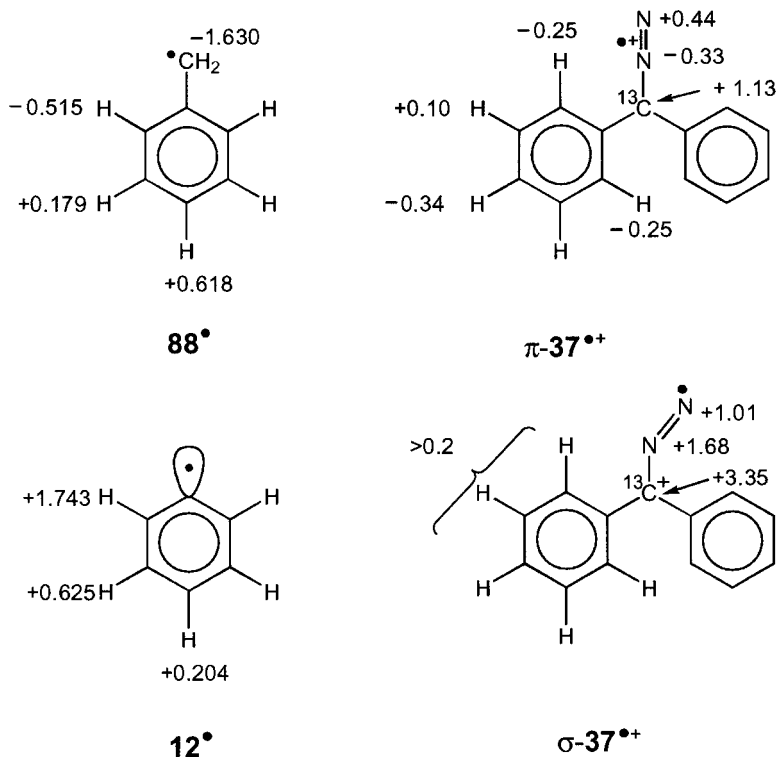


Very large ^1H -coupling constants were also found in the ESR spectra of radical cations generated from n -alkanes in rigid matrices, in particular for two protons, each located in a terminal methyl group and marking an end of a zigzag chain (Chapt. 10.1). The coupling constant of such protons is as large as $+15.2$ mT for the radical cation of ethane and only gradually decreases with intervening methylene groups in the radical cations of higher n -alkanes (Table 10.1) [306, 313].

The ^{13}C -coupling constant for the formyl radical is $+13.5$ mT. An even larger a_{C} value of $+27.16$ mT was observed for the “pyramidal” trifluoromethyl radical $\text{F}_3\text{C}^{\bullet}$ (**87'**) (Table 7.1) [482]. This value is 7 times greater than its counterpart, $+3.83$ mT, for the planar methyl radical $\text{H}_3\text{C}^{\bullet}$ (**58'**) [438]. Because the ^{13}C -coupling constant calculated for a spin population of $+1$ in a $2s$ -AO of the C atom is $+134.7$ mT [476], an a_{C} value of $+27.2$ mT corresponds to $\rho_{\text{C}}^{2\text{s}} \approx 0.2$, which may be considered as the $2s$ share in the spin-bearing σ orbital of (**87'**) (roughly an sp^3 hybrid).

In contrast to π radicals, in which the spin distribution over the centers μ follows the pattern indicated by the shape of the π -SOMO, spin population in “genuine” σ radicals is restricted to atoms next to the spin-bearing orbital and decreases more or less monotonously with distance from this orbital. As an illustration, the ^1H -coupling constants of the ring protons are compared for the benzyl (**88'**) [42] and phenyl (**12'**) [112] radicals, representing π and σ species *par excellence*. Another

example of differing spin distribution is provided by the ^1H - and ^{13}C - and ^{14}N -hyperfine data for π - and σ -radical cations of the same compound, diphenyldiazomethane (37); the π or σ structure of these radical cations depends on the conditions under which they are generated [245].



Because of their low persistence, most σ radicals are generated in solid media. The substantial s-character of the spin-bearing orbital causes the hyperfine anisotropy to be less pronounced than might be expected from the large size of the coupling constant. Thus, the observed anisotropic values for the proton in the formyl radical (13°) are $A_{\text{H},z} = +14.2$, $A_{\text{H},y} = +13.6$, and $A_{\text{H},x} = +13.3$ mT [113]; these values yield +13.7 mT as the ^1H -isotropic coupling constant a_{H} and +0.5 (z), -0.1 (y), and -0.4 mT (x) as the principal values of the anisotropy tensor $A_{\text{H,dip}}$. The anisotropic contributions to the ^{13}C -coupling constant a_{C} of +13.5 mT for 13° were not reported. Such contributions are, however, known for a ^{13}C isotope in the carbonyl C atom of a structurally related acyl radical generated from deuterated glutaric acid [483, 484]. The pertinent values are $A_{\text{C},z} = +16.3$, $A_{\text{C},y} = +11.4$, and $A_{\text{C},x} = +10.7$ mT, which yield an a_{C} value of +12.8 mT as the isotropic ^{13}C -coupling constant and +3.5 (z), -1.4 (y), and -2.1 (x) mT as the principal values of $A_{\text{C,dip}}$.

4.4 Triplet States

Because the two unpaired electrons in triplet-state molecules generally occupy π -MOs, only such species are considered in this chapter. We note that, despite the presence of two unpaired electrons, the sum of the π -spin populations, $\rho_{\mu}^{\pi}(\text{tr})$, at the centers μ of the triplet molecule is not +2 but is still +1, as in Eq. 4.4. for doublet π radicals. A $\rho_{\mu}^{\pi}(\text{tr})$ value can be represented as an average of $\rho_{\mu}^{\pi}(\psi_j)$ and $\rho_{\mu}^{\pi}(\psi_{j'})$, pertinent to the two MOs singly occupied by the unpaired electrons 1 and 2.

$$\rho_{\mu}^{\pi}(\text{tr}) = (1/2)[\rho_{\mu}^{\pi}(\psi_j) + \rho_{\mu}^{\pi}(\psi_{j'})] \quad (4.33)$$

The π -spin distribution in a triplet molecule is thus comparable to that in a structurally similar π radical, and the formulae presented in Chapt. 4.2, which relate the coupling constants a_X with the π -spin populations ρ_{μ}^{π} , can also be used for triplet states. Experimental confirmation of this statement is rather rare, because ESR studies of triplet molecules must generally be carried out in viscous or solid media, so that their hyperfine pattern is not resolved. The resolution has usually been better for the “half-field” signal, due to the nearly isotropic “ $\Delta M_S = \pm 2$ ” transition, than for signals in the “normal” field arising from the anisotropic “ $\Delta M_S = \pm 1$ ” counterparts (Chapt. 2.4). In some cases, such as radicals in rigid media, the triplet molecules were amenable to the ENDOR technique (Chapt. 5.2) [15e], which proved to be valuable for determining coupling constants a_X in poorly resolved ESR spectra.

For electronically excited triplets of π systems, the two singly occupied MOs (SOMOs) are the highest occupied MO (HOMO) and the lowest unoccupied MO (LUMO) of the unexcited molecule. In alternant π systems, these orbitals are related by “pairing” properties and, therefore, give rise to closely similar π -spin populations ρ_{μ}^{π} in the corresponding radical anion and radical cation (Chapts 8.1 and 8.4). In the excited triplets of alternant π systems, the π -spin distribution must thus be almost the same as in the two radical ions. This statement is confirmed by studies of the electronically excited alternant π system naphthalene (**83**) in a single crystal of durene (for zero-field splitting parameters D and E see Table 11.1), in which analysis of variously deuterated samples yielded the values, $|a_{\text{H}1,4,5,8}| = 0.561$ and $|a_{\text{H}2,3,6,7}| = 0.229$ mT [485]. These values compare favorably with those for the radical anion $\mathbf{83}^{\cdot-}$ ($a_{\text{H}1,4,5,8} = -0.495$ and $a_{\text{H}2,3,6,7} = -0.181$ mT) [135] and the radical cation $\mathbf{83}^{\cdot+}$ ($a_{\text{H}1,4,5,8} = -0.587$ and $a_{\text{H}2,3,6,7} = -0.166$ mT) [480]. It was thus concluded that the π -spin populations $\rho_{\mu}^{\pi}(\text{tr})$ are almost the same as the corresponding ρ_{μ}^{π} values for $\mathbf{83}^{\cdot-}$ and $\mathbf{83}^{\cdot+}$. This statement also holds for the electronically excited triplet states of other π systems (Chapt. 11.2).

Trimethylenemethane (TMM; $\mathbf{42}^{\cdot\cdot}$) (Table 11.6) is an example of a ground-state triplet molecule with axial symmetry. The value, $|a_{\text{H}}| = 0.89$ mT, of six equivalent protons was determined from the half-field signal of $\mathbf{42}^{\cdot\cdot}$, when a single crystal of 3-methylenecyclobutanone was UV-irradiated at low temperature [486]. Later, a similar $|a_{\text{H}}|$ value of 0.91 mT was observed for $\mathbf{42}^{\cdot\cdot}$ at 90 K ($|D'| = 26.1$ mT)

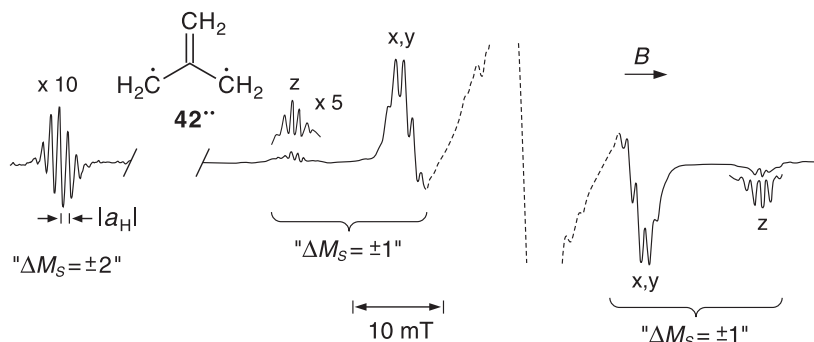


Fig. 4.9. ESR spectrum of the triplet trimethylenemethane (TMM; **42''**). For clarity, the central, very intense absorption due to mixtures of radical cations has been omitted. Hyperfine data in the text and zero-field-splitting parameters in Table 11.6. Taken from [487].

upon γ -irradiation of a CF_3CCl_3 matrix containing methylenecyclopropane [487]. The triplet **42''** was obtained in low concentration as a by-product, along with a mixture of radical cations. As shown in Figure 4.9, not only the half-field signal for “ $\Delta M_S = \pm 2$ ” exhibits the pertinent hyperfine splitting, but also the parallel and perpendicular features due to “ $\Delta M_S = \pm 1$ ” transitions. When a methylenecyclopropane **42-d₂'**, dideuterated at the CH_2 group, was used as the starting material, the hyperfine splitting arose from only four equivalent protons, while the small splitting, 0.14 mT, from the two deuterons was unresolved [487]. The observed $|a_{\text{H}}|$ value was only slightly affected by hyperfine anisotropy. The coupling constant of -0.9 mT (it is certainly negative) corresponds to the π -spin population of $+1/3$ at the three equivalent proton-bearing centers μ , if the small (and presumably negative) $\rho_{\mu}^{\pi}(\text{tr})$ value at the inner blind center is ignored. The π -spin population of $+1/3$ is tantamount to a “reasonable” parameter $Q_{\text{H}}^{\text{C},\text{H},\mu}$ of -2.7 mT in the McConnell Eq. 4.5.

4.5

Calculations of Spin Populations

Hückel-McLachlan

Persistent neutral π radicals, like phenalenyl (**4'**) and triphenylmethyl (**1'**), and π -radical ions of aromatic hydrocarbons were among the first organic species to be studied by ESR spectroscopy. Their spin distributions are, on the whole, well reproduced by the shape of the SOMO ψ_j , as described by the *Hückel molecular orbital* (Hückel-MO) model [488, 489], in which the π -spin populations ρ_{μ}^{π} are represented by the squares of the LCAO coefficients $c_{j,\mu}$ at the π centers μ (Chapt. 4.2). However, the Hückel-MO model does not make allowance for π,π -spin polarization

and thus fails to account for the negative spin populations ρ_{μ}^{π} that occur at centers μ having zero or very small $c_{j,\mu}^2$ values. This deficiency is redressed by a refinement introduced by McLachlan [490], which makes use of the so-called atom–atom polarizabilities $\pi_{\mu,v}$ of the Hückel-MO model [488, 489]. In the McLachlan procedure, the spin populations are expressed by

$$\rho_{\mu}^{\pi} = c_{j,\mu}^2 + \lambda \sum_{v=1}^n \pi_{\mu,v} c_{j,v}^2 \quad (4.34)$$

where λ is a dimensionless number, usually close to 1, and the summing is carried out over all centers v including $v = \mu$. Eq. 4.7 was used in Chapt. 4.2 to calculate the π -spin distribution in the allyl radical, for which the SOMO is ψ_2 with squared LCAO coefficients $c_{2,1}^2 = c_{2,3}^2 = 0.5$ and $c_{2,2}^2 = 0$. Because the atom–atom polarizabilities are $\pi_{1,1} = \pi_{3,3} = +0.442$, $\pi_{2,2} = +0.353$, $\pi_{1,2} = \pi_{2,3} = -0.177$, and $\pi_{1,3} = -0.265$, Eq. 4.34 with $\lambda = 1$ yields $\rho_1^{\pi} = 0.5 + 0.442 \cdot 0.5 - 0.177 \cdot 0 - 0.265 \cdot 0.5 = +0.5885 = \rho_3^{\pi}$, and $\rho_2^{\pi} = 0 + 0.353 \cdot 0 - 2 \cdot 0.177 \cdot 0.5 = -0.177$.

The spin populations are readily converted into the coupling constants $a_{X_{\mu}}$ by use of the McConnell equation and other relations considered in Section 4.2.

Some advantageous features of the Hückel model, such as the pairing properties of the antibonding and bonding MOs in alternant π systems (see Chapt. 8.1), are retained in the McLachlan procedure. Perturbation by introduction of a hetero- π center X, alkyl substitution at a center μ' , or a change in the bond length $\mu-v$ can be simulated by $\alpha_X = \alpha + h_X\beta$, $\alpha_{\mu'} = \alpha + h_{\mu'}\beta$, or $\beta_{\mu,v} = k_{\mu,v}\beta$; where α and β stand for the conventional Hückel-energy parameters (Chapt. 8.1), and h_X , $h_{\mu'}$, and $k_{\mu,v}$ are dimensionless numbers. For example, for X = N, O, and S, the numbers $h_N = +0.5$ to $+1.5$, $h_O = +1.0$ to $+2.5$, and $h_S = +0.5$ to $+1.0$ were proposed, which vary with the particular hetero- π system. An $h_{\mu'}$ value of -0.1 to -0.5 is appropriate to account for the electron-repulsion induced by an alkyl substituent at the center μ' , and an increase or decrease in the double-bond character of the $\mu-v$ linkage can be taken in consideration by setting $k_{\mu,v}$ larger or smaller than 1. The McLachlan procedure has been successfully applied to calculations of π -spin populations in planar π radicals [6], for which it is hardly surpassed by more sophisticated methods. A plot of the coupling constants $a_{H_{\mu}}$ of α protons in alternant benzenoid radical ions is shown in Figure 8.4.

Semiempirical and Nonempirical Methods

σ radicals and π radicals beyond the conventional planar systems require a treatment of all valence-shell orbitals, for which several MO methods have been devised. Presentation of the theory underlying them, which has been described in many papers, reviews, and monographs, greatly exceeds the scope of an introduction to ESR spectroscopy, especially since relevant computer programs are available in many laboratories. The methods can be classified as *semiempirical* and *non-empirical*. Semiempirical methods use empirical energy parameters to circumvent

laborious and time-consuming integrations, and the nonempirical ones do not make such approximations. Because spin distribution in open-shell systems, such as organic radicals, requires an adequate allowance for spin polarization, the methods must be based on the *unrestricted Hartree-Fock* (UHF) theory, which implies different orbitals for different spins (DODS). Two such semiempirical methods have been applied most frequently to radicals, namely Pople's *intermediate neglect of differential overlap* (INDO) procedure [491, 492] and AM1-UHF [493], which is a reparametrized version of Dewar's *modified neglect of differential diatomic overlap* (MNDO) procedure [494]. The calculations start from a given geometry of the radicals under study, which can be optimized using molecular mechanics [495, 496], as well as with the same or other MO methods. The s-spin populations are converted into isotropic coupling constants by parameters appropriate for the s-AO of the atom in question. For protons in the INDO method, a conversion factor of +53.9 mT was proposed, which is somewhat higher than the a_{H} value of +50.7 mT for the unit 1s-spin population in H \cdot . In Nelsen's AM1-UHF procedure [493], the corresponding factor was estimated empirically to be as large as +117.7 mT for α and β protons. In particular, good results with both semiempirical methods have been obtained for some polycyclic radicals having a rigid carbon framework [273, 317, 339, 497].

Nonempirical MO methods, which do not require empirical parameters, are generally referred to as *ab initio* methods. Because of their high computational expense, they were originally restricted to very small radicals. However, by using the more-easily-integrated Gaussian functions instead of the Slater functions and with the advent of high-performance computers, larger species can also be studied. In contrast to the Slater s-orbitals, which have a sharp maximum at the nucleus (the so-called "cusp"), the Gaussian functions are much flatter at this position. Because the Fermi contact term critically depends just on the s-spin density at the nucleus, a single Gaussian function fails to reproduce it, and several must be used for one Slater orbital. Ab-initio calculations can be carried out at varying levels of theory, generally the smaller the radical the higher the level. The level is specified by the notation of the ab-initio method: e.g., in 6-31G*, 6 and 31 signify the number of Gaussians used for the inner- and valence-shell Slater orbitals, respectively, and the asterisk indicates the extent of admixture of higher orbitals [498].

In the past few years, the *density functional theory* (DFT) formalism, first introduced by Kahn [499, 500], has been shown to be very appropriate for calculation of spin populations, even at heavy atoms, and, with the use of Gaussian functions [501], it has become the most popular method for this purpose [235, 361, 502–505]. Frequently, after the geometry has been optimized by other methods, such as INDO, AM1-UHF, and 6-31G*, the s-spin populations are calculated by the DFT procedure at single points in the radical. The DFT calculations can be also carried out at various levels of theory. For example, BLYP/6-31G* stands for functionals, due to Becke [506] and others [507], with a 6-31G* basis set.

5 Multiresonance

5.1 Historical Note

The first successful experiment in paramagnetic resonance was carried out on salts of transition metals by Zavoisky in Kazan, Russia, in 1944 [17c, 508]. After the Second World War, following this discovery, several research groups began to study organic radicals [1–3] with the use of ESR spectroscopy. These studies were performed on stable radicals, like triphenylmethyl (trityl; **1'**) [509, 510], 2,2-diphenyl-1-picrylhydrazyl (DPPH; **5'**) [92, 511, 512], phenalenyl (**4'**) [86], the radical anion of *p*-benzoquinone (**19**) (semiquinone) and its derivatives [513–515], the radical cations of *N,N'*-tetramethyl-*p*-phenylenediamine (**17**) (Wurster's blue) [516, 517] and thianthrene [17d, 518], and both radical ions of many aromatics [17e, 124–129, 220, 519, 520]; the groups involved in these studies were mostly located in the United States. The first spectra then taken on home-built instruments were poorly resolved, but their quality substantially improved in the 1960s, when more elaborate instruments became commercially available from Varian Associates [17q]. The rich hyperfine pattern revealed by the higher resolution is demonstrated by the ESR spectrum (Figure 5.1) of the radical anion of cycl[3.2.2]azine (pyrrolo[2,1,5-*cd*]indolizine; **89**) (Table 9.28) recorded on a Varian V-4502-spectrometer in 1963 [160]. This resolution was not essentially improved in the following decades, but progress was achieved by multiresonance techniques that greatly enhanced the efficiency of ESR spectroscopy.

For studies of organic radicals, by far the most important multiresonance technique is *electron-nuclear double resonance* (ENDOR) discovered by Feher in 1956 on a phosphorus-doped silicon system [17o, 521]. Several years later, it was applied to radicals in solution by Hyde and Maki [522, 523], as well as by Möbius and colleagues [17p, 524], who also introduced *TRIPLE-resonance* techniques [15f, 525]. The reason that the application of ENDOR spectroscopy to radicals in solution lagged behind its use on paramagnetic species in solids was partly due to a lack of interest in the liquid phase by the physicists who first used this technique. Even more important were problems of instrumentation, because liquids require much higher radio frequency (RF) power to saturate NMR transitions than solids [15c]. Although ENDOR has not attained a popularity comparable to ESR, it is now used by an increasing number of research groups, especially since ENDOR accessories

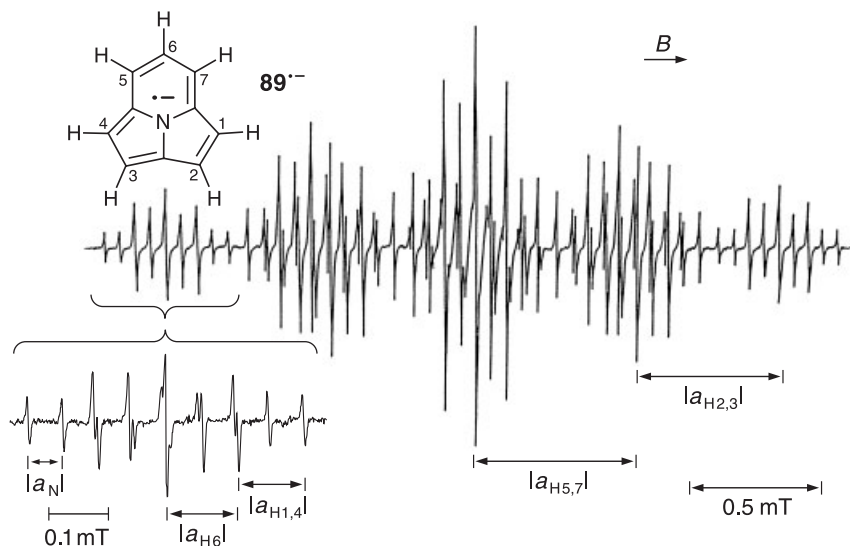


Fig. 5.1. ESR spectrum of the radical anion of cycl[3.2.2]azine (**89**). Solvent DME, counterion Li^+ , temperature 213 K. The part of the spectrum at the lowest field, reproduced below it and exhibiting still higher resolution, was taken with a “superheterodyne adapter” accessory. The coupling constants, in mT, are

$a_{\text{H}_{1,4}} = -0.113$, $a_{\text{H}_{2,3}} = -0.534$, and $a_{\text{H}_{5,7}} = -0.602$, each for two α protons, $a_{\text{H}_6} = +0.120$ for a single α proton, and $a_{\text{N}} = -0.60$ for the ^{14}N nucleus (the signs are those required by theory; Table 9.28). Reproduced by permission from [160].

became commercially available from Varian [17q] in the 1970s and from Bruker GmbH [17r] in the 1980s.

Another double-resonance technique *electron-electron double resonance* (ELDOR) [15a] was first applied in 1968 to radicals in solution [526, 527]. Unlike ENDOR, studies of organic radicals by ELDOR have only rarely been reported since then.

5.2 ENDOR

Physical Fundamentals of ENDOR

The ENDOR technique has been dealt with briefly in several early monographs on ESR spectroscopy [4, 5, 8, 10, 11] and at some length in a few more recent books specializing in multiresonance [12, 15]. An excellent introduction into the ENDOR technique, as used for organic radicals in solution, is a review article [528] and, in more detail, a book, both by Kurreck, Kirste, and Lubitz [16]. Their book also contains a comprehensive account of relevant ENDOR studies up to 1988.

The physical principles underlying this double-resonance technique can be grasped by considering the so-called *transient*-ENDOR effect in the way presented

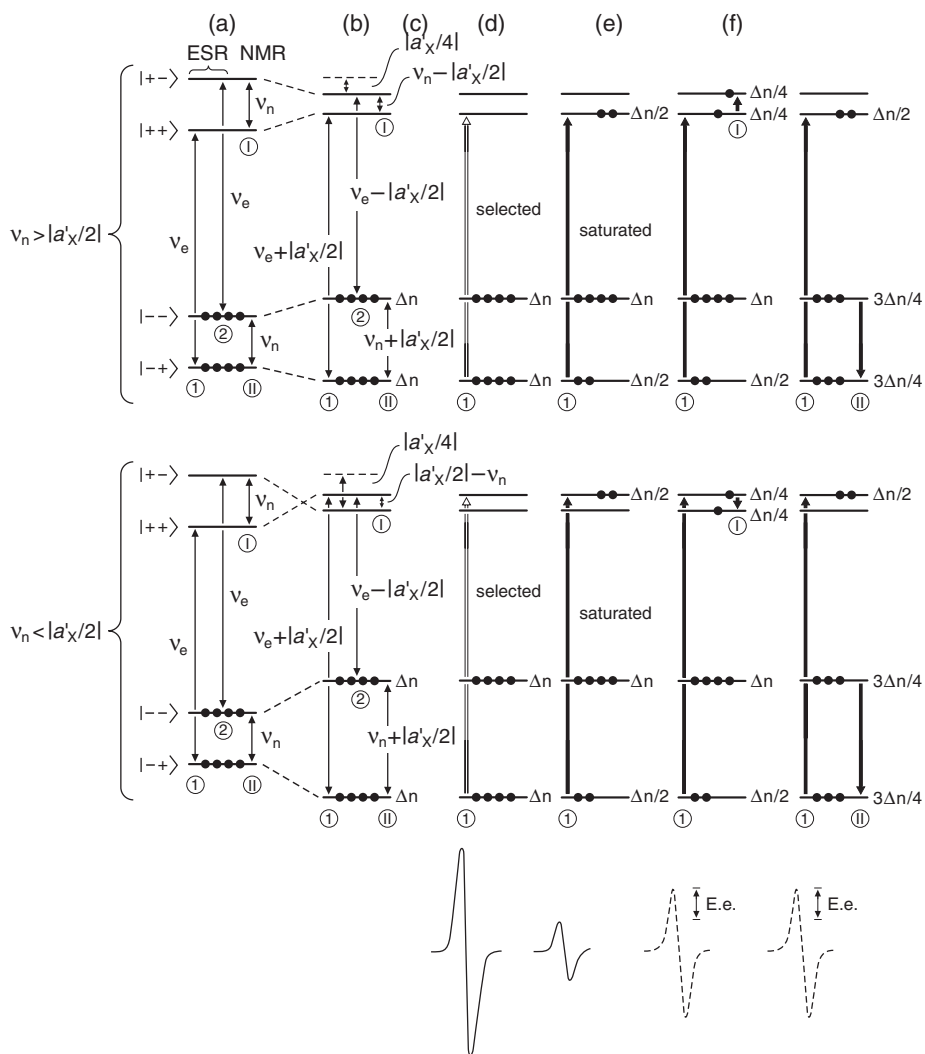


Fig. 5.2. Schemes relevant to the transient ENDOR effect for a paramagnetic system consisting of one unpaired electron and one magnetic nucleus with $I = 1/2$ and $g_n > 0$. (a) and (b): Energy levels in the presence and absence, respectively, of the hyperfine

interaction. (c): ESR transition ① selected for saturation. (d): Effect of saturation of ① on the populations. (e) and (f): Effect of saturation of NMR transitions ① and ②, respectively, on the populations.

in that book [16]. Schemes a–f (Figure 5.2) depict four Zeeman-energy levels which, at a given field strength B , are characteristic of a paramagnetic system consisting of one unpaired electron and one magnetic nucleus X , such as a proton, with the spin quantum number $I = 1/2$ and a positive g_n factor. The four levels, $|++\rangle$, $|+-\rangle$, $|-\rangle$, and $|--\rangle$, are specified by the signs of the magnetic spin quantum numbers, $+1/2$ (spin up; α) or $-1/2$ (spin down; β), in which the first sign relates to the number, M_S , of the electron and the second sign to that, M_I ,

of the nucleus. It is here advisable to recall some essential differences in the magnetic properties of the two particles, as pointed out in Chapt. 3.1. Because of its positive charge, the plus-level of a nucleus with $g_n > 0$ lies lower than its minus-counterpart, a situation that is opposite to that of the negatively charged electron. Moreover, at the same field strength B , the Zeeman splitting is about three orders of magnitude smaller for the nucleus than for the electron, and so is the population excess of spins in their respective lower levels, (if, as in the present case, the total number of spins is equal for both particles, and the temperature is also the same). Therefore, the excess, Δn_n , of nuclear spins in the levels $|++\rangle$ and $|+-\rangle$ relative to $|+-\rangle$ and $|--\rangle$, respectively, is neglected, and only the excess, $\Delta n (\equiv \Delta n_e)$, of electron spins in the levels $|+-\rangle$ and $|--\rangle$ relative to $|++\rangle$ and $|+-\rangle$, is considered. This excess, Δn , is symbolized by four dots in the levels $|+-\rangle$ and $|--\rangle$, each dot standing for $\Delta n/4$. For convenience, the Zeeman splittings are given in frequencies ν , and the hyperfine-coupling constant, $a'_X = \gamma_e a_X$, of the nucleus X also has the dimension of ν ($\gamma_e = 28.04$ MHz/mT is the gyromagnetic ratio of an electron; see Chapt 1.2). According to the selection rules, $\Delta M_S = \pm 1$ and $\Delta M_I = 0$, for the electron and $\Delta M_S = 0$ and $\Delta M_I = \pm 1$ for the nucleus, two ESR (① and ②) and two NMR transitions (Ⓐ and Ⓑ) are allowed.

In the absence of hyperfine interaction, the ESR transitions ① and ② require equal frequencies ν_e , as do the two NMR transitions with respect to the common frequency ν_n , as indicated in schemes a of Figure 5.2. Hyperfine interaction lowers the levels $|+-\rangle$ and $|+-\rangle$, for which the signs of M_S and M_I are opposite, and raises $|++\rangle$ and $|--\rangle$, with the same signs of these quantum numbers; the shift is $|a'_X/4|$ for each level. The resulting schemes b–f depend on whether $|a'_X/2|$ is smaller or larger than ν_n . When $\nu_n > |a'_X/2|$, which is mostly the case for protons in π radicals, the level $|++\rangle$ remains below $|+-\rangle$, and the NMR transition ① has the frequency $\nu_n - |a'_X/2|$ (Figure 5.2, top). When $\nu_n < |a'_X/2|$, the level $|+-\rangle$ is shifted to below $|++\rangle$, and the frequency of ① becomes $|a'_X/2| - \nu_n$ (Figure 5.2, bottom). In either case, the level $|+-\rangle$ lies below $|--\rangle$, so that the NMR transition ② has the frequency $\nu_n + |a'_X/2|$. The frequencies of the ESR transitions ① and ② are throughout $\nu_e + |a'_X/2|$ and $\nu_e - |a'_X/2|$, respectively, thus differing by $|a'_X|$, as expected.

In an ENDOR experiment, one ESR transition is selected for further study; it is here ①, as specified in scheme c. After having been locked at its frequency, $\nu_e + |a'_X/2|$, this transition is saturated by an intense microwave (MW) irradiation. Consequently, as indicated in scheme d, the populations in the two levels relevant to ①, $|+-\rangle$ and $|++\rangle$, become equal. Both levels then exhibit an excess $\Delta n/2$, and the intensity of the pertinent ESR signal is strongly reduced. In the next step, the system is subjected to an intense radio-frequency (RF) irradiation, which is scanned from 0 to higher values. At two frequencies, the NMR transitions become saturated, first ① at $\nu_n - |a'_X/2|$ or $|a'_X/2| - \nu_n$ and, subsequently, ② at $\nu_n + |a'_X/2|$. As a result, the populations in the pairs of the affected levels are equalized, as shown in schemes e and f for transitions ① and ②, respectively. Saturation of transition ① leads to an excess $\Delta n/4$ in each of the levels $|+-\rangle$ and $|++\rangle$, and saturation in ② yields $3\Delta n/4$ in $|+-\rangle$ and $|--\rangle$. Thus, either of the two satura-

tion processes makes the population in level $| - + \rangle$ higher by $\Delta n/4$ than the population in $| + + \rangle$, so that, in either case, the ESR transition ① is slightly desaturated, and the intensity of the ESR signal exhibits a small increase, the so-called *ENDOR enhancement*. Such an enhancement is, however, not directly verified, but its occurrence is confirmed by the NMR absorptions observed for the transitions ① and ②.

ENDOR Spectra

The records showing the signals that arise from NMR transitions ① and ② while scanning the RF ν are schematically presented in Figure 5.3. These records are called *ENDOR spectra*, because, in contrast to the NMR experiment, their intensity is due to a population excess of electron spins that is several orders of magnitude larger than that of nuclear spins. The sensitivity of ENDOR is thus much higher than that of NMR, although it is lower than that of EPR. For $\nu_n > |a'_X/2|$, the two ENDOR signals appear at $\nu_n \pm |a'_X/2|$; they are centered on the frequency, ν_n , of the “free” nucleus X and separated by the coupling constant $|a'_X| = \gamma_e |a_X|$. For $\nu_n < |a'_X/2|$, the two signals occur at $|a'_X/2| \pm \nu_n$; they are centered on $|a'_X/2|$ and separated by $2\nu_n$. The ENDOR signals can be recorded as absorption A or as its first derivative $dA/d\nu$ as a function of ν , depending on whether modulation is applied to the magnetic field or to the frequency.

Although ENDOR is less sensitive than ESR, this deficiency is more than compensated by the enormous *increase in spectral resolution*. Because the width, $\Delta\nu$, of the ENDOR signals (line-width) of ca 0.3 MHz is comparable to the $\Delta B (= \Delta\nu/\gamma_e)$ of ca 0.01 mT, generally achieved for ESR lines in a well-resolved spectrum of an organic radical in fluid solution, the increase in resolution by ENDOR relative to ESR spectroscopy is due to a drastic *decrease in the number of lines*. It can readily be verified that any magnetic nucleus X or any set of n equivalent nuclei with a coupling constant a_X gives rise to a single pair of ENDOR signals, irrespective of

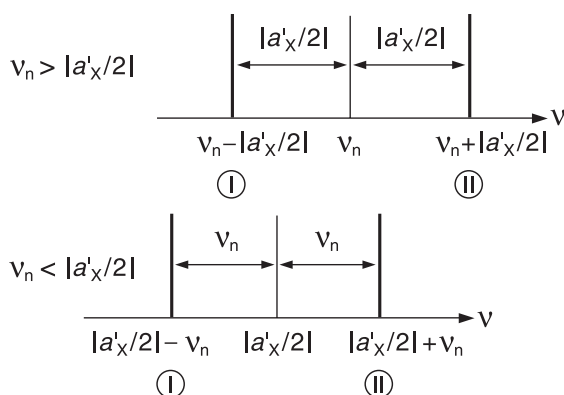


Fig. 5.3. Schematic presentation of an ENDOR spectrum arising from one nucleus X or a set of equivalent nuclei X with coupling constants $|a'_X| = \gamma_e |a_X|$.

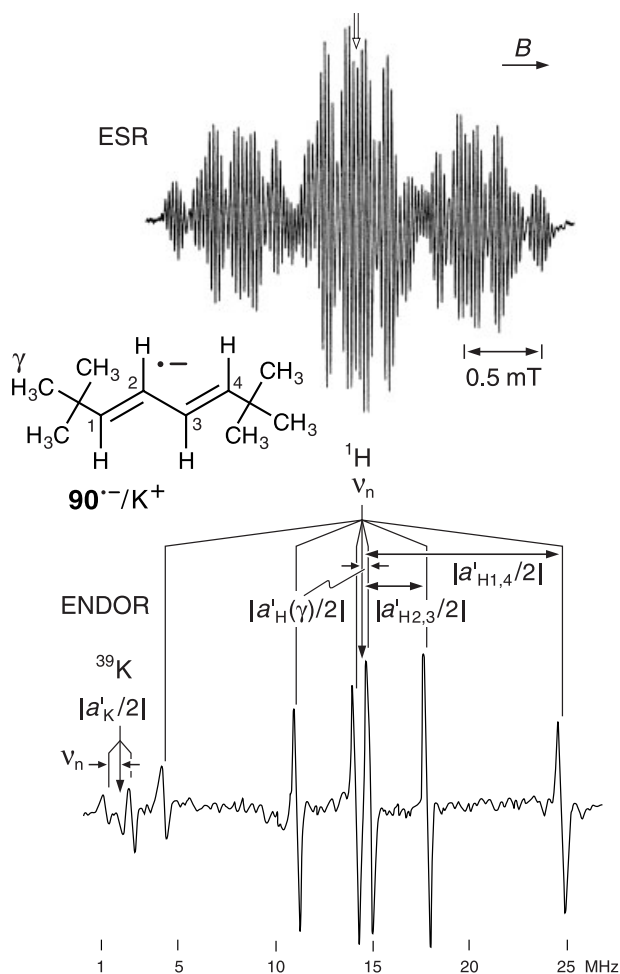


Fig. 5.4. ESR spectrum (top) and ^1H - and ^{39}K -ENDOR spectra (bottom) of the radical anion of 1,4-di-*tert*-butyl-*trans*-buta-1,3-diene (**90**). Solvent DME, counterion K^+ , temperature 200 K. The outline-arrow above the ESR spectrum indicates the line selected for saturation. Hyperfine data in the text and in Tables 8.6 and A.2.1. Reproduced by permission from [529].

the spin quantum number I and the g_n factor. This pair of signals generally appears in a separate NMR frequency range characteristic of X. With each further set, the number of lines grows *additively*, not *multiplicatively* as in ESR. Independent of n and I , the total number of ENDOR lines for k sets is thus $2k$ and not $(2n_1I + 1)(2n_2I + 1) \dots (2n_kI + 1)$ (Eq. 3.15).

Successful ENDOR experiments have been performed for most magnetic nuclei listed in Table 3.1 [16]. According to the resonance condition of NMR, the frequency, ν_n , of a “free” nucleus X at a given field strength B is specified by the nuclear gyromagnetic ratio $\gamma_n = \nu_n/B$ which, in turn, depends on the g_n factor of X

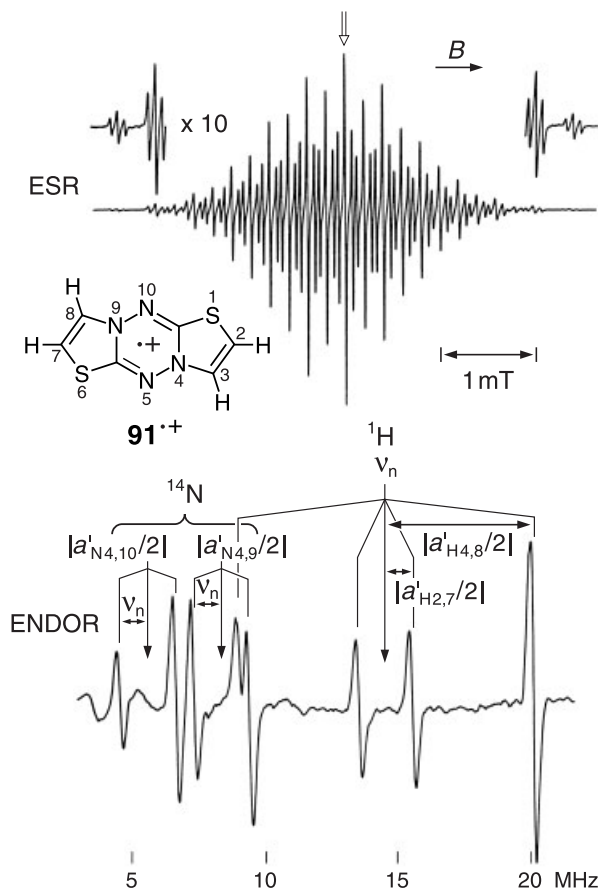


Fig. 5.5. ESR spectrum (top) and ^1H - and ^{14}N -ENDOR spectra (bottom) of the radical cation of dithieno[2,3-*b,e*]tetra-1,2,4,5-azine (**91**) (used as the salt $\mathbf{91}^{+\cdot}$ ClO_4^-). Solvent dichloromethane/TFA 1:2, counterions ClO_4^-

and CF_3COO^- , temperature 253 K. The outline-arrow above the ESR spectrum indicates the line selected for saturation. Hyperfine data in Table 9.33. Reproduced by permission from [530].

(Chapt. 3.1). The value of $\gamma_n = g_n \cdot 7.6226 \cdot 10^{-3}$ MHz/mT can be readily calculated from the g_n factors in Table 3.1. For a proton with g_n of 5.5854, γ_n is $4.2575 \cdot 10^{-2}$ MHz/mT. Examples are the ESR and ENDOR spectra of the radical anion of *trans*-1,4-di-*tert*-butylbuta-1,3-diene (**90**) closely associated with its counterion K^+ (Figure 5.4) [529] and of the radical cation of dithieno[2,3-*b,e*]tetra-1,2,4,5-azine (**91**) (Figure 5.5) [530]. For $\mathbf{90}^{\cdot-}/\text{K}^+$ with two pairs of α protons ($I = 1/2$), 18 γ protons in the two *tert*-butyl substituents, and one ^{39}K nucleus ($I = 3/2$) of the counterion, the number of ENDOR lines is $4 \cdot 2 = 8$ vs $3^2 \cdot 19 \cdot 4 = 684$ in ESR. The analogous numbers for $\mathbf{91}^{+\cdot}$ with two pairs of α protons and two pairs of ^{14}N nuclei ($I = 1$) are $4 \cdot 2 = 8$ vs $3^2 \cdot 5^2 = 225$ (hyperfine splitting from the ^{33}S isotopes of low abundance is not observed). In the ENDOR spectra taken in our Basel laboratory,

the frequency, ν_n , of a free proton, the so-called proton-ENDOR frequency is 14.56 MHz, corresponding to $B = \nu_n/\gamma_n = 342$ mT. In these spectra, the ENDOR frequency, ν_n , of a nucleus X other than proton is calculated from 14.56 MHz and $|g_n(X)|/g_n(H)$, i.e., by multiplying $|g_n(X)|$ by 14.56 MHz/5.5854 = 2.6068 MHz. Thus, the ν_n value of ^{39}K with $g_n = +0.2606$ is 0.68 MHz in the ENDOR spectrum of $\mathbf{90}^-/\text{K}^+$ (Figure 5.4), and that of ^{14}N with $g_n = +0.4036$ is 1.05 MHz in the spectrum of $\mathbf{91}^+$ (Figure 5.5). The coupling constants $|a'_H|$ are 20.47 and 6.79 MHz for the α protons in the 1,4- and 2,3-positions of $\mathbf{90}^-$, respectively, and the *tert*-butyl γ protons of this radical anion have an $|a'_H|$ value of 0.73 MHz. For the α protons in the 2,7- and 3,8-positions of $\mathbf{91}^+$, the two coupling constants $|a'_H|$ are 11.04 and 2.07 MHz, respectively. The relation $\nu_n > |a'_X/2|$ holds, therefore, for the protons in both radical ions. In contrast, because the coupling constant $|a'_K|$ for the ^{39}K nucleus in the counterion K^+ of $\mathbf{90}^-$ is 5.53 MHz, and because the two $|a'_N|$ values for the ^{14}N nuclei in the 4,9- and 5,10-positions of $\mathbf{91}^+$ are 11.22 and 16.71 MHz, respectively, the alternative relation $\nu_n < |a'_X/2|$ is valid for these nuclei.

A disadvantage of ENDOR spectroscopy is, that, unlike NMR, the intensity of a signal is not a reliable measure of the number of interacting nuclei giving rise to it. Such a shortcoming is evident from the ENDOR spectrum of $\mathbf{90}^-/\text{K}^+$, in which the signals from the 18 *tert*-butyl γ protons are as intense as those from the two α protons in the 2,3-positions. In this case, the relatively low intensity of the signals from the γ protons is due to insufficient separation of the ESR transitions ① and ② (Figure 5.2) by the small value $|a'_H|$ of the coupling constant, so that the selected transition ① can only be incompletely saturated. Moreover, as indicated by the spectra in Figures 5.4 and 5.5, even ENDOR signals from the same sort and the same number of nuclei can exhibit strikingly different intensities. This is because the ENDOR enhancement and, along with it, the intensity of the ENDOR signals, depends on whether the processes responsible for saturation of the NMR transitions ① and ② can compete with the electron spin-lattice relaxation (SLR) saturating the selected transition ① (Chapt. 1.3). Apart from nuclear SLR, which takes care of inversions of nuclear spins ($\Delta M_I = \pm 1$) with specific time T_{1n} , analogous to T_{1e} for the electron ($\Delta M_S = \pm 1$), more complicated cross-relaxation processes with $\Delta(M_S + M_I) = 0$ must be taken into account; times characteristics of these processes are denoted T_x . Usually, the relaxation of the electron spins is much more efficient than that of the nuclear spins, so that $T_{1e} \ll T_x \ll T_{1n}$. Because a successful ENDOR experiment requires that these times be comparable, electron relaxation must be slowed by appropriate experimental conditions. When the cross-relaxations with their times T_x can be neglected, as can often be done with protons in organic radicals, an increase of T_{1e} relative to T_{1n} is achieved in solutions by using viscous solvents and/or low temperatures. The ENDOR experiment is impeded by enhanced electron relaxation, e.g., in the presence of heavy nuclei (Chapt. 1.3) or by a dynamic Jahn–Teller effect (Chapt. 6.7). Instrument sensitivity also influences the intensity of ENDOR signals, because it differs in particular frequency ranges. For example, on going from ca 5 MHz downward, the sensitivity steadily decreases, so that the low-frequency signal is often weaker than its high-frequency counterpart.

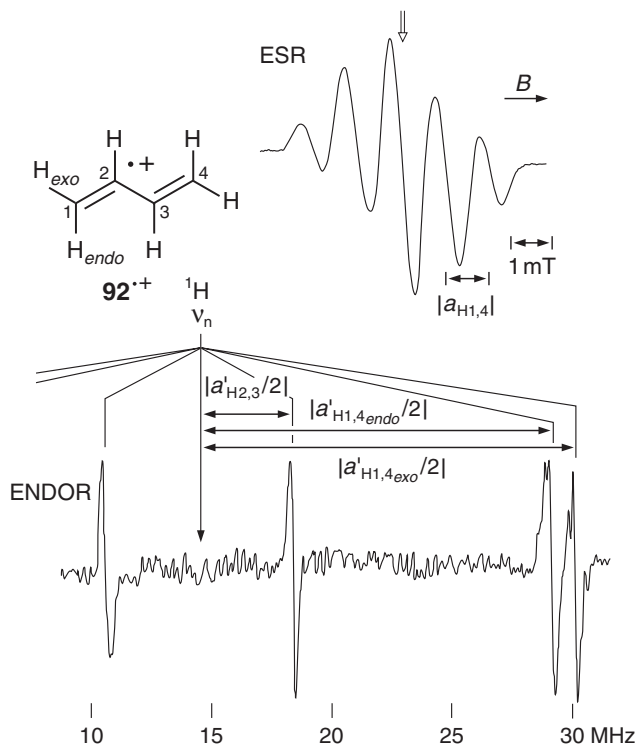


Fig. 5.6. ESR spectrum (top) and ^1H -ENDOR spectrum (bottom) of the radical cation of *trans*-buta-1,3-diene (**92**). Solvent CFCl_3 (matrix), counterions undefinable, temperature 130 K. The outline-arrow above the ESR

spectrum indicates the line selected for saturation. The baseline in the original ENDOR spectrum has been rectified. Hyperfine data in Table 8.6. Reproduced by permission from [316].

The ENDOR technique has proved to be particularly useful for radicals of low symmetry having many overlapping and/or incompletely resolved ESR lines [155, 481, 531, 532] and for radicals in solid media in which these lines are broadened by hyperfine anisotropy. Among the latter, studies of organic radicals generated by high-energy irradiation in biological systems [15d] and in Freon matrices are noteworthy [310]. The resolving power of ENDOR for these matrices is demonstrated by the spectra of the radical cation produced from *trans*-buta-1,3-diene (**92**) by γ -rays in a CFCl_3 glass (Figure 5.6) [316]. Whereas in the ESR spectrum of $92^{+\cdot}$ only five broad hyperfine components due the four α protons in the 1,4-positions are observed, the corresponding ENDOR spectrum exhibits signals from all protons. These ENDOR signals include not only those from the two α protons in the 2,3-positions with a small coupling constant $|a'_\text{H}|$, but they also make it possible to distinguish between the $|a'_\text{H}|$ values of the *exo* and *endo* protons in the 1,4-positions. For the protons in the 2,3-positions, both ENDOR signals at $\nu_n \pm |a'_\text{H}|/2$ (10.59 and 18.51 MHz) appear, yielding $|a'_\text{H}| = 7.92$ MHz. For the pairs of *exo* and *endo* protons in the 1,4-positions, only the high-frequency signals

at $\nu_n + |a'_{\text{H}}/2|$ (30.25 for *exo* and 29.28 MHz for *endo*) were observed, and their low-frequency counterparts in the range below 1.5 MHz were not detected. Nevertheless, the pertinent coupling constants $|a'_{\text{H}}|$, 31.38 and 29.44 MHz, of the *exo*- and *endo*-protons, respectively, were readily determined from the observed frequencies and the free-proton value of 14.56 MHz. Note that the ENDOR lines of 92^{+} are only ca 0.4 MHz wide, corresponding to 0.014 mT, whereas the five ESR components have a line-width of ca 0.7 mT. Thus, in contrast to ESR, for which this width increases more than ten-fold on going from a fluid solution to a glass, ENDOR spectra retain their resolution upon such a change in medium.

Because of its lower sensitivity relative to ESR spectroscopy, the ENDOR technique requires somewhat larger radical concentrations, and its application to transient radicals is, therefore, more problematic. To increase the signal-to-noise ratio, the ENDOR spectra are usually accumulated by repeated recording and addition. Radical ions, which are electrolytically generated inside a cavity, cannot be studied by the ENDOR technique, because the electrodes interfere with the RF coils.

The number of the nuclei X giving rise to an ENDOR signal must be verified by examination, preferably simulation of the corresponding ESR spectrum (Chapt. 6.4). Analysis of the ENDOR spectrum alone [533] may lead to misinterpretations [534]. Other procedures can likewise be used for verification, e.g., isotopic substitution, which also serves for the assignment of coupling constants to sets of equivalent nuclei (Chapt. 6.5) [155]. ENDOR spectroscopy is particularly suited for such an assignment, because the ENDOR signals of different isotopes appear in separate frequency regions. Relative numbers of nuclei responsible for an ENDOR signal can be determined by techniques that take advantage of such effects as nuclear–nuclear coherence [15b, 16, 531] and by *special*-TRIPLE resonance [15f, 16, 528].

Only absolute values of the coupling constants a'_X are derived directly from the ENDOR spectra, a feature in common with ESR. Relative signs of a'_X are amenable to *general*-TRIPLE resonance [15f, 16, 525, 528], which is considered in Chapt. 5.3 along with the *special*-TRIPLE resonance. Under favorable conditions, the absolute signs of the ^1H -coupling constants are derived from the ENDOR spectra of radical cations in Freon matrices, as shown below. In a few studies, which are cited in Chapt. 6.4, second-order splitting was also observed in ENDOR spectra.

Hyperfine Anisotropy in ENDOR

The ^1H ENDOR signals of 92^{+} in a CFCl_3 matrix (Figure 5.6) have a “quasi-isotropic” shape, i.e., the hyperfine anisotropy is averaged out by molecular motion despite the rigidity of the medium. Such isotropic signals are often observed for protons in radical cations of hydrocarbons in Freon matrices, especially in frozen $\text{CF}_2\text{ClCFCl}_2$ which is, therefore, denoted as a “mobile” matrix. Otherwise, ENDOR signals have an anisotropic shape, and, in some spectra of small hydrocarbon radical cations, the incompletely averaged (residual) hyperfine anisotropy can be resolved, in contrast to the corresponding ESR spectrum. Usually, the signal is split into two components associated with the anisotropic values, $|A'_{\text{H}\parallel}|$ and $|A'_{\text{H}\perp}|$,

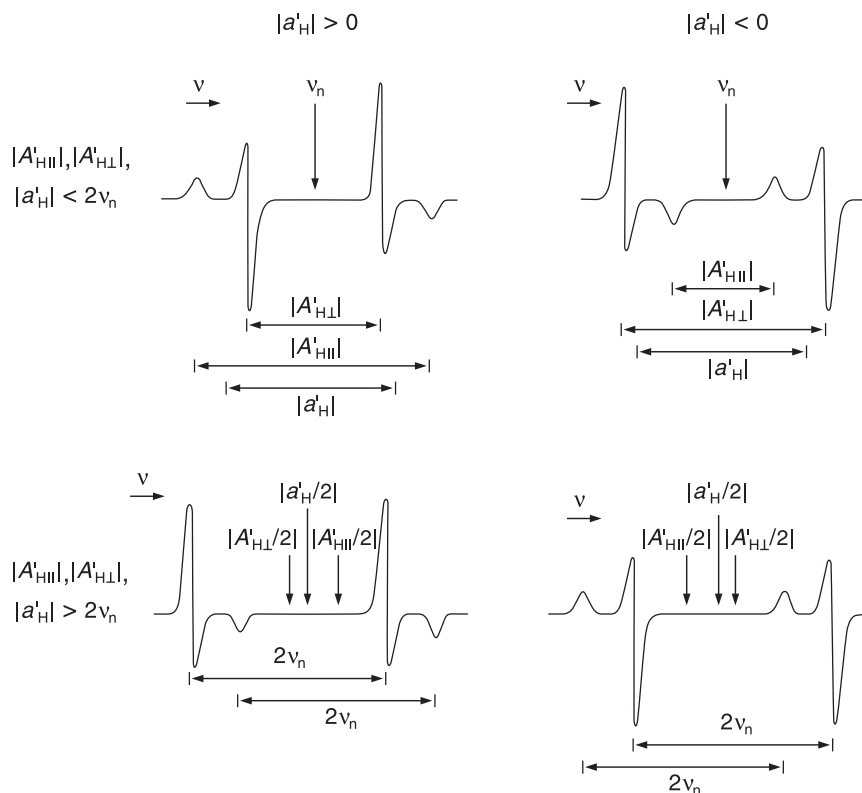


Fig. 5.7. ^1H -ENDOR signals of an idealized shape for axial or quasi-axial hyperfine tensors of small hydrocarbon radicals in a Freon matrix. Reproduced by permission from [329].

of the ^1H -coupling constant for an axial or a quasi-axial tensor; they represent the parallel and perpendicular features in the z and x, y directions, respectively, relative to the magnetic field. $A'_{H||}$ and $A'_{H\perp}$ are expressed in MHz, being convertible into the corresponding values $A_{H||}$ and $A_{H\perp}$ in mT by $A_{H||} = A'_{H||}/\gamma_e$ and $A_{H\perp} = A'_{H\perp}/\gamma_e$. The relations, which were formulated in Chapt. 3.2, between the isotropic and anisotropic coupling constants in mT, hold also for these values in MHz. Thus, $a'_H = (1/3)(A'_{H||} + 2A'_{H\perp})$, $A'_{H||} = a'_H + 2B'_{H,\text{dip}}$, and $A'_{H\perp} = a'_H - B'_{H,\text{dip}}$, where $2B'_{H,\text{dip}}$, $-B'_{H,\text{dip}}$, and $-B'_{H,\text{dip}}$ are the anisotropic contributions to a'_H representing the principal values, in MHz, of the traceless tensor $\mathbf{A}_{H,\text{dip}}$. According to the alternatives, $2v_n > |A'_{H||}|$, $|a'_H|$, $|A'_{H\perp}|$ or $2v_n < |A'_{H||}|$, $|a'_H|$, $|A'_{H\perp}|$, and $|A'_{H||}| > |A'_{H\perp}|$ or $|A'_{H||}| < |A'_{H\perp}|$, four cases have to be considered. The idealized shapes of ENDOR signals, observed in these cases, are shown in Figure 5.7 [310, 329]. It has been found that $|A'_{H||}| > |A'_{H\perp}|$ when the ^1H -coupling constant a'_H is expected to be positive, whereas $|A'_{H||}| < |A'_{H\perp}|$ when this constant should be negative. This is because $A'_{H||}$, a'_H , and $A'_{H\perp}$ have the same sign, and their absolute values are larger than $B'_{H,\text{dip}} = (1/3)|A'_{H||} - A'_{H\perp}|$, which is positive throughout.

Hence, when a'_H is positive, $|A'_{H\parallel}| = |a'_{H\parallel} + 2B'_{H,\text{dip}}|$ is larger than $|A'_{H\perp}| = |a'_H - B'_{H,\text{dip}}|$, whereas the opposite relation holds for a negative a'_H value. This statement is independent of the unit, MHz or mT, used for the coupling constants.

Triplet States by ENDOR

The ENDOR technique is also applicable to biradicals and triplet molecules in both the electronically excited and the ground-state [15e, 16].

Because π -spin populations are almost the same as in the corresponding monoradicals (Chapt. 4.4), the ENDOR signals for biradicals, which contain two equivalent π moieties and can be studied in fluid solution, appear at the frequencies usually observed for these monoradicals [435, 535, 536].

Most often, photoexcited triplet states of aromatics (Table 11.1) were investigated by ENDOR in single crystals, e.g., naphthalene in durene [537], benzene in perdeuteriobenzene [538], anthracene in phenazine [379], diphenyl in perdeuteriodiphenyl [539], and perdeuteriophenanthrene in diphenyl [540]. According to the observed ^1H -hyperfine data, the symmetry of these molecules in the excited triplet state seems to be reduced relative to that in the singlet ground state.

For ground-state triplets, ^1H -ENDOR studies were also performed for the structurally related fluorenylidene [541] and diphenylmethylene [542] (Table 11.3) produced by photolysis of their diazo precursors, fluorenylidene in a host crystal of diazofluorene and diphenylmethylene in a host of diphenylethylene crystal. ^{13}C -hyperfine data observed by ESR spectroscopy confirmed that, in both triplet molecules, the bulk of the π -spin population resides at the central C atom. The hyperfine splittings by protons could not be resolved in their ESR spectra, but the spin distribution over the remaining π centers was determined by ^1H -ENDOR studies.

5.3

TRIPLE Resonance

In the *special TRIPLE*-resonance or double ENDOR experiment [15f, 16, 528], the sample is irradiated simultaneously with two RF fields, in addition to the saturating MW irradiation, so that both NMR transitions ① and ② (Figure 5.2) are excited at the same time. According to schemes e and f in Figure 5.2, this procedure should double the ENDOR enhancement, because it leads simultaneously to $3\Delta n/4$ in $|-\rangle$ and $\Delta n/4$ in $|+\rangle$, thus yielding a difference $\Delta n/2$ instead of the $\Delta n/4$ achieved with a single RF source. The main advantage of special-TRIPLE resonance is that signal intensities reflect better the number of nuclei giving rise to them than they do in ENDOR spectroscopy. The special-TRIPLE resonance signal, associated with the coupling constant a'_X , appears separated from the origin (NMR frequency $\nu = 0$) by $|a'_X/2|$ in units of ν . As shown in Figure 5.8 for the phenalenyl radical (4') (Table 8.4) [528], the intensities of the special TRIPLE signals from the α protons in the 1,3,4,6,7,9- and 2,5,8-positions exhibit the expected ratio 2, although this ratio in ENDOR is only ca 1.4.

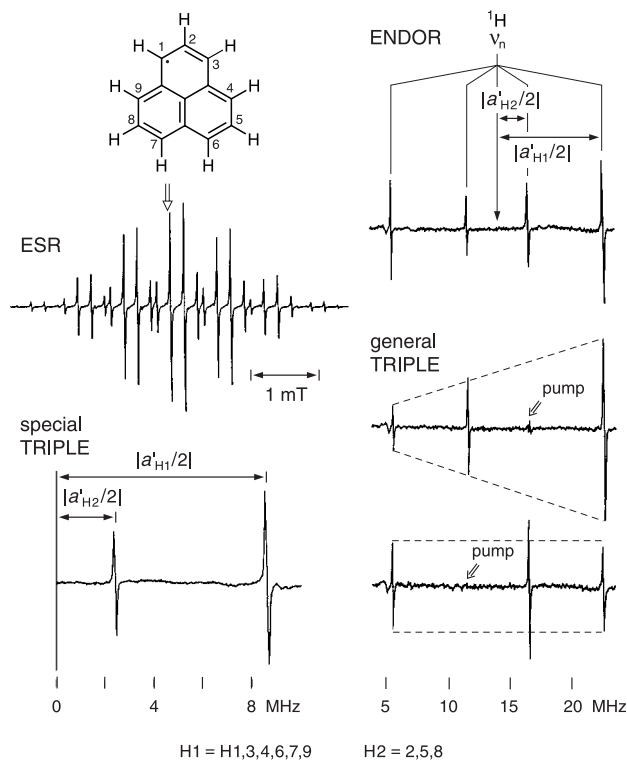


Fig. 5.8. Top: ESR (left center), ^1H -ENDOR (right top), special-TRIPLE resonance (left bottom), and general-TRIPLE resonance (right center and bottom) spectra of the phenalenyl radical (**4'**). Solvent mineral oil, temperature 300 K. The outline-arrow above the ESR

spectrum indicates the line selected for saturation, and those in the general-TRIPLE-resonance spectra mark the ENDOR signal chosen for pumping. Hyperfine data in the text and Table 8.4. Reproduced by permission from [528].

Whereas in special-TRIPLE-resonance, the NMR transitions of the *same* set of protons are irradiated (*homonuclear-TRIPLE* resonance), in general-TRIPLE resonance, transitions of different sets of nuclei are saturated simultaneously (*heteronuclear-TRIPLE* resonance). One NMR transition is “pumped” with the first (unmodulated) RF frequency, while the second (modulated) RF field is scanned over the whole range of NMR resonances. The “pumping” causes characteristic intensity changes in the high- and low-frequency signals relative to those observed by ENDOR. When the high- (or low-) frequency signal is pumped, its intensity is strongly reduced, while that of the low- (or high-) frequency partner, associated with the same coupling constant, is enhanced, because for this partner, the pumping corresponds to a special-TRIPLE-resonance experiment. Figure 5.8 demonstrates the effect of pumping the signals separated by the smaller coupling constant, $|a'_{\text{H}_{2,5,8}}|$, of the three α protons in **4'** [16, 528]. (In Figure 5.8, H1,3,4,6,7,9 and H2,5,8 are abbreviated to H1 and H2, respectively.) When the high-frequency signal at $\nu_n + |a'_{\text{H}_{2,5,8}}/2|$ is pumped, it nearly disappears, while its low-frequency

partner at $\nu_n - |a'_{\text{H}2,5,8}/2|$ increases substantially. An opposite effect on the intensities is observed on pumping the low-frequency signal. Simultaneously, striking intensity changes are observed for the pair of signals separated by the larger coupling constant, $|a'_{\text{H}1,3,4,6,7,9}|$ of the six α protons in **4'**, although neither of these signals is subjected to pumping. As evident from Figure 5.8, such changes follow a pattern that is diametrically opposed to those induced on the signals separated by $|a'_{\text{H}2,5,8}|$. The ratio of the intensity of the high-frequency signal at $\nu_n + |a'_{\text{H}1,3,4,6,7,9}/2|$ to that of its low-frequency partner at $\nu_n - |a'_{\text{H}1,3,4,6,7,9}/2|$ increases relative to the pattern in ENDOR, when the high-frequency signal at $\nu_n + |a'_{\text{H}2,5,8}|$ is pumped. In contrast, this ratio decreases when the pumping is carried out on the low-frequency signal at $\nu_n - |a'_{\text{H}2,5,8}|$. This behavior points to opposite signs of the two coupling constants, to $a'_{\text{H}1,3,4,6,7,9} = -17.64$ and $a'_{\text{H}2,5,8} = +5.08$ MHz, corresponding to $a_{\text{H}1,3,4,6,7,9} = -0.629$ and $a_{\text{H}2,5,8} = +0.181$ mT (Chapt. 4.2) [88]. Another example of the use of the general-TRIPLE-resonance technique to determine the relative signs of coupling constants is presented in Chapt. 6.3. This technique has often been applied to ENDOR spectra of organic radicals in solution, although its results are sometimes not fully conclusive.

5.4

ELDOR

The physical principles underlying ELDOR are similar to those presented above for ENDOR. Along with ENDOR, they were briefly introduced in some of the monographs on ESR spectroscopy [8, 10, 11] and more fully described in the two books on multiresonance [12, 15a, b]. Similar to ENDOR, one ESR transition (corresponding to ① in Figure 5.2) is saturated, and the intensity of the pertinent signal is reduced. However, unlike ENDOR, the second saturating irradiation in the ELDOR experiment makes use of an additional MW frequency, which is scanned over an ESR range. This second MW irradiation can alter the population of spins in the two levels relevant to the first saturated transition when its frequency agrees with that of another allowed ESR transition (② in Figure 5.2). The change in intensity of the ESR signal due to the first transition, while scanning the second MW frequency, is called *ELDOR effect*. Although the transitions induced by the two MW irradiations have no level in common, they may be coupled by various processes such as cross-relaxation (Chapt. 5.2) or by Heisenberg exchange at high radical concentrations (Chapt. 1.3); chemical exchange, to be considered in Chapt. 6.7, can also be effective in this respect. Thus, ELDOR is particularly suitable for studies of relaxation processes and their dependence on radical concentration, temperature, and MW power [543]. Furthermore, this technique has proved to be useful for determination of large coupling constants, especially those of ^{14}N nuclei in persistent radicals like nitroxyls and 2,2-diphenyl-1-picrylhydrazyl (DPPH; **5'**) (Table 9.3). In an ELDOR study of **5'**, the two $|a_{\text{N}}|$ values (0.974 and 0.794 mT) were measured exactly, for the first time [527].

6 Taking and Analyzing ESR Spectra

6.1 Instrumentation

ESR Spectrometer

The standard instrument consists of several components (Figure 6.1). The main components are an electromagnet and a resonant cavity connected by a waveguide to a klystron and to a crystal detector. Between the cavity and the klystron are an attenuator and a ferrite isolator, and the crystal detector is connected to a recorder via an amplifier. The spectrometer usually also includes a field modulator, which also operates on the cavity.

The field \vec{B} of the most widely used electromagnet can generally be scanned up to 1 T and must be homogeneous in 1 part per 10^5 – 10^6 . The field strength B is usually measured by means of an NMR proton probe placed beside or inside the resonant cavity, which is located in the homogeneous region of the field. This cavity is the heart of the spectrometer, as it houses the *sample cell*. The shape of the cavity can be parallelepiped (usually called rectangular) or cylindrical, and its quality is measured by its ability to store the energy $h\nu$ of radiation supplied to it. In this respect, a rectangular cavity is slightly better, but, in some cases, e.g. for special electrolytic cell [204] or for ENDOR spectroscopy (next section), use of a cylindrical cavity is indicated. Energy losses occur particularly when the sample contains a polar liquid with a high dielectric constant. These dielectric losses increase as the temperature of the fluid solution is lowered, but rapidly decrease when it freezes. The losses can be diminished by reducing the cross section of the sample cell or, in a rectangular cavity, by changing the shape of the cell to better fit the electric and magnetic field lines.

The *klystron*, which represents by far the most common source of energy, is a vacuum tube producing microwave oscillations in a small range of frequencies. The emitted microwave (MW) energy $h\nu$ is directed to the sample through the *waveguide* and an adjustable hole in the cavity, the *iris*. The dimensions of both the klystron and the waveguide match the length of the transmitted microwaves. This wavelength depends on the type of the klystron, which can be tuned within a limited range. A conventional X-band klystron is characterized by a frequency ν of about 9500 MHz, or a wavelength λ of ca 3 cm, which, for organic radicals having

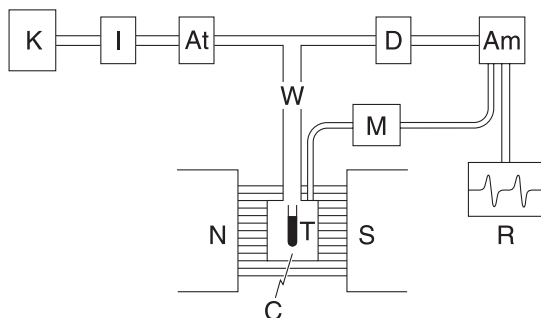


Fig. 6.1. Basic components of an ESR spectrometer. N and S = poles of electromagnet; C = resonance cavity; T = sample tube; W = waveguide; K = klystron; I = ferrite isolator; At = attenuator; D = crystal detector; Am = amplifier; R = recorder; M = modulator.

a g_e factor close to 2, meets the resonance condition at a field strength B of ca 0.34 T (340 mT). ESR studies at stronger (or weaker) fields require klystrons operating at higher (or lower) frequencies, e.g., a Q-band klystron with $\nu \approx 36000$ MHz, or $\lambda \approx 8$ mm, operates at $B \approx 1.3$ T. An advantage of a higher field strength B is a more favorable Boltzmann distribution, which leads to enhanced magnetization (see Chapt. 1.3). However, for radicals in fluid solution, this advantage is partially cancelled by the necessity of using a cavity matching the smaller wavelength λ , which means a narrower sample cell with fewer unpaired spins.

The *attenuator* adjusts the level of microwave power incident on the sample, and the *ferrite isolator* protects the klystron from reflected radiation.

The *detector* is a silicon crystal diode in contact with a tungsten wire. The noise, which appears even in the absence of ESR absorption, is the usual background of the signal; it is partly the intrinsic noise of the detector and partly the frequency noise of the klystron.

The *amplifier* enhances the registered signal without, however, markedly changing the signal-to-noise ratio. This ratio is greatly improved by the *field modulator*, which consists of small Helmholtz coils placed on each side of the cavity along the direction of the field. Because of the modulation, the ESR-absorption curve has the familiar shape of its first derivative dA/dB (see Chapt. 1.4).

A more detailed description of ESR instrumentation is found in general textbooks on ESR spectroscopy [4, 10, 11] and in two early specialized monographs [544, 545].

Although the resolving power of ESR spectrometers has not been markedly enhanced since the first commercially available instruments were produced by Varian Associates [17q] in the 1960s, their performance has greatly increased. Modern instruments, like those produced today by Bruker GmbH [17r], are largely computerized, so that many operations are carried out automatically, and additional functions, such as accumulating, storing, and manipulating the spectra, can be performed. Although these modern instruments may have more user-friendly

interfaces, they are black boxes internally, so any trouble calls for the assistance of a highly specialized expert.

Special Accessories

As discussed in Chapt. 5.2, substantial progress in analyzing complex or poorly resolved hyperfine patterns was not achieved by ESR spectroscopy itself, but by introducing complementary multiresonance techniques, such as ENDOR, TRIPLE, and ELDOR, which were considered in Chapt. 5.2–5.4. The accessories required for these techniques are being used by an increasing number of research groups, especially since ENDOR accessories became commercially available from Varian in the 1970s and from Bruker in the 1980s.

ENDOR spectroscopy requires, in addition to a standard ESR spectrometer, a powerful radio-frequency (RF) generator and a special cylindrical cavity, on which this second source of energy can also operate via RF coils inserted into the cavity. To perform an ENDOR experiment, the spectrometer is first configured as a conventional ESR instrument. Further procedures are outlined in Chapt. 5.2. A selected ESR line, usually the strongest one, is saturated by intense MW irradiation from the klystron, and the magnetic field is adjusted to this line and kept constant by a field-frequency lock. The RF generator then steps into action, and the spectrum is swept over the NMR frequency range of 0 to 35 or 400 MHz, depending on the generator used. ENDOR signals are registered as an increase in the intensity of the saturated line.

An apparatus employed in ENDOR and its extension to special- or general-TRIPLE-resonance, in which two RF frequencies operate via coils on an ESR signal, are described in more detail in [12, 15a, 16]. In electron-electron double resonance (ELDOR), the resonant cavity has to be tunable to two different MW frequencies separated by a multiple hyperfine splitting [12, 15a, 543].

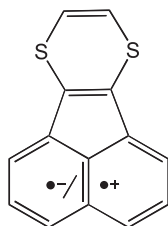
6.2

g_e Factor

The resonance condition (Eq. 1.5) implies that, for a constant MW frequency ν and a variable field strength B , the position of the ESR signal in the field \vec{B} depends on the factor g_e of the electron. For organic radicals in fluid solutions, this factor is isotropic like the hyperfine-coupling constants, because the g_e anisotropy also is averaged out by molecular motion. In a multiline ESR spectrum, the g_e factor is measured at the center of the spectrum, which may coincide with the position of the main line (as in a hyperfine pattern arising from an even number of protons) or fall in between lines (as a hyperfine pattern arising from an odd number of protons). Departure from the center results from second-order hyperfine splitting, which occurs with large coupling constants and was considered in Chapt. 3.2. In this case, the observed value must be corrected for this splitting (Figure 3.4). An asymmetric hyperfine pattern may arise from superposition of the ESR spectra of

two or more radicals with different g_e values. When this asymmetry occurs, conspicuous changes are observed upon replacing the X (9500 MHz) by the Q band (36000 MHz), as such superimposed spectra move apart. This is because the positions of the spectra in the magnetic field of strength B , as characterized by the g_e factors of the pertinent radicals, depend on the MW frequency ν (Eq. 1.5), whereas their hyperfine patterns do not (Eq. 3.14).

For paramagnetic species containing heavy atoms, such as complexes of organic ligands with transition metals, the g_e factor provides important structural information, which is particularly valuable when hyperfine splittings are not observed. However, for organic radicals without heavy atoms, the g_e factor is much less informative than the hyperfine interaction, and it is not specified in many reports on ESR studies of such radicals. This is because the g_e factor of organic radicals is close to 2 or, more exactly, to the free-electron value of 2.0023. It lies within the rather narrow range of 2.00 to 2.01 in the absence of atoms heavier than Cl. As was stated in Chapt. 2.1, deviations of g_e from the free-electron value are due an orbital admixture to the spin magnetism. Such an admixture is brought about by spin-orbit coupling, which is particularly effective in heavy atoms. Thus, within the narrow range of 2.00 to 2.01 deviations from 2.0023 occur when the radical contains heteroatoms, and these deviations are the largest for heavier heteroatoms like P and S, with high π -spin population (which is a measure of the probability of finding the unpaired electron at these atoms). For example, the radical cation of acenaphtho[1,2-*b*][1,4]dithiine (**93**) (Table 9.32) has an isotropic g_e factor of 2.0071, whereas the corresponding value for the radical anion of the same compound is 2.0026 [546].



93 •- / •+

The substantially larger g_e factor for **93**⁺ than for **93**⁻ is due to the much higher π -spin population, $2 \cdot (+0.25) = +0.50$, at the two S atoms in the radical cation, as compared to the radical anion, in which this population is smaller than 0.01 (sign uncertain). The g_e factors of various classes of organic radicals are indicated in Part B of this book, along with the hyperfine data. Some characteristic values are also given below.

For alkyl radicals, like methyl (**58**[•]) and ethyl (**59**[•]), the g_e factor is 2.0026 within a range of ± 0.0001 [547]. Hydrocarbon π radicals have a g_e factor between 2.0025 and 2.0028. Typically, for the radical cations of anthracene, tetracene, pentacene, and perylene, this factor is close to 2.00257 within a range ± 0.00003 , and for the corresponding radical anions, it is about 2.00267, also within ± 0.00003 [548, 549].

The anions thus exhibit a slightly but significantly larger g_e factor than the cations. The g_e factor of neutral π radicals lies in between, e.g., it is 2.00260 for triphenylmethyl (trityl; 1^{\cdot}) and 2.00265 for phenalenyl (4^{\cdot}) [548, 549]. Exceptions are π radicals with a degenerate ground state, such as the radical anions of benzene and coronene, for which the g_e factor is somewhat higher, namely 2.00284 and 2.00305, respectively [548, 549]. The presence of a diacetylene moiety in a π -radical anion seems to somewhat decrease the g_e factor below the free-electron value of 2.0023 [550] (Chapt. 8.3).

As stated above, introduction of a heteroatom into a π radical generally increases the g_e factor. For radical anions of azaaromatics, the range is apparently 2.0030–2.0035, and for those of azo compounds 2.0035–2.0042 [551, 552], respectively, and for the radical anions of the phospho derivatives it is 2.0040–2.0050 [165, 181]. The radical anions of nitro compounds exhibit a g_e factor of 2.0045–2.0055, and that of nitroxyls lies between 2.0055 and 2.0065 (part d1 of [18]). The g_e factor of semidione, semiquinone, and ketyl anions is in the range 2.0040–2.0060 (part c1 of [18]), and, for radical cations of 1,4-dithiine and 1,4,5,8-tetrathia-1,4,5,8-tetrahydrofulvalene (TTF; **23**), as well as for those of S-containing compounds structurally related to them, this value is as large as 2.0070 to 2.0080 [469].

For σ radicals, the g_e factor is usually lower than for their π counterparts, e.g., it is 2.0022 for vinyl (11^{\cdot}) [34] and 2.0023 for phenyl (12^{\cdot}) [112]. Such a decrease is particularly pronounced for acyl radicals like formyl (13^{\cdot}), for which the g_e factor is 2.0003 [553].

The g_e values can be determined indirectly by comparison with those of standard species, such as 2,2-diphenyl-1-picrylhydrazyl (DPPH; 5^{\cdot}) (2.0036), or $(\text{NO}^{\cdot})(\text{SO}_3^-)_2\text{K}^+$ (Frémy salt) in sat. Na_2CO_3 soln. (2.00550 ± 0.00005), or the radical anion of pyrene in DME with counterion K^+ (2.002710) [547], or the radical cation of perylene in conc. H_2SO_4 (2.002583 ± 0.000006) [548]. Such a measurement is best carried out in a dual cavity, where the spectra of the sample and the reference are recorded side by side. A direct method implies simultaneous determination of the field strength B with an NMR probe and of the MW frequency ν with a wavemeter.

According to the resonance condition, the g_e factor is then calculated as

$$g_e = (h/\mu_B)\nu/B = 7.144775 \cdot 10^{-2}\nu/B \quad (6.1)$$

where ν is MHz and B is in mT.

g_e Anisotropy

Thus far, the isotropic g_e factor has been considered. However, like other characteristics of paramagnetic species, the g_e factor is anisotropic. Because the anisotropy is averaged out in fluid solution, it must be studied in a rigid medium, preferably in single crystal. Similar to deviations of the isotropic g_e factor from the free-electron value, anisotropy contributions to this factor depend on the extent of spin-orbit coupling, and thus on the presence of heavier atoms accommodating high spin populations. The anisotropic g_e factor can be represented by a tensor \mathbf{G}_e ,

of which the principal values, $g_{e,z}$, $g_{e,y}$, and $g_{e,x}$, apply to the orientation of the radical in the three principal directions of space with respect to the magnetic field $\vec{\mathbf{B}}$. By subtracting the isotropic g_e factor from these three values, a traceless tensor $\mathbf{G}_{e,\text{aniso}}$ is obtained, with the anisotropic contributions as its principal values. Such contributions are usually very small for hydrocarbon radicals. For example, the anisotropic contributions for the ethyl radical (**59'**) (generated by photolysis of HI in the presence of ethene in xenon at 4.2 K) amount to -0.0010 , $+0.0005$, and $+0.0005$ in the z , y , and x direction, respectively, because the corresponding principal values, $g_{e,z}$, $g_{e,y}$, and $g_{e,x}$, of the \mathbf{G}_e tensor are 2.0016, 2.0031, and 2.0031, respectively, and the isotropic factor is 2.0026 [444, 554]. The z direction is the axis of the spin-bearing $2p$ -orbital at the methylene atom, which is parallel to the field $\vec{\mathbf{B}}$, and x and y are perpendicular to it. Therefore, $g_{e,z}$ can be denoted $g_{e\parallel}$, and $g_{e\perp} = g_{e,x} = g_{e,y}$ for an axial tensor \mathbf{G}_e or, in general, $g_{e\perp} = (1/2)(g_{e,x} + g_{e,y})$. This notation is used, in particular, for π radicals in which the z direction is parallel to the p_z axes at the centers μ of the π system, and x and y lie in the molecular plane perpendicular to these axes. The $g_{e,z}$ component is generally the lowest one, being closest to the free-electron value of 2.0023, so that $\Delta g_e = g_{e\parallel} - g_{e\perp} = g_{e,z} - (1/2)(g_{e,x} + g_{e,y})$ is negative. For hydrocarbon π radicals, $|\Delta g_e|$ is usually smaller than 0.001, and its effect on the spectrum becomes evident only when combined with that of hyperfine anisotropy (Chapt. 6.5). For example, the radical cation of naphthalene (**83**) in a CFCl_3 matrix has $g_e = 2.0025$ which is nearly isotropic, with anisotropy contributions less than 0.0003 [480]. The axes of \mathbf{G}_e often coincide with those of a hyperfine tensor \mathbf{A}_X .

Upon introduction of a heavier atom as a hetero- π center, the g_e anisotropy becomes more pronounced, as for the radical anion of 2,4,6-tri-*tert*-butylphosphabenzene (**82**) (Table 9.11) [165]. ESR spectra of **82** $^{\cdot-}$ are shown in Figure 4.8, along with the axes of the hyperfine tensor \mathbf{A}_P , which are also those of the g_e tensor \mathbf{G}_e . Due to the marked g_e anisotropy, the spectrum taken in glassy MTHF is not centrosymmetric, because the centers of each pair of the hyperfine components $A_{P\parallel}$ and $A_{P\perp}$, also relevant to $g_{e\parallel}$ and $g_{e\perp}$, are separated by 0.55 mT. This difference corresponds to Δg_e of -0.00325 . The sign of Δg_e is negative, because $g_{e\parallel}$ is smaller than $g_{e\perp}$, the former being measured at higher field than the latter (Figure 4.8). The three principal values are $g_{e,z} = 2.0026$, $g_{e,y} = 2.0069$, and $g_{e,x} = 2.0048$, equivalent to $g_{e\parallel} = 2.0026$, $g_{e\perp} = (1/2)(2.0069 + 2.0048) = 2.00585$, and $\Delta g_e = 2.0026 - 2.00585 = -0.00325$. The isotropic g_e factor is thus $(1/3)(2.0026 + 2.0069 + 2.0048) = (1/3)(2.0026 + 2 \cdot 2.00585) = 2.0048$, and the anisotropic contributions to this factor in the z , y , and x directions, as the principal values of $\mathbf{G}_{e,\text{aniso}}$, amount to ca. -0.0022 , $+0.0021$, and 0, respectively.

6.3

Optimal Conditions

A high-quality ESR spectrum is needed for providing reliable structural information. Two features characterize such a spectrum, maximal signal-to-noise ratio and minimal width of hyperfine lines. (Because the intensity of the absorption A is

proportional to the area under the signal, which, for the first derivative dA/dB , is the double integral over B , decrease in the line-width implies an increase in height of the line. In practice, under the experimental conditions considered below, the spectrum can often be optimized in favor of one desirable feature only at the expense of the other.

Microwave Power and Concentration

The theory underlying the effect of these two factors on the height and width of hyperfine lines was introduced in Chapt. 1.3 and 1.4. It involves spin-lattice relaxation (SLR) and spin-spin relaxation (SSR), with their characteristic relaxation times T_{1e} and T_{2e} , respectively. Enhancing the microwave (MW) power of the irradiation increases the probability, P , of electron-spin transitions and therefore also the excess, Δn , of spin population in the lower Zeeman level, so that the ESR signal should grow stronger. Yet, because the term $1 + PT_{1e}$ determines the extent of saturation (Eq. 1.11), enhancement of the MW power leads to a more intense signal only when T_{1e} is short, which does not occur for organic radicals lacking heavy atoms. Consequently, to avoid saturation, the MW power must be attenuated until the maximal height of the ESR signal is attained. Because of its dependence on T_{1e} , which is an individual property of the sample, the optimal attenuation should be determined in each experiment. In practice, this task is less troublesome, as structurally related radicals studied under similar conditions (solvent, temperature) have comparable SLR times T_{1e} , so that the same attenuation can be applied to them.

Because the number of unpaired electron spins increases with that of the paramagnetic molecules in the sample, generating a radical in high concentration seems to be a prerequisite for observing a high-quality ESR spectrum. However, an increase in radical concentration diminishes the average distance, r , between two unpaired electron spins, so that their interactions become stronger. Not only does the Heisenberg exchange, which occurs when the orbitals of two proximate electrons overlap, become more efficient but so does the dipolar magnetic interaction. Depending on r^{-3} , this intermolecular interaction of two radicals corresponds to the intramolecular interaction of the two unpaired electron spins in a triplet state (Eq. 2.5). All these interactions shorten the effective SSR time T_{2e} , which, in view of the long T_{1e} for organic radicals, is the main contributor to the line-width (Eq. 1.15). In particular, for persistent radicals that can be generated in high concentration, the solution must be diluted to achieve a reasonable compromise, i.e., an optimal resolution at an acceptable signal-to-noise ratio. As stated in Chapt. 5.2, because of its lower sensitivity and higher resolving power, somewhat higher concentrations are recommended for ENDOR than for ESR. Application to transient radicals is, therefore, more problematic in ENDOR than in ESR.

Solvent and Temperature

The choice of solvent is largely determined by conditions under which the radicals are generated (Chapt. 2.2–2.4). This statement especially holds for radical ions,

while for neutral radicals the solvent choice is less restricted. The solvent should dissolve the reagent and the precursor of the neutral radical and must be sufficiently inert not to react with this radical. Thus, for reactive neutral radicals in fluid solution, inert solvents, like cyclopropane at low temperatures, are preferred. Persistent neutral radicals can often be transferred from one solvent into another.

On the other hand, for radical anions produced with an alkali metal, ethereal solvents, such as 1,2-dimethoxyethane (DME), tetrahydrofuran (THF), 2-methyltetrahydrofuran (MTHF), or diethylether (DEE), must be used (their solvating power for the metallic counterion decreases in the order listed). Thus, if complications caused by close association of the radical anion with its counterion (ion pairing) must be avoided, the solvent of choice is DME, which can be partially or totally replaced by the more polar *N,N,N',N'*-hexamethylphosphoric triamide (HMPT). Studies of radical anions in matrices generally use MTHF, which form a glass on freezing. Electrolytic reduction require relatively polar solvents, like acetonitrile (ACN), *N,N*-dimethylformamide (DMF), or dimethylsulfoxide (DMSO), which have to dissolve the supporting salt.

The favorite solvent for radical cations (whether produced with chemical reagents or electrolytically) is dichloromethane, either pure or mixed with trifluoroacetic acid (TFA). As mentioned in Chapt. 2.3, Freons are used as matrices for radical cations generated by γ -irradiation. These solvents are inert halocarbons of high ionization energy ($IE \approx 12$ eV) and low freezing point (ca 160 K), namely $CFCl_3$ (F-11), CF_3CCl_3 (F-113A), $CF_2ClCFCl_2$ (F-113), CF_2ClCF_2Cl (F-114), and CF_2BrCF_2Br (F-114B2). Other inert solvents, especially for small radical cations are rare gases at cryogenic temperatures (e.g., Ne with $IE = 21.6$ eV) and sulfur hexafluoride ($IE = 15.7$ eV).

Raising the temperature has a variety of effects on the solvent, such as a *decrease* in viscosity and polarity. Depending on the sample, these effects can improve or worsen the quality of the ESR spectrum. Because a decrease in viscosity promotes molecular motion and, thus, an averaging out of dipolar interactions, the linewidths of radicals in solution tend to narrow at higher temperatures. Therefore, many persistent neutral radicals and radical cations yield better resolved spectra upon warming the solution. However, for less-persistent species, the upper limit of temperature is determined by decay of the radical. As mentioned in Chapt. 5.2, solvents of higher viscosity are usually required for ENDOR spectroscopy, to lengthen the electron SLR time T_{1e} . For ENDOR studies of neutral radicals, viscous mineral oil is often used as the solvent, whereas for such studies of radical ions, like anions in an ethereal solvent, an increase in viscosity must be achieved by lowering the temperature. Immobility of the solvent molecules is required for triplet-state species; it is brought about by fully freezing the solution or, in some cases [156], by cooling it almost to the freezing point.

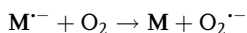
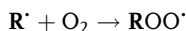
The decrease in solvent polarity on raising the temperature strengthens the association of the radical anions with their alkali-metal counterions and complicates the analysis (Chapt. 6.6). Generally, both ESR and ENDOR spectra of these species in ethereal solvents are thus preferably observed at ca 200 K; conveniently, DME serves as the solvent and K^+ as the counterion (due to the small magnetic

moment of the ^{39}K nucleus, the appearance of an additional splitting is usually avoided).

Changing the temperature affects the performance of the resonant cavity. On cooling the solution, its performance deteriorates because of increasing polar losses. Interestingly, polar losses strikingly decrease on freezing due to of the reduced mobility of the solvent molecules. As mentioned in Chapt. 6.1, an increase in polar losses needs to be compensated for by a decreased cross-section of the sample tube or by orienting a flat cell in the rectangular cavity in such a way as to diminish these losses.

Paramagnetic and Protic Impurities

The most common paramagnetic impurity found in an insufficiently degassed solution of radicals is dioxygen. It is detrimental to neutral radicals (converting them into peroxides) and to radical anions (oxidizing them to their diamagnetic precursors).

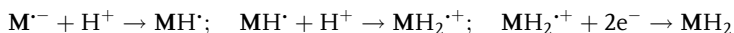


It is, in general, less harmful to radical cations.

In addition to its chemical reactivity, dioxygen interacts magnetically with any neutral radical or radical ion, by virtue of the two unpaired electron spins in its triplet ground state. The dipolar interaction of the two electron spins with those in the radical broadens the ESR lines and blurs the hyperfine pattern [17]. This effect is demonstrated in the ESR spectrum of the radical cation of *N,N'*-tetramethyl-1,4-phenylenediamine (**17**) (Wurster's blue (Table 9.34)) in Figure 6.2 [555]. Although the integrity of this highly persistent radical cation is not affected by saturating the solution with dioxygen, the finer hyperfine splittings are wiped out.

Less common paramagnetic impurities to be avoided are ions of transition metals, stemming from the reagents used for generating radicals and radical ions.

Protic impurities are mostly due to water in an incompletely dried solution of a radical. They react with radical anions $\text{M}^{\cdot-}$, thus yielding mono- and diprotonated species, respectively.



Diprotonation of π -radical anions usually takes place at the centers of highest charge, e.g., at the 9,10-positions of anthracene and phenanthrene. Under prevailing reductive conditions, the corresponding dihydro derivatives are produced. This dihydrogenation is equivalent to the well-known Birch reduction. Clearly, generation of a radical anion in ethereal solutions containing an alkali metal as the reducing agent must be carried out in as good a vacuum as possible or under a dry inert-gas atmosphere. Small water impurities are eliminated by the metallic mirror, but larger quantities destroy its surface, which is essential for the reduction

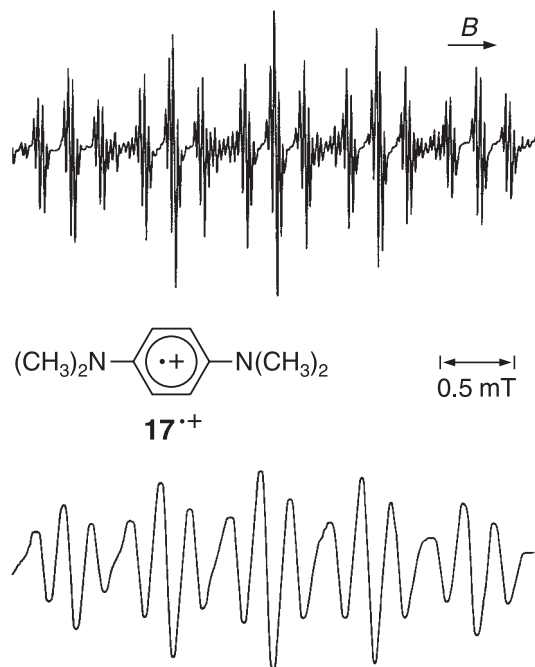


Fig. 6.2. Central part of the ESR spectrum of Wurster's blue ($17^{\bullet+}$) in oxygen-free (top) and in air-saturated ethanol (bottom). Hyperfine data in Table 9.34. Reproduced with permission from [555].

process. The mirror surface can sometimes be regenerated by sublimation of underlying pure metal.

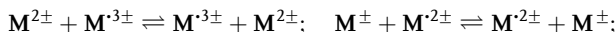
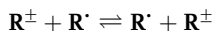
A particular case is that of the radical anions of several quinones and diazaaromatics, mentioned in Chapt. 2.3. Upon reduction in an acidic solution, these radical anions $M^{\bullet-}$ become diprotonated at the two O and N atoms, respectively, and the radical cations $MH_2^{\bullet+}$ thus formed are persistent [264–267].

In general, solutions of radical cations, which are often produced by oxidation with acids, contain substantial concentration of protons.

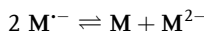
Chemical Exchange

Diamagnetic compounds other than water and acids do not usually interfere with radicals in solution. Exceptions are diamagnetic precursors of radicals, when they differ structurally from their paramagnetic redox products by only one electron. The fast electron exchange between the two species leads to shortening of the SSR time T_{2e} and to broadening of the hyperfine lines. Such exchange occurs between a diamagnetic ion (R^{\pm}) and the neutral radical (R^{\bullet}), between a diamagnetic neutral

compound (M) and its radical ion ($M^{\cdot\pm}$), between $M^{\cdot\pm}$ and the diamagnetic diion ($M^{2\pm}$), between $M^{2\pm}$ and the radical triion ($M^{\cdot 3\pm}$), and between a diamagnetic ion (M^{\pm}) and the radical diion ($M^{\cdot 2\pm}$).

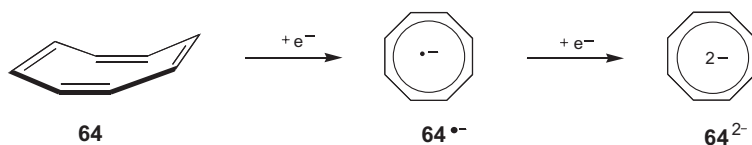


The most frequently observed electron exchange takes place between a neutral diamagnetic compound (M) and its radical anion ($M^{\cdot -}$), as well as between $M^{\cdot -}$ and the diamagnetic dianion M^{2-} . Compounds M , which are not readily reduced to dianions M^{2-} , can be almost completely converted into $M^{\cdot -}$. However, with better electron acceptors M , reduction should not be pushed too far because of the formation of M^{2-} . In this case, the situation becomes even more complicated due to an equilibrium:



Thus, reduction has to be carried out in such a way that this equilibrium is, as much as possible, shifted to the left. In a simple model, electrostatic attraction of M , $M^{\cdot -}$, and M^{2-} by the uncharged or the +1 or +2 charged counterions is 0, $-e^2$, or $-4e^2$, respectively, resulting in $-2e^2$ on the left vs $-4e^2$ on the right of the equilibrium equation. Formation of M^{2-} is thus promoted by association with the counterions and can be weakened by using solvents with higher cation-solvating power, by replacing alkali-metal cations with a tetraalkylammonium, and by lowering the temperature.

For example, conversion of the tub-shaped cyclooctatetraene (COT; **64**) [556, 567] into the planar dianion (**64**²⁻) is energetically favored [558].



ESR spectra of the intermediate radical anion (**64**^{•-}) (Table 8.10) are observed upon electrolysis in DMF (counterion $n\text{-Pr}_4\text{N}^+$ or $n\text{-Bu}_4\text{N}^+$) [559, 560] and upon reduction with an alkali metal in DME or THF (counterion Li^+ , Na^+ , or K^+) [449, 561–563] but not with potassium in MTHF, which has a relatively low cation-solvating power (counterion K^+) (footnote 6 in [183]). The ^1H - and ^{13}C -coupling constants for **64**^{•-} have led to the conclusion that this radical anion is essentially planar, although its flattening is energetically less favored than that of **64**²⁻. This

conclusion is corroborated by studies of electron exchange between 64 and $64^{\cdot-}$ and between $64^{\cdot-}$ and 64^{2-} . The electron exchange between 64 and $64^{\cdot-}$ is slow and does not markedly affect the lines in the ESR spectrum of $64^{\cdot-}$; however, the exchange between $64^{\cdot-}$ and 64^{2-} is fast and clearly broadens them [182]. This finding points to a planar structure of both $64^{\cdot-}$ and 64^{2-} , in contrast to the tub-shaped 64 .

Enhancement of Signal-to-Noise Ratio

Detection of transient radicals is often difficult because they cannot be produced in high concentration and, consequently, the signal-to-noise ratio in their ESR spectra is low. A procedure allowing observation of such spectra is the flow method, in which the solutions containing the precursor and the reagent are mixed only while flowing through the cell inside the cavity [59–65, 258–260]. In this way the decay of the radical is compensated for by its formation from new material, and a steady concentration is attained. However, a flow procedure requires a continuous supply of the precursor, which is not possible in large quantities for many radicals of interest. A method less demanding with respect to the amount of starting material is generation of transient radicals by high-energy irradiation in chemically inert rigid media, in which decay of this reactive species is largely impeded. Radical cations in Freon or rare-gas matrices are notable examples.

(Here, we should note that the flow method must also be used when radical ions are electrolytically generated, if these species are studied by the ENDOR technique [564–566]. The electrolysis takes place outside the ESR cell, because, as mentioned in Chapt. 5.2, the electrodes interfere with the RF coils inside the cavity. The radical ion has to be sufficiently persistent to survive the transfer of the solution.)

As stated in Chapt. 6.1, the signal-to-noise ratio can be greatly improved by raising the modulation amplitude. This amplitude, measured in mT, should be only a small fraction of the line-width ΔB . Moreover, the modulation frequency, which is usually 100 kHz (0.1 MHz), should not approach the line-width $\Delta\nu$ (ΔB is ca 0.01 mT and $\Delta\nu = \gamma_e \Delta B$ is ca 0.3 MHz for a well-resolved ESR spectrum of a radical in fluid solution). An increase in the amplitude and/or frequency of the modulation above these limits leads to a distortion and/or broadening of the lines, and the small hyperfine splittings are lost. This disadvantage, however, does not matter when the lines are very broad, and it is taken into account when the main purpose of the experiment is proving the formation of a transient radical.

Accumulation of spectra by repeated recording and addition should improve the signal-to-noise ratio by a factor \sqrt{n} , where n is the number of runs. This procedure is appropriate when a radical is generated in a low concentration that can be maintained during the period of time required for data accumulation. The risk that small hyperfine splitting may be blurred by this technique is not fully excluded. Accumulation of spectra has become routine for most ENDOR studies, because the sensitivity of this technique is inferior to that of ESR and the number of lines is less.

6.4

Unravelling Hyperfine Pattern

To begin this Chapter, a few useful tips for analysis of ESR spectra of radicals in solution are appropriate:

- (1) In general, the hyperfine lines are symmetric with respect to the center of the spectrum. Asymmetry can be caused by
 - (a) superposition of spectra with different g_e factors (Chapt. 6.2);
 - (b) second-order splitting observed for large coupling constants a_X (Chapt. 3.2);
 - (c) incomplete averaging out of g_e and hyperfine anisotropies, which usually affects the width of lines without changing their positions (Chapt. 6.5).
- (2) The absence of an intense central line indicates a hyperfine interaction with an odd number of equivalent nuclei X having a spin quantum number I that is an odd multiple of $1/2$. However, the presence of a fairly intense central line does not exclude an interaction with such nuclei, because of accidental relations between the coupling constants a_X .
- (3) As expressed in Eqs. 3.15 and 3.16, for k sets, each of n_k equivalent nuclei with I_k and a_{X_k} , the total number of lines is equal to the product $(2n_1I_1 + 1)(2n_2I_2 + 1) \cdots (2n_kI_k + 1)$, and the extent of the spectrum is given by the sum of $2n_1I_1|a_{X_1}| + 2n_2I_2|a_{X_2}| \cdots + 2n_kI_k|a_{X_k}|$. For nuclei with $I = 1/2$, like protons, this product and sum simplify to $(n_1 + 1)(n_2 + 1) \cdots (n_k + 1)$ and $n_1|a_{X_1}| + n_2|a_{X_2}| + \cdots + n_k|a_{X_k}|$, respectively. Unfortunately, the total number of lines can be determined only for a minority of radicals, which have only a few sets of equivalent nuclei and which exhibit fully resolved spectra. Better chances exist for measuring the extent of the spectrum as the separation of the two outermost lines, although such lines, being the weakest ones, are often difficult to identify.
- (4) The coupling constant with the smallest $|a_X|$ value is derived from the separation between an outermost line and the one next to it.

Simple Patterns

Analysis of the spectrum is trivial when the radical contains only one set of equivalent nuclei, like the semiquinone anion formed from 1,4-benzoquinone (**19**) (Table 9.17) in 80% alkaline ethanol [567] and the radical anion of benzene (**62**) (Table 8.8) produced by reduction of the neutral compound with potassium in DME [132, 568]. Due to their sets of four and six equivalent α protons, respectively, their spectra (Figure 6.3) exhibit five and seven lines with the expected binomial intensity distributions, 1:4:6:4:1 and 1:6:15:20:15:6:1. The pertinent coupling constants, including their signs as required by theory, are $a_{H2,3,5,6} = -0.237$ for **19** $^{\cdot-}$ and $a_{H1-6} = -0.375$ mT for **62** $^{\cdot-}$, and the corresponding extent of the spectra amounts to $4 \cdot 0.237$ mT = 0.95 mT and $6 \cdot 0.375$ mT = 2.25 mT.

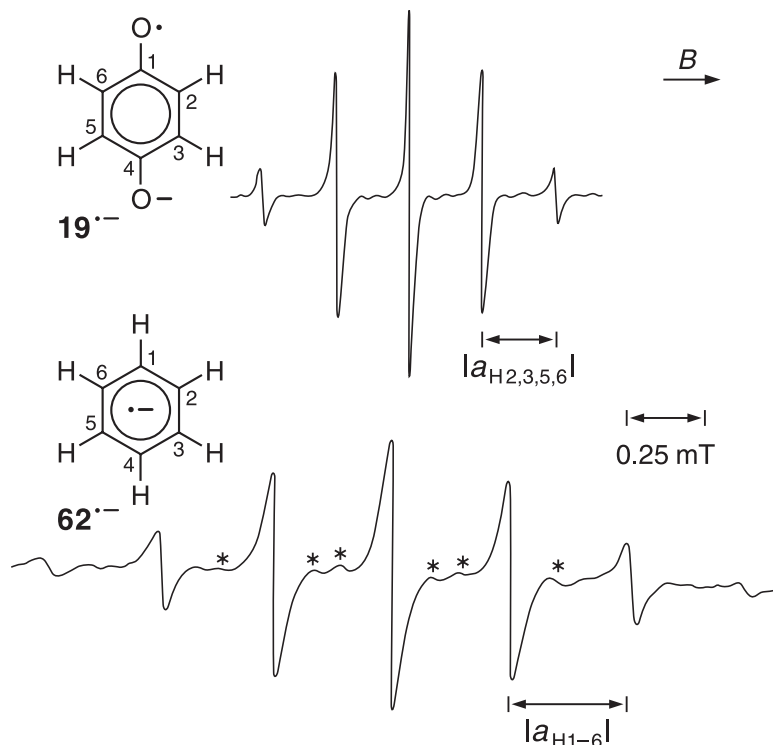


Fig. 6.3. ESR spectra of the radical anions of *p*-benzoquinone (**19**) and benzene (**62**). Top, **19**^{•−}; solvent 80% ethanol, counterion Na⁺, temperature 298 K. Bottom, **62**^{•−}; solvent DME, counterion K⁺, temperature 193 K. The

most conspicuous ¹³C satellites in the center of the spectrum of **62**^{•−} are marked by asterisks. Hyperfine data in the text and Tables 9.17 and 8.8, respectively. The lower spectrum is reproduced by permission from [132].

Also straightforward is an analysis of the hyperfine pattern for the phenalenyl radical (**4**[•]) (Table 8.4) with two sets of equivalent α protons. The spectrum of **4**[•], generated by air oxidation in tetrachlorocarbon solution [88], is shown in Figure 6.4. (A spectrum of **4**[•] produced under different conditions was shown in Figure 5.8). The hyperfine pattern is composed of seven distinct main groups with intensity ratios of 1:6:15:20:15:6:1; these groups are due to the six equivalent protons having the coupling constant $a_{H_{1,3,4,6,7,9}} = -0.629$ mT with a larger absolute value. Each of these seven groups is split into a 1:3:3:1-quartet arising from the three equivalent protons with $a_{H_{2,5,8}} = +0.181$ mT. The opposite sign of the two a_H values is predicted by theory and has been amply confirmed by experiment [90, 462]. The number of lines is $7 \cdot 4 = 28$ and the extent of the spectrum is $(6 \cdot 0.629 + 3 \cdot 0.181)$ mT = 4.32 mT. An intense central line is missing, because one set has an odd number of protons.

Slightly more demanding is an analysis of the hyperfine pattern of the radical anion of 1,4,5,8-tetraazaphthalene (**57**) [162]. This radical anion, produced with sodium in DME and associated with the counterion Na⁺, was briefly dealt with in

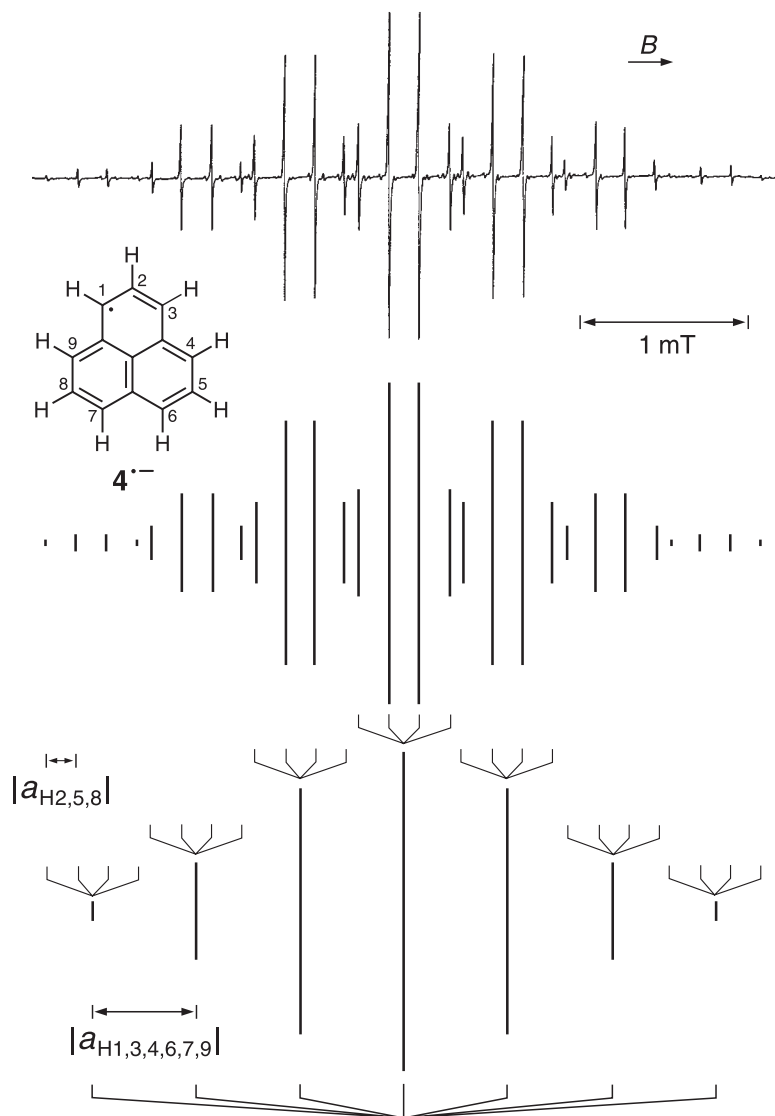


Fig. 6.4. ESR spectrum of the phenalenyl radical ($4^{\bullet-}$). Solvent tetrachloromethane, temperature 298 K. Below, a stick diagram using the coupling constants indicated in the text and Table 8.4. Reproduced with permission from [88].

Chapt. 3.2. Figure 6.5 shows the spectrum of $57^{\bullet-}$ generated electrolytically in DMF with tetraethylammonium perchlorate as the supporting salt. Therefore, this spectrum does not exhibit a hyperfine splitting by an interaction with the nucleus of the counterion, and its hyperfine pattern is simpler, being exclusively due to the two sets of magnetic nuclei in $57^{\bullet-}$ itself. The two sets of the four equivalent ^{14}N

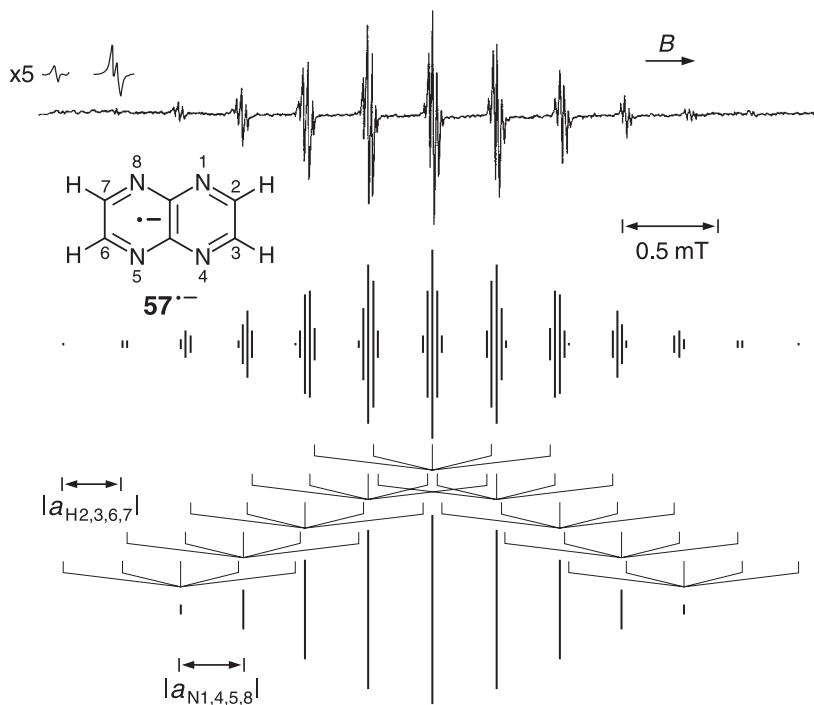


Fig. 6.5. ESR spectrum of the radical anion of 1,4,5,8-tetraazanaphthalene (**57**). Solvent DMF, counterion Et_4N^+ , temperature 298 K. Below, a stick diagram diagram using the coupling constants indicated in the text and Table 9.9. Reproduced with permission from [162].

nuclei and the four equivalent α protons should give rise to nine and five lines with intensity distributions of 1:4:10:16:19:16:10:4:1 and 1:4:6:4:1, respectively. Of the expected total number, $9 \cdot 5 = 45$, the outermost lines have only $1/(19 \cdot 6) = (1/114)$ the intensity of the central line. These and a few other weak lines can be unequivocally identified in somewhat less resolved but more intense spectra taken in solutions with higher radical concentration. The feature that makes the analysis of the hyperfine pattern less straightforward for **57**⁻ than for **4**[•] is the similar size of $|a_{\text{N}}|$ and $|a_{\text{H}}|$, so that the small omnipresent line separation of 0.023 mT is neither of the two values but their difference. The values themselves, 0.314 and 0.337 mT, can be determined by measuring the distances between an outermost line and the two following ones. However, because the intensity ratio of the outermost line to each of the two is 1:4, it is impossible to decide by this criterion which of these values should be assigned to the four ^{14}N nuclei and which to the four protons. This choice can be made by comparing the intensities of the two lines separated by 0.314 and 0.337 mT from the central, most intense line. Because the nearer and the slightly more distant line have intensity ratios of 4:6 and 16:19, respectively, relative to the central line, the absolutely larger coupling constant is that of the ^{14}N nuclei, leaving the smaller one for the protons. This conclusion is

verified by exactly measuring the extent of the spectrum, which is 3.95 mT. This value agrees with $(8 \cdot 0.337 + 4 \cdot 0.314)$ mT, whereas the alternative assignment yields $(8 \cdot 0.314 + 4 \cdot 0.337)$ mT = 3.86 mT. The result of the analysis is, therefore, that $a_{\text{N}1,4,5,8} = +0.337$ and $a_{\text{H}2,3,6,7} = -0.314$ mT. The signs are again those required by theory, and that of a_{N} arising from the positive ρ_{μ}^{π} at the N atoms is confirmed experimentally by the somewhat larger width of the lines at the high than at the low field (Chapt. 6.5).

The similar size of $|a_{\text{N}}|$ and $|a_{\text{H}}|$ is also responsible for the 13 observed groups of lines (including the two outermost single lines). This number is obtained with the formula $2 \cdot 4[1 + (1/2)] + 1$, where 4 is the number, n , of nuclei, common to both sets, and 1 and 1/2 are the respective I values of ^{14}N and ^1H . With poorer resolution, the two $|a_{\text{N}}|$ and $|a_{\text{H}}|$ values would appear equal, and the spectrum would consist of 13 broad hyperfine components spaced by ca. 0.33 mT. Such an apparent equality of the $|a_{\text{X}}|$ values of two coupling constants is often observed in ESR spectra. It is called *accidental degeneracy*, because it is removed by higher resolution. This notation distinguishes it from the *real* degeneracy that occurs for the same sort of nuclei X but is due to symmetry of the radical.

More frequent than an accidental equality of two $|a_{\text{X}}|$ values are relations in which one value is a multiple of another. These, also accidentally occurring relations, often give rise to an unusual distribution of intensities. An early and well-known example is the ESR spectrum of the radical anion of biphenyl (**94**) (Table 8.11) generated by reduction of the neutral compound with potassium in DME or THF [127, 159, 569]. The hyperfine pattern of **94**⁻ (Figure 6.6) consists of nine groups of lines spaced by 0.270 mT and having the relative intensities 1:4:8:12:14:12:8:4:1. Including the small 1:4:6:4:1-quintet splitting by 0.039 mT within each group, this pattern exhibits $9 \cdot 5 = 45$ instead of the $5^2 \cdot 3 = 75$ lines expected for two sets of four and one pair of equivalent α protons. While the small 0.039-mT splitting is due to one set of four, the two coupling constants of four and two protons with the larger absolute value must be derived from the spacing of the nine groups and their relative intensities. A correct analysis is based on the assumption that the two-proton $|a_{\text{H}}|$ value is twice as large (0.540 mT) as the four-proton value (0.270 mT), which appears as the spacing of the nine groups. The unusual intensity distribution of these groups is derived as follows:

	$ a_{\text{H}}(2\text{H}) $ $ \longleftarrow \quad \longrightarrow $								
splitting by 2H	1				2				1
multiplied by 6	6				12				6
	$ a_{\text{H}}(4\text{H}) $ $ \longleftarrow \quad \longrightarrow $								
splitting by 4H	1	4	6	4	1				
			2	8	12	8	2		
					1	4	6	4	1
summing up	1	4	8	12	14	12	8	4	1

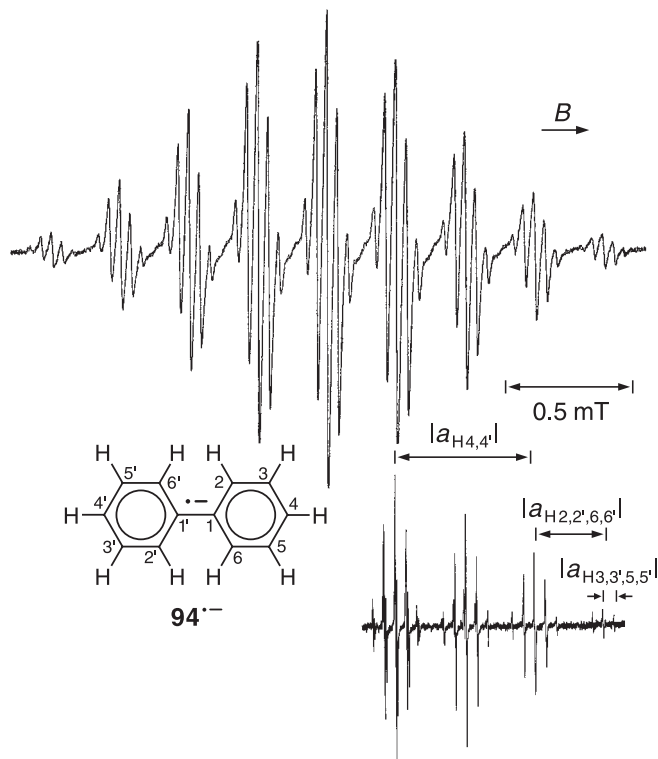


Fig. 6.6. ESR spectrum of the radical anion of biphenyl (**94**⁻). Solvent DME, counterion K⁺, temperature K. Below, the high-field half of the spectrum at higher resolution. Hyperfine data in the text and Table 8.11. Reproduced with permission from [569].

At higher resolution (Figure 6.6), all lines expected for **94**⁻ are resolved, and the above relation $|a_{\text{H}}(2\text{H})| = 2|a_{\text{H}}(4\text{H})|$ no longer holds exactly. The precise coupling constants are $a_{\text{H}4,4'} = -0.5387$, $a_{\text{H}2,2',6,6'} = -0.2675$ mT, and $a_{\text{H}3,3',5,5'} = +0.0394$ mT [569]. The assignment of the two four-proton coupling constants, which cannot be derived from the spectrum, is verified by deuterations [570, 571] and the signs of all values are based on theory and NMR studies (Chapt. 6.5 and Figure 6.6).

A careful reader might have noticed that, for the spectrum of the radical anion of cycl[3.2.2]azine (**89**) (Table 9.28) shown in Figure 5.1, the following relation holds: $|a_{\text{H}1,4}| = |a_{\text{H}6}| = 0.120$ mT = $2|a_{\text{N}}| = 2 \cdot 0.060$ mT. This accidental relation gives rise to an unusual 1:1:4:3:6:3:4:1:1 pattern marked by a brace at the low-field end of the spectrum and derived below.

As shown by the inset in Figure 5.1, higher resolution again removes the equality $|a_{\text{H}1,4}| = |a_{\text{H}6}|$, but it still fails to do so for the relation $|a_{\text{H}6}| = 2|a_{\text{N}}|$.

	$ a_{H_{1,4}} = a_{H_6} $				
	←→				
splitting by 2H + 1H = 3H	1	3	3	1	
	$ a_N $				
	←→				
splitting by 1N	1	1	1		
			3	3	3
				3	3
					3
					1
					1
					1
summing up	1	1	4	3	6
					3
					4
					1
					1

Complex Patterns

The simple hyperfine patterns of 4^{\cdot} and $57^{\cdot-}$ are reproduced in Figures 6.4 and 6.5 by means of *stick diagrams*. However, this procedure is too laborious and less informative for complex spectra consisting of many overlapping lines. The hyperfine patterns of such spectra are simulated by using generally available computer programs. In addition to the $|a_X|$ values of the coupling constants, the input must include the numbers, n , of equivalent nuclei X giving rise to these values, with the spin quantum numbers, I , of X, as well as the width (ΔB in mT) and shape of the hyperfine lines (Lorentzian, Gaussian, or a mixture of the two functions). Lorentzian line-shapes are generally used for fairly well resolved spectra, whereas Gaussian line-shapes are more appropriate for lines that are broadened by unresolved splittings. The most reliable $|a_X|$ values are obtained for radicals amenable to the ENDOR technique. Some programs can analyze the observed hyperfine pattern by starting with rough $|a_X|$ values and optimizing them by repeated simulations [572, 573]. These rough $|a_X|$ values can be derived from the ESR spectrum by inspection or must be taken from the data of structurally related radicals.

An example of a complex hyperfine pattern is the very well-resolved multiline ESR spectrum of the relatively persistent radical cation of adamantylideneadamantane (**25**) generated by electrolytic oxidation of the neutral compound in a 10:1:1 mixture of dichloromethane, TFA, and its anhydride [272]. This spectrum is shown in Figure 6.7, along with its computer simulation. The expected total number of lines is $9^2 \cdot 5^3 = 10\,125$, due to interaction with the two sets of eight and the three sets of four protons. Despite the high resolution, the hyperfine pattern could not be completely resolved in the range of 5.69 mT, representing the extent of the spectrum, due to the line density of nearly 18 per 0.01 mT, which is about the same as the line-width ΔB in a well-resolved spectrum. Because $25^{\cdot+}$ was generated electrolytically, the analysis was not amenable to the ENDOR technique. Nevertheless, the hyperfine pattern could be reproduced well by computer simulation with $|a_H(\beta)| = 0.058$, $|a_{H_{eq}}(\gamma)| = 0.327$, $|a_{H_{ax}}(\gamma)| = 0.047$, $|a_{H_{eq}}(\delta)| = 0.605$,

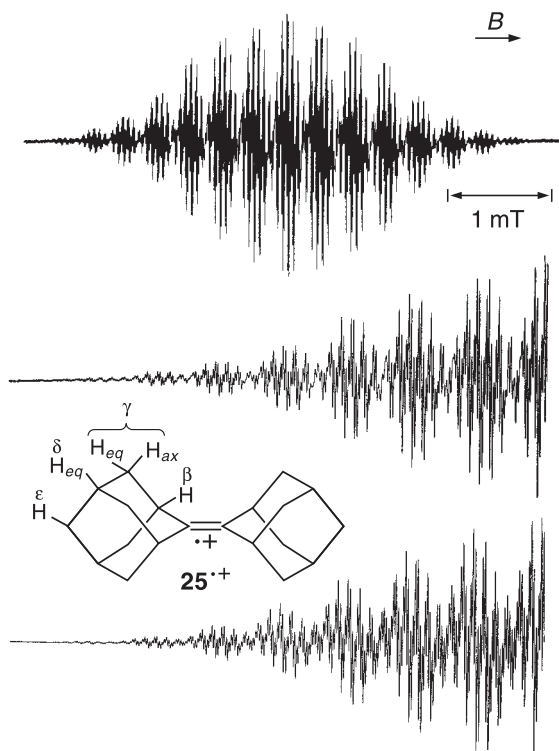


Fig. 6.7. ESR spectrum of the radical cation of adamantylideneadamantane (**25**) (top). Solvent $\text{CH}_2\text{Cl}_2/\text{TFA}/(\text{CF}_3\text{CO})_2$ mixture (10:1:1), counterion CF_3COO^- , temperature 193 K. Below, the low-field half of the spectrum on an expanded scale (middle) and its computer simulation (bottom) using the coupling constants indicated in the text and Table 7.15. Reproduced with permission from [272].

and $|a_{\text{H}}(\varepsilon)| = 0.012$ for sets of 4, 8, 8, 4, and 4 protons, respectively, and $\Delta B = 0.009$ mT (line-shape Lorentzian). Assignment of the coupling constants is based on deuteration and INDO calculations.

The ENDOR technique could be successfully applied to unravelling another multiline hyperfine pattern in the ESR spectrum shown in Figure 6.8 (top). This relatively poorly resolved spectrum arises from the kinetically and thermodynamically rather unstable radical anion of [2.2]metaparacyclophane (**95**), produced from the neutral compound with potassium in a 4:1 mixture of DME/THF at a very low temperature [155]. The $|a_{\text{H}}|$ values of the coupling constants for **95**⁻ are due to the seven pairs of protons, two single protons, and the ³⁹K nucleus of the counterion; and the expected number of hyperfine lines is as large as $3^7 \cdot 2^2 \cdot 4 = 34\,992$ per 1.68 mT or ca 208 per 0.01 mT. Computer simulation, also reproduced in Figure 6.8, made use of $|a_{\text{H}}|$ values derived from the corresponding ENDOR spectrum, 0.238, 0.182, 0.131, 0.106, 0.065, 0.065 (accidental degeneracy), and 0.007 mT for the seven pairs of protons, and 0.044 and 0.036 mT for the two single protons, along with $|a_{\text{K}}| = 0.062$ mT and $\Delta B = 0.020$ mT (line-shape Lorentzian).

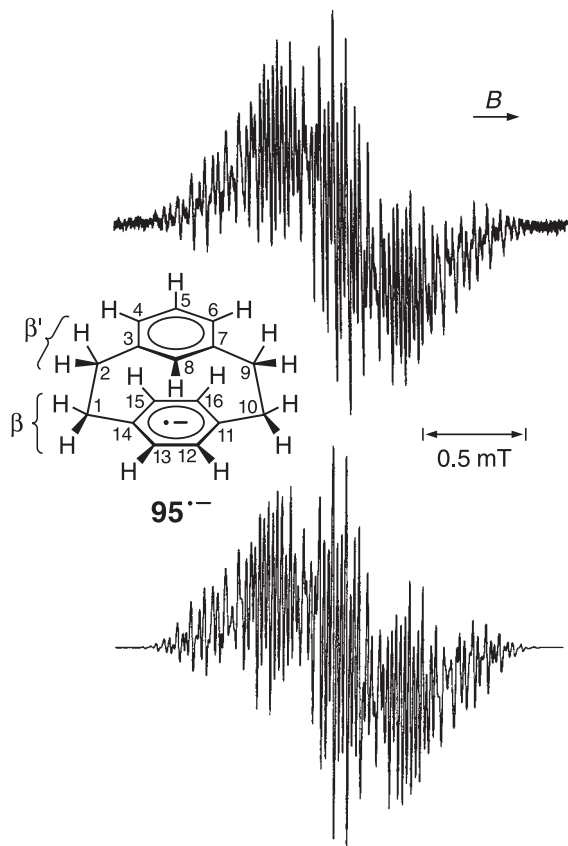
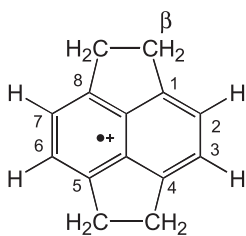
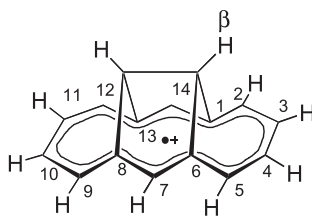


Fig. 6.8. ESR spectrum of the radical anion of [2.2]metapara-cyclophane (**95**). Solvent DMF/THF (4:1), counterion K^+ , temperature 168 K. Below: computer simulation using the coupling constants indicated in the text and Table 8.22. Reproduced with permission from [155].

Assignment of coupling constants to protons in specific positions was based on comparison of the 1H -ENDOR spectrum of $95^{\cdot-}$ with those of radical anions of three deuterio derivatives. The relative signs of these values were determined by the general-TRIPLE-resonance technique applied to the ENDOR signals. The ENDOR spectra of $95^{\cdot-}$ and the deuterated species, as well as the TRIPLE-resonance spectrum of this radical anion, are presented in Figures 6.16 and 6.17 of the next chapter. The complete results of the analysis are as follows (all values in mT): $a_{H12,13} = +0.106$ and $a_{H15,16} = +0.131$ for the two pairs of α protons in the *para*-bridged benzene ring; $a_{H4,6} = \pm 0.007$, $a_{H5} = -0.036$, and $a_{H8} = -0.044$ for the one pair and two single α protons the *meta*-bridged ring; $a_H(\beta) = +0.268$ and $+0.182$ for the two pairs of β protons in the methylene bridging groups adjacent to the the *para*-bridged ring (1,10); $a_H(\beta') = +0.065, -0.065$ for the remaining pairs of β -protons in such groups (2,9) close to the *meta*-bridged ring.

Second-order Splitting

As stated in Chapt. 3.2, second-order splitting occurs in well-resolved ESR spectra with large $|a_X|$ values. It was observed for simple alkyl radicals like ethyl (**59**[•]) [33], but it is rather rarely found for hydrocarbon π radicals with an unpaired electron delocalized over many centers. Because the $|a_H|$ values of the α protons in such radicals are usually less than 1 mT, a greater chance of observing a second-order splitting exists for the large and, generally, positive coupling constants of β protons, particularly in the spectra of radical cations. The first example of this kind was provided by the radical cation of pyracene (**96**) (Table 8.9) obtained by dissolving the neutral hydrocarbon in conc. sulfuric acid [574]. The spectrum of **96**^{•+} exhibits nine groups of lines having the intensity ratio 1:8:26:52:70:52:26:8:1 and spaced by the coupling constant, +1.280 mT, of the eight methylene β protons. The 1:4:6:4:1-quintet within each group stems from the four α protons with $a_{H2,3,6,7} = -0.200$ mT. Higher resolution reveals additional weak lines, in accord with the pattern predicted by Eq. 3.18 for a second-order splitting from eight protons with an $|a_H|$ value of 1.280 mT.

**96**^{•+}**97**^{•+}

H atoms at $\mu = 12$ and 14 are omitted for clarity

A larger $|a_H|$ value is required for observation of second-order splitting from only two equivalent protons. Such a splitting was found for the radical cation of 1,6:8,13-ethanediylidene[14]annulene (**97**) generated by oxidation of the neutral compound with aluminum trichloride in dichloromethane [233]. The prominent features of the spectrum of **97**^{•+} (Figure 6.9, top) are the three groups of lines spaced by the unusually large coupling constant, $a_H(\beta) = +2.815$ mT, of the two equivalent methine β protons in the ethanediylidene bridge. The apparent intensity ratio of these groups, as derived from the line-heights is only 1:1.4:1 instead of the expected 1:2:1. This is because the lines of the central groups are broader than those of the lateral groups, due to an unresolved second-order splitting, $a_H^2/B = (2.815 \text{ mT})^2/320 \text{ mT} = 0.025 \text{ mT}$, from the pertinent large coupling constant (Figure 3.4). The splitting in question becomes evident at higher resolution (Figure 6.9, bottom), together with the smallest value of two α protons, $a_{H2,5,9,12} =$

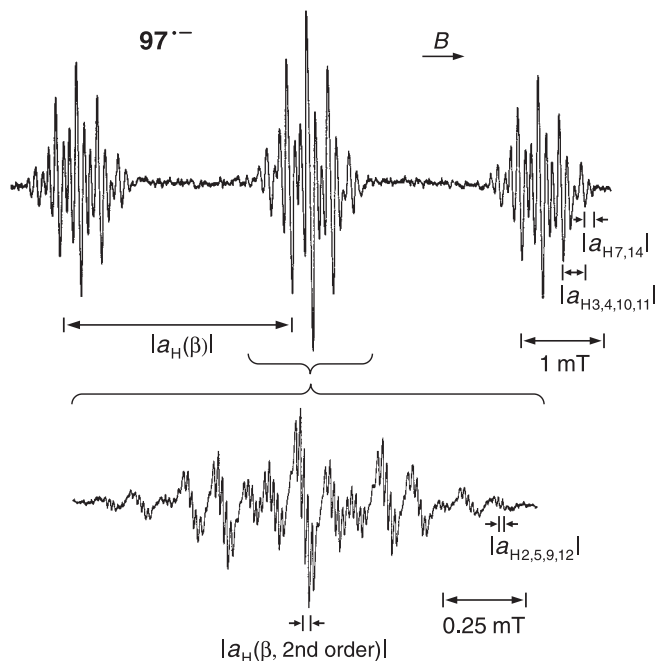


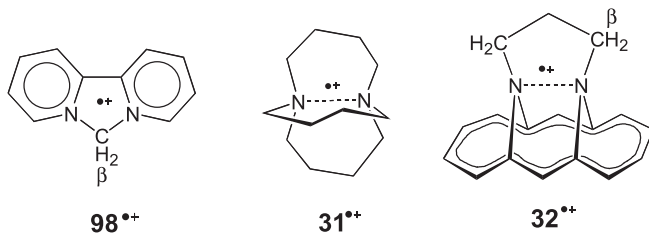
Fig. 6.9. ESR spectrum of the radical cation of 1,6:8,13-ethanediylidene[14]annulene (**97**) (structural formula on the preceding page). Solvent dichloromethane, counterion presumably ACL_4^- , temperature 213 K.

Below: central group of lines on an expanded scale and at higher resolution. Hyperfine data in the text and Table 8.20. Reproduced with permission from [233].

$+0.014 \approx (1/2)0.025$ mT. Other coupling constants of pairs of α protons, including signs as required by theory, are $a_{\text{H}3,4,10,11} = -0.248$ and $a_{\text{H}7,14} = +0.092$ mT. It is noteworthy that the large value, $a_{\text{H}}(\beta) = +2.815$ mT, is due to the “Whiffen effect” (Eq. 3.24), because each of the β -proton-bearing C atoms is linked to two bridged centers μ' and μ'' with a high population $\rho_{\mu'}^\pi = \rho_{\mu''}^\pi$ and with LCAO coefficients $c_{3,\mu'} = c_{3,\mu''}$ for the SOMO ψ_3^- (Chapt. 8.6 and Figure 8.12) having the same sign ($\mu', \mu'' = 1, 6$ and $8, 13$).

The ENDOR technique can also be useful for observation of second-order splitting (Chapt. 5.2). Only a few reports on such splitting in ENDOR spectra are found in the literature. One deals with the two equivalent ^{14}N or ^{15}N nuclei in the radical cation of 1,6-diazabicyclo[4.4.4]tetradecane (**31**) (Table 7.18) dissolved as a salt in a toluene/TFA mixture [300]. Two papers report on second-order splitting found in the ENDOR spectra for methylene β protons in groups linked to N atoms bearing π -spin populations. These splittings were observed for the two β protons in the radical cation of 6-hydrodipyrido[1,2-*c*:2',1'-*e*]imidazole (**98**) (dication known as monomethylene diquat), obtained with zinc from the 6-iodide derivative in TFA (Table 9.30) [575], and for one pair of “quasi-axial” β protons in the radical cation

of *N,N'*-trimethylene-*syn*-1,6;8,13-diimino[14]annulene (**32**) (Table 9.40) [244], generated by oxidation of the neutral compound with AlCl_3 in dichloromethane.



Satellite Lines

The hyperfine patterns considered so far are due to interaction with abundant magnetic nuclei like protons and ^{14}N . Other such nuclei often found in organic radicals are ^{19}F and ^{31}P . Careful examination of many spectra with a high signal-to-noise ratio reveals that these spectra exhibit very weak superposed patterns. Such secondary patterns stem from a small number of radicals, in which rare magnetic isotopes in natural abundance replace the abundant nonmagnetic nuclei of the same element, giving rise to additional hyperfine splitting. The most common among these organic radicals are those in which one nonmagnetic ^{12}C nucleus is substituted by a ^{13}C isotope ($I = 1/2$), thus doubling of the number of hyperfine lines. On superposing the secondary pattern of such radicals on the main hyperfine pattern due to radicals with only ^{12}C nuclei, each line of the main pattern becomes symmetrically flanked by two very weak lines separated from it by half the $|a_{\text{C}}|$ value of the ^{13}C -coupling constant. The two lines, spaced by this $|a_{\text{C}}|$ value are therefore called ^{13}C *satellites*.

When an element has several isotopes X_1, X_2, X_3, \dots with natural abundances x_1, x_2, x_3, \dots , their distribution is given by $(x_1 + x_2 + x_3 + \dots)^n$, where n is the number of equivalent atoms of this element in the radical. For two isotopes, x_1 and x_2 , the distribution is binomial:

$$(x_1 + x_2)^n = x_1^n + nx_1^{n-1}x_2 + [n(n-1)/2]x_1^{n-2}x_2^2 + \dots \quad (6.1)$$

$x_1 = 0.989$ for ^{12}C and $x_2 = 0.011$ for ^{13}C , so that Eq. 6.1 becomes

$$(0.989 + 0.011)^n = 0.989^n + n0.989^{n-1}0.011 + [n(n-1)/2]0.989^{n-2}0.011^2 + \dots$$

Because the radical anion of benzene (**62**) has six equivalent C atoms, the distribution of the two isotopes is

$$\begin{aligned} (0.989 + 0.011)^6 &= 0.989^6 + 6 \cdot 0.989^5 \cdot 0.011 + 15 \cdot 0.989^4 \cdot 0.011^2 + \dots \\ &= 0.936 + 0.062 + 0.0017 + \dots \end{aligned}$$

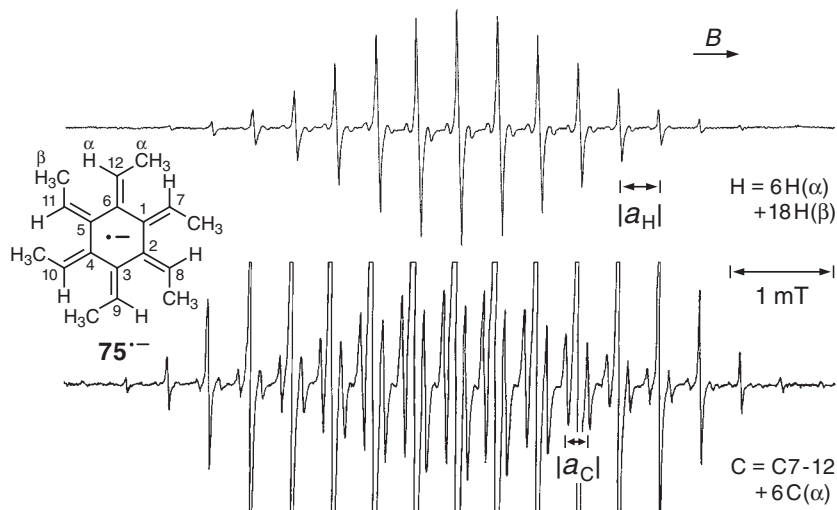


Fig. 6.10. ESR spectrum of the radical anion of 7,8,9,10,11,12-hexamethyl[6]radialene (**75**). Solvent DME, counterion K^+ , temperature 213 K. Below: amplified spectrum showing

^{13}C satellites in natural abundance. Hyperfine data in the text and Table 8.24. Reproduced with permission from [465].

This means that the probability of having only ^{12}C nuclei in all six C atoms of $62^{\cdot-}$ is ca 94% and that of finding a ^{13}C isotope in one atom is ca 6%, because this isotope can occur in any of the six equivalent positions. The probability of $62^{\cdot-}$ containing more than one ^{13}C isotope decreases rapidly with their increasing number. Thus, the probability of two ^{13}C isotopes is less than 0.2%, although there are 15 alternatives for replacing two ^{12}C nuclei in the six-membered ring. The ^{13}C -coupling constant for $62^{\cdot-}$ is +0.28 mT [132], with the positive sign required by theory (Chapt. 4.2). In Figure 6.3, the ^{13}C satellites flanking the three central lines of $62^{\cdot-}$ are marked by asterisks. They can be made more evident by higher modulation. The relative intensity of the satellites relative to that of the pertinent main line is only 3%, because the total of 6%, expected for one ^{13}C isotope per one radical anion, is shared by two satellites.

An example of readily observable ^{13}C satellites is the radical anion of 7,8,9,10,11,12-hexamethyl[6]radialene (**75**) produced by reduction of the neutral compound with potassium in DME [465]. In the spectrum of $75^{\cdot-}$ shown in Figure 6.10, the main hyperfine pattern consists of 25 equidistant lines with a binomial intensity distribution; it arises from the six α protons at the exocyclic π centers 7–12 and the 18 β protons in the six methyl substituents, having a common $|a_H| = 0.382$ mT (accidental degeneracy). With a fairly concentrated solution, 19 of the 25 lines can be identified. Even when the nine strongest central lines are off-scale, the six outermost lines are much too weak to be detected. Each line of the main hyperfine pattern is flanked by two ^{13}C satellites with relative intensity of ca 12%, or 6% per satellite. Hence these satellites stem from ^{13}C nuclei in two sets each of six equivalent C atoms with the same $|a_C|$ value of 0.200 mT. These two

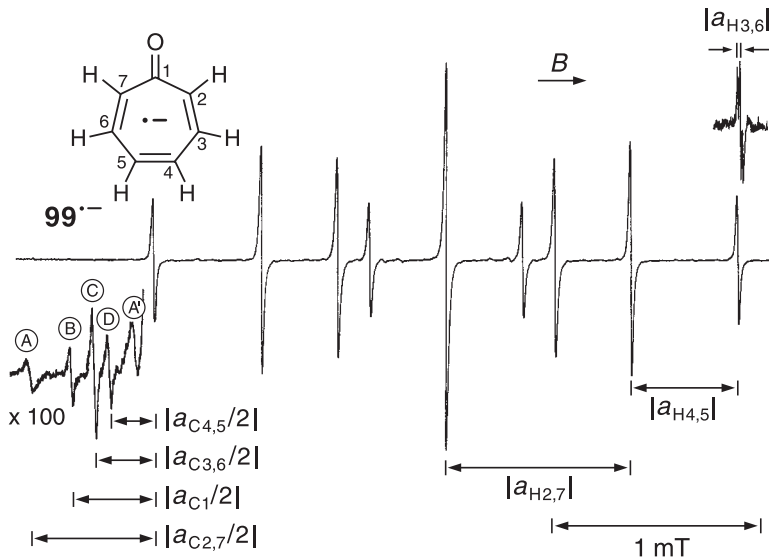


Fig. 6.11. ESR spectrum of the radical anion of tropone (**99**). Solvent DME, counterion Na^+ , temperature 203 K. Above right: the outermost satellites in natural abundance. Hyperfine data in the text and Table 9.14. Reproduced with permission from [214].

sets are tentatively identified with the C atoms in the six π centers 7–12 of the ring and those in the six methyl groups, (another case of accidental degeneracy), whereas the $|a_{\text{C}}|$ value of the ^{13}C nuclei in the six exocyclic π centers 1–6, which is predicted to be larger, is concealed by the main ^1H -hyperfine pattern.

For persistent radicals of lower symmetry with relatively intense outermost lines, the satellites are most conveniently observed at the periphery of the spectrum. An example is the radical anion of tropone (**99**) (Table 9.14), generated by electrolytic reduction of the neutral compound in DMF with tetraethylammonium perchlorate as the supporting salt [214]. The ESR spectrum of **99** $^{\cdot-}$ is presented in Figure 6.11. Its main hyperfine pattern should consist of $3^3 = 27$ lines from three pairs of α protons, but the very small splitting of 0.01 mT from one pair appears only at higher resolution (top, right), so that only $3^2 = 9$ lines from two pairs are usually observed. The pertinent coupling constants are $a_{\text{H}_{2,7}} = -0.875$, $a_{\text{H}_{4,5}} = -0.510$, and $a_{\text{H}_{3,6}} = +0.010$ mT. Their assignment and signs are readily derived from simple theoretical calculations, such as the McLachlan procedure. Each of these nine lines is flanked by several ^{13}C satellites which are made evident by amplification at the low-field end of the spectrum (bottom, left). Because these satellites, marked **A**, **B**, **C**, and **D**, have different line-widths, their intensities relative to that of the outermost line of the main hyperfine pattern have to be determined by integration. The integrated intensities are ca 1% for **A**, **C**, and **D**, corresponding to those expected for radical anions with the ^{13}C isotope in two equivalent sites. The coupling constants a_{C_i} associated with these satellites can be assigned by

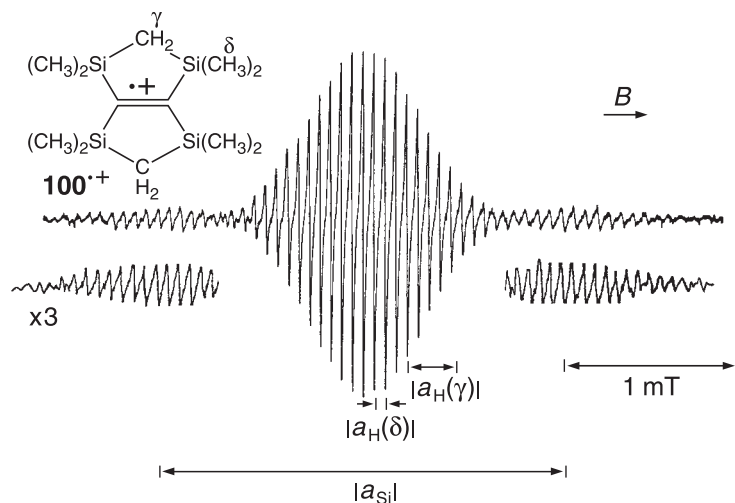


Fig. 6.12. ESR spectrum of the radical cation of 2,2,4,4,6,6,8,8-octamethyl-2,4,6,8-tetrasilabicyclo[3.3.0]oct-1(5)-ene (**100**). Solvent dichloromethane, counterion presumably

AlCl_4^- , temperature 180 K. Below: amplified ^{29}Si satellite groups. Hyperfine data in the text and Table 9.38. Reproduced with permission from [576].

considering the line-widths that correlate with the $a_{\text{H}_\mu}^2$ values: the larger the $|a_{\text{H}_\mu}|$ value, the broader the satellite line. (The principle underlying this correlation is considered in Chapt. 6.4.) Thus **(A)**, **(C)**, and **(D)** are associated with $|a_{\text{H}_{2,7}}|$, $|a_{\text{H}_{4,5}}|$, and $|a_{\text{H}_{3,6}}|$, respectively, and the ^{13}C -coupling constants are, in this sequence, $a_{\text{C}_{2,7}} = +1.233$, $a_{\text{C}_{4,5}} = +0.454$, and $a_{\text{C}_{3,6}} = -0.602$ mT. Their signs (positive for **(A)** and **(C)** and negative for **(D)**) are required by the relations between the coupling constants a_{C_μ} and spin populations ρ_μ^π , as formulated in Eqs. 4.16–4.18. The a_{C_μ} values thus obtained agree with the observed coupling constants. This statement also holds for the coupling constant $a_{\text{C}_1} = -0.832$ associated with the satellite **(B)**; its relative intensity of 0.5% qualifies it as stemming from the ^{13}C isotope in the single site 1. The satellite denoted **(A)** in Figure 6.11 represents the next line in the same hyperfine pattern as **(A)**.

Besides ^{13}C , three magnetic isotopes of low natural abundance are important for organic radicals. These isotopes are ^{17}O , ^{29}Si , and ^{33}S , which occur along with their abundant nonmagnetic counterparts, ^{16}O , ^{28}Si , and ^{32}S . The most readily detected are ^{29}Si satellites, because the natural abundance of the ^{29}Si isotope is 0.047 and its spin quantum number I is 1/2. Figure 6.12 shows the ESR spectrum of the radical cation of 2,2,4,4,6,6,8,8-octamethyl-2,4,6,8-tetrasilabicyclo[3.3.0]oct-1(5)-ene (**100**) (Table 9.38) generated from the neutral compound with aluminum trichloride in dichloromethane [576, 577]. The main hyperfine pattern of **100** $^{+}$ is due to the sets of 4 methylene and 24 methyl protons with $|a_{\text{H}(\delta)}| = 0.062$ and $|a_{\text{H}(\gamma)}| = 4 \cdot 0.062 = 0.248$ mT, respectively (accidental relation). Superimposed on this pattern, and arising from radical cations with only ^{28}Si nuclei, is a secondary pattern stemming from radical cations having a ^{29}Si isotope in one Si

atom of the four equivalent dimethylsilyl groups. The distribution ratio of ^{29}Si to ^{28}Si is, according to Eq. 6.1, 0.953^4 to $4 \cdot 0.953^3 \cdot 0.047$, or 0.825 to 0.163. This means that each of the two groups of lines flanking the main pattern should have a relative intensity of $(1/2)0.163/0.825 = 0.10$, or 10%. However, the observed ratio of line-heights is lower, because the line-width of the satellites is larger, due to incomplete averaging out of the ^{29}Si hyperfine anisotropy. The value $|a_{\text{Si}}|$ of the ^{29}Si -coupling constant is 2.271 mT. Keeping in mind that the g_n factor of this Si isotope is negative, this large a_{Si} value should also have a negative sign.

The appearance of satellite lines is less favorable for ^{33}S than for ^{29}Si , because the natural abundance of ^{33}S , 0.0074, is less, and its spin quantum number, $I = 3/2$, is larger. Nevertheless, ^{33}S satellites are readily observed, especially for the highly persistent radical cations of "S-donors" having large π -spin populations at the S atoms. The radical cation of 1,4,5,8-tetrahydro-1,4,5,8-tetrathiafulvalene (TTF; **24**), produced with aluminum trichloride in dichloromethane [230], provides an appropriate example (Figure 6.13). The spectrum of **24** $^{+\cdot}$ exhibits a simple 1:4:6:4:1-pattern from the four equivalent protons with the value $|a_{\text{H}_{2,3,6,7}}| = 0.125$ mT of their coupling constant. On amplification, two satellite groups are observed, which represent the two outer components of the 1:1:1:1-quartet due to radical cations with a ^{33}S isotope in one of the four equivalent S atoms. The two inner components remain concealed by the main hyperfine pattern. The distribution ratio of radical cations with only ^{32}S nuclei to those with one ^{33}S isotope is 0.9926^4 to $4 \cdot 0.9926^3 \cdot 0.0074$ or 0.971 to 0.029, leading to a relative intensity of $(1/4)0.029/0.971 = 0.0075$ or 0.75% for each of the four ^{33}S -component groups. Again, due to incomplete averaging out of the ^{33}S -hyperfine anisotropy, the lines of these components generally are broader than those of the main hyperfine pattern. Moreover, the ^{33}S -satellite lines on the high-field side are distinctly broader than their low-field counterparts. Because the local spin population ρ_u^π at the S atoms is positive, this finding indicates a positive sign for the ^{33}S -coupling constant $a_{\text{S}} = +0.425$ mT (Chapt. 6.5), while a_{H} is predicted to be negative.

The natural abundance of the ^{17}O isotope is only 0.00037, and its spin quantum number I is as large as $5/2$. Therefore, to observe ^{17}O satellites, enrichment in this isotope is required. A notable exception is the radical anion of dithieno[3,4-*b*; 3',4'-*e*]paradithiin-1,3,5,7-tetraone (**81**) produced by reduction of the neutral compound with potassium in DME [172]. This radical anion, which was mentioned in Chapt. 4.2, has no H atoms, but contains other atoms in equivalent sites, namely, two sets of four C, two pairs of S, and one set of four O. In the absence of protons, the main hyperfine pattern of **81** $^{\cdot-}$ consists of a single line. Owing to this feature, a large number of satellites due to rare magnetic isotopes in natural abundance can be detected. Not only satellites arising from one ^{13}C or ^{33}S isotope per radical anion were observed, but also those stemming from two such isotopes, that is, from two ^{13}C in the same set or each in a different set, as well as satellites arising simultaneously from one ^{13}C and one ^{33}S . For the spectrum of **81** $^{\cdot-}$ in Figure 6.14, amplification of the signals is progressively enhanced on going from the top to the bottom. The ^{13}C and even ^{33}S satellites can be observed at moderate amplification.

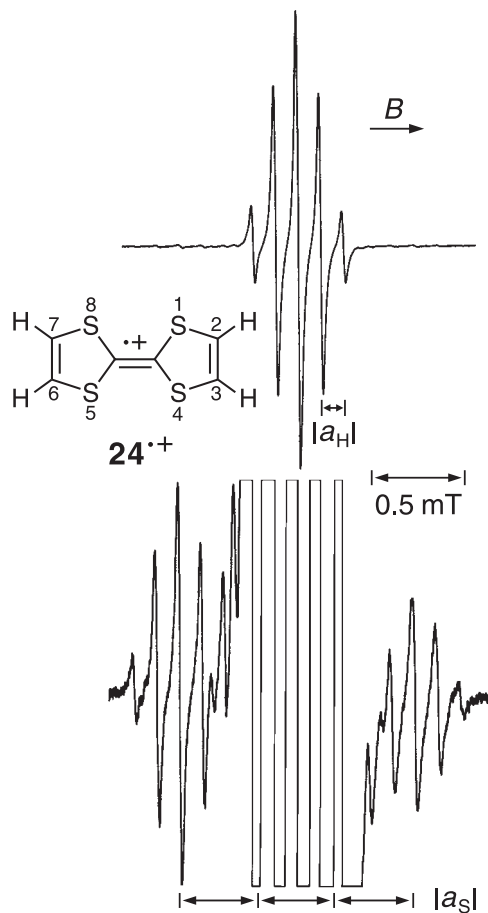


Fig. 6.13. ESR spectrum of the radical cation of 1,4,5,8-tetrahydro-1,4,5,8-tetrathiafulvalene (**24**). Solvent dichloromethane, counterion presumably AlCl_4^- , temperature 233 K. Below:

amplified spectrum showing ^{33}S satellites in natural abundance. Hyperfine data in the text and Table 9.31. Reproduced with permission from [230].

For the satellites associated with the larger $|a_{C_\mu}|$ value, the lines on the high-field side are broader than those at low field, but for satellites associated with the smaller $|a_{C_\mu}|$ value, the high-field lines are narrower than their low-field counterparts. Broader line-widths in the high- than in the low-field half are exhibited by ^{33}S satellites associated with both coupling constants a_{S_μ} . The distribution ratio for the ^{16}O and ^{17}O isotopes (the share of ^{18}O can be ignored) is 0.99963^4 to $4 \cdot 0.99963^3 \cdot 0.00037$, or 0.9985 to 0.0015, yielding a relative intensity for one ^{17}O satellite of $(1/6)0.0015/0.9985 = 0.00025$, or only 0.025%. Accordingly, the highest amplification and overmodulation were necessary to reveal satellite lines due to ^{17}O isotopes in natural abundance. Of the 1:1:1:1:1:1-sextet, the four outermost components were observed, but the two inner ones were hidden by the strong

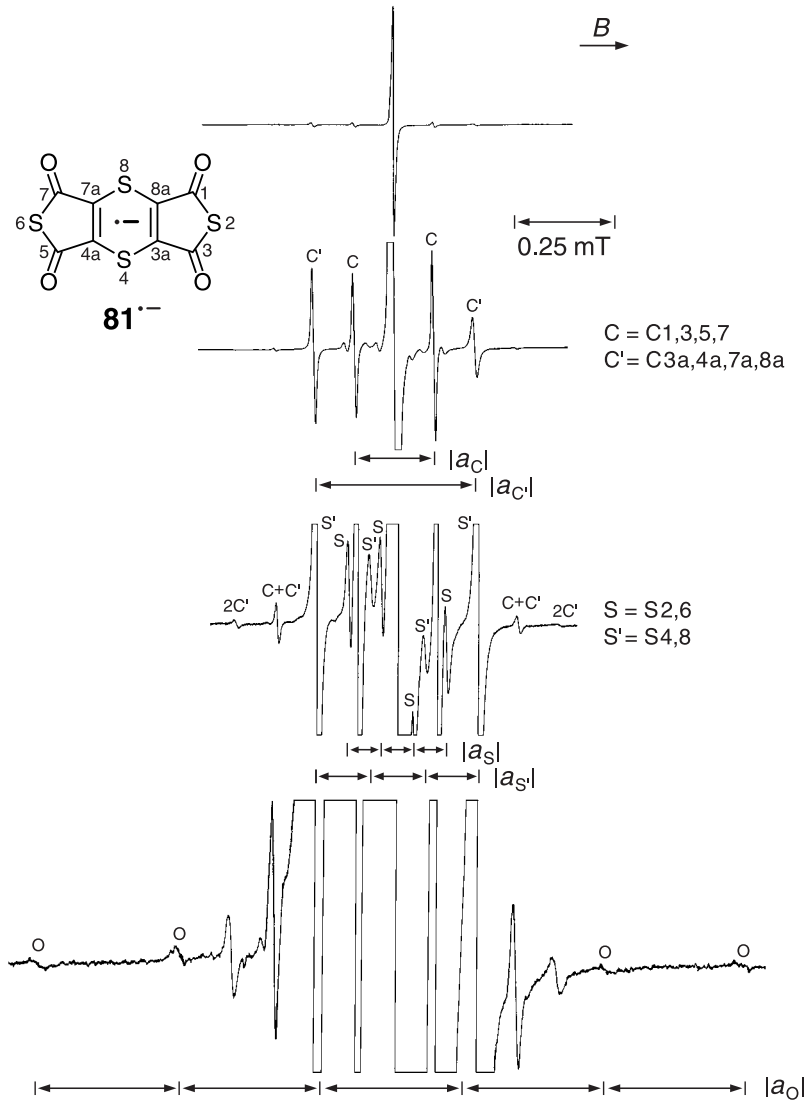


Fig. 6.14. ESR spectrum of the radical anion of dithieno[3,4-*b*;3'-4'-*e*]paradithiin-1,3,5,7-tetra-one (**81**). Solvent DME, counterion K^+ , temperature 183 K. Amplification and modulation amplitude increase on going from top to bottom, revealing successive ^{13}C , ^{33}S , and ^{17}O satellites in natural abundance. The letters above the satellite lines indicate the isotope and its occurrence in the equivalent positions of the radical anion; C = one ^{13}C in 1, 3, 5, 7; C' = one ^{13}C in 3a, 4a, 7a, 8a; S = one ^{33}S in 4,8; O = one ^{17}O ; 2C' two ^{13}C in 3a, 4a, 7a, 8a; C + C' = one ^{13}C in 1, 3, 5, 7 and one in 3a, 4a, 7a, 8a. Hyperfine data in the text. Reproduced with permission from [172].

main signal and its ^{13}C and ^{33}S satellites. The ^{17}O satellites at the high field are broader than their counterparts at the low field. A MO model predicts positive spin populations ρ_{μ}^{π} at all π centers μ of $81^{\cdot-}$, except at the S atoms that are located in the vertical nodal planes of the SOMO and bear negative ρ_{μ}^{π} values. Signs can now be allotted to the ^{13}C -, ^{33}S - and ^{17}O -coupling constants by considering the line-widths of the satellites, as well as the positive spin population ρ_{μ}^{π} values at the C and O atoms and the negative ρ_{μ}^{π} values at the S atoms (Chapt. 6.5). Because of the positive g_n factors of the ^{13}C and ^{33}S isotopes, the larger coupling constant $a_{C_{\mu}}$, assigned to ^{13}C nuclei in the centers $\mu = 3a, 4a, 7a, 8a$, is positive, the smaller $a_{C_{\mu}}$ value for the ^{13}C isotopes in the centers $\mu = 1, 3, 5, 7$ is negative; both $a_{S_{\mu}}$ values are negative. In view of the positive spin population ρ_{μ}^{π} at the O atoms and the negative g_n factor of the ^{17}O isotope, the coupling constants a_{O} must be negative. The complete result of the analysis for $81^{\cdot-}$, including assignment and sign of the coupling constants, is $a_{C1,3,5,7} = -0.202$, $a_{C3a,4a,7a,8a} = +0.410$, $a_{S2,6} = -0.083$, $a_{S4,8} = -0.138$, and $a_{O1,3,5,7} = -0.361$ mT.

^{13}C - and ^{29}Si -ENDOR spectra from these isotopes in natural abundance were also reported for several π radicals [16, 578–581].

6.5

Assignment and Sign of Coupling Constants

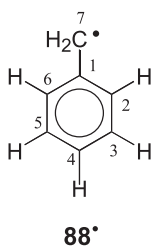
Analysis of an ESR spectrum is successful if its hyperfine pattern can be reproduced in terms of k sets, each consisting of n_k equivalent nuclei X_k with a spin quantum number I_k and a $|a_{X_k}|$ value of their coupling constant. Assignment of these values to nuclei X_k in specific positions of the radical is problematic if more than one set has the same number, n_k , of equivalent nuclei with the the same I_k , because such sets give rise to identical splitting patterns. In addition to an unequivocal assignment of the absolute values $|a_{X_k}|$, full information on the structure of a radical requires knowledge of the signs of its coupling constants, which, as stated several times in this book, is not directly available from an ESR spectrum.

Several methods, theoretical, experimental, or combinations of both, make it possible to assign the coupling constants and to determine their sign. These methods are considered below.

Theoretical Calculations

We pointed out in Chapt. 4.5 that the spin distribution in a radical and, accordingly, the coupling constants of its magnetic nuclei X , can be calculated by appropriate empirical, semiempirical, and nonempirical quantum-chemical procedures. Calculations that account for spin polarization yield both the assignment and the sign of coupling constants by their correlation with the observed $|a_X|$ values. In general, the higher the level of the theoretical procedure, the more reliable is the result of such correlation. If the calculated values completely fail to correlate with the experimental data, one must suspect that the structure of the radical charac-

terized by its ESR spectrum is different from that predicted theoretically. Such a discrepancy can arise if the radical generated under the given conditions is not the anticipated one or if the shape of the SOMO as indicated by calculations does not correspond to that actually occupied by the unpaired electron in the radical. In the latter case, experimental data may not correlate with the calculated values for a radical that has two close-lying orbitals as candidates for the SOMO, and in which some effect relevant to their energetic sequence is not accounted for by the calculations; such a situation was reported for the radical cation of binaphthylene (Table 8.10) [582]. Merits and shortcomings of theoretical calculations as a method of assigning the observed $|a_X|$ values of coupling constants to nuclei X in specific positions are demonstrated here, using the benzyl radical (**88'**) (Table 8.1) as an example.



For a simple π radical like **88'** with seven centers μ , an empirical quantum-chemical procedure should be appropriate for predicting the spin populations ρ_μ^π . Because this π system is odd and alternant, its SOMO in the Hückel model is a nonbonding π -orbital ψ_4 for which the squared LCAO coefficients $c_{4,\mu}$ at the centers $\mu = 1-7$ are readily derived as $c_{4,1}^2 = c_{4,3}^2 = c_{4,5}^2 = 0$, $c_{4,2}^2 = c_{4,4}^2 = c_{4,6}^2 = 1/7$, and $c_{4,7}^2 = 4/7$ (Chapt. 8.1). Applying the McLachlan procedure with the parameter $\lambda = 1$ (Eq. 4.34) transforms these values into $\rho_1^\pi = -0.102$, $\rho_2^\pi = \rho_6^\pi = +0.161$, $\rho_4^\pi = +0.136$, $\rho_3^\pi = \rho_5^\pi = -0.062$, and $\rho_7^\pi = +0.769$. By using the proportionality factor $Q_{\text{H}}^{C,\text{H}\mu} = -2.8$ mT in the McConnell equation (Eq. 4.5), the spin populations ρ_μ^π at the proton-bearing centers $\mu = 2-7$ are converted into the coupling constants of the α protons, $a_{\text{H}2,6} = -0.451$ and $a_{\text{H}3,5} = +0.174$ mT for the pairs of protons in the two *ortho* and *meta* positions, respectively, $a_{\text{H}4} = -0.381$ mT for the single proton in the *para* position, and $a_{\text{H}7}(2\text{H}) = -2.153$ mT for the two protons in the exocyclic methylene group. Experimentally, $|a_{\text{H}\mu}|$ values of 1.630, 0.515, and 0.179 mT were observed for the three proton pairs and 0.618 mT for the single proton [42] (Chapt. 4.3). Although the agreement between theory and experiment is only modest, the predicted sequence of the two-proton values, $|a_{\text{H}7}(2\text{H})| \gg |a_{\text{H}2,6}| \gg |a_{\text{H}3,5}|$, clearly corresponds to that found by ESR spectroscopy ($1.630 \gg 0.515 \gg 0.179$ mT). Such correspondence enables one not only to assign these three observed values to specific positions but also to allot signs to them, as well as to the single-proton value $|a_{\text{H}4}| = 0.618$ mT. The result of the complete analysis for **88'** is thus $a_{\text{H}2,6} = -0.515$, $a_{\text{H}3,5} = +0.179$, $a_{\text{H}4} = -0.618$, and $a_{\text{H}7}(2\text{H}) = -1.630$ mT. A serious shortcoming of the Hückel-McLachlan procedure is the prediction that

$|a_{\text{H}_{2,6}}|$ is distinctly larger than $|a_{\text{H}_4}|$, in contrast with the experimental finding. This defect cannot be corrected by reasonably modifying the empirical procedure nor by applying a semiempirical treatment like INDO [583]. The take-home lesson is that simple theoretical calculations function properly as a method for assigning coupling constants if the $|a_{\text{X}}|$ values differ greatly in size, but they are less satisfactory if these values are similar. In the particular case of **88'**, where the two pertinent values $|a_{\text{H}_{2,6}}|$ and $|a_{\text{H}_4}|$ arise from different numbers of nuclei, a wrong assignment is excluded, but generally caution is needed for $|a_{\text{X}}|$ values of comparable size. Also unreliable are theoretical calculations for assignment of small $|a_{\text{X}}|$ values if a radical has several such coupling constants, and they are not trustworthy for allotting signs to them.

Isotopic Replacement

The most reliable method of assigning the observed coupling constants to specific nuclei X in the radical is to replace one or several of these nuclei by their less-abundant isotopes X' in specific positions. As pointed out in Chapt. 3.2, such a replacement strongly changes the hyperfine pattern, because X' differs from X in its g_{n} factor and, usually, also in its spin-quantum number I . The usual assumption that the electronic structure of the radical is not markedly affected by this replacement is generally valid, except for radicals having a degenerate ground-state, like the benzene radical anion **62**⁻, of which the structure can be affected by the slightest perturbation (Chapts. 8.1 and 8.6). In organic radicals, the most frequent replacement of a nucleus X by its isotope X' is that of a proton (¹H = H) by deuterium (²H = D). One of the earliest π -radical ions to be studied by ESR spectroscopy was the anion of naphthalene (**83**) (Table 8.8), which has two sets of four equivalent α protons [520]. Assignment of the observed larger $|a_{\text{H}_\mu}|$ value of 0.495 mT to the protons at the centers $\mu = 1, 4, 5, 8$ and the smaller value of 0.183 mT to those at $\mu = 2, 3, 6, 7$ [135] is not to be doubted, because even the Hückel model exactly reproduces their ratio of 2.7. This assignment is corroborated by replacing the four protons in the 1,4,5,8-positions by deuterons, whereby $|a_{\text{H}_{1,4,5,8}}| = 0.495$ mT for **83**⁻ changes to $|a_{\text{D}_{1,4,5,8}}| = |a_{\text{H}_{1,4,5,8}}|g_{\text{n}}(\text{D})/g_{\text{n}}(\text{H}) = 0.495 \text{ mT} \cdot 0.1535 = 0.076 \text{ mT}$ for **83-d₄**⁻. It is evident from the ESR spectra of **83**⁻ and **83-d₄**⁻ [149] (Figure 6.15), that this isotopic replacement makes the hyperfine pattern less simple, because the number of lines *increases* from $5^2 = 25$ to $9 \cdot 5 = 45$, and the extent of the spectrum *decreases* from $(4 \cdot 0.495 + 4 \cdot 0.183) \text{ mT} = 2.71 \text{ mT}$ to $(8 \cdot 0.076 + 4 \cdot 0.183) \text{ mT} = 1.34 \text{ mT}$. (Of course, both coupling constants a_{H_μ} and a_{D_μ} are negative.)

Complication of the spectrum as a consequence of deuteration is not encountered with the ENDOR technique. On the contrary, replacement of equivalent protons by deuterons leads to removal of the pertinent signals from the ¹H-ENDOR spectrum, because those due to the ²H isotopes appear in a different frequency range. The power of the ENDOR technique in this respect is demonstrated with the radical anion of [2.2]metaparacyclophane (**95**) (Chapt. 6.3). Its complex hyper-

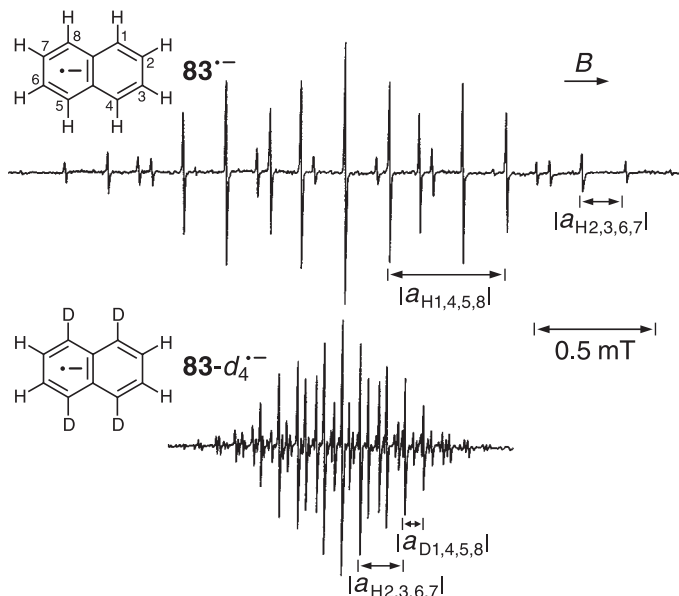


Fig. 6.15. ESR spectra of the radical anions of naphthalene (**83**) and 1,4,5,8-tetradeuterionaphthalene (**83-d₄**). Solvent DME, counterion Na⁺, temperature 203 K. Hyperfine data in the text and Table 8.8. Reproduced with permission from [149].

fine pattern was computer-simulated with the use of $|a_{\text{H}}|$ values derived from its ¹H-ENDOR spectrum, and their assignment was made with the aid of specific deuterations [155]. The three deuterio derivatives were isotopically labelled in the 8-position of the *meta*-bridged ring (**95-d**), or in the *para*-bridged ring and the two adjacent methylene groups (**95-d₈**), or in the both ethylene bridges (**95-d'₈**). Even if the ESR hyperfine patterns of **95-d^{•-}**, **95-d₈^{•-}**, and **95-d'₈^{•-}** were more complex than that of **95^{•-}** and less resolved, examination of their ¹H-ENDOR spectra allowed straightforward analysis. These ENDOR spectra are displayed in Figure 6.16 below that of **95^{•-}**. Although the intensity of an ENDOR signal is not a reliable measure of the number of nuclei giving rise to it, most signals of **95^{•-}** do reflect such a relation. Thus, the signals **Ⓐ**, **Ⓑ**, **Ⓒ**, and **Ⓓ**, associated with the two-proton values, 0.268, 0.182, 0.131, and 0.106 mT, respectively, have similar intensities. The signals **Ⓔ** of double intensity are due to two pairs of protons with the same $|a_{\text{H}}|$ value of 0.065 mT (accidental degeneracy), and the half-as-intense signals **Ⓕ** and **Ⓖ** stem from single protons with 0.044 and 0.036 mT. The very weak absorption **Ⓗ** at the frequency, ν_{n} , of the free proton, must belong to the remaining proton pair with 0.007 mT, with the strong reduction in its intensity being caused by the smallness of this value, as explained in Chapt. 5.2. The ENDOR spectrum of **95-d^{•-}** differs from that of **95^{•-}** by the absence of signals **Ⓕ** (0.044 mT), which are thus attributed to the single α proton in the 8-position of the *meta*-bridged ring, leaving **Ⓖ** (0.036 mT) for that in the 5-position of this ring. The ENDOR spectra of both

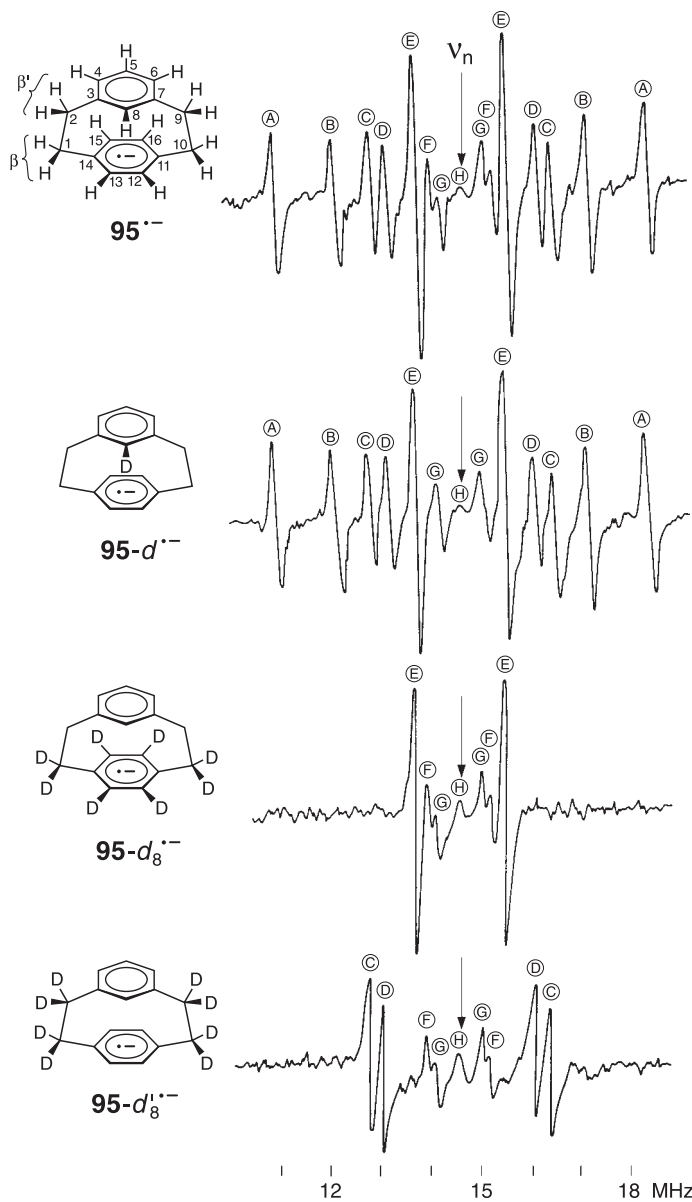


Fig. 6.16. ^1H -EENDOR spectra of the radical anions of [2.2]metaparacyclophane (**95**), as well as its 8-deuterio (**95-d**), 1,1,10,10,12,13,15,16-octadeuterio (**95-d₈**), and 1,1,2,2,9,9,10,10-octadeuterio (**95-d'₈**)

derivatives. Solvent DMF/THF (4:1), counterion K^+ , temperature 168 K. Hyperfine data in the text and Table 8.22. Reproduced with permission from [155].

$95-d_8^{\cdot-}$ and $95-d'_8^{\cdot-}$ lack the signals \textcircled{A} (0.268 mT) and \textcircled{B} (0.182 mT), which must, consequently, arise from the two β -proton pairs in the methylene groups (1,10) adjacent to the *para*-bridged benzene ring. In addition, the absence of the signals \textcircled{C} (0.131 mT) and \textcircled{D} (0.106 mT) in the ENDOR spectrum of $95-d_8^{\cdot-}$ requires that they stem from the α -proton pairs at this *para*-bridged ring (12,13- and 15,16-positions), and the missing of signals \textcircled{E} in the spectrum of $95-d'_8^{\cdot-}$ indicates their connection with the two β' -proton pairs in the methylene groups (2,9) close to the *meta*-bridged ring. Finally, the weak signal \textcircled{H} has to be associated with the α -proton pairs in the 4,6-position of the *meta*-bridged ring (1,10), because these protons are the only ones not yet accounted for.

Observation of the ENDOR spectra is more difficult for deuterons than for protons, because of the longer nuclear SLR relaxation times T_{1n} and the lower frequency range in which their signals occur, where the ENDOR technique is less sensitive (Chapt. 5.2). Not only are the coupling constants a_D reduced by a factor $g_n(D)/g_n(H) = 0.1535$ with respect to the corresponding a_H values, but also the frequency, ν_n , of the free deuteron is lowered by this factor relative to its proton counterpart. For example, in the ^1H -ENDOR spectrum of $95^{\cdot-}$, $\nu_n(H) = 14.56$ MHz and the largest value $|a_H|$ is 0.268 mT, or $|a'_H| = |a_H|\gamma_e = 0.268 \text{ mT} \cdot 28.04 \text{ MHz/mT} = 7.51 \text{ MHz}$, so that $\nu_n(D) = 14.56 \text{ MHz} \cdot 0.1535 = 2.23 \text{ MHz}$ and $|a'_D| = 7.51 \text{ MHz} \cdot 0.1535 = 1.15 \text{ MHz}$. Thus, in the ^2H -ENDOR spectrum of $95^{\cdot-}$, the signals are expected to appear in the frequency range of low sensitivity between 1.65 and 2.81 MHz, which represent $\nu_n(D) \pm |a'_D|/2$. Despite these rather unfavorable conditions, ^2H -ENDOR spectra have been reported for several radicals [192, 584–587].

Replacement of ^{14}N by ^{15}N isotopes has also been used for assigning coupling constants. The most prominent example of such a replacement is 2,2-diphenyl-1-picrylhydrazyl (DPPH; 5^{\cdot}) (Table 9.3), in which ^{15}N -labeling served to distinguish between the similar $|a_N|$ values of the two ^{14}N nuclei [587].

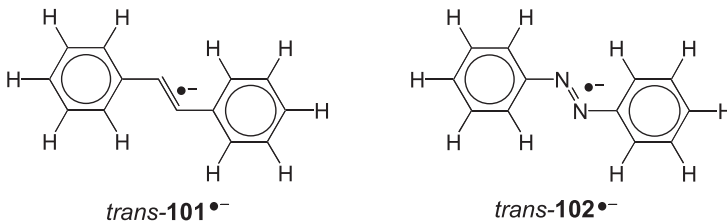
Studies of radicals containing deuterons (natural abundance 0.015%) requires, in general, preparation of labeled precursors. Only “acidic” protons, especially those in OH and NH groups or in certain positions of π radicals can be replaced by H/D exchange in a deuteron-rich solution. For other radicals, specifically labeled precursors must be synthesized in several reaction steps, starting from suitable precursors, which is expensive with respect to time and finances. This expenditure prevents the more general use of deuteration as the most reliable method for assigning ^1H -coupling constants. Great expenditure is also needed for replacement of ^{14}N by ^{15}N isotopes, although in favorable cases, ^{15}N satellites in natural abundance (0.37%) can be observed for some radicals with a NO^{\cdot} group [588, 589].

Enrichment in ^{13}C isotopes is often required for a radical, not only if satellites from these nuclei in natural abundance are difficult to detect, but also to secure assignment of an $|a_C|$ value to specific positions. Such an enrichment is synthetically even more demanding than introduction of deuterons [361, 463, 586, 590, 591].

Alkyl Substitution

Alkyl derivatives of radicals are, in general, more readily available than species that are deuterated in specific positions. Use of alkyl substitution seems, therefore, an attractive alternative to isotopic replacement as a method of assigning ^1H -coupling constants. Unfortunately, in contrast to isotopic replacement, alkyl substitution can markedly alter the spin distribution in any radical, not only in those in a degenerate ground state. Although the effect of such a substitution is, in the first place, electronic (inductive and hyperconjugative), the steric consequences of introducing an alkyl group must also be considered. Replacement of n equivalent α protons by methyl groups in a π radical replaces a binomial splitting from these protons with splitting from $3n$ β protons having coupling constants of opposite sign but similar $|a_{\text{H}}|$ value (Chapt. 4.2). If the alkyl substituents are *tert*-butyl groups, the number of protons giving rise to the pertinent splitting increases ninefold. However, because the *tert*-butyl protons are γ , their $|a_{\text{H}}|$ values are more than ten-fold smaller, and this splitting is often unresolved. *tert*-Butyl substitution then leads to elimination of the coupling constant of the α protons, along with an increased line-width.

Alkylation proved to be a suitable method to distinguish the coupling constants of protons in *exo*- vs *endo*- and in *syn*- vs *anti*- positions. Major examples are the 1,3-*exo,endo*-positions in the allyl radical (**65** \cdot) [43] and the 7-*syn,anti*-positions in the radical anion of bicyclo[2.2.1]heptane-2,3-dione (**72**) (semidione; Table 9.15) [7c]. In addition, introduction of alkyl groups into the radical anions of *trans*-stilbene (*trans*-**101**) (Table 8.12) [592] and *trans*-azobenzene (*trans*-**102**) (Table 9.13) [551, 593] allowed assignment of the coupling constants to phenyl protons in the two nonequivalent *ortho*- and the two likewise nonequivalent *meta*-positions. These protons appear nonequivalent, because rotation of the phenyl groups is slow on the hyperfine time-scale, so deuteration is here of no avail for the purpose of assignment.



General-TRIPLE Resonance

As exemplified by the ENDOR signals of the phenalenyl radical (**4** \cdot) in Figure 5.7, the relative signs of the coupling constants a_{X} can be determined by an electron–nuclear–nuclear-resonance technique denoted general TRIPLE. Another example of the use of this technique is provided by the radical anion of [2.2]metaparacyclophane (**95**) [155], of which the ENDOR spectrum was shown in Figure 6.16.

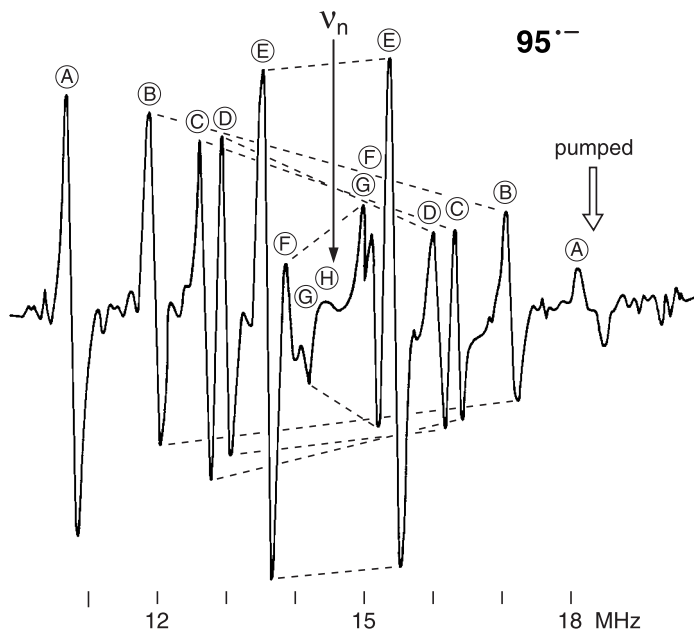


Fig. 6.17. General-TRIPLE-resonance spectrum of the radical anion of [2.2]metaparacyclophane (**95**^{•-}). Experimental conditions as for the ¹H-ENDOR spectrum in Figure 6.16 (complete structural formulas in Figures 6.8 and 6.16). Hyperfine data in the text and Table 8.22. Reproduced with permission from [155].

The corresponding general-TRIPLE-resonance spectrum (Figure 6.17) demonstrates how pumping the high-frequency component of the signals **A** changes the high- to low-frequency intensity ratio of the ENDOR signals. This ratio *decreases* for **B**, **C**, and **D** but *increases* for **F** and **G**. Thus, the three two-proton values 0.182, 0.131, and 0.106 mT, associated with **B**, **C**, and **D**, respectively, have the *same* sign as the fourth one of 0.268 mT responsible for **A**. In contrast, an *opposite* sign is indicated for the one-proton values 0.044 and 0.036 mT represented by **F** and **G**, respectively. The lack of response of the signals **E** to the TRIPLE-resonance experiment supports the assignment of the pertinent four-proton value 0.065 mT to two pairs having coupling constants of the same absolute value but opposite sign. No information could be gleaned about the sign of the two-proton value 0.007 mT attributed to the weak ENDOR absorption **H** because of the vanishingly small size of this coupling constant. Results of INDO calculations on **95**^{•-}, which are in an overall accord with the experimental data, require a positive sign for 0.268 mT. Therefore, 0.182, 0.131, and 0.106 mT must likewise be positive, and 0.044 and 0.036 mT have a negative sign. The complete analysis of the hyperfine pattern of **95**^{•-} (Figure 5.8), including both the assignment of coupling constants a_H by ENDOR by the use of isotopic labeling and the allotment of sign to these values by TRIPLE resonance, is presented in Chapt. 6.4 and in Table 8.22.

Nuclear Magnetic Resonance

Electron–nuclear magnetic interaction in solution affects NMR spectra of organic radicals so that signals are generally broadened beyond recognition. Nevertheless, ^1H - and ^2H -NMR spectra have been reported for several persistent radicals, which belong to two classes: (1) radical anions generated from π -electron compounds with an alkali-metal in ethereal solvents, and (2) heavily substituted nitroxyls and phenoxylys.

An efficient electron spin-lattice relaxation (SLR) with a short time T_{1e} is a condition for fast spin inversion and therefore for observation of an NMR spectrum of radicals in fluid solution. If this condition is met, the shift δ_{Fc} arises merely from the excess, Δn , of spins in the lower Zeeman level and, being mainly due to the Fermi-contact (Fc) term (Chapt. 3.2), is expressed in mT as [9b]

$$\delta_{\text{Fc}} = -a_{\text{X}}[(g_e\mu_{\text{B}})^2/(g_n\mu_{\text{N}})](4kT)^{-1} \quad (6.2)$$

where g_n is the g factor of X, and all symbols have their usual meanings specified in Chapters 1.1 and 3.1. The shift δ_{Fc} is measured relative to an appropriate diamagnetic compound as reference. The importance of Eq. 6.2 is that, unlike the hyperfine splitting in an ESR spectrum, not only is $|\delta_{\text{Fc}}|$ proportional to the $|a_{\text{X}}|$ value of the coupling constant, but the direction of δ_{Fc} depends on the *sign* of a_{X} . A *positive* coupling constant a_{X} shifts an NMR signal to a *lower* magnetic-field strength B , and a *negative* a_{X} value to a *higher* B . Thus, apart from line-broadening, which is roughly proportional to a_{X}^2 and can sometimes serve for the assignment of $|a_{\text{X}}|$ values, NMR spectra provide the absolute sign of the coupling constant a_{X} . Replacement of X by its isotope X' and of a_{X} by $a_{\text{X}'} = a_{\text{X}}g_n'/g_n$, where g_n' is the g_n factor of X', converts the quotient a_{X}/g_n of Eq. 6.2 into $a_{\text{X}'}/g_n' = (a_{\text{X}}g_n'/g_n)/g_n' = a_{\text{X}}g_n$. Therefore, such a replacement leaves δ_{Fc} unchanged, and this statement holds, in particular, for X = ^1H (=H) and X' = ^2H (=D). The advantage of replacing protons by deuterons in an NMR spectrum of a radical is a striking reduction in the line-width of the signals, by a factor of ca $g_n'^2(\text{D})/g_n^2(\text{H}) = 1/40$, while the shift δ_{Fc} remains the same [594].

Figure 6.18 shows the ^2H -NMR spectrum of a 1.1 M solution of perdeuteriobiphenyl (**94-d**₁₀) completely reduced with sodium in DME [9b, 595]. The high concentration of **94-d**₁₀ and its radical anion **94-d**₁₀^{•−} results in an enhanced electron-SLR. The coupling constants a_{D_μ} for **94-d**₁₀^{•−}, derived from their counterparts a_{H_μ} in the ESR spectrum of **94**^{•−} (Figure 6.6), including signs as required by theory, are $a_{\text{D}_{2,2'},6,6'} = -0.041$, $a_{\text{D}_{3,3'},5,5'} = +0.006$, and $a_{\text{D}_{4,4'}} = -0.082$ mT. The observed shifts are, relative to the signals of THF-*d*₈, added to the solution as an internal reference. In the general case of a partial reduction, they have to be scaled up by the proportion of **94-d**₁₀^{•−} in the total concentration, **94-d**₁₀ + **94-d**₁₀^{•−}, to obtain the full shifts δ_{Fc} diagnostic of the radical anion. The shifts are in accord with the expected $|a_{\text{D}_\mu}|$ values, and the line-widths of the signals associated with

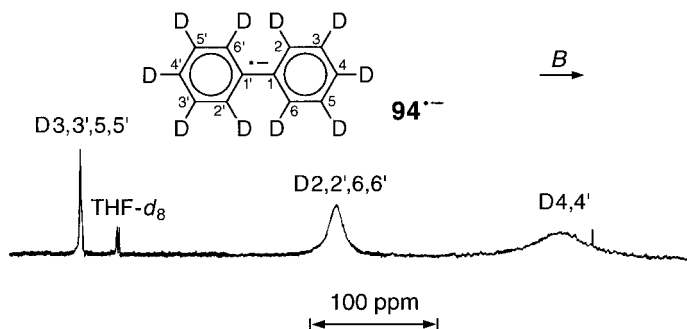


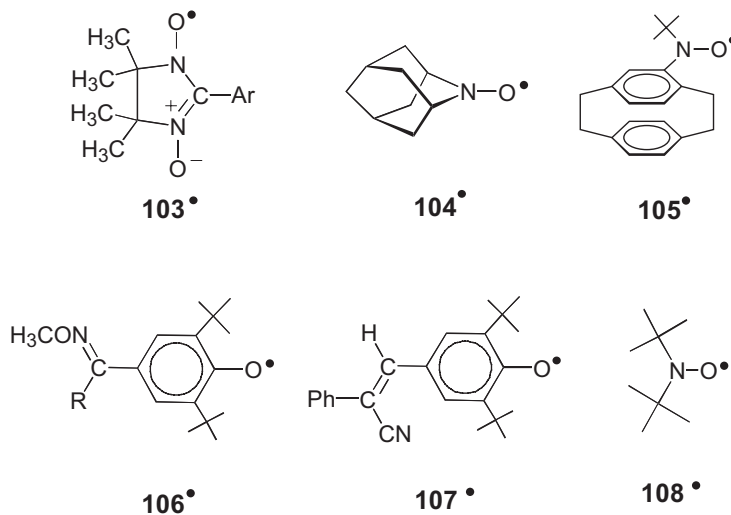
Fig. 6.18. ^2H -NMR spectrum of a 1.1 M solution of perdeuteriobiphenyl ($\mathbf{94-d}_{10}$) completely reduced with sodium in DME at 303 K. THF- d_8 added as internal reference. Hyperfine data in the text and Table 8.11. Reproduced with permission from [595].

these values reflect their size. The low-field shift of the signals from the deuterons in the *meta*-positions is consistent with the positive sign of $a_{\text{D}3,3',5,5'}$, in contrast to the high-field shift of the signals from the deuterons in the *ortho*- and *para*-positions, which have negative coupling constants $a_{\text{D}2,2',6,6'}$ and $a_{\text{D}4,4'}$.

Besides $\mathbf{94-d}_{10}^{\cdot-}$, radical anions of biphenyl itself [594, 595], its 3,3'-dimethyl derivative [596], naphthalene, perdeuterionaphthalene [9b], phenanthrene, perdeuteriophenanthrene, and fluorenone [595], have been studied by NMR, as well as radical anions of ethyl-, isopropyl-, and *tert*-butylbenzenes [597, 598].

Because the line-widths in the NMR spectra are enlarged so strongly with increasing $|a_X|$ value, this resonance technique is particularly suitable for determination of very small coupling constants, including their signs which cannot, in general, be measured by ESR and ENDOR. To this end, NMR spectroscopy has been applied to alkali-metal nuclei in cations associated with the radical anions of naphthalene, phenanthrene, biphenyl, fluorenone, and 2,2'-dipyridyl [9b, 595, 599, 600] (ion pairing; Chapt. 6.6). The results of these studies agree with the corresponding ESR data $|a_X|$ ($X = {}^6\text{Li}, {}^7\text{Li}, {}^{23}\text{Na}, {}^{39}\text{K}, {}^{85}\text{Rb}, {}^{87}\text{Rb}, \text{and } {}^{133}\text{Cs}$) where the latter are available (Tables A.2.1 and A.2.2); deviations are caused by different concentrations used in the two spectroscopic methods. The signs of these coupling constants a_X can change upon varying the solvent and/or the temperature, which influences the strength of association between the counterion and the radical anion (Chapt. 6.6).

Small coupling constants a_X occur in heavily substituted nitroxyls and phenoxyls like 2,2,6,6-tetramethyl-4-oxopiperidinyl-1-oxyl (TEMPO; $\mathbf{8}^{\cdot}$) [601], the nitronyl-nitroxyls $\mathbf{103}^{\cdot}$ [602], *N*-oxy-aza-2-adamantane ($\mathbf{104}^{\cdot}$) [603], [2.2]paracyclophane-4-yl-*tert*-butyl-nitroxyl ($\mathbf{105}^{\cdot}$) [604], and *para*-substituted derivatives $\mathbf{106}^{\cdot}$ [605] and $\mathbf{107}^{\cdot}$ [606] of the 2,6-di-*tert*-butylphenoxyl. Such radicals are, therefore, particularly amenable to NMR studies.



Interestingly, a liquid radical, di-*tert*-butylnitroxyl (**108**•) (Table 7.20), proved to be an appropriate solvent for achieving efficient electron-SLR in these studies, and it was used for **103**• and **105**•–**107**•. Coupling constants a_{H} and, in some cases, a_{D} were determined, inclusive of their signs, for protons and deuterons situated in the γ -positions of **8**• [601], in the aromatic group Ar of **103**• (Ar = Ph or 2-, 3- or 4-pyridinyl) [602], in the γ - and δ -positions of **104**• [603], in the [2.2]paracyclophane moiety of **105**• [604], and in the alkyl group R of **106**• [605]. In addition, ^{19}F -NMR spectra served for determination of coupling constants a_{F} for the fluorinated phenyl group Ph of **107**• [606], and a pulsed ^{13}C -NMR technique was applied to measure the coupling constants a_{C} for the aromatic group Ar of **103**• [607]; absolute values and sign of a_{F} and a_{C} were thus derived. All these ^1H , ^2H , ^{19}F , and ^{13}C nuclei are rather remote from the spin-bearing NO• or PhO• moiety, and their hyperfine interaction with the unpaired electron at this radical center is relatively weak.

Line-Broadening by Anisotropies

Line-widths in ESR spectra of organic radicals in solution are enlarged by incomplete averaging-out of hyperfine and g_{e} anisotropies. For a given radical, line-broadening increases when the viscosity of the solution is higher, i.e., by using more viscous solvents and/or by lowering the temperature. As an example, Figure 6.19 shows the ESR spectrum of the di-*tert*-butylnitroxyl radical (**108**•) in ethanol at 292 and 142 K [608]. The observed hyperfine pattern of this spectrum is solely due to interaction with the ^{14}N nucleus, because splittings by the 18 γ -protons of the two *tert*-butyl groups are unresolved. The origin of the characteristic line-broadening at the lower temperature is indicated by the stick diagram below the spectrum. In the stick diagram, the differences $A_{\text{N}\parallel} - A_{\text{N}\perp} = A_{\text{N},z} -$

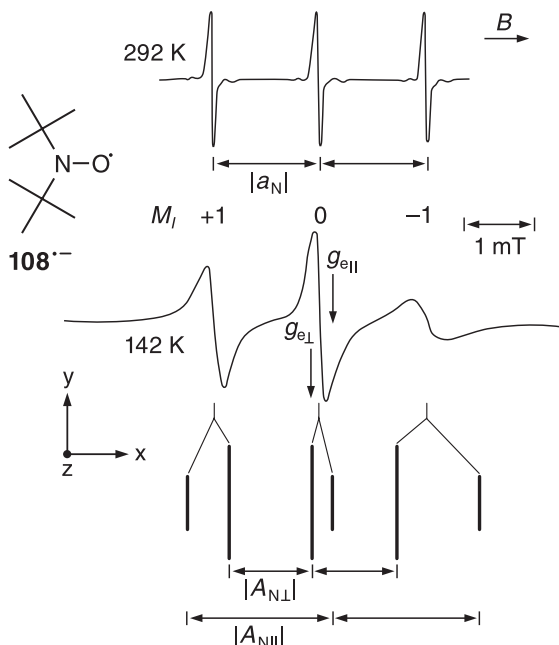


Fig. 6.19. ESR spectrum of the di-*tert*-butyl nitroxyl radical (**108•**) in ethanol at 292 and 142 K. Hyperfine data in the text and Table 7.20. Reproduced with permission from [608].

$(1/2)(A_{N,x} + A_{N,y})$ and $g_{e||} - g_{e\perp} = g_{e,z} - (1/2)(g_{e,x} + g_{e,y})$, derived for **108•** from data on a single crystal [609], were (somewhat arbitrarily) scaled down by a factor 3 to account for the partial averaging-out of ^{14}N -hyperfine and g_e anisotropies in solution. The axis of the tensors \mathbf{A}_N and \mathbf{G}_e (Chapts. 4.2 and 6.2), which were assumed to coincide, are shown in Figure 6.19 (x, y is the nodal π plane of the NO group, and z is perpendicular to it). The dependence of the line-width on the viscosity of the environment, as illustrated in Figure 6.19, underlies the use of nitroxyl radicals as spin labels in biological materials (Appendix A.1).

In addition to the viscosity of the solution, the structure of the radical plays an important role in line-broadening by anisotropies. As stated in Chapt. 4.2, magnetic dipolar nuclear–electron interaction, which is responsible for hyperfine anisotropy, depends on r^{-3} , where r is the distance between the nucleus and the unpaired electron. That is why hyperfine anisotropy is especially pronounced for nuclei in atoms bearing substantial “local” π -spin population. Accordingly, line-broadening by this anisotropy is often observed for ^{13}C , ^{14}N , ^{17}O , ^{31}P , and ^{33}S nuclei in π radicals but has been reported in only a few cases for protons, e.g., for those in the radical cation of pyracene (**96**) in viscous conc. sulfuric acid at 263 K [574].

Because hyperfine anisotropy broadens the lines in proportion to the square of the “local” spin population ρ_μ^π at the π center μ , the coupling constants a_{X_μ} of the

nuclei $X = {}^{13}\text{C}$, ${}^{14}\text{N}$, ${}^{17}\text{O}$, ${}^{31}\text{P}$, or ${}^{33}\text{S}$ can be assigned to specific positions μ by means of this relation. For example, the coupling constants, a_{C_μ} , associated with the ${}^{13}\text{C}$ satellites in the ESR spectrum of the radical anion of tropone (**99**) [214] (Figure 6.11) were assigned by correlation of their widths with the squares of the coupling constants, a_{H_μ} , of the α protons at the centers μ in virtue of the simple proportionality of the a_{H_μ} values to the spin populations ρ_μ^π , as expressed by the McConnell equation (Eq. 4.5). (The a_{C_μ} values themselves could not be used for this purpose, considering the substantial contributions to them by spin populations, ρ_ν^π , at the adjacent centers ν ; Eqs. 4.15–4.17).

Because g_e anisotropy is relatively small for organic radicals without heavy atoms, its effect on the line-widths is appreciable when it is combined with hyperfine anisotropy. The contribution of both anisotropies to the line-widths of radicals in solution can be formulated as a function of the spin quantum number M_I of the nucleus X [165, 574, 610]:





$$\Delta B(M_I) = U + VM_I + WM_I^2 \quad (6.3)$$

where the number $M_I = M_I(X)$ of a single nucleus X is replaced by $\sum M_I(X)$ for a set of equivalent nuclei X.

As is evident from the spectrum of **108** \cdot (Figure 6.19), the dependence on M_I is essential, because it gives rise to different line-widths in the same hyperfine pattern due to the nucleus X or to a set of these nuclei. Apart from the rotational correlation time of the radicals $\tau_r \propto \eta/T$ (where η is the viscosity of the solvent and T is the absolute temperature), the parameters U, V, and W are determined by the hyperfine and g_e anisotropy tensors, $\mathbf{A}_{X,\text{dip}}$ and $\mathbf{G}_{e,\text{aniso}}$ (Chapts. 4.2 and 6.2). The parameter U, to which the squares of $\mathbf{A}_{X,\text{dip}}$ and $\mathbf{G}_{e,\text{aniso}}$ contribute is *positive* and, being independent of M_I , is *constant* for all lines of the hyperfine pattern under the given conditions. Likewise *positive* are the parameter W, which is proportional to the square of $\mathbf{A}_{X,\text{dip}}$, and so is the third term WM_I^2 . Varying M_I^2 causes the lines to broaden progressively on going from the middle part of the hyperfine pattern (small $|M_I|$) to its peripheries (large $|M_I|$). Most interesting is the second term VM_I , because it can be positive or negative and thus cause the line-widths in the high-field half of the hyperfine pattern to differ from the line-widths in the low-field half. The parameter V is proportional to the product of $\mathbf{A}_{X,\text{dip}}$ and $\mathbf{G}_{e,\text{aniso}}$, and its sign depends on those of the spin population ρ_μ^π at the center μ with the nucleus X, on the g_n factor of X, and on the difference $\Delta g_e = g_{e\parallel} - g_{e\perp}$ or $\Delta g_e = g_{e,z} - (1/2)(g_{e,x} + g_{e,y})$, i.e. $\text{sign } V = \text{sign } \rho_\mu^\pi \cdot \text{sign } g_n \cdot \text{sign } \Delta g_e$. In principle, all three values ρ_μ^π , g_n , and Δg_e can have either sign, but, because Δg_e is negative in planar π radicals, $\text{sign } V = -\text{sign } \rho_\mu^\pi \cdot \text{sign } g_n$ in this case.

Now, for a *positive* coupling constant a_X , the spin quantum numbers M_I are *positive* in the low-field half of the hyperfine pattern and *negative* in its high-field half (Figures 3.1 and 3.2). The opposite holds for the sign of M_I when a_X is negative. Therefore, the term VM_I has the *same* sign as V in the low-field half and the *opposite* sign in the high-field half when a_X is *positive*, whereas its sign is *opposite* to that of V in the low-field and the *same* in the high-field half when a_X is *negative*. Clearly,

a *negative* term VM_I causes the line-width to narrow and a positive one to broaden. In conclusion, for a negative value of Δg_e , the relation between line-broadening and the sign of a_X can be expressed by the following rules:

Field							
low	high		ρ_μ^π	g_n of X	V	a_X	case
		}	+	+	-	+	①
			-	+	+	-	②
			+	-	+	-	③
			-	-	-	+	④
		}	+	+	-	-	⑤
			-	+	+	+	⑥
			+	-	+	+	⑦
			-	-	-	-	⑧

In words: a_X is positive when ρ_μ^π and g_n have the same sign and the high-field lines are broader (① and ④), or when ρ_μ^π and g_n have opposite signs and the low-field lines are broader (⑥ and ⑦); a_X is negative when ρ_μ^π and g_n have opposite signs and the high-field lines are broader (② and ③), or when ρ_μ^π and g_n have the same sign and the low-field lines are broader (⑤ and ⑧).

Case ① is by far the most frequently encountered, because the substantial local spin population ρ_μ^π at the atom in question is usually positive, and so is the sign of the g_n factor for the majority of nuclei like X = ^{13}C , ^{14}N , ^{31}P , and ^{33}S . Less common are cases ② or ③, where either ρ_μ^π or g_n (as for X = ^{17}O) is negative, and still fewer are the remaining cases. Examples have been presented throughout this book.

Case ① occurs for coupling constants of ^{14}N , ^{31}P , and ^{33}S nuclei in the radical anions of 1,4,5,8-tetraazaphtalene (57) [162] and 2,4,6-tri-*tert*-butylphosphabenzene (82) [165], and in the radical cation of 1,4,5,8-tetrahydro-1,4,5,8-tetrathiofulvalene (24) [230], respectively. The pertinent coupling constants are $a_N = +0.337$ for 57^- (Figure 6.5), $a_P = +2.27$ for 82^- (Figure 4.8), and $a_S = +0.425$ mT for 24^{+} (Figure 6.13). Case ① also holds for the larger coupling constant, $a_{\text{C}3a,4a,6a,7a} = +0.410$ mT, of the ^{13}C isotope in the radical anion of dithieno[3,4-*b*; 3'-4'*e*]paradithiin-1,3,5,7-tetraone (81) [172] (Figure 6.14). For this radical anion, the smaller ^{13}C -coupling constant, $a_{\text{C}1,3,5,7} = -0.202$ mT, represents case ⑤, and both ^{33}S -coupling constants, $a_{\text{S}2,6} = -0.083$ and $a_{\text{S}4,8} = -0.138$ mT, exemplify case ②. Finally, the coupling constant, $a_{\text{O}1,3,5,7} = -0.361$ mT, of the ^{17}O isotopes in 81^- is an illustration of case ③.

Returning to the spectrum of di-*tert*-butylnitroxyl (**108**[•]) in Figure 6.19 with the conspicuously larger line-broadening at high field, we note that it is an example of the most frequent case ①. Because the spin population ρ_{μ}^{π} at the N atoms and the g_n factor of ¹⁴N are certainly positive, the ¹⁴N-coupling constant, $a_N = +1.53$ mT, also has a positive sign. Applying Eq. 6.3 to the spectrum of **108**[•] at 142 K in Figure 6.19, the contribution $\Delta B(M_I)$ to the line-widths is $U + V + W$ for the low-field line ($M_I = +1$), is U for the central line ($M_I = 0$), and is $U - V + W$ for the high-field line ($M_I = -1$). Because $V < 0$ and the low-field line is broader than the central one, $|W|$ must be larger than $|V|$. From the observed line-widths, the values of U , V , and W can be estimated as $+0.25$, -0.15 , and $+0.30$ mT, respectively.

Miscellaneous

Because the contributions of hyperfine anisotropy to a coupling constant a_X can often be reliably calculated, the changes that result from adding such contributions to an isotropic a_X value indicate the absolute sign of this value. Use of liquid crystals as the solvent, which partially orders the molecules, prevents the hyperfine anisotropy from being completely averaged-out in solution while avoiding the cumbersome line-broadening of radicals in solid media. In the isotropic phase, the coupling constants a_X are similar to those observed in fluid solution, but, upon lowering the temperature and passing to the nematic phase, these values exhibit characteristic changes which make it possible to derive their sign. The reported studies were applied to nuclei in atoms with a substantial local spin population ρ_{μ}^{π} in a few very persistent π radicals, such as ¹⁴N nuclei in the radical anion of tetracyanoethene (TCNE; **18**) (Table 9.19) and in 2,2-diphenyl-1-picrylhydrazyl (DPPH; **5**[•]) (Table 9.3) [611], as well as to ¹³C isotopes in phenalenyl (**4**[•]) (Table 8.4) [90, 91, 462]. In accordance with theory, the positive signs of the coupling constants a_N ($+0.158$ for **18**^{•-} and $+0.92$ mT as an average value for the two central ¹⁴N nuclei in **5**[•]) were confirmed, and so were the positive signs of $a_{C1,3,4,6,7,9}$ ($+0.966$ mT) and the negative sign of $a_{C2,5,8} \approx a_{C3a,6a,9a}$ (-0.784 mT) for **4**[•].

As described in Chapt. 5.2, the absolute sign of coupling constants a_H can be derived from ENDOR spectra of radical cations in Freon matrices when the residual ¹H-hyperfine anisotropy is resolved [310, 329].

6.6 Ion Pairing

The fact that ions of opposite charge tend to associate in solution (ion pairing) is of great importance in the course of organic reactions [9]. The method of choice for studies of such pairing in which paramagnetic ions are involved is ESR spectroscopy. In particular, this tool has been applied to ion pairs formed by radical anions associated with their positively charged alkali-metal counterions [9a, b, c].

Loose and Tight Ion Pairs

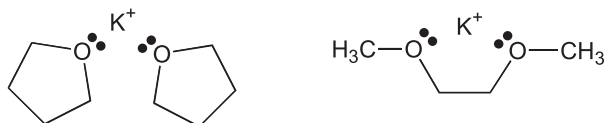
According to the strength of association, the ion pairs of radical anions and their alkali-metal counterions are considered to be *tight* or *loose*. Tight ion pairs are also often denoted *contact* pairs, because the cation directly contacts the radical anion, whereas loose ion pairs are mostly *solvent-separated*, because the two ions are separated by molecules of the solvent. The strength of association depends on several factors, such as the structure of the radical anion, the nature and concentration of the alkali-metal, and, last but not least, the cation-solvating power of the solvent.

Tight ion pairs of radical anions with lone σ -electron pairs at heteroatoms, especially at N or O, are generally contact pairs, because the cation is strongly attached to these electrons without intervening molecules of solvent. On the other hand, the loose ion pairs of radical anions of hydrocarbons are usually solvent-separated, because the cation is weakly bound to the π system, so that the molecules of the solvent successfully compete with this system for the cation. In addition to the electronic structure of the radical anion, steric factors can favor or hinder the approach of the counterion and thus influence ion pairing.

In the absence of intervening solvent molecules, as for counterions attached to lone σ -electron pairs, the smaller the cation, the closer can it interact with the radical anion, so that the strength of association generally *decreases* with the *increasing* size of the alkali-metal cation in the sequence Li^+ , Na^+ , K^+ , Rb^+ , Cs^+ . By contrast, in ion pairs of hydrocarbons, the strength of association usually *increases* in this order, because the larger the cation, the less it is solvated by the molecules of the solvent and the deeper it penetrates into the π -electron cloud. Radical anions with lone pairs at heteroatoms can be considered *hard* bases having a preference for *harder* acids such as Li^+ . On the other hand, radical anions of hydrocarbons may be regarded as *soft* bases which favor *softer* acids like K^+ [215, 612].

Ion pairing is obviously promoted by higher concentrations of alkali-metal cations, which are most efficiently achieved by adding a salt of the cation involved, such as sodium tetraphenylborate or potassium chloride soluble in many organic ethers. An increase in the concentration of both radical anion and counterion is also effective.

The cation-solvating power *decreases* in the sequence HMPT, DME, THF, MTHF, DEE and the association of the radical with the counterion is strengthened in the same order. For a given solvent, raising the temperature has a similar effect. The solvating power cannot, however, be equated just to the polarity of the solvent, as represented by its dielectric constant. Although THF and DME have almost the same dielectric constant, the former is better suited for strengthening the association.



This is because THF, with only one O atom, can solvate an alkali-metal cation only *intermolecularly*, whereas DME, by virtue of its two O atoms, can do so *intramolecularly* in a chelate-like fashion, especially for K^+ .

As expected, the cation-solvating power of the solvent has a greater effect on loose ion pairs, in which the counterion is separated from the radical anion by solvent molecules, than on tight ion pairs (particularly for those of radical anions with lone pairs at heteroatoms), in which the counterion directly contacts the radical anion.

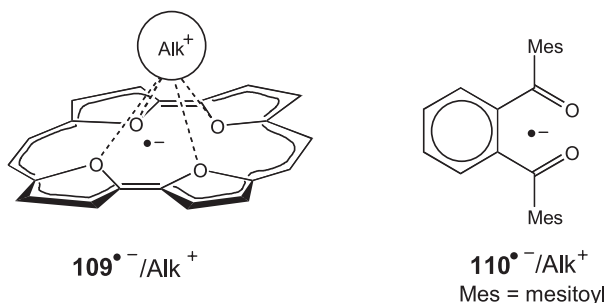
Slight enhancement of the g_e factor and line-broadening caused by the movement of the cation relative to the radical anion are often observed as evidence of appreciable ion pairing. However, the principal feature indicating the occurrence of ion pairs is the appearance of a conspicuous hyperfine splitting by the magnetic nuclei of the alkali-metal counterion.

Hyperfine Splitting by Alkali-metal Nuclei of Counterions

Since the report on a ^{23}Na -hyperfine splitting in the ESR spectra of naphthalene reduced with sodium to its radical anion in THF or MTHF [140], many papers describing similar findings have appeared. Although a fairly large splitting by a magnetic nucleus of the counterion is the clearest evidence for the formation of tight ion pairs, the smallness of this splitting or even its non-observance does not necessarily mean that the ion pairing in question is loose. The alkali-metal splitting can be small (even too small to be resolved in the ESR spectrum) when the counterion is, e.g., situated in the nodal plane of the radical anion. From the data in Table 3.1, it is obvious that the magnetic nucleus of the counterion is usually the isotope with high natural abundance, namely ^7Li , ^{23}Na , ^{39}K , ^{85}Rb , ^{87}Rb , and ^{133}Cs . The spin quantum numbers I are $3/2$ for ^7Li , ^{23}Na , ^{39}K , and ^{87}Rb , $5/2$ for ^{85}Rb , and $7/2$ for ^{133}Cs , so that an additional splitting into 4, 6, or 8 lines leads to a more complex hyperfine pattern. The g_n factors of all the alkali-metal nuclei are positive but greatly differ in magnitude, as do the coupling constants calculated for a spin population of $+1$ in the ns-AOs of these metals: $+13.0$ for ^7Li ($n = 2$), $+33.1$ for ^{23}Na ($n = 3$), $+8.1$ for ^{39}K ($n = 4$), $+37.0$ for ^{85}Rb ($n = 5$), $+125.4$ for ^{87}Rb , and $+88.0$ mT for ^{133}Cs ($n = 6$) [476].

Due to its predominant s-character, the tiny spin population, $\rho_{\text{Alk}}^{\text{ns}}$, at the alkali-metal cations often gives rise to observable $|a_X|$ values of the coupling constants, which vary widely from ca 0.01 mT for $X = ^{39}\text{K}$ in loose ion pairs of π -radical anions of hydrocarbons to more than 1 mT for $X = ^{87}\text{Rb}$ or ^{133}Cs in tight pairs. A compilation of these values is presented in Tables A.2.1 and A.2.2 for ion pairs of radical anions of hydrocarbons and compounds with heteroatoms, respectively. The simplest model accounting for the appearance of $\rho_{\text{Alk}}^{\text{ns}}$ is that of spin transfer from the SOMO of the radical anion to the outer s-AO of the alkali-metal cation. Such a back-transfer of charge and spin, which requires an adequate overlap between the two orbitals, is favored by low ionization potential of the radical anion and high electron affinity of the cation. It can be considered a small contribution of

the structure $\mathbf{M}/\text{Alk}^\bullet$ to $\mathbf{M}^-/\text{Alk}^+$, where \mathbf{M} is the organic molecule and Alk stands for an alkali-metal atom. Direct spin transfer to a metal ns-AO should lead to a positive spin population $\rho_{\text{Alk}}^{\text{ns}}$ in this AO and thus to a positive a_X value for the metal nucleus X as the product of $\rho_{\text{Alk}}^{\text{ns}}$ and the coupling constant calculated for a ns-spin population of +1. Indeed, for many tight ion pairs, the $|a_X|$ values of different alkali-metal nuclei X for the same radical anion and under the same conditions are roughly proportional to these calculated values, a finding that points to a similar structure of ion pairs. However, as indicated by alkali-metal NMR studies [9b, c], the pertinent coupling constant a_X can also be negative. When the $|a_X|$ value of an alkali metal nucleus increases upon raising the temperature, the coupling constant should be positive, whereas it is expected to be negative when this value decreases on warming the solution. A change in sign of the coupling constant with temperature is also observed, in which case the $|a_X|$ value exhibits an extremum. Because all alkali-metal nuclei have positive g_n factors, a negative sign of a_X arises when the spin population $\rho_{\text{Alk}}^{\text{ns}}$ transferred from the SOMO of the radical anion to the ns-AO of the alkali-metal is negative, i.e., when such a transfer occurs indirectly by spin polarization. Small, negative coupling constants for $X = {}^7\text{Li}$, ${}^{23}\text{Na}$, ${}^{39}\text{K}$, and ${}^{133}\text{Cs}$ nuclei of alkali-metal counterions (Table A.2.2) were observed in tight ion pairs of the radical anions of tetraoxaporphycene (**109**) (Table 9.42) [613]. Here, the cations are in close contact with the lone electron pairs of the four O atoms, but they lie in a vertical nodal plane of the π -SOMO. The $|a_{\text{Li}}|$, $|a_{\text{Na}}|$, $|a_{\text{K}}|$, and $|a_{\text{Cs}}|$ values have a ratio comparable to that of the coupling constants calculated for the ns-spin populations of +1.



The very large (and presumably positive) coupling constants a_X of alkali-metal nuclei in the tight ion pairs of *o*-dimesitylbenzene (**110**) (Table 9.16) served for years as a paradigm. With DME, these values are +0.375, +0.695, +0.133 [614], +0.491, +1.66 [615], and +1.02 mT [614] for $X = {}^7\text{Li}$, ${}^{23}\text{Na}$, ${}^{39}\text{K}$, ${}^{85}\text{Rb}$, ${}^{87}\text{Rb}$, and ${}^{133}\text{Cs}$, respectively (Table A.A.2). They are 10–100 times greater than those generally observed under the same conditions in loose ion pairs of π -radical anions of polycyclic alternant hydrocarbons (PAHs) like naphthalene. Surprisingly, coupling constants of alkali-metal nuclei comparable to those for **110**^{•-} were recently found for the tight ion pairs of the radical anion of the hydrocarbon, 1,4-di-*tert*-butylbuta-

1,3-diene (**90**) with K^+ , Rb^+ , and Cs^+ [529] (Table A.2.1) (ESR and ENDOR spectra of $90^{\cdot-}/K^+$ were shown in Figure 5.4). Even larger values are exhibited by the corresponding ion pairs of the radical anion of the 2,3-disubstituted isomer (**111**) (Table A.2.1) [529]. With DME as the solvent, the coupling constants are +0.155, +0.840, and +2.84 mT for ^{39}K , ^{85}Rb , and ^{87}Rb , respectively, at 260 K, and +2.47 mT for ^{133}Cs at 300 K (their positive sign is in accordance with the temperature dependence of a_X , and also with the result of a general-TRIPLE-resonance experiment). These values, unusually large for radical anions of hydrocarbons, point to very strong association of $90^{\cdot-}$ and $111^{\cdot-}$ with their alkali-metal counterions. Such an association has been traced to the particular structure of the ion pairs, in which electronic (smallness of the π system, shape of the SOMO) and steric (flanking of the cation by bulky *tert*-butyl groups) factors promote close contact between the oppositely charged particles. In Figure 6.20, spectra of $111^{\cdot-}/K^+$ in DME are shown at 175, 195, and 220 K. At the lowest temperature, the hyperfine pattern consists of merely a 1:4:6:4:1 quintet spaced by 0.71 mT and arising from the four α protons in the 1,4-positions. The hyperfine splitting by the 18 γ protons in the 2,3-*tert*-butyl substituents and the difference in the coupling constants of the 1,4-*endo*- and *exo*-protons are too small to be resolved. The absence of a detectable ^{39}K -hyperfine splitting and the rapid decrease in intensity of the five lines upon raising the temperature justify their attribution to a loose (solvent-separated) ion pair $111^{\cdot-}/K^+$. With the weakening of these five components, marked by asterisks in Figure 6.20, a well-resolved multiline hyperfine pattern appears, which exhibits substantial ^{39}K -hyperfine splitting and is therefore attributed to a tight ion pair $111^{\cdot-}/K^+$. This pattern is the only one present in the ESR spectrum at 220 K. It is important to note that, in the intermediate range of 180–200 K, both hyperfine patterns are observable, which means that both loose and tight ion pairs *coexist* in the same solution. The two ion pairs should thus have different structures, so that their exchange is slow on the hyperfine time-scale. This difference is indicated by the finding that, in addition to the appearance of the ^{39}K -hyperfine splitting, the coupling constants of the α protons in the 1,4-positions strikingly change on going from the loose to the tight ion pair. Whereas for the loose ion pair, the a_H values of both the *endo*- and the *exo*-protons are -0.71 mT, the coupling constant of the *endo*-protons in the tight ion pair no longer has such a value (which is common to α protons in the 1,4-positions of radical anions of buta-1,3-dienes), but is changed to ca -0.4 mT. This change is also characteristic of ion pairs $111^{\cdot-}/Rb^+$ and $111^{\cdot-}/Cs^+$, which are tight in the whole temperature range of investigation, and which exhibit the very large ^{85}Rb -, ^{87}Rb -, and ^{133}Cs -hyperfine splittings cited above. Pertinent ESR spectra (Figure 6.21) demonstrate that these splittings dominate the hyperfine patterns, particularly for ^{133}Cs . The ENDOR technique can readily be applied to ^{133}Cs and the two Rb isotopes, for which the frequencies ν_n of the free nuclei are smaller than the $|a'_X/2|$ values of the coupling constants in MHz. With $\nu_n = 14.56$ MHz for the proton, such frequencies are 1.39, 4.73, and 1.91 MHz for ^{85}Rb , ^{87}Rb , and ^{133}Cs , respectively, whereas the corresponding $|a'_X/2|$ values lie in the ranges 7–12, 23–40, and 20–36 MHz, respectively, depending on solvent (DME or THF) and temperature.

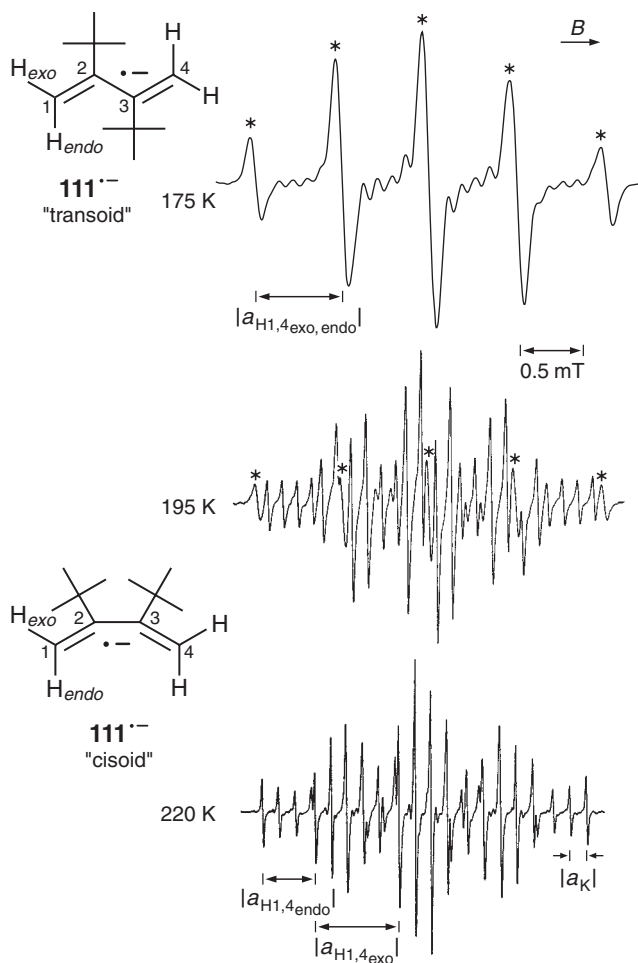


Fig. 6.20. ESR spectra of the radical anion of 2,3-di-*tert*-butylbuta-1,3-diene (**111**). Solvent DME, counterion K^+ , temperatures as indicated. The five broad lines due to the loose ion pair are marked by asterisks. The structural

formulas represent the assumed different geometries of the tight and loose ion pairs. Hyperfine data in the text and Tables 8.6 and A.2.1. Reproduced with permission from [529].

Spin Redistribution

Changes in the hyperfine patterns of radical anions due to electrostatic attraction by the positively charged counterion are relatively small for the loose ion pairs of the radical anions of benzenoids but become more pronounced in the tighter ion pairs of polarizable nonalternant hydrocarbons [147]. Thus, the coupling constants, a_H , of the α protons in the radical anions of azulene (**112**) and acenaphthylene (**113**) markedly change on going from non-associated to ion-paired species (values in mT, signs as required by theory).

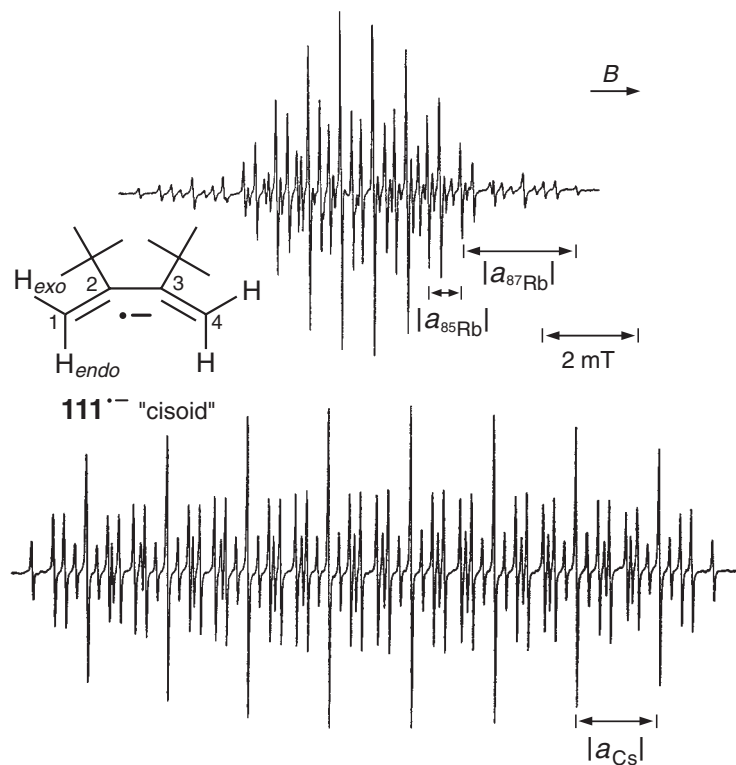
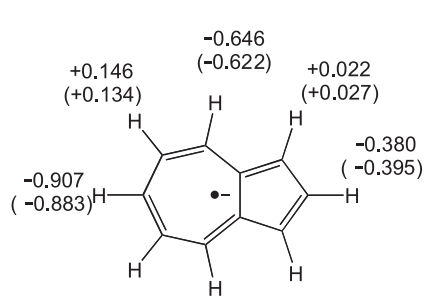


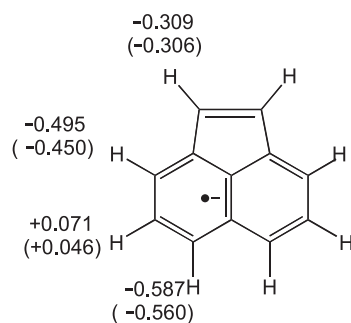
Fig. 6.21. ESR spectra of the radical anion of 2,3-di-*tert*-butylbuta-1,3-diene (**111**). Top: solvent DME, counterion Rb⁺, temperature 220 K. Bottom: solvent THF, counterion Cs⁺, temperature 210 K. The upper spectrum is a

mixture of hyperfine patterns due to both isotopes ⁸⁵Rb and ⁸⁷Rb in the concentration ratio, 72.17/27.83, of their natural abundances. Hyperfine data in the text and Tables 8.6 and A.2.1. Reproduced with permission from [529].



112^{•-}

ion-paired: DME, Li⁺, DME, 293K [616]
non-associated, in parentheses:
n-Pr₄N⁺, DMF, 298 K [298]

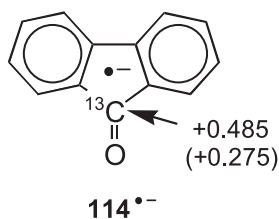


113^{•-}

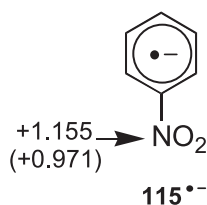
ion-paired: Na⁺, THF, 298K [617]
non-associated, in parentheses:
n-Pr₄⁺, DMF, 298 K [617]

For $112^{\cdot-}$, ion pairing increases the $|a_H|$ values of the protons at the seven-membered ring, and decreases those at the five-membered ring, but for $113^{\cdot-}$ ion pairing enhances the $|a_H|$ values of the protons at the six-membered rings without significantly changing those at the five-membered ring.

Even more sensitive to association with alkali-metal counterions are radical ions having carbonyl and nitro groups, in which the cation is tightly attached to lone electron pairs of O atoms. For a carbonyl group, the most striking change is the large increase in the coupling constant, a_C , of the ^{13}C isotope in this group. Such an increase can be interpreted as a greater weight of the structure $>\text{C}^{\cdot-}\text{O}^-$ relative to $>\text{C}^{\cdot-}\text{O}^{\cdot}$, because the electron-attracting power of the O atom is enhanced by contact with the alkali-metal cation. For a similar reason, the a_N value of the ^{14}N nucleus in the nitro group increases by favoring the structure $-\overset{\cdot-}{\text{N}}\langle\text{O}^-$ relative to $-\text{N}\langle\text{O}^{\cdot}$. Examples are provided by a_C and a_N values for the radical anions of fluorenone (**114**) (Table 9.14) and nitrobenzene (**115**) (Table 9.21), respectively (values in mT, signs as required by theory).

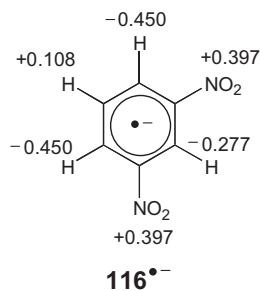


ion-paired: Na^+ , DME, 298 K [7b, 591, 618]
non-associated, in parentheses:
 Na^+ , DMF, 298 K [7b, 591, 618]

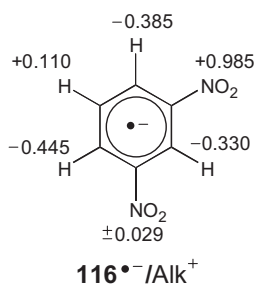


ion-paired: Li^+ , DME, 273 K [619]
non-associated, in parentheses:
 Et_4N^+ , DMF, 298 K [620]

The hyperfine pattern can change strikingly upon association with an alkali-metal counterion when the radical anion has two equivalent functional groups with lone electron pairs contacting the cation, as in 1,3-dinitrobenzene (**116**) (Tables 9.21 and A.2.2). On going from the non-associated species to paired spe-



non-associated:
 $n\text{-Pr}_4\text{N}^+$, DMF, 198 K [196]



ion-paired:
 Na^+ , DME, 298 K [620a]

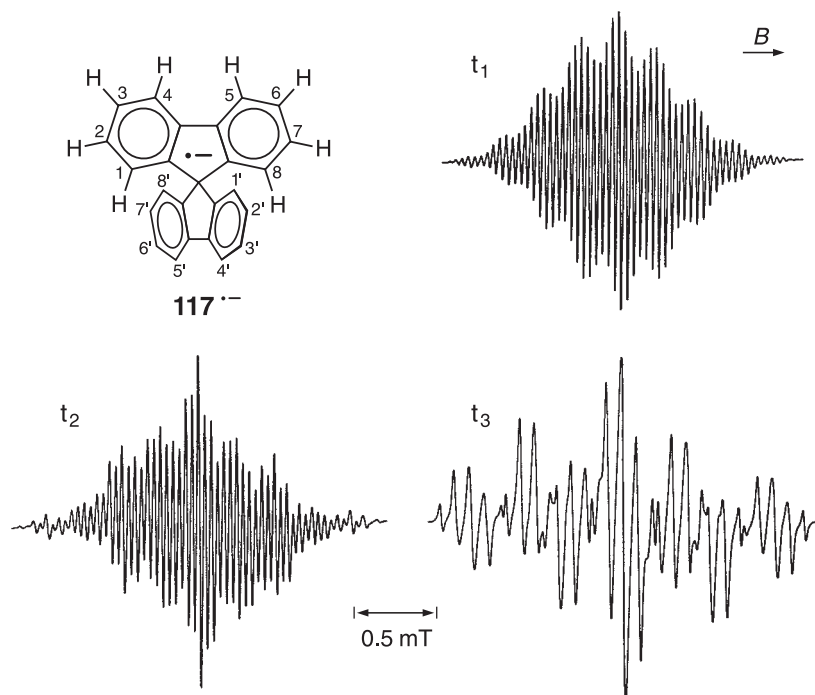


Fig. 6.22. ESR spectra of the radical anion of spirobifluorene (**117**) (the H atoms in one moiety are omitted for clarity). Solvent THF, counterion K^+ , temperature 213 K. The period,

t , of exposure to the potassium mirror increased in the order $t_1 < t_2 < t_3$. Hyperfine data in the text. Reproduced with permission from [141].

cies, the symmetry C_{2v} is lowered to C_s by an apparent partial spin localization on one nitro group, because in tight ion pairs, migration of the cation between the two groups is slow on the hyperfine time-scale.

Lowering of symmetry by spin localization, as a consequence of association with alkali-metal counterions, is also encountered with radical anions of hydrocarbons having two distinct and equivalent π moieties to accommodate the unpaired electron. This phenomenon is illustrated by the ESR spectra of the radical anion of bis(*o,o'*-biphenylene)methane (spirobifluorene; **117**) [141] (Figure 6.22). Prolonged reduction of the neutral compound by potassium in THF and, in consequence, a gradual increase in concentration of $117^{\bullet-}$ and K^+ , leads to conspicuous changes in the original hyperfine pattern (t_1) arising from four sets of four α protons: $a_{H1,1',8,8'} = +0.042$ or $+0.039$; $a_{H2,2',7,7'} = -0.266$; $a_{H3,3',6,6'} = +0.039$ or $+0.042$; $a_{H4,4',5,5'} = -0.193$ mT. With every second line decreasing in intensity (t_2), a final pattern (t_3) is obtained in which the number of lines is reduced from $5^4 = 125$ to $3^4 = 81$, due to interaction with four pairs of protons, albeit with coupling constants that are twice as large: $a_{H1,8} = +0.080$ or $+0.078$; $a_{H2,7} = -0.533$; $a_{H3,6} = +0.078$ or $+0.080$; $a_{H4,5} = -0.382$ mT. Clearly, protons of both biphenylene moieties contribute to the original hyperfine pattern, whereas only those of one moiety give rise to

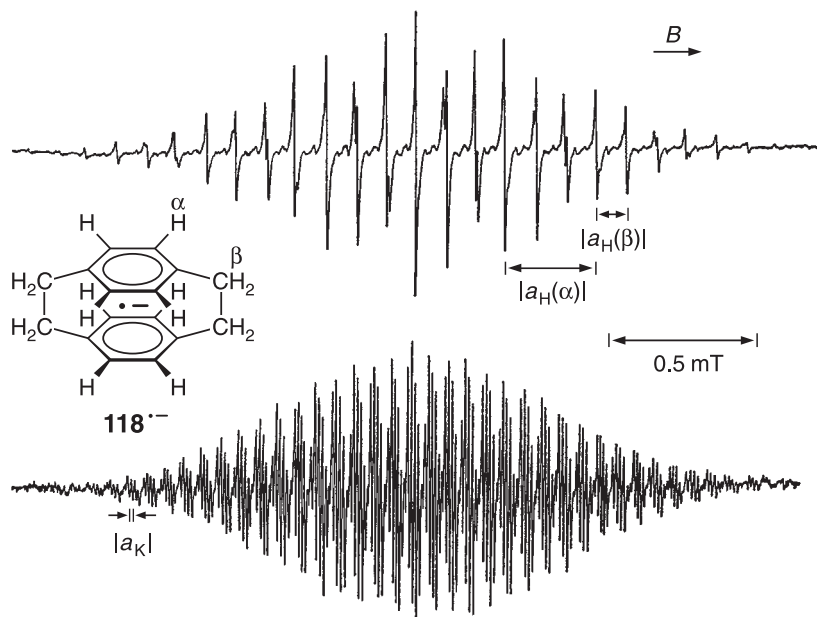


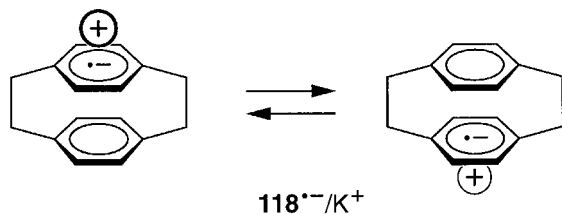
Fig. 6.23. ESR spectra of the radical anion of [2.2]paracyclophane (**118**). Top: solvent DME/HMPT (ca 40:1), counterion K^+ , temperature 188 K. Bottom: solvent THF, counterion K^+ , temperature 178 K. Hyperfine data in the text and Table 8.22. Reproduced with permission from [152].

the final pattern. Evidently, the symmetry is lowered from D_{2d} to C_{2v} by an apparent spin localization on this moiety. Although no ^{39}K -hyperfine splitting is detected, this finding signalizes a transition from loose to tighter ion pairs as the concentration increases, whereby the rate of migration of the cation is slowed to below the hyperfine time-scale. When MTHF is used as the solvent instead of THF and the solution is frozen after prolonged reduction with potassium, an ESR spectrum of a ground or low-lying triplet state of the dianion 117^{2-} is observed ($|D'| \approx 6$ mT), along with that of the tight ion pair $117^-/K^+$. In this triplet state, each biphenylene moiety takes up one unpaired electron and is associated with one K^+ .

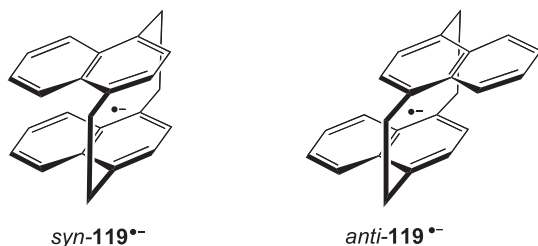
In [2.2]paracyclophane (**118**), two benzene rings rigidly face each other at a distance of ca 300 pm, so that its radical anion (Table 8.22) is an appropriate system in which to probe electron interaction. Figure 6.23 shows the spectrum of 118^- generated by reaction of the neutral compound with potassium in two different solvents [152, 621, 622]. The upper spectrum was taken with DME to which a small amount of HMPT was added to enhance its cation-solvating power. The relatively simple hyperfine pattern of this spectrum arises from a set of eight α protons at the two benzene rings with $a_H(\alpha) = -0.297$ mT and a set of eight β protons in the two methylene bridging groups with $a_H(\beta) = +0.103$ mT. The much more complex lower spectrum, taken with THF, exhibits $5^4 \cdot 4 = 2500$ instead of only $9^2 = 81$ lines, due to interaction with two sets of four α protons having $a_H(\alpha) = -0.378$ and -0.196 mT, two sets of four β protons with $a_H(\beta) = +0.127$ and $+0.068$ mT, and

one ^{39}K nucleus of the counterion with $|a_{\text{K}}| = 0.012$ mT. Note that the average of each pair of the four-proton coupling constants is almost equal to the corresponding two eight-proton values, and that the latter values seem to be subdivided in a ratio of ca 2:1 to yield the former values. Undoubtedly, the drastic change in the spectrum of $118^{\cdot-}$ on going from DME/HMPT to THF is caused by transition from a loose to a tighter ion pair, in which the symmetry is lowered from D_{2h} to C_{2v} by partial localization of the spin population on one moiety. The rate of migration of the cation between the two moieties, which determines this apparent spin localization, is fast on the hyperfine time-scale in the loose ion pairs and slow in the tighter pairs. In a DME/THF mixture the rate is comparable to this time-scale, which causes characteristic line-broadening in the ESR spectrum (Chapt. 6.7).

The K^+ counterion is too large to be placed in the center of $118^{\cdot-}$ inside the rings, although such a “sandwich” structure is esthetically appealing. To account for the lower symmetry C_{2v} , three pairs of structures are conceivable, in which the cation assumes an outside position on one of the three twofold C_2 axes of $118^{\cdot-}$ in the D_{2h} symmetry. Studies of $118\text{-}d_8^{\cdot-}$, in which one benzene ring and the two methylene groups linked to it are deuterated [621, 622], established that the preferred structure of the ion pair $118^{\cdot-}/\text{K}^+$ is the most expected one. In this ion pair, the cation is located on the C_2 axis perpendicular to the benzene rings, and it migrates between two equivalent positions above and below one ring.

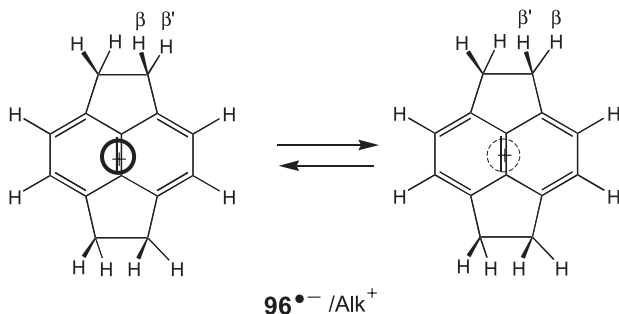


Ion pairs of similar structure were obtained for the radical anions of *syn*- and *anti*-[2.2](1,4)naphthalenophanes (*syn*-119 and *anti*-119) with K^+ as the counterion (Table 8.23) [142, 623].



A special case is that of the radical anion of pyracene (**96**) (Table 8.9), which has only one naphthalene π system to accommodate the unpaired electron. Upon going from DME to MTHF, with Na^+ or K^+ as the counterion, the hyperfine pattern of $96^{\cdot-}$ indicates a lowering of symmetry from D_{2h} to C_{2v} , due to transition

from a loose to a tighter ion pair [624]. This lowering does not involve spin redistribution, because the coupling constant (-0.163 mT) of the four α protons does not undergo marked changes due to the transition. The lowering of symmetry is caused by the eight methylene β protons, for which the coupling constant $a_{\text{H}}(\beta) = +0.658$ mT splits into two four-proton values $a_{\text{H}}(\beta_1) = +0.693$ and $a_{\text{H}}(\beta_2) = +0.637$ mT (with Na^+ , a ^{23}Na -splitting of 0.176 mT is observed). ESR studies of $96\text{-}d_2^{\cdot-}$ and $96\text{-}d_4^{\cdot-}$, in which one methylene or dimethylene group, respectively, is deuterated, indicate that the preferred sites of the cation are on the vertical twofold C_2 axis above or below the center of the naphthalene π system [625]. Thus, location of the cation at one of these sites makes the the four β protons above the molecular plane and those below it (β') nonequivalent. When the rate of migration of the counterion between the two sites is comparable to the hyperfine time-scale, as in the solvent THF, line-broadening effects are observed. These effects are considered in Chapt. 6.7.



Supplementary Notes

As mentioned in Chapt. 2.3, strong association with alkali-metal counterions favors formation of di- and trianions, which are associated with two and three cations, respectively. It also shifts the equilibrium $2\text{M}^{\cdot-} \rightleftharpoons \text{M} + \text{M}^{2-}$ to the right. In some studies, temporary association with two counterions was detected for radical anions like benzo-1,4-semiquinone ($19^{\cdot-}$), in which cations can be attached to both O atoms with lone electron pairs [626, 627]. For some ketyls, clusters consisting of two radical anions and two alkali-metal cations were reported [591, 618]. Two such counterions can be replaced by an alkaline-earth cation without, however, causing additional hyperfine splitting, because the most abundant isotopes of Mg, Ca, Sr, and Ba are nonmagnetic [591, 618]. Radical dianions [67, 188, 189] are associated with two positively charged counterions in equivalent or nonequivalent positions. Coupling constants of alkali-metal nuclei in such ion pairs of some radical dianions are given in Table A.2.3.

The nature of the alkali-metal used to generate a dianion in a triplet state has a strong effect on the zero-field parameters D and E by association with three pertinent counterions, although no hyperfine splitting by metal nuclei is resolved in the ESR spectra taken on solid matrices [175, 628].

In contrast to the radical anions, effects of ion pairing are rarely observed for radical cations [629–631], which are usually generated in polar solvents and have negatively charged counterions less appropriate for close association.

6.7 Intramolecular Dynamic Processes

As stated in Chapt. 1.4, line-widths in ESR spectra are primarily determined by electron relaxation times, T_{1e} of SLR and T_{2e} of SSR, where the latter is by far more effective for organic radicals without heavy atoms. Line-broadening by these mechanisms is denoted *homogeneous*, while it is called *inhomogeneous* when caused by other factors. The shape of the lines is reproduced better by the Lorentzian function for homogeneous broadening and by the Gaussian function for inhomogeneous broadening.

Inhomogeneous line broadening can arise by a lack of homogeneity in the magnetic field, by incompletely averaged-out g_e and/or hyperfine anisotropies (particularly in solid and viscous media; Chapt. 6.5), and by unresolved hyperfine splittings. For organic chemists, the most interesting causes of line-width effects are *dynamic*, i.e., time-dependent, phenomena which can be either *intermolecular* or *intramolecular*. Intermolecular phenomena comprise such processes as electron exchange between radicals and their diamagnetic precursors or products, which was considered in Chapt. 6.3. From the structural point of view, intramolecular phenomena are more informative. They involve processes in which the hyperfine pattern changes by time-dependent alterations in the coupling constants a_X . Usually, two equivalent forms, I and II, of a radical interconvert; the rate of their interconversion is the inverse of the lifetime, τ , of the individual forms I and II and is proportional to the difference in the coupling constants, $|a_X^I|$ and $|a_X^{II}|$ of a nucleus X in I and II.

$$\tau^{-1} \approx 2\pi(a_X^I - a_X^{II}) = 2\pi\gamma_e(|a_X^I| - |a_X^{II}|) \quad (6.3)$$

Eq. 6.3 complies with the uncertainty relation (Chapt. 1.4; Eq. 1.12). Differences $|a_X^I| - |a_X^{II}|$ of ca 0.006 to 0.6 mT correspond to a rate τ^{-1} of ca 10^6 to 10^8 s⁻¹, which is comparable to the hyperfine time-scale. The temperature range in which organic radicals are usually studied is 200 to 300 K. In this range, when $|a_X^I|$ and $|a_X^{II}|$ differ by less than ca 0.006 mT, they exhibit an averaged value, $|a_X| = (1/2)(|a_X^I + a_X^{II}|)$, of the two coupling constants. Temperatures below 200 K are then required to attain an interconversion rate slower than 10^6 s⁻¹, at which the two values can be distinguished. On the other hand, for $|a_X^I| - |a_X^{II}|$ larger than ca 0.6 mT, the temperature must be raised above 300 K to achieve an interconversion rate faster than 10^8 s⁻¹ and an average value $|a_X|$ of the two coupling constants. At temperatures where this rate is comparable to the hyperfine time-scale, “anomalous” hyperfine patterns can be observed.

Although, upon interconversion $I \rightleftharpoons II$, two nuclei X_1 and X_2 exchange their coupling constants a_{X_1} and a_{X_2} , they retain their spin quantum numbers $M_I(X_1)$ and $M_I(X_2)$, so that

$$a_{X_1}^I = a_{X_2}^{II} \quad \text{and} \quad a_{X_1}^{II} = a_{X_2}^I$$

but

$$M_I^I(X_1) = M_I^{II}(X_1) = M_I(X_1) \quad \text{and} \quad M_I^I(X_2) = M_I^{II}(X_2) = M_I(X_2)$$

The position of a hyperfine line relative to the center of the spectrum can thus be specified as

$$a_{X_1} M_I(X_1) + a_{X_2} M_I(X_2) \quad \text{in I}$$

$$a_{X_2} M_I(X_1) + a_{X_1} M_I(X_2) \quad \text{in II}$$

The contribution to the line-width, $(\Delta\nu)_{\text{exch}} = \gamma_e(\Delta B)_{\text{exch}}$, due to the $I \rightleftharpoons II$ interconversion depends on the shift:

$$\begin{aligned} & [a_{X_1} M_I(X_1) + a_{X_2} M_I(X_2)] - [a_{X_2} M_I(X_1) + a_{X_1} M_I(X_2)] \\ & = (a_{X_1} - a_{X_2}) [M_I(X_1) - M_I(X_2)] \end{aligned}$$

For fast interconversion, the line-width is proportional to the lifetime τ and the square of this shift

$$(\Delta\nu)_{\text{exch}} \propto (\tau \cdot \gamma_e^2) (a_{X_1} - a_{X_2})^2 [M_I(X_1) - M_I(X_2)]^2 \quad (6.4)$$

in which $M_I(X_1)$ and $M_I(X_2)$ have to be replaced by $\sum M_I(X_1)$ and $\sum M_I(X_2)$ if there are more than two nuclei exchanging their coupling constants a_{X_1} and a_{X_2} . Figure 6.24 shows hyperfine patterns undergoing a $I \rightleftharpoons II$ interconversion for two pairs of nuclei X_1 and X_2 with $I = 1/2$, e.g., protons i.e. with $\sum M_I(X_1)$ and $\sum M_I(X_2)$ each of $+1$, 0 , and -1 . It is evident that the hyperfine lines exhibiting the largest differences $|\sum M_I(X_1) - \sum M_I(X_2)|$ are subjected to the most extensive shifts and to the most pronounced broadening, as required by Eq. 6.4. Only the three lines of which positions and associated numbers $\sum M_I$ are unchanged remain narrow when the interconversion rate τ^{-1} is comparable to the hyperfine time-scale. These lines can always be observed in the ESR spectrum, whereas the other six are often broadened beyond recognition. The relative intensities of the three lines are then 1:4:1, and their separation is $|a_{X_1} + a_{X_2}|$, i.e., it is $|a_{X_1}| + |a_{X_2}|$ or $|a_{X_1}| - |a_{X_2}|$, according to whether the two coupling constants have the same or opposite signs; the former situation is by far more frequently encountered.

One does not often come across ESR studies in which hyperfine patterns with both distinct and averaged coupling constants a_{X_1} and a_{X_2} are observed, because they require temperatures beyond the usual range of 200 to 300 K.

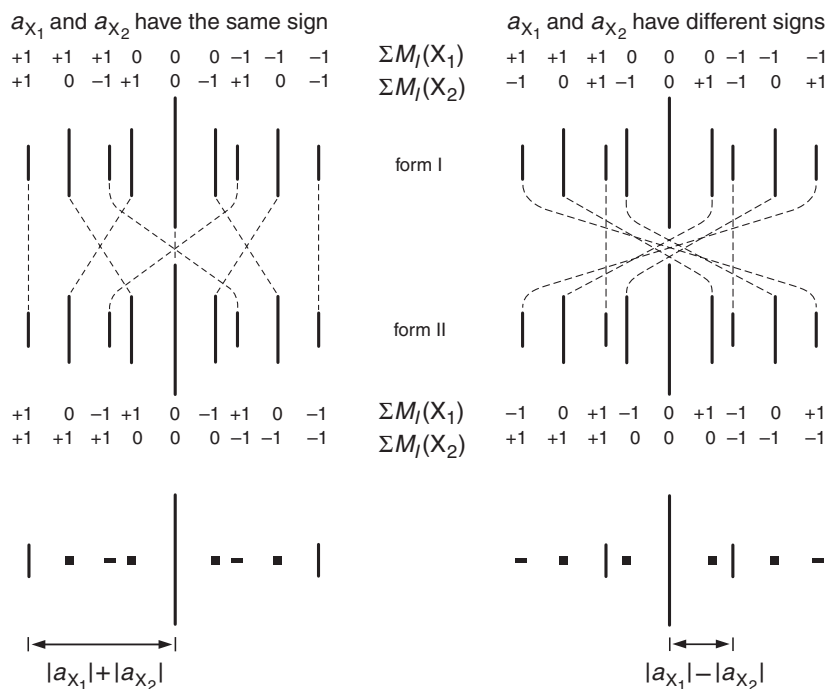


Fig. 6.24. Line-broadening due to exchange of coupling constants a_{X_1} and a_{X_2} of two nuclei with $l = 1/2$ when two equivalent forms I and II interconvert with a rate comparable to the hyperfine time-scale.

Conformational Interconversion

Due to its extraordinary persistence, the 1,2,3-trihydropyrenyl radical (120^{\bullet}) (Table 8.4) [89], of which ESR spectra are displayed in Figure 6.25, is amenable to studies in a temperature range extending from 200 K to as high as 600 K. This radical is 1,9-trimethylenephthalenyl, and, accordingly, the coupling constants of the α protons in 120^{\bullet} , $a_{H_{3,7}} = a_{H_{4,6}} = -0.614$ and $a_{H_{2,8}} = a_{H_5} = +0.174$ mT, are similar to the corresponding values, -0.629 and $+0.181$ mT, for phenalenyl (4^{\bullet}). The trimethylene chain bridging two π centers undergoes a half-chair-like conformational interconversion, by which the two pairs of β protons and the two γ protons exchange their coupling constants for the quasi-axial and quasi-equatorial positions. However, the difference $|a_{H_{ax}}(\gamma)| - |a_{H_{eq}}(\gamma)|$ for the two γ protons is too small to be observed on the hyperfine time-scale at temperatures as low as 203 K, and only the averaged coupling constant, $\bar{a}_{H(\gamma)} = \pm 0.047$ mT (sign undetermined), is apparent. The striking temperature dependence of the spectrum of 120^{\bullet} upon conformational interconversion is caused by the exchange of the coupling constants, $a_{H_{ax}}(\beta) = +1.197$ and $a_{H_{eq}}(\beta) = +0.299$ mT, of the two pairs of β protons. At 203 K, these values can be clearly distinguished, and they contribute $3^2 = 9$ components to the hyperfine pattern consisting of $3^6 \cdot 2 = 1458$ lines. On raising

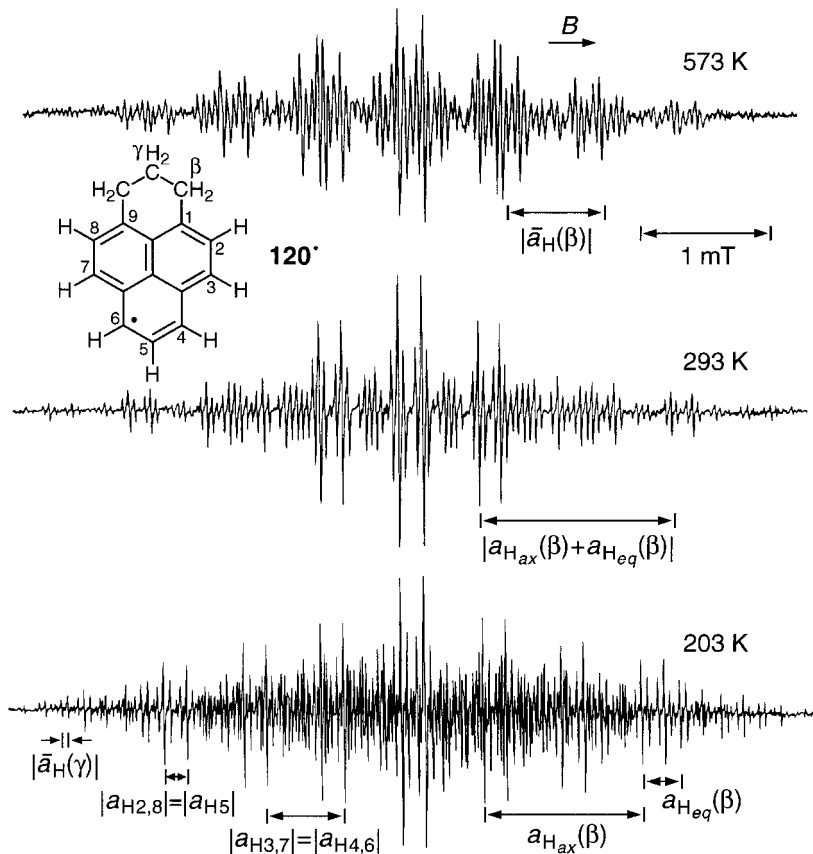


Fig. 6.25. ESR spectra of the 1,2,3-trihydropyrenyl radical ($120'$). Solvent 1-bromonaphthalene (top and center) and DME (bottom). Temperatures as indicated. Hyperfine data in the text and Table 8.4. Reproduced with permission from [89].

the temperature, characteristic line-broadening sets on, and, at 293 K, one observes a typical anomalous hyperfine pattern with the 1:4:1 intensity ratio of lines associated with the coupling constants of the β protons. These lines are spaced by the sum $|a_{H_{ax}}(\beta) + a_{H_{eq}}(\beta)| = 1.496$ mT, and the total number of lines is apparently reduced by 3 to $3^5 \cdot 2 = 486$. Heating the solution leads to averaging of these $a_H(\beta)$ values, and, at 573 K, the spectrum exhibits hyperfine pattern for four seemingly equivalent β protons, with the coupling constant $\bar{a}_H(\beta) = +0.719$ mT, which contributes 5 components to the $5 \cdot 3^4 \cdot 2 = 810$ lines. The somewhat smaller value of $\bar{a}_H(\beta)$ relative to the expected one of $(1/2)[a_{H_{ax}}(\beta) + a_{H_{eq}}(\beta)] = (1/2)(+1.197 + 0.299)$ mT = +0.748 mT, is due to a change in solvent and temperature on going from DME at 203 to 1-bromonaphthalene at 573 K.

According to Eq. 4.9 for β protons, the ratio, $a_{H_{ax}}(\beta)/a_{H_{eq}}(\beta) = +1.197$ mT / +0.299 mT = 4, should be equal to $\langle \cos^2 \theta_{ax} \rangle / \langle \cos^2 \theta_{eq} \rangle$, where θ_{ax} and θ_{eq} are

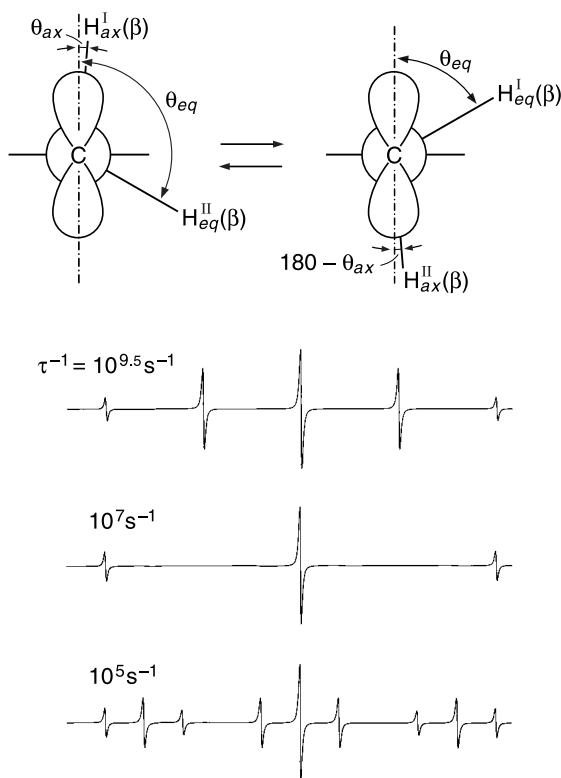


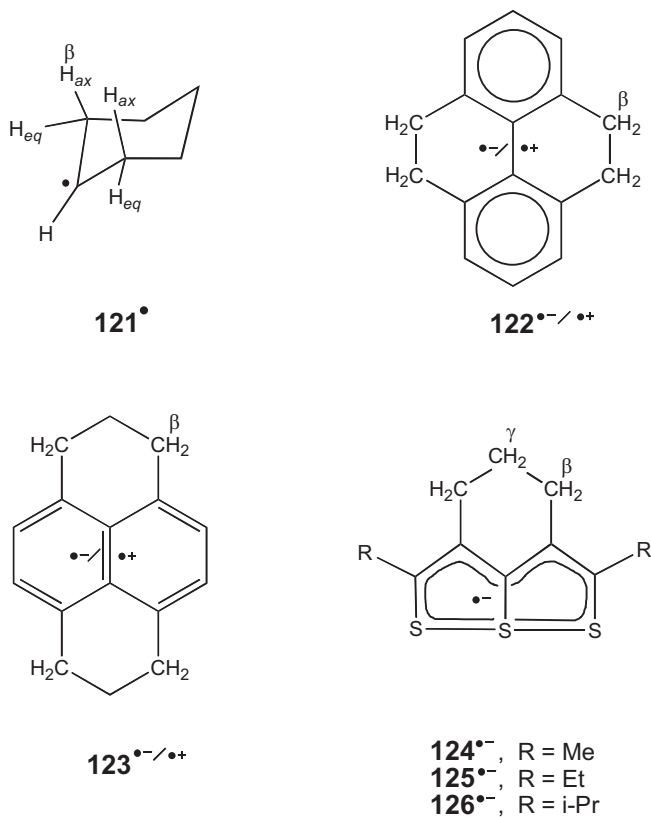
Fig. 6.26. Top: Newman projections in the direction of a $C_{\mu'}-CH_2(\beta)$ bond in the 1,2,3-trihydropyrenyl radical (**120'**) showing the changes in the dihedral angles θ_{ax} and θ_{eq} upon conformational interconversion. Below: computed hyperfine patterns for various rates, τ^{-1} , of this interconversion.

the dihedral angles between the $2p_z$ axes at the bridged π centers and the directions of the $C-H_{ax}(\beta)$ and $C-H_{eq}(\beta)$ bonds; this is because both coupling constants are proportional to the spin population $\rho_{\mu'}^{\pi}$ at the bridged centers μ' . Taking into account that the sum $\theta_{ax} + \theta_{eq}$ must be close to 120° , we arrive at $\langle \cos^2 \theta_{ax} \rangle \approx 1$ and $\langle \cos^2 \theta_{eq} \rangle \approx 0.25$, with $\theta_{ax} \approx 0$ and $\theta_{eq} \approx 120^\circ$ in one conformation and $\theta_{ax} \approx 180$ and $\theta_{eq} \approx 60^\circ$, in the other, as depicted at the top of Figure 6.26. When the two coupling constants of the β protons in **120'** are inserted into Eq. 4.9, together with $\rho_{\mu'}^{\pi} = +0.225$ as the spin population at the corresponding centers in **4'** (Chapt. 4.2), the parameter $B_H^{C_{\mu'}, CH_{\mu'}} = +5.3$ mT is obtained, which lies in the range appropriate for neutral π radicals.

The derivative curves calculated by a computer program [632] for two coupling constants in the ratio $a_{H_{ax}(\beta)}/a_{H_{eq}(\beta)} = 4$ are reproduced in Figure 6.26 for exchange rates, τ^{-1} , of 10^{-5} , 10^{-7} and $10^{-9.5}$ s^{-1} , which correspond to the hyperfine patterns due to $a_{H_{ax}(\beta)}$ and $a_{H_{eq}(\beta)}$ and observed for **120'** at 203, 293, and 573 K, respectively. Using the Arrhenius plot of $\log(\tau^{-1})$ vs $1/T$, the activation bar-

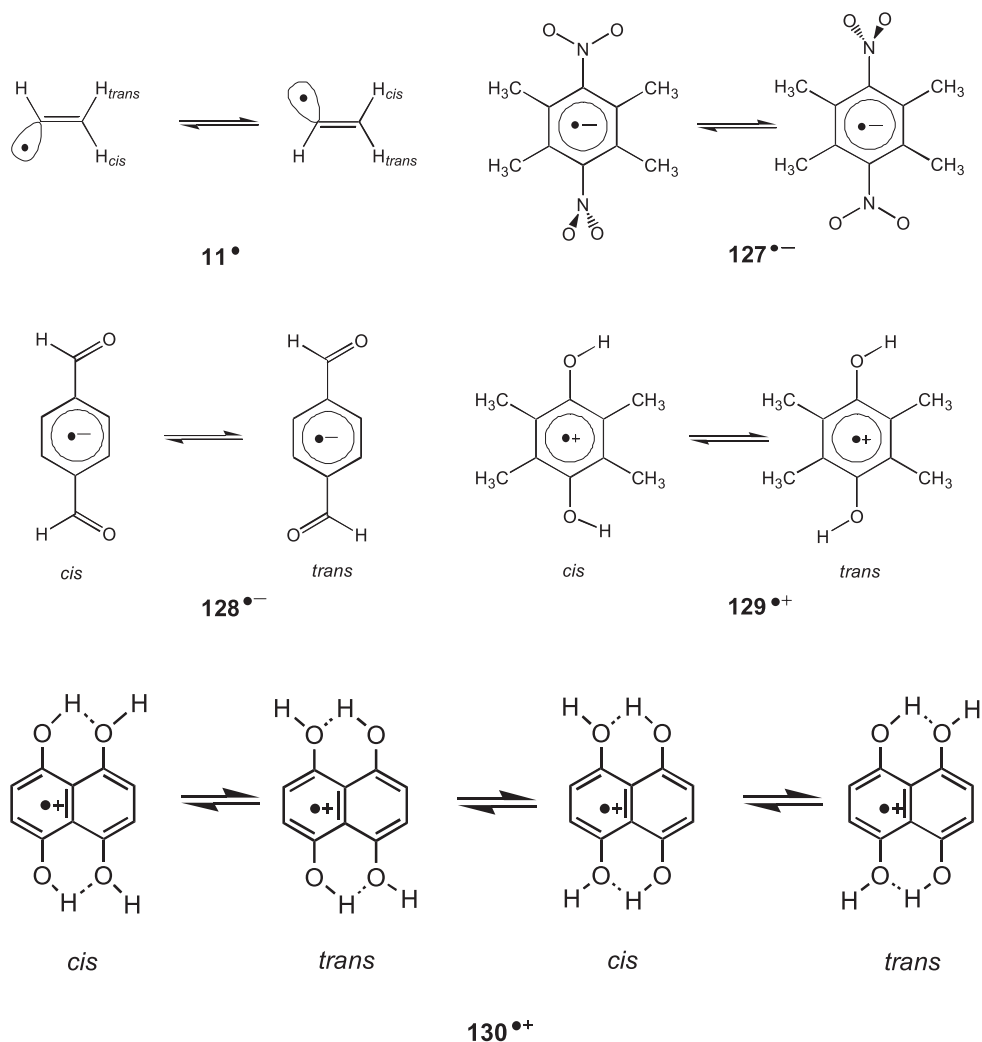
rier for the interconversion of the trimethylene chain in 120^{\bullet} is estimated as $27 \text{ kJ}\cdot\text{mol}^{-1}$.

Exchange of the coupling constants of methylene β protons for quasi-axial and quasi-equatorial positions has often been observed in ESR spectra upon conformational interconversion of π radicals. Some early examples were the cyclohexyl radical (121^{\bullet}) (Table 7.2) [633], as well as both radical ions of 4,5,9,10-tetrahydropyrene (122) [634, 635] and 1,2,3,6,7,8-hexahydropyrene (123) (Table 8.9) [636], and the radical anions of some derivatives, 124 (Table 9.12)– 126 , of 6a-thiathiophenes [209].



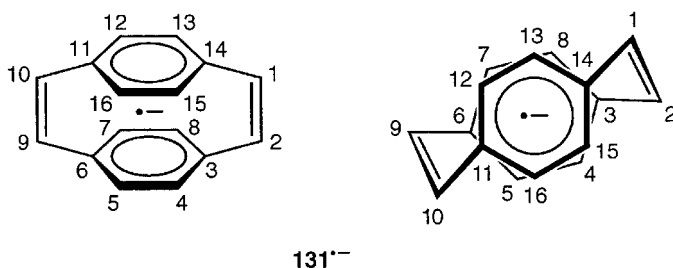
Other conformational interconversions, such as those of *cis* and *trans* isomers, due to restricted rotation about a single bond, have also been investigated by ESR spectroscopy. Examples are the radical anions of dinitrodurene (127) (Table 9.21) [637] and terephthalaldehyde (128) (Table 9.14) [638, 639] in DMF (i.e., not associated with their counterions), and the radical cations of dihydroxydurene (129) (Table 9.36) [640] and 1,4,5,8-tetrahydroxynaphtalene (130) (Table 9.37) [641]. For $128^{\bullet-}$, $129^{\bullet+}$, and $130^{\bullet+}$, four isomers, two *cis* and two *trans*, exist, and the inter-

conversions may be considered a *four-jump* process, in contrast to the *two-jump* processes considered thus far. Such four-isomer sets are shown below for $130^{+\bullet}$. The vinyl radical (11^\bullet) of σ structure (Table 7.9) also undergoes *cis-trans* interconversion [34] which is, however, configurational and not conformational, because it is due to restricted rotation about the double bond.



An unexpected conformational interconversion was observed for the radical anion of [2.2]paracyclophane-1,9-diene (131) (Table 8.22). Although, in contrast to the radical anion of [2.2]paracyclophane (118), the ESR spectrum of $131^{•-}$ [642]

does not exhibit observable effects of association with alkali-metal counterions, it is strongly temperature-dependent, due to interconversion of two conformations I and II. The interconversion does not affect the coupling constant, -0.422 mT, arising from the four olefinic α protons in the 1,2,9,10-positions of the bridging ethylene groups. This finding and the results of an ESR study on the radical anion $131\text{-d}_6^{\cdot-}$, in which one moiety (positions 2, 4, 5, 7, 8, and 9) was deuterated, indicate that two sets of four α protons, one pair in each benzene ring, exchange their coupling constants ± 0.046 and ∓ 0.020 mT. Two features of this exchange are noteworthy: First, due to the rather small difference, 0.026 mT, of the two $|a_{\text{H}}|$ values, hyperfine patterns characteristic of slow, intermediate, and fast exchange can be observed in the temperature range of 178 to 273 K at an interconversion rate τ^{-1} of 10^5 to $3 \cdot 10^8$ s $^{-1}$. Second, the two values represent a rather rare case in which the coupling constants involved in the exchange have opposite signs (see also [643]). This finding is indicated by the anomalous hyperfine pattern, in which the pertinent lines are spaced by the difference of the two absolute values and not by their sum. Such a pattern is also in accordance with the very small average value of the coupling constants of the eight protons, $\bar{a}_{\text{H}} = (1/2)(\pm 0.046 \mp 0.020)$ mT = ± 0.013 mT.



The two interconverting conformations of $131^{\cdot-}$ are assumed to have D_2 symmetry, in which the two benzene rings are twisted by 5° in opposite directions about the twofold C_2 axis perpendicular to the rings. The two sets of four α protons exchanging their coupling constants are those in positions 4, 7, 13, 16 and 5, 8, 12, 15. An Arrhenius plot yields an energy barrier of 33 kJ \cdot mol $^{-1}$ for the interconversion.

In some ESR spectra of two forms I and II, which interconvert at a rate τ^{-1} comparable to the hyperfine time-scale, *alternating line-widths* are observed, as narrow single components or groups of lines alternate with broadened ones. Such spectra are illustrated in Figure 6.27 by the ESR spectrum of the radical anion of dinitrodurene (127) in DMF (counterion $i\text{-Pr}_4\text{N}^+$) [637], for which the line-width effects are caused by modulation of the coupling constant of the ^{14}N nuclei in the two nitro groups. The activation barriers are in the range of 20 to 35 kJ \cdot mol $^{-1}$.

Note that intramolecular dynamic processes such as conformational interconversion must have activation barriers higher than 40 kJ \cdot mol $^{-1}$ in order to be studied by $^1\text{H-NMR}$ spectroscopy. This is because the pertinent differences in

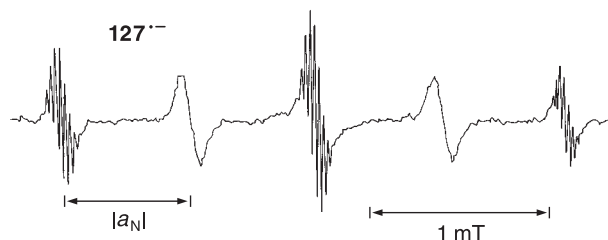


Fig. 6.27. ESR spectra of the radical anion of dinitrofluorene (**127**) (structural formulas in text). Solvent, DMF counterion Et_4N^+ , temperature 298 K. Hyperfine data in Table 9.21. Reproduced with permission from [637].

chemical shifts δ are ca 1 ppm, which corresponds to an interconversion rate τ^{-1} of only 100 s^{-1} for a 100 MHz-spectrometer. The NMR time-scale is thus 4 to 6 orders of magnitude less than that the hyperfine time-scale, a fact which requires higher activation barriers in order to observe processes in an accessible temperature range.

Jahn-Teller Effect

The theorem bearing this name predicts that, to lower its energy, a nonlinear molecule in a degenerate ground-state will deform to species in which the symmetry is reduced and the degeneracy is removed. Such molecule is a neutral radical or a radical ion, like the benzene anion $\mathbf{62}^{\bullet-}$, which has an axial symmetry, i.e., a rotational axis C_n with $n \geq 3$. In general, for each radical, two or more deformed species of lower symmetry (“Jahn–Teller species”) must be considered, which differ in their geometry, symmetry, and spin distribution. Because these species have the same or nearly the same energy, they interconvert rapidly on the hyperfine time-scale (“dynamic Jahn–Teller effect”), so that the higher axial symmetry does not appear to be reduced in the observed ESR spectrum (effective symmetry). As mentioned in Chapt. 5.2, the Jahn–Teller effect is then often revealed by broadening of the ESR lines, which saturate at higher than usual MW intensities.

Occasionally, a Jahn–Teller species can be stabilized and its ESR spectrum observed under particular conditions (“static Jahn–Teller effect”). For example, such spectra have been reported for the radical cation of benzene (D_{6h} symmetry of $\mathbf{62}^{\bullet+}$ reduced to D_{2h}) [644] and for radical cations of saturated hydrocarbons of axial symmetry (Chapt. 10.1), when $\mathbf{62}^{\bullet+}$ and these radical cations were generated by γ -irradiation in Freon matrices at very low temperatures.

Electron Transfer and Counterion Migration

Intramolecular transfer of an electron between a donor and an acceptor connected by a spacer can be induced thermally, photolytically, and radiolytically, and its rate depends on the distance and orientation of the two π systems involved. ESR spec-

troscopy seems to be a tool of choice for investigating electron transfer in paramagnetic species, because the pertinent rate often lies within the hyperfine time-scale of 10^6 to 10^8 s⁻¹. Consequently, this technique has been applied to radical anions containing two equivalent moieties and a spacer. One of the moieties accommodating the unpaired electron functions as a donor, while the other, the neutral moiety, is an acceptor. In interpreting the results of such ESR studies, special care must be paid to the experimental conditions, to assure that the observed rate of spin redistribution really represents that of true electron transfer. Generally, because of the association of the radical anion with its counterion, the rate of electron transfer is governed by the synchronous migration of the counterion between preferred sites at the two equivalent moieties of the radical anion. Raising the temperature need not give rise to a higher electron-transfer rate, because it decreases the cation-solvating power of the solvent, thus strengthening the association and slowing the migration of the counterion.

An example of this kind was presented in Chapt. 6.6 by the radical anion of [2.2]paracyclophane (**118**), in which the electron-spin transfer between the two benzene rings follows the cation migration between two sites above and below one ring. The two dimethylene bridging groups do not really serve as spacers, because the unpaired electron is more readily transferred directly via the π -electron clouds of the two rings, which are separated by only ca 300 pm.

A further example is provided by the radical anion of *cis*-10,11-dimethyldi-phensuccindan-9,12-dione (**132**), in which two acetophenone-like moieties are joined by C–C single bonds acting as spacers [215]. Reaction of **132** with potassium in ethereal solvents leads to a radical anion, in which the counterion K⁺ is tightly attached to the lone pair of the O atom in one moiety. A partial spin localization on this moiety is displayed in Figure 6.28 in the spectrum of **132**^{•-} in DME with the counterion K⁺ (bottom left). The coupling constants of the four single α protons in one moiety, $a_{H1} = +0.106$, $a_{H2} = -0.544$, $a_{H3} = +0.077$, and $a_{H4} = -0.394$ mT, are much larger than their counterparts, $a_{H5} = +0.028$, $a_{H6} = -0.082$, $a_{H7} = +0.009$, and $a_{H8} = -0.028$ mT, in the other moiety (assignments and signs as required by theory). Splitting by the alkali-metal nucleus is not observed even if DME is replaced by THF or MTHF and K⁺ by Li⁺ or Na⁺. A dramatic change in the hyperfine pattern occurs when a substantial amount of HMPT (ca 1/3 per volume) is added to the solution of **132**^{•-} in DME, as demonstrated by the spectrum shown in the upper left of Figure 6.28. The counterion is now preferably surrounded by molecules of HMPT with its high cation-solvating power, and the association of K⁺ with the radical anion is so weakened that the rate of counterion migration becomes fast on the hyperfine time-scale; the spectrum then exhibits coupling constants, $a_{H1,5} = +0.059$, $a_{H2,6} = -0.312$, $a_{H3,7} = +0.040$, and $a_{H4,8} = -0.193$ mT, for pairs of α protons (some deviations from the averages of the values given above for the single protons are again due to the change in solvent).

For the electrolytically generated radical anion **132**^{•-} in DMF with Et₄N⁺ as the counterion, where ion pairing plays only a secondary role, studies in the range 193 to 298 K revealed a clear-cut dependence of the rate of counterion migration on temperature (addition of a small amount of ACN prevented freezing of the solu-

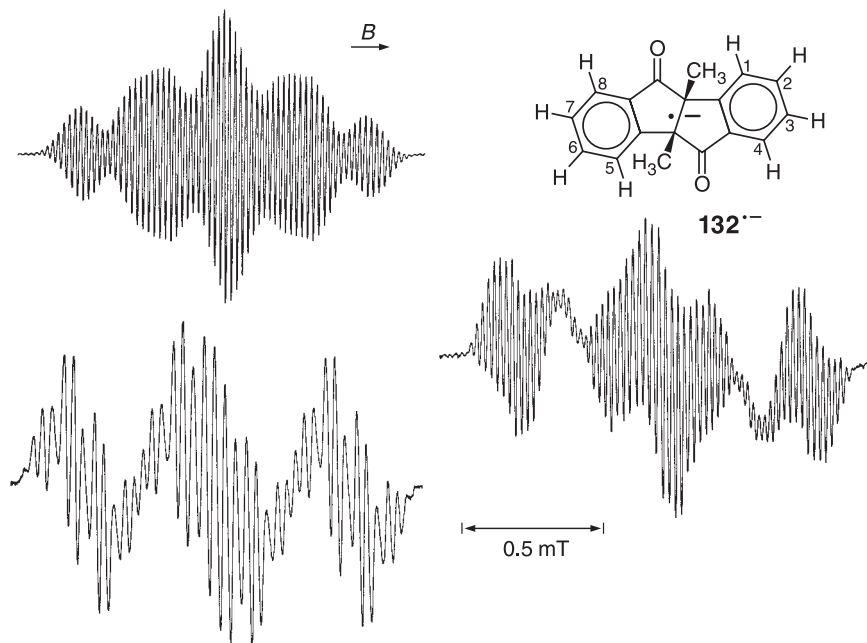
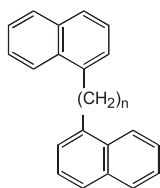
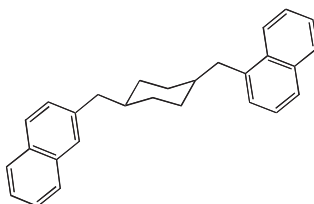


Fig. 6.28. ESR spectra of the radical anion of *cis*-10,11-dimethyldiphensuccindan-9,12-dione (**132**), Solvent, counterion, and temperature as follows: top left: DME/HMPT 2:1, K^+ 183 K;

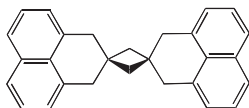
bottom left: DME, K^+ , 183 K; right: DMF, Et_4N^+ , 213 K. Hyperfine data in the text. Reproduced with permission from [215].

tion below 210 K). This rate varied from $5.3 \cdot 10^6$ at 193 K to $3.5 \cdot 10^8$ at 253 K, and an Arrhenius plot yielded an activation barrier of $29 \text{ kJ} \cdot \text{mol}^{-1}$. At the temperature where the rate is comparable to the hyperfine time-scale characteristic patterns were observed, as illustrated in Figure 6.28 (right) for the rate $2.8 \cdot 10^7 \text{ s}^{-1}$ at 213 K. Above 253 K, the rate is fast enough to give rise to a spectrum resembling that observed with DME/HMPT and diagnostic of spin delocalized over both moieties.

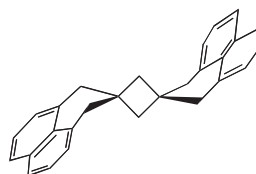
To determine the dependence of electron transfer on the donor–acceptor distance, several ESR studies were performed on radical anions in which two equivalent moieties are connected by spacers of various lengths. In most of these studies, the moieties were represented by naphthalene π systems linked by spacers, for which rigidity increases in the sequence **133** [9d, 645, 646] < **134** [647] < **135** [423] < **136** [424]. Each of the formulas **135** and **136** stands for a series of three compounds additionally specified by (1), (2), and (3); those in the **135** series can exist in experimentally non-separable *syn* and *anti* conformations. The distances between centers of the two naphthalene π systems are estimated as 740, 1190, and 1640 pm in the *syn* conformation of **135**(1), **135**(2), and **135**(3), respectively; for their *anti* counterparts these distances are 880, 1280, and 1710 pm. In the series **136**(1), **136**(2), and **136**(3), the analogous values are 630, 800, and 1030 pm.

133, $n = 3-6, 8, 10, 12$ 

134



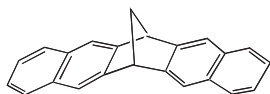
135 (1)

*syn*-135 (1)*anti*-135 (1)

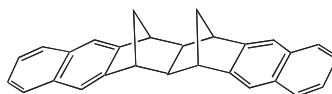
135 (2)



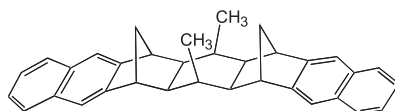
135 (3)



136 (1)



136 (2)



136 (3)

The radical anions of all six compounds **135** and **136** were generated by reaction with potassium in DME, MTHF, and mixtures of DME with HMPT, and they were investigated by ESR and ENDOR spectroscopy in the range 200 to 290 K. The hyperfine patterns of **135(1)**^{•-} in DME and MTHF, as well as those of **135(2)**^{•-} and **135(3)**^{•-} in all these solvents, indicated spin localization on one naphthalene moiety. The ESR and ENDOR spectra of **135(1)**^{•-} in DME/HMPT (1:3) revealed the occurrence of a radical anion, in which the spin population is delocalized over both moieties. In the second series, the hyperfine pattern of **136(1)**^{•-} resembled that of

the radical anion of binaphthylene, irrespective of the solvent, so that **136(1)**^{•-} can be considered a homo derivative of the latter, with the spin population homonjugatively delocalized through two C–C single bonds. The two larger radical anions **136(2)**^{•-} and **136(3)**^{•-} exhibited greater dependence on the solvent. With MTHF, spin localization in one moiety is found exclusively, but with DME and DME/HMPT, radical anions exhibiting localized spin population and those having this population delocalized over both moieties coexist in solution. Thereby, as expected, the radical anions with spin localization are more favored in **136(3)**^{•-} than in **136(2)**^{•-}. In each study, concentration of the radical anions exhibiting spin localization increased upon prolonged contact of the solution with potassium, but it decreased in favor of the radical anions with delocalized spin population when the proportion of HMPT in the solvent was increased.

The results for the radical anions in both series, **135**^{•-} and **136**^{•-}, suggest that the rate of electron transfer in such radical anions containing two π moieties connected by spacer is dependent on the synchronous counterion migration, even in solvents of high cation-solvating power and in the absence of appreciable ion pairing. This rate can exceed 10^7 s^{-1} when a rigid spacer with as many as 6 C–C single bonds holds the two π systems at a distance farther than 700 pm.

ESR spectra of dianions in a ground- or low-lying triplet state were observed for **135(1)**, **136(2)**, and **136(3)** in frozen MTHF upon prolonged contact of the compounds with potassium [423, 424]. The zero-field splittings for nearly axial tensors **D** of the triplet dianions **135(1)**^{••2-}, **136(2)**^{••2-}, and **136(3)**^{••2-} are $|D'| = 4.7, 5.7,$ and 2.5 mT, respectively, in accord with the distances (given above) between the centers of the two naphthalene moieties (Eq. 2.7). This accord indicates that each of the two moieties accommodates one unpaired electron.

B Special Part

This part, consisting of Chapt. 7.1 through 11.3 and the Appendix, is a review of the vast field of organic radicals that have been studied by ESR spectroscopy. Needless to say, the hyperfine data given in this review and characteristic of representative radicals are only an infinitesimal fraction of their total number; a comprehensive collection is being published elsewhere [18]. All coupling constants, a_X , of the nuclei X listed in the Tables are isotropic values in mT, unless otherwise stated. Signs have been allotted to them when it is obvious and verified by experiment and/or theory. Absolute values $|a_X|$ without a sign are quoted when the sign is not certain.

7

Organic Radicals Centered on One, Two, or Three Atoms

It is often difficult to unequivocally classify organic radicals as centered at specific atoms. Clearly, a radical should be regarded as centered on a restricted number of C or heteroatoms if the bulk of the spin population resides on these atoms. However, how should “bulk” be interpreted? As more than 50% or as much as 90% of the spin population?

Alkyl radicals of the general formula $R^1R^2R^3C^\cdot$ meet the condition for C-centered species when R^i are H atoms or an alkyl group. The classification as such alkyl radicals becomes less secure when the C^\cdot atom is linked to a heteroatom. Radical anions of alkylaldehydes or alkylketones, $R^1R^2CO^\cdot$, can still be considered C-centered (Chapt. 7.1), because the unpaired electron is preferentially accommodated by the C atom of the electron-accepting $>C=O$ group, according to the formula $R^1R^2C^\cdot-O^-$. This preference is even accentuated in the protonated radical anions of such compounds, $R^1R^2C^\cdot-OH$, which may be called C-centered hydroxyalkyl radicals. On the other hand, in the radical cations of aldehydes and ketones, $R^1R^2C=O^{+\cdot}$, the unpaired electron is localized on the O atom, so that these species should be treated as O-centered.

Similar ambiguity also exists in other classes of organic radicals. For example, alkylsulfinyl radicals can be formulated as S-centered, according to the formula $R-S^\cdot=O$. In Chapt. 7.5, however, classification as SO-centered is preferred, considering the large share of the O atom in the spin population, and to differentiate them from the alkylthiyl radicals $R^1R^2S^\cdot$.

Despite the presence of a conjugated π system, some σ radicals, such as aryls, arylimines and aryliminoxyls, are also classified as C-, N-, and NO-centered, respectively, because the spin population is largely restricted to one or two AOs bearing the unpaired electron (Chapt. 7.1).

7.1

C-, N-, and O-centered Radicals

Alkyl Radicals

These C-centered radicals may be considered to be derivatives of methyl H_3C^\cdot (58') in which the unpaired electron is accommodated in the $2p_z$ -AO of the C atom

(Chapt. 4.1). The *acyclic* alkyl radicals $R^1R^2R^3C^\cdot$ have one ($R^1 = R^2 = H$), two ($R^1 = H$), or all three H atoms of H_3C^\cdot substituted by alkyl groups R^i , but in *cyclic* alkyl radicals, the spin-bearing C $^\cdot$ atom is incorporated into one or more rings. According to whether the bonds to one, two, or three H atoms in H_3C^\cdot are replaced by bonds to C or other atoms, one speaks about *primary*, *secondary*, or *tertiary* alkyl radicals, respectively.

A feature relevant to the structure and hyperfine data of alkyl radicals is the geometry at the radical center C $^\cdot$. Diagnostic of a planar geometry at C $^\cdot$ are the coupling constants of the α protons linked to C $^\cdot$ and those of the ^{13}C isotopes in this atom. The pertinent values are $a_H = -2.304$ and $a_C = +3.834$ mT for the planar methyl **58'**, which is considered to be a π radical with its spin population localized in the $2p_z$ -AO of C $^\cdot$, the "single π center" (Chapt. 4.1). Increasing deviations from planarity ("pyramidalization") at this center imply a growing s-contribution to the spin-bearing orbital of C $^\cdot$, i.e., a gradual transition from a $2p_z$ -AO to a sp^n -hybrid or, in general, from a π - to a σ -type radical. The implications of such a transition are considered in Chapt. 4.3. Because the s contribution to the coupling constants is positive throughout, the a_H values of the α protons at C $^\cdot$ become less negative. Thus, their absolute values first decrease with enhanced pyramidalization, and, after reaching zero, increase continuously, because the coupling constants turn positive. In contrast, because the coupling constants of the ^{13}C isotope in C $^\cdot$ are positive for planar geometry, both a_C and its absolute value steadily increase with enhanced pyramidalization. The tendency of an alkyl radical to achieve planar geometry at C $^\cdot$ is in some radicals counteracted by electronic and/or steric factors.

Hyperfine data for several acyclic alkyl radicals are given in Table 7.1 [34, 38, 54, 438, 482, 553, 648–650]. The two simplest radicals, methyl (**58'**) and ethyl (**59'**), are dealt with in Chapt. 4.1. Like **58'**, alkyl radicals are usually planar at the spin-bearing C $^\cdot$ atom. On going from *n*-butyl (**137'**) to *n*-pentyl (**138'**) and *n*-hexyl (**139'**), the coupling constants of the methylene α , β , and γ protons do not markedly change. Substitution of H atoms in H_3C^\cdot by any group R^i ($i = 1-3$) that does not impair the planarity lowers the $|a_H(\alpha)|$ value of the coupling constant, because the $2p_z$ -spin population at C $^\cdot$ decreases according to the formula

$$\rho_C^{2p} = \prod_i [1 - \Delta(R^i)] \quad (7.1)$$

where $\Delta(R^i)$ is a parameter characteristic of the substituent R^i . $\Delta(R^i)$ values of 0.081, 0.148, and 0.160 were suggested for $R^i = CH_3$, CN, and OH, respectively [651].

Slight deviations from planarity were considered for the *tert*-butyl radical (**141'**) [652], because its coupling constant, $a_C = +4.52$ mT, exceeds the corresponding value for **58'**. More striking is the gradually enhanced pyramidalization at the C $^\cdot$ atom with successive substitution of H by F atoms. On passing from **58'** to its mono- (**144'**), di- (**145'**), and trifluoro- (**87'**) derivatives, the coupling constant a_C increases from +3.83 to +5.48, +14.88, and +27.16 mT, respectively; the last value corresponds to sp^3 -hybridization of the C atom (Chapt. 4.3). The coupling con-

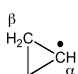
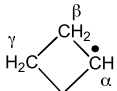
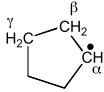
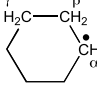
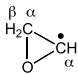
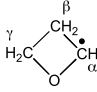
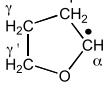
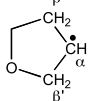
Tab. 7.1. Hyperfine Data for Some Acyclic Alkyl Radicals

Methyl 58 [•]	$\overset{\alpha}{\text{H}_3\text{C}}\cdot$	3H(α) $^{13}\text{C}\cdot$	-2.304 +3.834	[34] [438]
Ethyl 59 [•]	$\overset{\alpha\beta}{\text{CH}_3}\overset{\cdot\alpha}{\text{CH}_2}$	2H(α) 3H(β) $^{13}\text{C}\cdot$ $^{13}\text{C}(\alpha)$	-2.238 +2.687 +3.907 -1.357	[34] [438]
<i>n</i> -Propyl 60 [•]	$\overset{\gamma}{\text{CH}_3}\overset{\beta}{\text{CH}_2}\overset{\cdot\alpha}{\text{CH}_2}$	2H(α) 2H(β) 3H(γ)	-2.208 +3.332 0.038	[34]
<i>n</i> -Butyl 137 [•]	$\overset{\gamma}{\text{CH}_3}\overset{\beta}{\text{CH}_2}\overset{\cdot\alpha}{\text{CH}_2}\text{CH}_2$	2H(α) 2H(β) 2H(γ)	-2.208 +2.933 0.074	[648]
<i>n</i> -Pentyl 138 [•]	$\overset{\gamma}{\text{C}_2\text{H}_5}\overset{\beta}{\text{CH}_2}\overset{\cdot\alpha}{\text{CH}_2}\text{CH}_2$	2H(α) 2H(β) 2H(γ)	-2.196 +2.857 0.075	[649]
<i>n</i> -Hexyl 139 [•]	$\overset{\gamma}{\text{C}_3\text{H}_7}\overset{\beta}{\text{CH}_2}\overset{\cdot\alpha}{\text{CH}_2}\text{CH}_2$	2H(α) 2H(β) 2H(γ)	-2.195 +2.854 0.075	[649]
Isopropyl 140 [•]	$\overset{\alpha\beta}{(\text{CH}_3)_2}\overset{\cdot\alpha}{\text{CH}}$	H(α) 6H(β) $^{13}\text{C}\cdot$ $2^{13}\text{C}(\alpha)$	-2.211 +2.468 +4.130 -1.320	[34] [553]
<i>tert</i> -Butyl 141 [•]	$\overset{\alpha\beta}{(\text{CH}_3)_3}\overset{\cdot}{\text{C}}$	9H(β) $^{13}\text{C}\cdot$ $3^{13}\text{C}(\alpha)$	-2.272 +4.520 -1.235	[34] [553]
Hydroxymethyl 142 [•]	$\overset{\cdot\alpha}{\text{HOCH}_2}$	2H(α) H(O) ^{13}C	-1.798 -0.115 +4.737	[54] [650]
Cyanomethyl 143 [•]	$\overset{\cdot\alpha}{\text{NCCH}_2}$	2H(α) ^{14}N	-2.098 +0.351	[651]
Fluoromethyl 144 [•]	$\overset{\cdot\alpha}{\text{FCH}_2}$	2H(α) ^{19}F ^{13}C	+2.11 +6.43 +5.48	[482]
Difluoromethyl 145 [•]	$\overset{\cdot\alpha}{\text{F}_2\text{CH}}$	H(α) 2^{19}F ^{13}C	+2.22 +8.42 +14.88	[482]
Trifluoromethyl 87 [•]	$\text{F}_3\text{C}\cdot$	3^{19}F ^{13}C	+14.45 +27.16	[482]

stants a_{H} for 144[•] and 145[•], are presumably positive, in contrast to the corresponding negative values for 58[•]–60[•] and 137[•]–140[•].

Table 7.2 lists the hyperfine data for the simplest monocyclic alkyl radicals, as well as for several related species, 147[•]–150[•], produced by abstraction of an H atom from oxirane, oxetane, and THF [34, 438, 653–656]. The $|a_{\text{H}}(\alpha)|$ value for cyclo-

Tab. 7.2. Hyperfine Data for Some Monocyclic Alkyl Radicals

Cyclopropyl 14[•]		H(α) 4H(β) ¹³ C [•]	−0.651 +2.342 +9.59	[34] [653]
Cyclobutyl 61[•]		H(α) 4H(β) 2H(γ)	−2.120 +3.666 0.112	[34]
Cyclopentyl 146[•]		H(α) 4H(β) 4H(γ)	−2.148 +3.516 0.053	[34]
Cyclohexyl 121[•]		H(α) 2H _{ax} (β) 2H _{eq} (β) 4H(γ) ¹³ C [•]	−2.13 +3.94 +0.53 0.071 +4.13	[34] [438]
Oxiranyl 147[•]		H(α) 2H(β) ¹³ C [•] ¹³ C(α)	+2.45 +0.53 +12.10 0.30	[654]
Oxetanyl 148[•]		H(α) 2H(β) 2H(γ)	0.805 +2.87 0.15	[655]
Tetrahydrofuran-2-yl 149[•]		H(α) 2H(β) 2H(γ) 2H(γ')	−1.210 +2.848 0.164 0.082	[656]
Tetrahydrofuran-3-yl 150[•]		H(α) 2H(β) 2H(β')	−2.12 +0.353	[656]

propyl (**14[•]**) is greatly reduced relative to those for larger cycloalkyl radicals. As pointed out in Chapt. 4.3, the C–H(α) bond does not lie in the plane of the three-membered ring, and the spin-bearing orbital at C[•] must be classified as between a 2p_z-AO and an sp³-hybrid. According to most refined post-HF calculations for **14[•]** [657, 658], the coupling constant $a_{\text{H}}(\alpha)$ should still be negative, but the values $a_{\text{H}}(\beta)$ and a_{C} are, as expected, positive. Whereas the rings in cyclobutyl (**61[•]**) and cyclopentyl (**146[•]**) are considered to be effectively planar, with the four β protons appearing equivalent on the hyperfine time-scale, cyclohexyl (**121[•]**) exhibits different $a_{\text{H}}(\beta)$ values for the axial and equatorial protons, which are subject to exchange by ring inversion (Chapt. 6.7).

The hyperfine data for oxiranyl (**147[•]**) were also studied by similar high-level theoretical calculations as those for cyclopropyl (**14[•]**) [658]. Replacement of one

methylene group in **14'** by an O atom in **147'** has far-reaching consequences, because $a_{\text{H}}(\alpha)$ increases from -0.651 to $+2.45$ mT, $a_{\text{H}}(\beta)$ decreases from $+2.342$ to $+0.53$ mT, and a_{C} increases from $+9.59$ to $+12.10$ mT. These changes should be due to geometric rather than to direct electronic effects, in particular, the strongly enhanced pyramidalization at C'. Note the relatively large positive coupling constant $a_{\text{H}}(\alpha)$, of which sign is opposite to those of the corresponding values for cyclopropyl and larger cycloalkyl radicals. The two β protons in **147'** appear equivalent on the hyperfine scale, but they can be distinguished in the radical **147-d'**, deuterated at C', for which the two-proton $a_{\text{H}}(\beta)$ value splits into $+0.523$ and $+0.474$ mT, each for a single proton [654].

Pyramidalization at C' also affects the coupling constants $a_{\text{H}}(\alpha)$ in **148'** and **149'**, with C' directly linked to the O atom. However, in **150'**, the C' atom is separated from O by a sp^3 -hybridized C atom, and the $a_{\text{H}}(\alpha)$ value of -2.12 mT indicates an essentially planar geometry at the radical center.

In Table 7.3, hyperfine data are given for some polycyclic alkyl radicals generated by abstraction of an H atom from bicyclo[1.1.0]butane, bicyclo[2.2.0]hexane, bicyclo[2.2.1]heptane (norbornane), adamantane, and cubane [41, 458, 659–666]. The ^1H -coupling constants for the bicyclo[1.1.0]but-2-yl radical (**151'**) exhibit remarkable features, which were investigated theoretically, along with those of cyclopropyl (**14'**) [658, 667]. The experimental data are compatible with the values calculated for **151'**, in which the C–H(α) bond is in the *exo* position, in contrast to the original assignment [458]. A positive sign is required for the coupling constant $a_{\text{H}}(\alpha) = 0.785$ mT, which indicates that the pyramidalization at the C' atom in **151'** is stronger than in **14'** with $a_{\text{H}}(\alpha) = -0.651$ mT but less pronounced than in oxiranyl (**147'**) with $a_{\text{H}}(\alpha) = +2.45$ mT. The small coupling constant $a_{\text{H}}(\beta)$ of $+0.440$ mT for the two methine protons indicates the C–H(β) bonds make a large dihedral angle θ (ca 75°) with the “nominal” 2p_z -axis at the C' atom, and the large $a_{\text{H}_{\text{endo}}}(\gamma)$ value of $+1.264$ mT for one methylene proton reveals an efficient long-range coupling. Surprisingly, theoretical calculations require that this value should be assigned to the γ -proton in the *endo* and not to that in the *exo* position with $a_{\text{H}_{\text{exo}}}(\gamma) = -0.081$ mT, because the W-arrangement for the long-range coupling (Chapt. 4.2) does not occur in this radical for the *exo* conformation of the C–H(α) bond.

The secondary alkyl radical 7-norbornyl (**155'**) is pyramidal at the C' atom, and this statement holds even more strictly for the tertiary alkyl radicals, bicyclo[2.2.0]hex-1-yl (**152'**), 1-norbornyl (**153'**), 1-adamantyl (**157'**), and cubyl (**159'**), in which the bridgehead C' atom is part of a rigid carbon framework that prevents planarization at this atom. However, such flattening does seem to occur in the secondary alkyl radicals 2-norbornyl (**154'**), bicyclo[2.2.2]oct-2-yl (**156'**), and 2-adamantyl (**158'**), for which the coupling constant $a_{\text{H}}(\alpha)$ is close to -2.1 mT. Because of their rigid frameworks, oligocyclic radicals such as **151'** to **159'** offer a favorable playground for studying effects of geometry on the electronic structure, which are disclosed by the hyperfine data of these species.

In fact, the radicals **142'**–**145'**, **87'**, and **147'**–**149'**, which have heteroatoms linked to C', cannot strictly be considered C-centered, because of some spin delo-

Tab. 7.3. Hyperfine Data for Some Polycyclic Alkyl Radicals

Bicyclo[1.1.0]but-2-yl 151 [•]		H(α) 2H(β) H _{endo} (γ) H _{exo} (γ)	+0.785 +0.440 +1.264 -0.081	[458]
Bicyclo[2.2.0]hex-1-yl 152 [•]		2H _{exo} (β) 2H _{endo} (β) H(β') 4H(γ)	+2.20 +1.07 +0.62 <0.15	[659]
1-Norbornyl 153 [•]		2H _{exo} (β) 2H _{endo} (β) 2H(β') 2H _{exo} (γ) 2H _{endo} (γ) H(δ)	+0.981 +0.049 +0.235 +0.123 0.036 +0.245	[660]
2-Norbornyl 154 [•]		H(α) H _{exo} (β) H _{endo} (β) H _{exo} (γ) H _{exo} (δ)	-2.06 +4.17 +2.56 +0.90 0.019	[661]
7-Norbornyl 155 [•]		H(α) 2H(β) 4H _{exo} (γ) 4H _{endo} (γ)	-1.678 +0.105 0.072 +0.353	[662]
Bicyclo[2.2.2]oct-2-yl 156 [•]		H(α) 2H(β) H _{exo} (γ)	-2.15 +3.70 +0.57	[663]
1-Adamantyl 157 [•]		6H(β) 3H(γ) 3H _{ax} (δ) 3H _{eq} (δ) 13C [•]	+0.658 +0.466 +0.308 0.080 +13.7	[41] [664]
2-Adamantyl 158 [•]		H(α) 2H(β) 4H _{ax} (γ) 4H _{eq} (γ) 2H(δ) 2H(ϵ)	-2.073 +0.193 0.098 +0.406 +0.278 0.012	[665]
Cubyl 159 [•]		3H(β) 3H(γ) H(δ)	+0.82 +1.24 0.03	[666]

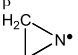
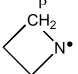
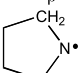
calization to these atoms. This statement holds, in particular, for $142'$ and $147'$ – $149'$ with C–O bonds. The hydroxymethyl radical $H_2C^{\bullet}-OH$ ($142'$) is a conjugate acid of the ketyl anion $H_2C-O^{\bullet-}$ which is presented in one of the following sections.

The g_e factor of alkyl radicals lacking heteroatoms is 2.0026–2.0027, as stated in Chapt. 6.2. It is 2.0029 for $142'$, and 2.0032–2.0033 for $143'$, $87'$, $147'$, and $148'$. With the exception of $153'$ and $158'$, generated by X- or γ -irradiation of the solid parent hydrocarbons, the alkyl radicals, for which the hyperfine data are given in Tables 7.1–7.3 were produced in fluid solution. Most of them were formed by H abstraction from corresponding hydrocarbons by high-energy electrons or by t -BuO $'$, but in some of them this abstraction was carried out by HO $'$ radicals.

Alkylaminyl Radicals and Radical Cations of Alkylamines

The N-centered aminyl radical H_2N^{\bullet} ($160'$) and the radical cation, $H_3N^{\bullet+}$, of ammonia (161) are isoelectronic with methyl H_3C^{\bullet} ($58'$). Substitution of the two H atoms in $160'$ by alkyl groups leads to dialkylaminyls, $R^1R^2N^{\bullet}$, and incorporation of the spin-bearing N atom into a ring yields cyclic aminyls. Only a few of these radicals have been characterized by ESR spectroscopy. Table 7.4 [668–671] presents the hyperfine data for some of them, both acyclic and cyclic aminyl radicals. The ammonia molecule H_3N (161) is pyramidal with C_{3v} symmetry, but aminyl radicals are predicted to have planar geometry. Thus, the two N–H or N–C bonds and the N-lone pair should be located in one plane, and the axis of the spin-bearing N- $2p_z$ -AO ought to be perpendicular to this plane. INDO calculations indicate that the

Tab. 7.4. Hyperfine Data for Some Alkylaminyl Radicals

Aminyl 160'	α H_2N^{\bullet}	^{14}N 2H(α)	+1.52 –2.54	[668]
Dimethylaminyl 162'	β $(CH_3)_2N^{\bullet}$	^{14}N 6H(β)	+1.478 +2.736	[669]
Diethylaminyl 163'	β $(CH_3CH_2)_2N^{\bullet}$	^{14}N 4H(β)	+1.427 +3.690	[669]
Diisopropylaminyl 164'	γ β [[$(CH_3)_2CH$] $_2N^{\bullet}$]	^{14}N 2H(β) 12H(γ)	+1.431 +1.431 0.066	[669]
1-Aziridinyl 165'	β 	^{14}N 4H(β)	+1.252 +3.070	[670]
1-Azetinidyl 166'	β 	^{14}N 4H(β)	+1.399 +3.825	[670]
1-Pyrrolidinyl 167'	β 	^{14}N 2H $_{ax}(\beta)$ 2H $_{eq}(\beta)$	+1.43 +5.42 +2.71	[671]

coupling constant a_N depends on the angle HNH. The reported hyperfine data for H_2N^\bullet (**160'**) are sensitive to the conditions used for its generation. They vary between +1.03 [672] and +1.52 mT [668] for a_N and between -2.39 [672] and -2.54 [668] mT for a_H . The coupling constants a_N for dialkylaminyls R_2N^\bullet with $R = Me, Et,$ and $i-Pr$ (**162'–164'**), as well as those for 1-azetidyl (**166'**) and 1-pyrrolinidyl (**167'**), lie in the range +1.4 to +1.5 mT; the a_N value is somewhat smaller, +1.25 mT, for 1-azirinidyl (**165'**) which is isoelectronic with cyclopropyl (**14'**). The $\cos^2 \theta$ -relation can be applied to the coupling constant $a_H(\beta)$, with the parameter $B_H^{N,CH'}$ of Eq. 4.12 being +5.5 mT, which is twice the $a_H(\beta)$ value of +2.74 mT for the freely rotating methyl substituents in **162'**. In addition, the conformations of the methylene groups in **163'** and **166'** are in line with those depicted for these groups in Figure 4.6 ($\theta \approx 30^\circ$).

The g_e factor of aminyl radicals is 2.0044–2.0048. Values of 2.0048 and 2.0046 were reported for the H_2N^\bullet radical (**160'**) which was generated from ammonia by photolysis in an argon matrix [672] or by high-energy bombardment in the gas phase [668]. With the exception of **167'** produced by γ -irradiation of pyrrolidine in a Freon matrix all radicals for which hyperfine data are given in Table 7.4 were formed in fluid solution, usually by abstraction of an H atom from the corresponding amine with $t-BuO^\bullet$ in cyclopropane.

Ammonia, H_3N (**161**), is rather difficult to ionize and its radical cation $H_3N^{\bullet+}$ has low persistence [333, 334]. Substitution of the H atoms by alkyl or other groups or incorporation of the spin-bearing N atom into a ring lowers the ionization energy and enhances the persistence of the corresponding radical cations. As for derivatives of methyl, amines are denoted *primary*, *secondary*, or *tertiary*, according to whether one, two, or three N–H bonds are replaced by bonds between N and other atoms. Reviews on radical cations of alkylamines have appeared in two publications [237, 673]; the more recent one [237] contains hyperfine data for many radical cations of trialkylamines, both acyclic and cyclic. A representative selection is presented in Tables 7.5 [237, 324, 333, 334, 674–676] and 7.6 [237, 246, 325, 348, 671, 677] for the radical cations of ammonia and several acyclic and cyclic, primary, secondary, and tertiary amines.

In general, alkyl-substituted amines are expected to have the pyramidal structure of the parent ammonia. This geometry was experimentally confirmed for trimethylamine (**169**) [678] and triethylamine (**171**) [679]. Planarity is promoted by isopropyl substituents, and pyramidalization is favored by cyclopropyl groups. Thus, triisopropylamine (**27**) is close to planarity [679], whereas tricyclopropylamine (**175**) is strongly pyramidal [676]. The monocyclic azetidine (**176**) and N-pyrrolidine (**177**) are predicted to be pyramidal, as are certainly the bicyclic 1-azanorbornane (**34**) and quinuclidine (**179**), and the tricyclic 1-azaadamantane (**180**) and azatriquinane (**182**). On the other hand, the bicyclic *N-tert*-butylbicyclo[3.3.1]nonane (**178**) and 1-azabicyclo[3.3.3]undecane (manxine; **181**) should be planar or nearly planar. Upon conversion to their radical cations, amines tend to flatten at the N atom, as does ammonia (**161**) upon ionization to $161^{\bullet+}$. However, planarity cannot be achieved for the radical cations of the bi- and tricyclic amines **34**, **179**, **180** and **182**, because flattening is impaired by the rigid molecular framework. A crite-

rior for the geometry at the N atom is the coupling constant a_N , which, due to s -contributions, increases with growing deviation from planarity. Substantial pyramidalization is indicated in radical cations for which the coupling constant a_N exceeds $+2.0 \pm 0.1$ mT, the value characteristic of planar geometry at the N atom. Thus, deviations from planarity should gradually become more pronounced in the sequence $180^{+\cdot} < 179^{+\cdot} \approx 182^{+\cdot} < 34^{+\cdot}$. The coupling constants $a_H(\beta)$ for the alkyl substituents exhibit $\cos^2 \theta$ -dependence (Eq. 4.11), with the parameter $B_H^{N_{\mu'}CH_{\mu'}} = +5.7$ mT for planar radical cations. This parameter is close to that for the aminyl radicals and is twice the $a_H(\beta)$ value for the freely rotating methyl groups in $169^{+\cdot}$. A lower value of $B_H^{N_{\mu'}CH_{\mu'}}$, $+4.0$ mT, seems appropriate for pyramidal radical cations such as $34^{+\cdot}$, $179^{+\cdot}$, $180^{+\cdot}$, and $182^{+\cdot}$ [237]. Usually, the alkyl substituents of the radical cations of amines retain the conformation of their neutral precursors. Striking exceptions are amines with cyclopropyl substituents, in which the conformation of the three-membered rings changes upon ionization, from “perpendicular” to “bisected”. Thus, the C–H(β) bonds eclipse the axis of the N-2p_z-AO in **175** (dihedral angle $\theta = 0^\circ$ or 180°) but assume a position in the nodal plane of this orbital in $175^{+\cdot}$ ($\theta = 90^\circ$) [676]. Long-range coupling is manifested by large values $a_H(\delta) = +1.43$ for $179^{+\cdot}$ and $a_H(\epsilon) = +0.60$ mT for $181^{+\cdot}$.

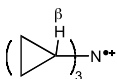
The g_e factor of amine radical cations is, in general, 2.0036–2.0038. Values of 2.0032, 2.0041, and 2.0035 were reported for $161^{+\cdot}$, $181^{+\cdot}$, and $182^{+\cdot}$, respectively. The radical cation $H_3N^{+\cdot}$ ($161^{+\cdot}$) was generated by γ -irradiation of NH_4ClO_4 powder [680] or by photolysis of ammonia in a neon matrix [333]. The radical cations of the amines for which hyperfine data are given in Tables 7.5 and 7.6 were produced by photolysis of their neutral precursors in strongly acidic solution, either in 90% H_2SO_4 [674] or in CF_3SO_3H [348]. Alternatively, they were formed by oxidation of the corresponding amines with SbF_5 or tris(4-bromophenyl)-ammoniumyl hexachloroantimonate (“magic blue”) in dichloromethane [236]. Only a few alkyl amines (**171**, **175**–**177**, and **182**) proved difficult to oxidize in solution and had to be converted into their radical cations by γ -irradiation in Freon matrices.

Alkoxy Radicals and Radical Cations of Alkylethers

The isoelectronic species corresponding to the aminyl radical, H_2N^\cdot (**160** $^\cdot$), and the radical cation, $H_3N^{+\cdot}$, of ammonia (**161**) are the hydroxyl radical, HO^\cdot (**183** $^\cdot$), and the radical cation, $H_2O^{+\cdot}$, of water (**184**).

Due to H-bonding differences, the coupling constant of the α -proton in the hydroxyl radical (**183**) varies considerably under different experimental conditions and so does the g_e factor. Here we confine to two studies on this radical produced by high-energy irradiation in single crystals of hexagonal ice [681] and $LiOAc \cdot H_2O$ [682]. In ice, three isotropic $a_H(\alpha)$ values of -2.32 , -2.21 , and -2.24 mT were measured for HO^\cdot in three distinguishable sites (the g_e factors are 2.0238, 2.0230, and 2.0232, respectively), and the isotropic $a_H(\alpha)$ value of HO^\cdot in $LiOAc \cdot H_2O$ was -2.03 mT ($g_e = 2.0285$). Substitution of the H atom in HO^\cdot by an alkyl group yields an alkoxy radical RO^\cdot . For the methoxy radical H_3CO^\cdot (**185** $^\cdot$), which was

Tab. 7.5. Hyperfine Data for Radical Cations of Some Acyclic Alkylamines

Ammonia 161 ⁺	α H ₃ N ^{•+}	¹⁴ N 3H(α)	+1.96 -2.74	[333, 334]
Dimethylamine 168 ⁺	β $\bullet\bullet$ α (CH ₃) ₂ NH	¹⁴ N H(α) 6H(β)	+1.928 -2.273 +3.427	[674]
Trimethylamine 169 ⁺	β (CH ₃) ₃ N ^{•+}	¹⁴ N 9H(β)	+2.07 +2.85	[675]
Diethylamine 170 ⁺	β $\bullet\bullet$ α (CH ₃ CH ₂) ₂ NH	¹⁴ N H(α) 4H(β)	+1.865 -2.224 +3.719	[674]
Triethylamine 171 ⁺	β (CH ₃ CH ₂) ₃ N ^{•+}	¹⁴ N 6H(β)	+2.08 +1.9	[324]
Di-n-propylamine 172 ⁺	β $\bullet\bullet$ α (C ₂ H ₅ CH ₂) ₂ NH	¹⁴ N H(α) 4H(β)	+1.858 -2.151 +3.421	[674]
Diisopropylamine 173 ⁺	γ β $\bullet\bullet$ α [(CH ₃) ₂ CH] ₂ NH	¹⁴ N H(α) 2H(β) 12H(γ)	+1.87 -2.25 +2.17 0.08	[674]
Ethyl-diisopropylamine 174 ⁺	β $\bullet\bullet$ β' CH ₃ CH ₂ N[CH(CH ₃) ₂] ₂	¹⁴ N 2H(β) 2H(β')	+2.02 +1.85 +0.44	[237]
Triisopropylamine 27 ⁺	$\beta\gamma$ β [(CH ₃) ₂ CH] ₃ N ^{•+}	¹⁴ N 3H(β) 18H(γ) 6 ¹³ C(β)	+2.02 +0.15 0.06 +1.38	[237]
Tricyclopropylamine 175 ⁺	β 	¹⁴ N 3H(β)	+2.01 +0.07	[676]

generated by X-irradiation of polycrystalline methyl alcohol ($g_{e,\max} = 2.088$; $g_{e,\min} = 1.999$), the $a_H(\beta)$ value of 5.2 mT is presumably positive [683]. This value is rather large for β protons in a freely rotating methyl group, because (assuming $\cos^2 \theta$ -dependence), it would require a parameter of +10.4 mT as the proportionality factor $B_H^{O_{\mu'}, CH_{\mu'}}$ analogous to $B_H^{N_{\mu'}, CH_{\mu'}}$ (Eq. 4.12) and $B_H^{C_{\mu'}, CH_{\mu'}}$ (Eq. 4.9). Worth mentioning are alkoxy radicals of more complex structure which were produced by irradiation of biological material such as sugars [684, 685].

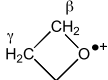
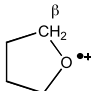
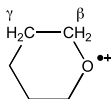
Replacement of one H atom in H₂O⁺ (184⁺) by an alkyl group R leads to the radical cation of an alcohol, and substitution of both H atoms yields the radical cations, R¹R²O⁺, of ethers. Hyperfine data for 184⁺ and the radical cations of water and some ethers are given in Table 7.7 [305, 320, 322, 686, 687]. The coupling constant $a_H(\alpha)$ for 184⁺ ought to be negative, and the $a_H(\beta)$ values for 186⁺–190⁺ are expected to have positive sign. The $a_H(\beta)$ values of the methylene

Tab. 7.6. Hyperfine Data for Radical Cations of Some Cyclic Alkylamines

Azetidine 176 ⁺		¹⁴ N H(α) 4H(β)	+1.91 -2.27 +5.41	[325]
N-Pyrrolidine 177 ⁺		¹⁴ N H(α) 2H _{ax} (β) 2H _{eq} (β)	+2.0 -2.45 +7.05 +3.40	[671]
N- <i>tert</i> -butylbicyclo[3.1.1]nonane 178 ⁺		¹⁴ N	+1.95	[246]
1-Azanorbornane 34 ⁺		¹⁴ N 2H _{exo} (β) 2H(β') 2H _{exo} (γ) H(δ)	+3.02 +1.51 +0.295 +0.295 +0.18	[348]
Quinuclidine 179 ⁺		¹⁴ N 6H(β) 6H(γ) H(δ)	+2.51 +0.939 +0.226 +1.43	[348]
1-Azaadamantane 180 ⁺		¹⁴ N 3H _{ax} (β) 3H(γ) 3H _{anti} (δ) 3H _{syn} (δ)	+2.16 +0.867 +0.702 +1.08 0.166	[348]
Manxine 181 ⁺		¹⁴ N 3H _{eq} (β) 3H _{ax} (β) 6H(γ) 6H(δ) H(ϵ)	+1.92 +3.85 0.023 0.18 0.16 +0.60	[237]
Azatriquinane 182 ⁺		¹⁴ N 3H(β)	+2.50 +4.00	[677]

β protons in 187⁺ and 188⁺ ($\theta \approx 30^\circ$) are, as expected, larger than those of the β protons in the freely rotating methyl groups in 186⁺. The sign of the coupling constant a_O (-3.98 mT) for 184⁺ is due to the negative g_n factor of the ¹⁷O isotope. The g_e factor of 184⁺ is 2.0093 and that of 186⁺ is 2.0085. The radical cation 184⁺ was produced by photolysis of water in a neon matrix, and 186⁺-190⁺ were formed by γ -irradiation of the neutral ethers in Freon matrices.

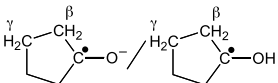
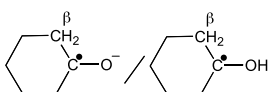
Tab. 7.7. Hyperfine Data for Radical Cations of Water and Some Dialkylethers

Water 184 ⁺	α H ₂ O ^{•+}	2H(α) ¹⁷ O	-2.63 -3.98	[686]
Dimethylether 186 ⁺	β (CH ₃) ₂ O ^{•+}	6H(β)	+4.3	[320]
Diethylether 187 ⁺	β (CH ₃ CH ₂) ₂ O ^{•+}	4H(β)	+6.87	[305, 322]
Oxetane 188 ⁺	β 	4H(β) 2H(γ)	+6.4 1.1	[305, 322]
Tetrahydrofuran 189 ⁺	β 	2H _{ax} (β) 2H _{eq} (β)	+8.9 +4.0	[305, 687]
Tetrahydropyran 190 ⁺	β γ 	2H _{ax} (β) 2H _{eq} (β) 2H _{ax} (γ) 2H _{eq} (γ)	+3.45 +1.4 1.1 0.3	[305, 322]

Radical Anions of Alkylaldehydes and Alkylketones (Ketyl Anions)

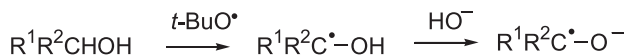
Because the keto group $>C=O$ is electron-withdrawing, aldehydes and ketones should readily accept an additional electron, which is accommodated by the antibonding π^* -MO of this group. The paramagnetic species thus resulting are called ketyl anions. In the bonding π -MO, $c_C\phi_C + c_O\phi_O$, of the keto group (represented as a linear combination of the $2p_z$ -AOs ϕ_C and ϕ_O), the contribution of the electronegative O atom prevails ($c_C < c_O$), according to the large weight of the ionic structural formula $>C^+-O^-$. In contrast, the C atom contributes more than O ($c_C > c_O$) to the antibonding π^* -MO, $c_C\phi_C - c_O\phi_O$, so that a ketyl radical anion can be adequately formulated as C-centered, $>C^{\cdot-}-O^-$. Table 7.8 [650, 688, 689] lists the hyperfine data for aliphatic ketyl radical anions, i.e. those of several simplest alkylaldehydes and dialkylketones of the general formula $R^1R^2C^{\cdot-}-O^-$ where R^i is H or alkyl. Radical anions of two cycloalkanones in which the C $^{\cdot-}$ atom is incorporated into a ring have also been included. The coupling constant, $a_{C^{\cdot-}} = +5.22$ mT, of the ¹³C isotope in the acetone radical anion $(CH_3)_2C^{\cdot-}-O^-$ (**196 $^{\cdot-}$**) is much larger than the corresponding value +3.83 mT, for the methyl radical H₃C $^{\cdot}$ (**58 $^{\cdot}$**), although in **196 $^{\cdot-}$** the C $^{\cdot-}$ atom shares some spin population with its O neighbor ($\rho_C^{\pi} < +1$). This increase in $a_{C^{\cdot-}}$ value is due to pyramidalization at the ketyl-C atom. In the series of aldehydes, H₂C $^{\cdot-}-O^-$ (**191 $^{\cdot-}$**) and RHC $^{\cdot-}-O^-$ (**192 $^{\cdot-}$** –**195 $^{\cdot-}$**), the coupling constant $a_H(\alpha) = -1.402$ mT for **191 $^{\cdot-}$** gradually decreases in absolute value with the introduction and growing size of the alkyl group R, a finding which may also indicate increasing deviation from planarity at the C $^{\cdot-}$ atom. On the other hand, the $a_H(\beta)$ value for **192 $^{\cdot-}$** –**194 $^{\cdot-}$** , which is less sensitive to such deviations, is

Tab. 7.8. Hyperfine Data for Radical Anions of Some Alkylaldehydes and Alkylketones (Ketyl Anions) and Their Conjugate Acids

Formaldehyde 191 ⁻ /191H [•]	$\overset{\alpha}{\text{H}_2\text{C}}\text{---}\overset{\bullet}{\text{O}}^- / \overset{\alpha}{\text{H}_2\text{C}}\text{---}\overset{\bullet}{\text{O}}\text{H}$	Base/Acid 2H(α) H(O) ¹³ C	-1.402/-1.727 [688] -0.111 +3.77/+4.737 [650]
Acetaldehyde 192 ⁻ /192H [•]	$\overset{\beta}{(\text{CH}_3)\text{HC}}\text{---}\overset{\bullet}{\text{O}}^- / \overset{\beta}{(\text{CH}_3)\text{HC}}\text{---}\overset{\alpha}{\text{O}}\text{H}$	Base/Acid H(α) 3H(β) H(O)	-1.205/-1.524 [688] +1.985/+2.211 -0.27
Propionaldehyde 193 ⁻ /193H [•]	$\overset{\gamma}{(\text{CH}_3\text{CH}_2)\text{HC}}\text{---}\overset{\beta}{\text{O}}\text{---}\overset{\alpha}{\text{C}}\text{---}\overset{\bullet}{\text{O}}^- / \overset{\gamma}{(\text{CH}_3\text{CH}_2)\text{HC}}\text{---}\overset{\beta}{\text{O}}\text{---}\overset{\alpha}{\text{C}}\text{---}\overset{\bullet}{\text{O}}\text{H}$	Base/Acid H(α) 2H(β) 3H(γ)	-1.172/-1.494 [688] +2.099/+2.114 0.040/0.032
Isobutyraldehyde 194 ⁻ /194H [•]	$\overset{\beta}{[(\text{CH}_3)_2\text{CH}]\text{HC}}\text{---}\overset{\bullet}{\text{O}}^- / \overset{\beta}{[(\text{CH}_3)_2\text{CH}]\text{HC}}\text{---}\overset{\alpha}{\text{O}}\text{H}$	Base/Acid H(α) H(β)	-1.092/-1.447 [688] +1.931/+2.139
2,2-Dimethylpropan- 1-one 195 ⁻ /195H [•]	$\overset{\gamma}{[(\text{CH}_3)_3\text{C}]\text{HC}}\text{---}\overset{\alpha}{\text{C}}\text{---}\overset{\bullet}{\text{O}}^- / \overset{\gamma}{[(\text{CH}_3)_3\text{C}]\text{HC}}\text{---}\overset{\alpha}{\text{C}}\text{---}\overset{\bullet}{\text{O}}\text{H}$	Base/Acid H(α) 9H(γ)	-0.865/-1.378 [688] 0.029/0.033
Acetone 196 ⁻ /196H [•]	$\overset{\beta}{(\text{CH}_3)_2\text{C}}\text{---}\overset{\bullet}{\text{O}}^- / \overset{\beta}{(\text{CH}_3)_2\text{C}}\text{---}\overset{\bullet}{\text{O}}\text{H}$	Base/Acid 6H(β) ¹³ C	+1.690/+1.962 [688] +5.22/+6.50 [688, 689]
Diethylketone 197 ⁻ /197H [•]	$\overset{\beta}{(\text{CH}_3\text{CH}_2)_2\text{C}}\text{---}\overset{\bullet}{\text{O}}^- / \overset{\beta}{(\text{CH}_3\text{CH}_2)_2\text{C}}\text{---}\overset{\bullet}{\text{O}}\text{H}$	Base/Acid 4H(β)	+1.430/+1.675 [688]
Cyclopentanone 198 ⁻ /198H [•]		Base/Acid 4H(β) 4H(γ)	+2.63/+2.80 [688] <0.02/0.032
Cyclohexanone 199 ⁻ /199H [•]		Base/Acid 2H _{ax} (β) 2H _{eq} (β)	+3.29/+3.55 [688] +0.84/+1.01

throughout $+2.0 \pm 0.1$ mT, thus indicating a lack of a preferred conformation of the alkyl group R. However, conformational preference for the alkyl groups is evident in the radical anions of ketones, because the coupling constant $a_{\text{H}}(\beta)$ changes from +1.690 for the freely rotating methyl groups of 196⁻ to +1.430 for the ethyl groups in 197⁻ (dihedral angle $\theta \approx 50^\circ$) and to +2.63 mT for the five-membered ring in 198⁻ ($\theta \approx 30^\circ$).

The g_e factor of 191⁻ is 2.0039 and that of the radical anions of alkylaldehydes and alkylketones ranges from 2.0032 to 2.0036. All these ketyl anions were generated by photolysis of a solution of potassium in the corresponding alcohol or by abstraction of a H atom from the alcohol by *t*-BuO[•] radical under strongly basic conditions. The latter reaction:

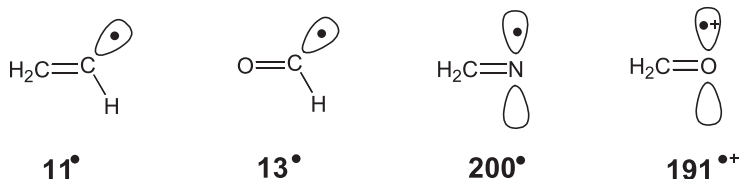


proceeds via the intermediate hydroxyalkyl radicals $\text{R}^1\text{R}^2\text{C}^\bullet\text{-OH}$ as the conjugate acids of $\text{R}^1\text{R}^2\text{C}^\bullet\text{-O}^-$. The ESR spectra of these radicals were observed under less basic conditions, and their hyperfine data are included in Table 7.8. The simplest radical $\text{H}_2\text{C}^\bullet\text{-OH}$ (**191H**[•]) is identical with the hydroxymethyl (**142**[•]) presented in Table 7.1. With respect to the π -spin population at the C[•] atom, the hydroxyalkyl radicals $\text{R}^1\text{R}^2\text{C}^\bullet\text{-OH}$ assume a position between the alkyl radicals $\text{R}^1\text{R}^2\text{HC}^\bullet$ (Table 7.1) and ketyl anions $\text{R}^1\text{R}^2\text{C}^\bullet\text{-O}^-$, with the $\rho_{\text{C}}^{\pi(2p)}$ values decreasing in this sequence. Thus, the coupling constants $a_{\text{H}}(\alpha)$ are -2.304 for $\text{H}_3\text{C}^\bullet$ (**58**[•]), -1.727 for $\text{H}_2\text{C}^\bullet\text{-OH}$ (**191H**[•] \equiv **142**[•]), and -1.402 mT for $\text{H}_2\text{C}^\bullet\text{-O}^-$ (**191**[•]). The $a_{\text{H}}(\beta)$ values behave similarly, decreasing from $+2.468$ for $(\text{CH}_3)_2\text{C}^\bullet\text{H}$ (**140**[•]) to $+1.962$ for $(\text{CH}_3)_2\text{C}^\bullet\text{-OH}$ (**196H**[•]) and $+1.690$ mT for $(\text{CH}_3)_2\text{C}^\bullet\text{-O}^-$ (**196**[•]).

The g_e factor of hydroxyalkyl radicals is lower than that of the corresponding ketyl anions, in line with the smaller share of the O atom in the π -spin population; it ranges from 2.0030 to 2.0033.

Vinyl, Acyl, and Iminyl Radicals and Radical Cations of Alkylaldehydes and Alkylketones

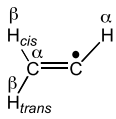
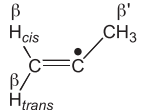
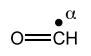
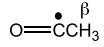
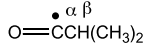
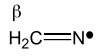
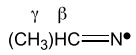
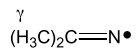
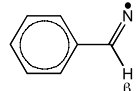
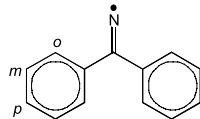
The vinyl (**11**[•]), formyl (**13**[•]), and methaniminyl (**200**[•]) radicals, as well as the formaldehyde radical cation (**191**^{•+}), have 11 valence electrons. While **11**[•] and **13**[•] are formally C-centered, **200**[•] and **191**^{•+} are N- and O-centered, respectively.



According to definition (Chapt. 4.3), the four isoelectronic species should be classified as σ radicals, because the spin-bearing nonbonding AO lies in the molecular plane that is the nodal plane of the double bond. They differ, however, in the “character” of this orbital, because the SOMO of **11**[•] and **13**[•] is a sp^n -hybrid with a substantial s contribution, whereas the SOMO of **200**[•] and **191**^{•+} must be considered as a nearly “pure” p-AO.

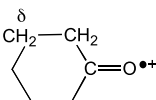
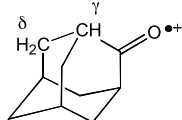
Tables 7.9 [34, 110, 438, 553, 690–694] and 7.10 [695–698] give the hyperfine data for **11**[•], **13**[•], **200**[•], and **191**^{•+}, along with those of some their alkyl derivatives. The classification of these radicals, of the general formulae $\text{R}^1\text{R}^2\text{C}=\text{C}^\bullet\text{R}^3$, $\text{O}=\text{C}^\bullet\text{R}$, $\text{R}^1\text{R}^2\text{C}=\text{N}^\bullet$, and $\text{R}^1\text{R}^2\text{C}=\text{O}^{\bullet+}$, as σ is justified by the large positive coupling constants of the α proton in formyl (**13**[•]) and of the β protons in vinyls (**11**[•] and **201**[•]), alkaniminyls (**200**[•] and **204**[•]), and alkylaldehyde radical cations (**191**^{•+}–**194**^{•+}). The much smaller $a_{\text{H}}(\alpha)$ value for **11**[•] (+1.33 mT) than for **13**[•] (+13.18 mT) is attributed to the CCH being narrower than the OCH angle and, thus, to a lower s con-

Tab. 7.9. Hyperfine Data for Some Vinyl, Acyl and Iminyl Radicals

Vinyl 11'		H(α) H _{cis} (β) H _{trans} (β) ¹³ C• ¹³ C(α)	+1.33 +6.85 +3.42 +10.76 -8.55	[34, 110, 438, 690]
Methylvinyl 201'		H _{cis} (β) H _{trans} (β) 3H(β')	+5.789 +1.948 +3.292	[34, 690]
Formyl 13'		H(α) ¹³ C ¹⁷ O	+13.175 +13.39 -1.51	[553]
Acetyl 202'		3H(β)	+0.40	[553]
2-Methylpropan-1-on-1-yl 203'		H(β) ¹³ C• ¹³ C(α)	<0.15 +11.36 +4.67	[553]
Methaniminyl 200'		¹⁴ N 2H(β)	+0.98 +8.52	[691]
Ethaniminyl 204'		¹⁴ N H(β) 3H(γ)	+1.020 +8.198 +0.249	[692]
Propan-2-iminyl 205'		¹⁴ N 6H(γ)	+0.96 +1.40	[691]
Phenylmethaniminyl 206'		¹⁴ N H(β)	+1.13 +7.8	[693]
Diphenylmethaniminyl 207'		¹⁴ N 4H _o , 4H _m 2H _p	+1.0 +0.037 <0.02	[694]

tribution. For 13', this contribution to the SOMO can be estimated as +13.18 mT/ +50.7 mT = 0.26, where the denominator is the ¹H-coupling constant of the H atom with the 1s-spin population of +1. (A valence-bond structure corresponding to such contribution is shown in Chapt. 4.3). The extremely large $a_{\text{H}}(\beta)$ values are due to the protons at the C(α) atom of the double bond $>\text{C}(\alpha)=\text{X}'$, where $\text{X}' = \text{C}'\text{H}$, N' , and O'^+ for vinyls, iminyls, and the aldehyde cations, respectively. The interaction giving rise to these values is a very efficient hyperconjugation across the double bond, which is favored by the small dihedral angle ($\theta \approx 0$; Eq. 4.8) and the shortness of this bond. As expected for σ radicals, the coupling constants $a_{\text{H}}(\beta)$ for

Tab. 7.10. Hyperfine Data for Radical Cations of Some Alkaldehydes and Alkylketones

Formaldehyde 191 ⁺	β $\text{H}_2\text{C}=\text{O}^{\bullet+}$	2H(β)	+9.03	[695]
Acetaldehyde 192 ⁺	β $(\text{CH}_3)\text{HC}=\text{O}^{\bullet+}$	H(β)	+13.65	[696, 697]
Propionaldehyde 193 ⁺	δ β $(\text{CH}_3\text{CH}_2)\text{HC}=\text{O}^{\bullet+}$	H(β) 1H(δ)	+13.5 +1.25	[696, 697]
Isobutyraldehyde 194 ⁺	δ β $[(\text{CH}_3)_2\text{CH}]\text{HC}=\text{O}^{\bullet+}$	H(β) 6H(δ)	+12.03 +2.04	[696, 697]
Acetone 196 ⁺	β γ $(\text{CH}_3)_2\text{C}=\text{O}^{\bullet+}$	1H(γ) 1H(γ) 2 ¹³ C(β)	0.15 0.03 1.53	[698]
Cyclohexanone 199 ⁺	δ 	2H _{eq} (δ)	+2.75	[696, 697]
Adamantan-2-one 208 ⁺	δ γ 	2H(γ) 4H _{eq} (δ)	0.69 +2.23	[697]

vinyls **11**[•] (+6.85 and +3.42 mT) and **201**[•] (+5.79 and 3.29 mT) strongly depend on the positions of the β protons (*trans* or *cis*) relative to the in-plane SOMO. The finding that these coupling constants increase on going from the vinyls **11**[•] and **201**[•] to the alkaniminyls **200**[•] (+8.52 mT) and **204**[•] (+8.20 mT) and to the aldehyde radical cations **191**⁺ (+9.03 mT) and **192**⁺–**194**⁺ (+12.0 to +13.7 mT) is interpreted in terms of the enhanced electronegativity of X[•] and the shortening of the double bond >C=X[•] in the sequence X[•] = C[•]H, N[•], O^{•+}.

The substantial s contribution to the SOMO in vinyls, and even more so in acyls, is also indicated by the large coupling constants of the ¹³C-isotopes in the C[•] atom, such as $a_{\text{C}^{\bullet}}$ = +10.76 for **11**[•], +13.39 for **13**[•], and +11.36 mT for **203**[•]. On the other hand, the relatively small ¹⁴N-coupling constants $a_{\text{N}} \approx +1.0$ mT for iminyls are in accord with the nearly pure p character of the SOMO. The rather modest $|a_{\text{O}}|$ value of the ¹⁷O isotope in **13**[•] confirms the essential spin localization on the C[•] atom in acetyls. The coupling constants of some δ protons in the radical cations of alkylaldehydes and ketones are relatively large (+1.25 to +2.75 mT), whereas those of their γ counterparts are very small and often escape detection. The C–H(δ) bonds of the pertinent protons are in a planar W arrangement with respect to the axis of the SOMO at the O^{•+} atom (Chapt. 4.2).

Linking the N atom of an iminyl group to a π system does not lead to noticeable spin delocalization, because the spin-bearing p-AO lies in the nodal π plane. For example, the coupling constants a_{N} and $a_{\text{H}}(\beta)$ for phenylmethaniminyl (**206**[•]) and the a_{N} value of diphenylmethaniminyl (**207**[•]) differ only slightly from the corre-

sponding data for alkaniminyls **200'**, **203'** and **204'**; while the phenyl protons in **206'** and **207'** gave rise to very small splittings which were not reported for **206'**.

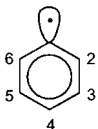
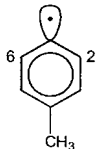
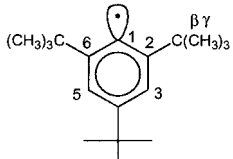
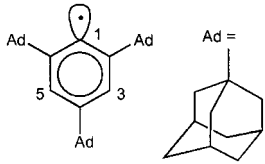
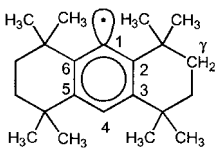
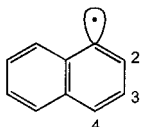
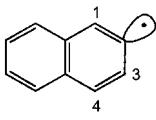
The g_e factors of vinyl and alkaniminyls are 2.0021 ± 0.0001 and 2.0029 ± 2.0002 , respectively. Those of acyls are as low as 2.0003–2.0007. For the radical cations of alkylaldehydes and alkylketones in Freon matrices, g_e factors of 2.003–2.005 were reported. Vinyl radicals **11'** and **201'** were generated from appropriate precursors both by photolysis in solid matrices [110] and with 2.8-MeV electrons in solution [34]. Formyl (**13'**) was first produced in solids [113] (Chapt. 2.2), but its formation, as well as that of the acetyls **202'** and **203'**, was later observed by photolysis of flowing solutions of ketones [553]. Alkaniminyls were generated in solution, namely **204'** from acetonitrile with 2.8-MeV electrons, and **200'** and **205'** from the corresponding azidoalkanes with *t*-BuO'. The phenyl-substituted iminyls **206'** and **207'** were formed by photolysis or thermolysis of the respective thiocarbamates. The radical cations of all alkylaldehydes and alkylketones were produced from the corresponding neutral compounds by γ -irradiation in matrices; with the exception of **191'** formed in solid sulfuric acid, CFCl₃ matrices were used.

Aryl Radicals

The aryl C-centered σ radicals are formally obtained when the ethenyl π moiety in vinyl (**11'**) is replaced by an aryl group. As in **11'**, the unpaired electron in aryl radicals is located in a nonbonding σ -AO when the pertinent C–H(α) or, generally, the C–X(α) σ bond in the aryl π system is cleaved. Because this spin-bearing AO lies in the nodal molecular plane of the π system, the spin population is largely confined to this AO and does not delocalize into the π -MOs. Table 7.11 [49, 112, 699–702] lists hyperfine data for phenyl and naphthyl radicals, and Table 7.12 gives data for some of their aza derivatives [703, 704]. The ¹H-coupling constants for the phenyl radical (**12'**) (Chapt. 4.3) decrease from the *ortho*- to the *meta*- and *para*-positions, i.e., with growing number of σ bonds separating the radical center from the protons in question. However, this interpretation does not suffice to account for the coupling constants of the ¹³C isotopes in the tri-*tert*-butyl derivative **16'**, where mechanisms such as σ - π and/or π - σ spin polarization must also be responsible for the spin transfer. The same statement also holds for the ¹H- and ¹³C-hyperfine data reported for the aryl radicals **210'**–**213'**.

The g_e factor of aryl radicals is in the range 2.0020–2.0025. As mentioned in Chapt. 2.2, the phenyl radical (**12'**) was obtained from solid iodide in a matrix by reaction with sodium [111] or photolysis [36] or from bromide by 2.8-MeV electrons in aqueous solution, a method also used for the formation of **214'** [112]. The sterically protected phenyl radicals **16'**, **210'**, and **211'** were generated in situ from the corresponding bromides with the photolytically produced Me₃Sn' radical in cyclopropane solution. They decayed, presumably by H tunnelling, **16'** to the 3,5-di-*tert*-butylneophyl, and **210'** and **211'** to unidentified radicals. Other less persistent, highly reactive aryl radicals were generated in the solid state. The radicals **212'**, **213'**, **215'**, **216'** and **220'**–**223'** were obtained by photolysis of corresponding halides in an argon matrix. γ -Irradiation of a single crystal of 4-toluenesulfonic acid

Tab. 7.11. Hyperfine Data for Some Phenyl and Naphthyl Radicals

Phenyl 12 [•]		H2,6 H3,5 H4	+1.743 +0.625 +0.204	[112]
<i>p</i> -Tolyl 209 [•]		H2,6	+1.82	[699]
2,4,6-Tri- <i>tert</i> -butylphenyl 16 [•]		H3,5 18H(γ) ¹³ C1 ¹³ C2,6 ¹³ C3,5 6 ¹³ C(β)	+0.731 0.030 +12.25 -0.616 +1.452 0.202	[49, 700, 701]
2,4,6-Tris(1-adamantyl)phenyl 210 [•]		H3,5 ¹³ C1	+0.71 +12.20	[700, 701]
1,1,4,4,5,5,8,8-Octamethyl- 1,2,3,4,5,6,7,8-octahydro- anthr-9-yl 211 [•]		H4 2H _{eq} (γ) ¹³ C1 ¹³ C2,6 ¹³ C3,5	+0.060 +0.060 +11.38 -0.600 +1.500	[701]
1-Naphthyl 212 [•]		H2 H3 H4	+1.9 +0.6 ~0.2	[702]
2-Naphthyl 213 [•]		H1 H3 H4	+1.57 +1.97 +5.8	[702]

led to 209[•], and 217[•]–219[•] were formed upon such irradiation of pyridazine, pyrimidine, and pyrazine, respectively, in a CFCl₃ matrix.

7.2

Si-, P-, and S-centered Radicals

These heteroatom-centered radicals are obtained when the spin-bearing atom in the C-, N-, and O-centered radicals is formally replaced by the corresponding

Tab. 7.12. Hyperfine Data for Some Azaphenyl and Azanaphthyl Radicals

Pyridin-2-yl 214 [•]		¹⁴ N H3 H4 H5 H6 ¹³ C2	+2.695 +0.499 +0.856 +0.412 +0.128 +17.0	[112] [703]
Pyridin-3-yl 215 [•]		H2,6 H4	+8.0 +1.9	[703]
Pyridin-4-yl 216 [•]		H2 H3	+1.0 +1.9	[703]
Pyridazin-3-yl 217 [•]		¹⁴ N2 H4,6	+2.8 +0.9	[704]
Pyrimidin-4-yl 218 [•]		¹⁴ N3 H5 H6	+2.8 +0.8 +1.3	[704]
Pyrazin-2-yl 219 [•]		¹⁴ N1 H3,6	+2.8 +0.8	[704]
Quinoxalin-2-yl 220 [•]		¹⁴ N1 H4	+2.6 +0.9	[703]
Quinoxalin-3-yl 221 [•]		H2 H4	+0.6 +1.9	[703]
Quinoxalin-4-yl 222 [•]		H2 H3 H8	+1.0 +2.0 +0.3	[703]
Isoquinoxalin-4-yl 223 [•]		H1 H3 H8	+0.5 +1.3 +0.5	[703]

Tab. 7.13. Hyperfine Data for Some Alkylsilyl Radicals

Silyl 224 [•]	α $\text{H}_3\text{Si}^\bullet$	3H(α) ^{29}Si	-0.796 -26.6	[705] [706]
Methylsilyl 225 [•]	β \bullet α CH_3SiH_2	2H(α) 3H(β) ^{29}Si	-1.182 +0.798 -18.1	[705] [707]
Dimethylsilyl 226 [•]	β \bullet α $(\text{CH}_3)_2\text{SiH}$	2H(α) 6H(β) ^{29}Si	-1.699 +0.719 -18.3	[705]
Trimethylsilyl 227 [•]	β $(\text{CH}_3)_3\text{Si}^\bullet$	9H(β) ^{29}Si	+0.628 -18.1	[705]
Triethylsilyl 228 [•]	γ β $(\text{CH}_3\text{CH}_2)_3\text{Si}^\bullet$	6H(β) 9H(γ)	+0.569 0.16	[705]

element of the next period. Such a replacement has a marked effect on the structure of the radicals, due to a lengthening and weakening of the bonds to the neighboring atoms, which diminish the tendency to flatten at the radical center and makes hyperconjugation less efficient. A few representative Si-, P-, and S-centered radicals are considered below.

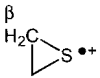
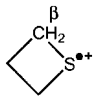
Alkylsilyl Radicals

Table 7.13 [705–707] lists hyperfine data for the silyl radical $\text{H}_3\text{Si}^\bullet$ (224[•]) and a few of its derivatives, in which one, two, or three H atoms are replaced by alkyl groups. In contrast to the alkyl radicals, their silyl counterparts are pyramidal at the spin-bearing atom. The $|a_{\text{H}}(\alpha)|$ values are much smaller than those for the corresponding alkyl radicals; the sign of these coupling constants should still be negative. Also, $a_{\text{H}}(\beta)$ values, which ought to be positive, are strongly reduced relative to those for alkyl radicals, as expected for the less efficient hyperconjugation. The large negative coupling constant, $a_{\text{Si}} = -18$ to -27 mT, of the ^{29}Si isotope (its g_{n} factor is negative) indicates considerable s contribution to the a spin-bearing Si-3p_z-AO. The g_{e} factor of alkylsilyl radicals is 2.0031–2.0032. These radicals were generated in solution by abstraction of a H atom from the corresponding silanes with *t*-BuO[•] or by γ -irradiation of these compounds in matrices.

Alkylphosphinyl Radicals

Only a few of these P-centered radicals $\text{R}^1\text{R}^2\text{P}^\bullet$ have been studied by ESR spectroscopy. Values $a_{\text{P}} = +9.7$ and $|A_{\text{H}}| = 1.3$ mT were reported for the ^{31}P nucleus and the two methine β protons in diisopropylphosphinyl $[(\text{CH}_3)_2\text{CH}]_2\text{P}^\bullet$ (229[•]) generated by γ -irradiation of the corresponding solid chloride [708]. The ratio, $a_{\text{P}}(229^\bullet)/a_{\text{N}}(164^\bullet) = +9.7 \text{ mT}/+1.43 \text{ mT} = 6.8$, of the coupling constants for this phosphinyl and the analogous diisopropylaminyl radical (Table 7.4), is similar to

Tab. 7.14. Hyperfine Data for Radical Cations of Some Thioethers

Dimethylsulfide 231 ⁺	β (CH ₃) ₂ S ^{•+}	6H(β)	+2.04	[712]
Thiirane 232 ⁺	β 	4H(β)	+1.61	[712]
Thietane 233 ⁺	β 	4H(β)	+3.11	[712]

the ratio of the values expected for the spin populations of +1 in the P-3p_z- and N-2p_z-AOs [476].

Alkylthiyl Radicals and Radical Cations of Alkylthioethers

Several thiyl radicals RS[•] ($g_e = 2.024$ to 2.030), in which R is an alkyl group, were produced by UV irradiation of the corresponding crystalline disulfides R₂S [709, 710]. In general, these radicals do not exhibit resolved hyperfine patterns. For the three methyl protons in methylthiyl H₃CS[•] (230[•]), an $|a_H(\beta)|$ value of 0.076 mT was reported [711], which is almost two orders of magnitude smaller than the corresponding value for the methoxyl radical H₃CO[•] (185[•]).

Hyperfine data for the radical cations of three thioethers are given in Table 7.14 [712]. The coupling constants $a_H(\beta)$ are generally smaller than those for the radical cations of the corresponding ethers. Analogous to 186⁺ and 188⁺, there is an increase in the $a_H(\beta)$ value of the methylene protons in 233⁺ relative to that of the protons in the freely rotating methyl groups in 231⁺. The much smaller $a_H(\beta)$ value for 232⁺ than for 233⁺ may be traced to the special geometry of the three-membered ring. The g_e factors are 2.014 for 231⁺ and 2.019 for 232⁺ and 233⁺. The radical cations of these three thioethers were generated by γ -irradiation in Freon matrices.

7.3

CC-, NN-, and OO-centered Radicals

Radical Cations of Alkyl Derivatives of Ethene

Although conjugated hydrocarbon radicals are dealt with in Chaps. 8.1–8.8, paramagnetic derivatives of ethene, a two-center π system, are considered here as CC-centered radicals. The radical ions of ethene tend to twist about the C–C linkage, of which the π -bond order is reduced from 1.0 in the neutral compound to 0.5 in the radical ions (anion: two electrons in the bonding π -MO and one in the antibonding π^* -MO; cation: one electron in the bonding π -MO). To our knowledge, the

structure of the radical ions of the parent ethene (**234**) has not yet been unequivocally established by ESR spectroscopy. An $|a_{\text{H}}|$ value of ca 0.3 mT was observed upon high-energy irradiation of ethene in a neon matrix at 4 K and was attributed to the four α protons in the radical cation **234**⁺ [713]. The $|a_{\text{H}}|$ value is very sensitive to twisting about the C–C bond and thus to deviations from planarity (Chapt. 4.4), as confirmed by high-level calculations which indicate that the 0.3 mT value with a negative sign corresponds to a twist angle of 28° [714]. This prediction can be interpreted as a result of interplay between π, σ -spin polarization and hyperconjugation (Eqs. 4.5 and 4.9):

$$a_{\text{H}} = \rho_{\mu}^{\pi} Q_{\text{H}}^{C_{\mu}H_{\mu}} + \rho_{\mu'}^{\pi} B_{\text{H}}^{C_{\mu'}CH_{\mu'}} \langle \cos^2 \theta \rangle$$

Setting $\rho_{\mu}^{\pi} = \rho_{\mu'}^{\pi} = +0.5$, $Q_{\text{H}}^{C_{\mu}H_{\mu}} = -2.5$ mT, $B_{\text{H}}^{C_{\mu'}CH_{\mu'}} = +8.7$ mT (see below), and $\theta = 90^{\circ} - 28^{\circ} = 62^{\circ}$, one obtains

$$a_{\text{H}} = 0.5(-2.5 + 8.7 \cdot 0.22) \text{ mT} = -0.3 \text{ mT}$$

Alkyl substitution of ethene strongly lowers its ionization energy and, accordingly, several radical cations of alkyl derivatives of ethene are sufficiently persistent to be studied by ESR spectroscopy. Table 7.15 [272, 273, 307, 340, 460, 715–720] lists the hyperfine data for some of them. Twisting of the radical cation about the C–C bond is, in a few cases, clearly indicated by a lowering of symmetry. For example, on passing from the neutral bicyclopropylidene (**241**) to its radical cation, the symmetry is reduced from D_{2h} to D_2 as the set of eight equivalent β protons in **241**⁺ splits into two sets of four. In contrast, ionization of bicyclobutylidene (**242**) seems not to affect the symmetry D_{2h} of the planar molecule, and the equivalence of the eight corresponding protons is apparently preserved in **242**⁺. In this case, as in many others, two equivalent twisted structures appear planar, because the interconversion barrier is low on the hyperfine time-scale [721]. In some radical cations, such as **246**⁺ and *syn*- and *anti*-**26**⁺, twisting can be hindered by embedding the double bond in a rigid molecular framework.

The π -spin population at the two π centers in the radical cations of the alkyl derivatives of ethene is not simply 0.5, but it decreases to an extent depending on the substituent. In analogy to Eq. 7.1 for substituted methyl radicals, a relation

$$\rho_{\mu'}^{\pi} = +0.5 \Pi_i [1 - \Delta(R^i)] \quad (7.2)$$

was proposed for the π -spin population $\rho_{\mu'}^{\pi}$ at an ethene center μ' substituted by alkyl groups R^i [273]. Parameters $\Delta(R^i) = 0.111$ and 0.237 were suggested for methyl and *tert*-butyl, respectively. The larger $\Delta(\text{Me})$ value for the radical cations (0.111) than for neutral radicals (0.081; Eq. 7.1) is consistent with the hyperconjugation being enhanced by the positive charge (Chapt. 4.2). Thus, a parameter $B_{\text{H}}^{C_{\mu'}CH_{\mu'}}$ as large as +8.72 mT is required in Eq. 4.8 for the coupling constant $a_{\text{H}}(\beta)$ in the freely rotating methyl groups of these radical cations. A $\Delta(R^i)$ value ($i = 1-2$) of 0.197 was derived for the bicyclic group in homoadamantene (**245**⁺),

Tab. 7.15. Hyperfine Data for Radical Cations of Some Alkyl Derivatives of Ethene

But-2-ene <i>cis</i> -235 ^{•+}		2H(α) 6H(β)	-0.90 +2.21	[307]
<i>trans</i> -235 ^{•+}		2H(α) 6H(β)	-0.88 +2.34	[307]
2,3-Dimethylbut-2-ene 236 ^{•+}		12H(β)	+1.72	[307]
2,2,3,4,5,5-Hexamethylbut-2-ene <i>cis</i> -237 ^{•+}		6H(β) 18H(γ)	+1.42 0.17	[715]
<i>trans</i> -237 ^{•+}		6H(β) 18H(γ)	+1.48 0.065	[715]
Cyclobutene 238 ^{•+}		2H(α) 4H(β)	-1.11 +2.80	[716]
Cyclopentene 239 ^{•+}		2H(α) 4H(β) 2H(γ)	-0.94 +4.73 0.70	[717]
Cyclohexene 240 ^{•+}		2H(α) 2H _{ax} (β) 2H _{eq} (β)	-0.88 +5.40 +2.25	[307]
Tricyclo[3.1.0.0 ^{2,6}]hex-3-ene (benzvalene) 73 ^{•+}		2H(α) 2H(β) 2H(γ)	-0.835 -0.158 +2.790	[460]
Bicyclopropylidene 241 ^{•+}		4H(β) 4H(β)	+2.24 -0.27	[340]
Bicyclobutylidene 242 ^{•+}		8H(β) 4H(γ)	+2.62 -0.27	[718]
2,2,2',2',4,4,4',4'-Octamethyl- bicyclobutylidene 243 ^{•+}		4H(γ) 24H(γ')	0.049 0.123	[719]

Tab. 7.15 (continued)

2,2,2',2',5,5,5',5',-Octamethyl- bicyclopentylidene 244 ^{•+}		4H(γ) 0.028 [719] 12H(γ') +0.203 12H(γ') <0.005 ¹³ C1,1' +0.88 [720]
Dimethylhomoadamantene 245 ^{•+}		2H(β) +0.062 [273] 6H(β') +1.555 4H _{eq} (γ) +0.454 4H _{ax} (γ) 0.050 2H(δ) +0.645
Sesquihomoadamantene 246 ^{•+}		4H(β) +0.043 [273] 8H _{eq} (γ) +0.486 8H _{ax} (γ) 0.043 4H(δ) +0.439
Sesquinorbornene <i>syn</i> -26 ^{•+}		4H(β) +0.392 [273] 2H _{anti} (γ) +0.746 2H _{syn} (γ) 0.083 4H _{exo} (γ') +0.353 4H _{endo} (γ') 0.076
<i>anti</i> -26 ^{•+}		4H(β) +0.326 [273] 2H _{anti} (γ) +1.346 2H _{syn} (γ) 0.103 4H _{exo} (γ') +0.311 4H _{endo} (γ') 0.068
Adamantylideneadamantane 25 ^{•+}		4H(β) +0.058 [272] 8H _{eq} (γ) +0.327 8H _{ax} (γ) 0.047 4H(δ) +0.605 4H(ϵ) 0.012

and similar values were estimated for such groups in adamantylidene (25^{•+}) and sesquinorbornenes (26^{•+}) [273].

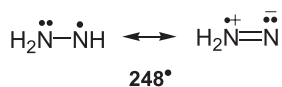
The coupling constant of the ¹³C isotopes in the two π centers of 244^{•+} is $a_C = +0.88$ mT [720]. This value agrees with that expected for this coupling constant in a derivative of an ethene radical ion, in which the spin population is evenly delocalized over both moieties. Originally, it has been suggested that the spin is localized on one cyclopentylidene moiety, because hyperfine interaction was observed for only half of the protons [719]. The observed coupling constants of the γ and δ protons in 25^{•+}, 73^{•+}, 245^{•+}, 246^{•+}, and *syn*- and *anti*-26^{•+} provide useful experimental data for long-range hyperfine interactions in rigid carbon frameworks (Chapt. 4.2).

The g_e factor reported for the radical cations presented in Table 7.15 varies considerably, from 2.0025 for *syn*-26^{•+} and 2.0026 for 244^{•+} to 2.0032 for 25^{•+}, 2.0028

for $241^{+\cdot}$, 2.0029 for $73^{+\cdot}$, 2.0033 for $246^{+\cdot}$, and 2.0037 for $242^{+\cdot}$. The radical cations $73^{+\cdot}$ and $235^{+\cdot}$ – $242^{+\cdot}$ were generated by γ -irradiation in Freon matrices, but the other, more persistent, species, $243^{+\cdot}$ – $246^{+\cdot}$, $25^{+\cdot}$, and *syn*- and *anti*- $26^{+\cdot}$, could be produced electrolytically in dichloromethane/TFA at a gold electrode. Substituents like adamantylidene, in which the C–H(β) bonds are forced to lie perpendicular to the $2p_z$ -axis at the π center, especially favor persistence. Radicals exhibiting this feature have been called “Bredt rule protected” [272]. For polycyclic radical cations, persistence increases in the order $245^{+\cdot} < \textit{anti}\text{-}26^{+\cdot} < \textit{syn}\text{-}26^{+\cdot} < 25^{+\cdot} < 246^{+\cdot}$. The presumably most stable radical cation among those listed in Table 7.15 is $244^{+\cdot}$, which can be readily generated from the neutral compound under a variety of conditions and persists for weeks if air is excluded. Radical cations with small rings are prone to ring-opening. Thus, $73^{+\cdot}$ isomerizes to the radical cation of benzene (**62**) [460], and $238^{+\cdot}$ and $241^{+\cdot}$ rearrange to the radical cations of *trans*-buta-1,3-diene (**92**) [716, 722] and tetramethyleneethane (TME; **43 \cdot**) [328], respectively. Whereas the rearrangement $238^{+\cdot} \rightarrow 92^{+\cdot}$ is photoinduced and occurs in any Freon matrix, ring-openings in $241^{+\cdot} \rightarrow 43^{+\cdot}$ are initiated thermally and require CFCl_3 as the matrix.

Alkylhydrazyl Radicals and Radical Cations of Alkylhydrazines

Starting from hydrazine, $\text{H}_2\text{N}-\text{NH}_2$ (**247**), the hydrazyl radical $\text{H}_2\text{N}-\dot{\text{N}}\text{H}$ (**248 \cdot**) and the radical cation $\text{H}_2\text{N}^{\pm}\text{NH}_2$ (**247 \cdot**) can be derived by abstraction of a H atom and removal of an electron from the N-lone pairs, respectively. Both radicals are analogous to the N-centered aminyl $\text{H}_2\text{N}\cdot$ (**160 \cdot**) and the ammonia cation H_3N^+ (**161 \cdot**), which also differ by a proton at one N atom. They are classified as NN-centered, because, in contrast to the aminyl and ammonia radical cations, with their unpaired electron localized on one N atom, the π -spin population is almost evenly shared by both N atoms. In hydrazyl (**248 \cdot**), with the unpaired electron formally centered at one N atom, the share of the second N atom can be represented by the substantial contribution of an ionic structural formula with a N=N double bond.

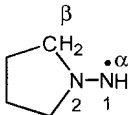


The hydrazyl radical thus has a N–N three-electron π bond like that in the iso-electronic hydrazine radical cation $\text{H}_2\text{N}^{\pm}\text{NH}_2$ (**247 \cdot**), which is considered in more detail below.

As in $\text{H}_2\text{N}\cdot$ (**160 \cdot**) and H_3N^+ (**161 \cdot**), the H atoms in **248 \cdot** and **247 \cdot** can be replaced by alkyl groups to yield $\text{R}^1\text{R}^2\text{N}-\text{N}\cdot\text{R}^3$ and $\text{R}^1\text{R}^2\text{N}^{\pm}\text{NR}^3\text{R}^4$, respectively, or the N atoms can be incorporated into a ring.

Although hydrazine (**247**) and its derivatives are pyramidal at the the N atoms, the corresponding radicals and radical cations are generally flattened at these atoms, as required for their π structure. Tables 7.16 [723–726] and 7.17 [272, 280,

Tab. 7.16. Hyperfine Data for Some Alkylhydrazyl Radicals

Hydrazyl 248 [•]	α' \bullet α H ₂ N-NH 2 1	¹⁴ N1 ¹⁴ N2 H(α) H(α') H(α')	+1.17 +0.88 -1.63 -0.43 -0.16	[723]
2,2-Dimethylhydrazyl 249 [•]	β \bullet α (CH ₃) ₂ N-NH 2 1	¹⁴ N1 ¹⁴ N2 H(α) 6H(β)	+0.960 +1.149 -1.367 +0.690	[724]
2,2-Diethylhydrazyl 250 [•]	β \bullet α (CH ₃ CH ₂) ₂ N-NH 2 1	¹⁴ N1 ¹⁴ N2 H(α) 4H(β)	+0.958 +1.114 -1.378 +0.673	[724]
2,2-Diisopropylhydrazyl 251 [•]	γ β \bullet α [(CH ₃) ₂ CH]N-NH 2 1	¹⁴ N1 ¹⁴ N2 H(α) 2H(β) 12H(γ)	+0.995 +1.166 -1.311 +0.22 0.025	[724]
Trimethylhydrazyl 252 [•]	β' \bullet β (CH ₃) ₂ N-NCH ₃ 2 1	¹⁴ N1 ¹⁴ N2 3H(β) 3H(β') 3H(β')	+1.17 +1.05 +1.76 +0.82 +0.59	[725]
(1-Pyrrolidinyl)aminyl 253 [•]	β \bullet α 	¹⁴ N1 ¹⁴ N2 H(α) 4H(β)	+1.06 +1.06 -1.34 +1.06	[726]

727–730] list hyperfine data for some of these hydrazyl radicals and hydrazine radical cations. The almost-even delocalization over both N atoms is indicated by the coupling constants a_N which are comparable for both ¹⁴N nuclei and lie in the range +0.9 to +1.2 mT for alkylhydrazyls and +1.3 to +1.5 mT for alkylhydrazine radical cations. The distinctly larger a_N values for the radical cations of some bicyclic hydrazines, such as **262**^{•+}, presumably arise from some pyramidalization at the N atoms. Due to spin delocalization on two N atoms, the radical cations of hydrazines are much more stable than their amine counterparts. Also, similar to the radical cations of amines, those of hydrazines become more persistent with an increased number of alkyl substituents. This statement holds, in particular, for the radical cations of tetraalkylhydrazines, and some of their oligocyclic analogues which, like **29**^{•+}, can be isolated as salts.

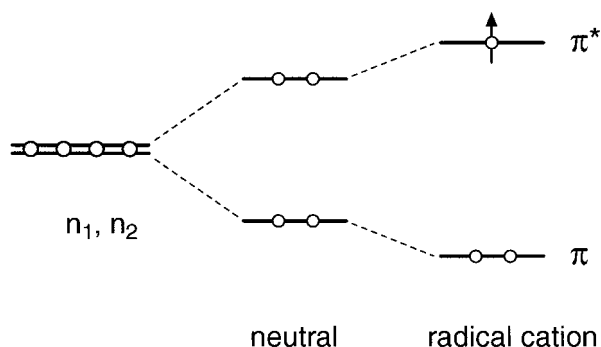
The g_e factor of hydrazyls and radical cations of hydrazines is 2.0032–2.0038. With the exception of **253**^{•+} produced by X-ray irradiation of 1-aminopyrrolidine in an adamantane matrix, the hydrazyl radicals were generated from the corresponding hydrazines in solution by H abstraction with *t*-BuO[•]. Electrolysis or reaction

Tab. 7.17. Hyperfine Data for Radical Cations of Some Alkylhydrazines

Hydrazine 247 ⁺		2 ¹⁴ N 4H(α)	+1.160 -1.154	[727]
1,2-Dimethylhydrazine <i>cis</i> -254 ⁺		2 ¹⁴ N 2H(α) 6H(β)	+1.47 -1.08 +1.26	[728]
<i>trans</i> -254 ⁺		2 ¹⁴ N 2H(α) 6H(β)	+1.303 -0.977 +1.219	[728]
1,1-Dimethylhydrazine 255 ⁺		¹⁴ N1 ¹⁴ N2 2H(α) 6H(β)	+0.969 +1.605 -0.691 +1.439	[729]
Tetramethylhydrazine 256 ⁺		2 ¹⁴ N 12H(β)	+1.338 +1.261	[729]
Tetraethylhydrazine 257 ⁺		2 ¹⁴ N 8H(β)	+1.315 +0.702	[280]
1,2-Dimethyl-1,2-azetidinium 258 ⁺		2 ¹⁴ N 6H(β) 4H(β')	+1.50 +1.31 +1.57	[730]
1,2-Dimethylpyrazolidinium 259 ⁺		2 ¹⁴ N 6H(β) 4H(β') 2H(γ)	+1.50 +1.28 +1.40 0.07	[280]
1,1-Biazetidinium 260 ⁺		2 ¹⁴ N 8H(β)	+1.48 +1.72	[280]
1,1-Bipyrrolidinium 261 ⁺		2 ¹⁴ N 8H(β) 8H(γ)	+1.29 +1.85 0.03	[280, 730]
1,5-Diazabicyclo[3.3.0]octane 262 ⁺		2 ¹⁴ N 8H(β) 4H(γ)	+1.76 +1.56 0.08	[280, 730]
2,3-Dimethyl-2,3-diazabicyclo- [2.2.1]heptane 263 ⁺		2 ¹⁴ N 6H(β) 2H _{exo} (γ') 1H _{anti} (γ') 1H _{syn} (γ')	+1.60 +1.31 +0.48 +0.17 0.08	[280]
2,3-Dimethyl-2,3-diaza- bicyclo[2.2.2]octane 264 ⁺		2 ¹⁴ N 6H(β) 4H _{exo} (γ)	+1.39 +1.27 +0.246	[280]
9,9'-Bis(9-azabicyclo- [3.3.1]nonane) 29 ⁺		2 ¹⁴ N 4H(β) 8H(γ) 8H(γ) 4H(δ) 4H(δ)	+1.33 +1.60 0.128 0.059 0.099 0.027	[272]

with tris(4-bromophenyl)ammoniumyl hexachloroantimonate (“magic blue”) in *n*-butyronitrile or ACN was used to generate the radical cations of tetraalkylhydrazines, and oxidation of less-substituted hydrazines was done with Ce(IV) ions in an acidic medium, using a flow system.

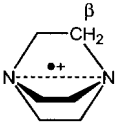
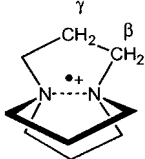
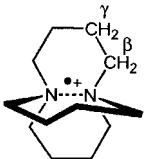
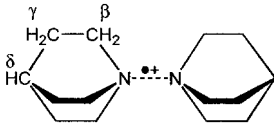
As stated above, formation of radical cations from hydrazines involves removal of an electron from the lone-electron pairs of the N atoms. Interaction between these nonbonding lone-pair AOs, n_1 and n_2 , leads to an energetically lower bonding π -MO and a higher-lying antibonding π^* -MO as the “plus” and “minus” combinations of the two AOs. In the neutral hydrazines having pyramidal geometry at the N atoms, this interaction is weak and so is the energy gap for the two MOs. Moreover, both MOs are occupied each by two lone-pair electrons. Thus, when the structure of the neutral hydrazines is considered, combining the lone-pair AOs into MOs can be disregarded from an energetic point of view. However in the radical cations, flattening at the N atoms leads to stronger interaction between n_1 and n_2 and to greater energetic splitting of π - and π^* -MOs. Therefore, removing an electron from the antibonding π^* -MO and leaving two electrons in the bonding π -MO results in substantial stabilization. This structural feature is referred to as a three-electron N–N π -bond. Actually, the overall order of the N–N bond is 1.5, because a half- π -bond (two bonding minus one antibonding electron) is added to the conventional σ bond.



Radical Cations of Alkyldiamines

An MO scheme analogous to that for hydrazines accounts for the formation of a three-electron N–N σ bond in the radical cations of several diamines, in which the two N atoms are formally not linked. Nevertheless, the nonbonding lone-pair AOs, n_1 and n_2 , at the two N atoms can interact through space and/or through methylene chains, combining to a bonding σ -MO and an antibonding σ^* -MO [730a]. Again, in contrast to the neutral diamines with both σ - and σ^* -MO's being doubly occupied, their radical cations have only one electron in the σ^* -MO, so that a three-electron N–N σ bond of order 0.5 is achieved. Hyperfine data for radical cations of three bicyclic alkyldiamines with this structural feature are given in Table 7.18 [297, 300, 349, 731]. The interaction of the N-lone pairs is essentially through bonds in $30^{+\cdot}$ [730a], but it is mainly through space in $31^{+\cdot}$ and $265^{+\cdot}$ [299]. The ^{14}N -

Tab. 7.18. Hyperfine Data for Radical Cations of Some Alkyldiamines

1,4-Diazabicyclo[2.2.2]octane (DABCO) $30^{+\cdot}$		2^{14}N +1.696 [297] 12H(β) +0.734
1,5-Diazabicyclo[3.3.3]undecane $265^{+\cdot}$		2^{14}N +1.47 [731] 12H(β) +2.22 6H(γ) 0.18
1,6-Diazabicyclo[4.4.4]tetradecane $31^{+\cdot}$		2^{14}N +3.59 [300] 6H(β) +1.76 6H(β) +0.086 6H(γ) -0.028 6H(γ) -0.01
Dimer of quinuclidine $(179)_2^{+\cdot}$		2^{14}N +3.87 [349] 12H(β) +0.337 12H(γ) 0.066 2H(δ) +0.406

coupling constant ranges from +1.47 in $265^{+\cdot}$ to +3.59 mT in $31^{+\cdot}$, because it strongly depends on the geometry at the N atoms which, in turn, determines the character of the σ^* -SOMO. More recently, such a dependence of the three-electron N–N σ bond in the radical cations of diamines has been systematically studied on the radical cations of more complex molecules [244] (Chapt. 9.4 and Table 9.40).

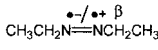
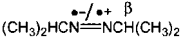
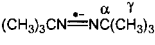
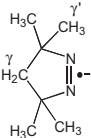
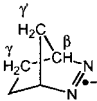
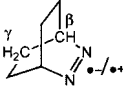
No g_e factors were reported for the radical cations of diamines. The three radical cations were generated by electrolytic or chemical oxidation of the corresponding diamines in ACN. Their ease of formation and persistence increased with growing size of the diamine. The two larger radical cations, $265^{+\cdot}$ and $31^{+\cdot}$, could be produced even with such mild oxidizing reagents as Ag(I) ion and care had to be taken to prevent their further oxidation to diamagnetic dication. Isolation of $31^{+\cdot}$ as a salt allowed its X-ray crystallographic structure analysis, which revealed the expected shortening of the N–N distance from 2.806 pm in neutral diamine 31 to 2.295 pm in $31^{+\cdot}$ [301].

A three-electron N–N σ bond can also be formed *intermolecularly*, as reported for the dimeric radical cation $(179)_2^{+\cdot}$ obtained by oxidation of quinuclidine (179) with $\text{O}_2^{+\cdot}$ SbF₆[−] in CHClF₂ (Table 7.18).

Radical Ions of Azoalkanes

The prototype of the azoalkanes is the hypothetical diimine HN=NH. The azo group –N=N– readily accepts an additional electron, which is accommodated in an

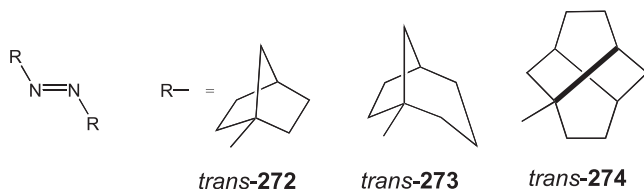
Tab. 7.19. Hyperfine Data for Radical Ions of Some Alkylazoalkanes

Diethyldiimine 266 ^{•-} /266 ^{•+}			Anion/Cation	
		² 14N	+0.775/+2.1	[732]/[733]
		4H(β)	+1.28/+1.78	
Diisopropyldiimine 267 ^{•-} /267 ^{•+}			Anion/Cation	
		² 14N	+0.80/+2.0	[732]/[733]
		2H(β)	+0.973/+1.60	
Di- <i>tert</i> -butyldiimine 268 ^{•-}			Anion	[734]
		² 14N	+0.824	
		18H(γ)	0.032	
		² 13C(α)	-0.480	
3,3,5,5-Tetramethyl-1-pyrazoline 269 ^{•-}			Anion	[552]
		² 14N	+0.923	
		2H(γ)	+0.048	
		12H(γ')	-0.072	
2,3-Diazabicyclo[2.2.1]hept-2-ene 270 ^{•-}			Anion	[552]
		² 14N	+0.855	
		2H(β)	+0.044	
		2H _{exo} (γ)	+0.340	
		2H _{endo} (γ)	-0.073	
		1H _{anti} (γ')	-0.223	
		1H _{syn} (γ')	-0.122	
2,3-Diazabicyclo[2.2.2]oct-2-ene 271 ^{•-} /271 ^{•+}			Anion/Cation	
		² 14N	+0.876/+3.14	[552]/[497, 735]
		2H(β)	-0.020/-0.336	
		4H _{exo} (γ)	+0.268/+1.51	
		4H _{endo} (γ)	-0.071/+0.135	

antibonding π^* -SOMO of this group. Hyperfine data for some of these radical anions are given in Table 7.19 [497, 552, 732–735]. The radical anions of acyclic and monocyclic azoalkanes are persistent only if they lack H atoms at the C atoms linked to the azo group. In acyclic radical anions of the general formula $R^1N=NR^2$, the alkyl groups are in the *trans* configuration, but in their cyclic counterparts, the azo group is constrained to the *cis* configuration. The ¹⁴N-coupling constant, which depends on experimental conditions, is +0.8 to +1.0 mT. Long-range hyperfine interactions are exhibited by the *exo* γ protons of the bicyclic radical anions **270^{•-}** and **271^{•-}**, but the corresponding $|a_H(\beta)|$ values are very small, because the pertinent protons lie in the nodal plane of the N=N π system.

The g_e value of radical anions of azoalkanes, which depends on the nature of the counterion, is 2.0037–2.0042. Radical anions that lack H atoms at the C atoms linked to the azo group were generated by reaction of the neutral compounds with an alkali metal in an ethereal solution, but the less persistent ones, like **266^{•-}** and **267^{•-}**, required some modifications of this method. The cyclic radical anions **269^{•-}**–**271^{•-}** form tight ion pairs with their alkali-metal counterions attached to

the azo group, and their ESR spectra exhibit substantial hyperfine splittings by the alkali-metal nuclei (Table A.2.2). In contrast to the radical anions of azoalkanes, the corresponding radical cations are not persistent in solution, because they rapidly lose dinitrogen upon oxidation. Thus, $266^{+\cdot}$, $267^{+\cdot}$ and $271^{+\cdot}$ were generated from the neutral azoalkanes by γ -irradiation in Freon matrices. Nevertheless, ESR spectra of radical cations of three *trans*-configured azoalkanes with two bulky oligocyclic alkyl groups, 1,1'-azonorbornane (**272**) [736, 737], 1,1'-azobicyclo[3.2.1]octane (**273**) [737], and 1,1'-azotwistane (1,1' azotricyclo[4.4.0.0^{3,8}]decane (**274**) [737], were observed in fluid solution. They were generated by oxidation of the neutral compounds with tris(2,4-dibromophenyl)ammoniumyl hexachloroantimonate ("magic green") in dichloromethane. The radical cation *trans*-**272**⁺ was also obtained by starting from the *cis* isomer [738].



The ^{14}N -coupling constants a_{N} for **272**⁺–**274**⁺ are +1.1 to +1.3 mT. The low g_{e} factor (2.0011 ± 0.0001) indicates that these radical cations are of σ -type, in contrast to their negatively charged π counterparts, **272**⁻–**274**⁻, with a_{N} and g_{e} values of $+0.80 \pm 0.02$ mT and 2.0041 ± 0.0001 . This statement is supported by the hyperfine data for the radical cations of the alkyldiimines, **266**⁺ and **267**⁺, and, in particular, by those for the radical cation of 2,3-diazabicyclo[2.2.2]oct-2-ene (**271**) ($g_{\text{e}} = 2.0022$). The coupling constants for **271**⁺ strikingly differ from those for the corresponding radical anion **271**⁻. The large increase in the coupling constant a_{N} , on going from the *trans*-configured radical cations **272**⁺–**274**⁺ to the bicyclic **271**⁺ (of which the azo group constrained to the *cis* configuration), is attributed to a marked decrease in the CNN angle.

Radical Cations of Diazoalkanes

These radical cations, in which the spin population is localized on the two N atoms of the diazo group, are not persistent because of the easy loss of dinitrogen [739, 740]. Their simplest representative, the unknown radical cation of diazomethane $\text{CH}_2\text{N}_2^{\cdot+}$, may have either a σ or a π structure, like those of its well-investigated phenyl and diphenyl derivatives (Chapt. 9.4).

Alkylperoxyl Radicals

The general formula of peroxyl radicals is ROO^{\cdot} , in which R is an alkyl or an aryl group. The simplest alkylperoxyls that have been studied by ESR spectroscopy are methylperoxyl $\text{CH}_3\text{OO}^{\cdot}$ (**275**[•]) [741], ethylperoxyl $\text{CH}_3\text{CH}_2\text{OO}^{\cdot}$ (**276**[•]) [742], 1-

propylperoxyl $\text{CH}_3\text{CH}_2\text{CH}_2\text{OO}^\cdot$ (**277'**) [743], 2-propylperoxyl $(\text{CH}_3)_2\text{CHOO}^\cdot$ (**278'**) [743], and *tert*-butylperoxyl $(\text{CH}_3)_3\text{COO}^\cdot$ (**279'**) [742]. Generally, alkylperoxyl radicals do not exhibit hyperfine splittings, but $|a_{\text{H}}(\beta)|$ values of ca 0.5 mT were observed for the methylene and methine protons at the C atoms adjacent to the peroxy group of **277'** and **278'**, respectively. With **279'**, enrichment in the ^{17}O isotope made it possible to measure coupling constants a_{O^1} and a_{O^2} of -2.18 and -1.64 mT for the $-\text{CO}^2\text{O}^1$ group. The g_e factor of the alkylperoxyls is rather high, 2.011–2.016, which confirms that they are π radicals with the unpaired electron in an antibonding π^* -MO. Autooxidation of many organic compounds proceed by chain processes that involve conversion of initially formed radicals R^\cdot into peroxyl radicals as an intermediate step: $\text{R}^\cdot + \text{O}_2 \rightarrow \text{ROO}^\cdot$ [744]. The peroxyalkyls mentioned above were generated in solution by photolysis of the corresponding peresters in the presence of dioxygen or by oxidation of hydroperoxides with Ce(IV) ions.

7.4

NO- and NO₂-centered Radicals

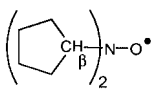
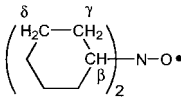
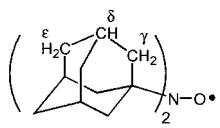
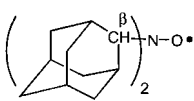
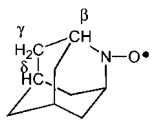
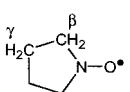
Alkylnitroxyl Radicals

The persistent nitroxyl π -radicals represent a large class of paramagnetic compounds, which have been extensively studied by ESR spectroscopy. Nitric oxide NO^\cdot (**280'**) has 11 valence electrons and is a stable inorganic radical with an unpaired electron in an antibonding π^* -MO. In dihydronitroxyl, $\text{H}_2\text{NO}^\cdot$ (**281'**), two electrons formally derived from one N-lone pair in NO^\cdot are engaged in two N–H bonds. In the acyclic alkylnitroxyls, $\text{R}^1\text{R}^2\text{NO}^\cdot$, the H atoms are substituted by alkyl groups, and in their cyclic counterparts the N atom is incorporated in a ring. Table 7.20 [98, 603, 745–759] lists hyperfine data for the gaseous NO^\cdot and several alkylnitroxyls in solution. The solvent- and temperature-dependent ^{14}N -coupling constant a_{N} varies, in general, from $+1.2$ to $+1.7$ mT. The $a_{\text{H}}(\alpha)$ value is -1.19 for **281'** and -1.38 mT for **282'**, and $a_{\text{H}}(\beta)$ is $+1.1$ to $+1.4$ mT for methyl and methylene protons in **282'**–**284'**, and ca $+0.4$ mT for methine protons in **285'**–**287'**. An ^{17}O -coupling constant a_{O} close to -2 mT was reported for **108'** and **8'**. Alkylnitroxyls are planar at the N atom, and the unpaired electron is almost entirely located in an antibonding π^* -SOMO of the NO^\cdot group. Although the precise spin distribution between the N and O centers is still uncertain, the spin population ρ_{N}^π and ρ_{O}^π values should be comparable, i.e., they are both near $+0.5$ [759]. A relation

$$a_{\text{N}} = Q_{\text{N}}\rho_{\text{N}}^\pi + Q_{\text{N}}^{\text{NO}}\rho_{\text{O}}^\pi \quad (7.3)$$

with the parameters $Q_{\text{N}} \approx +2.8$ mT and $|Q_{\text{N}}^{\text{NO}}| \ll |Q_{\text{N}}|$ is expected to hold for the ^{14}N -coupling constant in nitroxyls. Setting the spin populations $\rho_{\text{N}}^\pi \approx +0.5$ and neglecting the second term, Eq. 7.3 yields $a_{\text{N}} \approx +1.4$ mT, in accord with

Tab. 7.20. Hyperfine Data for Some Alkylnitroxyl Radicals

Nitrogen oxide 280 [•]	N-O [•]	¹⁴ N	+1.06	[745]
Dihydrornitroxyl 281 [•]	α H ₂ N-O [•]	¹⁴ N	+1.19	[746]
		2H(α)	-1.19	
Methylnitroxyl 282 [•]	β α (CH ₃)NH-O [•]	¹⁴ N	+1.38	[746]
		H(α)	-1.38	
		3H(β)	+1.38	
Dimethylnitroxyl 283 [•]	β (CH ₃) ₂ N-O [•]	¹⁴ N	+1.52	[746]
		6H(β)	+1.23	
Diethylnitroxyl 284 [•]	γ β (CH ₃ CH ₂) ₂ N-O [•]	¹⁴ N	+1.67	[98]
		4H(β)	+1.12	
		6H(γ)	0.032	
Diisopropylnitroxyl 285 [•]	β [(CH ₃) ₂ CH] ₂ N-O [•]	¹⁴ N	+1.59	[98]
		2H(β)	+0.405	
Di- <i>tert</i> -butylnitroxyl 108 [•]	β α [(CH ₃) ₃ C] ₂ N-O [•]	¹⁴ N	+1.62	[747]
		9H(γ)	-0.095	[748]
		¹³ C(α)	-0.469 ^a	[749]
		3 ¹³ C(β)	0.450 ^a	
		¹⁷ O	-1.941	[750]
Dicyclopentylnitroxyl 286 [•]		¹⁴ N	+1.49	[751]
		2H(β)	+0.44	
Dicyclohexylnitroxyl 287 [•]		¹⁴ N	+1.44	[752]
		2H(β)	+0.44	
		8H(γ)	0.043	
		4H _{eq} (δ)	0.083	
Bis(1-adamantyl)nitroxyl 288 [•]		¹⁴ N	+1.52	[753]
		12H(γ)	-0.041 ^a	
		6H(δ)	+0.054	
		6H(ϵ)	-0.0035	
		6H(ϵ)	-0.0015	
Bis(2-adamantyl)nitroxyl 289 [•]		¹⁴ N	+1.41	[754]
		2H(β)	+1.41	
N-oxy-2-azaadamantane 104 [•]		¹⁴ N	+1.975	[603]
		2H(β)	+0.295 ^a	
		4H _{eq} (γ)	+0.180	
		4H _{ax} (γ)	+0.095	
		2H(δ)	+0.19	
Pyrrolidinyl-1-oxyl 290 [•]		¹⁴ N	+1.66	[755]
		4H(β)	+2.23	
		4H(γ)	0.047	

Tab. 7.20 (continued)

Piperidinyl-1-oxyl 291 [•]		¹⁴ N 2H _{ax} (β) 2H _{eq} (β) 2H _{ax} (γ) 1H _{eq} (δ)	+1.69 +2.015 +0.345 0.065	[756]
2,2,6,6-Tetramethylpiperidinyl-1-oxyl 292 [•]		¹⁴ N 4H(γ) 12H(γ') 2H(δ) 2 ¹³ C(α) 2 ¹³ C(β) ¹³ C(γ) 2 ¹³ C _{ax} (β') 2 ¹³ C _{eq} (β') ¹⁷ O	+1.615 -0.039 ^a -0.023 +0.018 -0.36 +0.49 -0.032 +0.49 +0.082 -1.805	[757] [758]
2,2,6,6-Tetramethyl-4-oxopiperidinyl-1-oxyl (TEMPO) 8 [•]		¹⁴ N 4H(γ) 12H(γ') 2 ¹³ C(α) 2 ¹³ C(β) 4 ¹³ C(β') ¹³ C(γ) ¹⁷ O	+1.445 -0.002 ^a -0.012 -0.51 +0.23(+0.25) +0.57(+0.61) -0.038 -1.929	[759] [758]

^a Hyperfine data by NMR

experiment. A value $\rho_{\text{O}}^{\pi} \approx +0.5$ also accounts for the coupling constant $a_{\text{O}} \approx -2$ mT if the parameter $Q_{\text{O}} = -4.1$ mT is used in Eq. 4.28. Polar solvents tend to increase ρ_{N}^{π} and a_{N} at the expense of ρ_{O}^{π} and $|a_{\text{O}}|$, because they favor the ionic structural formula over the covalent one.



The polycyclic nitroxyl **104'** represents an exception, because its a_{N} value is close to +2 mT, which indicates a nonplanar geometry at the N atom. The coupling constants of the protons in the rigid adamantane framework exemplify long-range hyperfine interactions, as do the corresponding values in other radicals (**157'** and **158'**) and radical cations (**25^{•+}**, **180^{•+}**, **208^{•+}**, **245^{•+}** and **246^{•+}**) containing this framework.

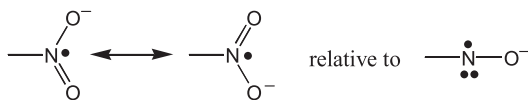
The most persistent nitroxyls radicals, like **108'**, **292'**, and **8'**, lack H atoms at the C atoms linked to the NO group. That is why such paramagnetic species are favored as spin labels and spin adducts (Appendix A.1). Among them, 2,2,6,6-tetramethyl-4-oxopiperidinyl-1-oxyl (TEMPO; **8'**) is included in Table 7.18 as the only alkylnitroxyl containing a heteroatom outside the NO[•] group. It is presumably

the best known and the most persistent nitroxyl radical and has been widely investigated.

As mentioned in Part A of this book, the g_e factor of nitroxyls is 2.0055 to 2.0065 (Chapt. 6.2), and they are generated by oxidation of the corresponding secondary amines or hydroxyamines with peroxides, Ag(I), Tl(III), Ce(IV) or Pb(IV) ions in various solvents (Chapt. 2.2).

Radical Anions of Nitrosoalkanes and Nitroalkanes

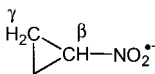
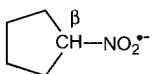
The prototypes of nitrosoalkanes $\text{RN}=\text{O}$ and nitroalkanes RNO_2 , in which R is an alkyl, are the hypothetical $\text{HN}=\text{O}$ (occurring as a dimer $\text{H}_2\text{N}_2\text{O}_2$), and nitrous acid HNO_2 , respectively. $\text{HN}=\text{O}$ is isoelectronic with diimine $\text{HN}=\text{NH}$, because the O atom in the former replaces the NH moiety in the latter. Addition of a second O atom to the nitroso group $-\text{N}=\text{O}$, yielding the nitro group $-\text{NO}_2$, has a stabilizing effect. Thus, HNO_2 , in contrast to HNO , is a well-known acid and, analogously, the nitroalkanes are more stable than their nitroso counterparts. Like $-\text{N}=\text{N}-$, the electron-attracting nitroso group, $-\text{N}=\text{O}$, readily takes up an additional π^* electron to yield the corresponding radical anion. This tendency is even more pronounced for the nitro group, $-\text{NO}_2$, in which the electron affinity is enhanced by a second O atom. Accordingly, the radical anions of nitroalkanes are much more frequently encountered than those of the energetically less favored nitrosoalkanes. The radical anion, $(\text{CH}_3)_3\text{CN}=\text{O}^{\cdot-}$ (**293**^{•-}) [760], of 2-nitroso-2-methylpropane has ¹⁴N- and ¹⁷O-coupling constants $a_{\text{N}} = +1.21$ and $a_{\text{O}} = -1.42$ mT, which are 20%–25% smaller than the corresponding values for alkyl nitroxyls. As shown in Table 7.21 [761–764], which gives hyperfine data for radical anions of some nitroalkanes, their ¹⁴N-coupling constant, $a_{\text{N}} = +2.3$ to $+2.7$ mT, is roughly twice as large as the value for **293**^{•-}. Simultaneously, the ¹⁷O-coupling constant changes from -1.42 mT for the single O atom in the nitroso group of **293**^{•-} to -0.51 mT for the two ¹⁷O nuclei in the nitro group of **279**^{•-}. The large increase in the a_{N} value on going from radical anions of nitrosoalkanes to those of nitroalkanes is not solely attributed to larger spin population ρ_{N}^{\cdot} at the N atom, as suggested by the greater weight of the two structural formulas



Whereas the radical anions of nitrosoalkanes, like alkyl nitroxides, are planar at the N atom, those of nitroalkanes should be slightly pyramidal.

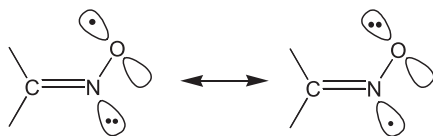
The g_e factor of radical anions of nitroalkanes ranges from 2.0050 to 2.0055. Although electrolytic reduction of the neutral nitrosoalkanes and nitroalkanes in DMF or ACN is a standard method to generate the corresponding radical anions, reaction of chemical reagents with various precursors, often in water and by means of a flow system, is also used.

Tab. 7.21. Hyperfine Data for Radical Anions of Some Nitroalkanes

Nitromethane 294 ⁻	β (CH ₃)NO ₂ ⁻	¹⁴ N 3H(β)	+2.555 +1.202	[761]
Nitroethane 295 ⁻	$\beta\gamma$ $\alpha\beta$ (CH ₃ CH ₂)NO ₂ ⁻	¹⁴ N 2H(β) 3H(γ) ¹³ C(α) ¹³ C(β)	+2.597 +0.963 0.045 <0.25 +0.605	[762]
2-Nitropropane 296 ⁻	$\beta\gamma$ $\alpha\beta$ [(CH ₃) ₂ CH]NO ₂ ⁻	¹⁴ N H(β) 6H(γ) ¹³ C(α) 2 ¹³ C(β)	+2.54 +0.48 0.03 <0.3 +0.511	[761] [762]
2-Nitro-2-methylpropane 297 ⁻	$\beta\gamma$ (CH ₃) ₃ CNO ₂ ⁻	¹⁴ N 9H(γ) 3 ¹³ C(β) 2 ¹⁷ O	+2.659 0.020 +0.37 -0.51	[762] [760]
Nitrocyclopropane 298 ⁻	γ β 	¹⁴ N H(β) 4H(γ)	+2.38 +0.73 0.06	[763]
Nitrocyclopentane 299 ⁻	β 	¹⁴ N H(β)	+2.70 +0.83	[764]

Iminoxyl Radicals

The general formula of acyclic alkaniminoxyls is R¹R²C=N-O[•], where Rⁱ is a H atom or an alkyl group; in cyclic alkaniminoxyls, the C atom of the double bond is incorporated into a ring. The electronic structure of these radicals is represented by the formulas below, in which the spin population is almost evenly shared by a 2p-AO at the O atom and an spⁿ-hybrid at the N atom.



Both AOs lie in the nodal plane of the C=N π -MO, so that iminoxyls are classified as σ radicals centered on the NO[•] group. Table 7.22 [765–770] lists hyperfine data for some alkaniminoxyls. Their σ character is indicated by ¹⁴N-coupling constants a_N of ca +3 mT, due to the substantial s contribution to the spin-bearing AO at the N atom. Like the corresponding values for vinyl σ radicals (Table 7.9), the coupling constants $a_H(\beta)$ of the protons at the in-plane C atom of the double bond differ strongly, according to their *cis* or *trans* position.

Tab. 7.22. Hyperfine Data for Some Alkaniminoxyl Radicals

Methaniminoxyl 300 [•]		¹⁴ N H _{cis} (β) H _{trans} (β)	+3.33 +2.62 +0.28	[765]
Ethaniminoxyl 301 [•]		¹⁴ N H _{trans} (β)	+3.25 +0.52	[766]
2,2-Dimethylpropaniminoxyl <i>trans</i> -302 [•]		¹⁴ N H _{cis} (β)	+3.05 +2.70	[767]
<i>cis</i> -302 [•]		¹⁴ N H _{trans} (β) 9H(δ)	+3.22 +0.74 0.0095	[767]
2,4-Dimethylpentan-3-iminoxyl 303 [•]		¹⁴ N H(γ), H(γ') 6H(δ), 6H(δ')	+3.07 0.12	[768]
2,2,4,4-Tetramethylpentan-3- iminoxyl 304 [•]		¹⁴ N 9H(δ) 9H(δ') ¹⁷ O	+3.132 +0.077 ^a +0.048 -2.26	[769] [770]
Bis(1-adamantyl)methaniminoxyl 305 [•]		¹⁴ N 12H(γ) 6H(δ) 6H _{ax} (ε)	+3.114 +0.055 ^a +0.019 +0.002	[769]
Cyclobutaniminoxyl 306 [•]		¹⁴ N	+3.16	[768]
Cyclopentaniminoxyl 307 [•]		¹⁴ N	+3.22	[768]
Cyclohexaniminoxyl 308 [•]		¹⁴ N 2H(β) 2H(β')	+3.07 +0.28 +0.14	[768]

^a Hyperfine data by NMR

Because the spin-bearing σ -AOs of the iminoxyl group do not conjugate with the π -MO of C=N, substitution of the C atom by phenyl or naphthyl moieties (R¹ and/or R² = aryl) leaves the spin population essentially localized in this group. Nevertheless, some of these substituted iminoxyls, for which hyperfine data are given in Table 7.23 [115, 767, 771, 772], exhibit remarkable features: Such aryliminoxyls

Tab. 7.23. Hyperfine Data for Some Aryl-substituted Iminoxyl Radicals

Phenylmethaniminoxyl <i>syn</i> -15 [•]		¹⁴ N H(β) 2H _o	+3.26 +0.65 +0.14	[115]
<i>anti</i> -15 [•]		¹⁴ N H(β) 2H _o	+3.00 +2.70 <0.05	
1-Phenylethan-1-iminoxyl 309 [•]		¹⁴ N 2H _o 3H(γ)	+3.16 +0.135 0.135	[771]
1-(2-Fluorophenyl)ethan-1-iminoxyl <i>syn</i> -310 [•]		¹⁴ N 3H(γ) ¹⁹ F	+3.195 0.150 +0.660	[767]
<i>anti</i> -310 [•]		¹⁴ N 3H(γ) ¹⁹ F	+3.20 0.14 <0.05	
Diphenylmethaniminoxyl 311 [•]		¹⁴ N H _o , H _{o'}	+3.15 +0.135	[771]
Fluoreniminoxyl 312 [•]		¹⁴ N H ₁ H ₈ ¹³ C ₉ ¹³ C _{9a}	+3.085 +0.270 +0.100 2.66 0.96	[772]
1-Fluorofluoreniminoxyl <i>syn</i> -313 [•]		¹⁴ N H ₈ ¹⁹ F	+3.110 +0.081 +1.350	[772]
<i>anti</i> -313 [•]		¹⁴ N H ₈ ¹⁹ F	+3.260 +0.285 +0.440	[772]

Tab. 7.23 (continued)

1-Naphthylmethaniminoxyl <i>syn</i> -314 [•]		¹⁴ N H(β) H2	+3.24 +0.705 +0.28	[767]
<i>anti</i> -314 [•]		¹⁴ N H(β) H2	+3.10 +2.75 <0.05	[767]

occur in two isomeric forms, *syn* (or *Z*) and *anti* (or *E*), which distinctly differ in their hyperfine patterns. Of particular interest is the through-space interaction between the unpaired electron at the O atom and magnetic nuclei of the π moieties linked to the iminoxyl group. In *syn*-phenylmethaniminoxyl (*syn*-15[•]), such a nucleus is represented by one *ortho* proton which is spatially close to the O atom. The reported coupling constant a_{H_o} of +0.14 mT is, however, less than the actual value of this single proton, because it arises as an average from both *ortho* protons H_o through rapid rotation of the phenyl group about the C–C bond. For *anti*-15[•], with large O–H_o distances, the corresponding value is too small to be observed. As in the alkyl derivatives (Table 7.22), the coupling constant, $a_{H(\beta)}$, of the proton at the C atom of the iminoxyl group also differs strongly according to its position in the *syn*- and *anti*-isomers. Interestingly, for steric reasons, 15[•] prefers the *anti* conformation, whereas for its N-methyl derivative 309[•] only the *syn*-isomer was detected. The coupling constants a_N and $a_{H(\beta)}$ for the *syn*- and *anti*-1-naphthylmethaniminoxyls (314[•]) are similar to those of the corresponding isomers of 15[•], because the protons at the fused ring do not contribute to the observed hyperfine pattern. Due to of the slower rotation of the naphthyl group, the coupling constant, $a_{H2} = +0.28$ mT, of the single proton close to the O atom in *syn*-314[•] is observed; it is twice the averaged a_{H_o} value of two protons in *syn*-15[•].

For diphenylmethaniminoxyl (311[•]), the corresponding coupling constant is an average value of two *ortho* protons in the phenyl group *syn* to the O atom. On the other hand, in fluoreniminoxyl (312[•]), with a similar spin distribution but with the two phenyl groups fixed by a C–C linkage the coupling constant, a_{H1} , of the pertinent proton is twice the corresponding two-proton value (+0.135 mT) for 311[•]. The difference in the hyperfine patterns for the conformations, *syn* (or *Z*) and *anti* (or *E*), of an iminoxyl is even more pronounced when the atom spatially close to the O atom is F. This finding is exemplified by 310[•] and 313[•], which are *ortho*-fluoro derivatives of 309[•] and 312[•], respectively. Whereas the ¹⁹F-coupling constant of in *syn*-310[•] is +0.66 mT, the corresponding a_F value for the *anti*-isomer is too

small to be observed. The analogous coupling constants for *syn*- and *anti*-**313'** are $a_F = +1.35$ and $+0.44$ mT, respectively.

The g_e factor of iminoxyls is 2.0051 to 2.0064. With the exception of **300'**, which was produced by photolysis of diazomethane in the presence of nitric oxide in an argon matrix, these radicals were generated in solution by abstraction of a H atom from the corresponding aldoxims or ketoximes in an organic solvent or in an aqueous acetone by means of Ce(IV) or Pb(IV) ions in a flow system, as already stated in Chapt. 2.2. An alternative procedure was trapping of transient radicals by benzonitrile; when applied to the formation of **309'** and **311'**, these transient radicals were methyl and phenyl, respectively.

7.5

PO-, PP-, SO-, SS-, and SO₂-centered Radicals

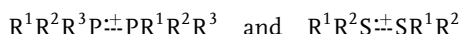
Alkylphosphonyl, Alkylsulfinyl, and Alkylsulfonyl Radicals

The general formulas of these phosphonyl, sulfinyl, and sulfonyl radicals are $R^1R^2P^{\cdot}=O$, $RS^{\cdot}=O$, and $RS^{\cdot}O_2$, respectively. Their simplest representatives are dimethylphosphonyl $(CH_3)_2P^{\cdot}=O$ (**315'**) [773], methylsulfinyl $CH_3S^{\cdot}=O$ (**316'**) [774], and methylsulfonyl $CH_3S^{\cdot}O_2$ (**317'**) [775]. The radical **315'** ($g_e = 2.005$) has a ^{31}P -coupling constant $a_P = +37.3$ mT and an $a_H(\beta)$ value of $+5.6$ mT for the six protons of the two methyl groups. The ratio, $a_P(\mathbf{315}')/a_N(\mathbf{283}') = +37.7$ mT/ $+1.52$ mT = 24.6, of the coupling constants for this phosphonyl and the analogous dimethylnitroxyl radical (Table 7.20) is three times larger than the values expected for the spin populations of $+1$ in the $P-3p_z$ - and $N-2p_z$ -AOs [476], a finding that indicates a pronounced pyramidal geometry of **315'** at the P atom in contrast to the planarity of **283'**. The coupling constants of the three methyl β -protons are $+1.16$ for **316'** ($g_e = 2.012$) and $+0.058$ mT for **317'** ($g_e = 2.049$). In addition, an ^{33}S -coupling constant $a_S = +0.8$ mT was reported for **316'**, which is isoelectronic with $SO_2^{\cdot-}$. This a_S value is rather small for such coupling constants and indicates a substantial contribution of the structural formula $-\ddot{S}-O^{\cdot}$ to $-S^{\cdot}=O$.

The radicals **315'** and **316'** were generated in the solid state by γ -irradiation of $(CH_3)_3PO$ and $(CH_3)_2SO$, respectively, and **317'** was produced in solution by photolysis of CH_3SO_2Cl with Et_3Si^{\cdot} formed from Et_3SiH and $t-BuO^{\cdot}$.

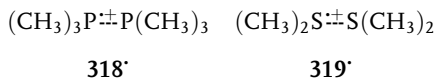
Radical Cations of Alkanediphosphines and Alkanedisulfides

Radical cations of these diphosphines and disulfides, which have, respectively, the general formulas



are usually formed as dimers by oxidation of the corresponding phosphines $R^1R^2R^3P$ and sulfides R^1R^2S . The two moieties are linked by a P–P or a S–S three-

electron σ bond, which is analogous to its N–N counterpart in the radical cations of diamines considered in a section above. The simplest radical cations of this kind are those of hexamethyldiphosphine and tetramethyldisulfide



The coupling constant, a_{P} , of the two ³¹P nuclei in **318**[·] ($g_e = 2.005$) is +48.2 mT, but only two of its 18 methyl β protons gave rise to an observable hyperfine splitting, of ca 2 mT, in the ESR spectrum of this radical cation formed by γ -irradiation of trimethylphosphine in a CH₂Cl₂ matrix [352]. For the 12 methyl protons in **319**[·] ($g_e = 2.0103$) generated from dimethylsulfide with Ti(III) ions and H₂O₂ in acidic solution by means of a flow system [353], a coupling constant $a_{\text{H}}(\beta) = +0.68$ mT was reported. As mentioned in Chapt. 2.3, additional radical cations with a P–P [350–353] or an S–S [354–357] three-electron σ bond were also obtained, as were those with an analogous Se–Se [358], or As–As [350, 359] bond.

8 Conjugated Hydrocarbon Radicals

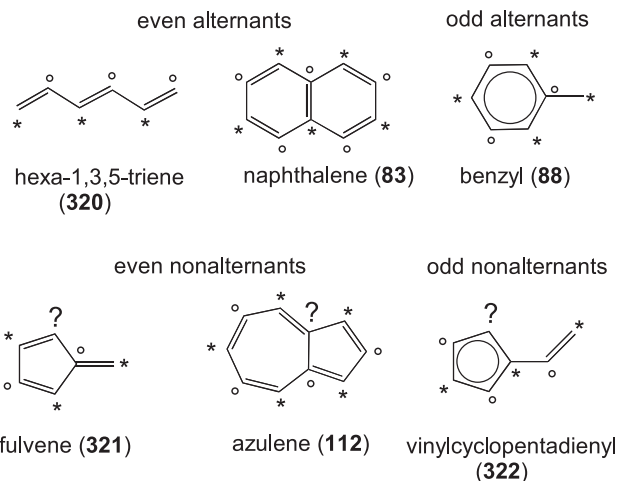
8.1

Theoretical Introduction

Paramagnetic conjugated hydrocarbons are π radicals *par excellence*, and their spin distribution is readily interpreted by simple theoretical models. These π radicals can be referred to as *even* or *odd* according to whether the number, n , of their carbon π centers is even or odd. Because the number of their π electrons, $N = n + \Delta N$, must be odd, the number ΔN is even for odd and odd for even radicals. $\Delta N = 0$ for neutral odd radicals, ± 1 for even radical ions, ± 2 for odd radical diions, and ± 3 for even radical triions, where the plus sign in front of ΔN refers to anions and the minus sign to cations.

Alternant and Nonalternant π Systems

With respect to topology, π systems are classified as *alternant* and *nonalternant*. In an alternant π system, the n π centers (μ) can be divided into starred (μ^*) and unstarred (μ°) centers in such a way that bonds occur only between μ^* and μ° [488, 489]. Obviously, a system of this kind cannot contain odd-membered rings, which would make it nonalternant. Below, examples are given for two even and one odd alternant system, as well as for their nonalternant counterparts with the same number, n , of centers.



By convention, the number of centers μ^* in an alternant π system is the same or larger than μ° , whereby the excess of μ^* must be even for an even and odd for an odd system. A common even alternant system has $n/2$ centers in each set, μ^* and μ° , and in a less common system made up of the so-called non-Kekulé hydrocarbons (Chapts. 2.4 and 11.3), $(n/2) + 1$ centers are μ^* and $(n/2) - 1$ are μ° . An odd alternant system has $(n + 1)/2$ centers μ^* and $(n - 1)/2$ centers μ° .

By virtue of its simplicity and lucidity, the Hückel-MO model is a useful tool for qualitative and semi-quantitative treatments of π systems. Such a system with n centers has n π -MOs, which for of an alternant system are related by *pairing* properties, because every bonding MO ψ_j is *paired* with an antibonding MO ψ_j . Their energies are

$$E(\psi_j) = \alpha + x_j\beta \quad \text{and} \quad E(\psi_j) = \alpha + x_j\beta \quad (8.1)$$

where α (≈ -8 eV) and β (≈ -2 eV) stand for the Coulomb and bond parameters, respectively. The number x_j , diagnostic of the energy of MO ψ_j , is dimensionless, being positive for bonding and negative for antibonding orbitals; x_j is zero for a nonbonding MO (NBMO) and can assume values between +3 and -3. Because

$$x_j = -x_j \quad (8.2)$$

the levels $E(\psi_j)$ and $E(\psi_j)$ lie symmetrically to the level of the NBMO, $E = \alpha$. In the LCAO presentation, the paired MOs are

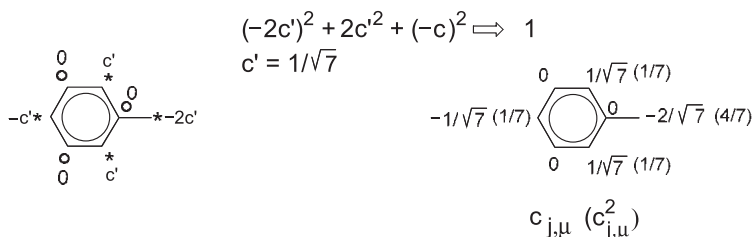
$$\psi_j = \sum_{\mu^*} c_{j,\mu^*} \phi_{\mu^*} + \sum_{\mu^\circ} c_{j,\mu^\circ} \phi_{\mu^\circ} \quad \text{and} \quad \psi_j = \sum_{\mu^*} c_{j,\mu^*} \phi_{\mu^*} + \sum_{\mu^\circ} c_{j,\mu^\circ} \phi_{\mu^\circ} \quad (8.3)$$

Their LCAO coefficients are related by

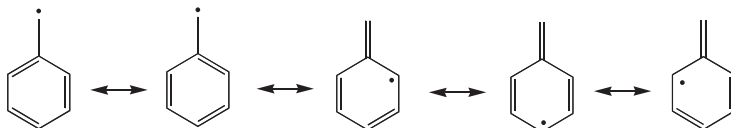
$$c_{j,\mu^*} = c_{j,\mu^*} \quad \text{and} \quad c_{j,\mu^\circ} = -c_{j,\mu^\circ} \quad (8.4)$$

so that $c_{j,\mu^*}^2 = c_{j,\mu^*}^2$ for all centers μ . For common even alternant π systems, which have $n/2$ bonding and $n/2$ antibonding MOs, it is essential that the lowest antibonding and the highest bonding MO be paired. Because of their occupancy in the neutral system, these two “frontier” MOs are usually referred as LUMO (lowest unoccupied) and HOMO (highest occupied), respectively. In the corresponding radical ions, one of them becomes the singly occupied MO (SOMO), namely, the LUMO in the anion and the HOMO in the cation. Because the squared LCAO coefficients, $c_{j,\mu}^2$, of the SOMO ψ_j represent the Hückel approximation of the spin populations ρ_μ^π at the centers μ (Chapt. 4.2), pairing of the LUMO with the HOMO means that the spin distribution in the radical anion and radical cation of the same alternant π system should be the same. This equality, which is also preserved in the McLachlan procedure and in some other more sophisticated MO methods, implies very similar hyperfine patterns in the ESR spectra of the two corresponding “alternant” radical ions.

In odd alternant π systems, $(n - 1)/2$ bonding MOs are paired with $(n - 1)/2$ antibonding MOs, so that a single MO remains without a partner. The pairing theorem requires that this “odd” MO should be “paired with itself”. Consequently, Eq. 8.2 becomes $x_j \equiv -x_j$, which requires x_j to be zero and this MO ψ_j to be a NBMO with $E(\psi_j) = \alpha$. Also, because Eq. 8.4 is now $c_{j,\mu^*} \equiv c_{j,\mu^*}$ and $c_{j,\mu^o} \equiv -c_{j,\mu^o}$, the LCAO coefficients and their squares should be zero at all unstarred centers μ^o . The sum of c_{j,μ^*} at the centers μ^* linked to the same center μ^o must vanish, which, together with the normalization condition (Eq. 4.7), makes it possible to derive the LCAO coefficients for such NBMO by means of a simple “back-of-the-envelope” calculation, as shown here for benzyl (**88'**):



It is evident that the ratio 2:1:0, of the values $|c_{j,\mu}|$ of the coefficients at the centers μ , reflects the number of mesomeric Kekulé formulas of **88'** in which the pertinent center bears the unpaired electron:



Because NBMO is the SOMO in a neutral odd alternant radical, the prediction that the squared coefficients c_{j,μ^o}^2 are zero means that the spin populations are expected to vanish at the centers μ^o in these radicals. Actually, as indicated by the McLachlan procedure and other methods, such $\rho_{\mu^o}^\pi$ values are small but, in general, not zero, and they have negative sign.

Figure 8.1 depicts the Hückel-energy schemes for naphthalene (**83**) and benzyl (**88'**) as examples of an *even* and an *odd* alternant π system, respectively, with no orbital degeneracy. Indicated are the single occupancy of the LUMO in the anion **83⁻**, of the HOMO in the cation **83⁺**, and of the NBMO in the neutral **88'**. In an *even* alternant radical trianion, the LUMO becomes doubly occupied and the unpaired electron is taken up by the next antibonding MO (NLUMO), while in an *even* alternant radical trication the HOMO is vacated and the next bonding MO (NHOMO) becomes the SOMO. Likewise, in an *odd* alternant radical dianion, the unpaired electron is accommodated by the LUMO after the NBMO has been filled, and an *odd* alternant radical dication has a vacant NBMO with the HOMO being singly occupied.

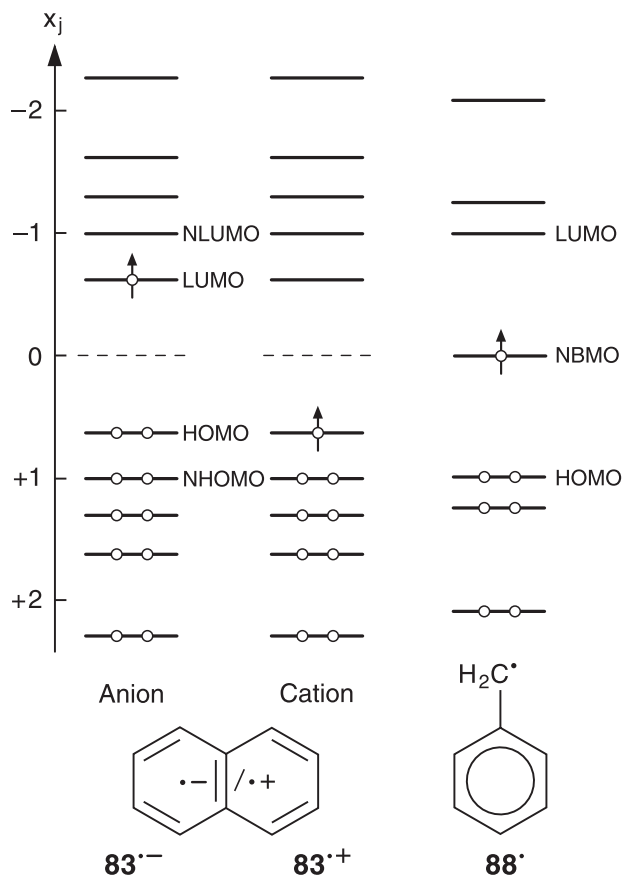


Fig. 8.1. Hückel energy schemes of naphthalene (**83**) and benzyl (**88 $^{\cdot}$**). Orbital occupancies in the radical ions **83 $^{\cdot-}$** and **83 $^{\cdot+}$** and in the radical **88 $^{\cdot}$** .

The energy scheme in Figure 8.1 does not apply to nonalternant π systems that lack the pairing properties of the MOs. Because the LUMO and the HOMO of an *even* nonalternant system, which become singly occupied in the radical anion and radical cation, respectively, are not paired, the spin populations ρ_{μ}^{π} in the two corresponding radical ions should strongly differ, and so should the hyperfine patterns of their ESR spectra. Moreover, because an *odd* nonalternant system generally has no NBMO, the SOMO of a neutral *odd* nonalternant radical is either the highest bonding or the lowest antibonding MO, with no simple prediction for the π -spin distribution and the hyperfine pattern.

Monocyclic π Systems (π Perimeters)

π -Electron systems of axial symmetry with a rotational axis C_n , where $n \geq 3$, can have more than one MO of the same energy (degenerate MOs). A special class of

such systems, in which all π centers lie on one cycle (π -perimeter), is particularly interesting. This is because, in the ideal case of a regular polygon, the π -MOs of the perimeter do not depend on the quantum chemical procedure used for their calculation, but are fully determined by their D_{nh} symmetry. In particular, for the radical or the radical ion with an n -membered perimeter, the π -spin population ρ_{μ}^{π} at all n centers μ is $+1/n$, by virtue of this symmetry. The coupling constants, $a_{H_{\mu}} = Q_{H}^{C_{\mu}H_{\mu}}/n$, of the ring α protons in paramagnetic π perimeters can thus be used to derive the value of the parameter Q in the McConnell Eq. 4.5, as was done in Table 4.1.

The *even*-membered perimeters are alternant π systems, whereas their odd-membered counterparts are nonalternant. The two sorts of π perimeters are exemplified in Figure 8.2, which shows the Hückel-energy schemes for five- and six-membered perimeters; the sequence and the degeneracies of the orbitals are determined by the D_{5h} and D_{6h} symmetries, respectively. The Hückel energies are

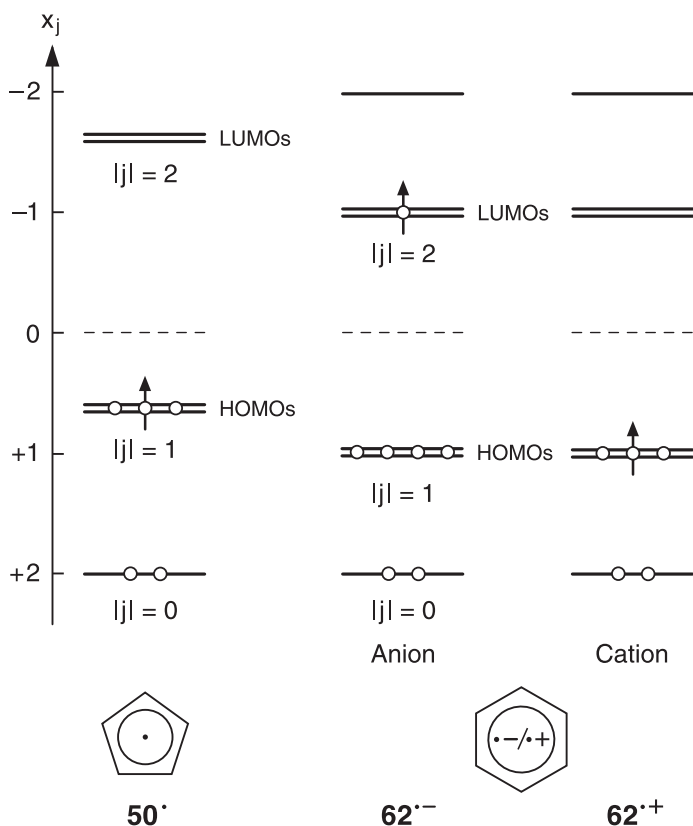


Fig. 8.2. Hückel-energy schemes of the five-membered π perimeter (cyclopentadienyl 50^{\bullet}) and the six-membered π perimeter (benzene 62). Orbital occupancies in the radical 50^{\bullet} and the radical ions $62^{\bullet-}$ and $62^{\bullet+}$.

$$E(\psi_j) = \alpha + 2\beta \cos[(2\pi/n)j] \quad (8.5)$$

where it is convenient to enumerate the perimeter π orbitals ψ_j by $|j| = 0, 1, 2, \dots$, so that the lowest nondegenerate MO is ψ_0 , and the following doubly degenerate MOs are ψ_1, ψ_2, \dots in order of increasing energy. MO-energy schemes, like those in Figure 8.2, are the basis for Hückel rule, which states that stable perimeters have a closed-shell configuration with $N = 2 + 4m$ π electrons, where m is an integer. Five- and six-membered perimeters of this kind with $N = 6$ and $m = 2$ are realized by the iso- π -electronic cyclopentadienyl anion (50^-) and benzene (62), respectively. These π systems are diamagnetic but they convert by oxidation or reduction into radicals, such as the neutral 50^\bullet and the ions $62^{\bullet-}$ and $62^{\bullet+}$. Figure 8.2 indicates the occupancy of the degenerate HOMOs ψ_1 in 50^\bullet and $62^{\bullet+}$ and of the likewise degenerate LUMOs ψ_2 in $62^{\bullet-}$.

Mathematically, the doubly degenerate perimeter-MOs ψ_j are pairs of complex-conjugated functions, but each pair can be expressed in a real form as the “plus” and “minus” combinations, ψ_{j+} and ψ_{j-} , of these two functions. The real MOs are symmetric (ψ_{j+}) or antisymmetric (ψ_{j-}) with respect to a vertical mirror plane that is perpendicular to the plane of the π system. This plane passes through two opposite centers μ in an *even*-numbered perimeter and through a center μ and the middle of the opposite bond in an odd-numbered perimeter. The MOs are represented by

$$\psi_{1+} = 0.632\phi_1 + 0.195(\phi_2 + \phi_5) - 0.512(\phi_3 + \phi_4)$$

and

$$\psi_{1-} = 0.602(\phi_2 - \phi_5) + 0.371(\phi_3 - \phi_4) \quad (8.6)$$

for the the pair of degenerate HOMOs in the five-membered perimeter, and by

$$\begin{aligned} \psi_{2+} &= 0.577(\phi_1 + \phi_4) - 0.289(\phi_2 + \phi_3 + \phi_5 + \phi_6) \quad \text{and} \\ \psi_{2-} &= 0.500(\phi_2 - \phi_3 + \phi_5 - \phi_6) \end{aligned} \quad (8.7)$$

for the pair of degenerate LUMOs in the six-membered perimeter.

In the six-membered perimeter, due to the pairing properties of an alternant π system, the pair ψ_{2+} and ψ_{2-} is related to the pair of likewise degenerate HOMOs ψ_{1+} and ψ_{1-} by

$$\begin{aligned} \psi_{i+} &= \psi_{2+} \quad \text{and} \quad \psi_{i-} = \psi_{2-}, \quad \text{along with} \\ c_{1+, \mu^*} &= c_{2+, \mu^*} \quad \text{and} \quad c_{1+, \mu^o} = -c_{2+, \mu^o} \quad \text{and} \\ c_{1-, \mu^*} &= c_{2-, \mu^*} \quad \text{and} \quad c_{1-, \mu^o} = -c_{2-, \mu^o} \end{aligned} \quad (8.8)$$

When ψ_j is doubly degenerate, a MO can be represented by

$$\psi_j = C_+ \psi_{j+} + C_- \psi_{j-} \quad (8.9)$$

with $C_+^2 + C_-^2 = 1$.

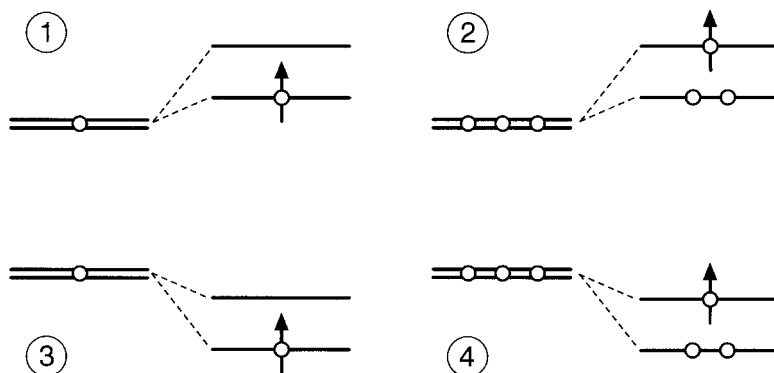
In particular, when the MO is singly occupied (SOMO), the spin populations ρ_μ^π and the hyperfine-coupling constants a_X are given by

$$\rho_\mu^\pi = C_+^2 \rho_\mu^\pi(\psi_{j+}) + C_-^2 \rho_\mu^\pi(\psi_{j-}) \quad \text{and} \quad (8.10)$$

$$a_X = C_+^2 a_X(\psi_{j+}) + C_-^2 a_X(\psi_{j-}) \quad (8.11)$$

where $\rho_\mu^\pi(\psi_{j+})$, $\rho_\mu^\pi(\psi_{j-})$, $a_X(\psi_{j+})$, and $a_X(\psi_{j-})$ are the values expected for an "exclusive" single occupancy of ψ_{j+} and ψ_{j-} .

For a radical with an unperturbed perimeter, $C_+ = C_- = 1/\sqrt{2}$, so that $\rho_\mu^\pi = +1/n$, i.e., $+1/5$ and $+1/6$ for the cyclopentadienyl radical (**50** \cdot) and benzene radical ions (**62** $^{\cdot-}$ and **62** $^{\cdot+}$), respectively. However, perturbation, such as introduction of an alkyl group or even simple replacement of a proton by a deuteron, reduces the symmetry of the perimeter and removes the degeneracy of ψ_j . The MOs ψ_{j+} and ψ_{j-} then no longer have the same energy, so that $C_+ \neq C_-$, and the spin populations ρ_μ^π strikingly differ from $+1/n$. For example, when a substituent has an inductive and electron-releasing effect that destabilizes the MO's, cases ① and ② are distinguishable when the degeneracy of ψ_j is removed.



In ①, because one electron has to be accommodated in ψ_{j+} and ψ_{j-} , the MO of lower energy is preferred for the SOMO, as in ψ_{2+} and ψ_{2-} of a perturbed radical anion **62** $^{\cdot-}$. In ②, where three electrons are taken up by ψ_{j+} and ψ_{j-} , it is the MO of higher energy that is favored for the SOMO, as in ψ_{1+} and ψ_{1-} of perturbed neutral radical **50** \cdot and the iso- π -electronic radical cation **62** $^{\cdot+}$. The energetic order of ψ_{j+} and ψ_{j-} should be opposite when the inductive effect of the substituent is electron-withdrawing and stabilizes the MOs (cases ③ and ④).

Depending on the shapes of ψ_{j+} and ψ_{j-} and on the position of the perturbation, it is straightforward to predict which of the two MOs, ψ_{j+} or ψ_{j-} , will be more strongly affected by the perturbation. Information as to whether the effect of the perturbation is stabilizing or destabilizing can be derived from the energetic

sequence of the two MOs, which is established by the ESR spectrum of the radical in question. This is because the π -spin distribution mapped by the hyperfine pattern reflects the shape of the SOMO, which is readily recognized as the MO that more strongly resembles either ψ_{j+} or ψ_{j-} .

As stated in Chapt. 6.7, the Jahn-Teller theorem predicts that, in order to lower its energy, a nonlinear molecule with a degenerate ground state deforms to a species in which the symmetry is reduced and the degeneracy is removed. For a neutral radical and radical ions, like 50^\cdot , $62^{+\cdot}$, and $62^{-\cdot}$, two such species, which differ in their geometry, symmetry, and π -spin distribution, correspond to those with single occupancy of either ψ_{j+} or ψ_{j-} . In the absence of perturbation ($C_+ = C_- = 1/\sqrt{2}$), these species have the same energy and usually interconvert rapidly on the hyperfine time-scale, so that, in most radicals with a degenerate ground state, an effective D_{nh} symmetry and π -spin populations of $+1/n$ are apparently retained. The “dynamic Jahn–Teller effect” thus observed is often revealed by line-broadening in the ESR spectra, which saturate at higher than usual microwave intensities. However, even if perturbation favors one of the two species, the energy gap is usually small and the interconversion is fast enough to yield spin population averaged over the two species, albeit in unequal weight according to Eq. 8.10 ($C_+ > C_-$ or vice versa).

The deformation to species of lower symmetry and their interconversion are brought about by molecular vibrations of symmetry appropriate to “mix” their electronic states. Such “vibronic mixing” is effective both in the absence of perturbation (degeneracy) and in its presence when the energy separating the two species is comparable to that of vibrations (“near-degeneracy”).

In the following (Chapts. 8.2–8.8), the hyperfine data for individual classes of conjugated hydrocarbons are considered. Included are some alkyl substituted π radicals particularly those with perturbed π -perimeters (Chapt. 8.6). In the accompanying structural formulas, H atoms directly attached to carbon π centers μ and relevant to the coupling constants, a_{H_μ} , of α protons are usually omitted. For the radical ions, the structural formulas are those of the neutral, diamagnetic or paramagnetic compounds, without the symbol of charge in the diions and without the symbols of unpaired electron and charge in monoions and triions.

8.2

Odd Alternant Radicals

Phenyl-substituted Methyl Radicals

When the H atoms in the methyl radical H_3C^\cdot (58^\cdot) are progressively replaced by phenyl groups, one obtains successively the benzyl $PhC^\cdot H_2$ (88^\cdot), diphenylmethyl $Ph_2C^\cdot H$ (323^\cdot), and triphenylmethyl Ph_3C^\cdot (trityl; 1^\cdot) radicals. Table 8.1 [42, 691, 776–789] lists hyperfine data for these radicals and some of their derivatives. In 88^\cdot , the largest positive π -spin population ρ_7^π , the similarly large positive ρ_4^π and $\rho_{2,6}^\pi$ values, and the small negative $\rho_{3,5}^\pi$ values, reflect the shape of the singly occupied

Tab. 8.1. Hyperfine Data for Some Phenyl-Substituted Methyl Radicals

Benzyl 88 [•]		H2,6	-0.515	[42]
		H3,5	+0.179	
		H4	-0.618	
		2H7	-1.630	
		¹³ C1	-1.445	[776]
		¹³ C7	+2.445	
4-Methylbenzyl 324 [•]		H2,6	-0.513	[777]
		H3,5	+0.175	
		2H7	-1.607	
		3H(beta)	+0.670	
7-Methylbenzyl 325 [•]		H2,6	-0.49	[691]
		H3,5	+0.17	
		H4	-0.61	
		H7	-1.63	
		3H(beta)	+1.79	
7,7-Dimethylbenzyl 326 [•]		H2,6	-0.52	[778]
		H3,5	+0.17	
		H4	-0.60	
		6H(beta)	+1.65	
7,7-Di-tert-butylbenzyl 327 [•]		H2,6	-0.091	[779]
		H3,5	+0.082	
		H4	-0.031	
		18H(gamma)	0.047	
		¹³ C1	-1.17	
		¹³ C2,6	+1.82	
		¹³ C7	+4.5	
		6 ¹³ C(beta)	+1.17	
Tetralin-1-yl 328 [•]		H2	-0.499	[780]
		H3,5	+0.167	
		H4	-0.606	
		H7	-1.573	
		H _{ax} (beta)	+3.33	
		H _{eq} (beta)	+1.218	
		H _{ax} (beta')	+0.790	
		H _{eq} (beta')	+0.156	
		2H(gamma)	0.067	
Diphenylmethyl 323 [•]		H2,2',6,6'	-0.37	[781]
		H3,3',5,5'	+0.135	
		H4,4'	-0.42	
		H7	-1.47	
Dimesitylmethyl 329 [•]		H3,3',5,5'	+0.145	[782]
		H7	-1.57	
		12H(beta)	+0.215	
		6H(beta')	+0.338	
		¹³ C7	+2.45	[783]

Tab. 8.1 (continued)

1,1-Diphenyl-1-ethyl 330 [•]		H2,2',6,6' H3,3',5,5' H4,4' 3H(β)	-0.324 +0.124 -0.335 +1.514	[784]
1,1-Diphenylneopentyl 331 [•]		H2,2',6,6' H3,3',5,5' H4,4' 9H(γ) ¹³ C7	-0.268 +0.111 -0.277 0.025 +2.93	[785]
Triphenylmethyl (trityl) 1 [•]		H2,2',2'',6,6',6'' H3,3',3'',5,5',5'' H4,4',4'' ¹³ C2,2',2'',6,6',6'' ¹³ C3,3',3'',5,5',5'' ¹³ C4,4',4'' ¹³ C7	-0.261 +0.114 -0.286 +0.64 -0.53 +0.61 +2.01	[786] [787]
Tris(4-methylphenyl)methyl 332 [•]		H2,2',2'',6,6',6'' H3,3',3'',5,5',5'' 9H(β)	-0.260 +0.114 +0.304	[788]
Tris(4-cyclopropylphenyl)methyl 333 [•]		H2,2',2'',6,6',6'' H3,3',3'',5,5',5'' 3H(β) 12H(γ)	-0.260 +0.114 +0.046 0.026	[788]
Tris(3-5-di- <i>tert</i> -butylphenyl)methyl 334 [•]		H2,2',2'',6,6',6'' H4,4',4'' ¹³ C1,1',1'' ¹³ C2,2',2'',6,6',6'' ¹³ C3,3',3'',5,5',5'' ¹³ C4,4',4'' ¹³ C7	-0.257 -0.280 -1.13 +0.65 -0.32 +0.41 +2.35	[789]
Tris(<i>p</i> -biphenyl)methyl 335 [•]		H2,2',2'',6,6',6'' H3,3',3'',5,5',5'' 6H _o , 3H _p 6H _m	-0.250 +0.114 -0.044 +0.017	[786]

NBMO of an alternant π system, as shown for this radical on p. 212. Increasing π -spin delocalization from the exocyclic C7 atom into the phenyl groups is demonstrated by the decreasing $|a_{H7}|$ and a_{C7} values of the protons and ¹³C-isotopes ($a_H = -2.30$ for **58[•]** vs $a_{H7} = -1.63$ for **88[•]** and -1.47 mT for **323[•]**; $a_C = +3.83$ for **58[•]** vs $a_{C7} = +2.45$ for **88[•]**, and $+2.01$ mT for **1[•]**). The π -spin population at C7 diminishes from +1 for **58[•]** to $\rho_7^\pi \approx +0.60$, $+0.55$, and $+0.52$ for **88[•]**, **323[•]**, and **1[•]**, respectively. The mono- and diphenylmethyl radicals, **88[•]** and **323[•]** are planar, whereas their triphenyl counterpart **1[•]** has a propeller form with a deviation by ca 30° from the molecular plane. This deviation is assumed to slightly decrease the

π -spin delocalization from the exocyclic atom C7 to the phenyl groups. In general, the spin distribution in all three radicals is not markedly altered by alkyl substitution, unless the planarity of the radical is very strongly affected by bulky substituents. A reduced spin delocalization from the C7 into the phenyl groups caused by such substituents, usually *tert*-butyl, is indicated by the increased coupling constants a_{C7} , e.g., in **331** \cdot (+2.93 mT) and, particularly, in **327** \cdot (+4.5 mT). On going from **88** \cdot to **327** \cdot , in which the phenyl group is almost perpendicular to the nodal plane of the $2p_z$ -AO at C7, the π -conjugation is impaired, so that **327** \cdot has to be considered a methyl-like radical with the spin population localized in this AO. Consequently, not only the coupling constant a_{C7} is increased but also the $|a_{H_r}|$ values of the phenyl protons in the *para*- (4-), *ortho*- (2,6-), and *meta*- (3,5-) positions of **327** \cdot are strongly decreased; they follow the sequence $|a_{H4}| < |a_{H2,6}| \approx |a_{H3,5}|$ instead of the order $|a_{H4}| \geq |a_{H2,6}| \gg |a_{H3,5}|$ found for **88** \cdot . The decrease in absolute value is most pronounced for a_{H4} , somewhat less for $a_{H2,6}$ (both negative), and much smaller for $a_{H3,5}$ (which has a positive sign). This behavior is characteristic of a phenyl ring that is twisted out of planarity (deviation larger than ca 60°) with respect to the spin-bearing radical center C \cdot and is caused by positive contributions to the ^1H -coupling constants due to such twisting.

The coupling constant, +0.046 mT, of the cyclopropyl β protons in **333** \cdot is much smaller than the corresponding value, +0.304 mT, of the methyl protons in **332** \cdot , but the other values are the same for both radicals. This finding indicates a “bisected” conformation for the cyclopropyl substituents, with the β protons close to the nodal plane of the π system.

The g_e factor of all the phenyl-substituted methyl radicals is 2.0026 ± 0.0001 . Due to π -spin delocalization, they are stabilized by successive phenyl substitution. Accordingly, generating them in solution becomes increasingly easier on going from $\text{H}_3\text{C}\cdot$ (**58** \cdot) to $\text{PhC}\cdot\text{H}_2$ (**88** \cdot), $\text{Ph}_2\text{C}\cdot\text{H}$ (**323** \cdot), and $\text{Ph}_3\text{C}\cdot$ (**1** \cdot), a statement which also holds for their alkyl derivatives. The radicals **88** \cdot , **324** \cdot , and **326** \cdot were generated by abstraction of an H atom from the corresponding hydrocarbons with *t*-BuO \cdot , and **325** \cdot was formed by decarboxylation of α -phenylpropionic acid. Halogen derivatives yielded **323** \cdot with $\text{Me}_3\text{Si}\cdot$ and **1** \cdot , **329** \cdot , and **331** \cdot with a metal like Zn, Ag, or Na; only **327** \cdot was formed by reaction of oxalic diester with Na/K alloy in benzene.

Here, some more recent findings concerning the benzyl radical (**88** \cdot) are mentioned. In the first place **88** \cdot , but also simple alkyl radicals, such as methyl (**58** \cdot), ethyl (**59** \cdot) and *tert*-butyl (**141** \cdot), generated photolytically with *t*-BuO \cdot or from corresponding esters, add to [60]fullerene (C_{60}) yielding secondary alternant π -radicals [75, 76, 790, 791] (Chapt. 2.2). In these adducts, the spin population is transferred from the primary radicals to specific centers of the C_{60} π -systems. Apart from monoadducts, highly symmetric tri- and pentaadducts are formed.

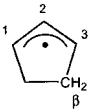
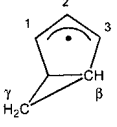
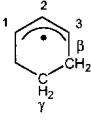
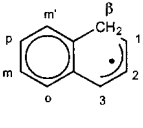
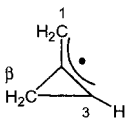
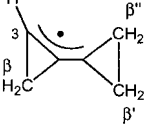
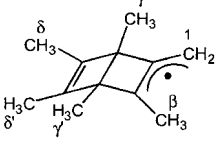
Allyl Radicals

Hyperfine data for allyl (**65** \cdot) and some of its derivatives are given in Table 8.2 [34, 42, 45, 337, 340, 458, 792–798]. The π -spin distribution in the parent **65** \cdot has

Tab. 8.2. Hyperfine Data for Some Allyl Radicals

Allyl 65 [•]		H1,3 _{exo} H1,3 _{endo} H2	-1.483 -1.393 +0.406	[34]
1-Methylallyl endo-336 [•]		H1 _{exo} H2 H3 _{exo} H3 _{endo} 3H(β)	-1.417 +0.383 -1.494 -1.352 +1.401	[42]
exo-336 [•]		H1,3 _{endo} H2 H3 _{exo} 3H(β)	-1.383 +0.385 -1.478 +1.643	[42]
2-Methylallyl 337 [•]		H1,3 _{exo} H1,3 _{endo} 3H(β)	-1.468 -1.382 -0.319	[42]
1,1-Dimethylallyl 338 [•]		H2 H3 _{exo} H3 _{endo} 3H(β) 3H(β')	+0.356 -1.406 -1.333 +1.535 +1.222	[792]
1-endo-2,3-exo-tri-tert-butylallyl 339 [•]		H1 _{exo} , H3 _{endo} 18H(γ, γ') ¹³ C1,3 ¹³ C2 6 ¹³ C(β, β')	-1.36 0.023 +2.39 -1.68 +0.58	[793]
1,1-Di-tert-butyl-2-methylallyl 340 [•]		H3 _{exo} H3 _{endo} 3H(β) 18H(γ, γ') ¹³ C1 ¹³ C2 ¹³ C3 2 ¹³ C(α, α') 6 ¹³ C(β, β')	-0.340 -0.096 -0.071 -0.045 +4.6 -1.2 +1.8 -1.2 +1.2	[794]
1,1,3,3-Tetraphenylallyl 341 [•]		H2 4H _o 4H _m 2H _p 4H _{o'} , 2H _{p'}	+0.881 -0.189 +0.070 -0.201 -0.117	[795]
Cyclobutenyl 71 [•]		H1,3 H2 2H(β)	-1.520 +0.241 0.445	[458]

Tab. 8.2 (continued)

Cyclopentenyl 342 [•]		H1,3 H2 4H(β)	-1.430 +0.277 +2.15	[45]
Bicyclo[3.1.0]hexenyl 343 [•]		H1,3 H2 2H(β) H _{syn} (γ) H _{anti} (γ)	-1.366 +0.254 +1.260 0.355 0.375	[796]
Cyclohexenyl 344 [•]		H1,3 H2 2H _{ax} (β) 2H _{eq} (β) 2H(γ)	-1.435 +0.338 +2.613 +0.827 0.094	[45]
1-Hydronaphthyl 345 [•]		H1 H2 H3 H(β) H(β) H _o H _m H _{m'} H _p	-1.07 +0.274 -1.301 +3.58 +3.23 -0.278 +0.099 +0.10 -0.309	[797]
Dehydromethylenecyclo- propane 346 [•]		H1 _{exo} , H1 _{endo} H3 2H(β)	-1.322 ^a -1.563 +1.936	[798]
Dehydrobicyclopropylidene 347 [•]		H3 2H(β) 2H(β') 2H(β'')	-1.71 +1.71 +1.57 +1.57	[340]
Hexamethyldehydro(Dewar) benzene 348 [•]		2H1 3H(β) 3H(γ) 3H(γ') 3H(δ) 3H(δ')	-1.50 +1.405 0.315 0.197 0.056 <0.02	[337]

^aDeuteriation indicates that previous assignment [799] was incorrect.

been amply discussed in Chapt. 4.3. Alkyl substitution does not greatly affect this distribution, except for a distorted methyl-like radical **340[•]** with two *tert*-butyl substituents ($a_{C1} = +4.5$ mT). In **341[•]**, tetraphenyl substitution at both terminal centers 1 and 3 leads to a twisting, by which the coupling constant a_{H2} increases from +0.406 in **65[•]** to +0.881 mT in **341[•]**. Such an increase must be due to a positive

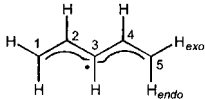
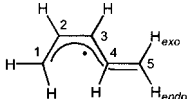
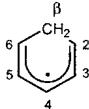
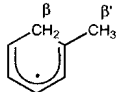
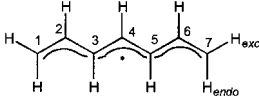
contribution by a direct spin transfer from the proximate phenyl rings, which are no longer situated in the molecular plane of the allyl π system.

The g_e factor of all allyl radicals is 2.0026 ± 0.0001 . Like phenyl-substituted methyl radicals, allyl and most of its alkyl-substituted derivatives were generated in solution by abstraction of a H atom from their hydrocarbon precursors by $t\text{-BuO}^\bullet$ or, alternatively, as for **339** $^\bullet$, from their bromo derivatives with $\text{Me}_3\text{Sn}^\bullet$. The radical **340** $^\bullet$ was produced from the oxalic acid ester of di-*tert*-butylallyl alcohol with Na/K alloy in benzene, and oxidation of the corresponding anion with Fe(III) ions in toluene or liquid paraffin yielded **341** $^\bullet$. X-irradiation of a single crystal of naphthalene led to **345** $^\bullet$, while **346** $^\bullet$, **347** $^\bullet$, and **348** $^\bullet$ were obtained as secondary paramagnetic species by loss of a H atom from methylenecyclopropane, bicyclopropylidene, and hexamethyl(Dewar)benzene, respectively, upon γ -irradiation in a $\text{CF}_2\text{ClCFCl}_2$ matrix.

Pentadienyl and Heptatrienyl Radicals

Hyperfine data of these radicals are presented in Table 8.3 [800–803]. The two isomeric pentadienyl radicals (all-*trans*- and *cis,trans*-**349** $^\bullet$) exist in equilibrium with

Tab. 8.3. Hyperfine Data for Some Pentadienyl and Heptatrienyl Radicals

Pentadienyl <i>all-trans</i> - 349 $^\bullet$		H1, ₅ <i>exo</i> H1, ₅ <i>endo</i> H2, ₄ H3	-1.040 -0.962 +0.332 -1.158	[800]
<i>cis,trans</i> - 349 $^\bullet$		H1 _{exo} H1 _{endo} H5 _{exo} H5 _{endo} H3 H2 H4	-1.012 -0.969 -0.918 -0.848 -1.438 +0.362 +0.308	[800]
Cyclohexadienyl 70 $^\bullet$		H2, ₆ H3, ₅ H4 2H(β)	-0.899 +0.265 -1.304 +4.771	[801]
2-Methylcyclohexadienyl 350 $^\bullet$		H3, ₅ H4 H6 2H(β) 3H(β')	+0.250 -1.270 -0.899 +4.420 +0.785	[802]
Heptatrienyl <i>all-trans</i> - 351 $^\bullet$		H1, ₇ <i>exo</i> H1, ₇ <i>endo</i> H2, ₆ H3, ₅ H4	-0.78 -0.73 +0.27 -0.95 +0.33	[803]

a low barrier to interconversion. They were generated by abstraction of a H atom from 1,3-pentadiene with *t*-BuO \cdot , and the heptatrienyl radical (**351 \cdot) was analogously produced from hepta-1,3,6-triene. The cyclic counterpart of **349 \cdot , the cyclohexadienyl radical (**70 \cdot), is frequently formed under various conditions, both by abstraction of a H atom from cyclohexa-1,3-diene with 2.8-eV electrons [801] or *t*-BuO \cdot [803a] and by addition of a H atom to benzene [804, 805]; it is also produced by loss of a proton from the radical cation of cyclohexa-1,3-diene in a γ -irradiated CF₂ClCFCl₂ matrix [329]. The large coupling constant, +4.77 mT, of the two β protons served as a paradigm of the “Whiffen effect” (Chapt. 4.2).******

The g_e factor of the two isomeric pentadienyl radicals **349 \cdot is 2.0026. That of **70 \cdot is slightly higher, 20027.****

Phenalenyl Radicals

The SOMO of the phenalenyl radical (**4 \cdot ; symmetry D_{3h}) is nondegenerate and characteristic of the NBMO of an odd alternant π system. Accordingly, both the electronic structure and chemistry of **4 \cdot are determined by specifying the nine proton-bearing π centers μ as six starred, $\mu^* = 1, 3, 4, 6, 7, 8$, and 9, and three unstarred, $\mu^\circ = 2, 5$, and 8. The spin distribution in **4 \cdot has been amply considered in Chapt. 4.2. The six proton-bearing centers μ^* , which are often denoted “active”, exhibit a large positive spin population $\rho_{\mu^*}^\pi$ (+0.225), whereas the corresponding $\rho_{\mu^\circ}^\pi$ value at the three remaining proton-bearing centers μ° is much smaller and negative (−0.065). This π -spin distribution pattern is, in general, retained in the 1-alkyl and 1-phenyl derivatives of phenalenyl, for which hyperfine data are given in Table 8.4 [88, 89, 806, 807]. 1,2,3-Trihydropyrenyl (**120 \cdot), a 1,9-trimethylenephthalenyl radical, is dealt with in Chapt. 6.7, where it served as an example for conformational interconversion of a six-membered ring, by which the coupling constants of the axial and equatorial β protons are exchanged.********

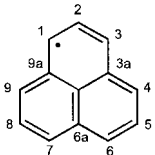
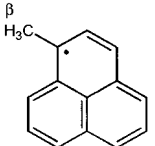
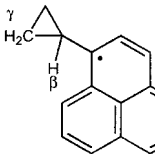
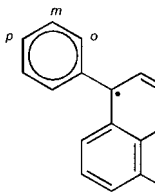
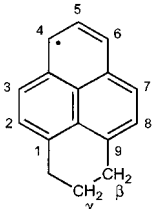
The g_e factor of phenalenyl radicals is 2.00265 ± 0.00005 . They are readily prepared in solution from the corresponding hydrocarbons by loss of a H atom from the corresponding hydrocarbon (some of them, like **4 \cdot and **120 \cdot , by merely contacting the solution with air).****

8.3

Odd Nonalternant Radicals and Radical Dianions

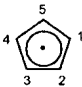
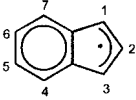
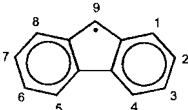
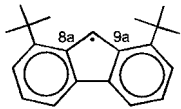
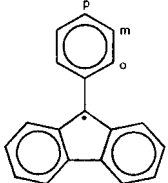
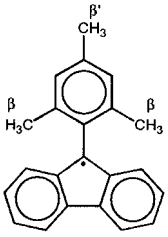
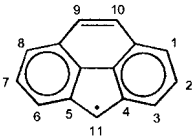
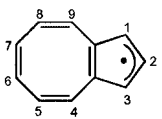
The number of odd nonalternant radicals studied by ESR spectroscopy is smaller than that of their alternant counterparts. Several of these neutral radicals can take up two additional electrons and yield the corresponding radical dianion, in which process, the SOMO of the neutral radical is filled and the next-higher-lying MO becomes singly occupied. Table 8.5 [67, 84, 144, 186–189, 446, 448, 808–815] lists hyperfine data for several radicals and radical dianions that contain a five- and/or a seven-membered ring. Not considered here are deuterio and alkyl derivatives of the cyclopentadienyl and cycloheptatrienyl radicals, which are dealt with in Chapt. 8.6.

Tab. 8.4. Hyperfine Data for Some Phenalenyl Radicals

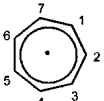
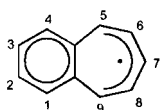
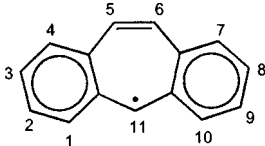
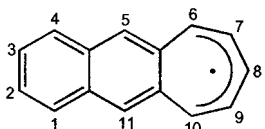
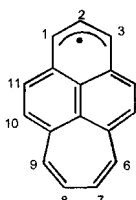
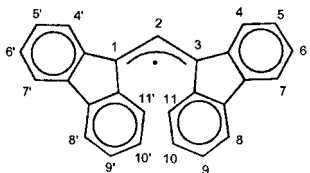
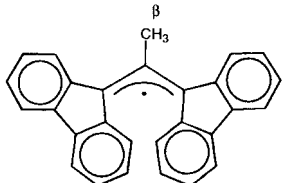
Phenalenyl 4 [•]		H1,3,4,6,7,9 H2,5,8 ¹³ C1,3,4,6,7,9 ¹³ C2,5,8 ¹³ C3a,6a,9a	-0.629 +0.181 +0.966 -0.784 -0.784	[88]
1-Methylphenalenyl 352 [•]		H2,5,8 H3 H4,6,7,9 3H(β)	+0.177 -0.648 -0.605 +0.627	[806]
1-Cyclopropylphenalenyl 353 [•]		H2,5,8 H3 H4,6,7,9 H(β) 2H(γ) 2H(γ)	+0.178 -0.596 -0.618 +0.581 -0.026 +0.020	[807]
1-Phenylphenalenyl 354 [•]		H2,5,8 H3,4,6,7,9 2H _o , H _p 2H _m	+0.178 -0.612 -0.048 +0.039	[806]
1,2,3-Trihydrodipyrnyl (1,9-trimethylenephalenyl) 120 [•]		H2,5,8 H3,4,6,7 2H _{ax} (β) 2H _{eq} (β) 2H(γ)	+0.173 -0.614 +1.197 +0.299 0.045	[89]

As expected, the shape of the SOMO differs strongly for the neutral radical and its radical dianion and so do their π -spin distributions. For example, in the fluorenyl radical (356[•]) with the largest spin population ρ_9^π , the π -spin distribution and the ¹H-hyperfine data closely resemble those in the alternant diphenylmethyl (323[•]). On the other hand, in the radical dianion 356^{•2-}, the SOMO has a vertical node at the pertinent center, so that the ρ_9^π and $|a_{H9}|$ values are very small. Analogously, for benzotropyl (362[•]), the bulk of the spin population is found in the seven-membered ring with the largest ρ_μ^π and $|a_{H_\mu}|$ values at $\mu = 5, 9$, and, especially, at 7. This spin distribution and ¹H-coupling constants are similar to the corresponding data for pentadienyls (349[•]) and cyclohexadienyl (70[•]). Again, the radical dianion exhibits completely different ρ_μ^π and $|a_{H_\mu}|$ values, because its SOMO has a vertical node at the center 7. The strongly differing hyperfine patterns of 362[•]

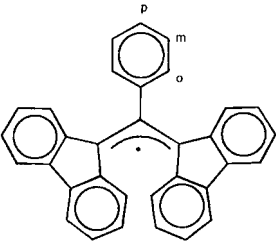
Tab. 8.5. Hyperfine Data for Some Odd Nonalternant Radicals and Radical Dianions

Cyclopentadienyl 50 [•]		H1-5 ¹³ C1-5	Neutral -0.602 +0.266	[446] [808]
Indenyl 355 [•]		H1,3 H2 H4,7 H5,6	Neutral -1.19 +0.218 -0.218 -0.147	[809]
Fluorenyl 356 [•] /356 ²⁻		H1,8 H2,7 H3,6 H4,5 H9	Neutral/Dianion -0.398/-0.305 +0.091/-0.305 -0.376/+0.035 +0.064/-0.453 -1.39/+0.053	[809]/[187]
1,8-Di- <i>tert</i> -butylfluorenyl 357 [•]		H2,7 H3,6 H4,5 H9 ¹³ C8a,9a ¹³ C9	Neutral +0.080 -0.347 +0.060 -1.347 -1.02 +1.982	[810]
9-Phenylfluorenyl 358 [•]		H1,8 H2,7 H3,6 H4,5 2H _o , H _p 2H _m	Neutral -0.328 +0.058 -0.347 +0.097 -0.195 +0.092	[811] [812]
9-Mesitylfluorenyl 359 [•]		H1,8 H2,7 H3,6 H4,5 2H _m 6H(β) 3H(β')	Neutral -0.377 +0.063 -0.359 +0.086 +0.097 +0.033 +0.043	[812]
4,5-Methylenephenanthrene 360 ²⁻		H1,8 H2,7 H3,6 H9,10 H11	/Dianion /-0.302 /+0.053 /-0.302 /-0.496 /+0.036	[186, 187]
Bicyclo[6.3.0]undeca- 1,3,5,7,9-pentaenyl 361 ²⁻		H1,3 H2 H4,9 H5,8 H6,7	/Dianion /-0.509 /+0.097 /-0.586 /+0.005 /-0.328	[144]

Tab. 8.5 (continued)

Cycloheptatrienyl (tropyli) $63^{\cdot}/63^{2-}$		H1-7 $^{13}\text{C}1-7$	Neutral/Dianion -0.392/-0.352 [448]/[188] +0.198 [808]
Benzotropyli $362^{\cdot}/362^{2-}$		H1,4 H2,3 H5,9 H6,8 H7	Neutral/Dianion -0.118/0.006 [67, 813]/ -0.114/-0.271 [67, 813] -0.816/-0.113 +0.292/-0.628 -1.103/+0.079
Dibenzo[1,2:4,5]tropyli 363^{2-}		H1,10 H2,9 H3,8 H4,7 H5,6 H11	/Dianion /+0.070 [189] /-0.306 /+0.070 /-0.212 /-0.534 /+0.092
2,3-Naphthotropyli $364^{\cdot}/364^{2-}$		H1,4 H2,3 H5,11 H6,10 H7,9 H8	Neutral/Dianion -0.062/<0.006 [67]/[67] -0.039/-0.128 -0.213/0.056 -0.778/-0.139 +0.289/-0.595 -1.042/+0.089
Cyclohepta[c,d]phenalenyl 365^{\cdot}		H1,3 H2 H4,11 H5,10 H6,9 H7,8	Neutral -0.501 [814] +0.136 -0.480 +0.155 +0.028 -0.295
1,3-Bis(diphenylene)allyl 366^{\cdot}		H2 H4,4',11,11' H5,5',10,10' H6,6',9,9' H7,7',8,8'	Neutral +1.340 [84] -0.201 +0.052 -0.196 +0.039
1,3-Bis(diphenylene)2-methylallyl 367^{\cdot}		H4,4',11,11' H5,5',10,10' H6,6',9,9' H7,7',8,8' 3H(β')	Neutral -0.176 [815] +0.041 -0.164 +0.032 -0.112

Tab. 8.5 (continued)

1,3-Bis(diphenylene)2-phenylallyl		Neutral		
2·		H4,4',11,11'	-0.203	[84]
		H5,5',10,10'	+0.050	
		H6,6',9,9'	-0.192	
		H7,7',8,8'	+0.036	
		2H _o , H _p	-0.018	
		2H _m	+0.010	

and 362^{2-} are illustrated by their ESR spectra in Figure 8.3. The total extent of these spectra is 3.78 for 362^{\cdot} vs 2.36 mT for 362^{2-} (including the additional splitting of 0.035 mT by two ^{39}K nuclei in the two K^+ counterions). The π -spin distribution in the radical dianions of methylenephenanthrene (360^{\cdot}) and dibenzotropyll (363^{\cdot}), in which the SOMOs have a vertical node at the center 11, is similar to that in the radical anions of *trans*- and *cis*-stilbenes (**101**) (Chapt. 8.4 and Table 8.12).

Upon replacement of phenyl by mesityl in the 9-position of fluorenyl, on going from 358^{\cdot} to 359^{\cdot} , the coupling constants of the protons at this substituent change from values compatible with a nearly coplanar phenyl group to those characteristic of one strongly twisted out of coplanarity (see comments above on the 7,7-di-*tert*-butylbenzyl radical 327^{\cdot}). The π -spin distribution in 1,3-bis(diphenylene)allyl (366^{\cdot}) is almost the same as in 1,1,3,3-tetraphenylallyl (341^{\cdot}) (Table 8.2). The nonalternant radical 366^{\cdot} is, however, even more twisted than its alternant counterpart 341^{\cdot} , and the coupling constant, $a_{\text{H}_2} = +0.401$ mT, for allyl (65^{\cdot}) is even more strongly increased by a direct spin transfer from the two rather rigid diphenylene moieties than by that from the four more flexible phenyl substituents. Consequently, this value is +1.340 mT for 366^{\cdot} , as compared with +0.881 mT for 341^{\cdot} . The ^1H -hyperfine data in Table 8.5 indicate that the π -spin distribution in 366^{\cdot} is not markedly altered by substitution in the 2-position either by a methyl (367^{\cdot}) or by a phenyl group (2^{\cdot}). The small value, $|a_{\text{H}}(\beta)| = 0.112$ mT (sign presumably negative), of the three methyl protons in 367^{\cdot} is thus a better measure of the spin population ρ_2^{π} than the corresponding a_{H_2} value of the α proton in 366^{\cdot} , because coupling constants of β protons are less sensitive to deviations of π radicals from planarity (see hyperfine data for the radical anions of 1,6-methano[10] annulene (**85**) and its 2-methyl derivative (**86**) in Chapt. 4.3). As mentioned in Chapt. 2.2, 1,3-bis(diphenylene)2-phenylallyl (2^{\cdot}), which can be isolated in crystalline form, is unusually persistent, due to the perfect shielding of the reactive allyl moiety by the one phenyl and two diphenylene groups.

The g_e factor of the nonalternant radicals is 2.0026 ± 0.0001 and that of the corresponding radical dianions is 2.0028 ± 0.0001 . The radicals 50^{\cdot} and 355^{\cdot} were generated by abstraction of a H atom with *t*-BuO $^{\cdot}$ from the corresponding hydrocarbons, 356^{\cdot} was formed from the 9-bromide with $\text{Et}_3\text{Si}^{\cdot}$, and 358^{\cdot} and 359^{\cdot} were obtained from the analogous chlorides with Hg or Zn. An alternative method is

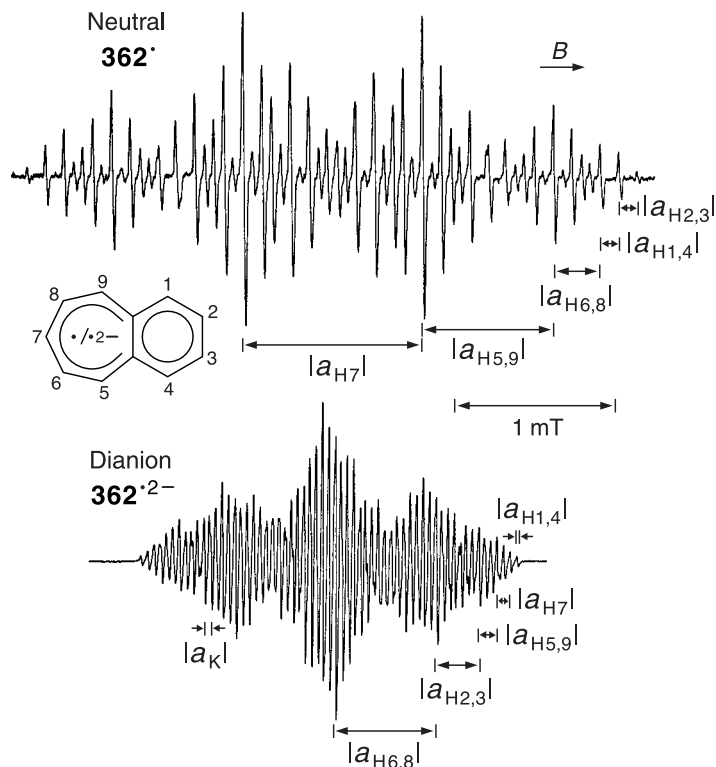


Fig. 8.3. ESR spectra of the neutral radical and radical dianion of benzotropyl ($362\cdot$). Top, neutral $362\cdot$: solvent high-boiling oil, temperature 423 K. Bottom, dianion $362\cdot^{2-}$: solvent DME, counterions K^+ , temperature 198 K. Hyperfine data in Table 8.5. Reproduced with permission from [813].

thermolysis, which yielded $63\cdot$ and $362\cdot$ from its dimer and $366\cdot$ from the percarbonic acid ester. Electrolytic reduction of the corresponding cation led to $365\cdot$. The radical dianions were produced with an alkali-metal from the corresponding methyl ethers or other precursors.

8.4

Even Alternant Radical Ions

Radical Ions of Polyenes

Tables 8.6 [199, 201, 202, 226, 316, 328, 529, 816, 817] and 8.7 [200, 201, 226, 307, 329, 337, 338, 529, 818–822] list the hyperfine data for the radical ions of some polyenes and their alkyl derivatives. The ^1H -coupling constants for the radical ions

Tab. 8.6. Hyperfine Data for Radical Ions of Some Acyclic Polyenes

<i>trans</i> -Buta-1,3-diene 92 ⁻ /92 ⁺		H1,4 _{exo} H1,4 _{endo} H2,3	Anion/Cation -0.762/-1.119 -0.762/-1.050 -0.279/-0.283	[199]/ [316]
<i>trans</i> -2,3-Dimethyl- buta-1,3-diene 368 ⁻		H1,4 _{exo} H1,4 _{endo} 6H(beta)	Anion -0.724 -0.700 +0.120	[201]
<i>trans</i> -1,4-Di- <i>tert</i> - butylbuta-1,3-diene 90 ⁻		H1,4 _{endo} H2,3 18H(gamma)	Anion -0.715 -0.240 +0.026	[529]
2,3-Di- <i>tert</i> -butylbuta- 1,3-diene "transoid"-111 ⁻		H1,4 _{exo} H1,4 _{endo}	Anion -0.71 -0.71	[529]
"cisoid"-111 ⁻		H1,4 _{exo} H1,4 _{endo}	-0.672 -0.398	[529]
<i>trans</i> -1,1,4,4- Tetramethylbuta- 1,3-diene 369 ⁻ /369 ⁺		H2,3 6H(beta) 6H(beta')	Anion/Cation -0.116/-0.300 +0.991/+1.290 +0.875/+1.075	[202]/ [226]
<i>trans</i> -Hexamethyl- buta-1,3-diene 370 ⁺		6H(beta) 6H(beta') 6H(beta'')	/Cation /+1.07 /+1.055 /+0.42	[226]
1,1,6,6,-Tetra- <i>tert</i> - butylhexa-1,3,5- triene <i>all-trans</i> -371 ⁻		H2,5 H3,4 18H(gamma) 18H(gamma')	Anion +0.108 -0.465 +0.019 <0.01	[816]
<i>trans,cis,trans</i> -371 ⁻		H2,5 H3,4 18H(gamma) 18H(gamma')	+0.090 -0.453 +0.019 <0.01	[816]
<i>all-trans</i> -1,1,8,8-Tetra- <i>tert</i> -butylocta- 1,3,5,7-tetraene 372 ⁻		H2,7 H3,6 H4,5 18H(gamma) 18H(gamma')	Anion +0.152 -0.515 -0.152 +0.017 <0.01	[816]
Tetramethyleneethane TME 43 ⁻ /43 ⁺		H1,1',3,3' _{exo} H1,1',3,3' _{endo}	Anion/Cation -0.765/-0.805 -0.765/-0.716	[817]/ [328]

Tab. 8.7. Hyperfine Data for Radical Ions of Some Cyclic and Bicyclic Polyenes

Cyclopenta-1,3-diene 373 ⁺		H1,4 H2,3 2H(β)	/Cation /−1.16 [307] /−0.35 /<0.02
Hexamethylcyclopenta-1,3-diene 374 ⁺		6H(β) 6H(β') 6H(γ)	/Cation /+1.44 [226] /+0.40 /0.13
Cyclohexa-1,3-diene 375 ⁻ /375 ⁺		H1,4 H2,3 2H _{ax} (β) 2H _{eq} (β)	Anion/Cation −0.821/−0.854 [201]/[329] −0.200/−0.407 +1.11/+3.187 +1.11/+2.909
1,4-Di- <i>tert</i> -butylcyclohexa-1,3-diene 376 ⁻		H2,3 2H _{ax} (β) 2H _{eq} (β)	Anion −0.20 [529] +1.23 +0.95
Cyclohepta-1,3-diene 377 ⁺		H1,4 H2,3 2H _{ax} (β) 2H _{eq} (β)	/Cation /−0.854 [329] /−0.255 /+2.814 /+1.028
Cyclohepta-1,3,5-triene 378 ⁻ /378 ⁺		H1,6 H2,5 H3,4 2H(β)	Anion/Cation −0.764/−0.78 [200]/[818] +0.059/<0.2 −0.490/−0.39 0.216/+6.98
Bicyclo[2.2.1]hepta-2,5-diene (norbornadiene) 379 ⁺		H2,3,5,6 2H(β) 2H(γ)	/Cation −0.780 [819] −0.049 +0.304
Bicyclo[2.2.2]hepta-2,5-diene (dihydrobarrelene) 380 ⁺		H2,3,5,6 2H(β) 4H(γ)	/Cation −0.676 [819] −0.108 +0.162
Bicyclo[2.2.2]hepta-2,5,7-triene (barrelene) 381 ⁺		H2,3,5,6,7,8 2H(β)	/Cation −0.603 [820] −0.115
Hexamethylbicyclo[2.2.0]hexa-2,5-diene (hexamethyl Dewar)benzene 382 ⁺		12H(β)	/Cation [337, 338, +0.92 821, 822]

of *trans*-buta-1,3-diene (**92**) still reflect the pairing properties of the MOs in the alternant π system. However, the ratio of the $a_{\text{H}1,4}$ values for $\mathbf{92}^{+\cdot}$ and $\mathbf{92}^{-\cdot}$ is $-1.085 \text{ mT}/-0.762 \text{ mT} = 1.42$, where -1.085 represents the average of the values for the protons in the *endo* and *exo* positions. This ratio exceeds that usually found for the coupling constants of α protons at the same centers μ in the two corresponding π -radical ions (see below). Note that the difference $\Delta a_{\text{H}1,4} = |a_{\text{H}1,4_{\text{exo}}} - a_{\text{H}1,4_{\text{endo}}}|$ is 0.069 mT for the cation $\mathbf{92}^{+\cdot}$, but it is too small ($<0.01 \text{ mT}$) to be resolved for the anion $\mathbf{92}^{-\cdot}$.

In general, the observed ^1H -hyperfine data for the polyene radical ions comply with the π -spin distribution as predicted by the simple MO methods, such as the Hückel model and the McLachlan procedure. The unusually tight association of the radical anions of 1,4- (**90**) and 2,3-di-*tert*-butylbuta-1,3-dienes (**111**) with their alkali-metal counterions is considered in Chapt. 6.6. The coupling constants of the two methylene β protons in the cyclohepta-1,3,5-triene radical ions $\mathbf{378}^{-\cdot}$ (0.216 mT ; sign undetermined) and $\mathbf{378}^{+\cdot}$ ($+6.98 \text{ mT}$) provide another example of the “Whiffen effect”. The SOMOs of these ions have the nodal properties of the LUMO ψ_4 and the HOMO ψ_3 , respectively, of the alternant hexa-1,3,5-triene. Whereas the LCAO coefficients $c_{4,1}$ and $c_{4,6}$ at the relevant terminal centers $\mu = 1$ and 6 for ψ_4 have opposite signs, the sign of $c_{3,1}$ and $c_{3,6}$ is the same for ψ_3 . (The first examples given in Chapt. 4.2 for the “Whiffen effect” are the analogous coupling constants for the neutral radicals cyclohexadienyl **70** \cdot and butenyl **71** \cdot .)

Tetramethyleneethane (TME, $\mathbf{43}^{\cdot\cdot}$) is a non-Kekulé diene with two unpaired electrons and a triplet ground state (Chapts. 2.4 and 11.3). The radical ions $\mathbf{43}^{-\cdot}$ and $\mathbf{43}^{+\cdot}$ are charged diallyls, in which the two allyl π moieties are presumably not coplanar. Their ^1H -coupling constants are each about half the corresponding values for the allyl radical (**65** \cdot) (Chapt. 4.2 and Table 8.2).

The bicyclic dienes **379**, **380**, and **382** and the triene **381** (which has D_{3h} symmetry and is the paradigm of a Möbius-type molecule [823]) have two or three nonconjugated double bonds which interact mainly through space. The SOMOs of the radical cations $\mathbf{379}^{+\cdot}$, $\mathbf{380}^{+\cdot}$, and $\mathbf{382}^{+\cdot}$ are antibonding combinations of two ethene π moieties, and the corresponding MO of $\mathbf{381}^{+\cdot}$ (which is nondegenerate) represents an analogous combination of three such π systems. The coupling constants of α protons in these bicyclic radical cations should be related to those for the radical cations of cyclic monoenes, which are close to -1.0 mT (Table 7.15). The $a_{\text{H},\alpha}$ values for the α -protons in the diene radical cations $\mathbf{379}^{+\cdot}$ and $\mathbf{380}^{+\cdot}$ greatly exceed the anticipated -0.5 mT , and that for the triene radical cation $\mathbf{381}^{+\cdot}$ considerably surpasses the expected -0.33 mT . This is because, in these bicyclic radicals, the intervening C–C bonds are situated outside the nodal π plane, and their σ -MOs contribute to $a_{\text{H}}(\alpha)$. On the other hand, the coupling constant $a_{\text{H}}(\beta)$ found for the methyl protons in $\mathbf{382}^{+\cdot}$ compares favorably with halves of the corresponding values for the monoene radical cations of alkenes (Table 7.15). Because the bridgehead β protons in $\mathbf{379}^{+\cdot}$ and $\mathbf{380}^{+\cdot}$ – $\mathbf{381}^{+\cdot}$ lie in the nodal π plane, hyperconjugation is not effective and spin polarization accounts for the negative sign of their small coupling constants.

The g_e factor of the polyene radical anions generated electrolytically or with

potassium in solution is 2.0027 ± 0.0001 . When K is replaced by a heavier alkali-metal as the reducing agent, the g_e factor of the tightly ion paired $92^{\cdot-}$ and $111^{\cdot-}$ becomes considerably higher for the former (Rb: 2.0036; Cs: 2.0056) and slightly lower for the latter radical anion (Rb: 2.0024; Cs: 2.0017). The g_e factor for the polyene radical cations is 2.0022–2.0027 and is enhanced for those generated in Freon matrices (2.0029–2.0037). Except for a few polyenes, for which both radical ions were studied, the anions and cations presented in Tables 8.6 and 8.7 were not generated from the same polyene. This is because reduction and oxidation of polyenes raise different problems. On the one hand, the electronegativity of these compounds is sufficient to undergo reduction with an alkali-metal in solution, but the radical anions thus formed are subject to polymerization if they are not sterically protected by bulky substituents like *tert*-butyl groups. An alternative method, which proved to be successful with **92**, **368**, **369**, and **378**, is electrolytic reduction under special conditions, such as the solvent liquid ammonia or THF at very low temperature. On the other hand, the ionization energy (IE) of polyenes is rather high, so that the radical cations had to be produced by γ -irradiation in Freon matrices. Only compounds heavily substituted by IE-lowering alkyl groups could be oxidized in solution, like **369**, **370**, and **374** which yielded the radical cations with Hg(II) ions upon photolysis in fluid TFA. Note that the radical ions $43^{\cdot-}$ and $43^{\cdot+}$ were not generated from tetramethyleneethane (TME) itself but from its precursors, dimethylenecyclobutane and bicyclopropylidene, respectively.

Radical Ions of Benzenoids

Stable polycyclic compounds containing fused benzene rings are known as polycyclic aromatic hydrocarbons (PAHs). Most are moderate electron acceptors and donors, and they yield fairly persistent π -radical anions and cations. These radical ions were among the first species to be studied by ESR spectroscopy, and the coupling constants a_{H_μ} of their ring α protons served to establish and verify the McConnell equation (Eq. 4.5). The hyperfine data for the radical ions of benzene and several polycyclic benzenoid hydrocarbons are given in Table 8.8 [131–135, 139, 222, 242, 287, 447, 480, 824–830]. A plot of the $a_{H_\mu}(\alpha)$ values for the radical anions and cations vs the π -spin populations ρ_μ^π , which were calculated by the McLachlan procedure ($\lambda = 1.0$), is shown in Figure 8.4. The equation of the regression line is, in mT:


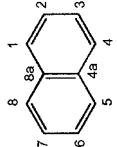
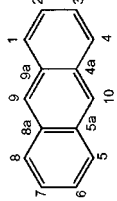
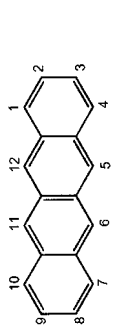
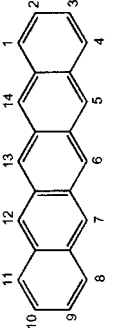
$$a_{H_\mu}(\alpha) = -0.02 - 2.37\rho_\mu^\pi \quad (8.12)$$

where -2.37 mT is an estimate of the π, σ -spin-polarization parameter $Q_H^{C_\mu H_\mu}$ in Eq. 4.5. When the radical anions and the radical cations are considered separately, the corresponding equations are

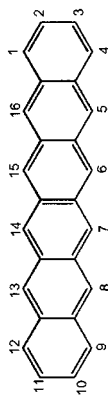
$$a_{H_\mu}(\alpha) = -0.03 - 2.15\rho_\mu^\pi \quad (8.13)$$

for the anions, and

Tab. 8.8. Hyperfine Data for Radical Ions of Some Benzenoid Hydrocarbons

			Anion/Cation	
Benzene			-0.375/-0.445 +0.28	[132]/[447]
$62^{\cdot-}/62^{\cdot+}$				
Naphthalene			Anion/Cation/Dim.Cat. ^a -0.495/-0.587/2× -0.276 -0.183/-0.167/2× -0.103 +0.726 -0.109 -0.573	[135]/[480]/[287] [824]
$83^{\cdot-}/83^{\cdot+}/83_2^{\cdot+}$				
Anthracene			Anion/Cation/Dim.Cat. ^a -0.274/-0.306/2× -0.142 -0.151/-0.138/2× -0.071 H9,10 -0.534/-0.653/2× -0.325 +0.357 -0.025/-0.037 +0.876/+0.848 -0.459/-0.450	[134]/[134]/[287]
$68^{\cdot-}/68^{\cdot+}/68_2^{\cdot+}$				
Naphthacene			Anion/Cation -0.154/-0.168 -0.116/-0.102 -0.423/-0.501	[242]/[242]
$383^{\cdot-}/383^{\cdot+}$				
Pentacene			Anion/Cation -0.092/-0.098 -0.087/-0.076 -0.303/-0.356 -0.426/-0.508	[242]/[242]
$384^{\cdot-}/384^{\cdot+}$				

Hexacene
385^{-•}/385^{+•}



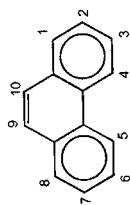
H1,4,9,12
H2,3,10,11
H5,8,13,16
H6,7,14,15

[139]/[139]

Anion/Cation

-0.063/-0.060
-0.057/-0.057
-0.210/-0.240
-0.365/-0.425

Phenanthrene
386^{-•}/386^{+•}



H1,8
H2,7
H3,6
H4,5
H9,10

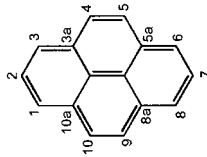
[131]/[825]

Anion/Cation

-0.360/-0.422
+0.032/+0.086
-0.288/-0.383
-0.072/-0.070
-0.432/-0.489

Pyrene

387^{-•}/387^{+•}/387₂^{+•}



H1,3,6,8
H2,7
H4,5,9,10
¹³C1,3,6,8
¹³C2,7
¹³C4,5,9,10
¹³C3a,5a,8a,10a

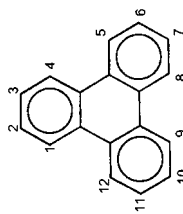
[242]/[242]/[287]

Anion/Cation/Dim.Cat.^a

-0.475/-0.538/2× -0.266
+0.109/+0.118/2× +0.058
-0.208/-0.212/2× -0.110
+0.710
-0.600
0.184
-0.258

[825a]

Triphenylene
388^{-•}/388₂^{+•}



H1,4,5,8,9,12
H2,3,6,7,10,11

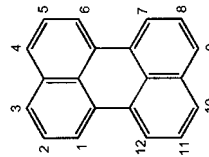
[826]/[827]

Anion/Dim.Cat.^a

-0.128/2× -0.059
-0.159/2× -0.092

Perylene

389^{-•}/389^{+•}/389₂^{+•}



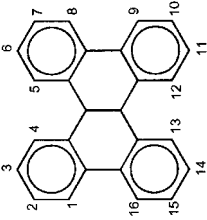
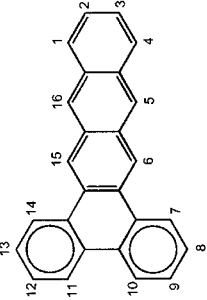
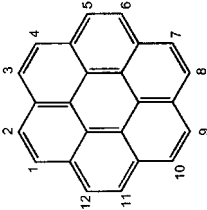
H1,6,7,12
H2,5,8,11
H3,4,9,10

[133]/[133]/[828]

Anion/Cation/Dim.Cat.^a

-0.308/-0.310/-0.149
+0.046/+0.046/+0.021
-0.353/-0.410/-0.191

Tab. 8.8 (continued)

Dibenzo[<i>a,c</i>]triphenylene 390 ^{••} /390 ^{•+}		H1,8,9,16 H2,7,10,15 H3,6,11,14 H4,5,12,13	Anion/Cation -0.062/-0.060 -0.171/-0.199 <0.003/<0.003 -0.206/-0.228	[242]/[242]
Dibenzo[<i>a,c</i>]naphthacene 391 ^{••} /391 ^{•+}		H1,4 H2,3 H5,16 H6,15 H7,14 H8,13 H9,12 H10,11	Anion/Cation -0.170/-0.208 -0.119/-0.112 -0.436/-0.544 -0.407/-0.431 +0.008/<0.005 -0.043/-0.020 -0.067/-0.052 +0.016/+0.008	[829]/[829]
Coronene 392 ^{••} /392 ^{•+} /389 ₂ ^{•+}		H1-12	Anion/Cation/Dim.Cat. ^a -0.147/-0.153/-0.076	[242]/[222]/[830]

^a Dimeric Radical Cation

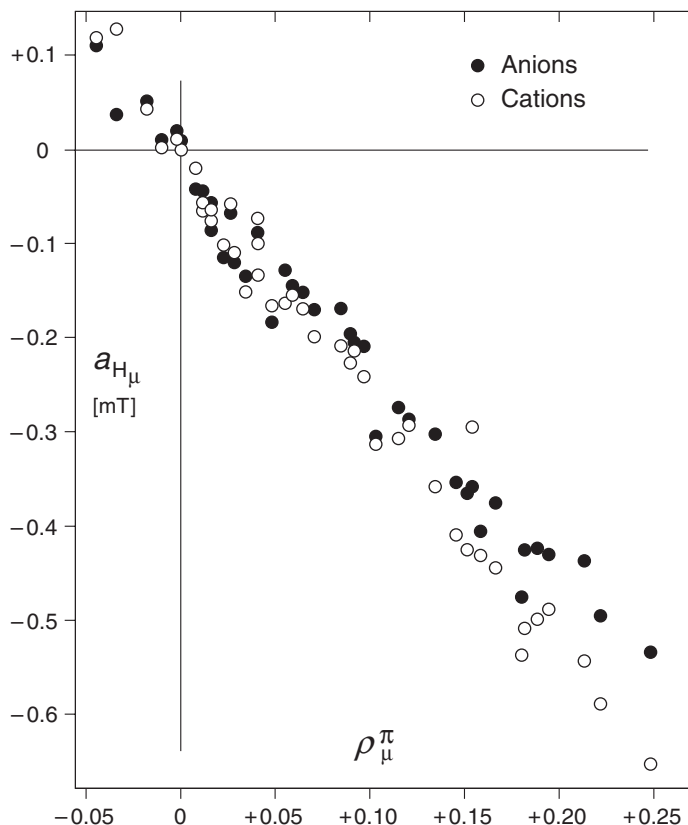


Fig. 8.4. Coupling constants, a_{H_μ} , of α protons in alternant benzenoid radical ions vs their π -spin populations ρ_μ^π . Hyperfine data in Table 8.8.

$$a_{H_\mu}(\alpha) = -0.01 - 2.60\rho_\mu^\pi \quad (8.14)$$

for the cations. The standard deviation is ± 0.06 mT for all three regression lines.

According to the pairing properties of the HOMO and the LUMO in alternant π systems, the π -spin populations in the radical cation and the radical anion of the same alternant hydrocarbon should be equal (Chapt. 8.1). This statement, which accounts for the similar observed hyperfine patterns of the two radical ions, is supported by the ESR spectra of 389^- and 389^+ reproduced in Figure 8.5. As indicated by the differing parameter $Q_H^{C_\mu H_\mu}$ (Eqs. 8.13 and 8.14), the $|a_{H_\mu}|$ values are generally larger for the radical cations than for the corresponding anions (Chapt. 4.2), although for small coupling constants the contrary is often true. (A careful reader may have noted that $Q_H^{C_\mu H_\mu}$ values obtained from the slopes of the regression lines in Eqs. 8.12–8.14 are at the lower limits of the ranges quoted for these values in Chapt. 4.2. This result is due to the nature of the regression: a_{H_μ} on ρ_μ^π .)

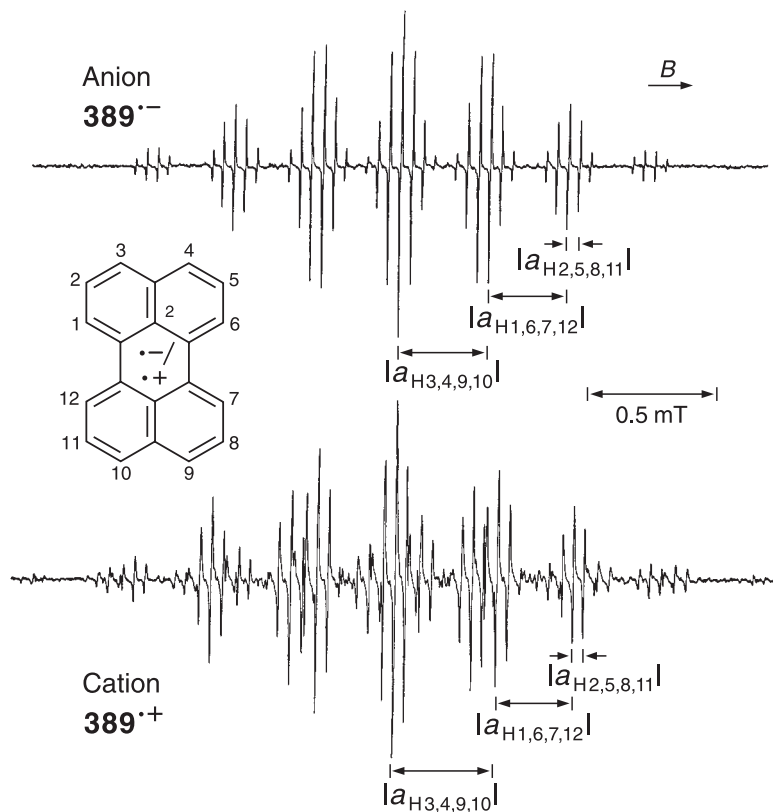


Fig. 8.5. ESR spectra of the radical ions of perylene (**389**). Top, anion $389^{\bullet-}$: solvent DME, counterion Na^+ , temperature 203 K. Bottom, cation $389^{\bullet+}$: solvent conc. sulfuric acid, counterion HSO_4^- , temperature 298 K. The apparently smaller number of lines for $389^{\bullet-}$ than for $389^{\bullet+}$ is due to the relation $|a_{\text{H}3,4,9,10}| \approx |a_{\text{H}1,6,7,12}| + |a_{\text{H}2,5,8,11}|$, holding for the anion. Hyperfine data in Table 8.8.

The dibenzonaphthacene **391** is an example of a benzenoid with as many as eight pairs of equivalent π centers μ . It can be considered as consisting of two fused π systems, those of anthracene and phenanthrene. The coupling constants $a_{\text{H},\mu}$ for $391^{\bullet-}$ and $391^{\bullet+}$ indicate that the bulk of the π -spin population resides in the anthracene system, as might be expected from the greater ease of reduction and oxidation of linearly-fused than of angularly-fused benzenoid hydrocarbons. Table 8.8 also gives hyperfine data for a few dimeric radical cations. Formation of such species $\text{M}_2^{\bullet+}$ from hydrocarbons **M** was also observed for other benzenoids in solution, where the dimeric cations occur alone or along with their monomeric counterparts $\text{M}^{\bullet+}$. Oxidation of naphthalene in fluid solution yields exclusively the dimer $83_2^{\bullet+}$.

The ESR spectrum of the dimeric pyrene radical cation $387_2^{\bullet+}$ is shown in Figure 8.6, together with that of the monomeric $387^{\bullet+}$.

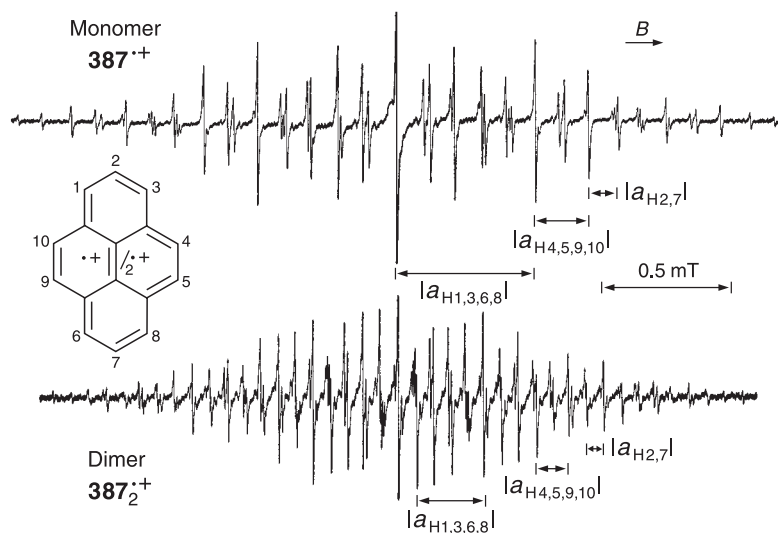
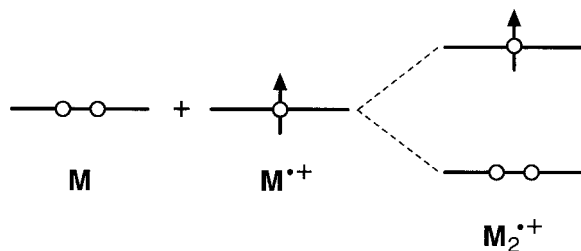


Fig. 8.6. ESR spectra of the monomeric and dimeric radical cations of pyrene (**387**). Top, monomer $387^{\bullet+}$ and bottom, dimer $387_2^{\bullet+}$: solvent dichloromethane, counterion SbCl_6^- ,

temperature 203 K. A large excess of SbCl_5 was used for the monomer. Hyperfine data in Table 8.8. Adapted with permission from [287].

As stated in Chapt. 2.3, dimerization is favored by a high IE value, increased concentration of M , and low temperature. The statement on IE holds, in particular, for hydrocarbons like **83** with a rather high IE value, because interaction between M and $M^{\bullet+}$ leads to the more stable dimer $M_2^{\bullet+}$, as shown for the HOMOs of these species:



In the dimeric radical cations, $M_2^{\bullet+}$, the two π moieties are situated in parallel planes at a distance comparable to that in the crystals (300–350 pm). The two moieties need not be eclipsed but can be twisted relative to each other as in $83_2^{\bullet+}$, in which the twist angle is 90° [831]. The number of interacting α protons in $M_2^{\bullet+}$ is twice that in the monomeric radical ions, but the larger coupling constants for $M_2^{\bullet+}$ are slightly less than one-half the corresponding values in the cations $M^{\bullet+}$ but more than one-half those in the anions $M^{\bullet-}$. Thus, the total extents $\sum |a_{H_i}|$ of the ESR spectra of the radical ions of pyrene are 2.95, 3.34, and 3.23 mT for $387^{\bullet-}$,

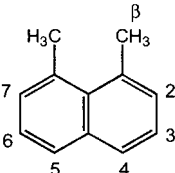
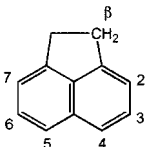
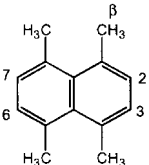
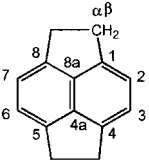
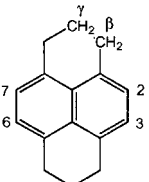
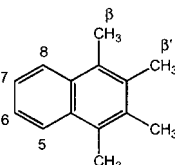
$387^{+\cdot}$, and $387_2^{+\cdot}$, respectively. These values reflect the charge dependence of the coupling constants $a_{H_\mu}(\alpha)$. (Due to the doubling of the number of centers μ , the positive π charge at the center μ in a dimeric radical cation is half as large as in the monomer.)

For alkyl-substituted benzenoid π systems having neither a degenerate nor a near-degenerate ground state (Chapts. 8.1 and 8.6) and in the absence of steric hindrance caused by the substituent, the pairing theorem still underlies the π -spin distribution in the two corresponding radical ions. However, the hyperfine patterns of the radical anion and the radical cation, even with no degenerate or near-degenerate ground state, may differ considerably, because the coupling constants of the alkyl β protons are enhanced much more by the positive π charge than those of their α counterparts. The positive $a_{H}(\beta)$ values for alkyl substituents at centers of high π charge can increase by as much as a factor of 2 on going from a radical anion to the corresponding cation. Such an increase, which was demonstrated in Chapt. 4.2 for the radical ions of 9,10-dimethylanthracene (**69**), is further exemplified by the hyperfine data in Table 8.9 [135, 288, 453, 477, 574, 624, 636, 824, 832, 833] for the radical anions and radical cations of several alkyl-substituted naphthalenes. The ^1H -coupling constants for the radical ions of 1,2,3,4-tetramethylnaphthalene (**394**) indicate that there is a shift of the π -spin population in the cation $394^{+\cdot}$ from the unsubstituted towards the alkyl-substituted ring, in accordance with the IE-lowering effect of the alkyl groups. The coupling constants $a_{H}(\beta)$, of $67^{\cdot-}$ and $67^{+\cdot}$ vs those of $66^{\cdot-}$ and $66^{+\cdot}$, on the one hand, and of $393^{\cdot-}$ and $393^{+\cdot}$ vs those of $96^{\cdot-}$ and $96^{+\cdot}$, on the other hand, illustrate the conformational dependence of $a_{H}(\beta)$, as already pointed out for $67^{\cdot-}$ vs $66^{\cdot-}$ in Chapt. 4.2. Dimeric radical cations were observed for the alkyl-substituted naphthalenes in Table 8.9, except for **123** and **393**; in the latter, steric hindrance by four methyl substituents presumably impairs formation of the dimers. The ^1H -coupling constants are given for $96_2^{+\cdot}$ and $394_2^{+\cdot}$; those for $66_2^{+\cdot}$ and $67_2^{+\cdot}$ have a rather complex hyperfine pattern due to a lowering of symmetry relative to the monomeric radical cations [477].

As mentioned in Chapt. 6.2, the g_e factor of π -radical anions is 2.0027 ± 0.0001 , and that of the corresponding cations and dimeric cations is 2.0026 ± 0.0001 ; however, radical ions with a degenerate ground state, like those of benzene (**62**) and coronene (**392**), have a higher g_e factor of 2.0028–2.0030.

The radical ions of polycyclic benzenoid hydrocarbons can be produced by a variety of methods in solution, as described in Chapt. 2.3. The most general method for reduction to the radical anions was contacting the neutral compound with an alkali-metal mirror in an ethereal solvent; alternatively, electrolysis of the compound at a cathode of mercury or of a gold amalgam can also be used. The radical cations were usually generated by dissolving the neutral compound in a protic acid like conc. sulfuric acid and TFA or by reacting it with a Lewis acid such as SbCl_5 or AlCl_3 in dichloromethane; they can also be generated electrolytically on a platinum or gold anode. For compounds that are hard to oxidize ($\text{IE} > 8$ eV), a more rigorous methods had to applied: $62^{+\cdot}$ and $83^{+\cdot}$ were obtained by high-energy irradiation in a Freon matrix or other frozen liquid, and $386^{+\cdot}$ was formed

Tab. 8.9. Hyperfine Data for Radical Ions of Some Alkyl Derivatives of Naphthalene

1,8-Dimethylnaphthalene $66^{\cdot-}/66^{\cdot+}$		H2,7 H3,6 H4,5 6H(β)	Anion/Cation -0.170/-0.245 -0.170/-0.116 -0.473/-0.573 +0.461/+0.825	[135]/[477]
Acenaphthene $67^{\cdot-}/67^{\cdot+}$		H2,7 H3,6 H4,5 4H(β)	Anion/Cation -0.104/-0.313 -0.242/-0.059 -0.417/-0.659 +0.753/+1.318	[453]/[477]
1,4,5,8-Tetramethylnaphthalene $393^{\cdot-}/393^{\cdot+}$		H2,3,6,7 12H(β)	Anion/Cation -0.141/-0.176 +0.435/+0.784	[832]/[288]
Pyracene $96^{\cdot-}/96^{\cdot+}/96_2^{\cdot+}$		H2,3,6,7 8H(β) $^{13}\text{C}1,4,5,8$ $^{13}\text{C}2,3,6,7$ $^{13}\text{C}4a,8a$ 4 $^{13}\text{C}(\alpha)$	Anion/Cation/Dim.Cat. ^a -0.158/-0.200/2 \times -0.115 +0.658/+1.280/2 \times +0.555 +0.732 -0.118 -0.518 -0.187/-0.266	[624]/[574]/ [477] [824]
1,2,3,6,7,8-Hexahydropyrene $123^{\cdot-}/123^{\cdot+}$		H2,3,6,7 4H _{ax} (β) 4H _{eq} (β) 4H(γ)	Anion/Cation -0.169/-0.190 +0.803/+1.463 +0.202/+0.390 0.050/0.040	[636]/[636]
1,2,3,4-Tetramethylnaphthalene $394^{\cdot-}/394^{\cdot+}/394_2^{\cdot+}$		H5,8 H6,7 6H(β) 6H(β')	Anion/Cation/Dim.Cat. ^a -0.532/-0.371/2 \times -0.222 -0.175/-0.133/2 \times -0.092 +0.374/+0.936/2 \times +0.349 +0.198/+0.241/2 \times +0.137	[833]/[833]/ [477]

^a Dimeric Cation

in solution by photolysis with Tl(III) ions in TFA. Owing to the alkyl substitution, all radical cations in Table 8.9 can be generated in fluid solution, either electrolytically or with AlCl_3 , in contrast to the parent species $83^{\cdot+}$. The dimeric radical cations $83_2^{\cdot+}$, $68_2^{\cdot+}$, and $387_2^{\cdot+}$ were produced with SbCl_5 in dichloromethane, and $388_2^{\cdot+}$ was formed with Hg(II) ions. In addition to a higher concentration of the

neutral precursor, electrolytic generation of dimeric radical cations, such as 96_2^{+} , and 394_2^{+} , required a lower oxidation potential than that used for the corresponding monomers.

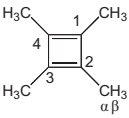
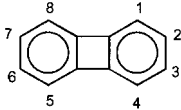
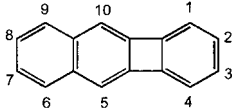
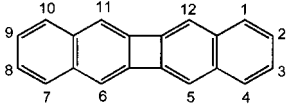
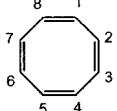
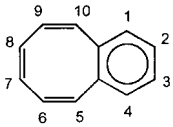
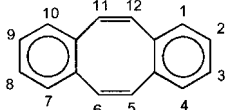
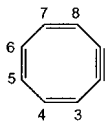
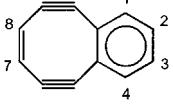
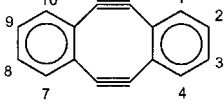
Radical Ions of Alternant Nonbenzenoids

These alternant hydrocarbons, which are less stable (aromatic) than their benzenoid (PAH) counterparts, contain at least one even-membered ring other than benzene. Table 8.10 [183, 224, 260, 263, 449, 559, 582, 834–839] gives hyperfine data for the radical ions of such hydrocarbons with a four- or eight-membered ring. The radical ions of the unsubstituted cyclobutadiene are unknown, and only the radical cations of the tetraalkyl-substituted derivatives, such as 395^{+} , have been studied by ESR spectroscopy. For the radical ions of biphenylene and benzobiphenylene, the pairing theorem is still valid, but the increase in the largest values, $|a_{H2,3,6,7}|$ for 396^{-} and $|a_{H2,3}|$ for 397^{-} , on passing to 396^{+} and 397^{+} , respectively, is larger than usually encountered with “purely” benzenoid radical ions. Presumably, the strain in the four-membered ring does not affect the HOMO and the LUMO to the same degree. For the radical ions of binaphthylene, however, the pairing theorem seems to fail completely, because the coupling constants a_{H_v} for 398^{-} and 398^{+} differ strikingly. Here, ring strain leads to a reverse in the sequence of the highest bonding π -MOs, so that the actual HOMO is no longer related to the LUMO by the pairing properties.

The radical anion of cyclooctatetraene (COT; **64**) was amply investigated and, in contrast to the tub-shaped neutral compound [556, 557] (Chapt. 6.3) found to be planar like the corresponding dianion 64^{2-} [182], of which the number of the π -electrons is conform with Hückel rule (Chapt. 8.1). The radical cation 64^{+} must also be tub-shaped, because the coupling constant a_{H1-8} for 64^{+} is markedly less negative than that for 64^{-} (Chapt. 4.4). An analogous change is observed for the $a_{H4,5,10,12}$ value of the protons in the eight-membered ring of the radical ions of dibenzo[*a,e*]cyclooctene (**400**). Here too, the cation 400^{+} ought to be tub-shaped like the neutral compound, in contrast to the anion 400^{-} which is planar. The planarity of the eight-membered ring is promoted by introduction of triple bonds. Thus, the neutral tetradehydrodibenzo[*a,e*]cyclooctene (**403**) is already planar, at least in the crystalline state [840]. The radical anion, of cyclooctatrienyne (**401**) can be considered a perturbed 64^{-} with a near-degenerate ground state. (Such species are dealt with in Chapt. 8.6.)

The g_e factors of the alternant nonbenzenoid radical ions are similar to those of their benzenoid counterparts. Also, the radical anions were generated by the same methods, namely, by reaction of the neutral hydrocarbon with an alkali-metal (the trianion 405^{3-} by prolonged contact) or electrolytically. Only 401^{-} and 402^{-} were obtained by elimination of HBr from bromocyclooctatetraene and 5,10-dibromobenzocyclooctene, respectively. The radical cations 396^{+} and 397^{+} were produced from the corresponding neutral compounds by dissolving them in conc. sulfuric acid, and 395^{+} was obtained from dimethylacetylene with $AlCl_3$ in dichloromethane. The remaining radical cations were formed in TFA by treating

Tab. 8.10. Hyperfine Data for Radical Ions of Some Alternant Nonbenzenoid Hydrocarbons

Tetramethylcyclobuta-1,3-diene 395 ⁺		12H(β) 13C1-4 413C(α)	/Cation /+0.870 /+0.404 /-0.404	[834]
Biphenylene 396 ⁻ /396 ⁺		H1,4,5,8 H2,3,6,7	Anion/Cation +0.021/+0.021 -0.286/-0.369	[224]/[224]
Benzo[b]biphenylene 397 ⁻ /397 ⁺		H1,4 H2,3 H5,10 H6,9 H7,8	Anion/Cation +0.110/+0.085 -0.247/-0.325 +0.141/+0.068 +0.047/+0.085 -0.152/-0.183	[835]/[835]
Binaphthylene 398 ⁻ /398 ⁺		H1,4,7,10 H2,3,8,9 H5,6,11,12	Anion/Cation -0.157/<0.04 -0.090/-0.173 -0.423/+0.061	[582]/[582]
Cycloocta-1,3,5,7-tetraene (COT) 64 ⁻ /64 ⁺		H1-8 13C1-8	Anion/Cation -0.321/-0.15 +0.130	[449]/[260] [559]
Benzocycloctene 399 ⁻		H1,4 H2,3 H5,10 H6,9 H7,8	Anion +0.036 -0.191 -0.370 -0.200 -0.312	[836]
Dibenzo[a,e]cyclooctene 400 ⁻ /400 ⁺		H1,4,7,10 H2,3,8,9 H5,6,11,12	Anion/Cation +0.022/<0.015 -0.184/-0.161 -0.260/-0.119	[183]/[263]
Cyclooctatriene 401 ⁻		H3,8 H4,7 H5,6	Anion -0.406 -0.292 -0.355	[837]
5,6,9,10-Tetradehydro- benzocyclooctene 402 ⁻		H1,4 H2,3 H7,8	Anion +0.031 -0.189 -0.473	[838]
5,6,11,12-Tetradehydro- dibenzo[a,c]cyclooctene 403 ⁻		H1,4,7,10 H2,3,8,9	Anion +0.016 -0.204	[183]

Tab. 8.10 (continued)

Octalene $404^{\cdot-}$		Anion	
		H1,6,7,12	0.012 [839]
		H2,5,8,11	-0.198
		H3,4,9,10	-0.081
Dibenzo[<i>c,j</i>]octalene $405^{\cdot-}/405^{\cdot3-}$		Anion/Trianion	
		H1,8,9,16	<0.01/-0.357 [839]/[839]
		H2,7,10,15	-0.261/-0.027
		H3,6,11,14	0.098/+0.046
		H4,5,12,13	0.069/-0.161

the neutral compound with Hg(II) ions (398^+ and 400^+) or with Co(IV) ions in a flow system (64^+).

Radical Ions of Polyaryls

Linking two aryl groups by a single bond is attended by steric hindrance of the H atoms in the *ortho* positions, which leads to twisting about this bond and deviation of the entire π system from coplanarity. Such a hindrance should increase in the sequence biphenyl (**94**) \approx 2,2'-binaphthyl (**415**) < 1,1'-binaphthyl < *o*-terphenyl (**407**) < 9,10-diphenylanthracene (**414**) < 9,9'-bianthryl (**416**) < 1,8-diphenylnaphthalene (**413**) < 1,5,11,12-tetraphenylnaphthacene (rubrene; **417**). Table 8.11 [534, 569, 585, 631, 827, 841–854] gives hyperfine data for the radical ions of these hydrocarbons, except for those of 1,1'-binaphthyl, for which no reliable data were reported. It is evident that, for $414^{\cdot-}$, $414^{\cdot+}$, and $417^{\cdot-}$ (but not for $413^{\cdot-}$), deviation from planarity leads to coupling constants characteristic of protons in phenyl groups perpendicular to the π system bearing the bulk of the the spin population (see comments on the 7,7'-di-*tert*-butylbenzyl radical **327** \cdot in Chapt. 8.2). For the radical ions $416^{\cdot-}$ and $416^{\cdot+}$ with two non-coplanar equivalent anthryl moieties, the π -spin population tends, on the hyperfine time-scale, to be localized in one of these moieties. Tetraphenylene is tub-shaped not only in the neutral compound but also in its radical ions $411^{\cdot-}$ and $411^{\cdot+}$, which must therefore be considered those of a cyclic polyphenyl. When $411^{\cdot-}$ is tightly associated with its alkali-metal counterion, π -spin population appears to be localized in one biphenyl-like moiety [854a]. Upon prolonged contact with potassium, the radical anion of 1,8-diphenylnaphthalene (**413**) accepts two further electrons to yield the radical trianion $413^{\cdot3-}$, in which the two almost-parallel phenyl substituents mimic the radical anion of an "open-chain cyclophane" linked to a naphthalene dianion.

The g_e factor of the radical ions of polyaryls is 2.0027 ± 0.0001 . The radical anions were generated from the neutral compounds with an alkali-metal in an ethereal solvent. The radical cations $94^{\cdot+}$ and $410^{\cdot+}$ were produced by photolysis of biphenyl (or benzene) and quaterphenyl, respectively, with Hg(II) ions in TFA, and $416^{\cdot+}$ was obtained by oxidation of bianthryl with Tl(III) in TFA or with DDQ in 1,1,1,3,3,3-hexafluoropropan-2-ol.

Radical Ions of Arylethenes and Arylpolyenes

Hyperfine data for some of these radical ions are listed in Table 8.12 [143, 550, 592, 825, 855–862]. In the radical anions of styrene (**420**) and the two isomeric stilbenes (**101**), the phenyl groups do not rotate freely about the C–C linkage to the double bond, at least on the hyperfine time-scale. As mentioned in Chapt. 6.5, the coupling constants of the phenyl protons at the two *ortho* and, likewise, the two *meta* positions of *trans*-**101**^{•−} can be distinguished by studies of alkyl-substituted radical anions like **421**^{•−}, in which the *ortho*-methyl groups should assume the less sterically hindered positions. A large twist about the double bond is predicted for the strongly congested radical anion **422**^{•−}, obtained from both the *trans*- and *cis*-isomer. The energy minima, roughly corresponding to either configuration of **422**^{•−}, should be separated by a low energy barrier, and the observed coupling constants of the phenyl protons are comparable to those for the unsubstituted *trans*- and *cis*-**101**^{•−}.

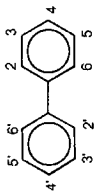
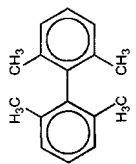
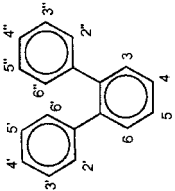
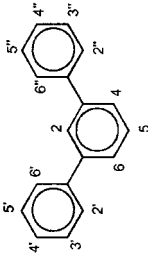
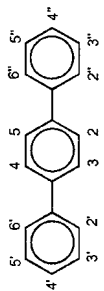
In general, radical anions of *cis*-stilbenes, which deviate much more from planarity than their *trans* counterparts, undergo rapid *cis* → *trans* isomerization. The ESR spectrum of *cis*-**101**^{•−} itself could be observed only under carefully controlled conditions. Interestingly, the coupling constants of the phenyl protons in *cis*- and *trans*-**101**^{•−} closely resemble each other, but that of the protons at the exocyclic C₇=C_{7'} bond is less negative for the *cis*-isomer, i.e., the absolute value is greatly reduced relative to that for its *trans* counterpart. This result indicates the same π -spin distribution in both isomeric radical anions, and the more pronounced nonplanarity in *cis*-**101**^{•−} is thus demonstrated merely by the reduced $|a_{\text{H}7,7'}|$ value (Chapt. 4.3). *cis* → *trans*-Isomerization of stilbene is impeded by incorporation of the exocyclic C₇=C_{7'} double bond into a ring to yield a 1,2-diphenylcycloalkane. ESR studies were reported for radical anions of such compounds which contain the π -system of *cis*-stilbene and in which the cyclic alkene is propene [863], butene [864], pentene [859] and hexene [865]. In Table 8.12, they are represented by the radical anion of 1,2-diphenylcyclopentene (**423**).

The g_e factor of the radical ions of arylpolyenes is 2.0027 ± 0.0001 . The radical anions were generated with an alkali-metal in an ethereal solvent except for the readily polymerizable styrene, of which radical anion **420**^{•−} had to be produced in liquid ammonia using a flow system. The corresponding radical cation **420**^{•+} was formed by γ -irradiation in a CFCl₃ matrix, and *trans*-**101**^{•+} was obtained by photolysis of both *trans*- and *cis*-stilbenes with Hg(II) ions in TFA.

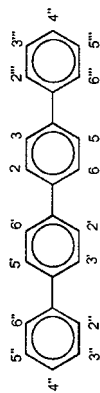
Radical Anions of Arylacetylenes and Aryldiacetylenes

Because both electron affinity (EA) and the ionization energy (IE) of acetylene are higher than those of ethene, arylacetylenes are easier to reduce to radical anions and harder to oxidize to radical cations than the corresponding arylethenes. However, due to the high reactivity of acetylene, radical anions of its alkyl derivatives are less amenable to ESR studies than their ethene counterparts (Table 7.15), and at least one aryl substituent is required to sufficiently stabilize the acetylene radical ion for such studies. Hyperfine data for radical ions of some arylacetylenes and arylacetylenes are listed in Table 8.13 [213, 226, 550, 866, 867].

Tab. 8.11. Hyperfine Data for Radical Ions of Some Polyaryls

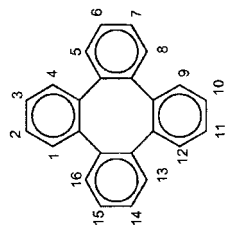
Biphenyl 94 ⁻ /94 ⁺		H2,2',6,6' H3,3',5,5' H4,4'	[569]/[841]	Anion/Cation -0.268/-0.315 +0.039/+0.051 -0.539/-0.630
2,2',6,6'-Tetramethylbiphenyl 406 ⁻		H3,3',5,5' H4,4' 12H(β)	[842]	Anion +0.033 -0.466 +0.222
o-Terphenyl 407 ⁻		H4,5 H3,6 H2',2'' H3',3'' H4',4'' H5',5'' H6',6''	[843]	Anion -0.267 +0.067 -0.194 +0.053 -0.296 +0.023 -0.140
m-Terphenyl 408 ⁻		H2 H4,6 H5 H2',2'',6',6'' H3',3'',5',5'' H4',4''	[843]	Anion +0.075 -0.505 +0.139 -0.098 +0.021 -0.246
p-Terphenyl 409 ⁻ /409 ⁺		H2,3,4,5 H2',2'',6',6'' H3',3'',5',5'' H4',4''	[843]/[827]	Anion/Cation -0.098/-0.122 -0.208/-0.228 +0.052/+0.061 -0.331/-0.365

p,p'-Quaterphenyl
410⁻/410⁺



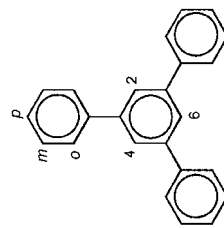
Anion/Cation	[844]/[845]
H2,2',6,6'	-0.147/-0.183
H3,3',5,5'	+0.011/+0.056
H2'',2''',6'',6'''	-0.147/-0.127
H3'',3''',5'',5'''	+0.042/+0.010
H4'',4'''	-0.210/-0.194

Tetraphenylene
411⁻/411⁺



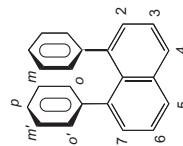
Anion/Cation	[846]/[847]
H1,4,5,8,9,12,13,16	+0.016/<0.001
H2,3,6,7,10,11,14,15	-0.134/-0.134

1,3,5-Triphenylbenzene
412⁻



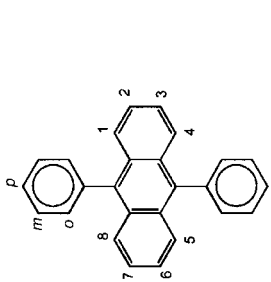
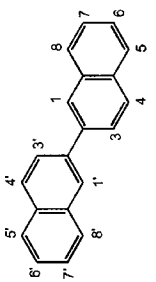
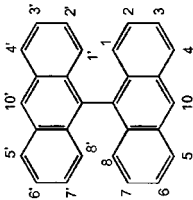
Anion	[848]
H2,4,6	-0.358
6H _o	-0.093
6H _m	+0.016
3H _p	-0.155

1,8-Diphenylnaphthalene
413⁻/413⁻

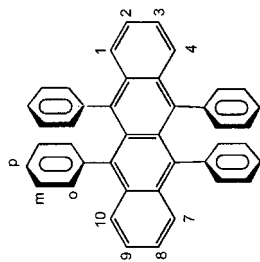


Anion/Triamion	[534]/[849]
H2,7	-0.261/-0.021
H3,6	-0.060/-0.021
H4,5	-0.459/-0.130
2H _o	{ -0.096/-0.189
2H _{o'}	{ -0.057/-0.070
2H _m	{ +0.035/+0.059
2H _{m'}	{ +0.019/+0.021
2H _p	-0.114/-0.301

Tab. 8.11 (continued)

9,10-Diphenylanthracene 414 ⁻ / 414 ⁺		H1,4,5,8 H2,3,6,7 4H _o 4H _m 2H _p	Anion/Cation -0.260/-0.267 -0.145/-0.126 -0.031/-0.044 +0.023/+0.044 -0.023/-0.044	[585]/[585]
2,2'-Binaphthyl 415 ⁻		H1,1' H3,3' H4,4' H5,5' H6,6' H7,7' H8,8'	Anion -0.471 -0.043 -0.238 -0.155 -0.043 -0.021 -0.258	[850]
9,9'-Bianthryl 416 ⁻ / 416 ⁺		localized H1,4,5,8 H2,3,6,7 H10 delocalized H1,1',4,4',5,5',8,8' H2,2',7,7' H3,3',6,6' H10,10'	Anion/Cation -0.264/-0.297 -0.144/-0.130 -0.574/-0.639 -0.133/-0.138 { -0.087/-0.059 -0.064/-0.059 -0.281/-0.353 }	[851]/[631]

5,6,11,12-Tetrabenzonaphthacene (rubrene)

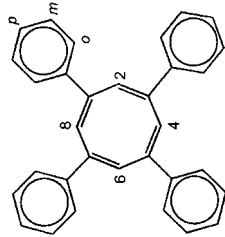
417⁻

Anion
 -0.134
 -0.106
 -0.020
 +0.022
 -0.020

H1,4,7,10
 H2,3,8,9
 8H_o
 8H_m
 4H_p

[852]

1,3,5,7-Tetraphenylcyclooctatetraene

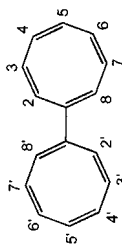
418⁻

Anion
 -0.330
 -0.040
 +0.020

H2,4,6,8
 8H_o, 4H_p
 8H_m

[853]

Bicyclooctatetraenyl

419⁻

Anion
 -0.238
 +0.028
 -0.238
 +0.028

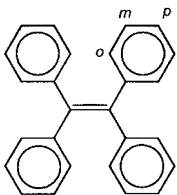
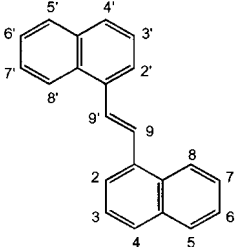
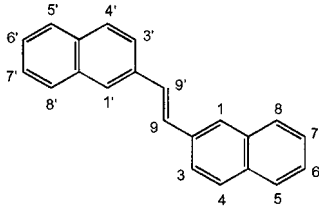
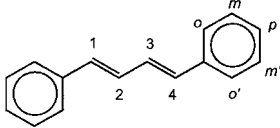
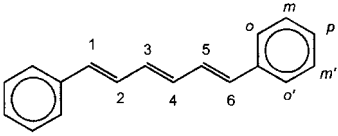
H2,2',8,8'
 H3,3',7,7'
 H4,4',6,6'
 H5,5'

[854]

Tab. 8.12. Hyperfine Data for Radical Ions of Some Arylethenes and Arylpolyenes

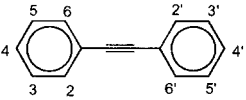
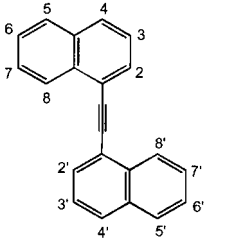
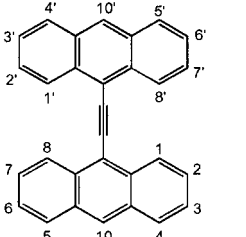
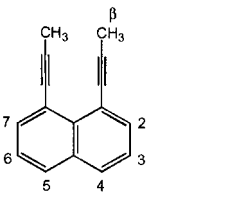
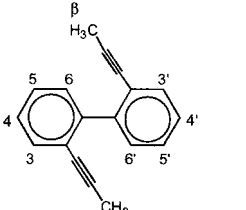
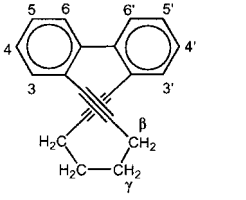
Styrene 420 ⁻ /420 ⁺		H2 H6 H3 H5 H4 H7 2H8	Anion/Cation { -0.382/-0.335 -0.200/-0.225 +0.086/<0.1 +0.059/<<0.1 -0.550/-0.675 -0.151/0.225 -0.735/-1.10	[855]/ [856]
Stilbene <i>trans</i> -101 ⁻ / <i>trans</i> -101 ⁺		H2,2' H3,3' H4,4' H5,5' H6,6' H7,7'	Anion/Cation -0.193/-0.278 +0.029/+0.072 -0.398/-0.453 +0.082/+0.072 -0.302/-0.278 -0.449/-0.453	[857]/ [825]
<i>cis</i> -101 ⁻		H2,2' H3,3' H4,4' H5,5' H6,6' H7,7'	Anion -0.194 +0.030 -0.386 +0.088 -0.291 -0.268	[857]
<i>trans</i> -2,2'-Dimethylstilbene 421 ⁻		H3,3' H4,4' H5,5' H6,6' H7,7' 6H(β)	Anion +0.039 -0.383 +0.082 -0.294 -0.460 +0.151	[592]
<i>trans</i> -7,7'-di- <i>tert</i> - butylstilbene 422 ⁻		H2,2' H3,3' H4,4' H5,5' H6,6' 18H(γ)	Anion -0.226 +0.025 -0.338 +0.085 -0.255 +0.085	[858]
1,2-Diphenylcyclopentene 423 ⁻		H2,2' H3,3' H4,4' H5,5' H6,6' 2H _{ax} (β) 2H _{eq} (β) 2H(γ)	Anion -0.206 +0.036 -0.381 +0.078 -0.263 +0.659 +0.293 0.036	[859]

Tab. 8.12 (continued)

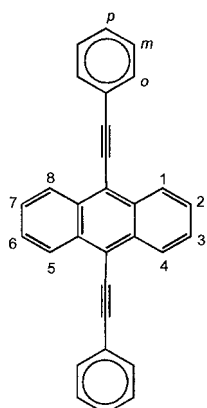
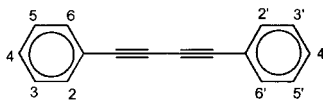
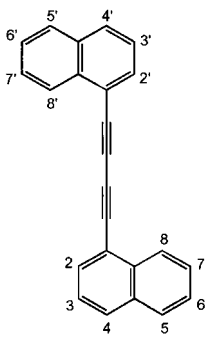
Tetraphenylethene 424 ⁻ /424 ⁺		8H _o 8H _m 4H _p	Anion/Cation -0.152/-0.206 +0.038/+0.052 -0.228/-0.293	[143]/ [860]
<i>trans</i> -1,2-Di(1-naphthyl)- ethene 425 ⁻		H2,2' H3,3' H4,4' H5,5' H6,6' H7,7' H8,8' H9,9'	Anion -0.326 +0.014 -0.420 -0.094 0.007 -0.076 -0.094 -0.348	[550]
<i>trans</i> -1,2-Di(2-naphthyl)- ethene 426 ⁻		H1,1' H3,3' H4,4' H5,5' H6,6' H7,7' H8,8' H9,9'	Anion -0.423 0.014 -0.046 0.046 -0.174 +0.022 -0.210 -0.373	[550]
<i>all-trans</i> -1,4-Diphenylbuta- 1,3-diene 427 ⁻		H1,4 H2,3 2H _o 2H _{o'} 2H _m 2H _{m'} 2H _p	Anion -0.489 -0.323 -0.193 -0.165 +0.076 +0.050 -0.248	[861]
<i>all-trans</i> -1,6-Diphenylhexa- 1,3,5-triene 428 ⁻		H1,6 H2,5 H3,4 2H _o 2H _{o'} 2H _m , 2H _{m'} 2H _p	Anion -0.492 +0.067 -0.265 -0.205 -0.171 +0.051 -0.252	[862]

Replacement of the double by a triple bond on going from arylenes to the corresponding arylacetylenes removes the steric hindrance present in arylenes, but, in general, does not greatly alter the π -spin distribution in the radical anions. Thus, the coupling constants of the α protons at the aryl groups in the radical

Tab. 8.13. Hyperfine Data for Radical Ions of Some Arylacetylenes and Aryldiacetylenes

Diphenylacetylene (tolane) 429 ⁻ / 429 ⁺		H2,2',6,6' H3,3',5,5' H4,4'	Anion/Cation -0.271/-0.222 [213]/ +0.059/+0.075 [226] -0.485/-0.314
Di(1-naphthyl)acetylene 430 ⁻		H2,2' H3,3' H4,4' H5,5' H6,6' H7,7' H8,8'	Anion -0.334 [550] +0.027 -0.475 -0.138 0.012 -0.041 -0.126
Di(9-anthryl)acetylene 431 ⁻		H1,1',8,8' H2,2',7,7' H3,3',6,6' H4,4',5,5' H10,10'	Anion 0.018 [550] -0.146 0.005 -0.159 -0.488
1,8-Di(propyn-1-yl)- naphthalene 432 ⁻		H2,7 H3,6 H4,5 6H(β)	Anion -0.293 [866] -0.069 -0.515 +0.220
2,2'-Di(propyn-1-yl)biphenyl 433 ⁻		H3,3' H4,4' H5,5' H6,6' 6H(β)	Anion +0.092 [866] -0.394 +0.084 -0.108 +0.261
5,6,11,12-tetrahydro-7,8,9,10- tetrahydridibenzo[a,c]- cyclodecene 434 ⁻		H3,3' H4,4' H5,5' H6,6' 2H(β) 2H(β) 2H(γ) 2H(γ)	Anion 0.005 [866] -0.131 -0.214 -0.126 +0.618 +0.455 0.175 0.036

Tab. 8.13 (continued)

9,10-bis(phenylethynyl)- anthracene 435 ⁻		H1,4,5,8	-0.137	[550]
		H2,3,6,8	-0.108	
		4H _o	-0.080	
		4H _m	+0.028	
		2H _p	-0.096	
Diphenyldiacetylene 436 ⁻ /436 ⁺		H2,2',6,6'	-0.247/-0.234	[867]/
		H3,3',5,5'	+0.066/+0.070	[226]
		H4,4'	-0.396/-0.320	
Di(1-naphthyl)diacetylene 437 ⁻		H2,2'	-0.331	[550]
		H3,3'	+0.022	
		H4,4'	-0.435	
		H5,5'	-0.107	
		H6,6'	<0.004	
		H7,7'	-0.063	
		H8,8'	-0.107	

anions of diphenylacetylene (tolane; **429**) and di(1-naphthyl)acetylene (**430**) resemble those in the radical anions of the two isomeric stilbenes (**101**) and 1,2-di(1-naphthyl)ethene (**425**), respectively (Table 8.12). On going to the radical anions of diphenyldiacetylene (**436**) and di(1-naphthyl)diacetylene (**437**), these values somewhat decrease, because the π -spin population is shared by two more centers. In the radical anions of 1,8-di(propyn-1-yl)naphthalene (**432**) and 5,6,11,12-tetrahydro-7,8,9,10-tetrahydridibenzo[*a,c*] cyclodecene (**434**), the two triple bonds are parallel and crossed, respectively. MO models suggest a weak bonding interaction between the two proximate acetylene moieties in these species.

The g_e factor of radical ions with monoacetylene groups is 2.0027 ± 0.0001 for **429⁻**–**435⁻** and 2.0024 for **429⁺**. It is markedly reduced by the presence of the diacetylene group in the radical anions: it is 2.0022 ± 0.0001 for **436⁻** and **437⁻** and 2.0013 for **436⁺**. This reduction was explained in terms of two orthogonal π

systems, one of them (π_z) embracing, as usual, all conjugated $2p_z$ -AOs, and the other (π_y) consisting of two $2p_y$ -AOs in the monoacetylene group and four $2p_y$ -AOs in the diacetylene group (the z direction is perpendicular to the molecular plane xy). Interaction between the systems (π_z and π_y) by spin-orbit coupling leads to a significant decrease in the x -component of the g_e factor for the radical anions with a diacetylene group relative to that for the radical anions with monoacetylene groups, because the four center π_y system in a diacetylene is energetically much closer to the extended π_z system than the two-center π_y counterpart in a monoacetylene. The radical anions were generated by reaction of the corresponding acetylenes or diacetylenes with potassium in DME, whereby $432^{\cdot-}$ – $434^{\cdot-}$, substituted in one of the two acetylene positions by alkyl instead of aryl groups, were less persistent. For the least stable $434^{\cdot-}$, electrolysis of the neutral compound at a helical cathode of gold amalgam proved to be more advantageous than reduction with potassium. The radical cations were produced by photolysis in TFA with ($436^{\cdot+}$) or without ($429^{\cdot+}$) Hg(II) ions.

8.5

Even Nonalternant Radical Ions

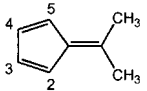
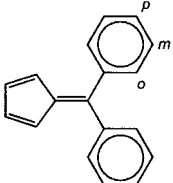
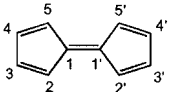
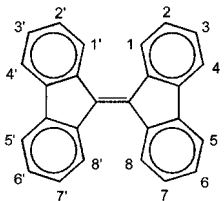
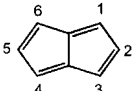
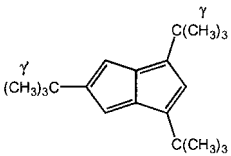

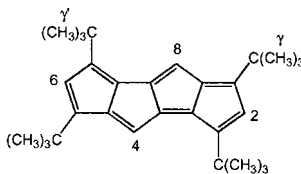
From the theoretical point of view, even nonalternant π systems are of much greater interest than their alternant counterparts because of the remarkable variety of their topography. As stated in Chapt. 8.2, nonalternant systems lack the pairing properties relating the antibonding with the bonding π -MOs of an alternant system. Therefore, the nodal characteristics and the shape of the LUMO and the HOMO are, in general, different for a nonalternant system, and so are the π -spin populations ρ_μ^π and the coupling constants a_{X_μ} for the radical anion and the radical cation of the same nonalternant hydrocarbon.

This difference is evident from the hyperfine data for such radical ions, given in Tables 8.14 [179, 184, 185, 239, 242, 868–878], 8.15 [259, 262, 814, 879–882], and 8.16 [136–138, 147, 239, 839, 883–886]. The nonalternant hydrocarbons and, in general, their radical ions are less stable than their alternant counterparts, and, in some cases, only their alkyl derivatives, in particular, the *tert*-butyl substituted ones, are available. Some of them have low-lying vacant π -MOs, so that they accept three additional electrons to form the radical trianions.

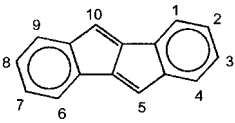
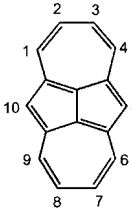
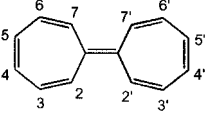
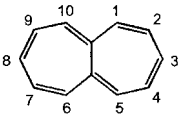
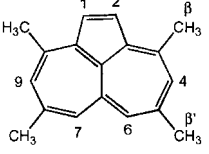
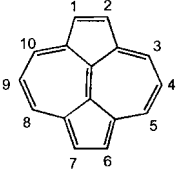
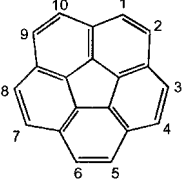
A paradigm of nonalternant hydrocarbon is azulene (**112**), an isomer of naphthalene (**83**). The chemical and physical properties of azulene depend on whether the four *even*- or the four *odd*-numbered centers μ are involved [887]. Thus, the π -spin populations ρ_μ^π in the radical anion $112^{\cdot-}$ are large and positive at $\mu = 2, 4, 6$, and 8, but small and negative at $\mu = 1, 3, 5$, and 7. Accordingly, large and negative coupling constants a_{H_μ} are found for the protons at the even-numbered centers but small and positive at the odd-numbered centers. The opposite statement with respect to the ρ_μ^π and a_{H_μ} values holds for the radical cation $112^{\cdot+}$.

In general, the π -spin distribution is much more sensitive to perturbations in nonalternant radical ions than in their alternant counterparts with a non-degenerate ground state. Such a sensitivity, which is pointed out in Chapt. 6.6 for

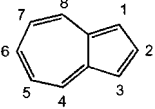
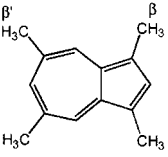
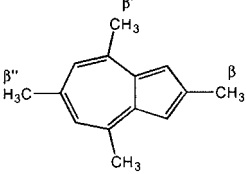
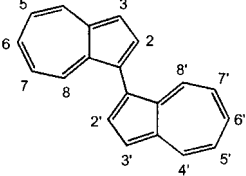
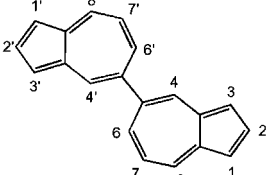
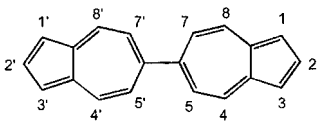
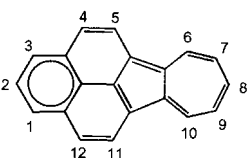
Tab. 8.14. Hyperfine Data for Radical Ions of Some Nonalternant Hydrocarbons Related to Fulvene, Fulvalene, Pentalene and Heptalene

6,6-Dimethylfulvene 438 ^{•+}		H2,5 H3,4	/Cation /−1.68 /−0.45	[868]
6,6-Diphenylfulvene 439 ^{•−}		H2,5 H3,4 4H _o 4H _m 2H _p	Anion −0.179 −0.200 −0.196 +0.085 −0.240	[869]
Fulvalene 440 ^{•−}		H2,2',5,5' H3,3',4,4' ¹³ C1,1' ¹³ C2,2',5,5' ¹³ C3,3',4,4'	Anion −0.155 −0.370 +0.290 −0.140 +0.215	[870]
Δ9,9'-Bifluorene 441 ^{•−} /441 ^{•+}		H1,1',8,8' H2,2',7,7' H3,3',6,6' H4,4',5,5'	Anion/Cation −0.151/−0.214 +0.054/+0.017 −0.193/−0.198 +0.027/+0.046	[861]/[242]
Pentalene 442 ^{•−}		H1,3,4,6 H2,5	Anion −0.776 +0.095	[184]
1,3,5-Tri- <i>tert</i> -butyl- pentalene 443 ^{•−} /443 ^{•+}		H2 H4,6 18H(γ) 9H(γ')	Anion/Cation +0.094/−0.918 −0.645/+0.040 0.018/0.006 0.003/0.045	[871]/[871]
Accepentalene 444 ^{•−}		H1–6	Anion −0.215	[185]
1,3,5,7-Tetra- <i>tert</i> -butyl- dicyclopenta[<i>a,e</i>]- pentalene 445 ^{•−} /445 ^{•+}		H2,6 H4,8 18H(γ) 18H(γ')	Anion/Cation −0.545/+0.045 −0.151/−0.169 +0.005/+0.017 +0.005/+0.017	[872]/[872]

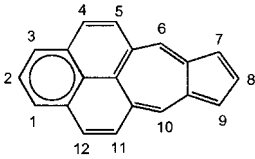
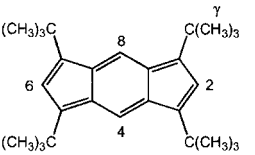
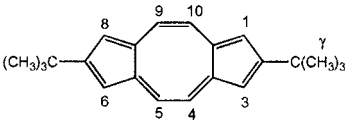
Tab. 8.14 (continued)

Dibenzo[<i>b,f</i>]pentalene 446 ⁻ /446 ⁺		H1,6 H2,7 H3,8 H4,9 H5,10	Anion/Cation -0.109/+0.058 +0.030/-0.353 -0.196/-0.005 +0.030/-0.147 -0.722/+0.033	[873]/[873]
Dicyclohepta[<i>cd,gh</i>]- pentalene 447 ⁻ /447 ³⁻		H1,4,6,9 H2,3,7,8 H5,10	Anion/Trianion -0.054/-0.305 -0.267/-0.064 +0.029/-0.190	[874]/[875]
Heptafulvalene 448 ⁻ /448 ⁺		localized H2,7 H3,6 H4,5 delocalized H2,2',7,7' H3,3',6,6' H4,4',5,5'	Anion/Cation -0.822/0.008 <0.03/-0.290 -0.502/-0.172 -0.410 <0.015 -0.249	[876]/[876]
Heptalene 449 ⁻		H1,5,6,10 H2,4,7,9 H3,8	Anion +0.069 -0.535 +0.079	[877]
3,5,8,10-Tetramethyl- cyclopenta[<i>ef</i>]- heptalene 450 ⁻ /450 ⁺		H1,2 H4,9 H6,7 6H(β) 6H(β')	Anion/Cation -0.032/-0.207 +0.128/-0.499 +0.099/-0.607 +0.544/-0.035 +0.512/-0.122	[239]/[239]
Dicyclopenta[<i>ef,kl</i>]- heptalene (Azupyrene) 451 ⁻ /451 ³⁻		H1,2,6,7 H3,5,8,10 H4,9	Anion/Trianion -0.064/-0.257 -0.423/-0.396 +0.094/+0.100	[878]/[875]
Corranullene 452 ⁻ /452 ³⁻		H1-10	Anion/Trianion -0.157/-0.162	[179]/[179]

Tab. 8.15. Hyperfine Data for Radical Ions of Some Nonalternant Hydrocarbons Related to Azulene and Indacene

Azulene 112 ⁻ /112 ⁺		H1,3 H2 H4,8 H5,7 H6	Anion/Cation +0.027/-1.065 -0.397/+0.152 -0.613/+0.038 +0.122/-0.415 -0.875/+0.112	[879]/ [259]
1,3,5,7-Tetramethylazulene 453 ⁻ /453 ⁺		H2 H4,8 H6 6H(β) 6H(β')	Anion/Cation -0.429/+0.123 -0.570/+0.022 -0.822/+0.103 -0.057/+1.170 -0.089/+0.485	[879]/ [262]
2,4,6,8-Tetramethylazulene 454 ⁻		H1,3 H5,7 3H(β) 6H(β') 3H(β'')	Anion +0.023 +0.134 +0.423 +0.642 +0.912	[879]
1,1'-Biazulenyl 455 ⁺		H2,2' H3,3' H4,4',8,8' H5,5',7,7' H6,6'	/Cation /+0.069 /-0.246 /+0.069 /-0.305 /+0.094	[262]
5,5'-Biazulenyl 456 ⁻		H1,1' H2,2' H3,3' H4,4' H6,6' H7,7' H8,8'	Anion +0.005 -0.209 +0.015 -0.259 -0.438 +0.054 -0.315	[880]
6,6'-Biazulenyl 457 ⁻		H1,1',3,3' H2,2' H4,4',8,8' H5,5',7,7'	Anion +0.050 -0.314 -0.151 -0.082	[880]
Azuleno[1,2,3-cd]- phenalene 458 ⁻ /458 ⁺		H1,3 H2 H4,12 H5,11 H6,10 H7,9 H8	Anion/Cation +0.02/-0.523 -0.08/+0.126 +0.01/-0.429 -0.08/+0.062 -0.67/+0.062 +0.16/-0.256 -0.90/+0.094	[814]/ [814]

Tab. 8.15 (continued)

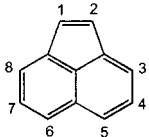
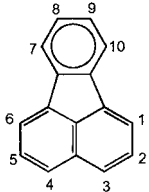
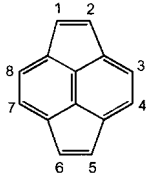
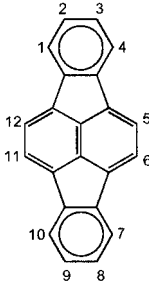
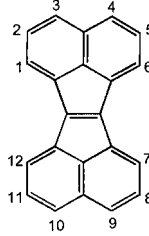
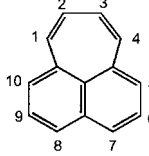
Azulen[5,6,7- <i>cd</i>]phenalene 459 ⁻		H1,3 H2 H4,12 H5,11 H6,10 H7,9 H8	Anion +0.073 -0.252 +0.031 -0.088 -0.504 +0.027 -0.419	[881]
1,3,5,7-Tetra- <i>tert</i> -butyl- <i>s</i> -indacene 460 ⁻ /460 ⁺		H2,6 H4,8 36H(γ)	Anion/Cation +0.109/+0.226 -0.395/+0.091 +0.005/+0.028	[882]/ [882]
2,7-Di- <i>tert</i> -butyldicyclo- penta[<i>a,e</i>]cyclooctene 461 ⁻ /461 ⁺		H1,3,6,8 H4,5,9,10 9H(γ)	Anion/Cation +0.038/-0.662 -0.196/-0.108 +0.017/-0.005	[882]/ [882]

nonalternant radical anions associated with their counterions, is also revealed by alkyl substitution in radical ions such as 453⁻, 453⁺, and 454⁻; the effect of the substitution again differs for even and odd-numbered centers. Whether the two azulene π systems are linked in even or odd positions is likewise important for the radical anions of 5,5'- (456) and 6,6'-biazulenyls (457). Although the π -spin distribution in 456⁻ is consistent with two weakly interacting azulenyl moieties, the π -spin populations in 457⁻ indicate appreciable conjugation between the two moieties. In the radical anions of the azulenophenalenyls 458 and 459, the π -spin distribution resembles that in the radical anions of 1- and 6-phenylazulenes, respectively, but the radical cation 458⁺ may be considered a phenalenyl radical (4⁺) linked by two bonds to the tropylium cation (63⁺).

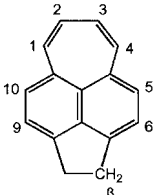
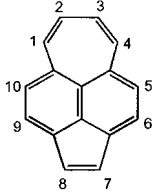
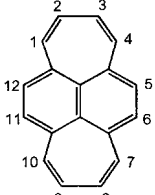
In contrast to the alternant radical ions, the total extents $\sum_{\mu} |a_{H_{\mu}}|$ of the ESR spectra of the radical anion and the radical cation of the same nonalternant hydrocarbon often differ strongly, as shown below.

		$\sum_{\mu} a_{H_{\mu}} $		
		Anion	Cation	Ratio cation/anion
Alternant:	anthracene (68)	2.77	3.08	1.12
	pyrene (387)	2.75	3.05	1.11
	perylene (389)	2.83	3.06	1.08
Nonalternant:	acenaphth[1,2- <i>a</i>]- acenaphthylene (465)	2.94	1.20	0.41
	acepleiadylene (468)	2.05	3.00	1.56

Tab. 8.16. Hyperfine Data for Radical Ions of Some Nonalternant Hydrocarbons Related to Acenaphthylene and Pleiadiene

Acenaphthylene 113 ⁻		H1,2 H3,8 H4,7 H5,6	Anion -0.309 -0.451 +0.045 -0.564	[137]
Fluoranthene 462 ⁻		H1,6 H2,5 H3,4 H7,10 H8,9	Anion -0.390 +0.017 -0.520 +0.008 -0.121	[147]
Pyracylene 463 ⁻		H1,2,5,6 H3,4,7,8	Anion -0.252 -0.188	[883]
Indeno[1,2,3- <i>cd</i>] fluoranthene 464 ⁻ /464 ⁺		H1,4,7,10 H2,3,8,9 H5,6,11,12	Anion/Cation -0.033/+0.015 -0.092/-0.199 -0.168/-0.070	[138]/[138]
Acenaphth[1,2- <i>a</i>]- acenaphthylene 465 ⁻ /465 ⁺		H1,6,7,12 H2,5,8,11 H3,4,9,10	Anion/Cation -0.330/-0.100 +0.071/+0.024 -0.335/-0.176	[136, 884]/ [136, 884]
Pleiadiene 466 ⁻ /466 ⁺		H1,4 H2,3 H5,10 H6,9 H7,8	Anion/Cation -0.659/-0.256 -0.255/-0.233 -0.093/-0.446 +0.031/+0.070 -0.192/-0.545	[885]

Tab. 8.16 (continued)

Acepleiadiene 467 ⁻ /467 ⁺		H1,4 H2,3 H5,10 H6,9 4H(β)	Anion/Cation -0.633/-0.244 -0.256/-0.112 -0.071/-0.350 +0.020/+0.017 +0.305/+1.006	[239]/[239]
Acepleiadylene 468 ⁻ /468 ⁺ / 468 ³⁻		H1,4 H2,3 H5,10 H6,9 H7,8	Anion/Cation/Trianion +0.021/-0.453/-0.625 -0.276/-0.213/-0.216 +0.080/-0.588/-0.068 -0.404/+0.078/+0.068 -0.244/-0.270/0.007	[136, 884]/ [136, 884]/ [839]
Dipleiadiene 469 ⁻ /469 ⁺		H1,4,7,10 H2,3,8,9 H5,6,11,12	Anion/Cation -0.253/-0.100 -0.200/-0.231 -0.043/-0.143	[886]

The most striking example of this difference is provided by the ESR spectra of the radical ions of acenaphth[1,2-*a*]acenaphthylene (**465**) (Figure 8.7). The LUMO of **465** has large squared LCAO coefficients $c_{j,\mu}$ at the peripheral proton-bearing centers $\mu = 1-12$ and small ones at the inner “blind” centers, whereas the HOMO exhibits diametrically opposite behavior. Accordingly, the a_{H_μ} values for **465**⁺ are 2–3 times smaller than those for **465**⁻. Calculations based on π -electron models, such as the McLachlan procedure, do not reproduce the observed hyperfine data for the nonalternant radical ions as well as those for their alternant counterparts. Some deviations of theory from experiment may be due to a dependence of the $Q_{H^{C_\mu H_\mu}}$ parameter of the McConnell equation (Eq. 4.5) on the CCC bond angles, which for five- and seven-membered rings are not close to 120°, as are those of benzenoid hydrocarbons. The π -spin distribution in the radical ions of 9,9'-bifluorene (**441**) is similar to that in the radical ions of the alternant tetraphenylethene (**424**) (Table 8.12).

The g_e factor of the nonalternant radical ions lies in the range 2.0025–2.0028. The radical anions were generated by conventional methods, i.e., reaction of the neutral compound with an alkali metal or by its electrolytic reduction, except for **442**⁻ and **444**⁻, which were produced by photooxidation of the pentalene and acepentalene dianions, respectively. The radical cations were, in general, formed by dissolution of the neutral precursor in conc. sulfuric acid, its electrolytic oxidation, or its reaction with SbCl₅ or AlCl₃ or in dichloromethane. Alkylazulenes like

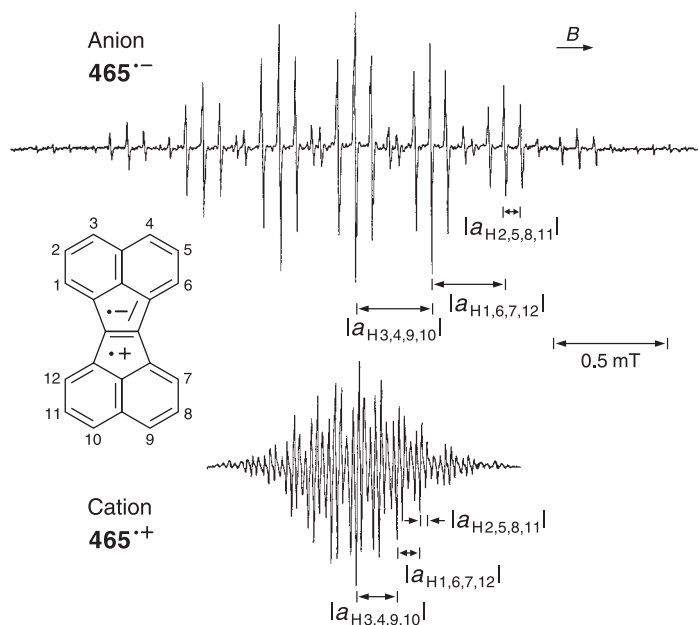


Fig. 8.7. ESR spectra of the radical ions of acenaphth[1,2-*a*]acenaphthylene (**465**). Top, anion $465^{\bullet-}$: solvent: DME, counterion Na^+ , temperature 213 K. Bottom, cation $465^{\bullet+}$:

solvent conc. sulfuric acid, counterion HSO_4^- , temperature 338 K. Hyperfine data in Table 8.16. Reproduced by permission from [884].

454 were converted to their radical cations by photolysis of their neutral precursors in dichloromethane containing $\text{Hg}(\text{CF}_3\text{CO}_2)_2$, whereas azulenes unsubstituted in the 1,3-positions yielded the radical cations of the corresponding 1,1'-biazulenyls under these conditions. Thus, $455^{\bullet+}$ was obtained starting from azulene, and the primary radical cation $112^{\bullet+}$ had to be generated by its oxidation with Co(IV) ions in a flowing solution.

8.6 Radicals and Radical Ions with a Perturbed π Perimeter

n -Membered π perimeters occur in $[n]$ annulenes, which have an even number n and are alternant, and in $[n]$ annulenylys, which have an odd n and are nonalternant. Unperturbed $[n]$ annulenylyl radicals and $[n]$ annulene radical ions of an effective D_{nh} symmetry have doubly-degenerate frontier π -MOs and exhibit π -spin population $\rho_{\mu}^{\pi} = +1/n$ at all n equivalent centers μ ; however, perturbation of these π systems lowers the symmetry and favors one of the two degenerate MOs, ψ_{j+} or ψ_{j-} . ESR spectra of these neutral radicals and radical ions indicate which one of the two orbitals is preferred as the SOMO and thus which effect is responsible for

the perturbation and removal of the degeneracy (Chapt. 8.1). Accordingly, the pertinent studies are of particular theoretical interest and will be dealt with in detail.

The π perimeters in $[n]$ annulenyls and $[n]$ annulenes with $n \leq 9$ assume ideal D_{nh} symmetry, in which all the π centers lie on a circle and are equivalent. These compounds are represented by cyclopropenyl ($n = 3$), cyclobutadiene ($n = 4$), cyclopentadienyl ($n = 5$), benzene ($n = 6$), cycloheptatrienyl (tropyli) ($n = 6$), planar cyclooctatetraene ($n = 8$), and cyclononatetraenyl ($n = 9$). In benzene, all CCC angles are 120° , as required by sp^2 -hybridization, whereas in the remaining $[n]$ annulenes and $[n]$ annulenyls of D_{nh} symmetry, deviation from this angle gradually increases with n differing from 6. When $n > 10$, instead of retaining the D_{nh} symmetry by adopting an all-*cis* configuration, $[n]$ annulenes and $[n]$ annulenyls can relinquish this symmetry by introducing *trans*-configurations, which make CCC angles of 120° possible. In fact, highly reactive all-*cis* and *trans-cis*-configured $[10]$ annulenes were synthesized [888], in which, however, sterical interference of the “inner” H atoms causes serious distortion from planarity along with conformational lability. These handicaps can be overcome by introducing “bridging” alkylidene groups or “stiffening” triple bonds. Like an alkyl substitution, such structural modifications function as perturbations, and the SOMOs in the pertinent neutral radicals and radical ions can be related to the perimeter MOs ψ_{j+} or ψ_{j-} .

Below, selectively deuterated, alkyl-substituted and bridged $[n]$ annulenyl radicals and radical ions of $[n]$ annulenes are considered, as well as radical ions of tetradehydro $[n]$ annulenes. ESR studies of radical ions of this kind were reviewed in 1984 [889].

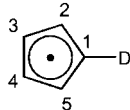
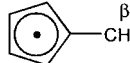
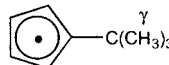
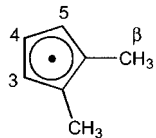
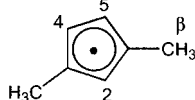
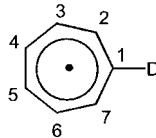
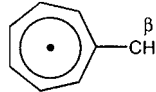
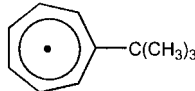
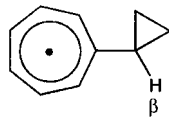
Deuterio and Alkyl Derivatives of $[n]$ Annulenyl Radicals and Radical Dianions

Table 8.17 [446, 890–894] lists hyperfine data for deuterio and alkyl derivatives of $[5]$ - and $[7]$ annulenyl. Those for the parent cyclopentadienyl ($\mathbf{50}^\bullet$) and cycloheptatrienyl (tropyli; $\mathbf{63}^\bullet$) are given in Table 8.5. The relevant degenerate HOMOs, ψ_{1+} and ψ_{1-} , of the five-membered π perimeter (Eq. 8.6) and the LUMOs, ψ_{2+} and ψ_{2-} , of the seven-membered π perimeter are shown in Figure 8.8, together with the spin populations $\rho_\mu^\pi(\psi_{j+})$ and $\rho_\mu^\pi(\psi_{j-})$ calculated by the McLachlan procedure ($\lambda = 1$) for the exclusively single occupancy of ψ_{j+} or ψ_{j-} ($C_+ = 1$, $C_- = 0$ or vice versa; Eq. 8.10).

These $\rho_\mu^\pi(\psi_{j+})$ and $\rho_\mu^\pi(\psi_{j-})$ values can be converted into the corresponding coupling constants $a_{H_\mu}(\psi_{j+})$ and $a_{H_\mu}(\psi_{j-})$ by means of the McConnell equation (Eq. 4.5), with the parameter $Q_{H^\mu}^{C_\mu H_\mu}$ set equal to -3.01 , -2.74 , and -2.44 for $\mathbf{50}^\bullet$, $\mathbf{63}^\bullet$, and $\mathbf{63}^{2-}$, respectively (Table 4.1). Comparison of these calculated coupling constants $a_{H_\mu}(\psi_{j+})$ and $a_{H_\mu}(\psi_{j-})$ with the data in Table 8.17 indicates which of the two MOs, ψ_{j+} or ψ_{j-} is favored as the SOMO in the derivatives of $\mathbf{50}^\bullet$ and $\mathbf{63}^\bullet$ (Eq. 8.11).

Perturbation of the MOs ψ_{j+} and ψ_{j-} by an inductive effect of the substituent at the center μ' is proportional to the squared coefficients $c_{j+, \mu'}^2$ and $c_{j-, \mu'}^2$ at this substituted center, so that the MO with the larger absolute value of the pertinent coefficient is more strongly perturbed than its partner. ESR studies on the radical anions of mono and dideuterio benzenes considered in the next section have

Tab. 8.17. Hyperfine Data for Some Deuterio and Alkyl Derivatives of Cyclopentadienyl Radicals and Cycloheptatrienyl Radicals and Radical Dianions

Deuteriocyclopentadienyl 49- <i>d</i> [•]		H2,5 H3,4 D1	Neutral -0.614 -0.600 -0.089	[446]
Methylcyclopentadienyl 470 [•]		H2,5 H3,4 3H(β)	Neutral -0.085 -0.780 +1.510	[890, 891]
<i>tert</i> -Butylcyclopentadienyl 471 [•]		H2,5 H3,4 9H(γ)	Neutral -0.120 -0.740 0.065	[890]
1,2-Dimethylcyclopentadienyl 472 [•]		H3,5 H4 6H(β)	Neutral +0.064 -1.200 +0.902	[891]
1,3-Dimethylcyclopentadienyl 473 [•]		H2 H4,5 6H(β)	Neutral +0.107 -0.378 +1.340	[891]
Deuteriocycloheptatrienyl 63- <i>d</i> [•]		H2,7 H3,6 H4,5 D1	Neutral -0.365 -0.365 -0.365 -0.056	[892]
Methylcycloheptatrienyl 474 [•] /474 ²⁻		H2,7 H3,6 H4,5 3H(β)	Neutral/Dianion -0.576/-0.024 -0.192/-0.567 -0.384/-0.268 +0.192/+0.720	[893]
<i>tert</i> -Butylcycloheptatrienyl 475 [•]		H2,7 H3,6 H4,5	Neutral -0.491 -0.277 -0.418	[894]
Cyclopropylcycloheptatrienyl 476 [•] /476 ²⁻		H2,7 H3,6 H4,5 H(β)	Neutral/Dianion -0.484/<0.02 -0.242/-0.558 -0.396/-0.278 +0.162/+0.323	[893]

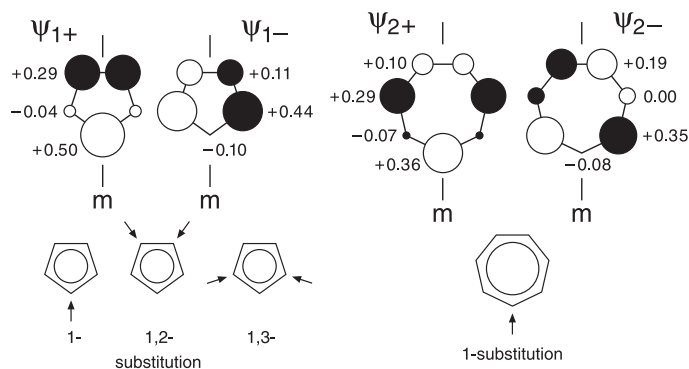


Fig. 8.8. Diagrams of degenerate HOMOs, ψ_{1+} and ψ_{1-} , of the five-membered π perimeter (cyclopentadienyl 50^\bullet) and of degenerate LUMOs, ψ_{2+} and ψ_{2-} , of the seven-membered π perimeter (cycloheptatrienyl 63^\bullet). π -Spin populations as expected for exclusive occupancy of one of these MOs. Positions of substitution as required by symmetry.

established that the weak substituent effect of deuterium is inductive and electron-releasing. Introducing one D atom in the position 1 of 50^\bullet to yield deuteriocyclopentadienyl radical ($50\text{-}d^\bullet$) should thus destabilize ψ_{1+} more strongly than ψ_{1-} (Eq. 8.6 and Figure 8.8). Experimentally, it was found that this deuteration very slightly affects the equivalency of the protons at the remaining positions 2–5. The coupling constant a_{D_1} of -0.089 mT for $50\text{-}d^\bullet$ corresponds to $a_{H_{1-6}}$ of -0.580 mT which is smaller than $a_{H_{1-6}}$ for 50^\bullet , a finding indicating that ψ_{1-} is slightly favored as the SOMO relative to its partner ψ_{1+} ($C_+ < C_-$). As ψ_{1+} and ψ_{1-} are occupied by three electrons, this preference means that the more strongly perturbed ψ_{1+} lies lower than ψ_{1-} (case ④ on p. 216) and, thus, it is at variance with the conclusion that the weak substituent effect of deuterium is inductive and electron-releasing. (case ② on p. 216). The contradiction is interpreted in terms of the dominant effect being here vibrational and not inductive (the amplitude of the out-of-plane vibration of the D atom is reduced relative to that of H atom) [446].

As for the deuteriocycloheptatrienyl radical ($63\text{-}d^\bullet$), perturbation by the D substitution is, within the limits of experimental resolution, not sufficiently large to affect the observed equivalency of the protons at the remaining positions 2–7.

Alkyl substitution in one position clearly removes the degeneracy by distinctly favoring ψ_{1+} as the SOMO in the derivatives of 50^\bullet ($C_+ > C_-$) and ψ_{2-} in those of 63^\bullet ($C_+ < C_-$). These findings are consistent with an inductive and electron-releasing effect of the alkyl substituent (Figure 8.8). With three electrons to be taken up by ψ_{1+} and ψ_{1-} in 50^\bullet and one electron to be accommodated by ψ_{2+} and ψ_{2-} in 63^\bullet , the effect on the energies of ψ_{j+} and ψ_{j-} thus provides examples of cases ② and ①, respectively, presented on p. 216.

The preference for ψ_{1+} in the monoalkyl derivatives of cyclopentadienyl (470^\bullet and 471^\bullet) and for ψ_{2-} in those of cycloheptatrienyl radicals (474^\bullet and 475^\bullet) is more

pronounced for methyl than for *tert*-butyl, an effect that is also observed for the radical anions of the alkyl-substituted benzenes (next section). By means of arguments analogous to those used for monoalkyl derivatives, we can predict that 1,2-dialkyl substitution of $50\cdot$ should also lead to a preferred single occupancy of ψ_{1+} ($C_+ > C_-$), whereas ψ_{1-} must be favored in its 1,3-isomer ($C_+ < C_-$) (Figure 8.8). This prediction is confirmed by the hyperfine data for $472\cdot$ and $473\cdot$ (Table 8.17). The coupling constants are strongly temperature-dependent (the values for $470\cdot$ – $473\cdot$ were observed at 213 K), whereby raising the temperature promotes orbital mixing, i.e., lessens the preference for one MO.

In the radical dianions 474^{2-} and 476^{2-} of monoalkyl derivatives of cycloheptatrienyl, the MO ψ_{2+} is preferred as the SOMO, in contrast to their neutral counterparts $474\cdot$ and $476\cdot$. This preference is another example of case ② on p. 216, because the dianions have two more electrons than the neutral radicals, i.e. ψ_{2+} and ψ_{2-} accommodate three electrons.

The g_e factor of $50\cdot$ and $63\cdot$ and its alkyl derivatives is 2.0026 ± 0.0001 . While alkylcycloheptatrienyls $470\cdot$ – $473\cdot$ were generated by photolysis of the corresponding hydrocarbons or their mercury derivatives, alkylcycloheptatrienyls $474\cdot$ – $476\cdot$ were formed by thermolysis of their dimers. Reaction of the dimers with alkali-metal yielded the radical dianions 474^{2-} and 476^{2-} .

Radical Ions of Deuterio and Alkyl Derivatives of [n]Annulenes

Table 8.18 [145, 228, 560, 563, 598, 776, 895–902] gives hyperfine data for radical ions of some deuterio and alkyl derivatives of benzene (**62**) ($n = 6$) and cyclooctatetraene (**64**) ($n = 8$). Figure 8.9 presents the relevant degenerate MOs ψ_{j+} and ψ_{j-} along with the spin populations $\rho_{\mu}^{\pi}(\psi_{j+})$ and $\rho_{\mu}^{\pi}(\psi_{j-})$. The parameter $Q_{\text{H}}^{C_{\mu}H_{\mu}}$ to be used in the McConnell equation is -2.25 , -2.66 and -2.57 mT for $62^{\cdot-}$, $62^{+\cdot}$, and $64^{\cdot-}$, respectively (Table 4.1).

Radical anions of many alkylbenzenes were among the first organic paramagnetic species to be studied by ESR spectroscopy, and their structures were adequately interpreted from their ^1H -hyperfine data (for an early review see [903]). This interpretation is based on the degenerate LUMOs, ψ_{2+} or ψ_{2-} , of in the six-membered π perimeter (Eq. 8.7 and Figure 8.9). The slightest perturbation, such as deuteration, proves sufficient to remove the degeneracy of these orbitals. Although very weak, the effect of a D/H replacement works in the same direction as does the alkyl substitution, i.e., it is inductive and electron-releasing. Thus, in the radical anions of both deuterio and alkyl derivatives, the MO, ψ_{2+} or ψ_{2-} , that has larger LCAO coefficients at the substituted centers, is more strongly destabilized. Because one electron has to be accommodated in the two MOs of $62^{\cdot-}$, it is an example of case ① on p. 216, with the less destabilized MO being singly occupied. For the mono- and 1,4-deuterated $62\cdot$ and $62\text{-}1,4\text{-}d_2^{\cdot-}$, such favored MO is clearly ψ_{2-} , whereas it is ψ_{2+} for the 1,3-derivative $62\text{-}1,3\text{-}d_2^{\cdot-}$ (Figure 8.9). The preference for ψ_{2-} is only slight ($C_+^2 \approx 0.47$, $C_-^2 \approx 0.53$ for $62\cdot$). In the series, $477^{\cdot-}$ – $484^{\cdot-}$, of the radical anions of monoalkyl-substituted benzenes, this preference becomes

Tab. 8.18. Hyperfine Data for Radical Ions of Some Deuterio and Alkyl Derivatives of Benzene and Cyclooctatetraene

Monodeuteriobenzene $62d^{\cdot-}$		H2,3,5,6 H4 D1	Anion -0.398 -0.345 -0.056	[895]
1-3-Dideuteriobenzene $62-1,3-d_2^{\cdot-}$		H2,5 H4,6 D1,3	Anion -0.419 -0.363 -0.058	[895]
1,4-Dideuteriobenzene $62-1,4-d_2^{\cdot-}$		H2,3,5,6 D1,4	Anion -0.416 -0.051	[895]
Toluene $477^{\cdot-}/477^{\cdot+}$		H2,6 H3,5 H4 3H(β) $^{13}\text{C}(\alpha)$	Anion/Cation -0.515/-0.193 -0.544 -0.051/-0.978 +0.077/+2.034 +0.079	[145, 598]/[896] [776]
Ethylbenzene $478^{\cdot-}/478^{\cdot+}$		H2,6 H3,5 H4 2H(β) 3H(γ)	Anion/Cation -0.499 -0.519 -0.085/-1.2 +0.079/+2.9 +0.002	[145, 598]/[896]
Isopropylbenzene $479^{\cdot-}/479^{\cdot+}$		H2,6 H3,5 H4 H(β) 6H(γ)	Anion/Cation -0.497 -0.508 -0.107/-1.2 +0.051/+2.1 <0.01/0.6	[145, 598]/[896]
<i>tert</i> -Butylbenzene $480^{\cdot-}$		H2,6 H3,5 H4 9H(γ)	Anion -0.467 -0.471 -0.177 <0.05	[145, 598]
Cyclobutylbenzene $481^{\cdot-}$		H2,6 H3,5 H4 H(β)	Anion -0.441 -0.449 -0.202 +0.100	[145]
Cyclopentylbenzene $482^{\cdot-}$		H2,6 H3,5 H4 H(β)	Anion -0.479 -0.495 -0.128 +0.054	[145]

Tab. 8.18 (continued)

Cyclohexylbenzene 483 ⁻		H2,6 H3,5 H4 H(β)	Anion -0.499 -0.517 -0.084 +0.020	[145]
Cycloheptylbenzene 484 ⁻		H2,6 H3,5 H4 H(β)	Anion -0.511 -0.538 -0.065 +0.015	[145]
<i>o</i> -Xylene 485 ⁻ /485 ⁺		H3,6 H4,5 6H(β)	Anion/Cation -0.693 -0.181/-0.544 +0.200/+1.376	[897]/[896]
<i>m</i> -Xylene 486 ⁻ /486 ⁺		H2 H4,6 H5 6H(β)	Anion/Cation -0.685 -0.146/-0.85 -0.772 +0.226/+1.20	[898]/[896]
<i>p</i> -Xylene 487 ⁻ /487 ⁺		H2,3,5,6 6H(β)	Anion/Cation -0.534/-0.373 -0.009/+1.894	[598, 898]/[899]
Durene 488 ⁺		H3,6 12H(β)	/Cation /+0.077 /+1.06	[228]
Deuteriocyclooctatetraene 64-d ⁻		H2,8 H3,7 H4,6 H5 D1	Anion -0.32 -0.32 -0.32 -0.32 -0.05	[900]
Methylcyclooctatetraene 489 ⁻		H2,8 H3,7 H4,6 H5 3H(β)	Anion -0.16 -0.48 -0.16 -0.48 +0.51	[563]
1,2-Dimethylcyclooctatetraene 490 ⁻		H3,8 H4,7 H5,6 6H(β)	Anion -0.295 -0.295 -0.262 +0.349	[901]

Tab. 8.18 (continued)

1,4-Dimethylcyclo-octatetraene 491 ^{·-}		H2,3 H5,8 H6,7 6H(β)	Anion -0.311 -0.311 -0.311 +0.350	[560]
1,5-Dimethylcyclo-octatetraene 492 ^{·-}		H2,4,6,8 H3,7 6H(β)	Anion 0.048 -0.585 +0.627	[560]
1,3,5,7-Tetramethyl-cyclooctatetraene 493 ^{·-}		H2,4,6,8 12H(β) ¹³ C1,3,5,7 ¹³ C2,4,6,8 4 ¹³ C(α)	Anion 0.045 +0.641 +0.937 -0.637 -0.423	[902]

less pronounced in the sequence methyl \approx cycloheptyl ($C_+^2 \approx 0.20$, $C_-^2 \approx 0.80$) > ethyl > cyclohexyl > isopropyl > cyclopentyl > *tert*-butyl > cyclobutyl ($C_+^2 \approx 0.35$, $C_-^2 \approx 0.65$).

Thus on going from methyl to ethyl, isopropyl, and *tert*-butyl as the substituents of radical anions in solution, the preference for ψ_{2-} decreases the larger the alkyl group, but in the corresponding cycloalkyl series it increases with the growing ring size of the cycloalkyl substituent.

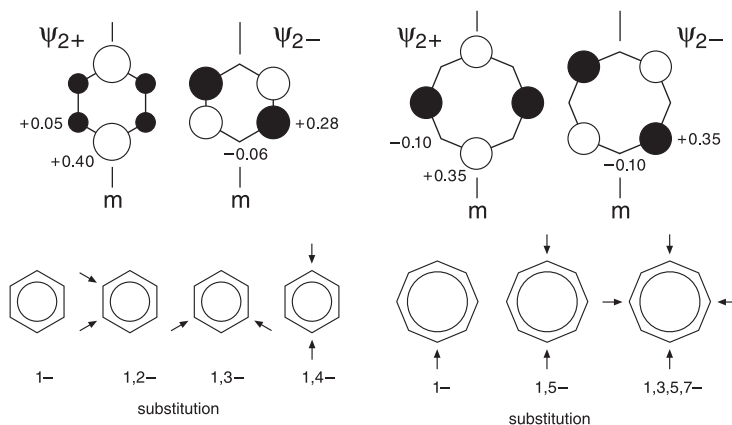


Fig. 8.9. Diagrams of degenerate LUMOs, ψ_{2+} and of ψ_{2-} , of the six-membered π perimeter (benzene **62**) and degenerate NBMOs, ψ_{2+} and ψ_{2-} , of the eight-membered π perimeter (planar cyclooctatetraene **64**). π -Spin populations as expected for exclusive occupancy of one of these MOs. Positions of substitution, as required by symmetry.

The coupling constants for $477^{\cdot-}$ – $484^{\cdot-}$ were observed at 183 K; upon raising the temperature, the share of ψ_{2-} vs ψ_{2+} becomes less dominant. In accordance with expectation (Figure 8.9), the single occupancy of ψ_{2-} is also favored in the 1,4-methyl substituted radical anion $487^{\cdot-}$, but in the 1,2- and 1,3-substituted anions, $485^{\cdot-}$ and $486^{\cdot-}$, ψ_{2+} is preferred as the SOMO.

For the radical cations of alkylbenzenes, the relevant HOMOs, ψ_{1+} and ψ_{1-} , are paired with ψ_{2+} and ψ_{2-} , respectively, so that their squared LCAO coefficients $c_{j,\mu}^2$, which determine the inductive substituent effect on the MO, are equal. Moreover, because the radical cations, with three electrons to be accommodated in ψ_{1+} and ψ_{1-} , represent case ② on p. 216, the preferred SOMO is ψ_{1+} in the radical cation when it is ψ_{2-} in the corresponding anion, and, similarly, ψ_{1-} is favored in the radical cation when ψ_{2+} is the SOMO in the anion. The ^1H -hyperfine data confirm the expected preference for ψ_{1+} in the 1- or 1,4-substituted radical cations, $477^{\cdot+}$ – $479^{\cdot+}$ and $487^{\cdot+}$, and favoring of ψ_{1-} in the 1,2-, 1,3-, or 1,2,4,5-substituted cations, $485^{\cdot+}$, $486^{\cdot+}$, and $488^{\cdot+}$.

The degenerate NBMOs, ψ_{2+} and ψ_{2-} , of planar cyclooctatetraene (Figure 8.9) convert into each other by simple rotation of 45° about the C_8 axis, so that they must be distinguished by the choice of the perpendicular mirror plane defining their symmetry [147]. Because three electrons are accommodated in these MOs, case ② on p. 216 has to be considered.

Within the limits of the resolution achieved, monodeuteration of cyclooctatetraene does not affect the equivalency of the protons in the remaining positions of $64\text{-}d^{\cdot-}$. The favored MO in the radical anions of the alkyl derivatives is ψ_{2+} for the 1-, 1,5-, or 1,3,5,7-substituted anions $489^{\cdot-}$, $492^{\cdot-}$, and $493^{\cdot-}$, whereas no marked preference is exhibited by the 1,2- and 1,4-substituted anions $490^{\cdot-}$ and $491^{\cdot-}$. These findings meet the expectation (Figure 8.9).

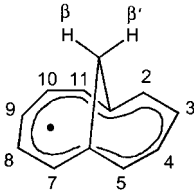
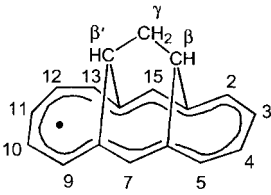
The g_e factor of the radical anions, which were generated in solution from the corresponding deuterio and alkyl substituted benzenes by reaction with an alkali metal and from these derivatives of cyclooctatetraenes mostly by electrolytical reduction, is 2.0027 ± 0.0001 . The g_e factor of the radical cations of alkyl-substituted benzenes, which were formed by γ -irradiation in Freon matrices, is 2.0029 ± 0.0002 . The radical cation, $488^{\cdot+}$, having four IE-lowering methyl substituents, was produced in solution by intense UV-irradiation of the neutral hydrocarbon in conc. sulfuric acid [225] or in $\text{FSO}_3\text{H}\text{-SO}_2$ mixtures [228].

Radicals and Radical Dianions of Bridged [n]Annulenyls

Table 8.19 [67] gives hyperfine data for bridged [11]- and [15]annulenyl radicals and the corresponding radical dianions. Figure 8.10 depicts the relevant degenerate LUMOs ψ_{3+} and ψ_{3-} of the 11-membered π perimeter and those, ψ_{4+} and ψ_{4-} , of the 15-membered π perimeter; the perimeters are drawn in the shapes characteristic of these bridged annulenyls.

Two effects of the bridging on the energies of ψ_{j+} and ψ_{j-} should be taken into account: (1) the already indicated inductive and electron-releasing effect, which destabilizes the MO proportionally to the squared LCAO coefficients at the bridged

Tab. 8.19. Hyperfine Data for Some Bridged [11]- and [15]Annulenyl Radicals and Radical Dianions

1,6-Methano[11]annulenyl 494 [•] /494 ²⁻			Neutral/Dianion	
		H2,5	-0.437/-0.232	[67]/[67]
		H3,4	<0.005/-0.357	
		H7,11	-0.638/+0.235	
		H8,10	+0.205/-0.492	
		H9	-0.764/+0.058	
		H(β)	-0.042/+0.060	
H(β')	-0.021/+0.017			
1,6:8,14-propane-1,3- diylidene[15]annulenyl 495 [•] /495 ²⁻			Neutral/Dianion	
		H2,5	-0.356/-0.234	[67]/[67]
		H3,4	0.025/-0.278	
		H7,15	-0.472/+0.044	
		H9,13	-0.495/-0.169	
		H10,12	+0.252/-0.485	
		H11	-0.609/+0.080	
		H(β)	-0.114/+0.038	
		H(β')	-0.025/<0.01	
2H(γ)	0.025/ 0.034			

centers, and (2) the homoconjugation between these spatially proximate centers, which is proportional to the product of the pertinent LCAO coefficients and acts to stabilize (or destabilize) when the sign of this product is positive (or negative). Clearly, the two effects work in the same direction for the MOs in Figure 8.10,

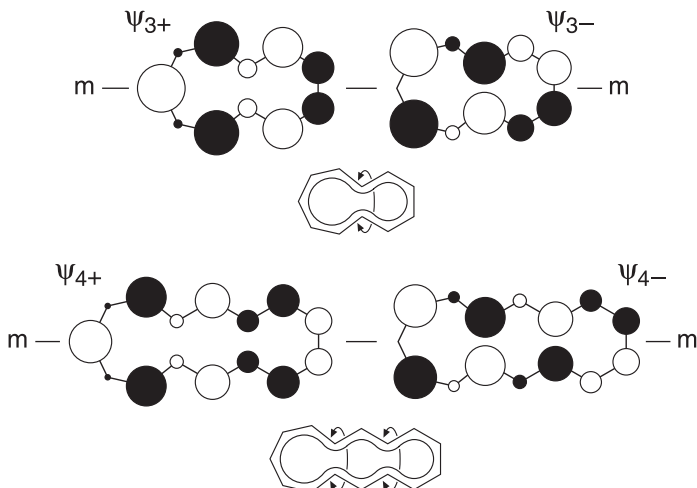


Fig. 8.10. Diagrams of degenerate LUMOs, ψ_{3+} and ψ_{3-} , of the 11-membered π perimeter and, ψ_{4+} and ψ_{4-} , of the 15-membered π perimeter. Shape and bridging of the two perimeters as in 494[•] (top) and 495[•] (bottom), respectively.

because both of them strongly destabilize ψ_{3-} and ψ_{4-} relative to ψ_{3+} and ψ_{4+} , respectively (large coefficients of different sign for ψ_{j-} vs small coefficients of the same sign for ψ_{j+} at the bridged centers). Because the two MOs have to accommodate one electron in the neutral radicals (case ① on p. 216) and three electrons in the corresponding radical dianions (case ② in that scheme), the lower-lying ψ_{3+} and ψ_{4+} should be favored in **494** \cdot and **495** \cdot , but the higher ψ_{3-} and ψ_{4-} should be preferred in **494** $^{2-}$ and **495** $^{2-}$. This prediction is in accordance with the observed ^1H -hyperfine data. The ESR spectra of the radical dianions exhibit resolved splitting from an alkali-metal nucleus of only one counterion. The two counterions are thus nonequivalent, being presumably situated above and below the bridging group (Table A.2.3).

The g_e factors pertinent to the two bridged [n]annulenylys and their radical dianions were not reported. The radicals were prepared by thermal homolysis of the dimers and by reduction of the cations with zinc. The radical dianions were produced with alkali-metal from various precursors, such as the above-mentioned dimers and cations, and also from the corresponding hydrocarbons.

Radical Ions of Bridged [n]Annulenes

Table 8.20 [144, 148–150, 210, 233, 457, 463] lists hyperfine data for radical ions of some bridged [10]- and [14]annulenes in which the neutral perimeter has a number of π electrons that conforms with Hückel rule. The LUMOs, ψ_{3+} and ψ_{3-} of the 10-membered π perimeter and ψ_{4+} and ψ_{4-} of the 14-membered one, relevant to the single occupancy in the radical anions, are illustrated in Figures 8.11 and 8.12. The perimeters are drawn in a naphthalene-, azulene-, anthracene-, or pyrene-like shape characteristic of the appropriate bridged annulene. The radical anions of the methano[10]annulenes **85** and **496** are iso- π -electronic with the [11]annulenyl radical **494** \cdot , and those of the bridged [14]annulenes **76**, **97**, and **497–500** are analogously related to the [15]annulenyl **495** \cdot , dealt with in the preceding section. For interpretation of the π -spin distribution in **85** $^{\cdot-}$ and **496** $^{\cdot-}$, as well as in **97** $^{\cdot-}$ and **497** $^{\cdot-}$ –**499** $^{\cdot-}$, it is sufficient to take account of the inductive and electron-releasing effect of the bridging group and the homoconjugation between the spatially proximate bridged centers. Similar to **494** \cdot and **495** \cdot , in five of these six radical anions, both effects work in the same direction by strongly destabilizing ψ_{3+} relative to ψ_{3-} in **85** $^{\cdot-}$ with a naphthalene-like perimeter (large LCAO coefficients of opposite sign at the bridged centers for ψ_{3+} vs vanishing ones for ψ_{3-} ; Figure 8.11, top) and also by strongly destabilizing ψ_{4-} relative to ψ_{4+} in **97** $^{\cdot-}$ and **497** $^{\cdot-}$ –**499** $^{\cdot-}$ with an anthracene-like perimeter (small coefficients of the same sign at the bridged centers for ψ_{4+} vs large ones of opposite sign for ψ_{4-} ; Figure 8.12, top). Only in **496** $^{\cdot-}$ with an azulene-like perimeter do the two effects work in opposite directions (large LCAO coefficients of the same sign for ψ_{3+} vs smaller ones of opposite sign for ψ_{3-} ; Figure 8.11, bottom). Here, homoconjugation overrides the inductive electron-releasing effect by stabilizing ψ_{3+} and destabilizing ψ_{3-} . Thus, with one electron to be accommodated in the two LUMOs (case ① on

Tab. 8.20. Hyperfine Data for Radical Ions of Some Bridged [10]- and [14]Annulenes

1,6-Methano[10]annulene 85 ⁻		H2,5,7,10 H3,4,8,9 2H(β)	Anion -0.270 -0.010 -0.115	[149]
1,5-Methano[10]annulene (homoazulene) 496 ⁻		H2,4 H3 H6,10 H7,9 H8 H _{exo} (β) H _{endo} (β)	Anion +0.091 -0.432 -0.367 +0.328 -0.685 +1.342 0.045	[144]
<i>syn</i> -1,6:8,13-Bismethano- [14]annulene 497 ⁻		H2,5,9,12 H3,4,10,11 H7,14 2H _{exo} (β) 2H _{endo} (γ)	Anion -0.239 -0.026 -0.281 -0.102 0.048	[150]
1,6:8,13-Propane-1,3- diylidene[14]annulene 498 ⁻ /498 ⁺		H2,5,9,12 H3,4,10,11 H7,14 2H(β) 2H(γ)	Anion/Cation -0.280/-0.325 -0.010/-0.058 -0.341/-0.457 -0.088/-0.140 <0.008/0.140	[150, 210]/ [233]
1,6:8,13-Ethane-1,3- diylidene[14]annulene 97 ⁻ /97 ⁺		H2,5,9,12 H3,4,10,11 H7,14 2H(β)	Anion/Cation -0.323/+0.014 -0.040/-0.248 -0.446/+0.092 -0.265/+2.815	[150/210] [233]
1,6:8,13-Cyclopropane- 1,3-diylidene[14]- annulene 499 ⁻		H2,5,9,12 H3,4,10,11 H7,14 2H(γ)	Anion -0.321 -0.078 -0.461 0.028	[150, 210]
<i>trans</i> -10b,10c- Dihydroxyrene 500 ⁻ /500 ⁺		H1,3,6,8 H2,7 H4,5,9,10 2H(β)	Anion +0.051 -0.548 -0.086 +1.910	[457]
<i>trans</i> -10b,10c-Dimethyl- 10b,10c-dihydroxyrene 76 ⁻ /76 ⁺		H1,3,6,8 H2,7 H4,5,9,10 6H(γ) ¹³ C(β)	Anion/Cation +0.078/+0.103 -0.546/-0.478 -0.078/-0.150 0.020/0.009 +1.34	[148]/ [148] [463]

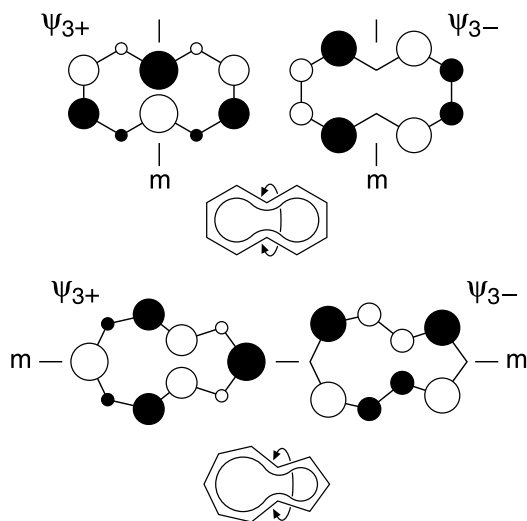


Fig. 8.11. Diagrams of degenerate LUMOs, ψ_{3+} and ψ_{3-} , of the 10-membered π perimeter. Shape and bridging of the perimeter as in **85** (top) and **496** (bottom).

p. 216), the MO that is favored as the SOMO is ψ_{3-} in **85**^{•−}, ψ_{3+} in **496**^{•−}, and ψ_{4+} in **97**^{•−} and **497**^{•−}–**499**^{•−}.

The radical anion of 1,6-methano[10]annulene (**85**) was presented in Chapt. 8.4 as an example of a paramagnetic species with a cyclic conjugation despite the considerable deviation of the π perimeter from planarity. Although the π -spin distribution is not markedly affected by this deviation, the nonplanarity causes a large decrease in the $|a_{H_\mu}|$ values of the α protons attached to the perimeter. These coupling constants are strongly temperature-dependent, in line with the expected diminishing preference for ψ_{3-} upon warming ($a_{H_{2,5,7,10}} = -0.278$ and -0.240 mT and $a_{H_{3,4,8,9}} = -0.006$ and -0.024 mT at 163 and 313 K, respectively) [147].

The deviation of the π perimeter from planarity in the radical anion of 1,5-methano[10]annulene (**496**) is at least as great as in the isomeric **85**^{•−}, but it has less impact on the coupling constants of the α protons because of the completely different π -spin distribution. The $a_{H_\mu}(\alpha)$ values for **496**^{•−} resemble those for the radical anion of azulene (**112**) (Table 8.14), which justifies the designation of the former as the radical anion of homoazulene. The largest difference is observed in the coupling constants $a_{H_{7,9}}$ for **496**^{•−} relative to the corresponding $a_{H_{5,7}}$ value for **112**^{•−}. These coupling constants are positive and, in contrast to those with a negative sign, their absolute values increase due to the likewise positive contributions by the nonplanarity.

Deviations from planarity are less pronounced for the larger π perimeters in bridged [14]annulenes. For those with an anthracene-like perimeter, a decrease in these deviations is indicated by the sums $\sum |a_{H_\mu}|$ of the α protons in the radical anions **497**^{•−}, **498**^{•−}, **97**^{•−}, and **499**^{•−}, which increase in this order from 1.62 to 1.84, 2.34, and 2.52 mT.

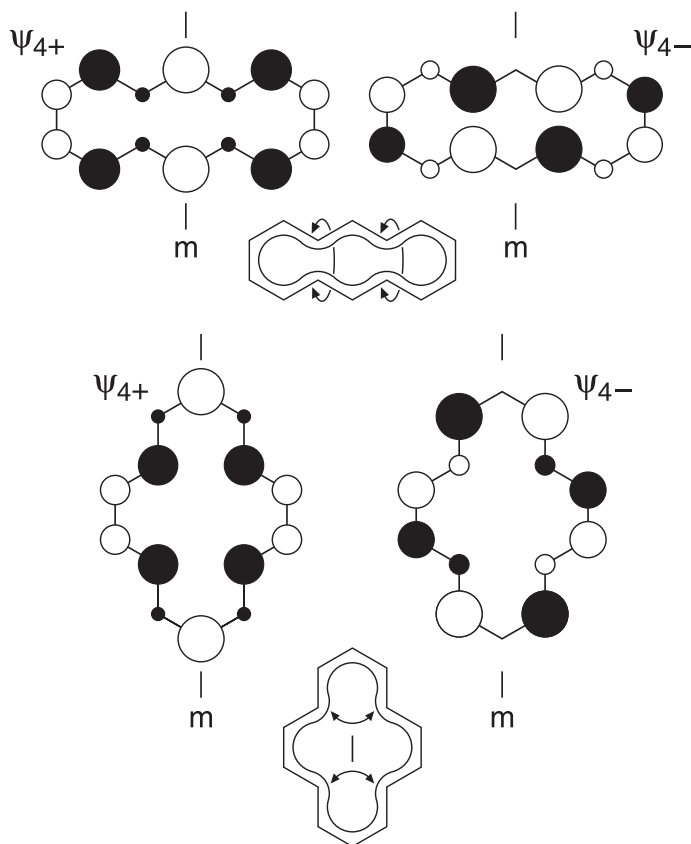


Fig. 8.12. Diagrams of degenerate LUMOs, ψ_{4+} and ψ_{4-} , of the 14-membered π perimeter. Shape and bridging of the perimeter as in **97** and **497–499** (top) and as in **76** and **500** (bottom).

In addition to the radical anions **97**^{•−} and **498**^{•−} dealt with above, the corresponding radical cations **97**^{•+} and **498**^{•+} were studied by ESR spectroscopy. The HOMOs, ψ_{3+} and ψ_{3-} , relevant to these radical cations, are paired with the LUMOs, ψ_{4+} and ψ_{4-} , respectively (Figure 8.12, top), which means that $c_{3+, \mu^*} = c_{4+, \mu^*}$ and $c_{3-, \mu^*} = c_{4-, \mu^*}$, but $c_{3+, \mu^o} = -c_{4+, \mu^o}$ and $c_{3-, \mu^o} = -c_{4-, \mu^o}$. Because $c_{3+, \mu}^2 = c_{4+, \mu}^2$ and $c_{3-, \mu}^2 = c_{4-, \mu}^2$ for all centers μ , the inductive and electron-releasing effect of the bridging group is the same for the HOMOs as for the LUMOs, thus destabilizing ψ_{3-} relative to ψ_{3+} . In contrast, the coefficients at the bridged centers in **97** and **498** have the same sign for the HOMOs ψ_{3+} and ψ_{3-} when they are of opposite sign for the LUMOs ψ_{4+} and ψ_{4-} and vice versa, so that the homoconjugation now stabilizes ψ_{3-} relative to ψ_{3+} . The two effects thus work in opposite directions, and the observed coupling constants indicate a switch in the energetic sequence of the orbitals on going from **498**^{•+} to **97**^{•+}. Whereas ψ_{3+} is

avored as the SOMO in 498^+ , ψ_{3-} is given preference in 97^+ . With three electrons to be accommodated by ψ_{3+} and ψ_{3-} (case ② on p. 216), this finding means that the inductive and electron-releasing effect is dominant in 97^+ , but that homoconjugation prevails in 498^+ . This conclusion is at variance with that drawn previously [233].

In the radical anions 500^- and 76^- with a pyrene-like perimeter, the inductive electron-releasing effect of the bridging alkylidene group destabilizes the LUMO ψ_{4+} relative to ψ_{4-} (Figure 8.12, bottom), and an equivalent statement holds for the HOMO ψ_{3+} relative to ψ_{3-} in the corresponding radical cations, because the LUMOs and HOMOs are again paired. Homoconjugation between the bridged centers is less important, in view of the rather large distance between them. Consequently, ψ_{4-} should be favored as the SOMO in the radical anions (case ① on p. 216), and ψ_{3+} should be preferred as such MO in the radical cations (case ② in that scheme).

Although these predictions are confirmed by the coupling constants for the radical cation 76^+ , they are at variance with experiment for the radical anions 500^- and 76^- , in which the SOMO resembles ψ_{4+} and not ψ_{4-} . Hyperconjugation of the two σ bonds C–H(β) and C(β)–CH₃ in the bridging groups of **500** and **76**, respectively, with the MOs of the 14-membered π perimeter has been suggested to account for this discrepancy. The pertinent bonds are almost perpendicular to the mean plane of the perimeter, and their bonding σ - and antibonding σ^* -MOs have the proper geometry and symmetry for effective hyperconjugation with the HOMO ψ_{3+} and the LUMO ψ_{4+} , respectively. Whereas such hyperconjugation should raise the energy of ψ_{3+} in 76^+ , and thus work in the same direction as the inductive effect, it is expected to lower the energy of ψ_{4+} . This stabilization can override the inductive effect and lead to the preference of ψ_{4+} over ψ_{4-} as the SOMO in 500^- and 76^- .

The effective hyperconjugation in 500^- is manifested by the large positive coupling constant of the two β protons in the bridging group (+1.910 mT). This value, as well as those of the two β protons in the bridging group of 97^+ (+2.815 mT) (Chapt. 4.2) and of one β proton in such a group of 496^- (+1.342 mT), are unusual for π radicals of that size. They represent another example of the “Whiffen effect”, because the bridged centers have LCAO coefficients of the same sign, and the relevant dihedral angles θ are small (ca 17° in **500**, 10° in **97**, and 40° in **496**).

The g_e factors of the radical ions of the bridged [10]- and [14]annulenes are in the ranges 2.0027–2.0030 for the anions and 2.0022–2.0027 for the cations. All the radical anions were generated by reaction of the neutral compounds with an alkali-metal in an ethereal solution or by their electrolysis in DMF, but special conditions had to be used for 496^- which, on prolonged reduction, easily converts to 361^{2-} and 362^{2-} , the radical dianions of bicyclo[6.3.0]undecapentaenyl and benzotropyyl (Table 8.5). Special precautions (method of solvated electrons) had to be used also for 500^- , because of its facile loss of the H atoms in the bridging group and conversion to the radical anion of pyrene (**387**) (Table 8.8). The radical cations were produced by dissolution of the neutral compounds in conc. sulfuric acid or by

their oxidation with AlCl_3 in dichloromethane. When generated by the latter method at 193 K, $76^{\cdot+}$ converts at 223 K (with loss of two H atoms) to a mixture of the radical cations of 1,6- and 1,8-dimethylpyrenes, which disproportionate to those of 1,3,6,8-tetramethylpyrene and less-substituted pyrenes [904].

Radical Ions of Tetradehydro[n]annulenes

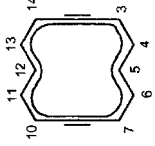
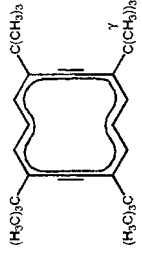
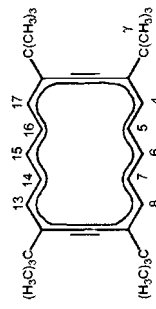
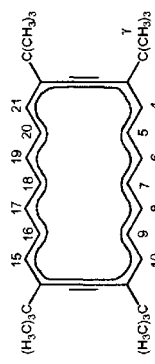
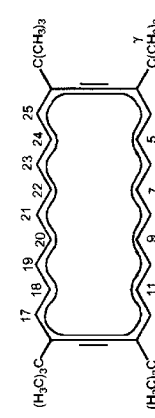
Table 8.21 [151, 905, 906] lists hyperfine data for radical ions of some tetradehydro[14]-, [18]-, [22]-, and [26]annulenes, in which the number of π electrons in the neutral perimeters conforms with Hückel rule. The perimeter LUMOs, ψ_{j+} and ψ_{j-} ($j = 4, 5, 6$, and 7 for $n = 14, 18, 22$, and 26 , respectively), relevant to the single occupancy in the radical anions, are depicted in Figure 8.13. The perturbation of the perimeter MOs by the *tert*-butyl substituents can be disregarded in comparison with the effect of the two triple bonds, a statement which is supported by the coupling constants of the ring α protons, which are very similar for $501^{\cdot-}$ and its *tetra-tert*-butyl-substituted derivative $502^{\cdot-}$. The introduction of triple bonds (μ and ν in Figure 8.13) is stabilizing when the LCAO coefficients at the two pertinent centers have the same sign and destabilizing when these signs are opposite. Thus, the direction of the effect alternates on going from $n = 14$ to 26 . For $501^{\cdot-}$ and $502^{\cdot-}$ ($n = 14$) and $504^{\cdot-}$ ($n = 22$), the two triple bonds stabilize the LUMO ψ_{j+} and destabilize ψ_{j-} , whereas the opposite statement holds for $503^{\cdot-}$ ($n = 18$) and $505^{\cdot-}$ ($n = 26$). With one electron to be taken up by ψ_{j+} and ψ_{j-} in the radical anions, the lower-lying MO is favored as the SOMO, namely, ψ_{4+} in $501^{\cdot-}$ and $502^{\cdot-}$, ψ_{5-} in $503^{\cdot-}$, ψ_{6+} in $504^{\cdot-}$, and ψ_{7-} in $505^{\cdot-}$.

Due to the pairing properties of even-membered π perimeters, the coefficients at the neighboring centers μ and ν in the HOMOs ψ_{j+} and ψ_{j-} ($j = 3, 4, 5$, and 6 for $n = 14, 18, 22$, and 26 , respectively) have absolute values equal to those at such centers in the corresponding LUMOs, but their signs are opposite for the HOMOs when they are the same for the LUMOs, and vice versa. As a result, the triple bonds destabilize the HOMO ψ_{j+} and stabilize ψ_{j-} for $n = 14$ and 22 but have the opposite effect for $n = 18$ and 26 . Nevertheless, because the HOMOs ψ_{j+} and ψ_{j-} in the radical cations accommodate three electrons, the lower-lying MO is now doubly occupied and the higher MO is the SOMO. Consequently, in the radical anion and the radical cation of a given tetradehydro[n]annulene, the SOMOs have the same symmetry with respect to the relevant mirror plane. In fact, the similar coupling constants for the two corresponding radical ions, $502^{\cdot-}/502^{\cdot+}$, $503^{\cdot-}/503^{\cdot+}$, and $504^{\cdot-}/504^{\cdot+}$, reflect the apparent pairing properties of alternant π systems.

In the radical trianions, $503^{\cdot 3-}$ and $504^{\cdot 3-}$, the lower-lying LUMO, which is the SOMO of the corresponding radical anions, is filled, and its less stable partner becomes singly occupied. This MO thus has a symmetry opposite to that of the SOMO of the monoanion, i.e., it is ψ_{5+} for $503^{\cdot 3-}$ and ψ_{6-} for $504^{\cdot 3-}$, as confirmed by the observed coupling constants.

The g_e factors of the radical ions of the annulenes **501**–**505** were not reported. Their radical anions and trianions were produced by reaction of the neutral compound with an alkali-metal in an ethereal solvent (short contact time for the anions

Tab. 8.21. Hyperfine Data for Radical Ions of Some Tetrahydro[4], [18], [22]- and [26]Annulenes

1,2,8,9-Tetrahydro[14]-annulene 501⁻		H3,7,10,14 H4,6,11,13 H5,12	Anion -0.454 +0.115 -0.515	[905]
3,7,10,14-Tetra- <i>tert</i> -butyl-1,2,8,9-tetrahydro[14]annulene 502⁻/502⁺		H4,6,11,13 H5,12 36H(γ)	Anion/Cation +0.108/+0.106 -0.514/-0.462 <0.01/0.019	[906]/[151]
3,9,12,18-Tetra- <i>tert</i> -butyl-1,2,10,11-tetrahydro[18]-annulene 503⁻/503⁺/503³⁻		H4,8,13,17 H5,7,14,16 H6,15 36H(γ)	Anion/Cation/Trianium +0.087/+0.086/-0.325 -0.402/-0.394/+0.120 +0.135/+0.129/-0.334 <0.01/0.018/<0.01	[906]/[151]/[151]
3,11,14,22-Tetra- <i>tert</i> -butyl-1,2,12,13-tetrahydro[22]-annulene 504⁻/504⁺/504³⁻		H4,10,15,21 H5,9,16,20 H6,8,17,19 H7,18 36H(γ)	Anion/Cation/Trianium +0.064/+0.069/-0.250 -0.337/-0.328/+0.057 +0.124/+0.123/-0.287 -0.399/-0.364/+0.093 <0.01/0.016/<0.01	[906]/[151]/[151]
3,13,16,26-Tetra- <i>tert</i> -butyl-1,2,14,15-tetrahydro[26]-annulene 505⁻		H4,12,17,25 H5,11,18,24 H6,10,19,23 H7,9,20,22 H8,21 36H(γ)	Anion +0.061 -0.285 +0.114 -0.310 +0.122 <0.01	[906]

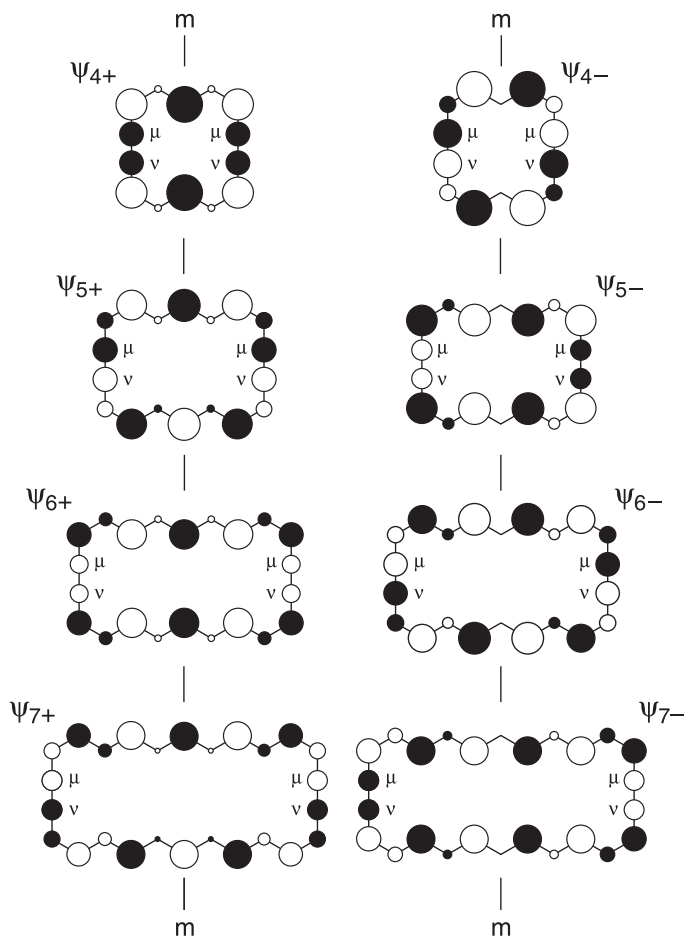


Fig. 8.13. Diagrams of degenerate LUMOs, ψ_{j+} and of ψ_{j-} , of the 14-, 18-, 22-, and 26-membered π perimeters ($j = 4, 5, 6$, and 7, respectively). Shapes of the perimeters as in the tetrahydro[n]annulenes **501–505**. The triply bonded centers are denoted μ and ν .

and prolonged contact for the trianions), and the radical cations were generated from these compounds with AlCl_3 in dichloromethane.

8.7

Radical Ions of Phanes

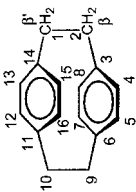
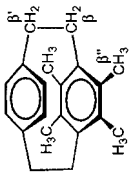
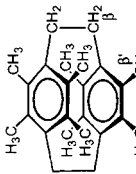
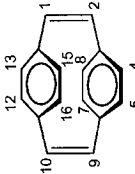
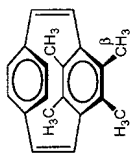
“Phanes” here means organic compounds containing two π moieties that are constrained to be close to each other by short linking chains of methylene or methine groups. Cyclophanes and arenophanes usually denote compounds in which the

two moieties are benzene rings and larger π systems, respectively. A review published in 1983 describes ESR studies on the radical ions of phanes carried out up to that date [621].

Table 8.22 [152, 154–156, 241, 270, 642, 907–909] lists hyperfine data for radical ions of some cyclophanes. The status of [2.2]paracyclophane (**118**) among the phanes is comparable to that of benzene among the aromatic compounds. As mentioned in Chapt. 6.6, the two benzene π moieties of **118** rigidly face each other at a distance of 300 pm, so that this molecule is an ideal system for probing the electron interaction. It is therefore not surprising that the first study of the radical anion $\mathbf{118}^{\cdot-}$ dates to the early decade of ESR spectroscopy [910]. No detailed analysis of the spectrum was reported in that study and following attempts to unravel the hyperfine pattern led to an erroneous interpretation [911]. The reason for this difficulty is the association of $\mathbf{118}^{\cdot-}$ with its alkali-metal counterion, considered in Chapt. 6.6. Although [2.2]paracyclophane accepts an extra electron more easily than benzene (reduction potential -3.0 vs -3.4 V) [912], its conversion to the radical anion likewise requires a strong reducing agent, like potassium. Tighter ion pairing of $\mathbf{118}^{\cdot-}$ with K^+ complicates the ESR spectrum by adding a hyperfine splitting (0.012 mT) from the alkali-metal nucleus of the counterion and, in particular, by lowering the symmetry from D_{2h} to C_{2v} , as a consequence of an apparent π -spin localization on one benzene moiety. The ESR spectra of $\mathbf{118}^{\cdot-}$ that is loosely or more tightly paired with K^+ are presented in Figure 6.23. Spin localization on one benzene moiety becomes more pronounced with decreasing cation-solvating power of the solvent in the order DME/HMPT (1.0) > DME (1.8) > THF (2.0) > MTHF (2.2), where the numbers in parentheses indicate the ratios of the coupling constants of the α protons at the two benzene moieties [621]. The structure of the ion pairs $\mathbf{118}^{\cdot-}/\text{K}^+$, in which the cation is situated on a C_2 axis above or below one benzene ring [622], is also presented in Chapt. 6.6. ESR spectra, which exhibit spin localization or delocalization, were likewise observed for radical anions of other cyclophanes structurally related to **118**, such as 1,2:9,10-dibenzo[2.2]paracyclophane-1,9-diene (**509**) and [2.2.2.2] (1,2,4,5)cyclophane (**511**).

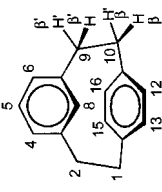
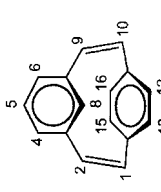
Radical anions of two additional cyclophanes, those of [2.2]paracyclophane-1,9-diene (**131**) and [2.2]metaparacyclophane (**95**), are dealt with in Chaps. 6.7 and 6.5, respectively. The radical anion $\mathbf{131}^{\cdot-}$ served as an example of a time-dependent exchange between two sets of protons with coupling constants of different sign (± 0.046 and ± 0.20 mT), and the ESR spectrum of $\mathbf{95}^{\cdot-}$ was used to demonstrate how a complex and only-partly-resolved hyperfine pattern can be analyzed by means of specific deuteration and the ENDOR technique. Note that the data for $\mathbf{95}^{\cdot-}$ and the radical anion of its 1,9-diene (**513**) indicate that the conformational flipping of the *meta*-bridged ring is slow on the hyperfine time-scale, at least at the low temperatures used for the ESR studies. The SOMO in $\mathbf{118}^{\cdot-}$ and its 1,2:9,10-dibenzo derivative $\mathbf{509}^{\cdot-}$ can be considered a combination of the LUMOs ψ_{2-} of the two benzene rings, whereas in $\mathbf{511}^{\cdot-}$ the relevant MO may be regarded as a combination of their partners ψ_{2+} (Figure 8.9). For the SOMO in $\mathbf{131}^{\cdot-}$, the LUMOs ψ_{2+} of the two benzene rings are assumed to interact with those of two ethene π systems.

Tab. 8.22. Hyperfine Data for Radical Ions of Some Para- and Metapara[2.2]cyclophanes (deloc. = delocalized; local. = localized)

		Anion deloc.	Anion local.		
[2.2]Paracyclophane 118 ⁻		-0.297	-0.379	H4,5,7,8 H12,13,15,16	[152]
		+0.103	+0.125	4H(β) 4H(β')	
			+0.070		
4,5,7,8-Tetramethyl- [2.2]paracyclophane 506 ⁻ / 506 ⁺		Anion			/Dim.Cat. ^a
		-0.295		H12,13,15,16	/2 \times 0.035 [241]/
		+0.015		4H(β)	/2 \times +0.168 [270]
		+0.168		4H(β')	/2 \times 0.018
		+0.099		12H(β'')	/2 \times +0.223
4,5,7,8,12,13,15,16- Octamethyl[2.2]- paracyclophane 507 ⁺					/Cation
				8H(β)	/+0.008 [907]
				24H(β')	/+0.435
				¹³ C4,5,7,8,12,13,15,16	/+0.328
				¹³ C3,6,11,14	/-0.128
[2.2]Paracyclophane-1,9- diene 131 ⁻		Anion			
		-0.422		H1,2,9,10	[642]
		\pm 0.046		H4,7,13,16	
		\mp 0.020		H5,8,12,15	
4,5,7,8-Tetramethyl[2.2]- paracyclophane-1,9- diene 508 ⁻		Anion			
		-0.560		H1,10	[642]
		-0.325		H2,9	
		<0.02		H12,13,15,16	
		<0.02		12H(β)	

1,2:9,10-Dibenzo[2.2]-paracyclophane-1,9-diene 509 ⁻		Anion /Anion deloc. local. $\left. \begin{array}{l} -0.158 \\ -0.120 \end{array} \right\} \begin{array}{l} \text{H4,9} \\ \text{H1,12} \end{array}$ $\left. \begin{array}{l} -0.094 \\ -0.077 \end{array} \right\} \begin{array}{l} \text{H3,10} \\ \text{H2,11} \end{array}$ $\left. \begin{array}{l} -0.018 \\ -0.324 \\ -0.235 \end{array} \right\} \begin{array}{l} \text{H5-8} \\ \text{H13-16} \end{array}$	[154]
4',4'',5',5''-Tetraphenyl-1,2,9,10-dibenzo[2.2]-paracyclophane-1,9-diene 510 ^{•-} / 510 ³⁻		Anion /Trianion $\left. \begin{array}{l} +0.042 \\ 0.005 \\ -0.076 \\ +0.023 \\ -0.126 \end{array} \right\} \begin{array}{l} \text{H1,4,9,12} \\ \text{H5-8,13-16} \\ 8\text{H}_o \\ 8\text{H}_m \\ 4\text{H}_p \end{array}$	[156]
[2.2.2.2](1,2,4,5)Cyclophane 511 ⁻		Anion /Anion deloc. local. $\left. \begin{array}{l} -0.598 \\ -0.409 \end{array} \right\} \begin{array}{l} \text{H3,6} \\ \text{H11,14} \end{array}$ $\left. \begin{array}{l} -0.259 \\ -0.213 \end{array} \right\} \begin{array}{l} 4\text{H}_{\text{exo}}(\beta) \\ 4\text{H}_{\text{exo}}(\beta') \end{array}$ $\left. \begin{array}{l} +0.038 \\ +0.033 \end{array} \right\} \begin{array}{l} 4\text{H}_{\text{endo}}(\beta) \\ 4\text{H}_{\text{endo}}(\beta') \end{array}$	[908]
[3.3]Paracyclophane 512 ⁻		Anion $\left. \begin{array}{l} -0.395 \\ -0.188 \\ +0.575 \\ +0.192 \end{array} \right\} \begin{array}{l} \text{H5,6,14,15} \\ \text{H8,9,17,18} \\ 4\text{H}_{\text{ax}}(\beta) \\ 4\text{H}_{\text{eq}}(\beta) \end{array}$	[152]

Tab. 8.22 (continued)

[2.2]Metaparacyclophane 95 ⁻		[155]
	Anion H4,6 0.007 H5 -0.036 H8 -0.044 H12,13 +0.106 H15,16 +0.131 2H(β) +0.268 2H'(β) +0.182 2H(β') -0.065 2H'(β') +0.065	
[2.2]Metaparacyclophane- 1,9-diene 513 ⁻		[909]
	Anion H2,9 +0.270 H1,10 -0.498 H4,6 +0.032 H5 0.015 H8 +0.301 H12,13 -0.316 H15,16 -0.087	

^a Dimeric cation

Alkyl substitution of the benzene rings in [2.2]paracyclophane, although making the compound harder to reduce, facilitates its oxidation. Thus, heavily substituted [2.2]paracyclophanes, such as the 4,5,7,8,12,13,15,16-octamethyl derivative (**507**), yield radical cations. The coupling constants of the methyl β protons in **507**⁺ are comparable to half the values of such protons in the radical cation of durene (**488**) (Table 8.8), with the benzene-HOMO ψ_{1-} being preferred as the SOMO.

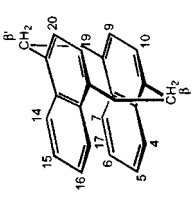
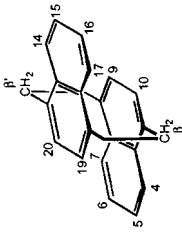
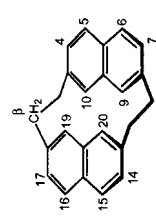
Owing to extension of the π system by tetraphenyl substitution in the lateral benzene rings, the derivative **510** of 1,2:9,10-dibenzo[2.2]paracyclophane-1,9-diene takes up more than one additional electron. Thus, prolonged contact of this compound with potassium yields, consecutively, the radical anion **510**^{•-}, the triplet dianion **510**^{••2-} (Chapt 11.3 and Table 11.7), and the radical trianion **510**^{•3-}. Whereas in **510**^{•-} and **510**^{••2-}, the π -spin population resides mainly on the two lateral *o*-terphenyl moieties, the bulk of this population in **510**^{•3-} is accommodated by the central [2.2]paracyclophane segment. This conclusion is drawn by comparison of the hyperfine data for **510**^{•-} and **510**^{•3-} with those for the radical anions of *o*-terphenyl (**407**) (Table 8.11) and dibenzo[2.2]paracyclophane-1,9-diene (**509**), respectively, and is in line with the reduction potentials of these constituent parts of **510**.

Splitting of the set of eight α protons at the two benzene rings into two sets of four in the radical anion, **512**^{•-}, of [3.3]paracyclophane is not due to ion pairing but to the flexibility of the longer trimethylene bridging group, which leads to a conformation of lower symmetry.

Table 8.23 [142, 153, 229, 623, 913–916] gives hyperfine data for radical ions of some arenophanes. Again, close association of the radical anion with its alkali-metal counterion is manifested by a lowering in the symmetry, as a consequence of the π -spin population being localized in one π moiety. However, replacement of two benzene rings in [2.2]paracyclophane by larger benzenoid π moieties like naphthalene, anthracene, and pyrene diminishes the tendency for such localization. Thus, unlike **118**^{•-}, the radical anions of the isomeric [2.2](1,4)naphthalenophanes (**119**) form tighter ion pairs with K⁺ counterions only in MTHF but not in DME and THF, and the corresponding ion pairs of the radical anion of [2.2](9,10)anthracenophane (**519**) are loose in all three solvents. Association of the radical anion with the alkali-metal cation is much tighter when the two π moieties are nonalternant and more polarizable than their alternant benzenoid counterparts (Chapt. 6.6). Accordingly, the three radical anions of azulenophanes, **521**^{•-} and *syn*- and *anti*-**522**^{•-}, all exhibit spin localization in one π moiety, as expected for tighter ion pairs. In both tight and loose ion pairs, the ¹H-hyperfine data for the radical anions of [2.2]arenophanes reflect the π -spin distribution in the radical anions of the respective arenes (Tables 8.8, 8.9, and 8.15). Analogously, the data for the radical anion of [2.2](2,7)naphthalenophane-1,11-diene (**516**) bear some resemblance to those for the radical anion of 1,2-di(2-naphthyl)ethene (**426**) (Table 8.12).

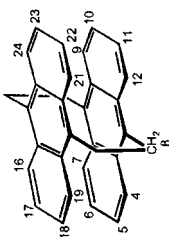
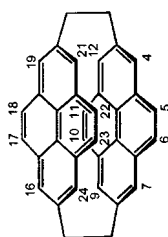
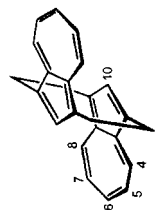
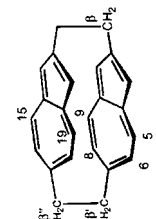
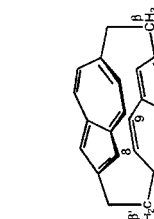
The coupling constants of the α protons at the π moieties in **519**^{•+} are close to the corresponding values for the dimeric cation, **68**₂^{•+}, of anthracene (Table 8.8). This finding supports a structure of these dimers in which the two anthracene π systems eclipse each other, as they do in **519**^{•+}. Introduction of the four methyl

Tab. 8.23. Hyperfine Data for Radical Ions of Some Arenophanes (deloc. = delocalized; local. = localized)

Radical Ion	Structure	Hyperfine Data																																											
[2,2]-(1,4)Naphthalenophane <i>syn</i> -119 ⁻		<table border="0"> <tr> <td>Anion deloc.</td> <td>-0.242</td> <td></td> <td></td> </tr> <tr> <td>Anion local.</td> <td>{ -0.364</td> <td>H4,7</td> <td rowspan="2">[142, 623]</td> </tr> <tr> <td></td> <td>{ -0.106</td> <td>H14,17</td> </tr> <tr> <td></td> <td>{ -0.191</td> <td>H5,6</td> <td></td> </tr> <tr> <td></td> <td>{ -0.060</td> <td>H15,16</td> <td></td> </tr> <tr> <td></td> <td>{ -0.143</td> <td>H9,10</td> <td></td> </tr> <tr> <td></td> <td>{ -0.055</td> <td>H19,20</td> <td></td> </tr> <tr> <td></td> <td>{ +0.232</td> <td>2H(β)</td> <td></td> </tr> <tr> <td></td> <td>{ +0.090</td> <td>2H(β')</td> <td></td> </tr> <tr> <td></td> <td>{ +0.050</td> <td>2H(β)</td> <td></td> </tr> <tr> <td></td> <td>{ +0.016</td> <td>2H(β')</td> <td></td> </tr> </table>	Anion deloc.	-0.242			Anion local.	{ -0.364	H4,7	[142, 623]		{ -0.106	H14,17		{ -0.191	H5,6			{ -0.060	H15,16			{ -0.143	H9,10			{ -0.055	H19,20			{ +0.232	2H(β)			{ +0.090	2H(β')			{ +0.050	2H(β)			{ +0.016	2H(β')	
Anion deloc.	-0.242																																												
Anion local.	{ -0.364	H4,7	[142, 623]																																										
	{ -0.106	H14,17																																											
	{ -0.191	H5,6																																											
	{ -0.060	H15,16																																											
	{ -0.143	H9,10																																											
	{ -0.055	H19,20																																											
	{ +0.232	2H(β)																																											
	{ +0.090	2H(β')																																											
	{ +0.050	2H(β)																																											
	{ +0.016	2H(β')																																											
<i>anti</i> -119 ⁻		<table border="0"> <tr> <td>Anion deloc.</td> <td>-0.300</td> <td></td> <td></td> </tr> <tr> <td>Anion local.</td> <td>{ -0.448</td> <td>H4,7</td> <td rowspan="2">[142, 623]</td> </tr> <tr> <td></td> <td>{ -0.109</td> <td>H14,17</td> </tr> <tr> <td></td> <td>{ -0.159</td> <td>H5,6</td> <td></td> </tr> <tr> <td></td> <td>{ -0.035</td> <td>H15,16</td> <td></td> </tr> <tr> <td></td> <td>{ -0.095</td> <td>H9,10</td> <td></td> </tr> <tr> <td></td> <td>{ -0.016</td> <td>H19,20</td> <td></td> </tr> <tr> <td></td> <td>{ +0.380</td> <td>2H(β)</td> <td></td> </tr> <tr> <td></td> <td>{ +0.042</td> <td>2H(β')</td> <td></td> </tr> <tr> <td></td> <td>{ +0.046</td> <td>2H(β)</td> <td></td> </tr> <tr> <td></td> <td>{ +0.004</td> <td>2H(β')</td> <td></td> </tr> </table>	Anion deloc.	-0.300			Anion local.	{ -0.448	H4,7	[142, 623]		{ -0.109	H14,17		{ -0.159	H5,6			{ -0.035	H15,16			{ -0.095	H9,10			{ -0.016	H19,20			{ +0.380	2H(β)			{ +0.042	2H(β')			{ +0.046	2H(β)			{ +0.004	2H(β')	
Anion deloc.	-0.300																																												
Anion local.	{ -0.448	H4,7	[142, 623]																																										
	{ -0.109	H14,17																																											
	{ -0.159	H5,6																																											
	{ -0.035	H15,16																																											
	{ -0.095	H9,10																																											
	{ -0.016	H19,20																																											
	{ +0.380	2H(β)																																											
	{ +0.042	2H(β')																																											
	{ +0.046	2H(β)																																											
	{ +0.004	2H(β')																																											
<i>anti</i> -[2,2]-(2,7)Naphthalenophane 514 ⁻		<table border="0"> <tr> <td>Anion deloc.</td> <td>-0.083</td> <td></td> <td></td> </tr> <tr> <td>Anion local.</td> <td>{ -0.194</td> <td>H4,7,14,17</td> <td rowspan="2">[153]</td> </tr> <tr> <td></td> <td>{ -0.268</td> <td>H5,6,15,16</td> </tr> <tr> <td></td> <td>{ +0.104</td> <td>H9,10,19,20</td> <td></td> </tr> <tr> <td></td> <td>{ +0.043</td> <td>4H(β)</td> <td></td> </tr> <tr> <td></td> <td></td> <td>4H(β')</td> <td></td> </tr> </table>	Anion deloc.	-0.083			Anion local.	{ -0.194	H4,7,14,17	[153]		{ -0.268	H5,6,15,16		{ +0.104	H9,10,19,20			{ +0.043	4H(β)				4H(β')																					
Anion deloc.	-0.083																																												
Anion local.	{ -0.194	H4,7,14,17	[153]																																										
	{ -0.268	H5,6,15,16																																											
	{ +0.104	H9,10,19,20																																											
	{ +0.043	4H(β)																																											
		4H(β')																																											

9,10,19,20-Tetramethyl- <i>anti</i> -[2.2](2,7)-naphthalenophane 515⁻		[913] Anion -0.055 -0.199 +0.077 +0.050 +0.293
<i>anti</i> -[2.2](2,7)Naphthalenophane-1,11-diene 516⁻		[153] Anion -0.087 -0.032 -0.108 -0.307
9,10,19,20-Tetramethyl- <i>anti</i> -[2.2](2,7)naphthalenophane-1,11-diene 517⁻/517⁺		[913] Anion/Cation -0.097/-0.054 -0.039/<0.01 -0.097/-0.225 +0.222/+0.316
[2.2](1,4)Anthracenophane <i>syn</i> - 518⁻		[914] Anion -0.268 -0.113 -0.077 -0.070 +0.090 +0.056
<i>anti</i> - 518⁻		[914] Anion -0.244 -0.111 -0.079 -0.073 +0.168 +0.015

Tab. 8.23 (continued)

[2.2](9,10)Anthracenophane 519 ⁻ / 519 ⁺		H4,7,9,12,16,19,21,24 H5,6,10,11,17,18,22,23 8H(β)	Anion/Cation -0.126/-0.110 -0.078/-0.065 +0.156/+0.098	[142, 229]/ [229]
[2.2](2,7)Pyrenophane 520 ⁻		H4,7,9,12,16,19,21,24 H5,6,10,11,17,18,22,23	Anion -0.225 -0.108	[915]
<i>anti</i> -[2.2](1,3)Azulenophane 521 ⁻		H4,8 H5,7 H6 H10	Anion local. -0.610 +0.110 -0.840 -0.367	[916]
[2.2](2,6)Azulenophane <i>syn</i> -522 ⁻		H5,9 H6,8 H15,19 2H(β) 2H(β') 2H(β'')	Anion local. -0.557 +0.251 -0.094 +0.291 +0.517 +0.050	[916]
<i>anti</i> -522 ⁻		H5,9 H6,8 2H(β) 2H(β')	Anion local. -0.599 +0.222 +0.349 +0.505	[916]

groups into [2.2](2,7)naphthalenophane-1,11-diene makes it amenable to oxidation in solution; the ^1H -hyperfine data for the radical cation $517^{+\cdot}$ thus formed exhibit some significant differences relative to those for the corresponding anion $517^{\cdot-}$, although the constituent π -systems, naphthalenes and ethenes, are alternant. These differences are presumably due to differing geometries, in particular to a slightly differing spatial demand of the sterically intervening methyl groups in the two radical ions.

The g_e factors of the radical anions and the radical cations ofphanes are 2.0027 ± 0.0001 and 2.0026 ± 0.0001 , respectively. The radical anions were generated from the neutral compounds with an alkali metal in an ethereal solvent. Their persistence decreased on going from [2.2]paracyclophanes to their metapara- and meta-counterparts. Thus, the radical anions of *anti*-[2.2]metacyclophane and its 1,9-diene were not amenable to ESR studies, because they rapidly lost two H atoms and converted into anions of 4,5,9,10-tetrahydropyrene (**122**) and pyrene (**387**), respectively. The ESR spectrum observed upon reaction of 4,5,7,8-tetramethyl[2.2]paracyclophane (**506**) with AlCl_3 in dichloromethane and first attributed to $506^{\cdot+}$ [241] proved to be that of the radical cation of 1,3,6,8-tetramethylpyrene formed by rearrangement (with several methyl shifts and loss of six H atoms) [904]. Under milder oxidation conditions, such as electrolysis on a gold anode in a mixture of dichloromethane with TFA and its anhydride, a dimeric radical cation $506_2^{\cdot+}$ with four eclipsed benzene π systems was obtained. For generation of $507^{\cdot+}$ and $517^{\cdot+}$ from the neutral compounds, electrolysis and reaction with AlCl_3 , respectively, were applied. Formation of $519^{\cdot+}$ was observed upon reaction of the anthracenophane in a mixture of dichloromethane or nitromethane with TFA and its anhydride. Interestingly, the radical anion of [2.2](2,7)naphthalenophane-1,11-diene (**516**) converts (with a loss of two H atoms) into that of *trans*-12b,12c-dihydrocoronene [153], which is structurally related to the radical anion of *trans*-10b,10c-dihydropyrene (**500**), a bridged [14]annulene (Table 8.20).

8.8

Radical Ions of Radialenes

[*n*]Radialenes contain *n*-membered rings of sp^2 hybridized C atoms, each of which bears a methylene group. They have D_{nh} symmetry in the planar geometry and are alternant π systems when *n* is even and nonalternant when *n* is odd. LUMOs of all planar [*n*]radialenes are nondegenerate, as are the HOMOs of the alternant [*n*]radialenes, whereas the HOMOs of the nonalternant [*n*]radialenes are doubly degenerate. Radialenes with *n* = 3, 4, and 6 were synthesized [917], and the radical ions of some of their alkyl- or phenyl-substituted derivatives were studied by ESR spectroscopy. The pertinent hyperfine data are given in Table 8.24 [464, 465, 918, 919]. The ESR spectrum of $75^{\cdot-}$ is shown in Figure 6.10.

The central rings in the substituted [4]- and [6]radialenes should be folded and have the symmetry D_{2d} and D_{3d} , respectively. However, for treatment of the spin

Tab. 8.24. Hyperfine Data for Radical Ions of Some [n]Radialenes

Hexamethyl[3]radialene 74 ⁻		18H(β) 6 ¹³ C(α)	Anion +0.757 -0.465	[464]
Octamethyl[4]radialene 523 ⁻ /523 ⁺		24H(β) ¹³ C1-4 8 ¹³ C(α)	Anion/Cation +0.567/+0.590 -0.16/-0.12 -0.37/-0.28	[918]
Octaphenyl[4]radialene 524 ⁻ /524 ⁺		8H _o } 8H _{o'} } 8H _m } 8H _{m'} } 8H _p	Anion/Cation -0.090/-0.045 -0.070/-0.045 +0.037/+0.066 +0.017/+0.066 -0.085/-0.023	[919]
7,8,9,10,11,12-Hexamethyl- [6]radialene 75 ⁻		H7-12 18H(β) ¹³ C1-6 6 ¹³ C(α)	Anion -0.382 +0.382 -0.200 -0.200	[465]
7,8,9,10,11,12-Hexaethyl- [6]radialene 525 ⁻		H7-12 6H(β) 6H(β) 24H(γ)	Anion -0.364 +0.468 +0.312 <0.02	[465]

distribution in their radical ions, they can be considered quasi-planar π systems. The bulk of π -spin population in the radical anions should be evenly distributed among the n exocyclic centers μ , yielding a ρ_{μ}^{π} value of ca 0.85/ n at each. Accordingly, the coupling constants of the methyl β protons in 74⁻, 523⁻, and 75⁻ are in the ratio (1/3):(1/4):(1/6), and this ratio is also roughly exhibited by the corresponding values of the ¹³C isotopes in the methyl-C atoms. The hyperfine data for the radical ions 523⁻ and 523⁺ reflect the pairing properties of the alternant [4]radialene, but those of their phenyl-substituted analogues 524⁻ and 524⁺ are less in line with such properties. According to the observed coupling constants, $|a_{H_p}| \approx |a_{H_o}| \gg |a_{H_m}|$ for 524⁻ and $|a_{H_m}| > |a_{H_o}| > |a_{H_p}|$ for 524⁺, the deviations of

the phenyl substituents from coplanarity with the [4]radialene π system are much larger for the radical cation than for the corresponding anion.

The g_e factors of the radical ions of [n]radialenes were not reported. The radical anions were generated from the neutral compound by reaction with potassium in DME or THF. The radical cations $523^{+\cdot}$ and $524^{+\cdot}$ were produced from the corresponding radialenes with AlCl_3 or Ti(III)trifluoroacetate, respectively, in dichloromethane.

9

Conjugated Radicals with Heteroatoms

A majority of conjugated organic radicals with heteroatoms can be thought as resulting either from combining a neutral hydrocarbon π system (Chapts. 8.1–8.8) with a spin-bearing heteroatom or a group of atoms (Chapts. 7.1–7.5) or from replacing carbon π -centers in a hydrocarbon radical by heteroatoms. The enormous number of ways to introduce “structural modifications” of this kind leads to the likewise enormous number of radicals. ESR data on some classes of radicals with heteroatoms, such as nitroxyls, semidione and semiquinone anions, and radical anions of nitro-substituted compounds fill hundreds of pages in the Landolt-Börnstein compilations [18]. Thus, the necessity to include only a few relatively simple, yet representative species is even more evident in this class of radicals than in those considered in the preceding Chapts. 7.1–7.5 and 8.1–8.8. Among such species are several highly persistent radicals, which have been mentioned in Chapts. 2.2 and 2.3. It is advisable to consider the neutral radicals and the radical ions separately. Like their hydrocarbon counterparts, a vast majority of conjugated radicals with heteroatoms have π structure. However, the presence of heteroatoms with lone-electron pairs makes it possible for some radical ions to form σ species.

For the radical ions and triions, the structural formulas in the Tables are again those of the neutral compounds without the symbols of unpaired electron and charge. Only in Tables 9.40 and 9.41 presenting radical cations of special structure, such symbols are used in the formulas.

9.1

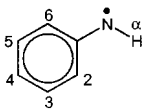
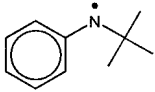
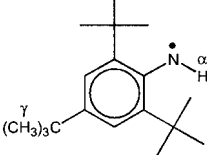
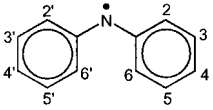
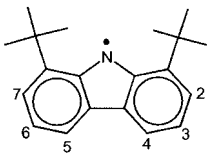
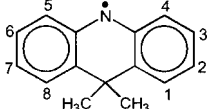
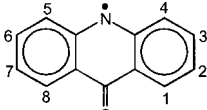
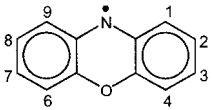
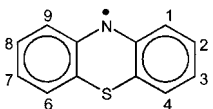
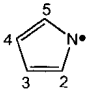
Neutral Radicals

In the neutral radicals dealt with below, the spin-bearing heteroatom or group of atoms, such as aminyl, oxyl, hydrazyl, tetrazolanyl, verdazyl, and nitroxyl, are linked to or incorporated into π systems.

Aminyl and Oxyl Radicals

Tables 9.1 [920–929] and 9.2 [580, 920, 930–938] list hyperfine data for some of these radicals. In phenylaminyl $\text{PhN}^{\cdot}\text{H}$ (526 \cdot) and phenoxyl PhO^{\cdot} (538 \cdot), the

Tab. 9.1. Hyperfine Data for Some Phenylaminyls and Related Radicals

Phenylaminyl 526 [•]		¹⁴ N H(α) H2,6 H3,5 H4	+0.795 -1.294 -0.618 +0.201 -0.822	[920]
<i>tert</i> -Butylphenylaminyl 527 [•]		¹⁴ N H2,6 H3,5 H4	+0.970 -0.584 +0.199 -0.709	[921]
(2,4,6-Tri- <i>tert</i> -butylphenyl)- aminyl 528 [•]		¹⁴ N H(α) H3,5 9H(γ)	+0.670 -1.175 +0.189 0.027	[922]
Diphenylaminyl 529 [•]		¹⁴ N H2,2',6,6' H3,3',5,5' H4,4'	+0.880 -0.368 +0.152 -0.428	[923]
1,8-Di- <i>tert</i> -butyl-9-carbazolyl 530 [•]		¹⁴ N H2,7 H3,6 H4,5	+0.697 +0.089 -0.430 +0.014	[924]
9,10-Dihydro-9,9-dimethyl- 10-acridinyl 531 [•]		¹⁴ N H1,3,6,8 H2,7 H4,5	+0.800 +0.128 -0.452 -0.367	[923]
9-Oxo-9,10-dihydro-10- acridinyl 532 [•]		¹⁴ N H1,8 H3,6 H2,7 H4,5	+0.698 +0.127 +0.076 -0.412 -0.367	[923]
10-Phenoxazinyl 533 [•]		¹⁴ N H1,9 H2,8 H3,7 H4,6	+0.803 -0.288 +0.097 -0.397 +0.065	[925]
10-Phenothiazinyl 534 [•]		¹⁴ N H1,9 H2,4,6,8 H3,7	+0.705 -0.285 +0.095 -0.366	[926]
1-Pyrrolyl 535 [•]		¹⁴ N H2,5 H3,4	-0.291 -1.326 -0.355	[927]

Tab. 9.1 (continued)

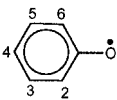
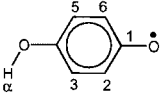
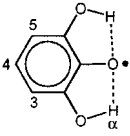
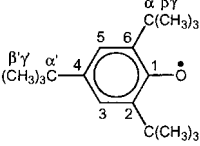
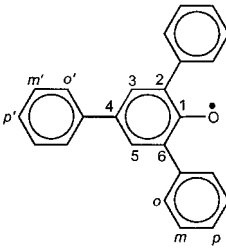
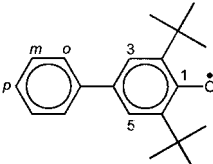
1-Methyl-4-carbomethoxy- pyridinyl 536 [•]		¹⁴ N	+0.625	[928]
		H2,6	-0.355	
		H3,5	+0.08	
		3H(β)	+0.555	
		3H(β')	+0.08	
1-Methyl-2-carboxymethoxy- pyridinyl 537 [•]		¹⁴ N	+0.658	[929]
		H3	+0.140	
		H5	+0.094	
		H4	-0.628	
		H6	-0.254	
		3H(β)	+0.564	
		3H(β')	+0.094	

exocyclic $\text{H}_2\text{C}^\bullet$ group of benzyl $\text{PhC}^\bullet\text{H}_2$ (**88[•]**) is replaced by HN^\bullet and O^\bullet , respectively, so that **526[•]** and **538[•]** are isoelectronic with **88[•]**. In the sequence $\text{H}_2\text{C}^\bullet$, HN^\bullet , O^\bullet , the π -spin population shifts from the exocyclic radical center to the phenyl ring, as indicated by the increasing $|a_{\text{H}}|$ values of the ring α protons (e.g., $a_{\text{H}4} = -0.617$, -0.822 , and -1.022 mT for **88[•]**, **526[•]**, and **538[•]**, respectively). In contrast to 7,7'-di-*tert*-butylbenzyl (**327[•]**), in which the two bulky substituents at the exocyclic C atom impair conjugation with the phenyl π system, introduction of one such substituent at the N atom in *tert*-butylphenylaminyl (**527[•]**) has only a moderate effect on the hyperfine data ($a_{\text{C}7} = +2.445$ and $a_{\text{H}4} = -0.617$ for **88[•]** vs $a_{\text{C}7} = +4.5$ and $a_{\text{H}4} = -0.031$ for **327[•]**, but $a_{\text{N}} = +0.795$ and $a_{\text{H}4} = -0.822$ for **526[•]** vs $a_{\text{N}} = +0.970$ and $a_{\text{H}4} = -0.709$ for **527[•]**).

Diphenylaminyl $\text{Ph}_2\text{N}^\bullet$ (**529[•]**) is isoelectronic with diphenylmethyl $\text{Ph}_2\text{C}^\bullet\text{H}$ (**323[•]**), and the two radicals have similar coupling constants for their phenyl α protons. With respect to the π -spin distribution, 9-carbazolyl (its 1,8-di-*tert*-butyl derivative **530[•]**) is presented in Table 9.1), as well as the two dihydroacridinyls **531[•]** and **532[•]**, the phenoxazinyl **533[•]**, and the phenothiazinyl **534[•]** are here considered to be bridged diphenylaminyl radicals. In general, due to π -spin delocalization into the phenyl groups, the ^{14}N -coupling constants for **526[•]**–**534[•]** ($a_{\text{N}} = +0.7$ to $+1.0$ mT) are smaller than those for alkylaminyls ($a_{\text{N}} = +1.2$ to $+1.5$ mT; Table 7.4).

In pyrrolyl and pyridinyl radicals, the aminyl-N atom is incorporated into a 5- and 6-membered cyclic π system, respectively. The small, negative a_{N} value for 1-pyrrolyl (**535[•]**) strongly differs from the ^{14}N -coupling constants in aminyl radicals, because the SOMO has a vertical node through the N atom. This radical must be regarded as azacyclopentadienyl, in which the SOMO resembles the HOMO ψ_{-1} of the five-membered π -perimeter (Figure 8.8). If the replacement of the CH group by an aza-N atom is considered as a perturbation by an electron-withdrawing substituent (Chapt. 8.2), the occupancy of the degenerate HOMOs ψ_{+1} and ψ_{-1} by three electrons in **535[•]** represents case ④ on p. 216. The π -spin distribution in **535[•]** is similar to that in the isoelectronic radical cation of pyrrole (**747**) (Table 9.29). On

Tab. 9.2. Hyperfine Data for Some Phenoxy and Related Radicals

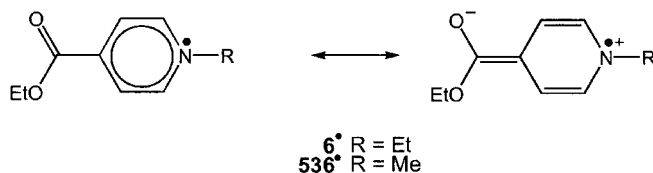
Phenoxy 538'		H2,6 H3,5 H4	-0.661 +0.185 -1.022	[920]
4-Hydroxyphenoxy 539'		H2,6 H3,5 H(α) $^{13}\text{C1}$ $^{13}\text{C4}$	-0.509 +0.029 -0.186 -0.35 +0.34	[930] [931]
2,6-Dihydroxyphenoxy 540'		H3,5 H4 2H(α)	+0.153 -0.762 -0.107	[932]
2,4,6-Tri- <i>tert</i> -butylphenoxy 9'		H3,5 18H(γ) 9H(γ') $^{13}\text{C1}$ $^{13}\text{C2,6}$ $^{13}\text{C3,5}$ $^{13}\text{C4}$ $2^{13}\text{C}(\alpha)$ $^{13}\text{C}(\alpha')$ $6^{13}\text{C}(\beta)$ $3^{13}\text{C}(\beta')$ ^{17}O	+0.160 +0.006 +0.039 -0.951 +0.813 -0.877 +1.391 -0.300 -0.444 +0.182 +0.453 -1.203	[580] [933]
1,3,5-Triphenylphenoxy 541'		H3,5 4H _o , 2H _p 4H _m 2H _{o'} 2H _{m'} H _{p'} $^{13}\text{C1}$ $^{13}\text{C2,6}$ $^{13}\text{C3,5}$ $^{13}\text{C4}$ ^{17}O	+0.168 -0.073 +0.038 -0.160 +0.059 -0.173 -1.25 +0.47 -0.87 +1.21 -0.97	[934] [935]
2,6-Di- <i>tert</i> -butyl-4-phenylphenoxy 542'		H3,5 2H _o 2H _m H _p $^{13}\text{C1}$	+0.169 ^a -0.175 +0.068 -0.192 -1.26	[936] [937]

Tab. 9.2. (continued)

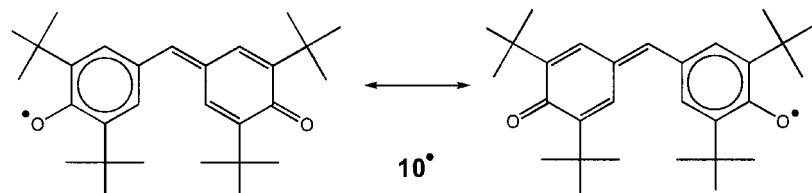
4-[(2',6'-Di- <i>tert</i> -butyl-1'-oxo-cyclohexa-2',5'-dien-4'-ylidene)methyl]-2,6-di- <i>tert</i> -butylphenoxy (galvinoxyl) 10^\bullet		H3,3',5,5'	+0.133	[938]
		H7	-0.559	
		36H(γ)	+0.005	
		$^{13}\text{C}1,1'$	-0.557	
		$^{13}\text{C}2,2',6,6'$	+0.499	
		$^{13}\text{C}3,3',5,5'$	-0.621	
		$^{13}\text{C}4,4'$	+1.073	
		$^{13}\text{C}7$	-0.995	
		$4^{13}\text{C}(\alpha)$	-0.18	
		$12^{13}\text{C}(\beta)$	+0.11	

^a Hyperfine data by NMR

the other hand, the pyridinyl radicals 536^\bullet and 537^\bullet have the coupling constants a_N and $a_H(\alpha)$ close to those of the radical anion of pyridine (**79**) (Table 9.8). The ESR spectrum of the highly persistent 1-ethyl-4-carboxypyridinyl (6^\bullet) (Chapt. 2.2) has not been analyzed in detail, but hyperfine data were reported for closely related radicals, such as the corresponding 1-methyl derivative 536^\bullet (Table 9.1). The stability of 6^\bullet and 536^\bullet is due to the electron-withdrawing carboxy substituent, and its contribution to the structure is expressed below by their ionic formulas. An analogous formula can be written for 1-methyl-2-carboxypyridinyl (537^\bullet), an isomer of 536^\bullet . The three pyridinyl radicals are in equilibrium with their diamagnetic dimers.



The reactive N'H and O' radical sites in phenylamiminyls and phenoxy radicals are shielded by bulky *ortho*-substituents, so that the 2,4,6-tri-*tert*-butyl derivatives 528^\bullet and 9^\bullet are persistent. Both phenoxy radicals, 9^\bullet and its triphenyl-substituted counterpart 541^\bullet , have been widely studied by ESR spectroscopy. High persistence and stability are also characteristic of the 4-[(2',6'-di-*tert*-butyl-1'-oxocyclohexa-2',5'-dien-4'-ylidene)methyl]-2,6-di-*tert*-butylphenoxy (galvinoxyl; 10^\bullet), the structure of which is properly described by two equivalent formulas:



For the hydroxyl-substituted phenoxy radicals 539^\bullet and 540^\bullet , the coupling constants depend strongly on experimental conditions, especially the pH and temperature.

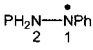
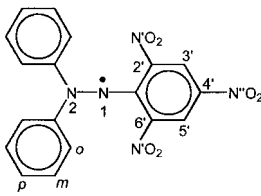
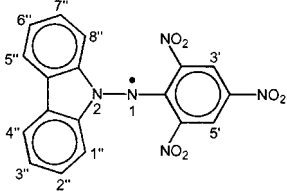
The g_e factor of most phenylaminy radicals is 2.0031–2.0035. That of 532 \cdot and 534 \cdot is higher, amounting to 2.0040 and 2.0046, respectively, whereas 535 \cdot , with a node at the N atom, has a much lower value of 2.0023. The g_e factor of phenoxy radicals is 2.0042–2.0046. The radicals of both classes presented in Tables 9.1 and 9.2 were generated in solution. The parent 526 \cdot and 538 \cdot were produced by reaction of radiolytically produced HO \cdot radicals with aniline and phenol, respectively. The former method was also used for generation of 535 \cdot from pyrrole. The sterically protected phenylaminy 528 \cdot and phenoxy 9 \cdot and 541 \cdot were obtained by oxidation with PbO $_2$ of the corresponding substituted aniline and phenols, respectively. Photolysis of tetrazene yielded 527 \cdot , and that of hydrazine/benzene mixtures in a flow system led to 529 \cdot . Thermal dissociation of the corresponding hydrazines gave 531 \cdot and 532 \cdot , and 533 \cdot and 534 \cdot were obtained by dehydrogenation of phenoxazine with air and of phenothiazine with PbO $_2$, respectively. Pyridinyls 6 \cdot , 536 \cdot , and 537 \cdot were produced by reduction of the salts of the corresponding cations with zinc. 1,4-Benzoquinone was the precursor of 539 \cdot and pyrogallol that of 540 \cdot . The galvinoxyl 10 \cdot could be formed from the corresponding phenol (galvinol) by various reagents, such as PbO $_2$ and K $_3$ Fe(CO) $_3$.

Hydrazyl Radicals

Only few hydrazyls with unsubstituted phenyl groups, such as the triphenyl derivative Ph $_2$ NN \cdot Ph (543 \cdot), have been studied by ESR spectroscopy. More widely known are hydrazyls having nitro-substituted phenyl groups, which bestow persistence on these radicals with their three-electron N–N π bond (Chapt. 7.3).

Among these hydrazyls, 2,2-diphenyl-1-picrylhydrazyl (DPPH; 5 \cdot) has become particularly prominent. This highly persistent radical is available in the crystalline state (Chapt. 2.2), and it was the first radical for which hyperfine splitting in an ESR spectrum was observed [511]. In view of its low symmetry and the expected $3^5 \cdot 2^{12} = 995328$ hyperfine lines, the splitting consisted of five broad lines due to two ^{14}N nuclei in the hydrazyl group with coupling constants of $+0.88 \pm 0.10$ mT. Later studies on 5 \cdot , using ELDOR [527], ENDOR [587, 939], TRIPLE resonance [587], and NMR [940], which were combined with isotopic $^{15}\text{N}/^{14}\text{N}$ and D/H replacements [527, 587] led to an unambiguous analysis of the hyperfine pattern and assignments of all coupling constants. The data are listed in Table 9.3 [527, 587, 940–942]. The a_{H} values are temperature-dependent, because the picryl and phenyl rings are subject to intermolecular motion about the C–N bonds. These values also slightly vary with the resonance-spectroscopic method employed. The coupling constants given in Table 9.3 for protons were measured by ENDOR at 295 K in the fast-motion range. The small a_{N} values for the nitro substituents were provided by ^{15}N -NMR (converted to ^{14}N by multiplication with -0.713 ; Chapt. 3.2), and ELDOR yielded the large ^{14}N -coupling constants for the hydrazo group. In addition to the hyperfine data for 5 \cdot , Table 9.3 lists those for the triphenylhydrazyl (543 \cdot) and 9-carbazolyl-(2,4,6-trinitrophenyl)aminy (544 \cdot), which has a π -spin distribution similar to 5 \cdot . As expected, some of the a_{N} values for 543 \cdot and 544 \cdot , with their extended π systems, are smaller than those of their alkyl counterparts ($+0.9$ to $+1.2$ mT; Table 7.16).

Tab. 9.3. Hyperfine Data for Some Triphenylhydrazyls and Related Radicals

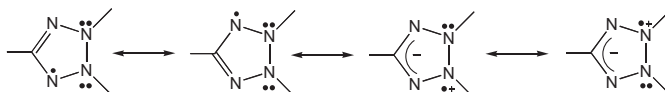
Triphenylhydrazyl 543 [•]		¹⁴ N1 ¹⁴ N2	+0.905 +0.428	[941]
2,2-Diphenyl-1-picrylhydrazyl (DPPH) 5 [•]		¹⁴ N1 ¹⁴ N2 H3',5' 4H _o 4H _m 2H _p 2 ¹⁴ N' ¹⁴ N''	+0.974 +0.795 +0.106 -0.155 +0.073 -0.158 +0.039 ^a +0.048	[527] [587] [940]
9-Carbazolyl-(2,4,6-trinitrophenyl)aminyl 544 [•]		¹⁴ N1 ¹⁴ N2 H3',5' H1'',8'' H2'',7'' H4'',5'' H3'',6''	+1.11 +0.60 +0.117 -0.192 +0.053 +0.041 -0.181	[942]

^aData by NMR

The g_e factor of DPPH (**10[•]**), mentioned in Chapt. 6.2, and that of **544[•]** is 2.0036. All three hydrazyls were readily produced from the corresponding hydrazines with PbO₂ in benzene.

Tetrazolinyl and Verdazyl Radicals

These radicals contain two equivalent hydrazine groups, in either of which a three-electron π bond can be formed. The two groups conjugate via a C atom to give a 5-centered 7-electron π system; their terminal N atoms are directly linked in the five-membered ring of tetrazolinyl, or they are separated by an sp³-hybridized C atom in the six-membered ring of verdazyl. The structure of tetrazolinyl is described by the following formulas, in which all four N atoms share the π -spin population:



Analogous formulas can be drawn for verdazyls.

The SOMO in radicals of both classes has a vertical nodal plane through the C center; in verdazyls, this plane also passes through the sp³-hybridized C atom. The π -spin distribution is thus similar in both classes of radicals, in which each of the four N atoms bears a population of ca +0.25. The radicals studied by ESR spectroscopy were particularly stable, because they are substituted by two phenyl groups (R = Ph) at the N atoms in positions 2 and 3 of tetrazolinyl or in the corresponding positions 1 and 5 of verdazyl. The chemical and physical properties of these radicals were reviewed in 1973 [943]. Table 9.4 [95, 944–950] lists hyperfine

Tab. 9.4. Hyperfine Data for Some Tetrazolinyl and Verdazyl Radicals

5- <i>tert</i> -Butyl-2,3-diphenyl tetrazolinyl 545 [•]		¹⁴ N _{1,4}	+0.57	[944]
		¹⁴ N _{2,3}	+0.75	
		4H _o , 2H _p	-0.095	
		4H _m	+0.05	
2,3,5-Triphenyltetrazolinyl 546 [•]		¹⁴ N _{1,4}	+0.56	[945]
		¹⁴ N _{2,3}	+0.75	
1- <i>H</i> -Benzo[<i>c</i>]tetrazolo- [2,3- <i>a</i>]cinnolin-1-yl 547 [•]		¹⁴ N _{1,3}	+0.385	[946]
		¹⁴ N _{4,13}	+0.77	
		H ₂	+0.04	
		H _{5,7,10,12}	-0.19	
1,5-Diphenylverdazyl 548 [•]		¹⁴ N _{1,2,4,5}	+0.60	[95]
		H ₃	+0.072 ^a	[947]
		4H _o	-0.110	
		4H _m	+0.040	
		2H _p	-0.116	
		2H(β)	-0.072	
3- <i>tert</i> -Butyl-1,5- diphenylverdazyl 549 [•]		¹⁴ N _{1,2,4,5}	+0.59	[948]
		4H _o , 2H _p	-0.108 ^a	[947]
		4H _m	+0.040	
		2H(β)	-0.008	
		9H(γ)	+0.011	
1,3,5-Triphenylverdazyl 7 [•]		¹⁴ N _{1,2,4,5}	+0.579	[949]
		4H _o	-0.112 ^a	[950]
		4H _m	+0.043	
		2H _p	-0.120	
		2H _{o'}	+0.043	
		2H _{m'}	-0.016	
		H _{p'}	+0.031	
2H(β)	-0.003			

^a Data by NMR

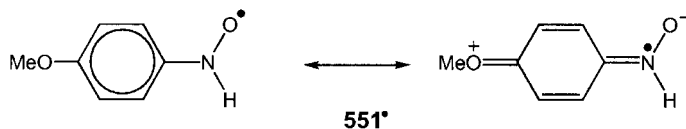
data for some of them. The ^{14}N -coupling constants for all tetrazolinyis are $a_{\text{N}1,4} = +0.5 \pm 0.1$ and $a_{\text{N}2,3} = +0.7 \pm 0.1$ mT, but the two corresponding values appear equal in the verdazyls, $a_{\text{N}2,4} \approx a_{\text{N}1,5} \approx +0.6$ mT. Only for the cinnolinyl derivative **547** \cdot , structurally related to 2,3-diphenyltetrazolinyil, is the coupling constant $a_{\text{N}1,3}$ (corresponding to $a_{\text{N}1,4}$ for **545** \cdot and **546** \cdot) considerably smaller. In general, the a_{N} values for tetrazolinyis and verdazyls are reduced relative to those for hydrazyls.

The g_e factor of tetrazolinyis and verdazyls is in the range 2.0034–2.0037 and thus similar to that of hydrazyls. The tetrazolinyis **545** \cdot and **546** \cdot were generated from the corresponding formazans with di-*p*-tolylaminyls, and the readily available verdazyls **7** \cdot , **548** \cdot , and **549** \cdot were synthesized by a variety of methods, such as alkylation of formazans in the presence of air and ring expansion of tetraazonium salts with diazoalkanes. Reduction of a corresponding tetrazolium salt with Na_2SO_4 yielded **547** \cdot .

Nitroxyl Radicals

The hyperfine data given in Tables 9.5 [749, 757, 923, 951–957] and 9.6 [958, 959] are only a narrow selection of those measured for hundreds of nitroxyls. Due to the delocalization of the π -spin population, the ^{14}N -coupling constant, which strongly depends on experimental conditions (Chapt. 7.4), decreases from a range $a_{\text{N}} = +1.2$ to $+1.7$ mT for alkylnitroxyls (Table 7.20) to $a_{\text{N}} = +0.7$ to $+1.1$ mT for phenylnitroxyls.

In phenylnitroxyls the ratio, $|a_{\text{N}}|/|a_{\text{H}}(\alpha)| = 0.75 \pm 0.1$, of this coupling constant to that of the proton at the N atom is largely independent of the solvent and of substitution at the phenyl group [960]. Both $|a_{\text{N}}|$ and $|a_{\text{H}}(\alpha)|$ values increase in protic solvents and decrease in aprotic ones; e.g., for **550** \cdot at room temperature, the pertinent coupling constants are, respectively, $+1.063$ and -1.315 mT with water [961], and $+0.889$ and -1.175 mT with DMSO [962]. For *para*-substituted phenylnitroxyls, the values increase when the substituent is electron-releasing and decrease when it is electron-withdrawing. Thus, in the solvent 1,2-dihydroxyethane at 293 K, the coupling constants a_{N} and $a_{\text{H}}(\alpha)$ are, respectively, $+1.015$ and -1.375 mT for the *p*-methoxy derivative (**551** \cdot) and $+0.750$ and -1.010 mT for its *p*-nitro substituted counterpart (**552** \cdot), compared with $+0.975$ and -1.275 mT for the parent phenylnitroxyl (**550** \cdot). This effect can be interpreted in terms of favoring (or disfavoring) the ionic formula of the nitroxyl group by electron-releasing (or withdrawing) substituents, as exemplified below for the *p*-methoxy group by the ionic formula of **551** \cdot .

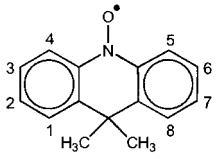
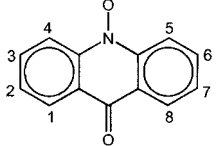
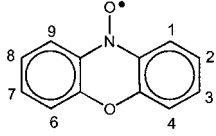
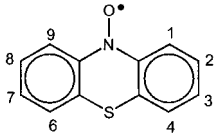


The coupling constant a_{N} is increased by the presence of bulky *N*-*tert*-butyl substituents at the N atom or in the phenyl *ortho* positions. These substituents twist the nitroxyl group out of coplanarity with the π system linked to it and thus impede

Tab. 9.5. Hyperfine Data for Some Phenylnitroxyls and Related Radicals

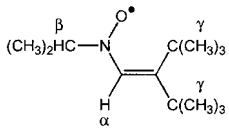
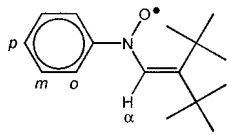
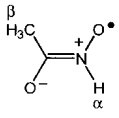
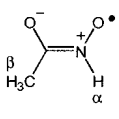
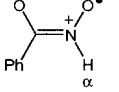
Phenylnitroxyl 550 [•]		¹⁴ N H(α) 2H _o , H _p 2H _m	+0.975 -1.275 -0.300 +0.100	[951]
<i>p</i> -Anisylnitroxyl 551 [•]		¹⁴ N H(α) 2H _o 2H _m 3H(β)	+1.015 -1.375 -0.337 ^a +0.100 +0.050	[951]
<i>p</i> -Nitrophenylnitroxyl 552 [•]		¹⁴ N H(α) 2H _o 2H _m ¹⁴ N'	+0.750 -1.010 -0.300 +0.085 +0.185	[951]
(2,4,6-Tri- <i>tert</i> - butylphenyl)nitroxyl 553 [•]		¹⁴ N H(α) 2H _m	+1.165 -1.296 +0.103	[952]
Methylphenylnitroxyl 554 [•]		¹⁴ N 2H _o , H _p 2H _m 3H(β) ¹³ C(α)	+1.065 -0.275 +0.101 +0.969 -0.60	[953] [749]
<i>tert</i> -Butylphenyl- nitroxyl 555 [•]		¹⁴ N 2H _o 2H _m H _p 9H(γ)	+1.208 -0.209 +0.089 -0.229 +0.009	[954]
Indolyl-1-nitroxyl 556 [•]		¹⁴ N H _{4,6} H _{5,7} 2H(β)	+1.175 +0.100 -0.374 +1.860	[955]
Diphenylnitroxyl 557 [•]		¹⁴ N 4H _o , 2H _p 4H _m	+0.966 -0.183 +0.079	[956]
Carbazolyl-9-oxyl 558 [•]		¹⁴ N H _{1,3,6,8} H _{2,4,5,7} ¹⁷ O	+0.665 -0.230 +0.055 -1.65	[757]

Tab. 9.5 (continued)

9,9-Dimethylacridinyl-10-oxyl 559 ^a		¹⁴ N H1,3,6,8 H2,4,5,7 ¹⁷ O	+0.875 +0.075 -0.230 -1.66	[757]
(9 <i>H</i>)-9-Oxoacridinyl-10-oxyl 560 ^a		¹⁴ N H1,3,6,8 H2,7 H4,5	+0.689 +0.069 -0.211 -0.203	[923]
Phenoxazinyl-10-oxyl 561 ^a		¹⁴ N H1,3,7,9 H2,4,6,8	+0.950 -0.240 +0.050	[757]
Phenothiazinyl-10-oxyl 562 ^a		¹⁴ N H1,3,7,9 H2,8 H4,6	+0.901 -0.220 +0.063 +0.050	[957]

^a Averaged value

Tab. 9.6. Hyperfine Data for Some Vinylnitroxyl and Acylnitroxyl Radicals

Isopropyl-2,2-di(<i>tert</i> -butyl)vinylnitroxyl 563 ^a		¹⁴ N H(α) H(β) 18H(γ)	+1.03 -0.75 +0.26 0.024	[958]
2,2-Di(<i>tert</i> -butyl)-vinylphenylnitroxyl 564 ^a		¹⁴ N H(α) 2H _o , H _p 2H _m	+1.00 -1.36 -0.25 +0.09	[958]
Acetylnitroxyl <i>trans</i> -565 ^a		¹⁴ N H(α) 3H(β)	+0.605 -1.060 +0.185	[959]
<i>cis</i> -565 ^a		¹⁴ N H(α) 3H(β)	+0.645 -1.085 <0.05	[959]
Benzoylnitroxyl 566 ^a		¹⁴ N H(α)	+0.610 -1.040	[959]

π -spin delocalization from the former into the latter, as demonstrated by the hyperfine data for **553** \cdot and **555** \cdot .

Analogous to what occurs in diphenylaminyl $\text{Ph}_2\text{N}\cdot\text{H}$ (**529** \cdot) and its tricyclic counterparts **530** \cdot –**534** \cdot , the π -spin distributions in carbazolyl-9-oxyl (**558** \cdot), the two acridinyloxy **559** \cdot and **560** \cdot , the phenoxazinyl **561** \cdot , and the phenothiazinyl **562** \cdot are similar to that in diphenylnitroxyl $\text{Ph}_2\text{NO}\cdot$ (**557** \cdot).

In vinylnitroxyls such as **563** \cdot and **564** \cdot , the $>\text{N}-\text{O}\cdot$ group conjugates with the double bond, and the coupling constant a_{N} is ca +1.0 mT. However, the polar structure ascribed to acylnitroxyls **565** \cdot and **566** \cdot discriminates against the spin at the N atom; the a_{N} value is reduced to ca +0.6 mT and the ratio $|a_{\text{N}}|/|a_{\text{H}}(\alpha)|$ is 0.58 ± 0.1 .

As mentioned previously, the g_{e} factor of all nitroxyls is 2.0055–2.0065 (Chapt. 6.2). These persistent radicals are readily generated from the corresponding amines and hydroxyamines with H_2O_2 , peroxyacids, Ag(I), Ce(IV), or Pb(IV) ions in various solvents (Chapts. 2.2 and 7.4). A flow system was required for the less persistent acylnitroxyls, and special reactions involving nitroso or nitro precursors were used for formation of the vinylnitroxyls.

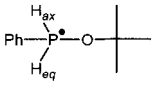
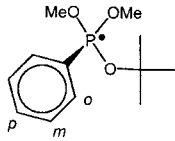
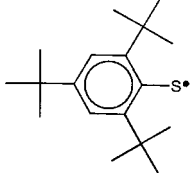
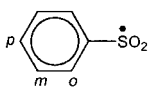
Phenyl-substituted Silyl, Phosphinyl, Phosphonyl, Phosphoranyl, Thiyl, and Sulfonyl Radicals

Table 9.7 [708, 775, 963–967] gives hyperfine data for some of these radicals in which at least one group linked to the heteroatom is phenyl. Because the silyl, phosphinyl, phosphonyl, and sulfonyl structures are generally pyramidal at the heteroatom, their radical centers do not effectively conjugate with the phenyl π system, and their ^{29}Si -, ^{31}P -, and ^{33}S -coupling constants should not be markedly reduced relative to their counterparts in alkyl derivatives (Chapts. 7.2 and 7.5). These expectations are borne out by experimental data, with the exception of the $|a_{\text{Si}}|$ value for the triphenylsilyl (**567** \cdot), which is much smaller than those for alkylsilyls (Table 7.13); this finding has not been accounted for theoretically.

Phenylphosphoranyl radicals fall into two types, which have drastically different ^{31}P -coupling constants, depending on the nature of the ligands. Radicals such as **570** \cdot , with a very large a_{P} value, are bipyramidal with the unpaired electron acting as a phantom ligand (the SOMO at the P atom has an appreciable 3s-contribution). An alternative, generally favored MO model of bipyramidal phosphoranyl radicals expresses the SOMO as a 3-centered nonbonding orbital involving both the axial ligands and the P atom [968]. In contrast, the radicals such as **571** \cdot with a rather small a_{P} value are tetrahedral; they usually have electron-releasing ligands like a methoxy group, which shifts the spin population into the phenyl π system.

For **567** \cdot , **568** \cdot , **569** \cdot , **572** \cdot , and **573** \cdot , g_{e} factors of 2.0029, 2.0051, 2.0035, 2.0103, and 2.0046, respectively, were reported; those for **570** \cdot and **571** \cdot are missing. The radicals **567** \cdot , **568** \cdot , and **569** \cdot were generated in solids by radiolysis of triphenylsilane, diphenylchlorophosphine, and diphenylhydrophosphone, respectively. The remaining radicals were produced in solution: **570** \cdot and **571** \cdot by addition of *t*-BuO \cdot

Tab. 9.7. Hyperfine Data for Some Phenyl-substituted Silyl, Phosphinyl, Phosphonyl, Phosphoranyl, Thiyl, and Sulphonyl Radicals

Triphenylsilyl 567 [•]	$\text{Ph}_3\text{Si}^\bullet$	^{29}Si	-7.96	[963]
Diphenylphosphinyl 568 [•]	$\text{Ph}_2\text{P}^\bullet$	^{31}P	+7.87	[708]
Diphenylphosphonyl 569 [•]	$\text{Ph}_2\text{P}^\bullet=\text{O}$	^{31}P	+36.16	[964]
<i>tert</i> -Butoxydihydro(phenyl)- phosphoranyl 570 [•]		^{31}P H_{ax} H_{eq}	+55.70 +12.65 +1.02	[965]
<i>tert</i> -Butoxydimethoxy(phenyl)- phosphoranyl 571 [•]		^{31}P 2H_o 2H_m H_p	+0.97 -0.55 +0.09 -0.97	[965]
2,4,6-tri- <i>tert</i> -butylphenylthiyl 572 [•]		^{33}S	+1.475	[966]
Phenylsulphonyl 573 [•]		^{33}S 2H_o 2H_m 2H_p	+8.32 -0.106 +0.033 -0.050	[967] [775]

to the corresponding phosphine, **572[•]** by oxidation of the thiophenol derivative with PbO_2 , and **573[•]** by reaction of phenylchlorosulfone with $\text{Et}_3\text{Si}^\bullet$.

9.2 Radical Anions of Electron Acceptors

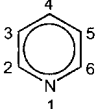
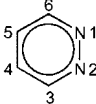
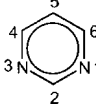
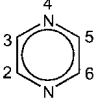
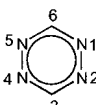
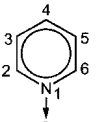
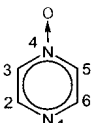
As pointed out in Chapt. 8.4 for benzenoid compounds, most conjugated hydrocarbons are both moderate electron acceptors and donors and can generally be converted into both radical anions and cations. Heteroatoms or groups containing heteroatoms endow these hydrocarbons with the properties of either a better acceptor or a better donor, which preferentially, and often exclusively, yield either the radical anion or the radical cation. When a C center in a hydrocarbon π system is replaced by a heteroatom, the nature and electronic structure (hybridization) of this atom determine whether the system becomes an acceptor or a donor. Linking a hydrocarbon π system with a functional group containing heteroatoms leads to an acceptor or a donor, according to whether the group is electron-withdrawing

or electron-releasing. In general, electron-withdrawing groups such as azo, keto, cyano, and nitro are those responsible for acceptor properties.

Radical Anions of Heterocycles

An aza-heterocycle is obtained when a C–H(α) segment in the corresponding hydrocarbon π system is replaced by an sp^2 -hybridized N atom, which has one electron in its $2p_z$ -AO contributing to the π system and a lone-electron pair in the molecular xy plane. Because almost any C–H(α) segment can be substituted by an isoelectronic aza-N atom of this structure, the number of possible aza-heterocycles is large. Tables 9.8 [157, 208, 467, 969], 9.9 [159, 162, 970–972], and 9.10 [159, 267,

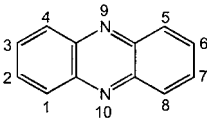
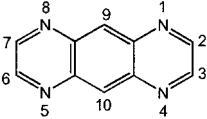
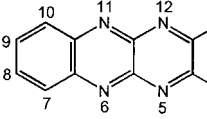
Tab. 9.8. Hyperfine Data for Radical Anions of Some Azabenzenes

Pyridine 79 $^{\cdot-}$		$^{14}\text{N}1$ H2,6 H3,5 H4	+0.628 –0.355 +0.082 –0.970	[467]
Pyridazine 574 $^{\cdot-}$		$^{14}\text{N}1,2$ H3,6 H4,5	+0.590 +0.016 –0.647	[208]
Pyrimidine 575 $^{\cdot-}$		$^{14}\text{N}1,3$ H2 H4,6 H5	+0.326 +0.072 –0.978 +0.131	[467]
Pyrazine 576 $^{\cdot-}$		$^{14}\text{N}1,4$ H2,3,5,6	+0.718 –0.264	[157]
<i>sym</i> -Tetrazine 577 $^{\cdot-}$		$^{14}\text{N}1,2,4,5$ H3,6	+0.528 +0.212	[208]
Pyridine- <i>N</i> -oxide 578 $^{\cdot-}$		$^{14}\text{N}1$ H2,6 H3,5 H4	+1.091 –0.301 +0.044 –0.851	[969]
Pyrazine-di- <i>N</i> -oxide 579 $^{\cdot-}$		$^{14}\text{N}1,4$ H2,3,5,6	+0.949 –0.137	[969]

Tab. 9.9. Hyperfine Data for Radical Anions of Some Azanaphthalenes, Azaanthracenes and Azanaphthacenes

Quinoline 580 ⁻		¹⁴ N1 H2 H3 H4 H5 H6 H7 H8	+0.395 -0.329 -0.126 -0.780 -0.390 -0.114 -0.202 -0.346	[970]
Isoquinoline 581 ⁻		¹⁴ N2 H1 H3 H4 H5 H6 H7 H8	+0.192 -0.538 -0.037 -0.401 -0.395 -0.326 0.004 -0.626	[970]
Quinoxaline 582 ⁻		¹⁴ N1,4 H2,3 H5,8 H6,7	+0.564 -0.332 -0.232 -0.100	[159]
1,5-Naphthyridine 583 ⁻		¹⁴ N1,5 H2,6 H3,7 H4,8	+0.336 -0.295 -0.169 -0.578	[971]
1,8-Naphthyridine 584 ⁻		¹⁴ N1,8 H2,7 H3,6 H4,5	+0.247 -0.407 +0.070 -0.654	[971]
Phthalazine 585 ⁻		¹⁴ N2,3 H1,4 H5,8 H6,7	+0.087 -0.578 -0.462 -0.209	[972]
1,4,5,8-Tetraazanaphthalene 57 ⁻		¹⁴ N1,4,5,8 H2,3,6,7	+0.337 -0.314	[162]
Acridine 586 ⁻		¹⁴ N9 H1,8 H2,7 H3,6 H4,5 H10	+0.372 -0.182 -0.202 -0.091 -0.278 -0.760	[159]

Tab. 9.9 (continued)

Phenazine 587 ^{•-}		¹⁴ N9,10 H1,4,5,8 H2,3,6,7	+0.514 -0.193 -0.161	[159]
1,4,5,8-Tetrazaanthracene 588 ^{•-}		¹⁴ N1,4,5,8 H2,3,6,7 H9,10	+0.241 -0.273 -0.396	[159]
5,6,11,12-Tetraaza-naphthalene 589 ^{•-}		¹⁴ N5,6,11,12 H1,4,7,10 H2,3,8,9	+0.298 -0.084 -0.140	[971]

970, 973–976] list hyperfine data for the radical anions of some aza derivatives of benzenoid hydrocarbons.

Introduction of aza-N atoms into the benzene ring affects the orbitals of the six-membered π perimeter too strongly to be considered a mere perturbation. Nevertheless, the effect of this modification on the degenerate perimeter LUMOs ψ_{2+} and ψ_{2-} (Figure 8.9) mimics that predicted for perturbation by an electron-attracting substituent at the pertinent position (Chapts. 8.1 and 8.6). Thus, with one electron in ψ_{2+} and ψ_{2-} (case ③ on p. 216), the shape of the SOMO is similar to ψ_{2+} in the radical anions of pyridine (79) and pyrazine (576) but resembles ψ_{2-} in those of pyridazine (574), pyrimidine (575), and *sym*-tetrazine (577).

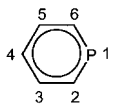
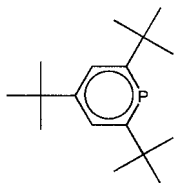
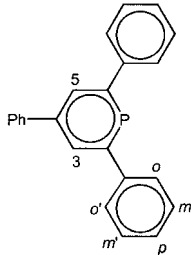
For π systems, which have no degenerate or nearly degenerate LUMOs, the shape of the SOMO in the radical anions of their aza-derivatives and, consequently, the π -spin distribution remains roughly the same as in those of the corresponding hydrocarbons. This statement holds for the radical anions of the aza derivatives, 57 and 580–596, of naphthalene, anthracene, naphthacene, phenanthrene, pyrene, and biphenyl. Their ¹⁴N-coupling constants $a_{N\mu}$ are comparable to the $|a_{H\mu}(\alpha)|$ values at the C center μ of the similar spin population ρ_{μ}^{π} , but their sign is opposite (Eqs. 4.5 and 4.22). Due to the presence of N-lone pairs, which do not participate in the π system, the radical anions of aza compounds function as bases and are prone to protonation in acid solution, whereby addition of two protons to N atoms in the proper positions leads to the formation of the radical cations of the dihydro adducts (Chapts. 2.3, 6.3, and 9.3 and Table 9.30). Protonation does not change the shape of the π -SOMO, but it enhances the electronegativity of the N atom. This effect is further promoted by addition of O atoms to the N-lone pairs, as demonstrated by the hyperfine data for the radical anions of pyridine-*N*-oxide (578) and pyrazine-di-*N*-oxide (579) (Table 9.8). Relative to the radical anions of the parent aza-heterocycles (79 and 576) the π -spin population at the N atoms in 578^{•-} and 579^{•-} is clearly increased at the expense of that at the C centers. The N-lone pairs are also responsible for tight association with alkali-metal counterions, in par-

Tab. 9.10. Hyperfine Data from Radical Anions of Some Azaphenanthrenes, Azapyrenes, and Azabiphenyls

1,10-Phenanthroline 590 ⁻		¹⁴ N1,10 H2,9 H3,8 H4,7 H5,6	+0.033 -0.277 +0.027 -0.317 -0.601	[973]
Benzo[c]cinnoline (9,10-diazaphenanthrene) 591 ⁻		¹⁴ N9,10 H1,8 H2,7 H3,6 H4,5	+0.494 -0.366 +0.017 -0.291 0.081	[970]
2,7-Diazapyrene 592 ⁻		¹⁴ N2,7 H1,3,6,8 H4,5,9,10	-0.157 -0.505 -0.215	[267]
1,3,6,8-Tetraazapyrene 593 ⁻		¹⁴ N1,3,6,8 H2,7 H4,5,9,10	+0.257 +0.036 -0.239	[974]
2,2'-Bipyridyl 594 ⁻		¹⁴ N1,1' H3,3' H4,4' H5,5' H6,6'	+0.254 -0.120 -0.105 -0.458 +0.054	[975]
4,4'-Bipyridyl 595 ⁻		¹⁴ N1,1' H2,2',6,6' H3,3',5,5'	+0.364 +0.043 -0.235	[159]
2,2'-Bipyrimidyl 596 ⁻		¹⁴ N1,1',3,3' H4,4',6,6' H5,5'	+0.141 +0.015 -0.493	[976]

ticular when the cation can be chelated by two such pairs in *peri* positions, as in 584⁻, 57⁻, and 589⁻, or in the “bay-region”, as in 590⁻, 594⁻, and 596⁻. 1,10-Phenanthroline (590) and 2,2'-bipyridyl (594) are known as favorite ligands for complexing cations of transition metals such as Cu(II).

Tab. 9.11. Hyperfine Data for Radical Anions and of Some Phosphabenzenes

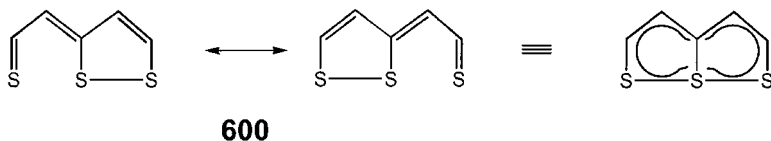
Phosphabenzene $80^{\cdot-}$		$^{31}\text{P}1$ H2,6 H3,5 H4 $^{13}\text{C}4$	Anion +3.56 -0.37 <0.1 -0.76 +1.20	[165]
2,4,6-Tri- <i>tert</i> -butyl- phosphabenzene $82^{\cdot-}$		$^{31}\text{P}1$	Anion +2.94	[165]
2,4,6-Triphenyl- phosphabenzene $597^{\cdot-}/597^{3-}$		$^{31}\text{P}1$ H3,5 2H_o $2\text{H}_{o'}$ 2H_m $2\text{H}_{m'}$ 2H_p	Anion /Trianion +3.31 / -0.267 <0.03 / -0.473 >0.3 / { -0.188 -0.075 <0.3 / { +0.043 +0.032 >0.3 / -0.249	[181]

Phosphabenzene (**80**) has a π -electronic structure similar to pyridine (**79**). The radical anion $80^{\cdot-}$ and those of 2,4,6-*tert*-butyl and triphenyl derivatives (**82** and **597**, respectively) were studied by ESR spectroscopy both in fluid and frozen solution (Chapt. 4.2). The ESR spectrum of $82^{\cdot-}$ in a MTHF glass is reproduced in Figure 4.8. The extension of the π system by three phenyl groups in **597** enables phosphabenzene to accept more than one electron, thus yielding the radical trianion 597^{3-} . Its hyperfine data are listed in Table 9.11 [165, 181], along with those for the radical anions $80^{\cdot-}$, $82^{\cdot-}$, and $597^{\cdot-}$. Like the LUMO of pyridine, that of phosphabenzene has a shape similar to the MO ψ_{2+} of benzene, whereas the NLUMO resembles ψ_{2-} , with a node through the P atom and the center 4. Thus, in contrast to $80^{\cdot-}$, $82^{\cdot-}$, and $597^{\cdot-}$, which exhibit a large positive ^{31}P -coupling constant of ca +3 mT, the trianion 597^{3-} has an a_p value of -0.267 mT and, in the absence of high-spin population on the heavier P atom (Chapt. 5.2), its hyperfine pattern was readily analyzed with the use of ENDOR spectroscopy.

In general, replacement of a C-H(α) segment by S atoms gives rise to electron-rich π systems, which are very good donors, easily yielding the radical cations (Chapt. 9.3). Notable exceptions are some derivatives of thiophene such as 2,2'-dithienyl (**598**), thieno[3,2-*b*]thienophene (**599**), and [1,2]dithiolo[1,5-*b*][1,2]dithiolo (6a-thiathiophene; **600**), which are readily converted to their radical anions. Their hyperfine data are given in Table 9.12 [209, 977-979]; the *cis* and *trans* rotamers are distinguished for $598^{\cdot-}$. The non-bond resonance compound **600** is an 8-centered 10-electron π system [980].

Tab. 9.12. Hyperfine Data for Radical Anions of Some Derivatives of Thiophene

2,2'-Dithienyl <i>cis</i> -598 ⁻		H3,3' H4,4' H5,5'	-0.421 +0.077 -0.488	[977]
<i>trans</i> -598 ⁻		H3,3' H4,4' H5,5'	-0.401 +0.075 -0.476	[977]
Thieno[3,2- <i>b</i>]thiophene 599 ⁻		H2,5 H3,6	-0.487 +0.052	[978]
1,2-Dithio[1,5- <i>b</i>][1,2]-dithiole (6a-thiathiophthene) 600 ⁻		H2,5 H3,4	-0.672 -0.173	[979]
2,5-Dimethyl-3,4-trimethylene- 6a-thiathiophthene 124 ⁻		2H _{ax} (β) 2H _{eq} (β) H _{ax} (γ) H _{eq} (γ) 6H(β')	+0.302 +0.124 0.052 0.013 +0.660	[209, 979]



The radical anion **600**⁻ undergoes *cis* → *trans* isomerization and yields the radical anion 4*H*-thiapyran-4-thione as the final product (with a loss of one of the three S atoms) [979]. The isomerization is hindered by bridging the 3- and 4-positions with a trimethylene chain to form a six-membered ring, so that radical anions such as **124**⁻ are more persistent.

The g_e factor was reported for radical anions of only few aza-heterocycles; it is in the range 2.0030–2.0035 and thus slightly higher than those for the radical anions of conjugated hydrocarbons. The radical anions of phosphabenzenes have a g_e factor of 2.0047 ± 0.0001 , and that of the trianion **597**³⁻ (with a very small π -spin population at the P atom) is 2.0027, as it is for most hydrocarbon radical anions. The three S atoms in the radical anions of 6a-thiathiophthenes **600** and **124** increase the g_e factor to 2.0074–2.0080. All radical anions presented in Tables 9.8–9.12 were generated from the corresponding heterocyclic compounds by the two conventional methods, i.e., by reaction with an alkali metal in an ethereal solvent or in HMPT and/or by electrolytic reduction in liquid ammonia, DMF, or ACN. The trianion **597**³⁻ was produced by prolonged contact of its neutral precursor with potassium in DME.

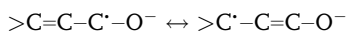
Radical Anions of Azoarenes

The radical anion of *trans*-azobenzene (*trans*-**102**), a 7,7'-diaz derivative of the isoelectronic stilbene (**101**), has been studied by ESR spectroscopy since the early 1960s, but analysis of its spectrum was complicated by line-broadening due to ¹⁴N-hyperfine anisotropy. Table 9.13 [551, 858, 981, 982] gives the hyperfine data for *trans*-**102**^{•−} and the radical anions of some azoarenes. All of these anions, except that of the cyclic 5*H*-dibenzo[*c,f*][1,2]diazepine (**602**), have the less sterically hindered *trans* configuration. Rapid *cis* → *trans* isomerization prevents *cis*-**102**^{•−} from being studied by ESR spectroscopy, in contrast to **101**^{•−}, for which both isomers could be characterized by their coupling constants (Table 8.12). The π system of *cis*-azobenzene is, however, contained in the essentially planar **602**. In *trans*-**102**^{•−}, as in *trans*- and *cis*-**101**^{•−}, rotation of the phenyl groups about the C–C linkage to the central double bond is not fast enough on the hyperfine time-scale to average the coupling constants of the *ortho* and *meta* protons. Also analogous to *trans*-**101**^{•−}, these protons were distinguished by investigations of the radical anions of *ortho*-substituted derivatives such as that of 2,2'-dimethylazobenzene (*trans*-**601**) in which the alkyl groups assume the less hindered positions. The π-spin distribution in the radical anions of azoarenes resemble that in their isoelectronic hydrocarbon counterparts (Table 8.12). The ¹⁴N-coupling constant for the acyclic radical anions generally decreases with increasing size of the aryl groups (from $a_N = +0.48$ for *trans*-**102**^{•−} to +0.32 mT for **605**^{•−}). It is lower than the corresponding value for the radical anions of azoalkanes ($a_N = +0.75$ to +0.95 mT; Table 7.19).

The g_e factor of *trans*-**102**^{•−} and *trans*-**601**^{•−} is 2.0035. The radical anions listed in Table 9.13 were generated by reaction of the neutral azoarenes with an alkali-metal in ethereal solvents. Their azo groups (similarly to these groups in azoalkanes) associate with counterions and their spectra also exhibit hyperfine splittings from the metal nuclei (Table A.2.2). Because azoarenes are better electron acceptors than their hydrocarbon counterparts, they readily form diamagnetic dianions, and the radical anions tend to disproportionate to the dianions and the neutral precursors (Chapts. 2.2 and 6.3).

Radical Anions of Aldehydes and Ketones (Ketyl Anions)

Hyperfine data for some of these radical anions are listed in Table 9.14 [213, 214, 218, 983–988]. As stated in Chapt. 7.1, the ketyl group is properly formulated as >C[•]–O[−], with the bulk of the π-spin population (ca 2/3) at the C atom. Deviation from planarity at this atom seems to play less of a role in the radical anions of conjugated aldehydes and ketones than in those of their alkyl counterparts, and the spin population is fully shared with the remaining π system. In the radical anions of enones and 2,5-dienones, such as **606**, **612–614** and **617**, a large part of the spin population is shifted to the π center next-but-one to the ketyl group:



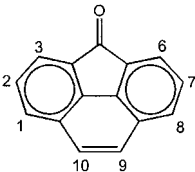
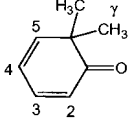
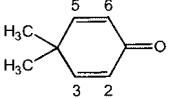
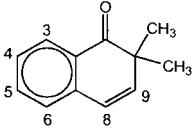
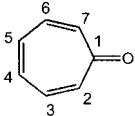
Tab. 9.13. Hyperfine Data for Radical Anions of Some Azoarenes

<i>trans</i> -Azobenzene <i>trans</i> -102 ^{•-}		¹⁴ N7,7'	+0.478	[551]
		H2,2'	-0.211	
		H3,3'	+0.062	
		H4,4'	-0.320	
		H5,5'	+0.089	
		H6,6'	-0.294	
<i>trans</i> -2,2'-Dimethylazobenzene <i>trans</i> -601 ^{•-}		¹⁴ N7,7'	+0.446	[551]
		H3,3'	+0.058	
		H4,4'	-0.321	
		H5,5'	+0.090	
		H6,6'	-0.297	
		6H(beta)	+0.151	
5 <i>H</i> -dibenzo[<i>c,f</i>][1,2] diazepine 602 ^{•-}		¹⁴ N7,7'	+0.664	[858]
		H2,2'	-0.234	
		H3,3'	+0.083	
		H4,4'	-0.305	
		H5,5'	+0.132	
		H _{ax} (beta)	0.132	
		H _{eq} (beta)	0.025	
1,1'-Azonaphthalene 603 ^{•-}		¹⁴ N9,9'	+0.444	[981]
		H2,2',4,4'	-0.24	
		H5,5',7,7'	-0.06	
2,2'-Azonaphthalene 604 ^{•-}		¹⁴ N9,9'	+0.485	[981]
		H1,1'	-0.285	
		H3,3',6,6'	-0.075	
		H8,8'	-0.075	
9,9'-Azoanthracene 605 ^{•-}		¹⁴ N11,11'	+0.320	[982]
		H2,2',4,4'	-0.095	
		H5,5',7,7'	-0.095	
		H9,9'	-0.370	

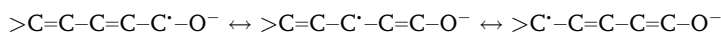
Tab. 9.14. Hyperfine Data for Radical Anions of Some Conjugated Aldehydes and Ketones

2,2,6,6-Tetramethyl-4-hepten-3-one 606 ⁻		H2 H3 9H(γ) 9H(γ')	<0.2 -1.167 0.039 0.027	[983]
Benzaldehyde 607 ⁻		H(α) H _o H _{o'} H _m H _{m'} H _p	-0.851 -0.469 -0.340 +0.131 +0.075 -0.647	[984]
Acetophenone 608 ⁻		H _o H _{o'} H _m H _{m'} H _p 3H(β)	-0.425 -0.379 +0.113 +0.091 -0.655 +0.674	[984]
Benzophenone 609 ⁻		4H _o 4H _m 2H _p 17O	-0.252 +0.082 -0.350 -0.818	[985] [986]
Diphenylcyclopropenone 611 ⁻		2H _o 2H _{o'} 2H _m 2H _{m'} 2H _p	-0.276 -0.311 +0.078 +0.096 -0.428	[213]
4,4,5,5-Tetramethylcyclopent-2-en-1-one 612 ⁻		H2 H3 6H(γ)	+0.045 -1.10 0.064	[987]
Cyclopentadienone 613 ⁻		H2,5 H3,4	-0.291 -0.527	[988]
Indene-1-one 614 ⁻		H2 H3 H4 H5 H6 H7	+0.020 -0.710 -0.115 -0.150 -0.204 -0.091	[988]
Fluorenone 114 ⁻		H1,8 H2,7 H3,6 H4,5 17O	-0.196 0.003 -0.308 +0.065 -0.921	[218] [986]

Tab. 9.14 (continued)

Phenanthrylene-4,5-ketone 615 ⁻		H1,8	-0.306	[218]
		H2,7	0.003	
		H3,6	-0.212	
		H9,10	0.010	
6,6-Dimethylcyclohexa-2,4-dien-1-one 616 ⁻		H2,4	+0.133	[987]
		H3	-0.808	
		H5	-0.940	
		6H(γ)	0.008	
4,4-Dimethylcyclohexa-2,5-dien-1-one 617 ⁻		H2,6	+0.114	[987]
		H3,5	-0.705	
2,3-Benzo-6,6-dimethylcyclohexa-2,4-dien-1-one 618 ⁻		H3	-0.120	[987]
		H4,8	+0.035	
		H5	-0.310	
		H6	+0.082	
		H9	-0.675	
Tropone 99 ⁻		H2,7	-0.867	[214]
		H3,6	+0.010	
		H4,5	-0.508	
		¹³ C1	-0.832	
		¹³ C2,7	+1.233	
		¹³ C3,6	-0.602	
¹³ C4,5	+0.454			

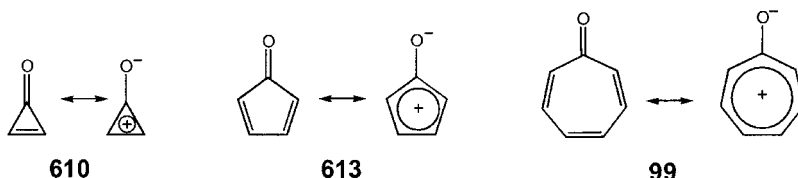
A similar part of spin population is also located at the terminal center of the ketyl anions of 2,4-dienones like **616**.



In the radical anions of benzaldehyde (**607**) and acetophenone (**608**), spin delocalization reduces the spin population at the ketyl-C atom to ca 1/3.

The π -spin distribution in the radical anions of fluorenone (**114**) and phenanthrene-4,5-ketone (**615**) resembles that in the benzophenone anion **609**⁻. However, in the radical anion of diphenylcyclopropanone (**611**), the SOMO has a vertical nodal plane through the ketyl group, so that the spin populations at the C centers are similar to those in the stilbene anions **101**⁻. The radical anion of cyclopropanone (**610**) itself is, to our knowledge, still unknown, but those of cyclopentadienone (**613**) and cycloheptatrienone (tropone; **99**) were studied by ESR spectroscopy (for the spectrum of **99**⁻ and its analysis, see Figure 6.11 and Chapt. 6.4). The positively charged π perimeters in the dipolar formulas of **610** and **99** comply with the Hückel $2 + 4m$ -rule (Chapt. 8.1), whereas that of **613** does not. Accordingly, **610** and **99**, which should be energetically favored are known, but **613**

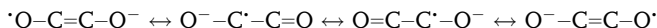
had not been isolated. However, because of the strained angles, **610** is stable only at low temperatures [989] so that solely **99** is an easily isolable compound.



The g_e factor of **611**^{•-}, with its SOMO having a node at the ketyl group, is 2.0026. Those of the remaining radical anions listed in Table 9.14 were not reported; they are expected to be in the same range, 2.0032–2.0035, as the corresponding values of the alkylketyl anions. Electrolytic reduction of conjugated aldehydes and ketones in DMF was the general method to produce their radical anions. The persistence of these ketyl anions required the absence of H atoms at the sp^3 -hybridized C atoms directly linked to the π system. The radical anions **614**^{•-}, **616**^{•-}, and **617**^{•-} were generated from the corresponding ketones in flowing DMSO containing *t*-BuOK, in which **613**^{•-} was prepared in situ from a bromo derivative of cyclopentadienone instead of from the nonisolable parent **613**.

Radical Anions of Dialdehydes and Diketones (Semidione and Semiquinone Anions)

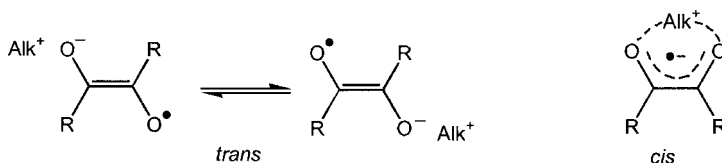
The simplest diketone is ethane-1,2-dione (glyoxal; **619**), a 4- π -center system. Its radical anion, the semidione **619**^{•-}, with 5 π electrons, can be formulated as



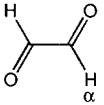
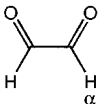
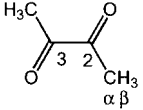
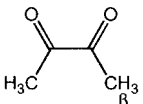
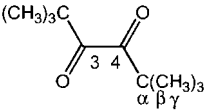
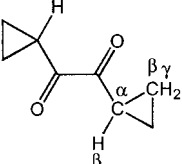
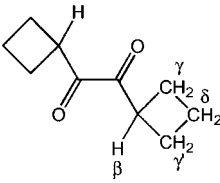
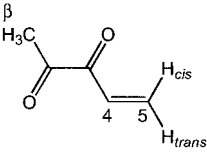
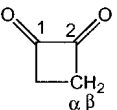
in which the π -spin populations at each of the two C and each of the two O atoms are ca +0.3 and +0.2, respectively.

Tables 9.15 [212, 459, 986, 990–998] and 9.16 [213, 614, 639, 999–1003] give hyperfine data for radical anions of some diones (semidione anions), for which early ESR studies were reviewed in 1968 [7c]. The π system of the dione is extended by conjugated double bonds in **624**^{•-}, **628**^{•-}, and **630**^{•-} and by phenyl and/or phenylene groups in **631**^{•-}–**635**^{•-}, **110**^{•-}, and **128**^{•-}.

The semidiones can exist in a *trans* and a *cis* form. Usually, the *trans*-form is preferred, particularly in the presence of bulky substituents such as *tert*-butyl groups in **621**^{•-}, for which only the *trans*-isomer was detected by ESR spectroscopy. The *cis*-form is favored by tight association with alkali-metal counterions (Alk^+), which are attached to both O atoms in a chelate-like fashion. The *cis*–*trans* equilibrium is thus very sensitive to ion pairing, which enhances the π -spin populations at the ketyl-C atoms at the expense of those at their O neighbors.



Tab. 9.15. Hyperfine data for Radical Anions of Some Alkanediones and Alkenediones

Ethan-1,2-dione (glyoxal) <i>trans</i> -619 ^{•-}		2H(α)	-0.76	[990]
<i>cis</i> -619 ^{•-}		2H(α)	-0.87	[991]
Butan-2,3-dione (biacetyl) <i>trans</i> -620 ^{•-}		6H(β) 13C2,3 213C(α)	+0.56 0.058 -0.45	[992] [993]
<i>cis</i> -620 ^{•-}		6H(β) 13C2,3 213C(α)	+0.70 0.114 -0.52	[992] [993]
2,2,5,5-Tetramethylhexan-3,4-dione <i>trans</i> -621 ^{•-}		18H(γ) 13C3,4 213C(α) 613C(β) 217O	0.029 0.14 -0.38 +0.243 -1.041	[994] [993] [986]
Dicyclopropylethan-1,2-dione 622 ^{•-}		2H(β) 4Hsyn(γ) 4Hanti(γ) 213C(α) 213C(β)	+0.057 0.020 0.037 -0.45 +0.81	[995] [993]
Dicyclobutylethan-1,2-dione 623 ^{•-}		2H(β) 4H(γ) 4H(γ') 4H(δ)	+0.222 0.045 0.023 0.08	[995]
Pent-4-ene-2,3-dione 624 ^{•-}		H4 H5trans H5cis 3H(β)	-0.125 -0.490 -0.500 +0.288	[995]
Cyclobutene-1,2-dione 625 ^{•-}		4H(β) 13C1,2 213C(α)	+1.395 0.14 -0.54	[996] [986]

Tab. 9.15 (continued)

Cyclopentane-1,2-dione 626 ⁻		4H(β) 2 ¹³ C(α)	+1.416 -0.56	[997] [986]
Cyclohexane-1,2-dione 627 ⁻		4H(β) 2 ¹³ C(α)	+0.982 -0.49	[997] [993]
Cyclohex-2-en-1,4-dione 628 ⁻		H2,3 4H(β)	-0.576 +0.236	[998]
Bicyclo[2.2.1]heptane-2,3-dione 72 ⁻		2H(β) 2H _{exo} (γ) 2H _{endo} (γ) H _{syn} (γ') H _{anti} (γ')	+0.249 +0.249 <0.01 0.036 +0.648	[459]
Bicyclo[2.2.1]hept-5-ene-2,3-dione 629 ⁻		2H(β) H5,6 H _{syn} (γ) H _{anti} (γ)	+0.110 0.073 0.210 +0.819	[459]
Spiro[5.5]undeca-1,4,6,9-tetraene-3,8-dione 630 ⁻		H1,5 H2,4 H6,10 H7,9	-0.762 +0.132 -0.087 +0.138	[212]

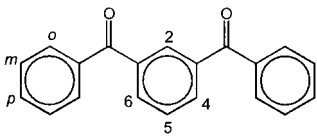
A paradigm for a tight ion pairing is the radical anion of *o*-dimesitylbenzene (**110**), for which alkali-metal nuclei in the associated counterions have very large coupling constants (Chapt. 6.6 and Table A.2.2). Long-range coupling with γ protons by W-plan interaction, which clearly differentiates between *syn*- and *anti*- as well as between *endo*- and *exo*-positions (Chapt. 4.2), is characteristic of the bicyclic semidiones **72**⁻ and **629**⁻. In the radical anion of the spiroundecatetraenedione **630**, the π -spin distribution resembles that in the ketyl anion **617**⁻ (Table 9.14), because the spin population is, on the hyperfine time-scale, largely localized in one moiety. A perturbation at one O atom by the counterion (Et₄N⁺) and/or by molecules of the solvent (DMF/ACN) is sufficient to bring about this localization.

When the C atoms of the two keto groups are parts of a fully conjugated cyclic π -system, like the hydrocarbons of which radical anions are considered in Chaps. 8.4–8.6, the diketone is called quinone. Its radical anion, denoted semiquinone,

Tab. 9.16. Hyperfine Data for Radical Anions of Some Phenyl-substituted Diones

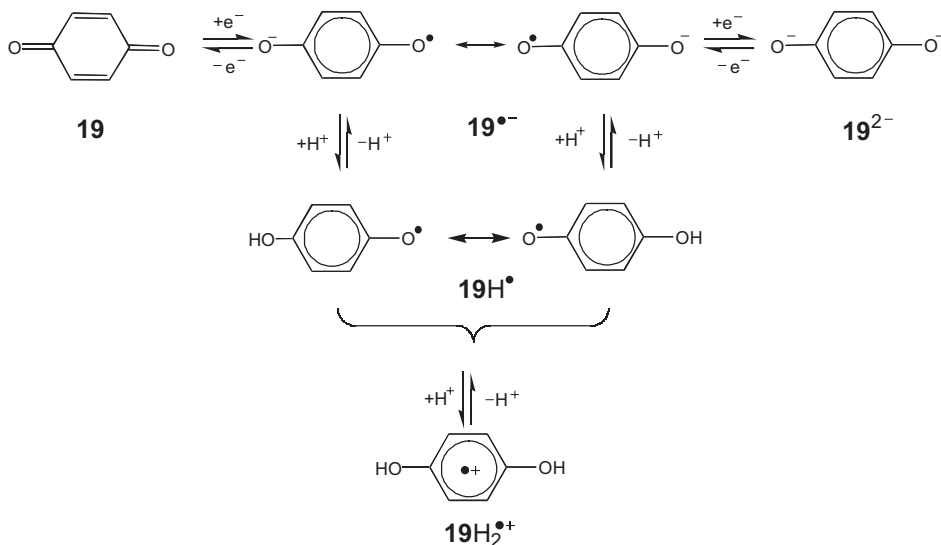
Phenylethane-1,2-dione <i>trans</i> -631 ^{•-}		H(α) 2H _o 2H _m H _p	-0.559 -0.134 +0.045 -0.152	[999]
<i>cis</i> -631 ^{•-}		H(α) 2H _o 2H _m H _p	-0.688 -0.150 +0.052 -0.170	[999]
Indane-1,2-dione 632 ^{•-}		H4 H5 H6 H7 2H(β)	-0.295 +0.056 -0.283 +0.073 +0.262	[1000]
Diphenylethane-1,2-dione (benzil) <i>trans</i> -633 ^{•-}		4H _o 4H _m 2H _p 2 ¹⁷ O	-0.100 +0.035 -0.111 -0.967	[213] [986]
<i>cis</i> -633 ^{•-}		4H _o 4H _m 2H _p	-0.109 ^a +0.047 -0.154	[1001]
1,2-Diformylbenzene (<i>o</i> -phthaldehyde) 634 ^{•-}		H(α) H(α') H3 H6 H4 H5	-0.462 -0.372 +0.049 +0.024 -0.291 -0.219	[639]
<i>o</i> -Dimesitylbenzene 110 ^{•-} (Mes = mesityl)		H4,5	-0.252	[614]
1,4-Diformylbenzene (Terephthaldehyde) <i>trans</i> -128 ^{•-}		2H(α) H2,5 H3,6	-0.395 -0.206 -0.072	[1002]
<i>cis</i> -128 ^{•-}		2H(α) H2,3 H5,6	-0.387 -0.154 -0.118	[1002]

Tab. 9.16 (continued)

<i>m</i> -Dibenzoylbenzene 635 ^{•-}		H2	+0.068	[1003]
		H4,6	-0.626	
		H5	+0.136	
		4H _o	-0.068	
		4H _m	+0.024	
		2 <i>p</i>	-0.096	

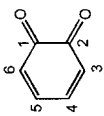
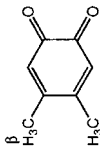

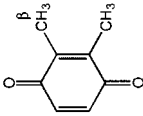
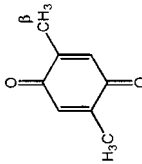
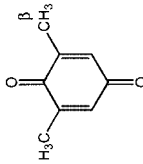
^a SnMe₃ complex

can be described by a formula in which the ketyl-O atoms are linked by single bonds to this hydrocarbon. Well-known examples are *p*-benzoquinone (**19**) and the corresponding semiquinone anion **19^{•-}**, which is an intermediate between **19** and the dianion **19²⁻**. Protonation of **19^{•-}** at one O atom yields the neutral 4-hydroxyphenoxyl radical **19H[•]** (\equiv **539[•]**) (Table 9.2), and addition of protons to both its O atoms leads to the radical cation **19H₂^{•+}** (\equiv **810^{•+}**) (Table 9.36).



Due to the presence of two electron-withdrawing keto groups, diones are better electron acceptors than aldehydes and ketones, which have only one such group. Incorporation of two keto groups into a conjugated cyclic π system enhances the tendency to take up additional electrons even more, so that quinones function as efficient acceptors in both chemistry and biology. Hyperfine data for some of their radical anions are listed in Tables 9.17 [986, 1004–1015] and 9.18 [148, 192, 567, 971, 1016–1025]. These semiquinone anions were readily generated by many methods (see below) and widely studied by ESR spectroscopy under various conditions, in particular **19^{•-}** and 9,10-anthrasemiquinone anion (**655^{•-}**). The extent of the pertinent spectra is rather narrow, because a large part of the π -spin population is accommodated by the keto group, of which nuclei do not contribute to the main

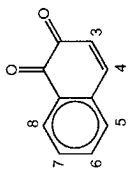
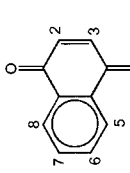
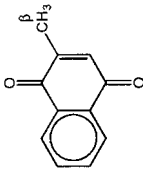
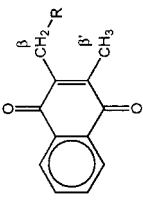
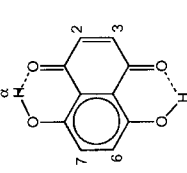
Tab. 9.17. Hyperfine Data for Radical Anions of Some Benzoquinones

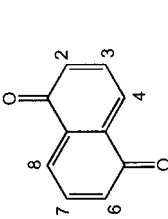
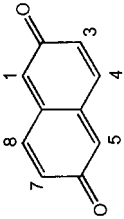
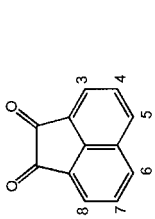
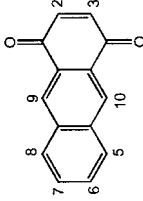
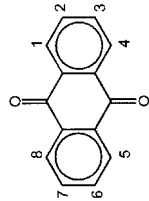
<i>o</i> -Benzoquinone 636 ⁻		H3,6 H4,5 ¹³ C1,2 ¹³ C3,6 ¹³ C4,5	+0.096 -0.350 -0.120 -0.216 +0.294	[1004]
4,5-Dimethyl- <i>o</i> -benzoquinone 637 ⁻		H3,6 6H(β)	+0.05 +0.42	[1005]
<i>p</i> -Benzoquinone 19 ⁻		H2,3,5,6 ¹³ C1,4 ¹³ C2,3,5,6 2 ¹⁷ O	DMSO Water -0.242 -0.236 -0.213 +0.024 -0.059 ^a -0.946 -0.870	[1006] [1007] [1008]
2,3-Dimethyl- <i>p</i> -benzoquinone 638 ⁻		H5,6 6H(β)	-0.262 +0.174	[1009]
2,5-Dimethyl- <i>p</i> -benzoquinone 639 ⁻		H3,6 6H(β)	-0.184 +0.232	[1009]
2,6-Dimethyl- <i>p</i> -benzoquinone 640 ⁻		H3,5 6H(β)	-0.193 +0.212	[1009]

2,3,5,6-Tetramethyl- <i>p</i> -benzoquinone (duroquinone) 641 ⁻		6H(β) } 6H(β') } 1 ³ C1,4 1 ³ C2,3,5,6 4 ^{1,3} C(α)	+0.190 { +0.291 ^a +0.093 ^b -0.107 -0.072 +0.138	[1010, 1011] [1010]
2,3,5,6-Tetrachloro- <i>p</i> -benzoquinone (chloranil) 642 ⁻		1 ³ C1,4 1 ³ C2,3,5,6 2 ¹⁷ O	-0.257; 0.48 0.28 -0.889 (DMF)	[1012, 1013] [986]
α -Tocopherol (vitamin E) quinone 643 ⁻		2H(β) } 3H(β') } 3H(β'') } 3H(β''') }	+0.091 +0.191	[1014]
Ubiquinone 644 ⁻	R = CH ₂ -C(OH)(CH ₃)[(CH ₂) ₅ CH(CH ₃) ₃]CH ₃ 	2H(β) 3H(β')	+0.102 +0.204	[1014]
Benzocyclobutane-1,2-dione 645 ⁻	R = C(CH ₃)(CH ₂) ₆ CH ₃ 	H3,6 H4,5	-0.374 -0.187	[1015]

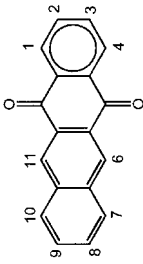
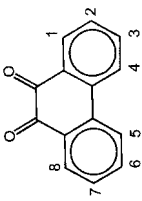
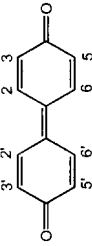
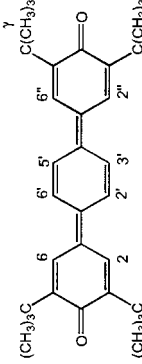
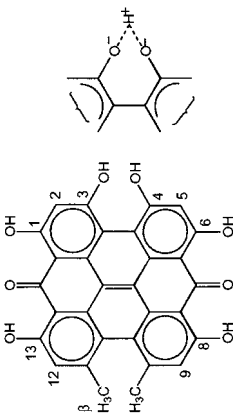
^a Aqueous alcohol^b Splitting for a tight ion pair

Tab. 9.18. Hyperfine Data for Radical Anions of Some Arenoquinones and Annulenoquinones

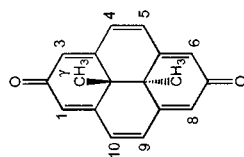
1,2-Naphthoquinone 646 ⁻		H3 H4 H5 H6 H7 H8	+0.042 -0.446 0.028 -0.142 0.014 -0.130	[1016]
1,4-Naphthoquinone 647 ⁻		H2,3 H5,8 H6,7 2 ¹⁷ O	-0.324 0.065 0.058 -0.858	[1016]
Menadiolone (vitamin K ₃ quinone) 648 ⁻		H3 H5 H6 H7 H8 3H(β)	-0.247 -0.048 -0.078 -0.056 -0.070 +0.291	[1014]
Phytonodione (vitamin K ₁ quinone) 649 ⁻		H5,8 H6,7 2H(β) 3H(β')	-0.052 -0.070 +0.127 +0.254	[1014]
5,8-Dihydroxy-1,4-naphthoquinone 650 ⁻		H2,3,6,7 2H(α)	-0.241 +0.052	[1017]

1,5-Naphthoquinone 651 ⁻		H2,6 H3,7 H4,8	-0.380 0.055 -0.525	[1018]
2,6-Naphthoquinone 652 ⁻		H1,4,5,8 H3,7	-0.425 0.130	[1018]
1,2-Acenaphthoquinone 653 ⁻		H3,8 H4,7 H5,6 2 ¹⁷ O	-0.118 +0.027 -0.128 -0.884	[1019] [986]
1,4-Anthraquinone 654 ⁻		H2,3 H5,6,7,8 H9,10	-0.26 0.04 0.11	[1020]
9,10-Anthraquinone 655 ⁻		H1,4,5,8 H2,3,6,7 ¹³ C1,4,5,8 ¹³ C2,3,6,7 2 ¹⁷ O	-0.055 -0.096 -0.137 0.070 -0.753	[567] [1021] [986]

Tab. 9.18 (continued)

5,12-Naphthacenequinone 656 ⁻		H1,4,8,9 H2,3 H6,11 H7,10	[1022]	-0.037 -0.111 -0.074 <0.01
9,10-Phenanthrenequinone 657 ⁻		H1,8 H2,7 H3,6 H4,5 2 ¹⁷ O	[1023]	-0.137 +0.022 -0.165 +0.042 -0.819
4,4'-Diphenoquinone 658 ⁻		H2,2',6,6' H3,3',5,5'	[971]	+0.053 -0.229
3,5,3'',5''-Tetra(<i>tert</i> -butyl)- <i>p</i> - terphenylquinone 659 ⁻		H2,2'',6,6'' H2',3',5',6'' 36H(γ)	[1024]	+0.019 -0.074 +0.004
Hypericin 660H ⁻ / 660 ²⁻		H2,5 H9,12 2H(1,6-O) 2H(8,13-O) 2H(3,4-O) 1H(3,4-O) 6H(β)	[192]	Anion/Conj.base -0.005/-0.05 -0.005/-0.094 -0.026/-0.027 -0.026/-0.017 -0.059 /+0.167 +0.119/+0.114
				660H ⁻ / 660 ²⁻

trans-10a,10b-Dimethyl-10a,10b-dihydrophenanthrene-2,7-dione
661⁻

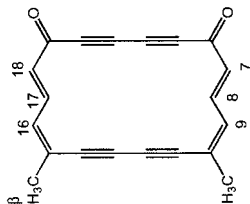


H1,3,6,8
H4,5,9,10
6H(γ)

0.022
-0.166
0.011

[148]

10,15-Dimethyl-2,3,4,5,11,12,13,14-octahydro[18]annulene-1,6-dione
662⁻

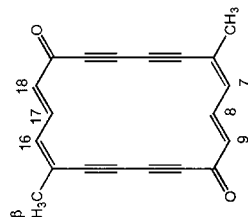


H7,9,16,18
H8,17
6H(β)

+0.034
-0.170
+0.198

[1025]

6,15-Dimethyl-2,3,4,5,11,12,13,14-octahydro[18]annulene-1,10-dione
663⁻

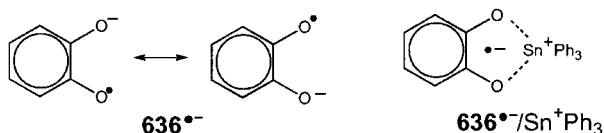


H7,16
H8,17
H9,18
6H(β)

+0.040
-0.156
+0.079
+0.198

[1025]

hyperfine pattern. In $19^{\cdot-}$, the calculated spin population on each of the two O atoms is +0.018, while the $\rho_{1,4}^{\pi}$ and $\rho_{2,3,5,6}^{\pi}$ values at each of the two and four C centers are ca +0.14 and +0.09, respectively [1008]. The spin distribution is sensitive to the solvent and counterion. The coupling constants of the α and β protons, and in particular, those of the ^{13}C and ^{17}O isotopes in the keto groups strongly depend on the solvent. For $19^{\cdot-}$ as an example, on going from DMSO to water, the coupling constant $a_{\text{C}_{1,4}}$ changes from -0.213 to $+0.024$ and the a_{O} value from -0.946 to -0.870 mT. This finding was interpreted in terms of complex formation between the solvent and the O-lone pairs, which alters the electronegativity of the O atoms and the π -spin distribution in the radical anion. In less polar solvents, association of the counterions with the O-lone pairs also has a strong effect on this distribution, especially for *ortho*-semiquinones. Thus, *o*-benzosemiquinone ($636^{\cdot-}$) forms chelate-like complexes not only with cations of alkali-metals (Table A.2.2) but also with those of other metals. Magnetic nuclei of these metals often give rise to large hyperfine splittings in ESR spectra (^{113}Sn : +1.013; ^{117}Sn : +0.968 mT [1026]).



The *p*-benzoquinone derivative, chloranil (**642**), in which the electron-acceptor properties are accentuated by the tetrachloro substitution, is used as an oxidizing agent in chemical reactions. As mentioned above, some quinones are also of biological relevance as electron acceptors, including the derivatives of *p*-benzoquinone, such as α -tocopherol (vitamin E quinone; **643**) and ubiquinone (**644**), or those of 1,4-naphthoquinone, such as menadione (vitamin K₃ quinone, **648**) and phytonadione (vitamin K₁ quinone, **649**). In addition, hypericin (**660H**), which contains a 4,4'-diphenylquinone π system, exhibits a vast range of pharmacological activities. The radical anion $660\text{H}^{\cdot-}$ had rather low persistence, even in neutral solution, and is rapidly converted to its conjugated base, the radical dianion $660^{\cdot 2-}$, in which one proton bridges the two 3,4-O atoms.

Radical anions of annulenediones larger than benzoquinones are also known. They are represented here by anions of the bridged [14]annulenedione **661** and the two isomeric octadehydro[18]annulenediones **662** and **663**.

The g_e factor of semidione, benzosemiquinone, and naphthosemiquinone anions is 2.0046–2.0052. It depends on the experimental conditions; e.g., that of $19^{\cdot-}$ is 2.0052 in DMSO but 2.0047 in water [1006]. For larger semiquinones, the g_e factor is lowered to 2.0037–2.0042.

Conversion of diones and quinones into their radical anions was readily carried out in solution by many methods. In addition to reaction with an alkali metal in an ethereal solvent and electrolytic reduction in DMF, ACN, DMSO, or their mixtures with water, less rigorous procedures have been used. Several semidione anions

were produced by treating an appropriate ketone precursor with *t*-BuOK in DMSO, or they formed spontaneously from the corresponding quinone in aqueous alkaline alcohol. Mild reagents, like glucose or zinc in DMF or alcohol, often sufficed to reduce larger quinones to their radical anions.

Radical Anions and Radical Trianions of Cyano-substituted Derivatives

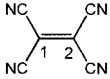
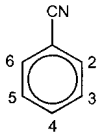
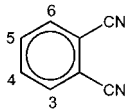
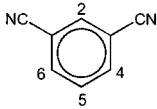
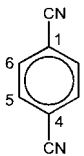
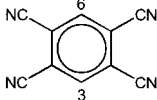
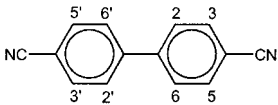
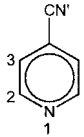
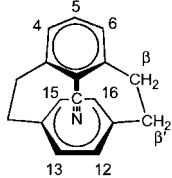
Hyperfine data for some of these radical anions are listed in Tables 9.19 [155, 206] and 9.20 [177, 207, 1027–1030]. The effect of the substitution by the electron-withdrawing cyano group on the degenerate LUMOs of benzene is similar to the replacement of the C–H(α) segment by an aza-N atom. This similarity is revealed by the coupling constants of the α protons in the radical anions of benzonitrile (**664**) and pyridine (**79**) ($a_{\text{H}4} = -0.842$ vs -0.970 mT), as well as in those of isophthalonitrile (**666**) and pyrimidine (**575**) ($a_{\text{H}4,6} = -0.829$ vs -0.978 mT) (Table 9.8). Accordingly, the shape of the SOMO at the proton-bearing C centers in **664**^{•−} and **667**^{•−} resembles the LUMO ψ_{2+} of the six-membered perimeter, but it is like ψ_{2-} at such centers in **665**^{•−}, **666**^{•−}, and **668**^{•−} (Chapt. 8.6 and Figure 8.9).

The steric effect of the rod-like cyano substituent is strikingly demonstrated by the hyperfine data for the radical anion of 8-cyano[2.2]metaparacyclophane (**671**), in comparison with those for the radical anion of the parent hydrocarbon **95** (Table 8.22). The two benzene rings in **671**^{•−} are forced into almost-parallel planes, with only slight interaction between their π systems. The π -spin population is localized in the *meta*-bridged ring bearing the electron-withdrawing cyano group, so that the spin distribution in this ring closely resembles that in the radical anion of benzonitrile (**664**).

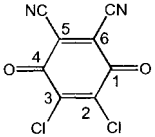
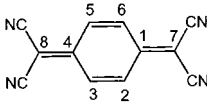
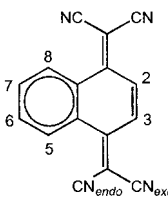
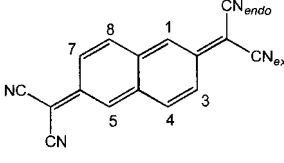
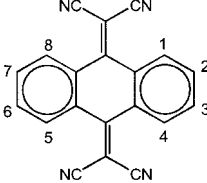
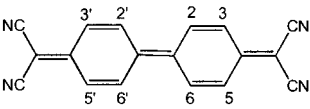
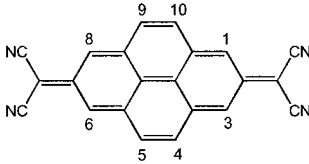
As an oxidizing agent in chemical reactions, 2,3-dichloro-5,6-dicyano-*p*-benzoquinone (DDQ; **672**) is even stronger than chloranil (**642**). Powerful electron acceptors are also obtained when the O atoms of quinones are replaced by C(CN)₂ groups to yield the corresponding tetracyanoquinodimethanes. It was mentioned in Chapt. 2.3 that the first-discovered “organic metal” is formed by the simplest of these compounds, 7,7,8,8-tetracyanobenzo-1,4-quinodimethane (TCNQ; **20**) with 1,4,5,8-tetrathia-1,4,5,8-tetrahydrofulvalene (TTF; **24**) as the electron donor.

Larger tetracyanoarenoquinodimethanes can readily be reduced, not only to the radical anions, but also (via the diamagnetic dianions) to the radical trianions. In the monoanions, the bulk of the π -spin population is located in the two C(CN)₂ groups, mostly at the two exocyclic C atoms, whereas in the radical trianions, each of the two C(CN)₂ groups bears negative charge but has no significant share in the spin distribution. The singly occupied orbitals in these trianions are NLUMOs and their shape at the arenediylidene moieties resembles that of the LUMOs, in the corresponding arenes. Thus the coupling constants of the α protons in **673**^{3−}, **674**^{3−}, and **677**^{3−} are comparable to those for the radical anions of these arenes (Table 8.8). In particular, the $a_{\text{H}1,3,6,7}$ and $a_{\text{H}4,5,9,10}$ values for the radical trianion of tetracyanopyreno-2,7-quinonodimethane (**677**), in which the SOMO has a node

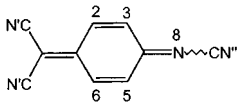
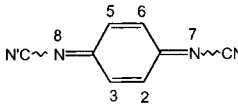
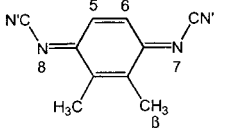
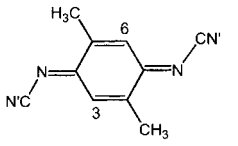
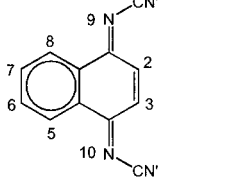
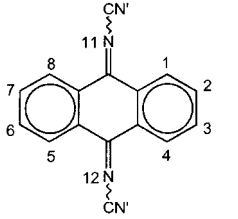
Tab. 9.19. Hyperfine Data for Radical Anions of Some Cyano Derivatives of Ethene, Benzene and Related Compounds

Tetracyanoethene (TCNE) 18^{•-}		4^{14}N $^{13}\text{C}_{1,2}$ $4^{13}\text{C}(\text{N})$	+0.157 +0.292 -0.945	[206]
Cyanobenzene (benzotrile) 664^{•-}		H _{2,6} H _{3,5} H ₄ ^{14}N $^{13}\text{C}(\text{N})$	-0.363 +0.030 -0.842 +0.215 -0.612	[206]
1,2-Dicyanobenzene (phthalonitrile) 665^{•-}		H _{3,6} H _{4,5} 2^{14}N	+0.042 -0.413 +0.159	[206]
1,3-Dicyanobenzene (isophthalonitrile) 666^{•-}		H ₂ H _{4,6} H ₅ 2^{14}N	+0.144 -0.829 <0.008 +0.102	[206]
1,4-Dicyanobenzene (terephthalonitrile) 667^{•-}		H _{2,3,4,5} 2^{14}N $^{13}\text{C}_{1,4}$ $^{13}\text{C}_{2,3,4,5}$ $2^{13}\text{C}(\text{N})$	-0.159 +0.181 +0.881 -0.198 -0.783	[206]
1,2,4,5-Tetracyano- benzene (pyromellitonitrile) 668^{•-}		H _{3,6} 4^{14}N	+0.111 +0.115	[206]
4,4'-Dicyanobiphenyl 669^{•-}		H _{2,2',6,6'} H _{3,3',5,5'} 2^{14}N	-0.181 0.029 +0.105	[206]
4-Cyanopyridine 670^{•-}		$^{14}\text{N}_1$ H _{2,6} H _{3,5} $^{14}\text{N}'$	+0.567 -0.140 -0.262 +0.233	[206]
8-Cyano-[2.2]metapara- cyclophane 671^{•-}		H _{4,6} H ₅ H _{12,13,15,16} 2H(β) 2H(β) 4H(β') ^{14}N	+0.047 -0.808 <0.01 +0.247 +0.159 0.022 +0.200	[155]

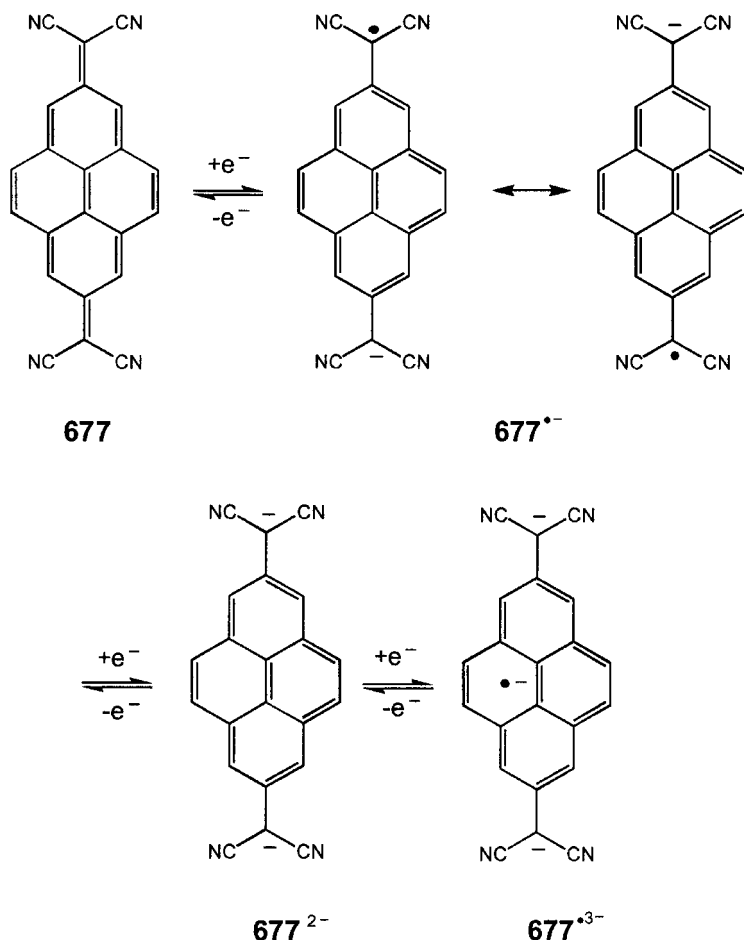
Tab. 9.20. Hyperfine Data for Radical Anions and Radical Trianions of Some Cyano Derivatives of *p*-Benzoquinone, Quinodimethanes, Quinomethane Imines and Quinone Diimines

2,3-Dichloro-5,6-dicyano- <i>p</i> -benzoquinone (DDQ) $672^{\cdot-}$		4^{14}N $^{13}\text{C}_{1,4}$ $^{13}\text{C}_{2,3}$ $2^{13}\text{C}(\text{N})$	Anion +0.057 -0.411 0.280 -0.458	[1027]
7,7,8,8-Tetracyano-benzo-1,4-quinodimethane (TCNQ) $20^{\cdot-}$		$\text{H}_{2,3,5,6}$ 4^{14}N $^{13}\text{C}_{1,4}$ $^{13}\text{C}_{2,3,5,6}$ $^{13}\text{C}_{7,8}$ $4^{13}\text{C}(\text{N})$	Anion -0.142 +0.099 -0.440 +0.062 +0.718 -0.638	[177] [207]
9,9,10,10-Tetracyano-naphtho-1,4-quinodimethane $673^{\cdot-}/673^{3-}$		$\text{H}_{2,3}$ $\text{H}_{5,8}$ $\text{H}_{6,7}$ $2^{14}\text{N}_{\text{exo}}$ $2^{14}\text{N}_{\text{endo}}$	Anion/Trianion -0.182/-0.163 0.040/-0.555 0.040/-0.163 +0.111/<0.03 +0.078/<0.03	[177]
9,9,10,10-Tetracyano-naphtho-2,6-quinodimethane $674^{\cdot-}/674^{3-}$		$\text{H}_{1,5}$ $\text{H}_{3,7}$ $\text{H}_{4,8}$ $2^{14}\text{N}_{\text{exo}}$ $2^{14}\text{N}_{\text{endo}}$	Anion/Trianion -0.259/-0.432 0.041/-0.390 -0.085/-0.432 +0.093/<0.015 +0.082/<0.015	[177]
11,11,12,12-Tetracyanoanthra-9,10-quinodimethane $675^{\cdot-}$		$\text{H}_{1,4,5,8}$ $\text{H}_{2,3,6,7}$ 4^{14}N	Anion -0.042 -0.070 +0.081	[1028]
7,7,7',7'-Tetracyano-dipheno-4,4'-quinodimethane $676^{\cdot-}$		$\text{H}_{2,2',6,6'}$ $\text{H}_{3,3',5,5'}$ 4^{14}N	Anion -0.033 -0.152 +0.082	[177]
11,11,12,12-Tetracyanopyreno-2,7-quinodimethane $677^{\cdot-}/677^{3-}$		$\text{H}_{1,3,6,8}$ $\text{H}_{4,5,9,10}$ 4^{14}N	Anion/Trianion -0.154/-0.487 0.018/-0.221 +0.088/<0.10	[177]

Tab. 9.20 (continued)

<i>N</i> ,7,7-Tricyanobenzo- 1,4-quinomethanimine 678 ⁻		H2,6 H3 H5 } ¹⁴ N8 2 ¹⁴ N', ¹⁴ N''	Anion -0.167 -0.167 -0.136 +0.395 +0.110	[1029]
<i>N</i> , <i>N</i> '-Dicyanobenzo- 1,4-quinone diimine 679 ⁻		H2,3,5,6 } ¹⁴ N7,8 2 ¹⁴ N'	Anion -0.201 (2H) -0.163 (2H) +0.442 +0.121	[1030]
<i>N</i> , <i>N</i> '-Dicyano-2,3- dimethylbenzo- 1,4-quinone diimine 680 ⁻		H5,6 6H(β) ¹⁴ N7,8 2 ¹⁴ N'	Anion -0.221 +0.107 +0.417 +0.115	[1030]
<i>N</i> , <i>N</i> '-Dicyano-2,5- dimethylbenzo- 1,4-quinone diimine 681 ⁻		H3,6 6H(β) ¹⁴ N7,8 2 ¹⁴ N'	Anion -0.138 +0.167 +0.405 +0.119	[1030]
<i>N</i> , <i>N</i> '-Dicyanonaphtho- 1,4-quinone diimine 682 ⁻		H2,3 H5,6,7,8 ¹⁴ N9,10 2 ¹⁴ N'	Anion -0.278 0.040 -0.382 +0.103	[1030]
<i>N</i> , <i>N</i> '-Dicyanoanthra- 9,10-quinone diimine 683 ⁻		H1,4,5,8 } H2,3,6,7 } ¹⁴ N11,12 2 ¹⁴ N'	Anion -0.052 (2H) -0.040 (2H) -0.085 (2H) -0.064 (2H) +0.321 +0.119	[1030]

at the centers 2 and 7, are almost identical to those for the radical anion of pyrene (**387**). The ESR spectra of **677**⁻ and **677**³⁻ in Figure 9.1 show how strikingly the hyperfine patterns of such radical monoanions and trianions differ. Whereas the spectrum of **677**⁻, like those of semiquinone anions, has an extent of only 1.0 mT, that of **677**³⁻ extends over 2.8 mT. The successive uptake of three additional electrons by **677** is schematically presented here:



Due to steric hindrance, the C(CN)₂ groups in tetracyanoquinodimethanes tend to twist out of coplanarity with the arene π system, which tendency is accentuated on going from the 1,4-benzo (20) to the 1,4-naphtho (673) and the 9,10-anthra (675) derivatives. The steric hindrance is alleviated in the corresponding *N,N'*-dicyanoquinone diimines, 679, 682, and 683, where the C(CN)₂ groups are replaced by NCN. The 1,4-benzo (679) and the 9,10-anthra (683) derivatives occur in *syn* and *anti* configurations which could not be distinguished for their radical anions 679^{•-} and 683^{•-}. Presumably, both configurations coexist on the hyperfine time-scale and give rise to identical coupling constants. However, the radical anions of 2,3-substituted dicyano-1,4-benzoquinone diimines, such as 680^{•-}, have the *syn* configuration, whereas the 2,5-substituted ones, like 681^{•-}, adopt the *anti* form. In contrast to 679^{•-} and 683^{•-}, the radical anion of dicyanonaphtho-1,4-quinone diimine (682) occurs only in the *syn* configuration.

With one C(CN)₂ and one NCN group, the tricyanoquinomethanimine 678 is a "hybrid" of 18 and 679. The tricyanoquinomethanimines and dicyanoquinone

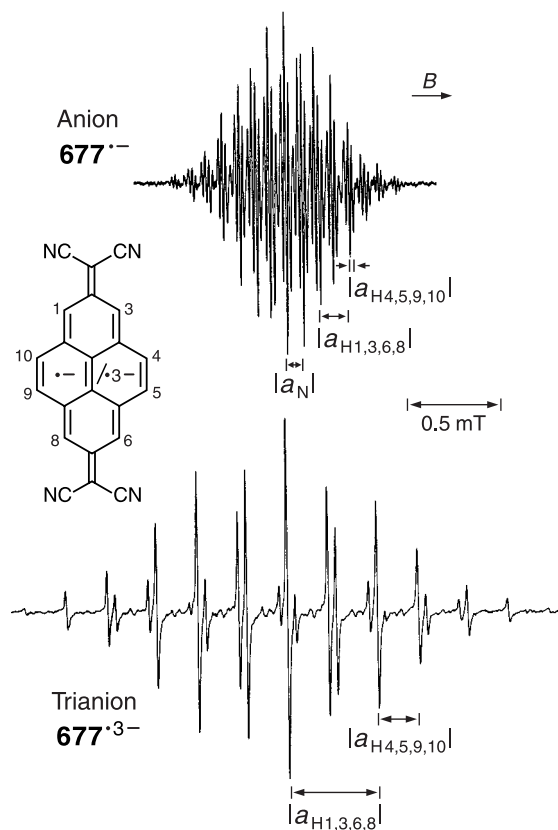


Fig. 9.1. ESR spectra of the radical anion and trianion of 11,11,12,12-tetracyanopyreno-2,7-quinodimethane (**677**). Top, anion **677**^{•-}; bottom, trianion **677**^{•3-}. Solvent DME, counterion K⁺; temperature 273 and 233 K for the anion the trianion, respectively. Reproduced by permission from [177].

diimines assume a position intermediate between the quinones and the tetracyanoquinodimethanes, and the unpaired electron in the radical anions increasingly favors these groups in the order O, NCN, C(CN)₂ at the expense of the arenediylidene moieties. Such a preference is indicated by the decreasing coupling constants of the four ring α protons in the radical anions of *p*-benzoquinone (**19**) and its analogues, the dicyanobenzoquinone dimine **679**, the tricyanobenzoquinomethanimine **678**, and the tetracyanobenzoquinodimethane **20**. The sum $\sum |a_{H_\mu}|$ for these four protons, 0.95, 0.73, 0.64, and 0.57 mT clearly diminishes in this sequence.

The g_e factor of the radical anions of cyano-substituted ethene, benzenes, biphenyl, and pyridine was not reported. They were generated by electrolytic reduction of the corresponding cyano derivatives in DMF, with the exception of **699**⁻, for which 4-amino- or 4-fluorobenzonitrile was the precursor (see reac-

tion scheme on p. 336). The g_e factors of the radical anion of DDQ (672) and of 8-cyano[2.2]metaparacyclophane (671) are 2.0052 and 2.0026, respectively. While 672 $^{\cdot-}$ can be formed from DDQ with any reducing agent, generation of 671 $^{\cdot-}$ from the neutral cyclophane was carried out electrolytically in DMF or by reaction with potassium in DME. The g_e factor is 2.0027 ± 0.0001 for the radical anions and trianions of tetracyanoquinodimethanes, 2.0032 for the radical anions of tricyanoquinomethanimines, and 2.0036 ± 0.0001 for those of dicyanoquinone diimines. Reaction of neutral precursors with potassium in an ethereal solvent or their electrolysis in DME was the usual method for generation of the radical anions and the trianion 673 $^{3-}$. Dihydro derivatives were the starting materials for producing 674 $^{\cdot-}$, 676 $^{\cdot-}$, and 677 $^{\cdot-}$, as well as 674 $^{3-}$ and 677 $^{3-}$. These derivatives were first deprotonated with *t*-BuOK to the dianions, which were subsequently oxidized with tris(4-bromophenyl)ammoniumyl hexachloroantimonate (“magic blue”) to the radical anions, or they were reduced with potassium to the radical trianions.

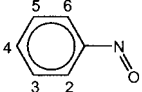
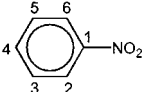
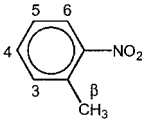
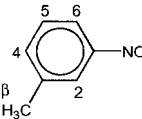
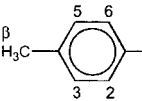
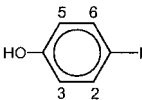
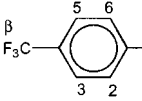
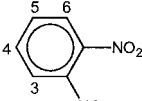
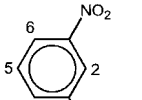
Radical Anions of Nitroso- and Nitro-substituted Derivatives

The electron-withdrawing property of the N=O group, with two electronegative heteroatoms, is further enhanced in the NO₂ group by the presence of an additional O atom (Chapt. 7.4). When linked to π systems, the nitro groups yield efficient electron acceptors that are very easily converted to their radical anions. The hyperfine data for some of them are listed in Tables 9.21 [196, 619, 620, 1031–1043] and 9.22 [1044–1051]. Their prototype, the radical anion of nitrobenzene (115), was widely investigated by ESR spectroscopy. The nitro group accommodates ca 2/3 of the spin population in the radical anion 115 $^{\cdot-}$, which can thus be considered a phenyl-substituted nitro-radical anion. Its ¹H- and ¹⁴N-coupling constants do not strongly differ from those for the radical anion of nitrosobenzene (35), also given in Table 9.20.

The coupling constant a_N for 115 $^{\cdot-}$, which is much smaller than the corresponding value (+2.2 to +2.4 mT) for the radical anions of nitroalkanes (Table 7.4), varies from +0.8 to +1.4 mT, because it strongly depends on the solvent and the temperature. The hyperfine data for 115 $^{\cdot-}$ in Table 9.21, like those for 35 $^{\cdot-}$, refer to DMF and 300 K. At this temperature, the coupling constant a_N , which is +0.971 mT for 115 $^{\cdot-}$ in DMF, increases to +1.387 mT with DMF/water (1:9) [1052], but decreases to +0.848 mT with HMPT [1053]; simultaneously, the a_{H4} value of –0.401 mT, changes to –0.355 and to –0.421 mT, respectively, but the ¹⁷O-coupling constant ($a_O = -0.884$) is only slightly affected.

To account for this effect, structural modifications of the nitro group must be considered, such as formation of H bonds with the solvent and pyramidalization at the N atom. (The latter structural feature has been invoked to rationalize increased coupling constants a_N for the radical anions of nitroalkanes relative to those for nitrosoalkanes; Chapt. 7.4). Linking to a π system should flatten the nitro group, and the extent of planarization may depend on the solvent and the temperature. The coupling constant a_N varies with the substituents at the phenyl moiety. As in phenylnitroxyl (550 $^{\cdot-}$; Table 9.5), electron-releasing substituents increase this value,

Tab. 9.21. Hyperfine Data for Radical Anions of Nitrosobenzene and Some Nitrobenzenes and Nitropyridines

Nitrosobenzene 35 ^{•-}		H2 H3,5 H4 H6 ¹⁴ N	-0.411 +0.103 -0.391 -0.302 +0.834	[1031]
Nitrobenzene 115 ^{•-}		H2,6 H3,5 H4 ¹⁴ N ¹³ C1 ¹³ C4 ¹⁷ O	-0.334 +0.106 -0.401 +0.971 -0.762 +0.595 -0.884	[620] [1032]
<i>o</i> -Nitrotoluene 684 ^{•-}		H3,5 H4 H6 3H(β) ¹⁴ N	+0.106 -0.387 -0.337 +0.324 +1.019	[1033]
<i>m</i> -Nitrotoluene 685 ^{•-}		H2,6 H4 H5 3H(β) ¹⁴ N	-0.339 -0.384 +0.109 -0.109 +1.07	[1034]
<i>p</i> -Nitrotoluene 686 ^{•-}		H2,6 H3,5 3H(β) ¹⁴ N	-0.340 +0.110 +0.394 +1.040	[1033]
<i>p</i> -Nitrophenol 687 ^{•-}		H2,6 H3,5 ¹⁴ N	-0.308 +0.073 +1.390	[1035]
4-Trifluoromethyl- nitrobenzene 688 ^{•-}		H2,6 H3,5 3 ¹⁹ F(β) ¹⁴ N	-0.313 +0.084 +0.905 +0.760	[1036]
1,2-Dinitrobenzene 689 ^{•-}		H3,6 H4,5 2 ¹⁴ N	+0.011 -0.172 +0.266	[196]
1,3-Dinitrobenzene 116 ^{•-}		H2 H4,6 H5 ¹⁴ N, ¹⁴ N'	-0.277 -0.450 +0.108 +0.397	[196]
		H2 H4 H6 H5 ¹⁴ N ¹⁴ N'	-0.330 ^a -0.445 -0.385 +0.110 +0.985 0.029	[619]

Tab. 9.21 (continued)

1,4-Dinitrobenzene 21 ⁻		H2,3,5,6 2 ¹⁴ N 13C1,4 4 ¹⁷ O	-0.114 +0.150 -0.236 -0.382	[1037] [1038]
2,3,5,6-Tetramethyl-1,4-dinitrobenzene (dinitrodurene) 127 ⁻		12H(β) 2 ¹⁴ N	+0.025 +0.698	[1039]
1,3,5-Trinitrobenzene 690 ⁻		H2,4,6 14N, 2 ¹⁴ N'	-0.421 +0.205	[1040]
		H2,6 H4 14N 2 ¹⁴ N'	-0.35 ^a -0.50 +0.825 +0.025	[1041]
4-Nitropyridine 691 ⁻		H2,6 H3,5 14N1 14N'	0.040 -0.302 +0.262 +0.886	[1042]
3,5-Dinitropyridine 692 ⁻		H2,6 H4 14N1 14N', 14N''	-0.485 -0.336 0.145 +0.352	[1043]
		H2 H4 H6 14N1 14N' 14N''	-0.353 ^a -0.363 -0.511 0.137 +0.882 0.027	[1043]

^aTight ion pair; spin localization on one nitrogen group.

and electron-withdrawing substituents decrease it. Thus, with DMF at 300 K, the coupling constants a_N are +1.390 and +0.760 mT for the radical anions of *p*-OH- (**687**) and *p*-CF₃-substituted nitrobenzene (**688**), respectively, as compared with the a_N value of +0.971 mT for **115**⁻.

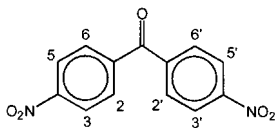
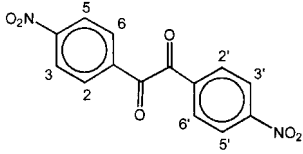
An increase in the spin population in the nitro group at the expense of that in the phenyl moiety can likewise be caused by twisting this group out of coplanarity with the benzene π system. A striking effect of such a twisting is demonstrated by the strongly differing coupling constants a_N for the radical anions of *p*-dinitrobenzene (**21**; +0.150 mT) and dinitrodurene (**127**; +0.698 mT).

The π -spin distribution in the radical anions of 4-nitro- (**691**) and 3,5-dinitropyridine (**692**) resembles that of their benzene counterparts **115**⁻ and **116**⁻, respectively, because it is governed by the position of the nitro groups rather than by aza-substitution.

Tab. 9.22. Hyperfine Data for Radical Anions of Some Nitro Derivatives of Arenes and Other Conjugated π -Systems

1,4-Dinitronaphthalene 693 ⁻		H2,3 H5,8 H6,7 2 ¹⁴ N	-0.169 -0.053 -0.041 +0.097	[1044]
1,5-Dinitronaphthalene 694 ⁻		H2,6 H3,7 H4,8 2 ¹⁴ N	-0.242 +0.044 -0.282 +0.230	[1044]
1,8-Dinitronaphthalene 695 ⁻		H2,7,4,5 H3,6 2 ¹⁴ N	-0.373 +0.100 +0.307	[1045]
1,4,5,8-Tetranitronaphthalene 696 ⁻		H2,3,6,7 4 ¹⁴ N	-0.149 +0.026	[1045]
9,10-Dinitroanthracene 697 ⁻		H1,4,5,8 H2,3,6,7 2 ¹⁴ N	-0.62 -0.43 +0.43	[1046]
2,2'-Dinitrobiphenyl 698 ⁻		H3,3' H4,4' H5,5' H6,6' 2 ¹⁴ N	-0.140 +0.023 -0.183 +0.035 +0.383	[1047]
4,4'-Dinitrobiphenyl 699 ⁻		H2,2',6,6' H3,3',5,5' 2 ¹⁴ N	-0.127 0.013 +0.304	[1048]
4,4'-Dinitrostilbene 700 ⁻		H2,2',6,6' H3,3',5,5' H7,7' 2 ¹⁴ N	<0.05 -0.24 -0.35 +0.12	[1049]
4,4'-Dinitrotolane 701 ⁻		H2,2',6,6' H3,3',5,5' 2 ¹⁴ N	<0.1 -0.131 +0.291	[1050]

Tab. 9.22 (continued)

4,4'-Dinitrobenzo- phenone 702 ^{•-}		H2,2',6,6' H3,3',5,5' 2 ¹⁴ N	<0.1 -0.094 +0.243	[1048]
4,4'-Dinitrobenzil 703 ^{•-}		H2,2',6,6' H3,3',5,5' 2 ¹⁴ N	<0.1 ^a -0.218 +0.482	[1051]

^a Presumably a dimer

When the radical anion has more than one nitro group, association with an alkali-metal counterion in a ethereal solvent leads (on the hyperfine time-scale) to localization of the spin population in a single group. Major examples of this localization are the radical anions of 1,3-dinitrobenzene (**116**) (Chapt. 6.6), 1,3,5-trinitrobenzene (**690**), and 3,5-dinitropyridine (**692**).

The coupling constant a_N is much smaller when the nitro group is linked to a larger π system having a higher electron affinity (EA) than benzene. In some of the pertinent radical anions, such as those of 1,8-dinitro- (**695**) and 1,4,5,8-tetranitronaphthalene (**696**), the nitro groups must be strongly twisted out of coplanarity with the naphthalene π system. Interestingly, the striking decrease in the a_N value on going from **695**^{•-} (+0.303 mT) to **696**^{•-} (+0.026 mT) runs parallel to that on passing from the radical anion of nitrobenzene (**115**) (+0.917 mT) to that of 1,4-dinitrobenzene (**21**) (+0.150 mT). In the radical anion of 2,2'-dinitrobiphenyl (**698**), the steric strain is relieved by twisting about the C-C bond between the two nitrophenylene moieties, so that the hyperfine data for **698**^{•-} approach half the corresponding values for **115**^{•-}.

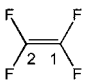
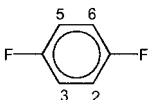

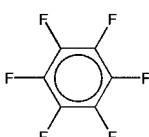
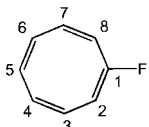
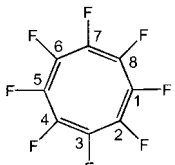
The g_e factors of **35**^{•-} and **115**^{•-} are also strongly dependent on the environment, as they vary from 2.0044 to 2.0054. Those of radical anions of other nitro derivatives also lie in this range.

Various procedures are appropriate for generation of **115**^{•-} and these radical anions. In addition to electrolysis of the neutral compounds in DMF, ACN, or DMSO (also in mixtures of these solvents with water) and their reduction with an alkali-metal in DME, THF, MTHF, or HMPT, some additional procedures have been used, such as their reaction with *t*-BuOK in DMSO.

Radical Anions of Fluoro- and Fluoroalkyl-substituted Derivatives

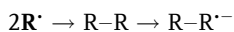
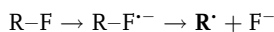
As stated in Chapt. 4.2, the coupling constant, a_{F_μ} , of the α -¹⁹F nucleus in a F atom directly attached to a π center μ is roughly proportional to the spin population at this center and has the same sign as ρ_μ^π (Eq. 4.30). The $|a_{F_\mu}|$ value should be 2–3 times larger than $|a_{H_\mu}|$ for an α proton when the ρ_μ^π values are comparable. However, this condition is rarely fulfilled upon a F/H replacement at the center μ ,

Tab. 9.23. Hyperfine Data for Radical Anions of Some Fluoro Derivatives of Ethene, Benzene and Cyclooctatetraene

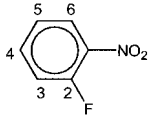
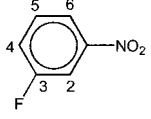
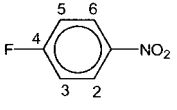
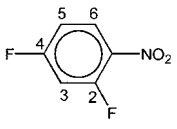
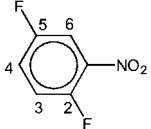
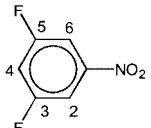
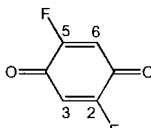
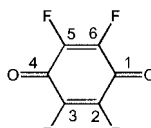
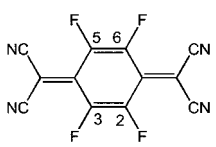
Tetrafluoroethene 704 ⁻		¹⁹ F1,1,2,2	+9.39	[1054]
1,4-Difluorobenzene 705 ⁻		H2,3,5,6 ¹⁹ F1,4	-0.530 0.175	[1055]
1,2,4,5-Tetrafluorobenzene 706 ⁻		H3,6 ¹⁹ F1,2,4,5	+0.780 +5.10	[1055]
Hexafluorobenzene 707 ⁻		¹⁹ F1-6 ¹³ C1-6	+13.7 +1.21	[1055, 1056]
Fluorocyclooctatetraene 708 ⁻		H3,5,7 H2,8 H4,6 ¹⁹ F1	-0.650 0.033 0.016 +1.301	[1057]
Octafluorocyclooctatetraene 709 ⁻		¹⁹ F1-8	+1.092	[1058]

because the fluoro substitution affects the π -spin distribution. This effect is not only inductively electron-withdrawing, in view of the high electronegativity of the F atom, but it is also conjugatively electron-releasing, due to the F-lone-electron pairs. In some derivatives, the fluoro substitution may also have a steric effect, because the F atom is larger than H. Thus, the ratio $|a_{F_\mu}|/|a_{H_\mu}|$ observed upon F/H replacement at the center μ varies considerably.

Tables 9.23 [1054–1058] and 9.24 [177, 986, 1012, 1059] give hyperfine data for radical anions of some fluoro derivatives of various π systems, which can be divided into two groups with respect to their generation. Fluoro derivatives of poor or moderate electron acceptors, like ethene and benzene, which require rather rigorous conditions for reduction, were converted into the radical anions in solid matrices, to prevent decomposition into a neutral radical and a fluoride anion.



Tab. 9.24. Hyperfine Data for Radical Anions of Some Fluoro Derivatives of Nitrobenzene, *p*-Benzoquinone and Tetracyanobenzoquinodimethane

2-Fluoronitrobenzene 710 ^{•-}		H3,5 H4 H6 ¹⁹ F2 ¹⁴ N	+0.101 -0.401 -0.347 +0.636 +0.982	[1059]
3-Fluoronitrobenzene 711 ^{•-}		H2 H4 H5 H6 ¹⁹ F3 ¹⁴ N	-0.337 -0.391 +0.101 -0.316 -0.292 +0.923	[1059]
4-Fluoronitrobenzene 712 ^{•-}		H2,6 H3,5 ¹⁹ F4 ¹⁴ N	-0.352 +0.114 +0.861 +0.995	[1059]
2,4-Difluoronitrobenzene 713 ^{•-}		H3,5 H6 ¹⁹ F2 ¹⁹ F4 ¹⁴ N	+0.111 -0.363 +0.640 +0.859 +0.981	[1059]
2,5-Difluoronitrobenzene 714 ^{•-}		H3 H4 H6 ¹⁹ F2 ¹⁹ F5 ¹⁴ N	+0.092 -0.419 -0.357 +0.624 -0.323 +0.844	[1059]
3,5-Difluoronitrobenzene 715 ^{•-}		H2,6 H4 ¹⁹ F3,5 ¹⁴ N	-0.326 -0.398 -0.273 +0.810	[1059]
2,5-Difluoro- <i>p</i> -benzoquinone 716 ^{•-}		H3,6 ¹⁹ F2,5	-0.141 +0.535	[1012]
2,3,5,6-Tetrafluoro- <i>p</i> - benzoquinone 717 ^{•-}		¹⁹ F2,3,5,6 ¹³ C1,4 ¹³ C2,3,5,6 ² 17O	+0.395 -0.219 -0.080 -0.953	[1012] [986]
7,7,8,8-tetracyano-2,3,5,6- tetrafluorobenzo-1,4- quinodimethane 718 ^{•-}		¹⁹ F2,3,5,6 4 ¹⁴ N	+0.153 +0.111	[177]

Thus, reduction of fluorobenzene ($R = \text{Ph}$) with an alkali metal in ethereal solution yields the radical anion of biphenyl (**94**; Table 8.11) [971]. However, such a reaction does not occur for the radical anions of fluoro derivatives of good electron acceptors like cyclooctatetraene, *p*-benzoquinone, tetracyanobenzoquinodimethane, and nitrobenzene, because these derivatives can be reduced by milder methods in fluid solution.

The ^1H - and ^{19}F -hyperfine data for the radical anion of 1,4-difluorobenzene (**705**) classify it as a π species. They are consistent with a SOMO similar to the LUMO ψ_{2-} of benzene (Figure 8.9), because the coupling constant, $a_{\text{H}2,3,5,6} = -0.530$ mT, is close to that of the radical anion of *p*-xylene (**487**; Table 8.18), and the relatively small $|a_{\text{F}1,4}|$ value of 0.175 is appropriate for ^{19}F nuclei in the vertical nodal plane of the LUMO. The overall effect of the fluoro substituents on the degenerate LUMOs, ψ_{2+} and ψ_{2-} , of benzene, which are occupied by one electron, is thus electron-releasing (case ① on p. 216). With larger number of these substituents at the benzene ring, there is a dramatic increase in the ^{19}F -coupling constants, which indicates transition to a σ structure: $a_{\text{F}1,2,4,5} = +5.10$ and $a_{\text{F}1-6} = +13.7$ mT for the radical anions of 1,2,4,5-tetra- and hexafluorobenzene (**706** and **707**, respectively). The structure of these species is still open to discussion, as is also true for the radical anion of tetrafluoroethene (**704**) ($a_{\text{F}} = +9.39$ mT).

It is noteworthy that radical anions of σ -structure with the spin population delocalized over the entire molecule were also obtained from formally saturated perfluorocycloalkanes [1060, 1061]. Their ESR spectra exhibit very large coupling constants which are due to all equivalent ^{19}F nuclei and decrease regularly with the growing size of the ring ($a_{\text{F}} = +19.8$, $+14.8$, and $+11.5$ mT for the six, eight, and ten ^{19}F nuclei in the radical anions of perfluorocyclopropane, perfluorocyclobutane, and perfluorocyclopentane, respectively).

The structure when good electron acceptors are fluoro-substituted is less problematic; their radical anions are all π species. The SOMO in the radical anion of fluorocyclooctatetraene (**708**) resembles the NBMO ψ_{2-} of the eight-membered π perimeter (Figure 8.9), and the large π -spin populations at the odd-membered centers are again in line with an overall electron-releasing effect of the fluoro substituent on the degenerate NBMOs, ψ_{2+} and ψ_{2-} , of planar cyclooctatetraene which are occupied by three electrons (case ② on p. 216). π -Structure is also indicated for the radical anion of octafluorocyclooctatetraene (**709**). Although the π -spin distribution in **710** $^{\cdot-}$ –**718** $^{\cdot-}$, the radical anions of fluoro substituted derivatives of nitrobenzene, *p*-benzoquinone, and tetracyanoquinodimethane, is governed by the strongly electron-withdrawing NO_2 , $\text{C}=\text{O}$, and $\text{C}(\text{CN})_2$ groups, the ratio $|a_{\text{F}_i}|/|a_{\text{H}_i}|$ depends sensitively on the position of substitution (a_{H_i} is here the coupling constant of the corresponding α proton in the unsubstituted radical anion). In this respect, the radical anions of mono- and difluoronitrobenzenes (**710**–**715**) provide a complete set for analysis. This ratio is 1.9, 2.5–3.0, and 2.1, respectively for the *ortho*-, *meta*-, and *para*-fluoro substituents of nitrobenzene (**115**; Table 9.21). The analogous ratio is 1.7 for the 2,5-difluoro (**716**) and 2.3 for the tetrafluoro (**717**) derivative of the radical anion of *p*-benzoquinone (**19**; Table 9.17), and it is as low as 1.1 for that the tetrafluoro derivative (**718**) of TCNQ (**20**; Table 9.20).

The g_e factor of the π -radical anions **704** \cdot^- and **706** \cdot^- is 2.0030 ± 0.0002 , that of **707** \cdot^- , presumably a σ -radical anion, is 2.0015. These radical anions were produced by high-energy irradiation of the neutral compounds in matrices, namely, by γ -rays in frozen methylcyclohexane- d_{14} (**704** \cdot^-) or by X-rays in solid adamantane doped with Me_3NBH_3 (**705** \cdot^- –**707** \cdot^-). The g_e factors of **708** \cdot^- and **710** \cdot^- –**717** \cdot^- were not reported; those of **710** \cdot^- –**717** \cdot^- should lie in the same ranges as those of non-fluorinated species of the same class, 2.0044–2.0054, and 20046–2.0052 for the radical anions of nitrobenzenes, and *p*-benzoquinones, respectively. A g_e factor of 2.0029 was measured for **718** \cdot^- . γ -Irradiation was used to produce the radical anions of perfluorocycloalkanes in neopentane or tetramethylsilane matrices ($g_e = 2.0024$ to 2.0031) and that of octafluorocyclooctatetraene (**709**) in a MTHF matrix ($g_e = 2.0049$). The radical anions **710** \cdot^- –**718** \cdot^- were generated electrolytically from the neutral compounds in various solvents, such as HMPT, DME, ACN, or DMF.

The effect of the trifluoromethyl and difluoromethylene substituents on the π system is strongly electron-withdrawing. Relatively few radical anions of this class of compounds have been studied by ESR spectroscopy. Hyperfine data for some of them are listed in Table 9.25 [193, 1062, 1063]. Those for the radical anions of the three isomeric trifluoromethylnitrobenzenes **719**, **720**, and **688** should be compared with the corresponding data for their nitrotoluene counterparts **684** \cdot^- –**686** \cdot^- (the coupling constants for the radical anion, **688** \cdot^- , of 4-trifluoromethylnitrobenzene are given in Table 9.21, along with the data of **684** \cdot^- –**686** \cdot^-). Whereas the π -spin distribution in the nitrobenzene radical anion **115** \cdot^- is only slightly affected by methyl substitution (the coupling constant a_N of +0.971 for **115** \cdot^- in DMF is increased to $+1.04 \pm 0.03$ mT for **684** \cdot^- –**686** \cdot^-), such distribution is substantially altered by introduction of trifluoromethyl groups, especially in the *ortho* and *para* positions, as the a_N value decreases to +0.767, +0.873, and +0.760 mT for **719** \cdot^- , **720** \cdot^- , and **688** \cdot^- , respectively. The ratios $|a_F(\beta)|/|a_H(\beta)|$ (i.e., 3.0, 1.2, and 2.3) of the ^{19}F -coupling constants for these radical anions relative to the corresponding values of the methyl protons in **684** \cdot^- –**686** \cdot^- reflect their dependence on the position of substitution, due to an interplay of the electronic (*ortho* and *para* vs *meta*) and the steric (*meta* and *para* vs *ortho*) effects.

Substitution by the electron-withdrawing difluoromethylene groups drastically enhances the electron-acceptor property of cyclooctatetraene (**64**) in its tetrakis(perfluorocycloalka) derivatives **721** and **722**, and that of [2.2]paracyclophane (**118**) in its 1,1,2,2,9,9,10,10-octafluoro derivative **723**. In particular, tetrakis(perfluorocyclobuta)cyclooctatetraene (**721**), which (in contrast to **64**) is planar already in the neutral form, represents one of the most powerful oxidants known, because it is reduced to its radical anion **721** \cdot^- and dianion **721** $^{2-}$ at positive potentials vs the saturated calomel electrode. The ^{19}F -coupling constants $a_F(\beta)$ for **721** \cdot^- and the radical anion of its cyclopenta analogue (**722**) are +0.320 and +0.956 mT (averaged values), respectively, with no proton counterparts for comparison. The smaller value for **721** \cdot^- is presumably due to the 1,3-interaction in the annelated four-membered rings. Replacement of the two weakly electron-releasing dimethylene bridging groups in **118** \cdot^- by the strongly electron-

Tab. 9.25. Hyperfine Data for Radical Anions of Some Trifluoromethylnitrobenzenes, Tetrakis(perfluorocycloalka)cyclooctatetraenes and 1,1,2,2,9,9,10,10-Octafluoro[2.2]paracyclophane

2-Trifluoromethylnitrobenzene 719⁻		H3 H4 H5 H6 $3^{19}\text{F}(\beta)$ ^{14}N	+0.087 -0.436 +0.126 -0.306 +0.964 +0.767	[1062]
3-Trifluoromethylnitrobenzene 720⁻		H2,6 H4 H5 $3^{19}\text{F}(\beta)$ ^{14}N	-0.327 -0.403 +0.101 -0.128 +0.873	[1062]
Tetrakis(perfluorocyclobuta)- cyclooctatetraene 721⁻		$16^{19}\text{F}(\beta)$ $^{13}\text{C}1-8$ $8^{13}\text{C}(\alpha)$	+0.315 +0.135 -0.191	[193]
Tetrakis(perfluorocyclopenta)- cyclooctatetraene 722⁻		$8^{19}\text{F}(\beta)$ $8^{19}\text{F}(\beta)$ $4^{19}\text{F}(\gamma)$ $4^{19}\text{F}(\gamma)$	+0.976 +0.935 0.090 0.059	[193]
1,1,2,2,9,9,10,10- Octafluoro[2.2]- paracyclophane 723⁻		H4,5,7,8,12,13,15,16 $8^{19}\text{F}(\beta)$	<0.10 +3.35	[1063]

withdrawing bis(difluoromethyl) groups in **723⁻** leads to a change in the SOMO that can no longer be considered a combination of two benzene-LUMOs ψ_{2-} , but must be regarded as a combination of their partners ψ_{2+} (Figure 8.9). Consequently, on going from **118⁻** to **723⁻**, the coupling constant $a_{\text{H}}(\alpha)$ of the eight protons at the benzene rings decreases from -0.297 mT to an (absolute) value smaller than 0.1 mT, and the coupling constant, $a_{\text{H}}(\beta) = +0.103$, of the eight methylene protons is replaced by the value, $a_{\text{F}}(\beta) = +3.35$ mT, of eight ^{19}F nuclei.

The g_e factors of the trifluoromethylnitrobenzene radical anions **719⁻**, **720⁻**, and **688⁻** were not reported; they also should lie in the range 2.0044 – 2.0054 . Those of the radical anions of tetrakis(perfluorocycloalka)cyclooctatetraenes are rather unusual, being 2.0010 for **721⁻** and 2.0021 for **722⁻**. No g_e value was given for **723⁻**. The radical anions were generated from the neutral compounds electrocyclically (**688⁻**, **719⁻**, **720⁻**, and **723⁻**), or they were produced by reaction with

potassium ($721^{\cdot-}$ and $722^{\cdot-}$). For $721^{\cdot-}$, radical-anion formation was also observed merely by shaking the DME solution of the neutral compound with mercury.

Radical Anions of Trimethylsilyl-substituted Derivatives

Hyperfine data for radical anions of some of these derivatives and of dimethylphenylphosphine are listed in Tables 9.26 [1064–1066] and 9.27 [734, 1067, 1068]. Because the Si atom is more electropositive than the C atom, the inductive effect of the trimethylsilyl substituent on a π system should be more strongly electron-releasing than that of the *tert*-butyl group. However, π -spin distribution in the radical anion of trimethylsilyl derivatives of benzene clearly indicates that, in contrast to an alkyl group, the overall effect of this substituent is electron-withdrawing. Thus, in the mono- and 1,4-disubstituted radical anions $726^{\cdot-}$ and $729^{\cdot-}$, the SOMO resembles the LUMO ψ_{2+} of benzene, but in the 1,2- and 1,3-disubstituted derivatives $727^{\cdot-}$ and $728^{\cdot-}$, it is like ψ_{2-} (Figure 8.9) (case ③ on p. 216). The electron-withdrawing effect of the trimethylsilyl group has been interpreted in terms of electron delocalization from the π system into the vacant Si-3d-AO of proper symmetry. Such an effect is also indicated for the dimethylphosphinyl substituent, in which replacing Si by P as the heteroatom has the same effect, because the coupling constants, a_{H_μ} , of the phenyl protons in $726^{\cdot-}$ and in the radical anion of dimethylphenylphosphine (733) are similar.

Surprisingly, the $|a_{\text{Si}_\mu}|$ values for trimethylsilyl substituents do not greatly differ from their α -proton counterparts $|a_{\text{H}_\mu}|$ at centers μ of comparable π -spin populations. Analysis of the hyperfine data for $724^{\cdot-}$ – $732^{\cdot-}$ [474] suggests that the coupling constants a_{Si_μ} are roughly proportional to the ρ_μ^π values at the substituted centers μ (Eq. 4.32), a relation that is analogous to the McConnell equation (Eq. 4.5) for the α protons. Because the ρ_μ^π values are positive in all the pertinent radical anions, the parameter $(Q_{\text{Si}}^{\text{C}_\mu\text{Si}_\mu})_{\text{eff}}$ in Eq. 4.32 has the same sign as the coupling constant a_{Si_μ} . The g_n factor of the ^{29}Si isotope is negative, and so presumably are the coupling constants a_{Si_μ} for $724^{\cdot-}$ – $732^{\cdot-}$ and the parameter $Q_{\text{Si}}^{\text{C}_\mu\text{Si}_\mu}$.

Spin delocalization into a trimethylsilyl substituent is enhanced when N is the substituted atom, probably due to the presence of the N-electron-lone pair. Thus, the coupling constant a_{N} (+0.625 mT) for the radical anion of bis(trimethylsilyl)diimine (737) is considerably smaller than the corresponding value (+0.824 mT) for $268^{\cdot-}$ with two *tert*-butyl instead of trimethylsilyl groups (Table 7.19). Due to the electron-withdrawing effect of the trimethylsilyl substituent, *N,N'*-bis(trimethylsilyl)aniline (739) and *N,N,N',N'*-tetrakis(trimethylsilyl)-*p*-phenylenediamine (740) can be reduced to their radical anions, whereas the corresponding dimethylamino-substituted benzenes are typical electron donors, yielding radical cations such as “Wurster’s blue” ($17^{\cdot+}$). The overall effect of the entire bis(trimethylsilyl)amino group on the benzene π system is, however, still electron-releasing, so that the coupling constants of the ring α protons in $739^{\cdot-}$ and $740^{\cdot-}$ are close to the corresponding values for the radical anions of toluene (477) and *p*-xylene (487) (Table 8.18). This means that the SOMO

Tab. 9.26. Hyperfine Data for Radical Anions of Some Trimethylsilyl-substituted Conjugated Hydrocarbons and of Dimethylphenylphosphine

<i>trans</i> -1,2-Bis(trimethylsilyl)-ethane 724 ⁻		H1,2 18H(γ) 2 ²⁹ Si 1 ¹³ C1,2	-0.749 0.036 -0.672 +0.56	[1064]
<i>trans</i> -1,4-Bis(trimethylsilyl)-buta-1,3-diene 725 ⁻		H1,4 H2,3 18H(γ) 2 ²⁹ Si	-0.671 -0.322 0.024 -0.573	[1064]
Trimethylsilylbenzene 726 ⁻		H2,6 H3,5 H4 9H(γ) 2 ²⁹ Si	-0.265 +0.106 -0.809 0.026 -0.518	[1064]
1,2-Bis(trimethylsilyl)benzene 727 ⁻		H3,6 H4,5 18H(γ) 2 ²⁹ Si	+0.046 -0.523 0.023 -0.448	[1064]
1,3-Bis(trimethylsilyl)benzene 728 ⁻		H2 H4,6 H5 18H(γ) 2 ²⁹ Si 1 ¹³ C4,6 1 ¹³ C5	+0.030 -0.694 +0.066 0.016 -0.406 +0.93 -0.93	[1064]
1,4-Bis(trimethylsilyl)benzene 729 ⁻		H2,3,5,6 18H(γ) 2 ²⁹ Si	-0.176 0.027 -0.617	[1064, 1065]
1,4-Bis(trimethylsilyl)-naphthalene 730 ⁻		H2,3 H5,8 H6,7 2 ²⁹ Si	-0.231 -0.319 -0.141 -0.463	[1064]
1,5-Bis(trimethylsilyl)-naphthalene 731 ⁻		H2,6 H3,7 H4,8 2 ²⁹ Si	-0.212 -0.166 -0.470 -0.353	[1064]
2,5-Bis(trimethylsilyl)-naphthalene 732 ⁻		H1,5 H3,7 H4,8 2 ²⁹ Si	-0.461 0.022 -0.449 -0.267	[1064]

Tab. 9.26. (continued)

Dimethylphenylphosphine 733 ⁻		H2,6	-0.331	[1066]
		H3,5	+0.039	
		H4	-0.906	
		6H(γ)	0.078	
		¹⁹ P	+0.828	

Tab. 9.27. Hyperfine Data for Radical Anions of Some Trimethylsilyl-substituted Hetero- π -Systems

Trimethylsilyl- <i>p</i> -benzoquinone 734 ⁻		H3	-0.268	[1067]
		H5	-0.210	
		H6	-0.252	
		9H(γ)	<0.01	
		²⁹ Si	-0.182	
2,5-Bis(trimethylsilyl)- <i>p</i> -benzoquinone 735 ⁻		H3,6	-0.279	[1067]
		9H(γ)	<0.01	
		²⁹ Si	-0.151	
Trimethylsilylphenylketone 736 ⁻		H2	-0.428	[1067]
		H3,5	+0.102	
		H4	-0.525	
		H6	-0.315	
		9H(γ)	0.013	
		²⁹ Si	-0.834	
Bis(trimethylsilyl)diimine 737 ⁻		18H(γ)	<0.01	[734]
		² ¹⁴ N	+0.625	
		²⁹ Si	-0.70	
<i>N,N'</i> -Bis(trimethylsilyl)- <i>p</i> -benzoquinomethane diimide 738 ⁻		H2,3,5,6	-0.200	[1067, 1068]
		18H(γ)	≤ 0.008	
		² ¹⁴ N	+0.402	
		²⁹ Si	-0.386	
		¹³ C _{2,3,5,6}	+0.160	
<i>N,N</i> -Bis(trimethylsilyl)aniline 739 ⁻		H2,6	-0.51	[1067, 1068]
		H3,5	-0.57	
		H4	≤ 0.05	
		9H(γ)	≤ 0.01	
		¹⁴ N	≤ 0.05	
<i>N,N,N',N'</i> -Tetrakis(trimethylsilyl)- <i>p</i> -phenylene diamine 740 ⁻		H2,3,5,6	-0.543	[1068]
		36H(γ)	≤ 0.1	
		² ¹⁴ N	≤ 0.05	

of $739^{\cdot-}$ and $740^{\cdot-}$ is similar to the LUMO ψ_{2-} of benzene because of a vertical nodal plane passing through the substituted C centers and the N atoms (Figure 8.9).

The g_e factors of $724^{\cdot-}$ – $740^{\cdot-}$ were not reported. These radical anions were generated by electrolytic reduction in DMF and/or by reaction with potassium or sodium in DME or THF.

Radical Anions of Heteroatom-bridged [n]Annulenes

Table 9.28 [149, 150, 160, 164, 1069, 1070] gives hyperfine data for some of these radical anions which are structurally related to the radical anions of [n]annulenes bridged by alkylidene groups (Table 8.20). The methano group bridging the [10]annulene in **85** is replaced by an imino and an oxido bridge in **741** and **742**, respectively. Analogously, the alkylidene groups bridging the [14]annulene in **497**–**499** and **97** are substituted by dimino bridges in **743**, **744**, and **32** and by oxido bridges in **745**. As indicated by the coupling constants of the perimeter protons in the radical anions, the imido and oxido bridging groups also have an electron-releasing effect on the π -MOs. Thus, the SOMOs of $741^{\cdot-}$ and $742^{\cdot-}$, like that of $85^{\cdot-}$, is similar to the LUMO ψ_{2-} of the naphthalene-like 10-membered perimeter (Figure 8.11), but in $743^{\cdot-}$ – $745^{\cdot-}$ and $32^{\cdot-}$, as in $497^{\cdot-}$ – $499^{\cdot-}$ and $97^{\cdot-}$, the SOMO resembles the LUMO ψ_{3+} of the anthracene-like 14-membered perimeter (Figure 8.12).

The sum $\sum |a_{\text{H}_i}|$ for the perimeter protons is a measure of the deviation of the perimeter from planarity (Chapt. 8.6). This sum increases on going from $85^{\cdot-}$ (1.12) to $741^{\cdot-}$ (1.31) and $742^{\cdot-}$ (1.54 mT), indicating a decrease in deviations from planarity by replacement of the methano by the more flexible imino and oxido groups bridging the [10]annulene. Less evident is such a structural effect for the bridged [14]annulenes, because the corresponding sums for $32^{\cdot-}$ and $743^{\cdot-}$ – $745^{\cdot-}$ are comparable to those for their alkadiylidene counterparts (Table 8.20).

Cycl[3.2.2]azine (**89**) and cycl[3.3.3]azine (**746**) represent a class of compounds in which a π perimeter is bridged by a central sp^2 -hybridized N atom. The lone pairs of this atom have an electron-releasing effect on the degenerate MOs ψ_{3+} and ψ_{3-} , which are the LUMOs of the 10-membered perimeter in **89** and the NBMOs of the 12-membered perimeter in **746**; these MOs are drawn in Figure 9.2 in a shape appropriate for the two cyclazines. For both of them, the MOs ψ_{3+} , which have the larger LCAO coefficients at the bridged centers, should be destabilized relative to their partners ψ_{3-} . In $89^{\cdot-}$, one electron has to be placed in the LUMOs of the 10-membered perimeter (case ① on p. 216), and, in $746^{\cdot-}$, three electrons must be accommodated by the NBMOs of the 12-membered perimeter (case ② in that scheme). Consequently, the SOMOs of $89^{\cdot-}$ and $746^{\cdot-}$ are expected to resemble the LUMO ψ_{3-} and the NBMO ψ_{3+} , respectively. This expectation is borne out by the hyperfine data for the two radical anions.

The g_e factors of $32^{\cdot-}$ and $743^{\cdot-}$, $745^{\cdot-}$ are in the range 2.0026–2.0029. They were not reported for the remaining radical anions in Table 9.28, but should lie in the same range. Generation of all radical anions was carried out by reaction of

Tab. 9.28. Hyperfine Data for Radical Anions of Some Heteroatom-bridged [n]Annulenes

1,6-Imino[10]annulene 741 ⁻		H2,5 H7,10 H3,4 H8,9 H' ¹⁴ N ¹³ C _{2,5,7,10} ¹³ C _{5a,10a}	-0.328 -0.286 -0.028 -0.014 0.058 <0.05 +0.70 -0.70	[1069]
1,6-Oxido[10]annulene 742 ⁻		H2,5,7,10 H3,4,8,9	-0.344 -0.042	[149]
<i>N,N</i> -Dimethyl- <i>syn</i> -1,6:8,13- diimino[14]annulene 743 ⁻		H2,5,9,12 H3,4,10,11 H7,14 6H' 2 ¹⁴ N	-0.244 -0.063 -0.204 0.021 0.040	[150]
<i>N,N</i> -Methano- <i>syn</i> -1,6:8,13- diimino[14]annulene 744 ⁻		H2,5,9,12 H3,4,10,11 H7,14 2H' 2 ¹⁴ N	-0.279 <0.008 -0.318 0.017 0.017	[150]
<i>N,N</i> -Trimethylene- <i>syn</i> - 1,6:8,13-diimino- [14]annulene 32 ⁻		H2,5,9,12 H3,4,10,11 H7,14 4H' 2 ¹⁴ N	-0.252 <0.008 -0.318 0.032 0.022	[150]
<i>syn</i> -1,6:8,13-Bisoxido- [14]annulene 745 ⁻		H2,5,9,12 H3,4,10,11 H7,14 ¹³ C _{1,6,8,13} ¹³ C _{2,5,9,12} ¹³ C _{7,14}	-0.297 -0.036 -0.289 +0.49 +0.57 +0.73	[1070]
Cycl[3.2.2]azine 89 ⁻		H1,4 H2,3 H5,7 H6 ¹⁴ N	-0.113 -0.534 -0.602 +0.120 -0.060	[160]
Cycl[3.3.3]azine 746 ⁻		H1,3,4,6,7,9 H2,5,8 ¹⁴ N ¹³ C _{1,3,4,6,7,9} ¹³ C _{2,5,8} ¹³ C _{3a,6a,9a}	+0.005 -0.484 +0.654 -0.447 +0.656 +0.162	[164]

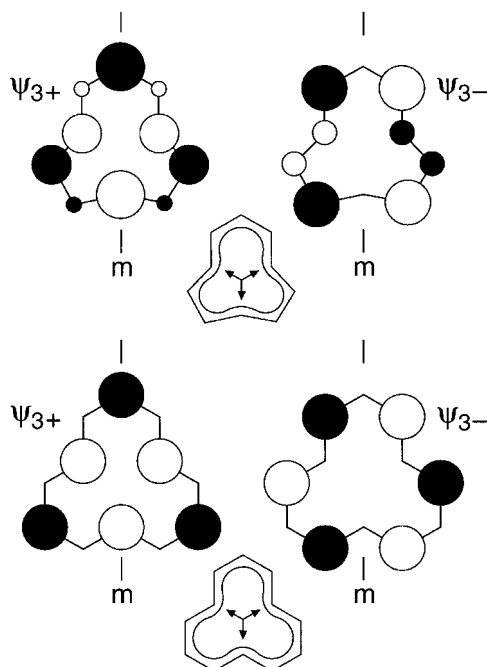


Fig. 9.2. Diagrams of degenerate LUMOs, ψ_{3+} and ψ_{3-} , of the 10-membered π perimeter and of the degenerate NBMOs, ψ_{3+} and ψ_{3-} , of the 12-membered π perimeter. Shape and bridging of the two perimeters as in cycl[3.2.2]azine (**89**) (top) and cycl[3.3.3]azine (**746**) (bottom).

the neutral bridged annulenes with potassium or sodium in DME and THF and/or by electrolytic reduction of these compounds in DMF. The radical anions **741**^{•-} and **742**^{•-} were rather nonpersistent, readily losing the bridging group to yield the radical anion of naphthalene (**83**). Interestingly, when the N-methyl derivative of **741** was reacted with sodium in DME, the radical anion of the isomeric azulene (**112**) was obtained instead of **83**^{•-} as the secondary paramagnetic species [1069].

9.3

Radical Cations of Electron Donors

Heteroatoms that bestow the properties of a good electron donor upon hydrocarbon π systems are usually N, O, and S and are linked to their neighbors C and/or H by three, two, and two formally single bonds, respectively. A lone pair of each atom enriches the π system with two additional electrons. They either replace C centers in a hydrocarbon π system or make part of a strongly electron-releasing substituent group such as amino, hydrazo, hydroxyl, alkoxy, or thyl.

Radical Cations of Heterocycles

Because each of the atoms N, O, and S contributes two electrons to the π system in heterocyclic donors, their radical cations are iso- π -electronic with the radicals, radical anions, radical dianions, and radical trianions of the corresponding hydrocarbons when they contain one, two, three, and four such heteroatoms, respectively.

Five-centered six-electron π systems, like pyrrole (747), furan (750), and thiophene (752), are hetero-counterparts of the “aromatic” benzene. Table 9.29 [253, 254, 1071] gives hyperfine data for their radical cations, along with those for some of their methyl derivatives. These radical cations with five π electrons are iso- π -electronic with the cyclopentadienyl radicals, and their SOMO has a shape similar to the LUMO ψ_{1-} of the five-membered π perimeter with a vertical node through the heteroatom (Figure 8.8). The preference for ψ_{1-} as the SOMO of $747^{+\cdot}$ – $753^{+\cdot}$ is in accordance with occupancy of the degenerate perimeter HOMOs, ψ_{1+} and ψ_{1-} by three electrons and with the electron-releasing effect of the heteroatom

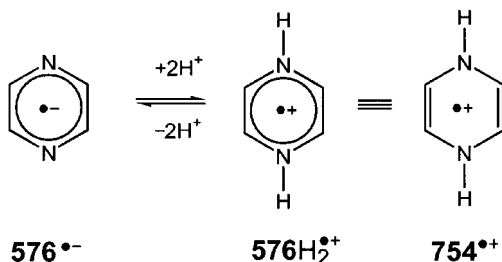
Tab. 9.29. Hyperfine Data for Radical Cations of Pyrrole, Furan and Thiophene and Some of Their Methyl Derivatives

Pyrrole 747 ^{•+}		¹⁴ N1 H1 H2,5 H3,4	~ -0.35 ~ +0.1 ~ -1.80 ~ -0.20	[1071]
2,5-Dimethylpyrrole 748 ^{•+}		¹⁴ N1 H1 H3,4 6H(β)	-0.40 +0.09 -0.36 +1.60	[253, 254]
N,2,5-Trimethylpyrrole 749 ^{•+}		¹⁴ N1 H3,4 6H(β) 3H(β')	-0.42 -0.34 +1.60 -0.15	[254]
Furan 750 ^{•+}		H2,5 H3,4	-1.44 -0.38	[1071]
2,5-Dimethylfuran 751 ^{•+}		H3,4 6H(β)	-0.36 +1.66	[253]
Thiophene 752 ^{•+}		H2,5 H3,4	-1.18 -0.32	[1071]
2,5-Dimethylthiophene 753 ^{•+}		H3,4 6H(β)	-0.31 +1.70	[253, 254]

(case ② on p. 216), and the coupling constants of the α -protons in $747^{+\cdot}$ – $753^{+\cdot}$ are similar to corresponding values for the radical cation of cyclopenta-1,3-diene (**373**) (Table 8.7) and the 1,3-dimethylcyclopentadienyl radical **473 \cdot** (Table 8.17).

Because the heteroatom lies in the vertical node of the SOMO, the g_e factor of the three radical cations and their derivatives is in the range 2.0023–2.0027, characteristic of hydrocarbon radicals. The unsubstituted radical cations $747^{+\cdot}$, $750^{+\cdot}$, and $752^{+\cdot}$ had to be generated by γ -irradiation in Freon or other matrices, whereas the more persistent methyl-substituted radical cations were produced in solution by photolysis in conc. sulfuric acid ($753^{+\cdot}$) or in TFA with Hg(II) ions ($748^{+\cdot}$ and $749^{+\cdot}$) or in TFA alone ($751^{+\cdot}$).

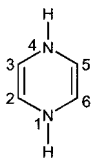
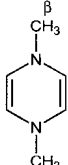
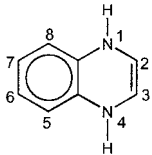
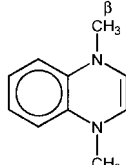
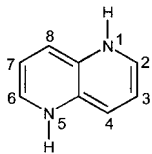
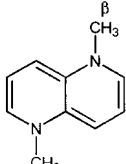
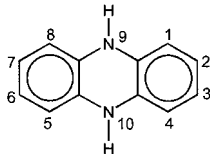
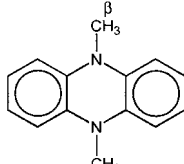
Replacement of two $>C-H(\alpha)$ segments in two appropriate positions of a cyclic hydrocarbon π system by $>N-H(\alpha)$ segments yields a dihydrodiazaheterocycle. Table 9.30 [266, 267, 1072–1078] lists hyperfine data for the radical cations of some of these heterocycles and their N,N' -dimethyl derivatives. The radical cations of the dihydrodiazaheterocycles are iso- π -electronic with the radical anions of the corresponding arenes (Table 8.8) and their aza derivatives (Tables 9.8–9.10) and, in fact, they are diprotonated radical anions of the parent diazaheterocycles (Chapts. 2.3 and 6.3). For example, the radical cation of 1,4-dihydropyrazine (**754**), a 7- π -electron species like the radical anion of benzene and its aza derivatives, is a diprotonated radical anion of pyrazine (**576**).



Consequently, the π -spin distribution in the radical cations of the dihydrodiazaheterocycles is similar to that in the radical anions of the parent diazaarenes, with the notable exception of 2,7-diazapyrene (**592**) (Table 9.10), because the coupling constant, $a_{N_{2,7}}$, is +0.404 for the radical cation of the dihydro derivative (**765**) vs -0.157 mT for **592 \cdot^-** (Table 9.10). In this particular case, the enhancement of the electronegativity of the two N atoms upon protonation leads to a reversal in the energy sequence of the relevant LUMOs. Thus, the SOMO of **765 \cdot^+** and that of its methoxy analogue **766 \cdot^+** is symmetric with respect to the vertical plane through the centers 2 and 7, whereas the corresponding MO of **592 \cdot^-** (like that of the pyrene radical ions **387 \cdot^-** and **387 \cdot^+**) (Table 8.8) is antisymmetric with respect to this plane. The ratio, $|a_{H_\mu}|/|a_{N_\mu}|$, for the α proton at the N atom and the ^{14}N nucleus is 1.10 ± 0.05 .

Substitution of the protons at the two N atoms by methyl groups has only a slight effect on the π -spin distribution. The coupling constant a_{N_μ} then increases by

Tab. 9.30. Radical Cations of Some Dihydrodiazaheterocyclics and Their *N*-Methyl Derivatives

1,4-Dihydropyrazine 754 ⁺		¹⁴ N1,4 H1,4 H2,3,5,6	+0.740 -0.794 -0.313	[266]
1,4-Dimethyl-1,4-dihydropyrazine 755 ⁺		¹⁴ N1,4 H2,3,5,6 6H(β)	+0.836 -0.285 +0.803	[1072]
1,4-Dihydroquinoxaline 756 ⁺		¹⁴ N1,4 H1,4 H2,3 H5,8 H6,7	+0.665 -0.717 -0.399 -0.075 -0.138	[266]
1,4-Dimethyl-1,4-dihydroquinoxaline 757 ⁺		¹⁴ N1,4 H2,3 H5,8 H6,7 6H(β)	+0.742 -0.370 -0.092 -0.142 +0.690	[1073]
1,5-Dihydro-1,5-naphthyridine 758 ⁺		¹⁴ N1,5 H1,5 H2,6 H3,7 H4,8	+0.286 -0.337 -0.464 -0.108 -0.625	[1074]
1,5-Dimethyl-1,5-dihydro-1,5-naphthyridine 759 ⁺		¹⁴ N1,5 H2,6 H3,7 H4,8 6H(β)	+0.340 -0.434 -0.130 -0.602 +0.221	[1074]
9,10-Dihydrophenazine 760 ⁺		¹⁴ N9,10 H1,4,5,8 H2,3,6,7 H9,10	+0.612 -0.066 -0.171 -0.649	[266]
9,10-Dimethyl-9,10-dihydrophenazine 761 ⁺		¹⁴ N9,10 H1,4,5,8 H2,3,6,7 6H(β)	+0.686 -0.062 -0.138 +0.620	[1075]

Tab. 9.30 (continued)

6-Hydrodipyrido[1,2-c:2',1'-e]-imidazole 98 ^{•+}		¹⁴ N _{2,2'} H _{3,3'} H _{4,4'} H _{5,5'} H _{6,6'} 2H(β)	+0.434 -0.239 -0.065 -0.281 -0.023 +2.424	[1076]
6,7-Dihydrodipyrido[1,2- <i>a</i> :2',1'-c]pyrazine 762 ^{•+}		¹⁴ N _{2,2'} H _{3,3'} H _{4,4'} H _{5,5'} H _{6,6'} 4H(β)	+0.408 -0.254 -0.058 -0.289 -0.036 +0.698	[1077]
1,1'-Dihydro-4,4'-dipyridine 763 ^{•+}		¹⁴ N _{1,1'} H _{1,1'} H _{2,2',6,6'} H _{3,3',5,5'}	+0.356 -0.406 -0.161 -0.145	[266]
1,1'-Dimethyl-1,1'-dihydro-4,4'-dipyridine 764 ^{•+}		¹⁴ N _{1,1'} H _{2,2',6,6'} H _{3,3',5,5'} 6H(β)	+0.423 -0.133 -0.157 +0.399	[1078]
2,7-Dihydro-2,7-diazapyrene 765 ^{•+}		¹⁴ N _{2,7} H _{1,3,6,8} H _{2,7} H _{4,5,9,10}	+0.404 -0.193 -0.452 -0.041	[267]
2,7-Dimethyl-2,7-dihydro-2,7-diazapyrene 766 ^{•+}		¹⁴ N _{2,7} H _{1,3,6,8} H _{4,5,9,10} 6H(β)	+0.470 -0.183 -0.040 +0.439	[267]

a factor of ca 1.15 and the ratio, $|a_{\text{H}}(\beta)|/|a_{\text{N}_i}|$, for the methyl β protons and the ¹⁴N nucleus is ca 0.95 (except for **759**^{•+}, in which this ratio is anomalous). The large coupling constant (+2.424 mT) of the two β -methylene protons in the radical cation of the hydrodipyridoimidazole **98** is noteworthy, because it represents an example of the “Whiffen effect” (Chapt. 4.2; Eq. 4.11) applied to such protons in a group bridging two N centers.

The g_e factor of the radical cations of the dihydrodiazaheterocycles and their dimethyl derivatives lies in the range 2.0029–2.0032. The former were usually generated by chemical or electrolytic reduction of the corresponding diaza compounds in acid solution, and the latter were produced either by oxidation of the neutral dimethyldihydrodiazaprecursors or by reduction of their dications, usually

with zinc. (Three of these dication, the diquats 98^{2+} and 762^{2+} , and the paraquat 764^{2+} , are powerful herbicides.)

Conjugated thia compounds that are π -electron-rich are often referred to as S-donors. Among them, 1,4,5,8-tetrathia-1,4,5,8-dihydrofulvalene (TTF; **24**), a 14- π -electron system, has become well known as a donor in superconducting crystals ("organic metals"). Its derivatives are also efficient electron donors, especially bis(ethylenedithio)-TTF (**768**). Hyperfine data for 24^{+} and 768^{+} and some related radical cations are listed in Table 9.31 [230, 284, 1079, 1080]. The bulk of their π -spin population resides in the central $S_2C=CS_2$ segment of 24^{+} and 767^{+} – 771^{+} or in the $S_2C=C-C=CS_2$ segment of 772^{+} and 773^{+} . In 770^{+} and 771^{+} , which contain two TTF moieties, this population is evenly shared by both moieties. In the corresponding radical trications 770^{3+} and 771^{3+} , one TTF moiety becomes doubly charged and the spin population is restricted to the second, singly charged moiety. When the phenyl group in these radical cations is replaced by a third TTF moiety, radical pentacations are formed in which two TTF moieties are doubly charged and the third TTF accommodates the unpaired electron [285].

Upon dissolving equimolar quantities of **773** and TCNQ (**20**) in acetonitrile at 295 K, electron transfer occurs from the donor **773** to the acceptor **20**, and ESR spectra for both the radical cation 773^{+} and the radical anion 20^{-} are observed simultaneously (Figure 9.3) [1080].

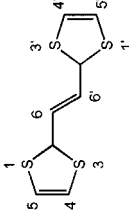
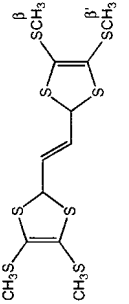
The g_e factor of 24^{+} is 2.0081. Those of the remaining radical cations and the radical trications 770^{3+} and 771^{3+} lie in the range 2.0074–2.0080. All radical cations were readily generated from the neutral compounds in dichloromethane with a variety of reagents like $AlCl_3$ or TFA or electrochemically. Even a mild oxidizing agent such as $Ag(I)$ ion was efficient in this respect, particularly in converting **770** and **771** into their radical monocations, whereas use of $AlCl_3$ or TFA led directly to the corresponding trications.

Table 9.32 [469, 546, 1081–1084] gives hyperfine data for radical cations of some thiaheterocycles not related to TTF. The radical cation of dithiine (**774**), a 7- π -electron species, is iso- π -electronic with the benzene radical anion (62^{-}), and its spin distribution is similar to that in the radical anion of pyrazine (**576**) (Table 9.8) and in the radical cation of the corresponding dihydrodiaz derivative (**754**) (Table 9.30). Analogously, other dithia-radical cations are iso- π -electronic with the radical anions of the corresponding arenes (Tables 8.8, 8.11, and 8.16), but the radical cations of tetrathiaheterocycles, such as **781**–**783**, are iso- π -electronic with the unknown radical trianions of their hydrocarbon counterparts. (For a historical review of ESR studies of the thianthrene radical cation 776^{+} , see [17d]). All these radical cations have a relatively high π -spin populations at each of the S atoms, which decrease with increasing extension of the π system.

The g_e factor of 774^{+} is 2.0080, but it is lower for larger dithia-radical cations (it is 2.0057 and 2.0055 for 777^{+} and 778^{+} , respectively). The tetrathia-radical cations have higher g_e factors (2.0094 for 783^{+}). The radical cations 774^{+} – 776^{+} were generated by dissolution of the neutral compounds in conc. sulfuric acid or by their reaction with $AlCl_3$ in nitromethane, and $AlCl_3$ in dichloromethane was used for formation of 777^{+} , 778^{+} , 93^{+} , and 781^{+} . Reduction of the correspond-

Tab. 9.31. Hyperfine Data for Radical Cations and Trications of Tetrathiatetrahydrofulvalene (TTF) and Related Compounds

1,4,5,8-Tetrathia-1,4,5,8-tetrahydrofulvalene (TTF) 24 ^{•+}		H2,3,6,7 13C8a,8b 33S1,4,5,8	-0.125 +0.285 +0.425	[230]
2,3,6,7-Tetramethyl-TTF 767 ^{•+}		12H(β) 33S1,4,5,8	+0.074 +0.395	[230]
Bis(ethylendithio)-TTF 768 ^{•+}		8H(β) 13C8a,8b 33S1,4,5,8 33S9,12,13,16	≤ 0.005 +0.255 +0.370 < 0.080	[230]
Dibenzo-TTF 769 ^{•+}		H9,12,13,16 H10,11,14,15 33S1,4,5,8	0.049 0.015 +0.410	[230]
Bis(TTF-yl)phenylphosphine 770 ^{•+} / 770 ³⁺		31P H2,2' H6,6',7,7'	Cation -0.054 -0.061 -0.061	[284]
Bis(dimethyl-TTF-yl)-phenylphosphine 771 ^{•+} / 771 ³⁺		β H2,2' 12H(β)	Cation -0.034 -0.045 +0.045	[284]

2,2'-Ethanediyldiene(1,3-dithiole) 772 ⁺		H4,4' H5,5' H6,6' ³³ S1,1' ³³ S3,3'	-0.123 -0.082 -0.313 +0.398 ~+0.32	[1079]
4,4',5,5'-Tetrakis(methylthio)-2,2'-ethanediyldiene(1,3-dithiole) 773 ⁺		H6,6' 6H(β) 6(H β') ³³ S1,1' ³³ S3,3'	-0.272 +0.072 +0.015 +0.383 +0.296	[1080]

^aSpin localization in one TTF moiety

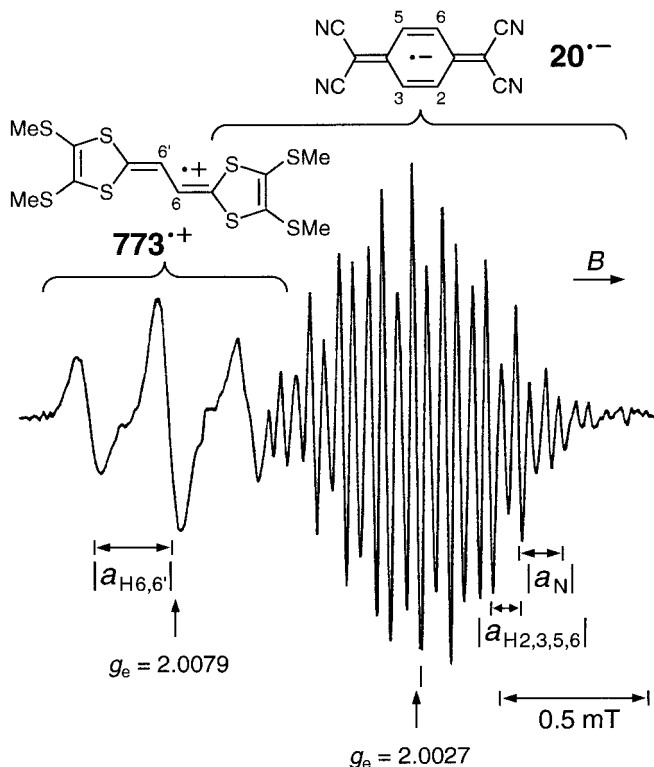
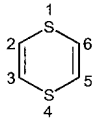
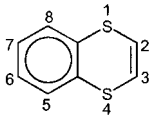
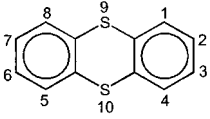
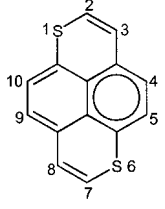
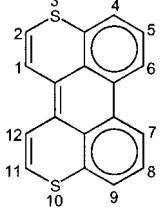
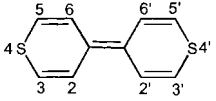
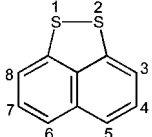
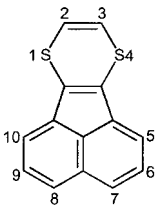


Fig. 9.3. ESR spectra of the radical cation of 4,4',5,5'-tetrakis(methylthio)-2,2'-ethanediylidene-(1,3-dithiole) (**773**) and the radical anion of 7,7,8,8-tetracyano-1,4-quinodimethane (TCNQ, **20**) formed as a donor-acceptor complex. Solvent ACN, temperature 295 K. Reproduced by permission from [1080].

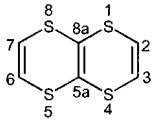
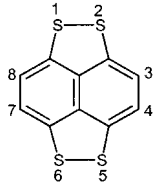
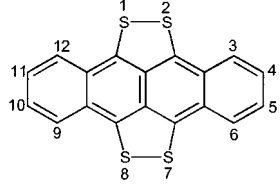
ing dication led to 780^{++} , and electrolytic oxidation of their neutral precursors yielded 782^{++} and 783^{++} .

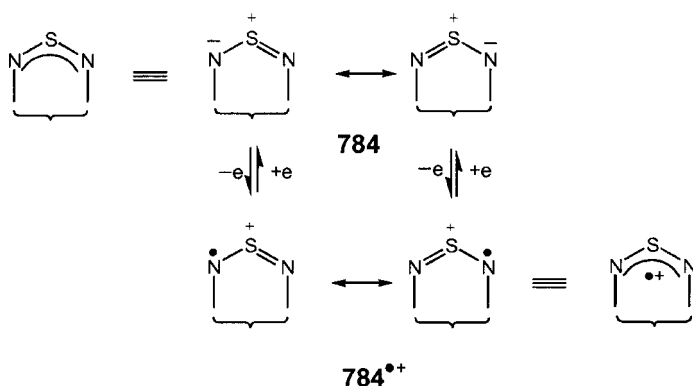
Hyperfine data for the not-yet-considered radical cations of some heterocyclics are collected in Table 9.33 [164, 469, 530, 1085–1087]. The radical anion of cycl[3.3.3]azine (**746**), a 12-membered perimeter bridged by a central N atom, is been discussed in Chapt. 9.2. As pointed out there, interaction of the N-lone pair destabilizes the perimeter NBMO ψ_{3+} relative to its partner ψ_{3-} (Figure 9.2). In $746^{\bullet-}$, with three electrons to be placed in ψ_{3+} and ψ_{3-} , the SOMO correlates with the less stable MO ψ_{3+} (case ② on p. 216), whereas in 746^{++} it resembles the lower-lying one ψ_{3-} (case ① in that scheme). The π -spin distribution in 746^{++} is thus almost the same as in the iso- π -electronic phenalenyl radical (**4'**) (Chapt. 4.2), and the ^1H - and ^{13}C -coupling constants for 746^{++} are very close to those for **4'** (Table 8.4). Also iso- π -electronic with **4'** is the radical cation of the naphthothiazine **784**, in which the NSN segment contributes three electrons to the π system.

Tab. 9.32. Hyperfine Data for Radical Cations of Some Thiaheterocycles not Related to Tetrathiatetrahydrofulvalene (TTF)

1,4-Dithiin 774 ⁺		H2,3,5,6 ³³ S1,4	-0.282 +0.984	[469]
Benzo-1,4-dithiin 775 ⁺		H2,3 H5,8 H6,7 ³³ S1,4	-0.332 -0.020 -0.106 +0.935	[469]
Thianthrene 776 ⁺		H1,4,5,8 H2,3,6,7 ³³ S9,10	-0.014 -0.128 +0.915	[469]
1,6-Dithio-1,6-dihydropyrene 777 ⁺		H2,7 H3,8 H4,9 H5,10 ³³ S1,6	-0.184 -0.126 -0.166 -0.126 +0.530	[1081]
3,10-Dithia-3,10-dihydroperylene 778 ⁺		H1,12 H2,11 H4,9 H5,8 H6,7 ³³ S3,10	-0.086 -0.247 -0.073 -0.030 -0.086 +0.46	[1081]
4,4'-Dithia-4,4'-dihydrobiphenyl 779 ⁺		H2,2',6,6' H3,3',5,5'	-0.237 0.060	[1082]
1,2-Dithia-acenaphthene 780 ⁺		H3,8 H4,7 H5,6 ³³ S1,2	-0.456 +0.096 -0.552 +0.716	[1083]
Acenaphtho[1,2-b][1,4]-dithine 93 ⁺		H2,3 H5,10 H6,9 H7,8 ³³ S1,4	-0.206 -0.034 <0.005 -0.054 +0.83	[546]

Tab. 9.32 (continued)

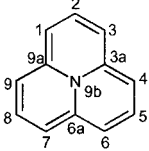
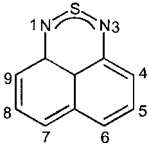
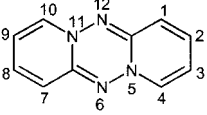
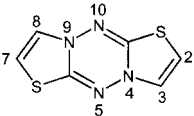
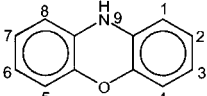
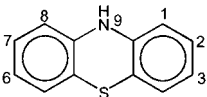
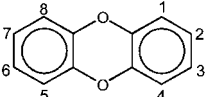
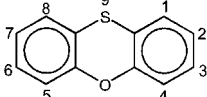
1,4,5,8-Tetrathiatetraline 781⁺		H2,3,6,7 ³³ S1,4,5,8	-0.03 +0.417	[1084]
1,2,5,6-Tetrathia- pyracene 782⁺		H3,4,7,8 ³³ S1,2,5,6	-0.151 +0.437	[1083]
1,2,5,6-Tetrathia- dibenzo[<i>c,i</i>]-pyracene 783⁺		H3,6,9,12 H4,5,10,11 ³³ S1,2,8,7	-0.055 -0.055 +0.336	[1083]



The ESR and ENDOR spectra of the radical cation of dithienotetrazine, **91**, are reproduced in Figure 5.5. The radical cations **91⁺** and **785⁺**–**789⁺** are iso- π -electronic with the radical anions of anthracene (**68**) (Table 8.8), acridine (**586**), and phenazine (**587**) (Table 9.9). In the radical cations of phenoxazine (**786**) and phenothiazine (**787**), the π -spin distribution is also related to that in the diphenylamine radical cation (next section).

The g_e factor of **746⁺** was not reported; it should be close to that of **4[•]** (2.0026). The remaining radical cations have g_e factors ranging from 2.0027 for **784⁺** to 2.0061 for **789⁺**. All of them are very persistent (**91⁺** and **785⁺** were isolated as perchlorate salts) and can be generated from the neutral compounds by a variety of methods, such as reaction with Ag(I) ions in ACN or DME (**746⁺**), reaction with AlCl_3 in dichloromethane (**784⁺**) or nitromethane (**789⁺**), dissolution in TFA/

Tab. 9.33. Hyperfine Data for Radical Cations of Some Heterotricyclics Isoelectronically Related to the Phenalenyl Radical and the Radical Anion of Anthracene

Cycl[3.3.3]azine 746 ⁺		¹⁴ N9b H1,3,4,6,7,9 H2,5,8 ¹³ C1,3,4,6,7,9 ¹³ C2,5,8 ¹³ C3a,6a,9a	+0.129 -0.645 +0.178 +0.969 -0.811 -0.773	[164]
Naphtho[1,8-cd][1,2,6] thiadiazine 784 ⁺		¹⁴ N1,3 H4,9 H5,8 H6,7 ¹³ C4,9 ¹³ C5,8 ¹³ C6,7	+0.196 -0.508 +0.077 -0.674 +0.75 -0.59 +0.93	[1085]
Dibenzo[<i>b,e</i>]tetra- 1,2,4,5-azine 785 ⁺		¹⁴ N5,11 ¹⁴ N6,12 H1,7 H2,8 H3,9 H4,10	+0.280 +0.618 -0.243 +0.099 -0.358 +0.117	[530]
Dithieno[2,3- <i>b,e</i>]tetra- 1,2,4,5-azine 91 ⁺		¹⁴ N4,9 ¹⁴ N5,10 H2,7 H3,8	+0.400 +0.596 -0.394 +0.074	[530]
Phenoxazine 786 ⁺		¹⁴ N9 H1,8 H2,7 H3,6 H4,5 H9	+0.783 -0.161 +0.044 -0.327 +0.066 -0.902	[1086]
Phenothiazine 787 ⁺		¹⁴ N9 H1,8 H2,4,5,7 H3,6 H9	+0.641 -0.114 +0.049 -0.250 -0.741	[1086]
Dibenzo- <i>p</i> -dioxine 788 ⁺		H1,4,5,8 H2,3,6,7	<0.01 -0.210	[1087]
Phenoxathiine 789 ⁺		H1,8 H2,7 H3,6 H4,5 ³³ S9	-0.056 -0.099 -0.214 +0.026 +1.191	[469]

dichloromethane (785^{+} and 91^{+}) or conc. sulfuric acid/nitromethane (786^{+} and 787^{+}), or electrolysis in ACN (788^{+}).

Radical Cations of Amino-substituted Derivatives

The strongly electron-releasing amino and alkylamino substituents are particularly effective in bestowing strong donor properties on π systems even as small as ethene. The most prominent representative of their persistent radical cations is that of *N,N,N',N'*-tetramethyl-*p*-phenylenediamine (**17**), which has been known for a long time as “Wurster’s blue”. Hyperfine data for the radical cations of these amines are given in Tables 9.34 [264, 274, 283, 517, 1088–1091] and 9.35 [282, 1092–1094]. Their amino groups accommodate a large part of the π -spin population, as indicated by the pertinent ^{14}N - and ^1H -coupling constants. Due to delocalization into the π systems linked to the amino groups, their $|a_{\text{N}}|$, $|a_{\text{H}}(\alpha)|$ and $|a_{\text{H}}(\beta)|$ values are strongly reduced relative to those for the radical cations of alkylamines (Tables 7.5 and 7.6). The largest ^{14}N - and ^1H -coupling constants in Table 9.34 are exhibited by the radical cations of 4-nitroaniline (792^{+} : $a_{\text{N}} = +0.801$, $a_{\text{H}}(\alpha) = -1.023$ mT) and its *N,N*-dimethyl derivative (794^{+} : $a_{\text{N}} = +1.280$, $a_{\text{H}}(\beta) = +1.483$ mT), in which the corresponding values for the radical cations of aniline (791^{+} : $a_{\text{N}} = +0.768$, $a_{\text{H}}(\alpha) = -0.958$) and *N,N*-dimethyl-*p*-toluidine (793^{+} : $a_{\text{N}} = +1.117$ and $a_{\text{H}}(\beta) = +1.222$ mT) are enhanced by the *para*-nitro substituent. (It is preferable to quote the data of 793^{+} instead of those for the radical cation of the parent *N,N*-dimethylaniline, because the values available for the phenyl α protons in this radical cation [1095] seem unrealistic.) As expected, the coupling constants a_{N} , $a_{\text{H}}(\alpha)$, and $a_{\text{H}}(\beta)$ decrease with expansion of the π system and/or introduction of a second amino group. The ratios $|a_{\text{H}}(\alpha)|/|a_{\text{N}}|$ and $|a_{\text{H}}(\beta)|/|a_{\text{N}}|$ are all 1.2 ± 0.1 and 1.0 ± 0.1 , respectively. Steric hindrance of the amino groups by the *ortho*-methyl substituents in the radical cation of diaminodurene (**796**) moderately reduces the $|a_{\text{N}}|$ and $|a_{\text{H}}(\alpha)|$ values relative to those in the radical cation of *p*-phenylenediamine (**795**). The hexaazaoctadecahydro-coronene **799** can be considered a derivative of hexaminobenzene. It was converted not only into its radical cation 799^{+} , but also into the corresponding trication 799^{3+} . Due to deviations from planarity, the two β proton in each methylene group are nonequivalent, but the chain inversion in 799^{3+} was fast on the hyperfine time-scale.

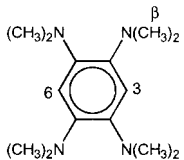
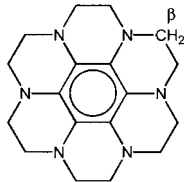
The π -spin distribution in the radical cation of diphenylamine (**802**) is generally preserved in the radical cation of the acridine derivative **803** and, to a lesser extent, in those of phenoxazine (**786**) and phenothiazine (**787**) (Table 9.33). The radical dication 805^{2+} is the oxidized triamino derivative of the cyclopropenium cation (the structural formula in Table 9.35 is that of the cation), the smallest π system that conforms to Hückel rule. It is iso- π -electronic with the radical anion of hexamethyl[3]radialene (**74**; Table 8.24), and, despite the difference in charge, the two radical ions have similar π -spin distributions, as indicated by the coupling constants of their methyl β protons ($+0.814$ for 805^{2+} vs $+0.757$ mT for 74^{-}).

To our knowledge, the radical cation of 1,8-bis(dimethylamino)naphthalene (**807**;

Tab. 9.34. Hyperfine Data for Radical Cations of Some Amino Derivatives of Ethene and Benzene

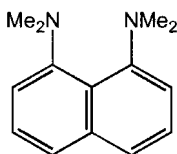
1,2-Bis(dimethyl-amino)ethene $790^{+\cdot}$		2^{14}N H1,2 12H(β)	+0.695 -0.435 +0.815	[1088]
Tetrakis(dimethyl-amino)ethene $23^{+\cdot}$		4^{14}N 12H(β) 12H(β)	+0.490 +0.328 +0.284	[1088]
Aniline $791^{+\cdot}$		^{14}N 2H(α) H2,6 H3,5 H4	+0.768 -0.958 -0.582 +0.152 -0.958	[276]
4-Nitroaniline $792^{+\cdot}$		^{14}N 2H(α) H2,6 H3,5 $^{14}\text{N}'$	+0.801 +1.023 -0.642 +0.206 +0.206	[276]
<i>N,N</i> -Dimethyl- <i>p</i> -toluidine $793^{+\cdot}$		^{14}N H2,6 H3,5 6H(β) 3H(β')	+1.117 -0.521 +0.136 +1.222 +0.997	[274]
<i>N,N</i> -Dimethyl-4-nitroaniline $794^{+\cdot}$		^{14}N H2,6 H3,5 6H(β) $^{14}\text{N}'$	+1.280 -0.586 +0.187 +1.483 +0.391	[274]
<i>p</i> -Phenylenediamine $795^{+\cdot}$		2^{14}N 4H(α) H2,3,5,6	+0.529 -0.588 -0.213	[269]
3,6-Diaminodurene $796^{+\cdot}$		2^{14}N 4H(α) 12H(β)	+0.472 -0.510 +0.513	[1089]
<i>N,N</i> -Dimethylamino- <i>p</i> -phenylenediamine $797^{+\cdot}$		^{14}N $^{14}\text{N}'$ 2H(α) H2,6 H3,5 6H(β)	+0.762 +0.473 -0.516 -0.265 -0.146 +0.775	[274]
<i>N,N,N',N'</i> -Tetra-methyl- <i>p</i> -phenylene-diamine $17^{+\cdot}$		2^{14}N H2,3,5,6 12H(β)	+0.702 -0.198 +0.674	[517, 1090]

Tab. 9.34 (continued)

1,2,4,5-Tetrakis-(dimethylamino)-benzene 798 ⁺		4 ¹⁴ N	+0.357	[1091]	
		H3,6	+0.034		
		12H(β)	+0.376		
		12H(β)	+0.256		
2a,4a,6a,8a,10a,12a-hexaaza-1,2,2a,3,4,4a,5,6,6a,7,8,8a,9,10,10a,11,12,12a-octadecahydro-coronene 799 ⁺		6 ¹⁴ N	+0.260	+0.281 ^a	[283]
		12H(β)	+0.422	}	
		12H(β)	+0.097		

^aTrication

“proton sponge”) has not been studied by ESR spectroscopy, although the radical anion **807**⁻ was characterized by its hyperfine data [1096]. However, such studies were reported for the radical cation of 1,4,5,8-tetrakis(dimethylamino)naphthalene (**806**; “double proton sponge”). As expected, free rotation of the dimethylamino groups in the *peri*-positions of **806**⁺ is sterically hindered.

**807**

The g_e factor of the radical cations of amino-substituted cyclic π systems lies in the range 2.0027–2.0034; that of the tetraminoethene radical cation (**23**⁺) is slightly higher (2.0036). Oxidation of the neutral amines to their radical cations was carried out electrolytically in ACN or DMF or with a variety of reagents, such as PbO₂ in TFA, bromine in ACN or DMF, or dichloromethane. A flow system with Ce(IV) or Pb(IV) ions had to be used with aniline (**791**) and *p*-nitroaniline (**792**) to form their radical cations. The radical dication **805**^{·2+} was generated from the corresponding diamagnetic cation by electrolysis in DMF or by dissolution in conc. sulfuric acid.

Radical Cations of Hydroxy-, Methoxy- and Methylthio-substituted Derivatives

The hydroxy, methoxy, and methylthio substituents have an electron-releasing effect which approaches that of the amino groups, and they are easily oxidized to their radical cations. Hyperfine data for some of these cations are listed in Tables 9.36 [231, 1097–1104] and 9.37 [641, 1105–1107]. Analogous to the radical cations

Tab. 9.35. Hyperfine Data for Radical Cations of Some Amino Derivatives of Conjugated Hydrocarbons other than Benzene

Benzidine 800 ^{•+}		2 ¹⁴ N 4H(α) H2,2',6,6' H3,3',5,5'	+0.360 -0.397 -0.162 -0.108	[1092]
<i>N,N,N',N'</i> -Tetramethylbenzidine 801 ^{•+}		2 ¹⁴ N H2,2',6,6' H3,3',5,5' 6H(β)	+0.488 -0.165 -0.073 +0.470	[1092]
Diphenylamine 802 ^{•+}		¹⁴ N H(α) 4H _o 4H _m 4H _p	+0.903 -1.098 -0.346 +0.131 -0.486	[1093]
9,9-Dimethyl-9,10-dihydroacridine 803 ^{•+}		¹⁴ N H(α) H1,1' H2,2' H3,3' H4,4'	+0.856 -1.106 +0.093 -0.473 +0.114 -0.319	[1093]
Triphenylamine 804 ^{•+}		¹⁴ N 6H _o 6H _m 3H _p	+1.019 -0.226 +0.122 -0.327	[1093]
Tris(dimethylamino)cyclopropenium 805 ^{•2+}		3 ¹⁴ N 18H(β)	+0.733 ^a +0.814	[282]
1,4,5,8-Tetrakis(dimethylamino)naphthalene 806 ^{•+}		4 ¹⁴ N H2,3,6,7 12H(β) 12H(β)	+0.265 -0.153 +0.354 +0.177	[1094]

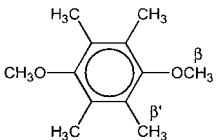
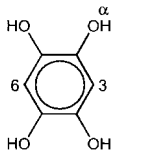
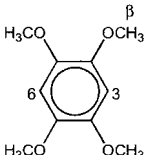
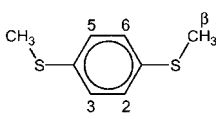
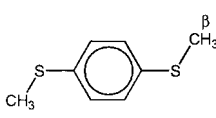
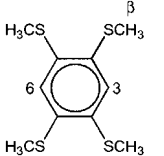
^a Dication

of dihydrodiazaheterocycles and the radical anions of the corresponding diazaarenes, the radical cations of several dihydroxy derivatives of cyclic π systems are diprotonated semiquinone anions with similar π -spin distributions (Chapts. 2.3 and 6.3). For example, $19^{\cdot-} + 2H^+ = 19H_2^{\cdot+} \equiv 810^{\cdot+}$, where 19 and 810 are *p*-benzoquinone and 1,4-dihydroxybenzene, respectively. In the same way, the radical cations $816^{\cdot+}$, $818^{\cdot+}$, and $820^{\cdot+}$ are related to the corresponding semiquinone anions $647^{\cdot-}$, $655^{\cdot-}$, and $658^{\cdot-}$ (Table 9.18).

Tab. 9.36. Hyperfine Data for Radical Cations of Some Hydroxy, Methoxy and Methylthio Derivatives of Benzenes

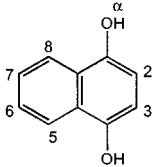
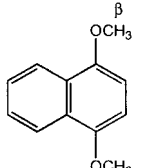
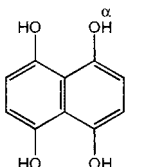
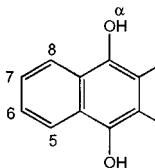
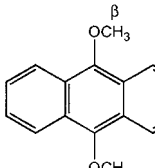
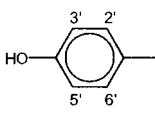
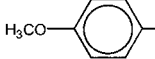
Anisole $808^{+\cdot}$		H2 } H6 } H3 } H5 } H4 3H(β)	-0.551 -0.452 +0.100 +0.021 -0.997 +0.483	[1097]
1,2-Dimethoxybenzene $809^{+\cdot}$		H3,6 H4,5 6H(β)	+0.016 -0.489 +0.333	[1097]
1,4-Dihydroxybenzene (hydroquinone) <i>cis</i> - $810^{+\cdot}$		H2,3 } H5,6 } H(α) $^{13}\text{C}_{1,4}$ $^{13}\text{C}_{2,3}$ } $^{13}\text{C}_{5,6}$ } 2^{17}O	-0.236 -0.215 -0.329 +0.423 -0.120 -0.165 -0.783	[1098] [1099]
<i>trans</i> - $810^{+\cdot}$		H2,5 } H3,6 } H(α) $^{13}\text{C}_{1,4}$ $^{13}\text{C}_{2,5}$ } $^{13}\text{C}_{3,6}$ } 2^{17}O	-0.246 -0.206 -0.329 +0.423 -0.120 -0.165 -0.783	[1098] [1099]
Dihydroxydurene- (duroquinol) <i>cis</i> - $129^{+\cdot}$		6H(β, β') } 6H(β'', β''') } 2H(α)	+0.217 +0.193 -0.289	[1100]
<i>trans</i> - $129^{+\cdot}$		6H(β, β'') } 6H(β', β''') } 2H(α)	+0.279 +0.139 -0.289	[1100]
1,4-Dimethoxybenzene <i>cis</i> - $811^{+\cdot}$		H2,3 } H5,6 } 6H(β)	-0.261 -0.188 +0.324	[1097]
<i>trans</i> - $811^{+\cdot}$		H2,5 } H3,6 } 6H(β)	-0.292 -0.159 +0.341	[1097]

Tab. 9.36 (continued)

1,4-Dimethoxydurene 812 ⁺		6H(β) 12H(β')	+0.276 +0.211	[231]
1,2,4,5-Tetrahydroxybenzene 813 ⁺		H3,6 4H(α)	+0.095 -0.171	[1101]
1,2,4,5-Tetramethoxybenzene 22 ⁺		H3,6 12H(β)	+0.086 +0.227	[1102]
1,4-Bis(methylthio)benzene <i>cis</i> - 814 ⁺		H2,3 } H5,6 } 6H(β)	-0.170 -0.112 +0.531	[1103]
<i>trans</i> - 814 ⁺		H2,5 } H3,6 } 6H(β)	-0.103 -0.179 +0.544	[1103]
1,2,4,5-Tetrakis(methylthio)- benzene 815 ⁺		H3,6 12H(β)	+0.071 +0.259	[1104]

The radical cation of phenol has not yet been studied by ESR spectroscopy, and only hyperfine data for the radical cation of anisole (**808**) have been reported. The π -spin distribution in **808**⁺ is similar to that in the aniline radical cation **791**⁺ (Table 9.34). In general, replacement of the hydroxy-H atoms by methyl groups has only a slight effect on the π -spin distribution. The ratio $|a_{\text{H}}(\beta)|/|a_{\text{H}}(\alpha)|$ for the methoxy- and hydroxy-protons is close to 1. Due to restricted rotation about the C–O bonds, the radical cations of both hydroxy and methoxy compounds exist as *cis* and *trans* conformers, which could be distinguished in a few cases, when the interconversion was slow on the hyperfine time-scale. The coupling constants, $a_{\text{H}}(\alpha)$, of the hydroxy protons are strongly dependent on the environment and temperature, not at least because of this interconversion. The radical cations of duroquinol (**129**) and naphthazarine (**130**), which exhibit line-width alternation in their ESR spectra, are cited in Chapt. 6.7 as examples of a four-jump process (p. 159). The *cis*–*trans* interconversion, as a four-jump process, also occurs in the

Tab. 9.37. Hyperfine Data for Radical Cations of Some Hydroxy- and Methoxy-substituted Arenes Other than Benzene

1,4-Dihydroxynaphthalene 816 ⁺		H2,3 H5,8 H6,7 2H(α)	-0.309 -0.164 -0.082 -0.245	[1105]
1,4-Dimethoxynaphthalene 817 ⁺		H2,3 H5,8 H6,7 6H(β)	-0.335 -0.146 -0.070 -0.219	[1106]
1,4,5,8-Tetrahydroxynaphthalene (naphthazarin) 130 ⁺		H2,3,6,7 4H(α)	-0.238 -0.12	[641]
9,10-Dihydroxyanthracene 818 ⁺		H1,4,5,8 H2,3,6,7 2H(α)	-0.155 -0.104 -0.128	[1105]
9,10-Dimethoxyanthracene 819 ⁺		H1,4,5,8 H2,3,6,7 6H(β)	-0.172 -0.108 +0.119	[1106]
4,4'-Dihydroxybiphenyl 820 ⁺		H2,2',6,6' H3,3',5,5' 2H(α)	-0.195 ^a +0.075 -0.168	[1107]
4,4'-Dimethoxybiphenyl 821 ⁺		H2,2',6,6' H3,3',5,5' 6H(β)	-0.191 ^a +0.078 +0.176	[1107]

^a Average values of *cis*- and *trans*-isomers; low barrier to rotation about C–O bond

radical cation of 1,2,4,5-tetrahydroxybenzene (**813**), although no specific line-width effects were observed here. The *cis*-conformation should be favored in the radical cations of 1,4-dihydroxy- (**816**) and 1,4-dimethoxynaphthalene (**817**). Both isomers were found for the radical cation of 1,4-bis(methylthio)benzene (**814**), but not for that of the corresponding 1,2,4,5-tetra-substituted derivative **815**.

The g_e factor of the radical cations of hydroxy- and methoxybenzenes is 2.0034–2.0039, and the radical cations of hydroxy and methoxy derivatives of naphthalene, anthracene, and biphenyl have a g_e value of 2.0031–2.0032. For the methylthio-substituted radical cations **814**^{•+} and **815**^{•+}, considerably higher g_e factors (2.0079–2.0087) are reported.

The standard method of generation was reaction of the neutral compounds with AlCl_3 in nitromethane, although their oxidation by dissolution in conc. sulfuric acid was effective for several radicals. The radical cations of methoxybenzenes, such as **809**^{•+}, **811**^{•+}, and **22**^{•+}, were also produced by pulse radiolysis of aqueous solutions containing the corresponding methoxybenzenes with Ti(II) or Ag(II) or $\text{SO}_4^{\cdot-}$ ions as reagents.

Radical Cations of Trimethylsilylmethyl-substituted Derivatives

The electron-releasing effect of these substituents (general formula $-\text{CH}_3\text{-}_n\text{SiMe}_n$) is comparable to that of dimethylamino, methoxy, and methylthio groups; even trimethylsilylmethyl derivatives of such π -systems as ethene and benzene are amenable to oxidation in solution. Table 9.38 [576, 577, 1108–1110] gives hyperfine data for some radical cations thus formed which, due to their bulky trimethylsilylmethyl substituents, are persistent (the ESR spectrum of **100**^{•+} is shown in Figure 6.12). These substituents assume a conformation reconciling maximum π -conjugation with the least steric hindrance. The large $|a_{\text{H}}(\beta)|$ and $|a_{\text{Si}}|$ values for the methylene protons and the ^{29}Si isotopes, as well as the still observable hyperfine splittings by the numerous Si-methyl δ protons, indicate substantial delocalization of the π -spin population into the trimethylsilylmethyl groups. ESR studies of organosilicon radical cations were reviewed in 1982 [232].

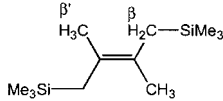
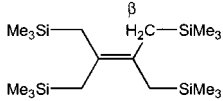
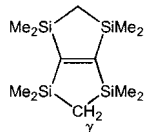
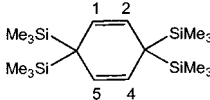
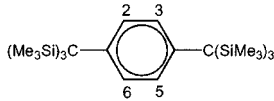
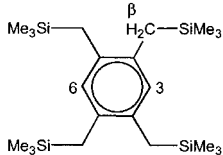
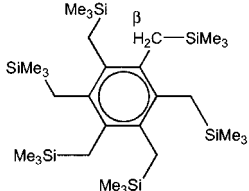
The g_e factors of the trimethylsilylmethyl-substituted radical cations **100**^{•+} and **822**^{•+}–**827**^{•+} were not reported. These cations were generated from the neutral compounds with AlCl_3 in dichloromethane.

Radical Cations of Dihydropyridazine and Phenylhydrazines

Ionized hydrazines, which have a three-electron N–N π bond, are considered in Chapt. 7.3 in the context of the radical cations of their alkyl derivatives. Hyperfine data for radical cations of dihydropyridazine and some phenylhydrazines are given in Table 9.39 [1111–1113]. The radical cation of dihydropyridazine (**828**) has a spin distribution similar to that of the isoelectronic radical anion of pyridazine (**574**) (Table 9.8). In the radical cations of the phenylhydrazines **829**–**832**, the π -spin population is delocalized into the phenyl groups, as indicated by the decrease of their ^{14}N -coupling constants from $+1.5 \pm 0.1$ mT for the alkylhydrazines (Table 7.17) to $+0.9 \pm 0.2$ mT in **829**^{•+}–**832**^{•+}.

The g_e factor of the phenylhydrazine radical cations is in the range 2.0030–2.0034. These radical cations were generated from the neutral compounds with Pb(IV) ions in TFA/dichloromethane (**832**^{•+} was formed by merely dissolving tetraphenylhydrazine in TFA) or by electrolysis in ACN.

Tab. 9.38. Hyperfine Data for Radical Cations of Some Trimethylsilylmethyl Derivatives of Ethene and Benzene, Me = CH(δ)₃

1,4-Bis(trimethylsilyl)-2,3-dimethyl-2-butene 822⁺		2H(β) 2H(β) 6H(β') 18H(δ) 2 ²⁹ Si	+1.072 +0.762 +1.072 0.046 -1.4	[1108]
Tetrakis(trimethylsilylmethyl)-ethene 823⁺		4H(β) 4H(β) 36H(δ) 4 ²⁹ Si	+0.855 +0.729 0.031 -1.25	[1108]
2,2,4,4,6,6,8,8-Octamethyl-2,4,6,8-tetrasilol[3.3.0]oct-1(5)-ene 100⁺		4H(γ) 24H(δ) 4 ²⁹ Si	0.248 0.062 -2.271	[576, 577]
3,3,6,6-Tetrakis(trimethylsilyl)-cyclohexa-1,4-diene 824⁺		H1,2,4,5 36H(δ) 4 ²⁹ Si	-0.303 0.018 -2.09	[1108]
1,4-Bis[tris(trimethylsilyl)methyl]benzene 825⁺		H2,3,5,6 54H(δ) 6 ²⁹ Si	-0.171 0.018 -0.63	[1109]
1,2,4,5-Tetrakis(trimethylsilylmethyl)benzene 826⁺		H3,6 8H(β) 36H(δ) 4 ²⁹ Si	+0.061 +0.579 0.018 -0.825	[1110]
Hexakis(trimethylsilylmethyl)-benzene 827⁺		12H(β) 54H(δ) 6 ²⁹ Si	+0.353 0.013 -0.54	[1110]

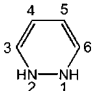
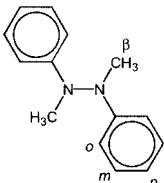
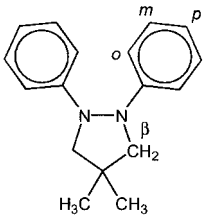
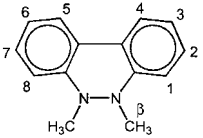
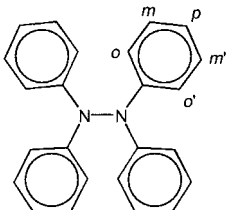
9.4

Radical Cations with Special Structures

Radical Cations of Nitrosobenzene and Diimino[14]annulenes

The common feature of these compounds is that they behave as electron acceptors in their reduction to π -radical anions (Chapt. 9.2), whereas the corresponding cations are σ radicals, in which the spin population is largely located at the two heteroatoms. Thus, the radical anion of nitrosobenzene (**35**), like that of nitrobenzene

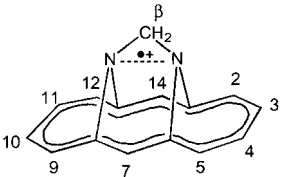
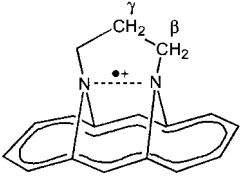
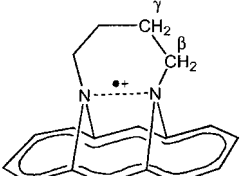
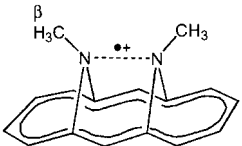
Tab. 9.39. Hyperfine Data for Radical Cations of Dihydropyrazine and Some Phenyl-substituted Hydrazines

<i>N,N'</i> -Dihydropyridazine 828 ^{•+}		¹⁴ N _{1,2} H _{1,2} H _{3,6} H _{4,5}	+0.781 -0.653 +0.092 -0.580	[1111]
1,2-Dimethyl-1,2-diphenylhydrazine 829 ^{•+}		2 ¹⁴ N 4H _o , 2H _p 4H _m 6H(β)	+1.085 -0.180 +0.08 +1.170	[1112]
4,4'-Dimethyl-1,2-diphenylpyrazolidine 830 ^{•+}		2 ¹⁴ N 4H _o , 2H _p 4H _m 4H(β)	+1.087 -0.195 +0.09 +1.185	[1112]
5,6-Dihydro-5,6-dimethylbenzo[<i>c</i>]cinnoline 831 ^{•+}		2 ¹⁴ N H _{1,8} H _{2,4,5,7} H _{3,6} 6H(β)	+0.879 -0.173 +0.055 -0.231 +0.822	[1112]
Tetraphenylhydrazine 832 ^{•+}		2 ¹⁴ N 4H _o } 4H _{o'} } 4H _m , 4H _{m'} 4H _p	+0.752 -0.137 -0.107 +0.048 -0.186	[1113]

(115), has a π structure (Table 9.21). However, the radical cation 35^{•+}, generated by electrolysis of nitrosobenzene in nitromethane or ACN ($g_e = 2.0007$) [360], is structurally related to the iminoxy σ radicals (Tables 7.22 and 7.23). This conclusion was drawn from its ¹⁴N- and ¹H-coupling constants, $a_N = +3.7$ and $a_H = +0.38$ mT (the latter value was observed for a single phenyl proton, presumably in the *meta* position).

In the radical anions of 1,6:8,13-diimino[14]annulenes (Table 9.28), as in both radical anions and cations of 1,6:8,13-dialkylidene[14]annulenes (Table 8.20), the spin distribution is that expected for a perturbed anthracene-like π perimeter (Figure 8.12). In contrast, the radical cations of these diimino[14]annulenes have a σ structure that is related to that of the radical cations of the bicycloalkane diamines 30, 31, and 265 and that of the quinuclidine dimer 179₂, with two formally non-

Tab. 9.40. Hyperfine Data for Radical Cations of Some 1,6:8,13-Diimino[14]annulenes

<i>N,N'</i> -Methano- <i>syn</i> -1,6:8,13-diimino[14]annulene 744 ^{•+}		2 ¹⁴ N	+0.633	[244]
		H2,5,9,12	+0.062	
		H3,4,10,11	-0.143	
		H7,14	<0.01	
		2H(β)	<0.01	
<i>N,N'</i> -Trimethylene- <i>syn</i> -1,6:8,13-diimino[14]annulene 32 ^{•+}		2 ¹⁴ N	+1.70	[244, 302]
		H2,5,9,12	{ +0.174 +0.154	
		H3,4,10,11	{ -0.210 -0.203	
		H7,14	{ 0.009 <0.005	
		2H(β)	+2.182	
		2H(β)	+0.059	
		H(γ)	-0.246	
H(γ)	-0.129			
<i>N,N'</i> -Tetramethylene- <i>syn</i> -1,6:8,13-diimino[14]annulene 33 ^{•+}		2 ¹⁴ N	+2.57	[244, 303]
		H2,5,9,12	+0.154 ^a	
		H3,4,10,11	-0.188 ^a	
		H7,14	0.012	
		4H(β)	+0.718 ^a	
4H(γ)	-0.051 ^a			
<i>N,N'</i> -Dimethyl- <i>syn</i> -1,6:8,13-diimino[14]annulene 743 ^{•+}		2 ¹⁴ N	+2.66	[244]
		H2,5,9,12	+0.172	
		H3,4,10,11	-0.189	
		H7,14	<0.02	
		6H(β)	+1.213	

^a Averaged values for two pairs of protons

linked amino groups in the neutral compounds (Table 7.18). This is because ionization of the lone pairs at the two heteroatoms of the diimine bridges gives rise to a N–N three-electron σ bond. The two nonbonding N-lone pairs interact through space, and the SOMO represents their antibonding combination σ^* (Chapt. 7.3).

ESR studies were performed on a series of radical cations of the diimino[14]annulenes, in which the two N atoms are linked by a chain of 1–7 methylene groups. Table 9.40 [244, 302, 303] gives hyperfine data for such radical cations with one (744), three (32), and four (33) methylene groups. The structure and properties of these radical cations critically depend on the number of methylene groups in the chain. The N-lone pairs in neutral diimino[14]annulenes are directed outward when the two N atoms are linked by a chain of one (744) or two methylene groups, but they are oriented inward when the chain contains three (32) or four (33) or more methylene groups. Their inward orientation is also indicated

for the N,N' -dimethyl derivative **743**; the hyperfine data for its radical cation are included in Table 9.40. Whereas the N–N three-electron σ bond formed upon oxidation to the radical cations is rather weak for the diimines with outward-directed lone pairs, it is strong for those with inward-oriented lone pairs. The radical cations with a strong bond of this kind are exceptionally stable, so that perchlorate salts of $32^{+\cdot}$ and $33^{+\cdot}$ were isolated and studied by X-ray crystallography. Formation of the N–N σ bond in the radical cations is in accordance with a decrease in the N–N interatomic distance from 270.5 pm in **32** to 216.0 pm in $32^{+\cdot}$ [302] and from 256.0 pm in **33** to 218.9 pm in $33^{+\cdot}$ [303]. The ^{14}N -coupling constant, which is +1.69 mT for $32^{+\cdot}$, as compared with +0.63 mT for $744^{+\cdot}$, reflects the strengthening of the N–N bond upon changing the orientation of the N-lone pairs from outward to inward orientation. In $32^{+\cdot}$, this N–N bond involves lone-pair AOs of an almost a “pure” p-character with axes nearly perpendicular to the “planes” of the approximately sp^2 -hybridized N atoms. A further increase in the a_{N} value to +2.57 in $33^{+\cdot}$ and +2.66 mT in $743^{+\cdot}$ is due to a deviation from this geometry, leading to an s-contribution to the character of the pertinent AOs. For reasons of symmetry, the singly-occupied MO σ^* of the N-lone pairs in the radical cations interacts with the HOMO ψ_{3-} of the 14-membered π perimeter (which is related to the LUMO ψ_{4-} by the pairing properties; Figure 8.12), whereas in the corresponding anions, the SOMO resembles the LUMO ψ_{4+} . The differing structures of these radical ions are dramatically manifested (Figure 9.4) by the total extents of their ESR spectra which are shown for $743^{+\cdot}$ and $743^{-\cdot}$ in Figure 9.4. These extents are 14.04 for the cation vs. 1.84 mT for the anion.

The g_e factor of $744^{+\cdot}$ is 2.0029, and that of the other radical cations of diimino[14]annulenes with a strong N–N bond is 2.0036 ± 0.0001 . Generation of all these radical cations from the neutral compounds was carried out in dichloromethane by electrolysis or by reaction with Ag(I) and Pb(IV) ions, as well as by oxidation with nitrosyletrafluoroborate or tris(*p*-bromophenyl)ammoniumyl hexachlorantimonate (“magic blue”).

Radical Cations of Diphenyldiazomethanes and Diphenylcarbene

We noted in the previous section that the radical cations of nitrosobenzene and 1,6:8,13-diimino[14]annulenes have σ structure, whereas the corresponding anions are π radicals. As mentioned in Chapt. 2.3, both σ and π structures were observed for the radical cation of diphenyldiazomethane (**37**). Under various conditions, this radical cation exhibits strikingly differing color, hyperfine pattern and photostability. Because of the dependence of its color on the environment, it has been called a “chemical chameleon”. Hyperfine data for $37^{+\cdot}$, which are shown on p. 78, are given again for convenience in Table 9.41, together with those for the radical cations of structurally related 9-diazo-9,10-dihydro-10,10-dimethylantracene (**833**) and 5-diazo-10,11-dihydro-5*H*-dibenzo[*a,d*]cycloheptene (**834**). The behavior of $37^{+\cdot}$, which occurs as a π - and σ -radical cation, is shared by $834^{+\cdot}$, but only the π structure was observed for $833^{+\cdot}$. The π -radical cations are expected to have a linear CNN group, which should be bent in their σ counterparts. The bending in the

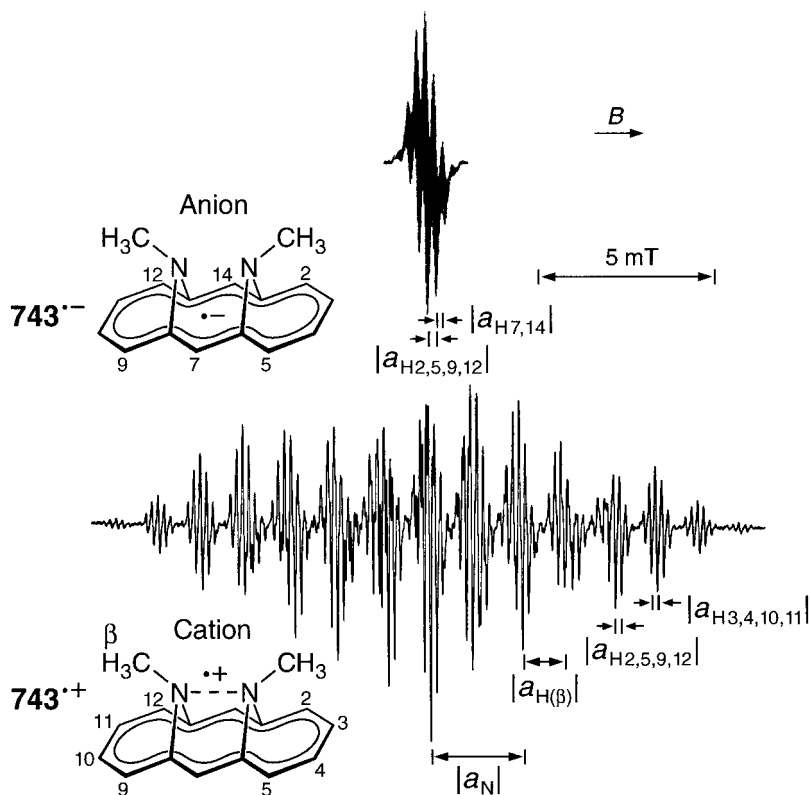


Fig. 9.4. ESR spectra of the radical ions of *N,N'*-dimethyl-*syn*-1,6:8,13-diimino[14]annulene (**743**). Top, anion **743**^{•-}: solvent DME, counterion K⁺, temperature 273 K. Bottom, cation **743**^{•+}: solvent: dichloromethane, counterion SbCl₆⁻, temperature 298 K. Spectrum of **743**^{•+} reproduced by permission from [244].

σ -radical cations σ -**37**⁺ and σ -**834**⁺ gives rise to large ¹⁴N-coupling constants ($a_N = +1$ to $+2$ mT) and vanishingly small ¹H-hyperfine splittings, whereas the π -radical cations π -**37**⁺, π -**833**⁺, and π -**834**⁺ have moderate and comparable $|a_N|$ and $|a_{H_{\alpha,p}}|$ values (0.25–0.45 mT). The coupling constant of the ¹³C isotope in the diazo-C atom is $+1.13$ for π -**37**⁺ but $+3.35$ mT for σ -**37**⁺. The drastically different hyperfine patterns of this radical cation in its π - and σ -structures are demonstrated by the ESR spectra in Figure 9.5. The dependence of the structure only on experimental conditions (see below) indicates that the π and σ states of **37**⁺ are energetically very close. However, this proximity is not found theoretically as an intrinsic property of **37**⁺ but must be due to some unidentified solvent (and/or counterion) effects acting to preferentially stabilize the σ states.

The g_e factors of the π - and σ -radical cations are 2.0027 ± 0.0002 and 2.0009 ± 0.0002 , respectively. The radical cations π -**37**⁺ and π -**834**⁺ were generated in

Tab. 9.41. Hyperfine Data for Radical Cations of Diphenyldiazomethane and Structurally Related Compounds

Diphenyldiazomethane π - $37^{+\bullet}$		$^{14}\text{N}1$ $^{14}\text{N}2$ 4H_o 4H_m 2H_p $^{13}\text{C}3$	+0.44 -0.33 -0.25 +0.10 -0.34 +1.13	[245]
σ - $37^{+\bullet}$		$^{14}\text{N}1$ $^{14}\text{N}2$ $4\text{H}_o, 4\text{H}_m, 2\text{H}_p$ $^{13}\text{C}3$	+1.01 +1.68 <0.2 +3.35	[245]
9-Diazo-9,10-dihydro-10,10-dimethylantracene $833^{+\bullet}$		$^{14}\text{N}1$ $^{14}\text{N}2$ 4H_o 4H_m 2H_p	+0.40 -0.32 -0.24 +0.076 -0.32	[245]
5-Diazo-10,11-dihydro-5H-dibenzo[<i>a,d</i>]cycloheptene π - $834^{+\bullet}$		$^{14}\text{N}1$ $^{14}\text{N}2$ 4H_o 4H_m 2H_p $2\text{H}_{ax}(\beta)$ $2\text{H}_{eq}(\beta)$	+0.44 -0.38 -0.26 +0.08 -0.35 +0.47 +0.18	[245]
σ - $834^{+\bullet}$		$^{14}\text{N}1$ $^{14}\text{N}2$ $4\text{H}_o, 4\text{H}_m, 2\text{H}_p$ $4\text{H}(\beta)$	+1.02 +1.84 <0.2	

solution from the neutral compounds in dichloromethane by reaction with tris(4-bromophenyl)- or tris(2,4-dibromophenyl)ammoniumyl hexachloroantimonate (magic blue and magic green, respectively), whereas σ - $37^{+\bullet}$ and σ - $834^{+\bullet}$ were obtained by electrolysis of these compounds in dichloromethane (supporting salt tetra-*n*-butylammonium tetrafluoroborate). With γ -irradiation of **37** and **834** in matrices, π -radical cations were formed in frozen $\text{CF}_2\text{BrCF}_2\text{Br}$, but their σ counterparts were produced in CFCl_3 glasses; the $\text{CF}_2\text{BrCF}_2\text{Br}$ matrix became blue and the CFCl_3 matrix light pink. Under all these conditions, only the π structure was observed for $833^{+\bullet}$. The primary radical cations were not persistent and readily lost a dinitrogen in solution. A secondary paramagnetic species from $37^{+\bullet}$ was identified as the radical cation of tetraphenylethene (**424**) (Table 8.12).

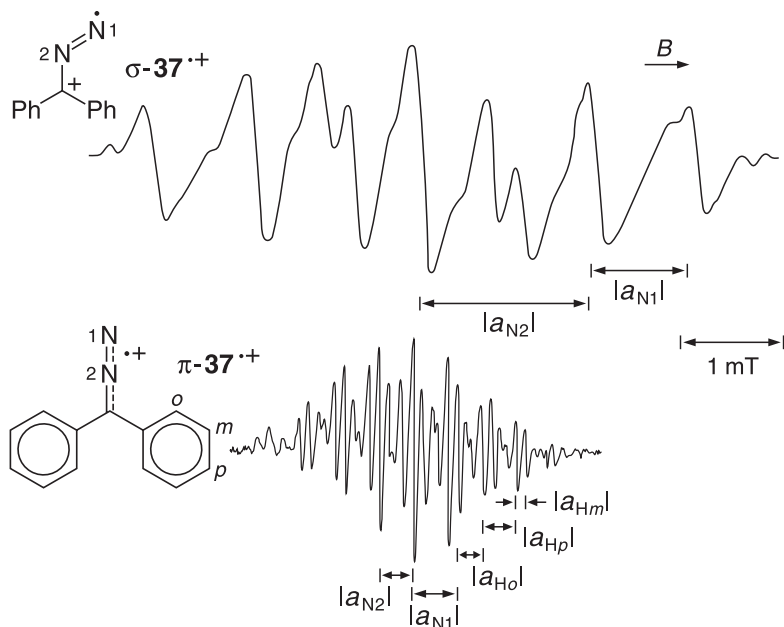


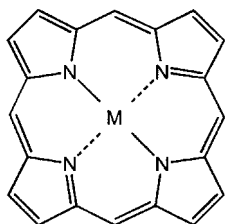
Fig. 9.5. ESR spectra of the π - and σ -radical cations of diphenyldiazomethane (**37**). Solvent dichloromethane. Top, $\sigma\text{-37}^{\cdot+}$ (generated electrolytically): counterion SbCl_6^- , temperature 198 K. Bottom, $\pi\text{-37}^{\cdot+}$ (generated “chemically”): counterion BF_4^- , temperature 183 K. Reproduced by permission from [245].

Photolysis of $\pi\text{-37}^{\cdot+}$ in a $\text{CF}_2\text{BrCF}_2\text{Br}$ matrix, but not that of $\sigma\text{-37}^{\cdot+}$ in a CFCl_3 glass, yielded the diphenylcarbene radical cation $36^{\cdot+}$, which is shown to have the σ structure, by virtue of its large coupling constant, $a_{\text{C}} = +9.83$ mT, observed for the ^{13}C isotope in the diazo-C atom [361]. This finding is in agreement with theoretical calculations which predict that the $\sigma^0\pi^0$ state is substantially more stable than the $\sigma^0\pi^{\cdot}$ state.

9.5 Radical Ions of Multi-redox Systems

Porphyrins are heterocyclics with an extended π system that are structurally related to bridged [18]- and [20]annulenes; they can function as both good electron donors and acceptors, yielding several redox stages, alternatively dia- and paramagnetic. Because their deeply colored metal complexes are biologically highly relevant, they have been called “pigments of life” [1114]. Surprisingly, only a few ESR studies were reported for the radical ions of unsubstituted porphyrin (**835**; $\text{M} = 2\text{H}$) and the corresponding metalloporphyrins (**835**; $\text{M} = \text{metal}$), which have an effective D_{4h} symmetry. Because of the dynamic Jahn–Teller effect in these

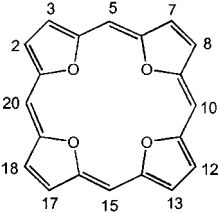
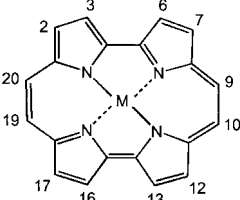
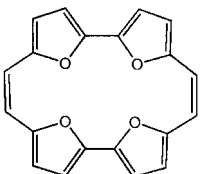
molecules with a degenerate ground state (Chapt. 6.6 and 8.2), the ESR spectra of their radical ions were poorly resolved and no ENDOR signals could be detected. A single unresolved ESR signal was observed for the anions $835^{\cdot-}$ ($M = 2H$ or metal) ($g_e = 2.0026$ for $M = 2H$) [1115], and, to our knowledge, no ESR studies on the corresponding cations $835^{\cdot+}$ were reported, although radical cations of chlorophyll α with low symmetry were investigated by 1H -ENDOR spectroscopy [1116].



835

Tetraoxaporphyrin (**836**), which also has D_{4h} symmetry, has five readily identifiable redox stages, namely, the dication (isolated as a salt), the radical cation, the neutral compound (tetraoxaisochlorin), the radical anion, and the dianion. These redox stages are isoelectronic with five redox stages of the free base porphyrin (**835**; $M = 2H$), namely the neutral compound, the radical anion, the dianion, the radical trianion and the tetranion, respectively. The radical ions $836^{\cdot-}$ and $836^{\cdot+}$, like those of porphyrins, have a degenerate ground state and gave rise to broad ESR signals with only slightly resolved hyperfine splittings. With the ENDOR technique being not applicable to these radical ions, their hyperfine patterns were analyzed by computer and yielded the 1H -coupling constants listed in Table 9.42 [268, 613, 1117]. In contrast to the radical ions of porphyrin and metalloporphyrins, the radical anions of the isomeric porphycene (**837**; $M = 2H$) and metalloporphycenes (**837**; $M = \text{metal}$) have an effective D_{2h} symmetry, and they exhibited well-resolved ESR spectra that were amenable to the ENDOR technique. The four ^{14}N nuclei $837^{\cdot-}$ appear equivalent, not only for the radical anions of metalloporphycenes ($M = \text{metal}$), but also for that of the free base ($M = 2H$), which indicates fast tautomerization of the two α protons on the hyperfine time-scale. Well-resolved ESR spectra and readily-observable ENDOR signals were also reported for the radical ions of tetraoxaporphycene (**109**), an isomer of tetraoxaporphyrin (**836**). The five redox stages of **109**, from the dication to the dianion, are isoelectronic with those of free base porphycene (**837**; $M = 2H$), from the neutral compound to the tetraanion, in analogous way to the five redox stages of tetraoxaporphyrin vs. those of the free base porphyrin. The hyperfine data for $109^{\cdot-}$ and $109^{\cdot+}$ are given in Table 9.41, together with those for $837^{\cdot+}$ ($M = 2H$ or Zn). As pointed out in Chapt. 6.6, the radical anion $109^{\cdot-}$ is tightly associated with alkali-metal cations in MTHF: the counterion lies on the fourfold axis and contacts the lone pairs of the four O atoms in a chelate-like fashion (p. 144). The 1H -coupling constants for $109^{\cdot-}$ change systematically as the ion pairs become tighter in order

Tab. 9.42. Hyperfine Data for Radical Ions of Tetraoxaporphyrin, Porphycene and Tetraoxaporphycene

Tetraoxaporphyrin $836^{\cdot-}/836^{\cdot+}$		H2,3,7,8,12,13,17,18 H5,10,15,20	Anion -0.129 -0.197	Cation -0.122 -0.198	[268]
Porphycene $837^{\cdot-}$		H2,7,12,17 H3,6,13,16 H9,10,19,20 2H(α) 4^{14}N	Anion M = 2H(α) -0.146 -0.182 -0.096 +0.018 -0.071	Anion M = Zn -0.165 -0.171 -0.083 -0.068	[1117]
Tetraoxaporphycene $109^{\cdot-}/109^{\cdot+}$		H2,7,12,17 H3,6,13,16 H9,10,19,20	Anion -0.085 -0.037 -0.234	Cation -0.145 -0.169 -0.123	[613]

of decreasing size of the counterion. (For the coupling constants of the alkali-metal nuclei in the counterions, see Table A.2.2). The similarity of the ^1H -coupling constants for the radical cation $109^{\cdot+}$ and the radical anion of the free base porphycene ($837^{\cdot-}$; M = 2H) is in accordance with their isoelectronic structure.

The g_e factors of $836^{\cdot-}$, $836^{\cdot+}$, $109^{\cdot-}$, and $109^{\cdot+}$ are 2.0031, 2.0027, 2.0032, and 2.0024, respectively. That of $837^{\cdot-}$ is 2.0025 (M = H₂) and 2.0024 (M = Zn). The radical anions $836^{\cdot-}$ and $109^{\cdot-}$ were generated from the neutral compounds or the dications with an alkali-metal in an ethereal solvent, and the radical cations $836^{\cdot+}$ and $109^{\cdot+}$ were produced from the neutral compounds with Tl(III) ions in TFA or with AlCl₃ in dichloromethane or from the dications with zinc or mercury. The radical anions $837^{\cdot-}$ (M = 2H or metal) were formed from the neutral precursors in THF by reaction with sodium or electrolytically.

10

Saturated Hydrocarbon Radicals

As stated in Chapt. 2.3, organic molecules that are difficult to ionize ($IE > 8$ eV) can be converted to their radical cations by high-energy irradiation in inert matrices; the reactive paramagnetic species formed under such conditions are sufficiently long-lived to be characterized by ESR spectroscopy. These statements hold, in particular, for saturated hydrocarbons and their radical cations, which are usually of σ -type with their SOMO being largely confined to a few C–C and C–H σ bonds. However, π -radical cations can also be formed as primary paramagnetic species upon ionization of some cycloalkanes and bicycloalkanes. For the radical cations in Tables 10.1–10.4, the formulas are those of the neutral alkanes without the symbols of unpaired electrons and charge.

10.1

Radical Cations of Alkanes

ESR studies on these radical cations in solid matrices were reviewed in 1987 [306].

Radical Cations of Acyclic Alkanes

Methane CH_4 (**838**) was ionized by bombardment with high-energy particles (atoms, electrons, or photons) in a neon matrix at 4 K [334, 335]. The ESR spectrum of the radical cation $\text{CH}_4^{+\cdot}$ (**838** $^{+\cdot}$), which, in the T_d symmetry, has a degenerate ground state and is subject to Jahn–Teller distortion, exhibited a hyperfine pattern from four protons with a coupling constant a_H of +5.48 mT ($g_e = 2.0029$). Under the same conditions, the radical cation $\text{CH}_2\text{D}_2^{+\cdot}$ (**838**- $d_2^{+\cdot}$), had $a_H = +12.17$ and $a_D = -0.222$ mT, due to the two protons and two deuterons; the a_D value is equivalent to $a_H = -0.222/0.1535 = -1.45$ mT. Ab initio calculations [1118, 1119] predict C_{2v} symmetry for **838** $^{+\cdot}$, with differing pairs of C–C bonds and HCH angles. The observed coupling constant of the four protons in this σ -radical cation thus represents a value averaged by a dynamic Jahn–Teller effect (Chapt. 6.7). The ^{13}C -coupling constant for **838** $^{+\cdot}$ was determined as $a_C = +0.14$ mT [1120].

Tab. 10.1. Hyperfine Data for Radical Cations of Some *n*-Alkanes

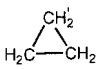
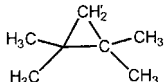
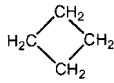
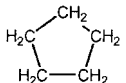
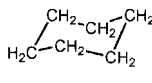
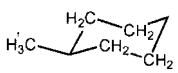
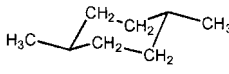
Ethane 839 ⁺	H ₃ CCH ₃	2H _{<i>ip</i>} 4H _{<i>op</i>}	+15.25 <0.2	} 6H	+5.03	[313]
Propane 840 ⁺	H ₃ CCH ₂ CH ₃	2H _{<i>ip</i>}	+9.50			
Butane 841 ⁺	H ₃ C(CH ₂) ₂ CH ₃	2H _{<i>ip</i>} 4H _{<i>op</i>}	+6.15 -1.05			[1121]
Pentane 842 ⁺	H ₃ C(CH ₂) ₃ CH ₃	2H _{<i>ip</i>}	+4.95			[1121]
Hexane 843 ⁺	H ₃ C(CH ₂) ₄ CH ₃	2H _{<i>ip</i>} 4H _{<i>op</i>} 4H _{<i>op</i>}	+4.08 -0.68 -0.36			[1121]
Heptane 844 ⁺	H ₃ C(CH ₂) ₅ CH ₃	2H _{<i>ip</i>}	+3.70			[1121]

The radical cations of higher alkanes were generated by γ -irradiation of the neutral compounds in solid SF₆ or various Freons, and their hyperfine patterns depend somewhat on the matrix and temperature. The data listed in Table 10.1 [313, 1121] for these σ species were all obtained in SF₆ matrices at 77 K; only the value of +15.25 mT for the radical cation of ethane H₃CCH₃ (**839**) was observed at 4 K. Like CH₄⁺ (**838**⁺), this radical cation is Jahn–Teller-distorted to avoid the degenerate ground state of *D*_{3h} symmetry. At 4 K, its hyperfine pattern is due to two protons with a large coupling constant of +15.25 mT, which corresponds to a 1s-spin population of ca +0.3 (Chapt. 4.1). At 77 K, this pattern changes reversibly

Tab. 10.2. Hyperfine Data for Radical Cations of Some Branched Alkanes

2-Methylpropane (isobutane) 845 ⁺	(H ₃ C) ₃ C	2H	+5.25	[313]
2-Methylbutane (isopentane) 846 ⁺	(H ₃ C) ₂ CHCH ₂ CH ₃	3H	+4.30	[1122]
2,2-Dimethylpropane (neopentane) 847 ⁺	(H ₃ C) ₄ C	3H	+3.98	[313]
2,2-Dimethylbutane 848 ⁺	(H ₃ C) ₃ CCH ₂ CH ₃	4H	+3.70	[1122]
2,3-Dimethylbutane 849 ⁺	(H ₃ C) ₂ CHCH(CH ₃) ₂	4H	+3.75	[1122]
2,2,3-Trimethylbutane 850 ⁺	(H ₃ C) ₃ CCH(CH ₃)CH ₃	5H	+3.20	[1122]
2,2,3,3-Tetramethylbutane (hexamethylethane) 851 ⁺	(H ₃ C) ₃ CC(CH ₃) ₃	6H	+2.90	[309]

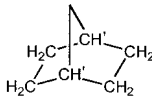
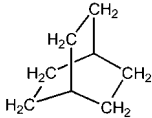
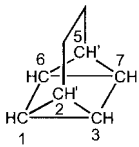
Tab. 10.3. Hyperfine Data for Radical Cations of Some Cycloalkanes and Their Methyl Derivatives

Cyclopropane 852 ⁺		4H 2H'	-1.25 +2.10			[1123]
1,1,2,2-Tetramethyl- cyclopropane 853 ⁺		12H 2H'	1.50 +1.87			[315]
Cyclobutane 854 ⁺		2H 2H 4H	+4.9 +1.4 -0.5	8H	+1.33	[1124]
Cyclopentane 855 ⁺		2H 8H	+2.24 <0.2			
Cyclohexane 856 ⁺		2H _{eq} 2H _{eq} 2H _{eq}	+8.5 +1.4 +3.4	4H _{eq} 2H _{eq}	+5.0 +2.9	[1126] [1125]
Methylcyclohexane 857 ⁺		2H _{eq} 2H _{eq} 1H'	+4.88 +4.22 2.10			6H _{eq}
1,4-Dimethylcyclo- hexane 858 ⁺		4H _{eq}	+5.62			[1128]

to that arising from all six protons and showing a coupling constant of +5.03 mT, which is nearly one-third the two-proton value observed at 77 K. Evidently, the symmetry of **839⁺** is lowered from D_{3h} to C_{2h} , but a dynamic Jahn–Teller effect averages the coupling constants upon raising the temperature.

A large coupling constant of two protons is a prominent feature of the radical cations of *n*-alkanes. It is attributed to two in-plane protons (H_{ip}) of the terminal

Tab. 10.4. Hyperfine Data for Radical Cations of Some Polycycloalkanes

Norbornane 859 ⁺		2H _{exo} 2H'	+6.51 -0.35			[1129]
Bicyclo[2.2.2]octane 860 ⁺		4H 4H 4H	+3.85 +1.58 +0.82	12H	+2.0	[1129]
Quadricyclane 861 ⁺		4H 2H'	+0.57 +0.27			

methyl groups; the pertinent plane contains the two C–H_{ip} and all C–C σ bonds in an extended chain structure. The symmetry should thus be C_{2h} when the number, n , of C atoms is even (including 839^{+} with $n = 2$) and C_{2v} when it is odd. The coupling constant $a_{H_{ip}}$ smoothly decreases as the chain length increases, from +15.25 for $n = 2$ to +3.70 mT for $n = 7$ (Table 10.1). Sometimes, additional, smaller coupling constants were observed and were assigned to the out-of-plane protons (H_{op}) in the methylene groups of the chain; their values differ in different matrices.

Table 10.2 [309, 313, 1122] gives hyperfine data for radical cations generated from several branched alkanes in Freon matrices and observed at 77 K. In contrast to their “linear” counterparts, their SOMO seems to be confined to one C–C linkage and to the methyl C–H σ bonds parallel to that C–C bond. In the radical cation of hexamethylethane (**851**), which has been studied often, each of the six protons giving rise to the observed main hyperfine splitting belongs to a different methyl group.

Upon illumination by visible light or raising the temperature, the alkane radical cations deprotonate to the corresponding alkyl radicals (Table 7.1). Thus, 839^{+} , 840^{+} , and 845^{+} , are converted into the ethyl (59^{\bullet}), n -propyl (60^{\bullet}) or isopropyl (140^{\bullet}), and *tert*-butyl radical (141^{\bullet}), respectively. Elimination of H_2 , CH_4 , or, in general, of C_nH_{2n+2} fragments also occurred.

Radical Cations of Cycloalkanes

Table 10.3 [315, 1123–1128] lists hyperfine data for some of these σ -radical cations which were generated from the neutral cycloalkanes by γ -irradiation in Freon matrices. The unsubstituted radical cations have a degenerate ground state and are subject to Jahn-Teller distortion, which lowers their symmetry. The hyperfine pattern of the radical cation of cyclopropane (**852**) in a $CFCl_2CF_2Cl$ matrix at 4 K is due to two and four protons with coupling constants of +2.10 and -1.25 mT, respectively. The symmetry of 852^{+} is thus reduced from D_{3h} to C_{2v} , with one of the C–C bonds becoming longer, and two shorter. At 77 K, averaging of the two values (which have opposite signs) yielded a hyperfine splitting that was too small to be resolved. Analogously, the radical cation of 1,1,2,2-tetramethylcyclopropane (**853**) in a $CFCl_3$ matrix at 145 K had coupling constants of +1.87 and 1.50 mT (sign undetermined) arising from two ring protons and 12 methyl protons, respectively. Cyclobutane (**854**) is puckered in the D_{2d} symmetry, and its radical cation distorts to a C_{2v} structure. In a $CFCl_3$ matrix at 4 K, 854^{+} exhibited coupling constants of +4.9, +1.4, and ca -0.5 mT arising from two, two, and four protons respectively; they yielded an averaged eight-proton value of +1.33 mT at 77 K. In the ESR spectrum of the radical cation of cyclopentane (**855**) in a CF_3CCl_3 matrix, only one hyperfine splitting by two protons was resolved at 6 K ($a_H = +2.24$ mT), but a binomial pattern arising from all 10 protons with a coupling constant of +0.63 mT was observed at 113 K.

Cyclohexane (**856**) has D_{3d} symmetry in its chair conformation, and the ground-state degeneracy of its radical cation is likewise removed by distortion to a structure of lower symmetry (C_{2h} or C_s). The observed hyperfine pattern of 856^{+} depends

on the matrix used. From an anisotropic ESR spectrum taken with CFCl_3 at 4 K, the isotropic values of three coupling constants +8.5, +3.4, and +1.4 mT, each of two protons, were derived. At 77 K, two of these values averaged to a four-proton coupling constant of +5.0 mT, leaving the third value at +2.9 mT. In a CF_3CCl_3 matrix at 141 K, a coupling constant of +4.3 mT was observed for six protons. The protons giving rise to an observable hyperfine splitting are assumed to be in the equatorial positions of cyclohexane. In a perfluoromethylcyclohexane matrix at 77 K, the radical cation of 1,4-dimethylcyclohexane (**858**) exhibited a hyperfine pattern due to four protons with a coupling constant of +5.62 mT, and for methylcyclohexane (**857**), values of +4.88 and +4.22, each arising from two ring protons, and 2.10 mT from a single proton (sign undetermined), were obtained. Assuming the methyl substituents to be in the equatorial positions, these results suggest C_{2h} and C_s symmetry for $\mathbf{858}^{\cdot+}$ and $\mathbf{857}^{\cdot+}$, respectively. Thus, the observed coupling constant for $\mathbf{858}^{\cdot+}$ and the two larger values for $\mathbf{857}^{\cdot+}$ were assigned to the four ring protons in the equatorial unsubstituted positions (the smallest coupling constant for $\mathbf{857}^{\cdot+}$ was attributed to one methyl proton).

Light and warming cause deprotonation of the cycloalkane radical cations to the corresponding cycloalkyl radicals (Table 7.2), such as cyclobutyl (**61** \cdot) and cyclohexyl (**121** \cdot) when starting from $\mathbf{854}^{\cdot+}$ and $\mathbf{856}^{\cdot+}$, respectively.

Radical Cations of Polycycloalkanes

Hyperfine data for radical cations of three polycycloalkanes, generated by γ -irradiation in Freon matrices, are given in Table 10.4 [1129, 1130]. The hyperfine pattern of the radical cation of norbornane (**859**) in a $\text{CF}_2\text{ClCFCl}_2$ matrix at 4 K is due to a coupling constant of +6.51 mT arising from the four methylene *exo* protons. Warming to 100 K led to observation of an additional smaller value of -0.35 mT belonging to the two bridgehead-methine protons. The radical cation of bicyclo[2.2.2]octane (**860**), which has D_{3h} symmetry, undergoes a Jahn–Teller distortion. Its ESR spectrum, taken with CFCl_3 at 4 K, is rather complicated because of incomplete averaging by the dynamic Jahn–Teller effect. Simulation yielded coupling constants of +3.85, +1.58, and +0.82 mT, each of four protons; these values were assigned to three sets of the four methylene protons in $\mathbf{860}^{\cdot+}$, which has C_{2v} symmetry. In a perfluorocyclohexane matrix at 77 K, a hyperfine splitting by all 12 methylene protons, with an averaged coupling constant of +2.0 mT, was observed. The radical cation of quadricyclane (**861**) was obtained as a photoproduct from the radical cation of isomeric norbornadiene (**379**) (Table 8.7), which was generated from the neutral diene by γ -irradiation in a CFCl_3 matrix. The ESR spectrum of $\mathbf{861}^{\cdot+}$ at 135 K exhibited coupling constants of +0.57 and +0.27 mT, assigned to four and two methine protons in the 1,6,7,8- and 2,5-positions, respectively.

Upon warming, $\mathbf{859}^{\cdot+}$ deprotonated to 2-norbornyl (**154** \cdot), $\mathbf{860}^{\cdot+}$ gave the bicyclo[2.2.2]oct-2-yl radical (**156** \cdot ; both Table 7.3), and $\mathbf{861}^{\cdot+}$ isomerized to $\mathbf{379}^{\cdot+}$.

The reported g_e factors of alkane radical cations in SF_6 and Freon matrices generally lie in the range 2.003 to 2.004, although lower or higher values were also observed. Relative to the g_e factors of hydrocarbon σ -radical cations in fluid solution, they seem to be enhanced by interaction with the matrix.

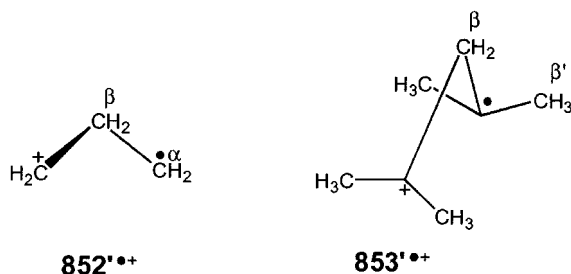
10.2

Structurally Modified Radical Cations

As mentioned above, formation of primary π -radical cations can occur upon ionization of some cycloalkanes and bicycloalkanes. An accompanying structural change involves a considerable elongation and, consequently, substantial weakening, of one C–C σ bond. Because the geometric integrity of the pertinent molecules **M** is otherwise conserved upon ionization, their formal notation has been retained for their structurally modified radical cations, which are referred to as $\mathbf{M}^{\prime+}$ (instead of $\mathbf{M}^{+\bullet}$).

“Ring-opened Forms” of Cyclopropane Radical Cations

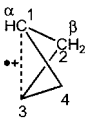
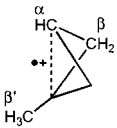
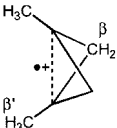
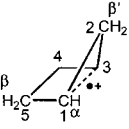
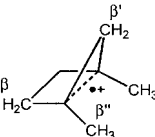
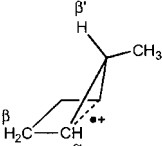
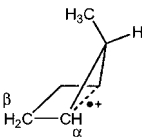
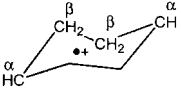
The structure of a trimethylene π -radical cation (**852** $^{\prime+}$) ($g_e = 2.0028$) was proposed for ionized cyclopropane (**852**) in a γ -irradiated $\text{CF}_2\text{ClCFCl}_2$ matrix above 80 K [1131], because the observed coupling constants $a_{\text{H}}(\alpha) = -2.24$ and $a_{\text{H}}(\beta) = +3.06$ mT, each for two methylene protons, are similar to those for the *n*-propyl radical (**60** \cdot) (Table 7.1). The “mobile” $\text{CF}_2\text{ClCFCl}_2$ matrix is particularly favorable for rearrangement of radicals, and the ring-opened structure results from further elongation of one σ bond in the Jahn–Teller-distorted cyclopropane radical cation (**852** $^{\prime+}$) (see above). An analogous form **853** $^{\prime+}$ ($g_e = 2.0032$) was observed for ionized 1,1,2,2-tetramethylcyclopropane (**853**) in a $\text{CF}_2\text{ClCFCl}_2$ matrix, although only above 120 K [315]. The hyperfine pattern of **853** $^{\prime+}$ is due to the coupling constants $a_{\text{H}}(\beta) = +2.33$ and $a_{\text{H}}(\beta') = +1.17$ mT for the two methylene and six methyl protons, respectively. A structure of a “distonic” radical cation was suggested for both **852** $^{\prime+}$ and **853** $^{\prime+}$ in which the unpaired electron and positive charge are separated (Chapt. 2.3). However, the two radical cations should differ in their conformations, **852** $^{\prime+}$ having a “bisected” and **853** $^{\prime+}$ an “eclipsed” conformation.



Diyl Radical Cations from Bicycloalkanes

For some ionized bicycloalkanes, one of the σ bonds is stretched to such an extent that the radical cation must be considered a diyl with two pertinent C atoms as π centers bearing the bulk of the spin population. Table 10.5 [317, 329, 330, 1132, 1133] presents hyperfine data for several examples of such 1,3-diyl cations **862** $^{\prime+}$ –**867** $^{\prime+}$ generated by γ -irradiation in Freon matrices from bicyclo[1.1.0]butane

Tab. 10.5. Hyperfine Data for Some Cycloalkane-1,3-diyl Radical Cations

Cyclobutane-1,3-diyl 862 ^{•+} (869 ^{•+})		2H(α) 2H _{ax} (β) 2H _{eq} (β)	-1.142 +7.71 +1.188	[317, 329]
1-Methylcyclobutane-1,3-diyl 863 ^{•+} (870 ^{•+})		H(α) 2H _{ax} (β) 2H _{eq} (β) 3H(β')	-0.92 +6.89 +0.92 +1.73	[329]
1,3-Dimethylcyclobutane-1,3-diyl 864 ^{•+} (871 ^{•+})		2H _{ax} (β) 2H _{eq} (β) 6H(β')	+6.51 +0.89 +1.65	[329]
Cyclopentane-1,3-diyl 865 ^{•+} (38 ^{•+})		2H(α) 2H _{exo} (β) H _{ax} (β')	-1.17 +3.35 +4.49	[717]
1,3-Dimethylcyclopentane-1,3-diyl 866 ^{•+} (872 ^{•+})		2H _{exo} (β) H _{ax} (β') 6H(β'')	+2.50 +4.21 +1.61	[330]
2- <i>eq</i> -Methylcyclopentane-1,3-diyl <i>eq</i> - 867 ^{•+} (<i>eq</i> - 873 ^{•+})		2H(α) 2H _{exo} (β) H _{ax} (β')	-1.17 +3.28 +4.39	[1132]
2- <i>ax</i> -Methylcyclopentane-1,3-diyl <i>ax</i> - 867 ^{•+} (<i>ax</i> - 873 ^{•+})		2H(α) 2H _{exo} (β)	-1.19 +3.25	[1132]
Cyclohexane-1,4-diyl 874 ^{•+} (868 ^{•+})		2H(α) 4H _{ax} (β)	-1.2 +1.2	[1133]

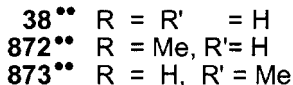
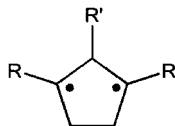
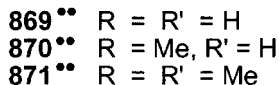
(**862**), bicyclo[2.1.0]pentane (housane; **865**), and some of their methyl derivatives. The cyclobutane-1,3-diyl cation **862**^{•+}, obtained from **862**, has two methine-C atoms as the spin-bearing π centers 1 and 3, and its geometry is intermediate between the planar triplet cyclobutane-1,3-diyl (**869**^{••}) and the buckled **862**. The prominent feature of its ESR spectrum is the coupling constant of +7.71 mT, arising from the two methylene β protons in the axial positions. This extremely

large value is due to the high spin population ($\rho_{1,3}^{\pi} \approx 0.5$) at the two π centers, the small dihedral angle ($\theta \approx 20^\circ$) between the C–H_{ax}(β) bonds and the 2p_z-axes at these centers, and the “Whiffen effect” for protons in bridging methylene groups (Eq. 4.11). The two methine α protons and the two methylene β protons in the equatorial positions give rise to smaller coupling constants of -1.188 and $+1.142$ mT, respectively. Substitution at the π centers by methyl groups leads to a decrease in all $|a_{\text{H}}|$ values by partial withdrawal (ca 15%) of the spin population to the substituents, as indicated by the hyperfine data for 1-methyl- and 1,3-dimethylcyclobutane-1,3-diyl cations **863**^{‘+’} and **864**^{‘+’} generated from 1-methyl (**863**) and 1,3-dimethylbicyclo[2.1.0]butane (**864**), respectively.

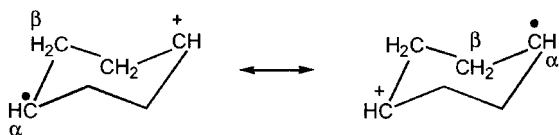
Similarly, the cyclopentane-1,3-diyl cation **865**^{‘+’} produced from housane (**865**) has two π -like centers 1 and 3, and its geometry is intermediate between the planar triplet cyclopentane-1,3-diyl (**38**^{••}) and the buckled **865**. Its ESR spectrum exhibits coupling constants of $+4.49$, $+3.35$, and -1.17 mT for the single methylene β' proton in the axial 2-position, the two methylene β protons in the 4,5-*exo* positions, and the two α protons at the spin-bearing centers 1 and 3. (The hyperfine splittings by the remaining protons were too small to be resolved.) The large values for the β' protons are again due to the high spin population $\rho_{1,3}^{\pi}$ and the small dihedral angle θ ; in addition, the 2-axial proton in the bridging methylene group benefits from the “Whiffen effect”. The hyperfine data for the 1,3-dimethylcyclopentane-1,3-diyl cation **866**^{‘+’} generated from 1,4-dimethylhousane (**866**) indicate that, here also, 1,3-dimethyl substitution at the π centers lowers their spin population. The isomeric 2-methylcyclopentane-1,3-diyl cations *eq*- and *ax*-**867**^{‘+’} were produced from 5-*anti*- and 5-*syn*-methylhousanes (*anti*- and *syn*-**867**), respectively. As might be expected for these radical cations in the absence of ring inversion, substitution by a methyl group in the equatorial 2 position (*eq*-**867**^{‘+’}) does not markedly change the hyperfine pattern of the parent diyl cation **865**^{‘+’}, but introducing a methyl group in the corresponding axial position (*ax*-**867**^{‘+’}) eliminates the large coupling constant ($+4.49$ mT) of the single β' proton.

The notation for the above buckled cycloalkane-1,3-diyl cations **862**^{‘+’}–**867**^{‘+’} emphasizes their structural relation to the corresponding, but even more strongly bent, bicycloalkanes **862**–**867** from which they were generated. As mentioned above, their geometry is intermediate between those of the buckled bicycloalkanes and the corresponding planar triplet cycloalkane-1,3-diyls **869**^{••}–**871**^{••}, **38**^{••}, **872**^{••}, and **873**^{••}, respectively. To emphasize that the diyl cations are formally derived from these triplet molecules by ionization, their alternative notation, **869**^{‘+’}–**871**^{‘+’}, **38**^{‘+’}, **872**^{‘+’}, and **873**^{‘+’}, is indicated in Table 10.5, along with **862**^{‘+’}–**867**^{‘+’}. The triplet cycloalkanediyIs are dealt with in Chapt. 11.3, and zero field splitting (ZFS) parameters and hyperfine data are given in Table 11.5 for those of them which were characterized by ESR spectroscopy.

The g_e factor of the cyclobutane-1,3-diyl cations in a CFCl₃ matrix is 2.0039. That of the cyclopentane-1,3-diyl cations ranges from 2.0033 to 2.0040, depending on the matrix. Whereas **862**^{‘+’}–**864**^{‘+’} are persistent up to the softening point of the CFCl₃ matrix, their unsubstituted cyclopentane analogue **865**^{‘+’} isomerizes rapidly above 90 K to the radical cation of cyclopentene (**239**) (Table 7.15) in all Freon



matrices used. Alkyl substitution at the π centers had a stabilizing effect, so that the 1,3-dimethylcyclopentane-1,3-diyl cation (**866^{'++}**) was resistant to isomerization under the same conditions. In contrast, methyl substitution in the 2-position does not prevent the 2-methylcyclopentane-1,3-diyl radical cations from isomerizing; thus, *eq*-**867^{'++}** is converted to the 1-methylcyclopentene, and *ax*-**867^{'++}** yields mainly the 3-isomer, a remarkable stereochemical memory effect.



868^{'••} (**874^{'••}**)

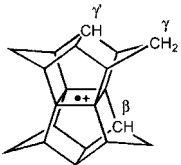
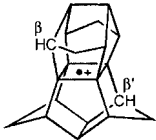
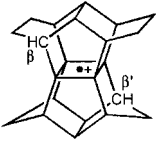
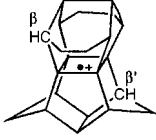
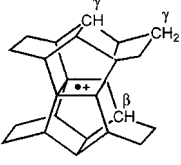
In addition to ESR spectra of **862^{'++}**–**867^{'++}**, that of a cyclohexane-1,4-diyl cation (**868^{'++}**) ($g_e = 2.0026$) was observed upon γ -irradiation and ring-opening of bicyclo[2.2.0]hexane (**868**) in Freon matrices [1133]. This diyl cation **868^{'++}** was also obtained as an intermediate in the cyclization of the radical cation of 1,5-hexadiene to that of cyclohexene (**240**) (Table 7.15) [1134]. It is in the chair form, and its geometry is intermediate between those of the buckled **868** and of a still-hypothetical, presumably more-planar, triplet cyclohexane-1,4-diyl (**874^{'••}**), so that it can be alternatively denoted **874^{'++}**. The six protons of **868^{'++}** giving rise to observable hyperfine splitting stem from the two methine α protons at the π centers 1 and 4 and the four methylene β protons in the axial positions of the chair form (coupling constants -1.2 and $+1.2$ mT, respectively). The interaction between the two methine π centers is through space [1135].

Upon warming the Freon matrix, the cyclohexane-1,3-diyl cation (**868^{'++}**) was converted into the radical cation of cyclohexene (**240**).

Radical Cations from “Cage” Hydrocarbons

The principal representatives of cage hydrocarbons are pagodanes which contain a cyclobutane ring incorporated into a rigid polycyclic carbon framework (the “cage”). Upon oxidation to their radical cations, two parallel C–C σ bonds in this ring are elongated to form a rectangle, by which two types of structure, “tight” and “extended”, can be discerned. In the tight structure, the two parallel short bonds

Tab. 10.6. Hyperfine Data for Radical Cations of Some Pagodanes

[1.1.1.1]Pagodane (7,8;12,19-bissecododecahedrane) 875 ^{•+}		8H(β) 4H(γ) 4H(γ) 4H(γ')	+1.544 -0.117 -0.065 +0.051	[1136]
[1.1.1.1]Isopagodane 876 ^{•+}		4H(β) 4H(β')	+0.95 +0.11	[1137]
[2.2.1.1]Pagodane 877 ^{•+}		4H(β) 4H(β')	+1.76 +0.96	[1136]
[2.2.1.1]Isopagodane 878 ^{•+}		4H(β) 4H(β')	+1.63 <0.08	[1138]
[2.2.2.2]Pagodane 879 ^{•+}		8H(β) 8H(γ) 8H(γ) 4H(γ')	-0.060 +0.582 -0.060 <0.05	[1139]

are theoretically calculated to be 175 pm apart, so that the four-membered ring remains "cyclobutanoid", whereas in the extended structure, the corresponding distance is predicted by theory to be 260 pm. The radical cations having the tight structure were short-lived, whereas their extended counterparts, also obtained from the corresponding pagodanes with a cyclobutadiene ring, proved to be persistent. Upon further oxidation, radical cations of both structures yielded dicationic species having two π electrons in the four-membered ring, which thus comply with the Hückel $2 + 4m$ -rule for π perimeters (Chapt. 8.1). Table 10.6 [1136–1139] gives hyperfine data for radical cations of five pagodanes. Comparison of theoretical and experimental ^1H coupling constants for 875^{•+}–879^{•+} makes it possible to distinguish the two types of structure. Such a comparison requires that the radical cations 875^{•+} and 878^{•+} from [1.1.1.1]pagodane (875) and [2.2.1.1]isopagodane (878) possess the extended structure, and that those, 876^{•+}, 877^{•+}, and 879^{•+}, from [1.1.1.1]isopagodane (876), [2.2.1.1]pagodane (877), and [2.2.2.2]pagodane (879) must have the tight structure. The dominant feature in the ESR spectrum of 875^{•+}

is the coupling constant of +1.544 mT arising from the eight methine β protons. Its large value is due to the high spin population ($\approx +0.25$) at each of the four centers μ and the small dihedral angle θ ($\approx 10^\circ$). The hyperfine data for the remaining radical cations **876'**^{•+}–**879'**^{•+} vary considerably, depending, in general, on the symmetry (D_{2h} or C_{2v}), and, in particular, on the geometry of the central four-membered ring (planar or pyramidal).

The g_e factors of **875'**^{•+} and **878'**^{•+} are 2.0031 and 2.0040, respectively; those of the other radical cations were not reported. The radical cation **875'**^{•+} is highly persistent and can be generated in dichloromethane solution from the pagodane or the corresponding diene by a variety of methods, such as reaction with AlCl_3 or tris(*p*-bromophenyl)ammoniumyl hexachloroantimonate (“magic blue”) or by electrolysis. The radical cation **878'**^{•+} and its less-persistent isomer **877'**^{•+} were also obtained from their neutral precursors in dichloromethane solution by reaction with AlCl_3 or magic blue, whereas short-lived radical cations **876'**^{•+} and **879'**^{•+} have to be produced by γ -irradiation of the corresponding pagodanes in a CFCl_3 matrix.

11

Biradicals and Triplet-state Molecules

Physical fundamentals, methods of generation, and representative examples of such organic molecules with two unpaired electrons in singly occupied MOs (open shells) are dealt with in Chapt. 2.4. When the interaction between the two electrons is negligible, the molecules can be considered as having two moieties in doublet spin states. With the strengthening of the interaction, the two doublets yield a singlet and a triplet state, according to whether the two electrons become paired or remain unpaired. The interaction is expressed by two quantities: (1) the exchange integral, J , over the orbital functions of the two electrons, which is responsible for the energetic difference of the singlet and triplet states, and (2) the zero-field-splitting (ZFS) parameter D which characterizes the (anisotropic) dipolar magnetic interaction between the two electron spins.

In Chapt. 2.4, molecules in an electronically excited triplet state are distinguished from those for which the triplet is a ground or thermally accessible state. Systematic and more detailed classification including the characteristic ZFS parameters of the individual molecules is given below. First, it is convenient to treat separately some special molecules which have two unpaired electrons in the ground state and may be considered biradicals.

11.1

Biradicals

The term “biradicals” refers here to molecules with two unpaired electrons which give rise to observable ESR spectra in fluid solution. This term presupposes a low value of the ZFS parameter D , so that the anisotropic electron–electron interaction is averaged out in solution, like the electron–nucleus interaction (Chapt. 3.2). Biradicals contain two, usually equivalent, spin-bearing π moieties that are separated by an “insulating” segment. Several such biradicals, in which the structure of the two moieties is closely related to that of well-known persistent monoradicals, were studied by ESR spectroscopy; for example, bisnitroxyls, bisverdazyls, and bisgalvinoxyls.

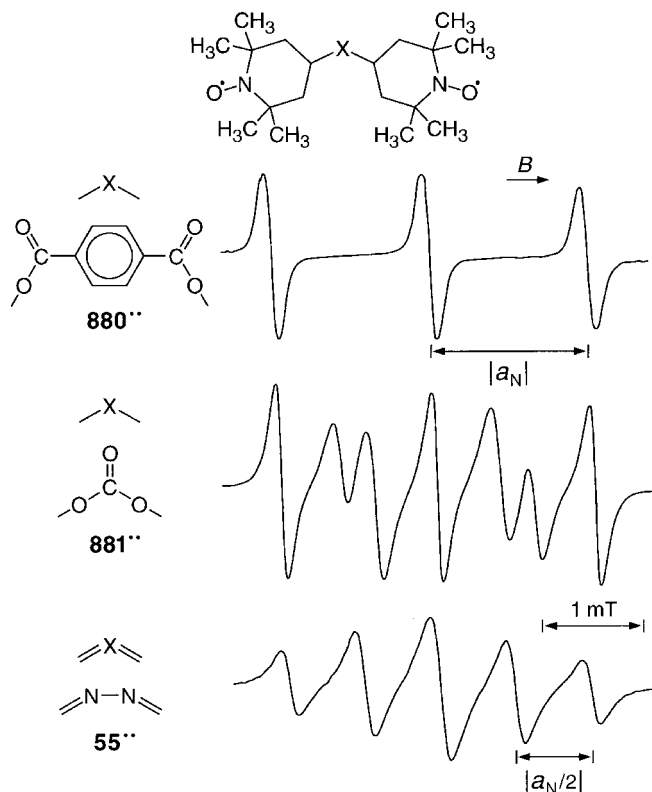


Fig. 11.1. ESR spectra of bisnitroxyls **880**^{••}, **881**^{••}, and **55**^{••} with different linking groups X. Solvent DMF, temperature 298 K. Reproduced with permission from [433].

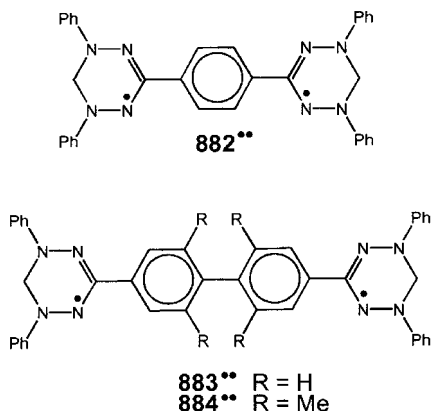
Bisnitroxyl Biradicals

Interaction between the two unpaired electrons in the two π moieties represented by 2,2,6,6-tetramethylpiperidinyl-1-oxyl (**292**[•]) and its 4-oxo-derivative (TEMPO; **8**[•]) (Table 7.20) was systematically studied on bisnitroxyls in solution. The formulas and ESR spectra of three of these bisnitroxyls, **55**^{••}, **880**^{••}, and **881**^{••}, [433, 434], are shown in Figure 11.1. The segment X separating the two nitroxyl moieties was varied to adjust the exchange integral J . For **880**^{••} with the longest group $-X- = -O-CO-C_6H_4-CO-O-$, $|J| \ll a'_N$, where J is in MHz and ^{14}N coupling constant $a'_N = +44$ MHz ($a_N = +1.56$ mT); accordingly, the observed hyperfine pattern was that of the nitroxyl monoradicals **292**[•] or **8**[•] (Figure 11.1, top). By contrast, for **55**^{••} with the group $=X= =N-N=$, $|J| \gg a'_N$, so that its hyperfine pattern arose from two equivalent ^{14}N nuclei at $+0.74$ mT, a value close to $a_N/2$ (Figure 11.1, bottom). In the intermediate range, exemplified by **881**^{••} with $-X- = -O-CO-O-$, $|J|$ is

comparable to a'_N , and more complex pattern was observed (Figure 11.1, middle). Such a pattern is predicted by a theoretical treatment in which the eigenfunctions of the singlet and triplet states are mixed by hyperfine interactions [1140]. Simulation of the spectrum of $881^{\bullet\bullet}$ yields the ratio $|J|/a'_N = 1.85$ from which (with $a'_N = +0.44$ MHz) a value of 81 MHz is obtained for $|J|$.

Bisverdazyl Biradicals

In $882^{\bullet\bullet}$ – $884^{\bullet\bullet}$ [1141], the two 2,5-diphenylverdazyl π moieties are linked by one or two phenylene groups; steric hindrance by the four methyl groups in $884^{\bullet\bullet}$ causes twisting about the inter-phenylene bond.

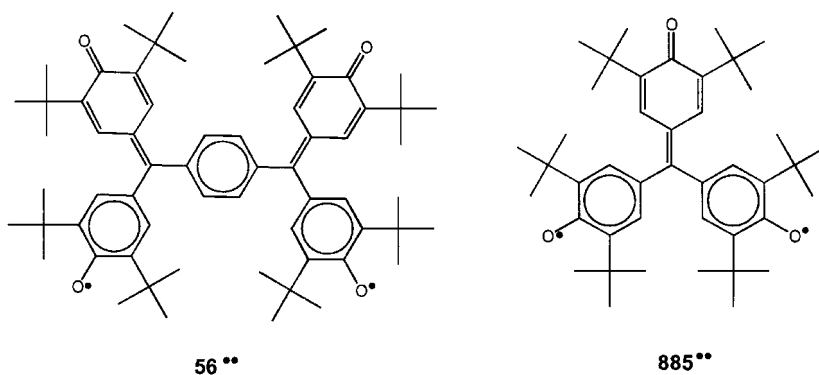


The ESR signal of $882^{\bullet\bullet}$ in benzene solution was unresolved, but those of $883^{\bullet\bullet}$ and $884^{\bullet\bullet}$ exhibited a hyperfine pattern due to the eight ^{14}N nuclei in both verdazyl moieties. The pertinent coupling constant of $+0.29$ mT, which is half as large as the a_N value of the four nuclei in the diphenylverdazyl monoradicals $548^{\bullet\bullet}$ and $549^{\bullet\bullet}$ (Table 9.4), indicates that $|J| \gg a'_N$. From the ESR spectra of the biradicals in an MTHF glass, the parameters D' of 4.6 mT for $882^{\bullet\bullet}$ and 1.55 mT for $883^{\bullet\bullet}$ and $884^{\bullet\bullet}$ were derived (E' is too small to be observed). The D' values correspond to average distances, r , of 850 and 1230 pm, respectively, between the two unpaired electrons (Eq. 2.7) in the verdazyl moieties.

Bisgalvinoxyl Biradicals

For *p*-phenylenebisgalvinoxyl ($56^{\bullet\bullet}$) in toluene solution [435], coupling constants of $+0.068$ and $+0.48$ mT were observed for the eight ring protons and the ^{13}C isotopes in two exocyclic C atoms, respectively. These coupling constants arise from nuclei in both π moieties and are half as large as the corresponding $a_{\text{H}3,3',5,5'}$ and $a_{\text{C}7}$ values for the galvinoxyl monoradical 10^{\bullet} (Table 9.2). However, Yang's biradical $885^{\bullet\bullet}$ [435, 436, 536], must be considered a "one-and-a-half galvinoxyl", because it contains one phenoxy group in addition to a 10^{\bullet} -like moiety. Accordingly, the cou-

pling constant of +0.85 mT, measured for the six protons of $885^{\bullet\bullet}$ in toluene solution, amount to two thirds of the $a_{\text{H}3,3',5,5'}$ value for 10^{\bullet} , and the ^{13}C isotopes in the single exocyclic C atom give rise to a value of +0.86 mT, which is 14% lower than a_{C_7} for 10^{\bullet} (Table 9.2). The parameters D' obtained for these biradicals in a toluene glass are 1.96 mT for $56^{\bullet\bullet}$ and 3.25 mT for $885^{\bullet\bullet}$ [1142], reflecting the smaller average distance between the two unpaired electrons in the galvinoxyl moieties in $885^{\bullet\bullet}$ relative to those in $56^{\bullet\bullet}$. (Again, E' is too small to be observed.)



The g_e factors of the biradicals and the methods of their generation are similar to those of the corresponding monoradicals.

11.2

Molecules in Photoexcited Triplet State

As stated in Chapt. 2.4, nearly all stable molecules have a singlet ground state, in which all electrons are paired in doubly occupied orbitals (closed shell); for π systems, this state is separated by several eV from electronically excited states. Excitation of electrons from the bonding π -MOs or the nonbonding n-MOs of heteroatoms to antibonding π^* -MOs ($\pi \rightarrow \pi^*$ or $n \rightarrow \pi^*$) by UV or visible light leads to a molecule with two SOMOs, albeit in a singlet state, because only electronic transitions with no change in spin multiplicity ($\Delta S = 0$) are allowed. The Jablonski diagram in Figure 2.5 illustrates the sequence of events that yield the first excited triplet state which, in general, lies energetically lower than its excited singlet counterpart. Such triplet states are characterized by the ZFS parameters, D and E , listed for some molecules in Tables 11.1 [379, 381–385, 387, 1143–1153] and 11.2 [175, 373, 395, 397, 398, 1154–1159]. By convention, these values are given in wave numbers cm^{-1} , which are proportional to the energy. (For $g_e \approx 2$, they are related to D' and E' , in the unit B of the magnetic-field strength, by 1 T, corresponding to 0.93 cm^{-1} .)

The problems that initially hindered ESR studies of triplet molecules are also pointed out in Chapt. 2.4. Precise values, including the signs of D and E (at least,

Tab. 11.1. Zero Field Splitting Parameters, D and E in cm^{-1} , for Some Molecules in Their Lowest Electronically Excited Triplet State; observed with Single Crystals. Footnotes indicate where the structural formulas are shown.

	<i>Host</i>	<i>D</i>	<i>E</i>	
Benzene ^a 62* ^{**}	borazole	+0.1568	+0.0199	[1143]
Perdeuteriobenzene ^a 62- <i>d</i> ₆ * ^{**}	borazole	+0.1581	-0.0064	[1143]
<i>p</i> -Xylene ^b 487* ^{**}	perdeuterio- <i>p</i> -xylene	+0.1416	-0.0554	[1144]
Naphthalene ^a 83* ^{**}	durene	+0.10119	-0.01411	[1145]
Anthracene ^a 68* ^{**}	diphenyl phenazine	+0.07156 ±0.07055	-0.00844 ∓0.00791	[1146] [379]
Naphthacene ^a 383* ^{**}	<i>p</i> -terphenyl	±0.0551	∓0.0047	[1147]
Pentacene ^a 384* ^{**}	<i>p</i> -terphenyl	+0.0460	-0.017	[1148]
Phenanthrene ^a 386* ^{**}	biphenyl	±0.10043	∓0.04658	[1145]
Perdeuteriopyrene ^a 387* ^{**}	fluorenone	±0.06577	∓0.003162	[382]
Biphenyl ^c 94- <i>d</i> ₁₀ * ^{**}	dibenzofurane	+0.11065	-0.00370	[383]
Diphenylacetylene ^d 429* ^{**}	benzophenone	±0.1426	∓0.0306	[387]
Quinoline ^e 580* ^{**}	durene	±0.1030	∓0.0162	[385]
Isoquinoline ^e 581* ^{**}	durene	+0.1004	0.0117	[385]
Quinoxaline ^e 582* ^{**}	durene	+0.1007	∓0.0182	[384]
1,5-Naphthyridine ^e 583* ^{**}	durene	+0.106	-0.017	[1149]
1,8-Naphthyridine ^e 584* ^{**}	durene	+0.1124	-0.01837	[1149]
Acridine ^e 586* ^{**}	biphenyl	+0.07366	-0.00872	[381]
Phenazine ^e 587* ^{**}	biphenyl	+0.0744	-0.0110	[1150]
Benzophenone ^f 609* ^{**}	4,4'-dibromophenylether	-0.156473	+0.017434	[1151]
Benzil ^g 633* ^{**}	benzophenone	0.092	0.021	[1152]

Tab. 11.1 (continued)

	Host	<i>D</i>	<i>E</i>	
9,10-Dihydrophenazine ^h 760* ^{••}	perdeuteriofluorene	0.1157	0.0090	[1153]

^aTable 8.8.^eTable 9.9.^bTable 8.18.^fTable 9.14^cTable 8.11.^gTable 9.16.^dTable 8.13.^hTable 9.30.

the relative ones of the two parameters) and their dependence on sample orientation in the magnetic field can be determined in single-crystal studies (Table 11.1), which were the first successful investigations in this field. However, because such studies involve growing single crystals of an appropriate host, in which the target molecule is embedded, most investigations have been of triplet molecules randomly oriented in solid matrices (Table 11.2). The *D* and *E* values measured by this method differ slightly from those determined for the same molecules in single crystals. The parameter *D*, which depends on the average distance, *r*, between the two unpaired electrons (see Eq. 2.7 for *D'* and *r*), generally decreases with the size of the π system of the molecule, and the *E* value accounts for deviation from axial symmetry. This value is ca 10 times smaller than *D* and, is usually of opposite sign; it vanishes (or nearly vanishes) for triplet-state molecules with axial symmetry (rotational axis C_n with $n \geq 3$), such as photoexcited triphenylene (388*^{••}), coronene (392*^{••}), 1,3,5-triphenylbenzene (412*^{••}), and decacyclene (886*^{••}). In contrast, a significant $|E|$ value was found for the excited benzene triplet (62*^{••}), which indicates a distorted geometry in this state, presumably, a quinoid structure of D_{2h} symmetry.

Hyperfine splittings are usually unresolved in the ESR spectra of electronically excited triplet molecules, but, in a few studies, ¹H-coupling constants were determined with single crystals, often by the ENDOR technique. Because such splittings by deuterons, with their smaller coupling constants, broaden the triplet components considerably less than those by protons, it has sometimes proved advantageous to work on perdeuterated molecules, particularly in matrix studies. As stated in Chapt. 4.4, the π -spin distribution in the electronically excited triplet states of benzenoid hydrocarbons is close to that in the corresponding radical ions (see, e.g., [1160]).

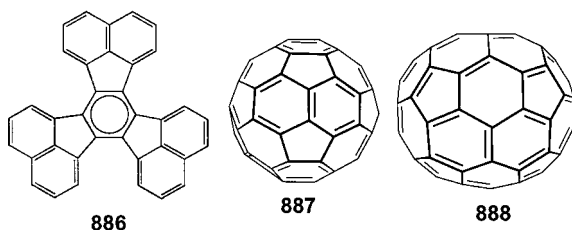
In general, g_e factors, which depend on the environment, were not explicitly given for molecules in an electronically excited triplet state, although they can be determined from their ESR spectra. The isotropic g_e values are similar to those for the corresponding radical ions, namely 2.0028 ± 0.0001 for the triplet hydrocarbons 62*^{••} and 68*^{••} and 2.0035 ± 0.0001 for the triplet azaarenes 586*^{••} and 587*^{••}. Photoexcitation was performed in situ (Chapt. 2.4); the host molecules for single crystals and the frozen solvents used for matrices are indicated in Tables 11.1 and 11.2, respectively.

Tab. 11.2. Zero-Field Splitting Parameters D and E in cm^{-1} for Some Molecules in Their Lowest Electronically Excited Triplet State; Derived from Matrix Studies. Footnotes indicate where the structural formulas are shown.

	<i>Matrix</i>	$ D $	$ E $	
Perdeuterionaphthalene ^a 83-d ₆ ^{**}	MTHF	0.10046	0.01536	[373]
Perdeuterioanthracene ^a 68-d ₁₀ ^{**}	MTHF	0.0724	0.0081	[373]
Phenanthrene ^a 386 ^{**}	ethanol	0.1042	0.0462	[393]
Triphenylene ^a 388 ^{**}	MTHF	0.1342	0	[373]
Coronene ^a 392 ^{**}	Ethanol/DMF	0.096	0	[393]
Biphenyl ^b 94 ^{**}	ethanol	0.1094	0.036	[1154]
<i>m</i> -Terphenyl ^b 408 ^{**}	3-methylpentane	0.110	0.004	[395]
Decacyclene ^c 886 ^{**}	MTHF	0.057	0	[175]
1,3,5-Triphenylbenzene ^b 412 ^{**}	3-methylpentane	0.111	<0.001	[395]
Acenaphthene ^d 67 ^{**}	ethanol	0.0966	0.0140	[1154]
Quinoline ^e 580 ^{**}	ethanol/water	0.1014	0.0164	[1155]
Protonated quinoline (580H ⁺) ^{**}	ethanol/water	0.0921	0.0150	[1155]
Isoquinoline ^e 581 ^{**}	ethanol/water	0.1003	0.0113	[1155]
Protonated isoquinoline (581H ⁺) ^{**}	ethanol/water	0.0941	0.0112	[1155]
Acridine ^e 586 ^{**}	polyethylene	0.0725	0.0084	[1156]
2,2'-Bipyridyl ^f <i>trans</i> -594 ^{**} <i>cis</i> -594 ^{**}	polyvinylalcohol polyvinylalcohol	0.1079 0.1092	0.123 0.122	[1157] [1157]
4,4'-Bipyridyl ^f 595 ^{**}	diethylether	0.1197	0.040	[1154]
Phenoxazine ^g 786 ^{**}	ethanol	0.1247	0.0119	[1158]
9,10-Anthraquinone ^h 655 ^{**}	ether/pentane/ethanol	0.351	0.005	[1159]
[2.2]Paracyclophane ⁱ 118 ^{**}	ether/pentane/ethanol	0.0059 ^j		[397]

Tab. 11.2 (continued)

	Matrix	D	E	
Fullerene C ₆₀ ^c 887* ^{••}	toluene	0.0114	0.00069	[398]
Fullerene C ₇₀ ^c 888* ^{••}	toluene	0.0052	0.00069	[398]

^aTable 8.8.^fTable 9.10.^bTable 8.11.^gTable 9.33.^cSee below.^hTable 9.18.^dTable 8.9.ⁱTable 8.22.^eTable 9.9.^j $D^* = (D^2 + 3E^2)^{1/2}$.

11.3

Molecules in Ground or Thermally Accessible Triplet State

Triplet Carbenes and Nitrenes

Carbenes have one divalent C atom with two electrons in NBMOs which give rise to a singlet or a triplet ground state. In the lowest singlet state (H₂C:; **40**:) of the simplest carbene, methylene, these two electrons are paired in the NBMO which is a spⁿ-hybrid of σ character, σ_y , with its axis lying in the molecular plane. In the corresponding triplet (H₂C*^{••}; **40***^{••}), which is the ground state of methylene, the two electrons occupy different NBMOs. One NBMO is σ_y , and the other, π_z , has an almost “pure” p-character and its axis is perpendicular to the molecular plane. As illustrated in Figure 11.2, the electron configuration of the singlet is thus $\sigma_y^2\pi_z^0$ (top, left) and that of the triplet is $\sigma_y^1\pi_z^1$ (top, right). The HCH angle is 102° for the singlet and 136° for the triplet **40***^{••}, which indicates that the C–H bonds have less and the hybrid NBMO σ_y has more p-contribution in the triplet than in the singlet, as theoretically predicted [408]. The triplet lies 38 kJ·mol⁻¹ below the singlet.

Table 11.3 [373, 402, 403, 406, 1161–1172] lists the ZFS for **40***^{••} and several other triplet carbenes, in which one or both H atoms are substituted by an alkyl or an aryl group, as well as for triplet carbenes having the spin-bearing C*^{••} atom incorporated into a ring. The angle about this C atom is approximately the same as in

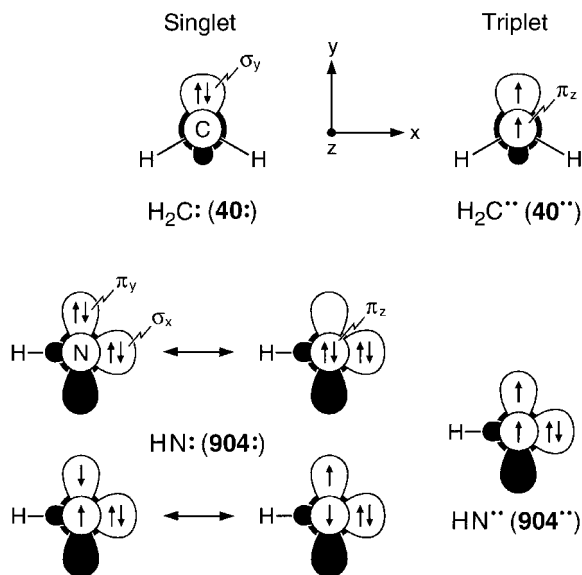


Fig. 11.2. NBMOs and their occupancy in the singlet H_2C : (40:) and triplet $\text{H}_2\text{C}^{\bullet\bullet}$ ($\text{40}^{\bullet\bullet}$) of the simplest carbene and in the singlet HN : (904:) and triplet $\text{HN}^{\bullet\bullet}$ ($\text{904}^{\bullet\bullet}$) of the simplest nitrene. Reproduced with permission from [408].

the parent $\text{40}^{\bullet\bullet}$, but the $|D|$ value decreases with substitution by an alkyl and even more by an aryl group, in the order of the extending π system. This is because the unpaired electron, which is originally in the NBMO π_z , delocalizes into the π system of the aryl substituent. Thus, the average distance to the second unpaired electron, which remains localized in the in-plane NBMO σ_y , is decreased.

A similar effect occurs upon incorporation of the $\text{C}^{\bullet\bullet}$ atom into a cyclic π system. The parameter $|D|$ of fluoren-9-ylidene ($\text{899}^{\bullet\bullet}$) is almost identical to that of diphenylmethylene ($\text{36}^{\bullet\bullet}$), but the $|D|$ value of dimesitylmethylene ($\text{891}^{\bullet\bullet}$) is considerably smaller. A strikingly low parameter $|D|$, much less than that expected, considering its value for the monoanthryl analogue ($\text{893}^{\bullet\bullet}$), was also found for dianthrylmethylene ($\text{895}^{\bullet\bullet}$). These findings were interpreted in terms of a sterical hindrance that forces the two aryl moieties in $\text{891}^{\bullet\bullet}$ and $\text{895}^{\bullet\bullet}$ to be nearly perpendicular to each other with a $\text{CC}^{\bullet\bullet}\text{C}$ angle approaching 180° . Thus the NBMO σ_y of the triplet carbene requires an “nearly pure” p-character and it should be renamed π_y ; its electron configuration is thus formulated as $\pi_y^{\uparrow}\pi_z^{\uparrow}$. Because each of the two unpaired electrons in the π_y - and π_z -NBMOs delocalizes into a separate mesityl or anthryl π system, the $|D|$ values are decreased relative to those of hypothetical planar dimesityl- and dianthrylmethylenes in which one electron remains localized (σ_y) and the second (π_z) is delocalized into both systems. The almost-perpendicular geometry, which implies a nearly axial symmetry D_{2d} , is in line with the very small E values, especially for $\text{895}^{\bullet\bullet}$. The geometric isomerism and spin distribution in

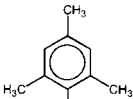
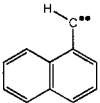
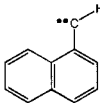
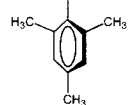
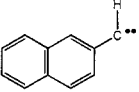
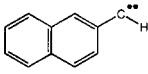
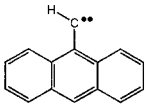
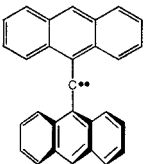
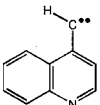
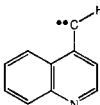
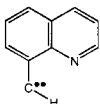
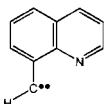

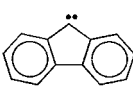
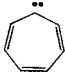
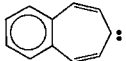
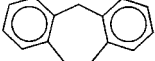
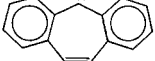
Tab. 11.3. Zero Field Splitting Parameters, D and E in cm^{-1} , for Some Triplet Carbenes. The structural formulas are shown below.

	<i>Matrix</i>	$ D $	$ E $	
Methylene 40 ^{••}	xenon	0.6964	0.0039	[402, 403]
Dideuteriomethylene 40- d_2 ^{••}	xenon	0.76	0.0046	[1161]
Di- <i>tert</i> -butylmethylene 889 ^{••}	MTHF	0.689	0.039	[1162]
Phenylmethylene 890 ^{••}	Fluorolube	0.518	0.024	[1163]
Diphenylmethylene 36 ^{••}	Fluorolube Benzophenone ^a	0.4055 +0.4078 ^a	0.0194 -0.0206 ^a	[373] [406]
Dimesitylmethylene 891 ^{••}	n-octane	0.3517	0.0115	[1164]
1-Naphthylmethylene <i>syn</i> -892 ^{••} <i>anti</i> -892 ^{••}	benzophenone benzophenone	0.4347 0.4555	0.0208 0.0202	[1165] [1165]
2-Naphthylmethylene <i>syn</i> -893 ^{••} <i>anti</i> -893 ^{••}	benzophenone benzophenone	0.4926 0.4711	0.0209 0.0243	[1165] [1165]
9-Anthrylmethylene 894 ^{••}	benzophenone	0.3008	0.0132	[1165]
9,9'-Dianthrylmethylene 895 ^{••}	9,9'-dianthryldiazomethane	0.113	0.0011	[1166]
4-Quinolylmethylene <i>syn</i> -896 ^{••} <i>anti</i> -896 ^{••}	fluorocarbone fluorocarbone	0.4666 0.4865	0.219 0.207	[1167] [1167]
8-Quinolylmethylene <i>syn</i> -897 ^{••} <i>anti</i> -897 ^{••}	fluorocarbone fluorocarbone	0.4434 0.4641	0.0225 0.0225	[1167] [1167]
Cyclopentadienylidene 898 ^{••}	hexafluorobenzene	0.4089	0.0120	[1168]
Fluoren-9-ylidene 899 ^{••}	hexafluorobenzene	0.4078	0.0283	[1168]
Cycloheptatrienylidene (tropyliidene) 900 ^{••}	argon	0.317 0.425	0.087 0.022	[1169] [1170]
4,5-Benzocyclohepta- trienylidene 901 ^{••}	corresp. diazocompound	0.52	0.021	[1171]
Dihydrodibenzo[<i>a,d</i>]- cycloheptenylidene 902 ^{••}	corresp. diazocompound	0.3932	0.017	[1172]

Tab. 11.3 (continued)

	Matrix	$ D $	$ E $	
Dibenzo[<i>a,d</i>]cycloheptenyliene 903 ^{**}	corresp. diazocompound	0.3787	0.0162	[1172]

^a Single crystals; signs of *D* and *E* determined.

RC ^{**} R'	R	R'			
40 ^{**}	H	H			
40-d ₂ ^{**}	D	D		<i>syn-892^{**}</i>	<i>anti-892^{**}</i>
889 ^{**}	<i>t</i> -Bu	<i>t</i> -Bu			
890 ^{**}	Ph	H			
36 ^{**}	Ph	Ph		<i>syn-893^{**}</i>	<i>anti-893^{**}</i>
			891^{**}		
					
894^{**}			895^{**}	<i>syn-896^{**}</i>	<i>anti-896^{**}</i>
					
<i>syni-897^{**}</i>	<i>anti-897^{**}</i>		898^{**}	899^{**}	
					
900^{**}	901^{**}	902^{**}	903^{**}		

some triplet carbenes, such as the naphthylmethylenes **892^{**}** and **893^{**}** and the quinolylmethylenes **896^{**}** and **897^{**}** were discussed in [1173]. Although the singlet–triplet energy gap for larger carbenes is less than that for the parent **40^{**}**, the triplet is the ground state of all hydrocarbon carbenes presented in Table 11.3.

However, the singlet can be the ground state for some carbenes having heteroatoms [437].

The singlet and triplet states, $\text{HN}:(\mathbf{904:})$ and $\text{HN}^{\cdot\cdot}(\mathbf{904}^{\cdot\cdot})$, respectively, of the simplest nitrene are isoelectronic with their carbene counterparts $\text{H}_2\text{C}:(\mathbf{40:})$ and $\text{H}_2\text{C}^{\cdot\cdot}(\mathbf{40}^{\cdot\cdot})$. However, replacement of the divalent C atom in carbenes by the also-divalent N atom in nitrenes, which implies replacement of the two electrons of one C–H σ bond in carbenes by a N-lone pair in nitrenes, has significant consequences. This is because, now in general, the two NBMOs are π_y and π_z , both of “pure” p-character and degenerate. As shown in Figure 11.2, the singlet state $\text{HN}:(\mathbf{904:})$ has a “closed-shell” component, $\pi_y^2 \leftrightarrow \pi_z^2$ (middle), and an “open-shell” one, $\pi_y^\uparrow\pi_z^\uparrow \leftrightarrow \pi_y^\downarrow\pi_z^\downarrow$ (bottom, left) and it lies $150 \text{ kJ}\cdot\text{mol}^{-1}$ higher than the triplet $\text{HN}^{\cdot\cdot}(\mathbf{904}^{\cdot\cdot})$ with the electronic configuration $\pi_y^\uparrow\pi_z^\uparrow$ (bottom, right). The singlet–triplet energy gap is thus four times larger than for the corresponding simplest carbene. Although this gap decreases for substituted nitrenes, it remains relatively large, so that the triplet appears to be the ground state for all nitrenes studied so far.

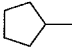
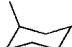
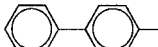
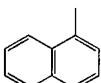
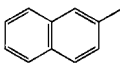
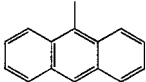
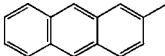
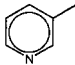
The ZFS parameters D and E for $\text{HN}^{\cdot\cdot}(\mathbf{904}^{\cdot\cdot})$ and some triplet alkyl and aryl nitrenes are given in Table 11.4 [1174–1177]. The triplet $\text{HN}^{\cdot\cdot}$ has not been characterized by ESR spectroscopy, but its $|D|$ value was derived from optical measurements in the gas phase. This value, which decreases with delocalization of the unpaired π_z electron into the alkyl and, particularly, into the aryl substituent, is roughly twice as large in nitrenes as in the corresponding carbenes (Table 11.3). Because D is proportional to r^{-3} , the average distance, r , between the two unpaired electrons, is ca 25% shorter in nitrenes than in carbenes. This is a consequence of the contraction of the NBMOs π_y and π_z due to the higher nuclear charge in the N relative to the C atom. Nitrenes were reviewed in 1971 [1175] and their physical and chemical properties, compared with those of carbenes, were recently discussed [408].

The carbenes and nitrenes were generated in matrices by photolysis of the corresponding diazo compounds and azides, respectively (Chapt. 2.4). Occasionally, aromatic ketones were used as a sensitizer.

Triplet Cycloalkane-1,3-diyls

The triplet cyclopentane-1,3-diyl ($\mathbf{38}^{\cdot\cdot}$) was the first one of this class to be characterized by its ZFS parameters. The ESR spectrum of the triplet cyclobutane-1,3-diyl ($\mathbf{869}^{\cdot\cdot}$) was not observed, but some of its derivatives, in which this state is stabilized by 1,3-substituents, were amenable to ESR studies. The parameters, D and E , for $\mathbf{38}^{\cdot\cdot}$ are given in Table 11.5, along with those of its 1,3-diphenyl derivative ($\mathbf{39}^{\cdot\cdot}$) and three 1,3-substituted cyclobutane-1,3-diyls [399–401, 1178]. Substitution in the spin-bearing 1,3-positions of the triplet cycloalkane-1,3-diyls by vinyl or phenyl groups reduces the $|D|$ values, as expected for delocalization of the two unpaired electrons into the π systems of the substituents, which increases the distance between the two electrons. This delocalization is confirmed by the observed ^1H -coupling constants, which were determined from the splitting of the less aniso-

Tab. 11.4. Zero-Field-Splitting Parameters, D and E in cm^{-1} , for Some Triplet Nitrenes. General formula $\text{RN}^{\bullet\bullet}$; the structure of R is given in the Table.

	R	$ D $	$ E $	
Nitrene 904$^{\bullet\bullet}$	H	1.86	0	[1174, 1175]
Methylnitrene 905$^{\bullet\bullet}$	Me	1.595	<0.003	[1175]
<i>n</i> -Propylnitrene 906$^{\bullet\bullet}$	<i>n</i> -Pr	1.607	0.0034	[1175, 1176]
<i>tert</i> -Butylnitrene 907$^{\bullet\bullet}$	<i>t</i> -Bu	1.625	<0.002	[1175, 1176]
Cyclopentylnitrene 908$^{\bullet\bullet}$		1.575	<0.002	[1175, 1176]
Cyclohexylnitrene 909$^{\bullet\bullet}$		1.599	<0.002	[1175, 1177]
Diphenylmethylnitrene 910$^{\bullet\bullet}$	Ph_2CH	1.636	<0.002	[1175, 1176]
Triphenylmethylnitrene 911$^{\bullet\bullet}$	Ph_3C	1.660	<0.002	[1175, 1177]
Phenylnitrene 41$^{\bullet\bullet}$	PhCH_2	0.9978	<0.002	[1175]
4-Biphenylnitrene 912$^{\bullet\bullet}$		0.9367	<0.003	[1175]
1-Naphthylnitrene 913$^{\bullet\bullet}$		0.7890	<0.002	[1175]
2-Naphthylnitrene 914$^{\bullet\bullet}$		1.0083	<0.003	[1175]
1-Anthrylnitrene 915$^{\bullet\bullet}$		0.6625	<0.003	[1175]
2-Anthrylnitrene 916$^{\bullet\bullet}$		0.7779	<0.003	[1175]
3-Pyridinylnitrene 917$^{\bullet\bullet}$		1.0048	<0.003	[1175]

tropic " $\Delta M_S = \pm 2$ " components in the half-field range of the ESR spectra; these a_{H} values are also given in Table 11.5.

The large coupling constants observed for the β protons in the methylene group bridging the spin-bearing 1,3-positions in **871 $^{\bullet\bullet}$** , **918 $^{\bullet\bullet}$** , **919 $^{\bullet\bullet}$** , and **39 $^{\bullet\bullet}$** are

Tab. 11.5. Zero Field Splitting Parameters, D and E in cm^{-1} , and Hyperfine Data for Some Cycloalkane-1,3-diyls.

1,3-Dimethylcyclobutane- 1,3-diyl 871 ^{••}		$ D $ $ E $ $4H(\beta)$ $6H(\beta')$	0.112 0.005 +3.2 +1.6	[1178]
1,3-Diphenylcyclobutane- 1,3-diyl 918 ^{••}		$ D $ $ E $ $4H(\beta)$ $4H_o, 2H_p$ $4H_m$	0.060 0.002 +2.25 -0.3 +0.05	[1178]
1,3-Divinylcyclobutane- 1,3-diyl 919 ^{••}		$ D $ $ E $ $4H(\beta)$ $H_{2,2'}$ $H_{1',1''}$ <i>exo,endo</i>	0.050 0.001 +1.9 +0.2 -0.7	[1178]
Cyclopenta-1,3-diyl 38 ^{••}		$ D $ $ E $	0.084 0.002	[399, 400]
1,3-Diphenylcyclopenta- 1,3-diyl 39 ^{••}		$ D $ $ E $ $2H(\beta)$ $4H(\beta')$ $4H_o, 2H_p$ $4H_m$	0.045 0.001 +2.4 +1.4 -0.3 <0.1	[401]

as expected for such protons (“Whiffen effect”, Eq. 4.11). These values are proportional to the π -spin populations $\rho_{1,3}^\pi$ and so (roughly) is the ZFS parameter $|D|$, as was found for a series of triplet 1,3-diyls structurally related to **39**^{••} [1179]. The coupling constants of the methyl β -protons in **871**^{••}, as well as those of the α protons in the vinyl group of **919**^{••} and in the phenyl groups of **39**^{••} and **318**^{••} are about half the corresponding values for ethyl (**59**[•]) (Table 7.1), allyl (**65**[•]) (Table 8.2), and benzyl (**88**[•]) (Table 8.1) radicals. All cycloalkane-1,3-diyls are assumed to be planar and have the triplet ground state. This assumption is supported by high-level calculations for the parent diyls **869**^{••} and **38**^{••}, which indicate that the singlet–triplet gap is almost twice as large for **869**^{••} (7.1 $\text{kJ}\cdot\text{mol}^{-1}$) than for **38**^{••} (3.8 $\text{kJ}\cdot\text{mol}^{-1}$) [1180]. Through-space interaction of the two electrons in the $\pi(2p_z)$ -NBMOs would lead to a singlet ground state, but it is overbalanced by the through-bond coupling mediated by the π -like orbitals of the methylene groups linking them. Both effects are more pronounced for the smaller ring and so is the preference for the triplet ground state in **869**^{••} relative to **38**^{••}. The spin distribution in cyclobutanediyls and in some non-Kekulé hydrocarbons (next section) was discussed in [1181].

The cycloalkane-1,3-diyls were generated by photolysis of the corresponding azo compounds in frozen MTHF or other glassy solvents.

Triplet Non-Kekulé Hydrocarbons

The term “non-Kekulé” is applied to even π systems (Chapt. 8.1) for which it is impossible to write a Kekulé formula with fewer than two non π -bonded C \cdot atoms (Chapt. 2.4). Such systems have two electrons singly occupying π -NBMOs (Chapt. 8.1). Their simplest representatives, of which formulas are shown in Chapt. 2.4, are trimethylenemethane (TMM; **42 $\cdot\cdot$**), tetramethyleneethane (TME; **43 $\cdot\cdot$**), *m*-xylylene (*m*-benzoquinodimethane; **44 $\cdot\cdot$**), and 1,8-naphthoquinodimethane; (**45 $\cdot\cdot$**). (An ESR spectrum of **42 $\cdot\cdot$** is reproduced in Figure 4.9). ZFS parameters *D* and *E* for **42 $\cdot\cdot$** –**45 $\cdot\cdot$** and some of their derivatives are given in Table 11.6. [410–417, 419, 420, 1182–1187]. The methylenecyclopenta-1,3-diyls **46 $\cdot\cdot$** and **920 $\cdot\cdot$** –**922 $\cdot\cdot$** are cyclic derivatives of TMM (**42 $\cdot\cdot$**), and the dimethylenecyclohexane-1,4-diyl **47 $\cdot\cdot$** is a cyclic analogue of TME (**43 $\cdot\cdot$**).

The *D* values decrease with extension of the π system and diminishing π -spin population at the spin-bearing centers. As mentioned in Chapt. 4.4, a coupling constant of 0.90 ± 0.01 mT was determined for the six protons in **42 $\cdot\cdot$** from the hyperfine splittings of the “ $\Delta M_S = \pm 2$ ” component in the half-field of the ESR spectrum, and it was later also observed in the “ $\Delta M_S = \pm 1$ ” components (Figure 4.9) [772]. A similar value was derived for the eight protons in **43 $\cdot\cdot$** from the splitting of the “ $\Delta M_S = \pm 2$ ” component. Both values are compatible with those expected for the π -spin populations at the three and four proton-bearing π centers of **42 $\cdot\cdot$** and **43 $\cdot\cdot$** , respectively. In the ESR spectrum of perinaphth-1,3-diyl (**49 $\cdot\cdot$**), all components exhibit splitting due to the two β protons having a large coupling constant of +2.6 mT, which is also in line with the value expected for such protons in a methylene group between two π centers (“Whiffen effect”).

According to Hund rule, non-Kekulé hydrocarbons should be paramagnetic in a triplet ground state. This rule is expected to hold for those non-Kekulé hydrocarbons in which the two NBMOs cannot be separated in such a way that they extend over different π centers (*non-disjoint* NBMOs). However, Hund rule is expected to fail, and non-Kekulé hydrocarbons should have the singlet ground state, when separation of this kind is possible for the two NBMOs (*disjoint* NBMOs) [409]. Ground state triplet is indicated by calculations for TMM (**42 $\cdot\cdot$**) [410, 1411, 1188–1191] and *m*-xylylene (**44 $\cdot\cdot$**) [1191, 1192], which have non-disjoint NBMOs, as predicted by Hund rule and confirmed experimentally [413, 1193]. In contrast, for a planar TME with disjoint NBMOs, the singlet (**43:**) and triplet (**43 $\cdot\cdot$**) states must be close in energy which sensitively depends on the coplanarity of the two allyl moieties [1194]; experimental evidence in favor of a triplet ground state or a singlet ground state with a thermally accessible triplet state is not conclusive [409].

Schlenck’s hydrocarbon (**48 $\cdot\cdot$**), a tetraphenyl derivative of *m*-xylylene (**44 $\cdot\cdot$**), as well as its isomer Chichibabin’s hydrocarbon (**923 $\cdot\cdot$**), contain two triphenylmethyl (trityl; 1 \cdot) moieties. The two compounds have been known for more than a century and bear the names of the chemists who first synthesized them [1195, 1196]. Their well-resolved ESR spectra, observed upon dissolving them in fluid solvents (which would classify them as biradicals), proved to be due to monoradicals formed by

Tab. 11.6. Zero-Field Splitting Parameters, D and E in cm^{-1} , for Some Non-Kekulé Hydrocarbons and Their Derivatives. Footnotes indicate where the structural formulas are shown.

	$ D $	$ E $	
Trimethylenemethane ^a (TMM)	0.025; 0.024 +0.0248	<0.001 0.0003 ^b	[410, 411] [1182]
42 ^{**}	0.0219	<0.0054 ^c	[1183]
2-Methylenecyclopentane-1,3-diyl ^d 920 ^{**}	0.0265	0.00550	[1184]
2-Isopropylidenecyclopentane-1,3-diyl ^{de} 46 ^{**}	0.0256	0.00340	[416, 1184]
2-Benzylidenecyclopentane-1,3-diyl ^d 921 ^{**}	0.0196	0.004	[1184]
2-Diphenylmethylenecyclopentane-1,3-diyl ^d 922 ^{**}	0.180	0.0025	[1184]
Tetramethyleneethane (TME) ^a 43 ^{**}	0.025	<0.001	[412]
2,3-Dimethylenecyclohexane-1,4-diyl ^e 47 ^{**}	0.0204	0.0016	[417]
<i>m</i> -Benzoquinodimethane ^e (<i>m</i> -xylylene) 44 ^{**}	0.011	<0.001	[413]
7,7,8,8-Tetraphenyl- <i>m</i> -benzoquinodimethane (Schlenk's hydrocarbon) ^{ef} 48 ^{**}	0.0064 0.0079	0.0006 <0.0005	[1185] [419]
7,7,8,8-Tetraphenyl- <i>p</i> -benzoquinodimethane (Chichibabin's hydrocarbon) ^e 923 ^{**}	0.0135	0.0005	[1186]
1,8-Naphthoquinodimethane ^e 45 ^{**}	0.0218	0.0021	[415]
Perinaphtha-1,3-diyl ^f 49 ^{**}	0.026	<0.002	[420]
1,4-Dihydronaphtho[1,8- <i>de</i>][1,2]diazepine (2,3-dihydropleiadiene) ^d 924 ^{**}	0.018	<0.003	[414, 1187]

^a P. 33, Chapt. 2.4.

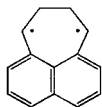
^b In single crystal of γ -irradiated methylenecyclopropane.

^c Triplet of lower symmetry appearing when temperature is raised from 196 to 133 K; this change is reversible.

^d See below.

^e P. 34, Chapt. 2.4.

^f See next page.



920^{**} R = R' = Ph

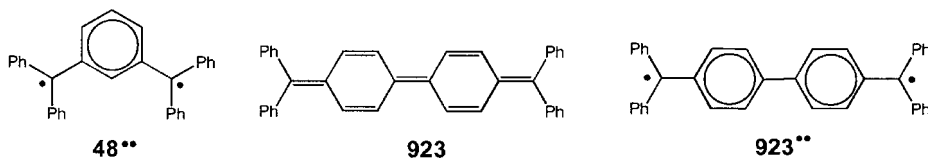
46^{**} R = R' = Me

921^{**} R = Ph, R' = H

922^{**} R = R' = Ph

924^{**}

reactions between themselves or with the solvent [1185, 1197, 1198]. Whereas Schlenk's hydrocarbon, like the parent *m*-xylylene (**44**^{••}), is certainly a non-Kekulé π system **48**^{••}, Chichibabin's hydrocarbon can be formulated either as quinoid molecule **923** with all electrons paired or as **923**^{••} with two unpaired electrons [419]. Accordingly, triplet **48**^{••} is the ground state and is 13 kJ·mol⁻¹ more stable than the singlet, but the thermally accessible triplet **923**^{••} lies 23 kJ·mol⁻¹ [1186] above the singlet. The two molecules deviate slightly from planarity, like their monoradical counterpart, the trityl **1**[•].



The two hydrocarbons, **48**^{••} and **923**^{••}, were produced from their halide precursors with zinc or by electrolysis of the corresponding cations, and the spectra of their triplets were observed in frozen toluene. The other triplet non-Kekulé hydrocarbons were usually generated by photolysis of the corresponding azo compounds in frozen MTHF (pp. 33 and 34).

Triplet Ions and Diions of Axial Molecules

Uptake of one π electron by the SOMO of a neutral odd radical produces an anion, and removal of one π electron from this MO (the NBMO in an alternant system) yields a cation. A radical anion is converted to a dianion when the SOMO (usually the LUMO) accepts an additional π electron, and a radical cation forms a dication upon releasing another π electron from the SOMO (usually the HOMO) (Figure 8.1). In general, the ions and diions thus obtained are closed-shell singlets with all their electrons paired. However, in axial molecules (rotational symmetry axis C_n with $n \geq 3$), frontier orbitals can be degenerate, so that these ions or diions have two π electrons in open shells, yielding a ground or thermally accessible triplet state. ESR studies were carried out on some ions and diions of this structure, and their ZFS parameters D and E are given in Table 11.7 [175, 285, 421, 425–428, 1199].

MO models (Chapt. 8.1) predict double degeneracy for the HOMO $\psi_{|1|}$ of the five- and six-membered π perimeters of D_{5h} and D_{6h} symmetry, respectively (Figure 8.2). With $\psi_{|1|}$ being fully occupied by four electrons, the cyclopentadienyl anion (**50**⁻) is a singlet that obeys Hückel $2 + 4$ m-rule, but the corresponding neutral radical (**50**[•]) (Table 8.5) with three electrons in $\psi_{|1|}$ is a doublet having a degenerate ground state. The prediction that the cyclopentadienyl cation with an unpaired electron in each of the two components of $\psi_{|1|}$ should be in a triplet ground state was verified by ESR studies on **50**^{•+} ($g_e = 2.0023$) and its pentachloro (**51**^{•+}) ($g_e = 2.0070$) and pentaphenyl (**52**^{•+}) derivatives. Removal of one electron from the fully occupied degenerate HOMOs $\psi_{|1|}$ of benzene, a paradigm of Hückel rule, leads to its radical cation **62**^{•+} (Table 8.8) with three electrons in this MO and a degenerate ground state, whereas loss of a second electron should yield the triplet

Tab. 11.7. Zero Field-Splitting Parameters, D and E in cm^{-1} , for Some Triplet Ions and Dianions. Footnotes indicate where structural formulas are shown.

	$ D $	$ E $	
Cyclopentadienyl ^a 50^{••+}	0.1844	0	[425]
Pentachlorocyclopentadienyl ^a 51^{••+}	0.1495	<0.002	[426, 427]
Pentaphenylcyclopentadienyl ^b 52^{••+}	0.1050	0	[427, 428]
Hexachlorobenzene ^b 53^{••2+}	0.1012	<0.003	[286]
Triphenylene ^c 388^{••2-}	0.0458	0.0089	[1199]
Coronene ^c 392^{••2-}	0.053	0	[421]
1,3,5-Triphenylbenzene ^d 412^{••2-}	0.111	<0.001	[175]
Decacyclene ^e 886^{••2-}	0.021	0	[175]
Hexaazaoctadecahydrocoronene ^f 799^{••2+}	0.0550	0.0024	[283]

^a P. 35; Chapt. 2.4.

^b P. 36; Chapt. 2.4.

^c Table 8.8.

^d Table 8.11.

^e Table 11.2.

^f Table 9.34.

dication **62^{••2+}** with an unpaired electron in each of the two components of $\psi_{|1|}$. This expectation, too, has been borne out by observation of the hexachlorobenzene radical dication (**53^{••+}**) ($g_e = 2.0116$) which has a triplet ground state as do **50^{••2+}** and **51^{••2+}**. The triplet state of **52^{••+}** and of crystalline **799^{••2+}** is thermally accessible.

Theoretical aspects of the cyclopentadienyl cation (**50^{••+}**) were discussed in a review, together with those of TMM (**42^{••}**) as another 4π -electron species [1190].

Dianions of several hydrocarbons with D_{3h} symmetry, such as triphenylene (**388**), 1,3,5-triphenyl benzene (**412**), and decacyclene (**886**), were found to be in a triplet ground state, but the triplet state of dianion of coronene (**392**) with the same symmetry is thermally accessible. The ZFE parameters $|D|$ and $|E|$ of **388^{••2-}**, **392^{••2-}**, **412^{••2-}**, and **886^{••2-}** (Table 11.7) are smaller than those for the corresponding neutral molecules **388^{••}**, **392^{••}**, **412^{••}**, and **886^{••}**, in a photoexcited triplet state (Table 11.2), because the repulsion of the two negative charges in the dianions increases the average distance, r , between the unpaired electrons.

The cyclopentadienyl cation (**50^{••+}**) and its hexachloro derivative **51^{••+}** were pre-

pared by reacting bromo- and hexachlorocyclopentadiene, respectively, with SbF_5 , and the corresponding pentaphenyl-substituted cation $52^{\cdot\cdot+}$ was obtained from pentaphenylcyclopentadiol with BF_3 . All samples were frozen for ESR studies. The dication ($53^{\cdot\cdot 2+}$) was produced by mixing solid hexachlorobenzene with a viscous solution of SbCl_5 saturated with chlorine. The dianions were generated from the neutral compounds by prolonged reduction with an alkali metal, preferentially in glassy MTHF.

Triplet Dianions of Molecules with Two π Moieties and a Spacer

When a molecule contains two (usually equivalent) π systems that are separated by spacer of an appropriate structure, reduction can lead to dianions in a ground or thermally accessible triplet state in which each of two π moieties bears an additional unpaired electron. In the triplet dianion of **510**, a tetraphenyl-substituted dibenzo[2.2]paracyclophane-1,9-diene, of which radical anion and trianion were presented in Table 8.22 [156], the cyclophane segment acts as spacer between two lateral *o*-terphenyl moieties. In the triplet dianions of **135(1)** [423] and **136(2)** [424] (for their formulas, see p. 164), the spacers are a spirobonded cyclobutane and a segment consisting of two annelated norbornyls, respectively, both linked to two naphthalene moieties in their 2,3-positions. A triplet dianion was also found for spirobifluorene (**117**) [141], of which radical anion gave rise to the ESR spectra shown in Figure 6.22. Spirobifluorene **117** has D_{2d} symmetry, with the two mutually orthogonal biphenyl-like moieties linked by a central spiro-C atom. A triplet is presumably the ground state of all four dianions, as verified experimentally for $510^{\cdot\cdot 2-}$.

The ESR spectra of $510^{\cdot\cdot 2-}$, $135(1)^{\cdot\cdot 2-}$, $136(2)^{\cdot\cdot 2-}$, and $117^{\cdot\cdot 2-}$ were observed after prolonged contact of the neutral compounds with potassium in MTHF and subsequent freezing of the solution. (Those of $510^{\cdot\cdot 2-}$ were also obtained with viscous THF at 150 K.) The ZFS parameters D' in mT are 3.35, 4.7, 5.7, and ca 6 mT, respectively, which correspond to average distances of 940 pm between the two *o*-terphenyl moieties in $510^{\cdot\cdot}$, 840 and 790 pm between the two naphthalene moieties in $135(1)^{\cdot\cdot}$ and $136(2)^{\cdot\cdot}$, respectively, and 780 pm between the two biphenyl moieties in $117^{\cdot\cdot 2-}$ (Eq. 2.7).

In general, g_e factors were not reported for molecules in a ground or thermally accessible triplet state.

Appendices

A.1

Nitroxyls as Spin Labels and Spin Adducts

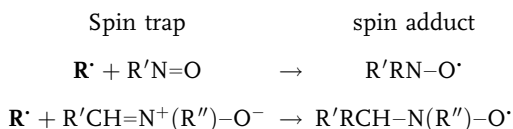
Spin Labeling

Small organic molecules, when inserted into biological macromolecules, can provide information about the molecular structure and biological function of these macromolecules. They have been called *labels*, and the information is complementary to that obtained by X-ray crystallographic analysis. The first labels were fluorescent and dye molecules, of which properties and behavior in biological materials were studied by optical emission and absorption spectroscopy [1200]. With the advent of ESR spectroscopy, this tool has become an alternative to optical studies. Suitable labels with an unpaired electron spin, the so-called *spin labels* [17k], are persistent neutral radicals, generally nitroxyls related to 2,2,6,6-tetramethylpiperidinyl-1-oxyl (**292'**) and its 4-oxo derivative (TEMPO; **8'**) (Table 7.20) [1201]. They can be incorporated into biological macromolecules covalently or by diffusion. The prominent hyperfine feature of nitroxyls is a three-line pattern due to the ^{14}N nucleus, in which the shape and width of the individual lines are governed by the combined contributions of the g_e and hyperfine anisotropies, as exemplified by *tert*-butylnitroxyl (**108'**; Figure 6.19). These contributions depend sensitively on the environment, which, for the spin label, is the surrounding biological material. The ESR spectra of a nitroxyl label thus reflect the structure of this material, in particular, its viscosity, which affects the mobility of the radical. Spin labeling was first briefly reviewed in 1968 [1202, 1203] and, several years later, more comprehensively treated by several authors in two volumes [1204]. It has been used to study the structure of lipids and membranes [1204b,c,d, 1205], proteins and nucleic acids [1202, 1204f, 1206,], enzymes [1204a], and polymers [1204e]. Applications to both *in vitro* and *in vivo* systems are possible under appropriate conditions [1207–1209].

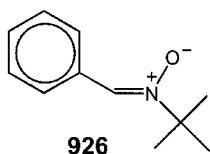
Spin Trapping

Direct identification of short-lived radicals in fluid solution by ESR spectroscopy is possible only if these radicals are produced in sufficient concentration, which

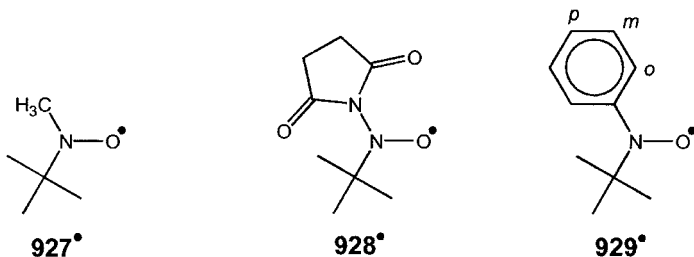
can sometimes be attained by generating them photolytically in situ, or, preferably, in rapid-mixing flow systems. An alternative method, particularly useful in chemical reactions, is addition of transient radicals to molecules of appropriate structure, thus yielding stable secondary radicals. The pertinent molecules have been called *spin traps*, and the addition of transient radicals to them is known as *spin trapping* [17g]. Conventional spin traps are nitroso compounds $R'N=O$ and nitrones $R'CH=N^+(R'')-O^-$ which add short-lived primary radicals R' to produce persistent nitroxyl radicals as *spin adducts*.



Nitroso-*tert*-butane (*t*-BuN=O; **925**) [1210–1212] and phenyl-*tert*-butylnitronone (**926**) [1213–1216] are the most common spin traps and react with a variety of short-lived radicals R' , such as alkyls, alkoxy, acyl, amyl, thiyl, benzyl, and even hydroxyl and phenyl.



The advantage of nitroso compounds $R'N=O$ as spin traps is the conspicuous appearance of additional splittings due to the nuclei of R' in the ESR spectrum of the spin adduct $R'RN-O\cdot$. Thus, the α protons of an alkyl radical become β protons in the adduct, and their hyperfine pattern indicates the number of these protons. The ^{14}N nucleus in a N-centered radical gives rise to another three-line pattern in addition to that of the nitroxyl. Upon trapping of the phenyl radical, the coupling constants of its protons are observed in the spin adduct in the order of their $|a_H|$ values *para* \geq *ortho* \gg *meta* (Chapt. 8.2). In this respect, **925** is particularly useful, because the small splitting by its nine *tert*-butyl γ protons generally remains unresolved; even more advantageous is the perdeuterated compound **925-d₉**. Addition of methyl, succinimidyl (as a N-centered radical), and phenyl to **925** yields the respective nitroxyl radicals **927** \cdot –**929** \cdot presented below:



Tab. A.2.1. Hyperfine Data for Alkali-Metal Nuclei in Counterions of Some Hydrocarbon Radical Anions in DME, THF, MTHF, and DEE (observed at room temperature unless otherwise stated). Footnotes indicate where the structural formulas are shown.

				<i>Temp. [K]</i>	
Benzene ^a 62 ^{•-}	⁷ Li	MTHF	0.169	220	[1218]
<i>o</i> -Xylene ^b 485 ^{•-}	³⁹ K	DME	0.017	193	[897]
<i>p</i> -Xylene ^b 487 ^{•-}	³⁹ K	DME	0.0100	182	[1219]
	¹³³ Cs	DME	0.3766		
Naphthalene ^a 83 ^{•-}	⁷ Li	THF	0.019		[140, 1220,
	⁷ Li	MTHF	0.046		1221]
	²³ Na	DME	0.041		
	²³ Na	THF	0.1036		
	²³ Na	MTHF	0.1115		
	⁸⁵ Rb	DME	0.0095		
	⁸⁷ Rb	DME	0.0316		
	⁸⁷ Rb	THF	0.0290		
	¹³³ Cs	DME	0.1071		
	¹³³ Cs	THF	0.1117		
Acenaphthene ^c 67 ^{•-}	²³ Na	DME	0.108		[1222]
Pyracene ^c 96 ^{•-}	²³ Na	THF	0.0146	243	[624, 1223]
	²³ Na	MTHF	0.0176	193	
Anthracene ^a 68 ^{•-}	²³ Na	THF	0.15		[1224, 1225]
	²³ Na	DEE	0.25		
	³⁹ K	THF	0.01		
	³⁹ K	DEE	0.262		
	¹³³ Cs	DME	0.047		
	¹³³ Cs	THF	0.055		
Phenanthrene ^a 386 ^{•-}	²³ Na	THF	0.040		[1226]
Pyrene ^a 387 ^{•-}	³⁹ K	MTHF	0.0057	249	[1227]
	¹³³ Cs	MTHF	0.0714		
Triphenylene ^a 388 ^{•-}	²³ Na	MTHF	0.060		[1228]
	²³ Na	DEE	0.085		
Biphenyl ^d 94 ^{•-}	³⁹ K	THF	0.0043	283	[1129]
	⁷ Li	THF	+0.0017 ^e		[1230]
	⁷ Li	MTHF	+0.0023 ^e		
	²³ Na	DME	+0.0015 ^e		
	²³ Na	THF	+0.0036 ^e		
	³⁹ K	DME	-0.0013 ^e		
	⁸⁵ Rb	DME	-0.016 ^e		
	⁸⁷ Rb	DME	-0.050 ^e		
Cyclooctatetraene ^f 64 ^{•-}	⁷ Li	THF	0.02		[562]
	²³ Na	THF	0.09		

Tab. A.2.1 (continued)

				<i>Temp. [K]</i>			
Biphenylene ^f	²³ Na	THF	0.012			[1231]	
396⁻	³⁹ K	THF	0.010				
	¹³³ Cs	THF	0.174				
Azulene ^g	⁷ Li	THF	0.0174			[1225]	
112⁻	²³ Na	THF	0.0538				
	³⁹ K	DEE	0.0202				
Acenaphthylene ^h	³⁹ K	THF	0.007			[617]	
113⁻	¹³³ Cs	DME	0.107				
	¹³³ Cs	THF	0.117				
Heptafulvalene ⁱ	³⁹ K	THF	0.023	183		[876]	
448⁻							
1,4-Di- <i>tert</i> -butyl-buta-1,3-diene ^j	³⁹ K	DME	+0.136	270		[529]	
	³⁹ K	THF	+0.146	280			
	90⁻	⁸⁵ Rb	DME	+0.495	240		
		⁸⁷ Rb	DME	+0.167	240		
		⁸⁵ Rb	THF	+0.620	280		
		⁸⁷ Rb	THF	+2.11	280		
		¹³³ Cs	DME	+0.80	240		
		¹³³ Cs	THF	+0.99	280		
2,3-Di- <i>tert</i> -butyl-buta-1,3-diene ^j	³⁹ K	DME	+0.155	260		[529]	
	111⁻	⁸⁵ Rb	DME	+0.840	260		
		⁸⁷ Rb	DME	+2.84	260		
		¹³³ Cs	DME	+1.65	240		
		¹³³ Cs	THF	+2.57	320		
1,6-Methano[10]annulene ^k	³⁹ K	THF	0.008	243		[1232]	
85⁻							
[2.2]Paracyclophane ^l	³⁹ K	THF	0.012	183		[152, 621]	
	118⁻	³⁹ K	MTHF	0.013	163		
		¹³³ Cs	THF	0.038	183		
[2.2]Metaparacyclophane ^l	³⁹ K	DME	0.062	168		[155]	
95⁻							
1,2:9,10-Dibenzo[2.2]-paracyclophane-1,9-diene ^l	³⁹ K	DEE	0.011	183		[154]	
	509⁻						
[2.2.2.2](1,2,4,5)Cyclophane ^l	³⁹ K	DME	0.075	183		[908]	
	511⁻	³⁹ K	MTHF	0.103	210		
3,7,10,14-Tetra- <i>tert</i> -butyl-1,2,8,9-tetrahydro[14]annulene ^m	⁷ Li	DEE	+0.913	270		[151]	
	502⁻	²³ Na	DEE	+0.781			
		³⁹ K	DEE	+0.235	210		
		¹³³ Cs	DEE	+1.920			
3,9,12,18-Tetra- <i>tert</i> -butyl-1,2,10,11-tetrahydro[18]annulene ^m	³⁹ K	DEE	+0.078	270		[151]	
	503⁻	¹³³ Cs	DEE	+0.655			

Tab. A.2.1 (continued)

			<i>Temp. [K]</i>		
3,11,14,22-Tetra- <i>tert</i> -butyl- 1,2,12,13-tetradec- hydro[22]annulene ^m	³⁹ K ¹³³ Cs	DEE DEE	+0.060 +0.388	270	[151]
504⁻					
^a Table 8.8.	^h Table 8.16.				
^b Table 8.18.	ⁱ Table 8.14.				
^c Table 8.9.	^j Table 8.6.				
^d Table 8.11.	^k Table 8.20.				
^e NMR.	^l Table 8.22.				
^f Table 8.10.	^m Table 8.21.				
^g Table 8.15.					

The coupling constant a_N of the nitroxyl varies with the electron-withdrawing power of the added group R. It is +2.7 to +2.8, +1.7 to +1.85, and +0.7 to +0.85 mT when alkoxy, thiyyl, and acyl radicals, respectively, become attached to R'N=O. Also, the g_e factor of the nitroxyl increases from ca 2.006 to 2.007 when the atom of the group R linked to N belongs to the second row of elements instead of the first. The disadvantage of nitroso spin traps is their instability to photolysis, leading to dimerization and side reactions, as well as the proneness of some of their spin adducts to split into a nitroso compound and a radical other than the original one.

Although the nitron spin traps R'CH=N⁺(R'')-O⁻ and the resulting nitroxyls R'RCH-N(R'')-O[•] are much more stable than their nitroso counterparts, identification of the primary radical R' is less straightforward. This is because, in addition to the three-line pattern of the ¹⁴N nucleus, the ESR spectrum of the nitroxyl adduct exhibits substantial splitting due to the methine β proton of the nitron spin trap, and the nuclei of the added group R give rise to only minor hyperfine features. More detailed data can, however, be obtained with the use of ¹H- and ¹⁴N-ENDOR spectroscopy and deuterated derivatives of **926** as spin traps [1216].

Spin trapping was repeatedly reviewed [77–79]. A recent survey [1217] describes the application of this technique to living cells for in-situ identification of transient C- and O-centered radicals and an insight into their role in biology.

A.2

Hyperfine Splitting by Alkali-Metal Nuclei in Counterions of Radical Anions

Association of radical anions with their alkali-metal counterions in ethereal solvents (ion pairing) is considered in Chapt. 6.6. As stated there, the structure of ion pairs is generally different for radical anions with and without heteroatoms. In ion pairs of hydrocarbon radical anions, the alkali-metal cation is solvated and is located in the π -electron cloud above or below the molecular plane. However, in ion pairs of radical anions containing heteroatoms, the cation directly contacts the in-

Tab. A.2.2. Hyperfine Data for Alkali-Metal Nuclei in Counterions of Some Radical Anions with Heteroatoms in DME, THF, and MTHF (observed at room temperature unless otherwise stated). Footnotes indicate where the structural formulas are shown.

		<i>Temp. [K]</i>		
Pyrazine ^a	⁷ Li	THF	0.070	[1233–1235]
576⁻	²³ Na	DME	0.052	
	²³ Na	THF	0.059	
	³⁹ K	DME	0.010	
	³⁹ K	THF	0.011	
	¹³³ Cs	THF	0.127	
1,4,5,8-Tetraazanaphthalene ^b	²³ Na	DME	0.095	[162]
	³⁹ K	DME	0.020	223
57⁻				
2,2'-Bipyridyl ^c	²³ Na	DME	0.058	265 [1236]
594⁻				
1,10-Phenanthroline ^c	²³ Na	DME	0.08	190 [973]
590⁻				
Bis(trimethylsilyl)diimine ^d	²³ Na	THF	0.105	190 [734]
737⁻				
Azobenzene ^e	³⁹ K	DME	+0.041	[551]
	³⁹ K	MTHF	+0.035	
3,3,5,5-Tetramethyl-1-pyrazoline ^f	²⁷ Li	DME	-0.116	203 [552]
	²³ Na	DME	+0.236	273
	³⁹ K	DME	+0.058	273
	¹³³ Cs	DME	+0.554	
2,3-Diazabicyclo[2.2.1]-hept-2-ene ^f	²⁷ Li	DME	-0.053	[552]
	³⁹ K	DME	+0.055	
	¹³³ Cs	DME	+0.493	
2,3-Diazabicyclo[2.2.2]-oct-2-ene ^f	²⁷ Li	DME	-0.112	203 [552]
	³⁹ K	DME	+0.061	
	¹³³ Cs	DME	+0.547	
Benzophenone ^g	⁷ Li	DME	0.0673	[169, 1237,
	⁷ Li	THF	0.032	1238]
	²³ Na	DME	0.1125	
	²³ Na	THF	0.118	
	³⁹ K	DME	0.039	
	³⁹ K	THF	0.024	
Fluorenone ^g	²³ Na	THF	+0.16	283 [169]
	⁷ Li	THF	+0.025 ^h	[1230]
	²³ Na	DME	+0.35 ^h	
	⁸⁵ Rb	THF	+0.09 ^h	333
	⁸⁷ Rb	THF	+0.31 ^h	333
	¹³³ Cs	THF	+0.06 ^h	333

Tab. A.2.2 (continued)

				<i>Temp. [K]</i>	
Benzil ⁱ 633 ^{•-}	²³ Na	DME	0.061	223	[1239]
<i>o</i> -Dimesitoylbenzene ⁱ 110 ^{•-}	⁷ Li	DME	+0.375		[614, 615]
	²³ Na	DME	+0.695		
	³⁹ K	DME	+0.133		
	⁸⁵ Rb	DME	+0.491	220	
	⁸⁷ Rb	DME	+1.66	220	
<i>o</i> -Benzoquinone ^j 636 ^{•-}	¹³³ Cs	DME	+1.02		
	⁷ Li	MTHF	0.064		[1004]
	²³ Na	MTHF	0.050		
	⁸⁵ Rb	MTHF	0.025		
<i>p</i> -Benzoquinone ^j 19 ^{•-}	¹³³ Cs	MTHF	0.093		
	²³ Na	DME	0.109		[1240]
2,3-Dimethyl- <i>p</i> - benzoquinone ^j 638 ^{•-}	¹³³ Cs	DME	0.026	383	[1241]
2,6-Dimethyl- <i>p</i> - benzoquinone ^j 640 ^{•-}	⁷ Li	DME	0.020	185	[1241]
	¹³³ Cs	DME	0.024	373	
Duroquinone ⁱ 641 ^{•-}	²³ Na	DME	0.0387		[1240]
	²³ Na	THF	0.0346		
1,2-Naphthoquinone ^k 646 ^{•-}	⁷ Li	DME	0.054	272	[1242]
	²³ Na	DME	0.049	272	
	⁸⁵ Rb	DME	0.010	272	
	⁸⁷ Rb	DME	0.029	272	
	¹³³ Cs	DME	0.056	272	
9,10-Anthraquinone ^k 655 ^{•-}	²³ Na	DME	0.041		[1243]
1,2-Acenaphthoquinone ^k 653 ^{•-}	⁷ Li	DME	0.053		[1242]
	²³ Na	DME	0.069		
	³⁹ K	DME	0.009		
	⁸⁵ Rb	DME	0.027		
	⁸⁷ Rb	DME	0.087		
	¹³³ Cs	DME	0.029		
Phthalonitrile ^l 665 ^{•-}	²³ Na	DME	0.030		[1244]
	²³ Na	MTHF	0.026		
Terephthalonitrile ^l 667 ^{•-}	²³ Na	DME	0.030		[1245]
	²³ Na	THF	0.038		
	²³ Na	MTHF	0.046		
	³⁹ K	MTHF	0.013		

Tab. A.2.2 (continued)

				<i>Temp. [K]</i>	
Nitrobenzene ^m 115 ⁻	⁷ Li	DME	0.0125	273	[619, 1246– 1247]
	²³ Na	DME	0.039		
	²³ Na	THF	0.036		
	³⁹ K	DME	0.023		
	³⁹ K	THF	0.025		
	⁸⁵ Rb	DME	0.110		
	⁸⁷ Rb	DME	0.345		
	¹³³ Cs	DME	0.295		
	¹³³ Cs	THF	0.323		
1,2-Dinitrobenzene ^m 689 ⁻	²³ Na	DME	0.038		[619]
	³⁹ K	DME	0.022		
	¹³³ Cs	DME	0.330		
1,3-Dinitrobenzene ^m 116 ⁻	⁷ Li	DME	0.125	273	[619, 1248]
	²³ Na	DME	0.029		
	³⁹ K	DME	0.021		
	⁸⁵ Rb	DME	0.09		
	⁸⁷ Rb	DME	0.21		
	¹³³ Cs	DME	0.246		
4-Nitropyridine ^m 691 ⁻	⁷ Li	DME	0.030	273	[1249]
	²³ Na	DME	0.034		
	³⁹ K	DME	0.021		
3,5-Dinitropyridine ^m 692 ⁻	²³ Na	THF	0.025		[1043]
	¹³³ Cs	THF	0.219		
2,2'-Dinitrobiphenyl ⁿ 698 ⁻	⁷ Li	DME	0.035		[1250]
	²³ Na	DME	0.018		
4,4'-Dinitrobenzo- phenone ⁿ 702 ⁻	²³ Na	DME	0.027		[1051]
	³⁹ K	DME	0.017		
<i>syn</i> -1,6:8,13-Bisoxido[14]- annulene ^o 745 ⁻	²³ Na	DME	0.020		[1070]
Tetraoxaporphycene ^p 109 ⁻	⁷ Li	MTHF	-0.019	198	[613]
	²³ Na	MTHF	-0.030		
	³⁹ K	MTHF	-0.009		
	¹³³ Cs	MTHF	-0.076		

^aTable 9.8.ⁱTable 9.16.^bTable 9.9.^jTable 9.17.^cTable 9.10.^kTable 9.18.^dTable 9.27.^lTable 9.19.^eTable 9.13.^mTable 9.21.^fTable 7.19.ⁿTable 9.22.^gTable 9.14.^oTable 9.28.^hNMR.^pTable 9.42.

Tab. A.2.3. Hyperfine Data for Alkali-Metal Nuclei in Counterions of Some Hydrocarbon Radical Dianions in DME. Footnotes indicate where the structural formulas are shown.

			<i>Temp. [K]</i>	
Cycloheptatrienyl (tropyli) ^a 63 ^{•2-}	²³ Na	0.176	183	[188]
Benzotropyli ^a 362 ^{•2-}	²³ Na	0.107	193	[67]
	³⁹ K	0.039	193	
Dibenzo[1,2:4,5]tropyli ^a 363 ^{•2-}	²³ Na	0.070	193	[189]
2,3-Naphthotropyli ^a 364 ^{•2-}	³⁹ K	0.038	193	[67]
1,6-Methano[11]annulenyl ^b 494 ^{•2-}	²³ Na	0.115	193	[67]
	³⁹ K	0.038	193	
1,6:8,13-Propane-1,3- diylidene[15]annulenyl ^b 495 ^{•2-}	²³ Na	0.066	193	[67]
	³⁹ K	0.038	183	

^aTable 8.5. ^bTable 8.19.

plane σ electrons of the lone pairs of these atoms. Hyperfine data for the alkali-metal nuclei in counterions associated with some radical anions of the two classes are listed in Tables A.2.1 [140, 151, 152, 154, 529, 562, 617, 621, 624, 876, 897, 908, 1218–1232] and A.2.2 [162, 169, 551, 552, 613–615, 619, 734, 973, 1004, 1043, 1051, 1070, 1230, 1233–1251], and, for some radical dianions, in Table A.2.3 [67, 188, 189]. In the ion pairs of radical monoanions, the nucleus of only one alkali-metal cation gives generally rise to hyperfine splitting. Rarely, such splitting appears to stem from two counterions, e.g., for the two ⁷Li nuclei in counterions associated with the radical anions of cyclic azoalkanes **269–271** (Tables 7.19 and A.2.2). ESR spectra of planar hydrocarbon radical dianions exhibit splitting by the nuclei of two equivalent counterions, above and below the molecular plane. However, the two counterions of a nonplanar radical dianion can be nonequivalent, as are those of the dianions of the bridged [11]- and [15]annulenyl (**494[•]** and **495[•]**) (Tables 8.19 and A.2.3), in which the ²³Na or ³⁹K nucleus of only one cation has an observable coupling constant.

Index

A

- Ab-initio methods 82
- Accumulation of spectra 108
- Acenaphth[1,2-*a*]acenaphthylene radical ions 259–261
 - ESR spectra of 261
- Acenaphthene
 - radical anion 62, 240, 241, 407
 - radical cation 240, 241
- Acenaphtho[1,2-*b*][1,4]dithiine
 - radical anion 100
 - radical cation 100, 355
- Acenaphtho-1,2-quinone (1,2-acenaphtho-quinone) radical anion 321, 411
- Acenaphthylene
 - radical anion 146, 147, 259, 408
 - related to 259
- Acetone radical anion 180, 181
- Acetonitrile (ACN) as solvent 22, 104
- Acetophenone radical anion 311, 312
- Acids, hard and soft 142
- Acridine
 - in photoexcited triplet state 32, 390, 392
 - radical anion 304, 356
- Activation barrier 157, 158, 160, 163
- Acyl radicals 182–185
- Acylnitroxyl radicals 300, 301
- Adamantane matrix 16
- 2-Adamantyl radical 173, 174
- Adamantylideneadamantane radical cation 25, 64, 65, 115, 116, 192
 - ESR spectrum of 116
- Aldehydes
 - radical anions 169, 180–182, 309, 311–313
 - radical cations 169, 182, 184, 185
- Alkali-metal
 - cations, association with radical anions 44, 104, 136, 141–153, 161, 279–283, 305, 315, 335, 373, 407–413
 - nuclei
 - hyperfine splitting 143–147, 199, 407–413
 - NMR studies 136, 144
- Alkanediphosphine radical cations 208, 209
- Alkane radical cations 77, 375–385
 - acyclic 375–378
 - branched 376–378
 - cyclic 378, 379
 - structurally modified 380–385
- Alkanedione radical anions 313–315
- Alkanedisulfide radical cations 208, 209
- Alkaniminyl radicals 182–185
- Alkaniminoxyl radicals 204, 205
- Alkoxy radicals 177, 178
- Alkyl radicals 100, 169–175
 - acyclic 170, 171
 - monocyclic 171–173
 - polycyclic 173–175
 - primary, secondary, tertiary 170
- Alkyl substituents at ethene radical cation, parameters 190
- Alkyl substitution 62, 133, 240, 258
 - effect on π perimeters 262–269
- Alkylaldehyde
 - radical anions 169, 180–182
 - radical cations 182–185
- Alkylamine radical cations 175–177
 - acyclic 178
 - cyclic 179
 - primary, secondary, tertiary 176
- Alkylaminyl radicals 175, 176
- Alkylazulene radical ions 257, 258
- Alkylbenzene radical ions 265–269
- Alkylcycloheptatrienyl radicals and radical dianions 263, 265
- Alkylcyclooctatetraene radical anions 265, 267–269
- Alkylcyclopentadienyl radicals 263, 265
- Alkyldiamine radical cations 196, 197

- Alkylether radical cations 177
 Alkylhydrazine radical cations 193–196
 Alkylhydrazyl radicals 193, 194, 196
 Alkylketones
 – radical anions 169, 180–182
 – radical cations 182–185
 Alkylnitroxyl radicals 200–203
 Alkylperoxyl radicals 199, 200
 Alkylphosphinyl radicals 188
 Alkylphosphonyl radicals 208
 Alkylsilyl radicals 188
 Alkylsulfinyl radicals 169, 208
 Alkylsulfonyl radicals 208
 Alkylthioether radical cations 189
 Alkylthiyl radicals 169, 189
 Allyl radical 14, 15, 59, 60, 81, 220, 221
 – derivatives of 220–223
 Aluminum trichloride as oxidizing agent 23
 AM1-UHF method 82
 Amino-substituted radical cations 358–361
 Aminyl radicals 16, 175, 176, 290–292, 294, 295
 Ammonia
 – molecule 175, 176
 – liquid, as solvent 22, 233
 – radical cation 176–178
 Amplifier 98
 Anisole radical cation 362, 363
 Anisotropic contributions to coupling constant
 – of ^{13}C nuclei 53
 – of α protons 53, 54
 – of protons other than α 56
 Anisotropy of (*see also* dipolar)
 – electron-electron magnetic interaction 27, 29
 – electron-nuclear magnetic interaction 40, 41, 73–75, 92–94
 – g_e factor 101, 102
p-Anisylnitroxyl 298, 299
 Annulene radical ions 261–274
 – bridged 271–276
 – heteroatom-bridged 344–346, 366–370, 372
 – with triple bonds 276–278
 Annulenyl radicals and radical dianions, bridged 269–271
 Annulenoquinone radical anions 323, 324
 Anode
 – helical, of gold 24
 – wire, of platinum 24
 Anthracene
 – in photoexcited triplet state 32, 390
 – perdeuterated, in photoexcited triplet state 392
 – radical anion 62, 234, 356, 407
 – radical cation 62, 234
 – – dimeric radical cation 234, 283
 [2.2]Anthracenophane radical ions 283, 286, 287
 9,10-Anthraquinone (anthra-9,10-quinone)
 radical anion 317, 321, 411
 9-Anthrylmethylene triplet 394–396
 Antimony
 – pentachloride as oxidizing agent 23
 – pentafluoride as oxidizing agent 23
 – trichloride (molten) as oxidizing agent 23
 Arenophane radical ions 278, 283–287
 Arenoquinone radical anions 320–322
 Arrhenius plot 157, 163
 Aryl radicals 169, 185–188
 Arylacetylene radical anions 245, 252–254
 Aryldiacetylene radical anions 245, 253, 254
 Arylethene radical ions 245, 250, 251
 Aryliminoxyl radicals 169, 205–208
 Aryliminyl radicals 169, 183
 Arylpolyene radical ions 245, 250, 251
 Atomic orbital (AO) 49
 Attenuation of MW intensity 8, 103
 Attenuator 98
 Autooxidation of organic compounds 200
 Axial symmetry 213, 402
 1,1'-Azabicyclo[3.2.1]octane radical ions 199
 Azaheterocycles, radical anions of 303–308
 Azanorbornane (1-azabicyclo[2.2.1]heptane)
 radical cation 27, 177, 179
 Azaphenyl radicals 187
 1-Azetinidyl radical 175, 176
 Azoarenes, radical anions of, 309, 310
 Azoalkane radical ions 197–199
 Azobenzene radical anion 133, 309, 310, 410
 1,1'-Azonorbornane radical ions 199
 1,1'-Azotwistane radical ions 199
 Azulene
 – π system 210, 254
 – radical anion 146, 147, 254, 257, 408
 – radical cation 23, 254, 257, 261
 – radical ions, related to 257, 258
 Azulenophane radical anions 283, 286
 Azulenophenalene radical ions 257, 258
- B**
 B parameter for coupling constant of β protons, charge dependence 62
 Barrelene (bicyclo[2.2.2]hepta-2,5,7-triene)
 radical cation 231, 232
 Bases, hard and soft 142
 Bay region 306
 Benzaldehyde radical anion 311, 312

- Benzene
 – in photoexcited triplet state 32, 390, 391
 – radical anion 57, 58, 67, 109, 110, 120, 121, 214, 215, 233, 234, 351, 407
 – – ESR spectrum of 110
 – radical cation 58, 161, 214, 215, 233, 234
 Benzenoid radical ions 233–242
 – alkylsubstituted 240–242
 Benzidine radical cations 361
 Benzil (diphenylethane-1,2-dione) radical anion 316, 411
 1-*H*-Benzo[*c*]tetrazolo[2,3-*a*]cinnolin-yl radical 297, 298
 Benzo-1,2-quinone (1,2-benzoquinone; *o*-benzoquinone) radical anion 318, 324, 411
 Benzo-1,4-quinone (1,4-benzoquinone; *p*-benzoquinone) 22
 – radical anion 83, 109, 110, 152, 317, 318, 411
 – – ESR spectrum of 110
 Benzo[*b*]biphenylene radical ions 242, 243
 Benzotrile radical anion 325, 326
 Benzophenone radical anion 311, 312, 410
 Benzotropyl
 – radical 225, 227, 229
 – radical dianion 225, 227, 229, 413
 – radical and radical dianion, ESR spectra of 229
 Benzvalene (tricyclo[3.1.10^{2,6}]hex-3-ene) radical cation 64, 65, 191, 193
 Benzyl
 – π system 210–213
 – radical 15, 77, 78, 128, 217–220
 – – “back-of-the-envelope” calculation 212
 Biazulenyl radical ions 257, 258
 Bicyclo[1.1.0]butane (cyclobutane-1,3-diyl) radical cation 380–382
 Bicyclo[1.1.0]but-2-yl radical 173, 174
 Bicyclo[2.2.1]heptane-2,3-dione radical anion 64, 65, 133, 315
 Bicyclo[2.2.0]hex-1-yl radical 173, 174
 Bicyclo[2.2.2]octane radical cation 377, 379
 Bicyclo[2.2.2]oct-2-yl radical 173, 174
 Bicyclobutylidene radical cation 190, 191
 Bicyclopropylidene radical cation 190, 191
 Δ 9,9'-Bifluorene radical ions 255, 260
 2,2'-Binaphthyl radical anion 244, 248
 Binaphthylene
 – radical anion 165, 242, 243
 – radical cation 242, 243
 Binomial distribution
 – of intensities 43, 109
 – of isotopes 120
 Biphenyl
 – in photoexcited triplet state 32, 390, 392
 – radical anion 113, 114, 338, 407
 – – ESR spectrum of 114
 – – of perdeuterio derivative 135, 136
 Biphenylene
 – radical anion 242, 243, 408
 – radical cation 242, 243
 2,2'-Bipyridyl radical anion 306, 410
 Biradicals 27, 36, 386–389
 8,8'-Bis(8-azabicyclo[3.2.1]octane) radical cation 25
 9,9'-Bis(9-azabicyclo[3.3.1]nonane) radical cation 25, 195
 1,8-Bis(dimethylamino)naphthalene radical anion 358, 360
 1,3-Bis(diphenylene)allyl 227, 228
 1,3-Bis(diphenylene)-2-phenylallyl 16, 228
 Bis(ethylenedithio)-1,4,5,8-tetrathia-1,4,5,8-tetrahydrofulvalene radical cation 351, 352
N,N-Bis(trimethylsilyl)aniline radical anion 341, 343
 1,4-Bis(methylthio)benzene radical cation 363, 364
 1,4-Bis(trimethylsilyl)buta-1,3-diene radical anion 342
N,N'-Bis(trimethylsilyl)-*p*-benzoquinodimethane diimide radical anion 343
 Bis(trimethylsilyl)diimine radical anion 343, 410
 1,2-Bis(trimethylsilyl)ethene radical anion 342
 Bis(TTF-yl)phenylphosphine radical cation and radical trication 24, 351, 352
 Bisgalvinoxyl radicals 36, 386, 388, 389
 Bisnitroxyl biradicals 36, 386–388
 1,6:8,13-Bisoxido[14]annulene radical anion 345, 412
 Bisverdazyl biradicals 386, 388
Bohr magneton 4
Boltzmann distribution 6, 98
 σ Bond of methyl radical 52
 Branching diagram for 1–4 unpaired electrons 11, 13
Bredt-rule protected radical cations 193
Brownian molecular motion 29, 41, 73, 99
Bruker GmbH 84, 98
trans-Buta-1,3-diene
 – radical anion 230, 232
 – radical cation 91, 92, 191, 193, 230, 232
 – – ESR and ENDOR spectra of 91
tert-Butoxyl radical 15
n-Butyl 170, 171

- tert*-Butyl radical 120, 121, 220, 378
tert-Butylphenylaminy radical 291, 292
- C**
- Cage-hydrocarbon radical cations *see* pagodane radical cations
- Calculation methods
 – empirical 80, 81, 127–129
 – semiempirical and nonempirical 81, 82, 129
- Carbazolyl-9-oxyl radical 299, 301
- 9-Carbazolyl-(2,4,6-trinitrophenyl)aminy radical 295, 296
- Carbene triplets 32, 393–397
- Cathode
 – helical, of amalgamated gold 22
 – mercury pool 22
- Cation-solvating power 107, 142, 143, 162, 279
- π -Centers of alternant π systems, starred and unstarred 210, 211
- Charge-transfer (donor-acceptor) complexes 24, 351, 354
- Chelate-like complexes 142, 143, 306, 324
- Chemical
 – exchange 106, 108
 – shift of organic radicals 135
- Chichibabin's* hydrocarbon (7,7,8,8-tetraphenyl-*p*-benzoquinodimethane) triplet 400–402
- Chlorophyll radical cations 373
- Choranil radical anion 319, 324
- Closed-shell configuration 215, 397
- Conformation of alkyl substituents 55, 56, 62
- Conformational
 – dependence of β proton-coupling constant 61–64, 240, 241
 – interconversion 155–161
- Coppinger's* radical (*see* galvinoxyl)
- Coronene
 – radical anion 101, 236
 – radical cation 236
 – dianion triplet 35, 403
 – in photoexcited triplet state 32, 392
- Corrannulene
 – radical anion 256
 – radical trianion 21, 256
- Counterion *see also* alkali-metal cations 44, 141–153, 324
 – migration 161–164
- Coupling
 – constant (*see also* individual radicals and/or classes of radicals)
 – anisotropic 47, 73–75, 92–94
 – assignment of 127–135
 – ^{13}C -coupling constant, parameters for calculation 65–67
 – ^{19}F -coupling constant, parameters for calculation 71, 72
 – isotropic 41–47, 73–75
 – ^{14}N -coupling constant, parameters for calculation 69
 – ^{17}O -coupling constant, parameters for calculation 70
 – ^{31}P -coupling constant, parameters for calculation 69
 – of α protons in alternant benzenoid radical ions vs π -spin populations 233, 237
 – ^{33}S -coupling constant, parameters for calculation 70
 – ^{29}Si -coupling constant, parameters for calculation 72, 73, 341
 – sign of 43, 93, 94, 127–135, 139, 140
 – to nuclei other than proton 65–72
 – to α protons 56–60
 – to β protons 61–64
 – to γ , β , and ϵ protons 64, 65
- Cross
 – relaxation 90, 96
 – section of sample tube 105
- Cryogenic temperatures 26
- Crystal detector 98
- 8-Cyano[2.2]metaparacyclophane radical anion 325, 326
- 4-Cyanopyridine radical anion 326
- Cyano-substituted
 – radical anions 69, 325–331
 – radical trianions 325, 327–331
- Cycl[3.2.2]azine radical anion 83, 84, 114, 115, 344, 345
 – ESR spectrum of 84
- Cycl[3.3.3]azine
 – radical anion 344, 345
 – radical cation 354, 356, 357
- Cycloalkane radical cations 378–383
- Cycloalkane-1,3-diyl
 – cations 380–383
 – triplets 381–383, 397–399
- Cyclobutane radical cation 377, 378
- Cyclobutene radical cation 191, 193
- Cyclobutenyl radical 63, 64, 221
- Cyclobutyl radical 56, 77, 172, 379
- Cycloheptatrienyl (tropylium)
 – radical 58, 224, 227, 264, 265
 – radical dianion 58, 224, 227, 413
- Cyclohexadienyl radical 63, 64, 223, 224
- Cyclohexane radical cation 377–379

- Cyclohexane-1,4-diyl radical cation (from bicyclo[2.2.0]hexane or 1,5-hexadiene) 383
- Cyclohexyl radical 158, 172, 379
- Cyclooctatetraene (COT)
- dianion 107, 108, 242
 - molecule 107
 - radical anion 58, 107, 108, 242, 243, 407
 - radical cation 23, 242, 243
- Cyclooctatrienyl radical anion 242, 243
- Cyclopenta-1,3-diene radical cation 231, 348
- Cyclopentadienone 313
- radical anion 311–313
- Cyclopentadienyl
- radical 58, 214–216, 264, 265
 - triplet dication 35, 402, 403
- Cyclopentane radical cation 377, 378
- Cyclopentane-1,3-diyls
- radical cations (from housanes) 381–383
 - triplets 33, 397, 399
- [2.2.2.2](1,2,4,5)Cyclophane radical anion 279, 281, 408
- Cyclophane radical ions 278–283
- Cyclopropane radical cation
- ring-closed form 377, 378
 - ring-opened form 380
- Cyclopropenone 313
- Cyclopropyl
- group, bisected and perpendicular conformation 177, 220
 - radical 19, 75, 77, 171–173
- D**
- Decacyclene
- dianion triplet 35, 403
 - in photoexcited triplet state 392
- Degenerate π perimeter MOs
- HOMOs 214, 215, 262–264, 269, 274–276, 292, 344, 369, 402
 - LUMOs 214, 215, 262, 264, 265, 268, 270, 271, 274–276, 278, 305, 325, 338, 341, 346, 347, 402
 - NBMOs 268, 269, 338, 344, 346, 354, 402
- Density functional theory (DFT) 82
- Deuteriobenzene radical anions 265, 266
- Deuteriocycloheptatrienyl radical 263, 264
- Deuteriocyclooctatetraene radical anion 265, 267, 269
- Deuterium substitution, effect on π perimeters 262–267
- Deviations from planarity 76, 170, 219, 273, 298, 309, 329, 358
- Di(1-naphthyl)acetylene radical anion 252, 253
- Di(1-naphthyl)diacetylene radical anion 253
- Dialdehyde radical anions 159, 316
- Dialkylaminyl radicals 175, 176
- Dialkylether radical cations 180
- Diamagnetic molecules 49, 106, 107
- Diamagnetism 10
- Dianions
- diamagnetic 21
 - in triplet state 21, 35, 165, 402, 404
- 9,9'-Dianthrylmethylene 394–396
- 2,3-Diazabicyclo[2.2.1]hept-2-ene radical anion 198, 410
- 2,3-Diazabicyclo[2.2.2]oct-2-ene
- radical anion 198, 410
 - radical cation 198, 199
- 1,4-Diazabicyclo[2.2.2]octane (DABCO) radical cation 25, 26, 75, 196, 197
- 1,6-Diazabicyclo[4.4.4]tetradecane radical cation 25, 26, 75, 119, 120, 197
- 2,7-Diazapyrene radical anion 306, 348
- 5-Diazo-10,11-dihydro-5*H*-dibenzo[*a,d*]cycloheptene radical cations 369–371
- 9-Diazo-9,10-dihydro-10,10-dimethylanthracene radical cation 369–371
- Diazoalkane radical cations 199
- 1,2:9,10-Dibenzo[2.2]paracyclophane-1,9-diene radical anion 279, 281, 408
- Dibenzo[*a,c*]naphthacene radical ions 236, 238
- Dibenzo[*a,e*]cyclooctene radical ions 242, 243
- Dibenzo[1,2:4,5]tropyl radical dianion 227, 228, 413
- 5*H*-Dibenzo[*c,f*][1,2]diazepine radical anion 309, 310
- 2,3-Dichloro-5,6-dicyano-*p*-benzoquinone (DDQ) radical anion 325, 327
- Dichloromethane as solvent 23
- N,N'*-Dicyanoarenoquinone diimine radical anions 328–330
- Dideuteriomethane radical cation 375
- Dielectric losses 97
- Dienone radical anions 309, 311, 312
- Diethylether (DEE) as solvent 104
- Different orbitals for different spins (DODS) 52, 82
- 1,4-Difluorobenzene radical anion 336, 338
- Difluoromethyl radical 170, 171
- Difluoronitrobenzene radical anions 337, 338
- Dihedral angle θ for β protons, $\cos^2\theta$ -dependence 55, 56, 61, 156, 157
- 2,7-Dihydro-2,7-diazapyrene radical cation 348, 350
- 9,10-Dihydro-9,9-dimethylacridinyl radical 291, 292

- Dihydrodiazaheterocycle radical cations 23, 348–350
 – *N,N'*-dimethyl derivatives 348–350
 Dihydrnitroxyl radical 200, 201
 1,4-Dihydropyrazine radical cation 348, 349
 10b,10c-Dihydropyrene radical anion 272, 275
N,N'-Dihydropyridazine (1,2-dihydropyridazine) radical cation 365, 367
 1,4-Dihydroxynaphthalene radical cation 364
 2,6-Dihydroxyphenoxyl radical 293, 294
 1,6:8,13-Diimino[14]annulenes
 – radical anions 344, 345, 367
 – radical cations 25, 26, 75, 367–369
 Diisopropylphosphinyl radical 188
 Diketone radical anions 313–325
 Dimeric radical cations 24, 234–236, 238–242
 o-Dimesitylbenzene radical anion 144, 315, 316, 411
 Dimesitylmethylene triplet 394–396
 Dimethoxybenzene radical cations 362
 1,2-Dimethoxyethane (DME) as solvent 20, 104, 142, 162–165
 1,4-Dimethoxynaphthalene radical cation 364
 1,3-Dimethylbicyclo[1.1.0]butane (1,3-dimethylcyclobutane-1,3-diyl) radical cation 380–382
 2,7-Dimethyl-2,7-dihydro-2,7-diazapyrene radical cation 348, 350
 9,9'-Dimethyl-9,10-dihydroacridine radical cation 358, 361
 2,5-Dimethyl-3,4-trimethylene-6a-thiathiophene radical anion 158, 308
 9,10-Dimethylanthracene radical ions 62
 2,2'-Dimethylazobenzene radical anion 133, 309, 310
 1,3-Dimethylcyclobutane-1,3-diyl triplet 381, 383, 397–400
 1,4-Dimethylcyclohexane radical cation 377, 379
 1,3-Dimethylcyclopentadienyl radical 263, 348
 1,3-Dimethylcyclopentane-1,3-diyl radical cation (from 1,4-dimethylhousane) 381–383
 10b,10c-Dimethyl-10b,10c-dihydropyrene
 – radical anion 68, 272, 275
 – radical cation 272, 275, 276
N,N'-Dimethyl-1,6:8,13-diimino[14]annulene
 – radical anion 344, 345
 – radical cation 368–370
 – radical ions, ESR spectra of 370
cis-10,11-Dimethyldiphensuccindan-9,12-dione radical anion 162, 163
 – ESR spectra of 163
 2,3-Dimethylenecyclohexane-1,4-diyl triplet 33, 34, 400, 401
N,N-Dimethylformamide (DMF) as solvent 22, 104
 1,8-Dimethylnaphthalene
 – radical anion 62, 240, 241
 – radical cation 240, 241
 Dimethyl-*p*-benzoquinone radical anions 318, 411
N,N-Dimethyl-*p*-toluidine radical cation 358, 359
 Dimethylphenylphosphine radical anion 341, 343
 Dimethylphosphonyl radical 208
 2,2'-Dimethylstilbene radical anion 245, 250
 Dimethylsulfoxide (DMSO) as solvent 22, 104
 1,2-Dinaphthyl ethene radical anions 251, 283
 1,3-Dinitrobenzene (*m*-dinitrobenzene) radical anion 148, 332, 333, 335, 412
 1,2-Dinitrobenzene (*o*-dinitrobenzene) radical anion 332, 412
 1,4-Dinitrobenzene (*p*-dinitrobenzene) 22
 – radical anion 333
 4,4'-Dinitrobenzophenone radical anion 335, 412
 2,2'-Dinitrobiphenyl radical anion 334, 412
 Dinitrodurene radical anion 158–161, 332
 – ESR spectrum of 161
 1,8-Dinitronaphthalene radical anion 334, 335
 3,5-Dinitropyridine radical anion 333, 335, 412
 Dione radical anions 313–317
 – phenyl-substituted 316, 317
 Dioxygen, effect on ESR spectrum 105, 106
 2,2-Diphenyl-1-picrylhydrazyl (DPPH) radical 17, 83, 94–96, 132, 141, 295, 296
 – as reference for g_e factor 101
 Diphenylamine radical cation 358, 361
 Diphenylaminyl radical 291, 292, 301
 9,10-Diphenylanthracene radical ions 244, 248
 1,3-Diphenylcyclobutane-1,3-diyl triplet 397, 400
 1,3-Diphenylcyclopentane-1,3-diyl triplet 33, 397, 399
 1,2-Diphenylcyclopentene radical anion 245, 250

- Diphenylcyclopropenone radical anion 311, 312
- Diphenyldiacetylene radical anion 253
- Diphenyldiazomethane radical cation 27, 78, 369–372
- ESR spectra of 372
- Diphenylmethaniminoxyl radical 206, 207
- Diphenylmethaniminyl radical 183, 184
- Diphenylmethyl radical 217–220, 292
- Diphenylmethylene (diphenylcarbene)
- radical cation 27, 369, 372
- triplet 33, 395, 396
- 1,8-Diphenylnaphthalene
- radical anion 244, 247
- radical trianion 21, 244, 247
- Diphenylnitroxyl 299, 301
- Diphosphopolyphenylene radical trianions 21
- Dipolar
- magnetic electron-nuclear interaction 40, 41, 92–94, 103, 138
- – of ^{13}C nucleus with unpaired electron spin in carbon p-AO 53
- – of proton with unpaired electron spin in carbon p-AO 53, 54
- 1,8-Di(propyn-1-yl)naphthalene radical anion 252
- Diprotonation of radical anions 23, 24, 105, 305, 317, 348
- Disproportionation of radical anions 21
- Distance of unpaired electrons 28
- Distonic radical cations 27, 380
- Di-*tert*-butylnitroxyl radical 137, 138, 141, 406
- ESR spectra of 138
- 1,8-Di-*tert*-butyl-9-carbazoyl radical 291, 292
- 7,7-Di-*tert*-butylbenzyl radical 218, 220, 244
- 1,4-Di-*tert*-butylbuta-1,3-diene radical anion 88–90, 144, 145, 230, 232, 408
- ESR and ENDOR spectra of 88
- 2,3-Di-*tert*-butylbuta-1,3-diene radical anion 145–147, 230, 232, 408
- ESR spectra of 146, 147
- 2,6-Di-*tert*-butylphenoxyl radical, *para*-substituted derivatives 136, 137
- Dithieno[2,3-*b,e*]tetra-1,2,4,5-azine radical cation 89, 90, 356, 357
- ESR and ENDOR spectra of 89
- Dithieno[3,4-*b*; 3',4'-*e*]paradithiin-1,3,5,7-tetraone radical ions 71
- radical anion 124–127
- – ESR spectra of 126
- 2,2'-Dithienyl radical anions 307, 308
- Dithiine radical cation 351, 355
- 1,3-Divinylcyclobutane-1,3-diyl triplet 399
- Diyl radical cations (from bicycloalkanes) 380–383
- Doublet-spin function 10
- Doubly occupied orbitals 50, 59
- Durene (1,2,4,5-tetramethylbenzene) radical cation 267, 269
- Duroquinol (dihydroxydurene) radical cation 158, 159, 362, 363
- Duroquinone (2,3,5,6-tetramethyl-*p*-benzoquinone) radical anion 319, 411
- Dynamic processes, intermolecular 153–165
- ## E
- Effective symmetry 217
- ELDOR (electron-electron double resonance) 84, 96, 295
- accessories 99
- Electromagnet 97, 98
- Electron
- acceptors 22, 161, 162, 233, 302, 317, 331, 336, 338, 339, 351
- – radical anions of 302–346
- affinity (EA) 19, 143, 245, 335
- correlation by spin 59
- donors 24, 25, 161, 162, 233, 302, 307, 351, 358
- – radical cations of 346–366
- exchange between diamagnetic and paramagnetic species 106–108
- spin (*see there*)
- transfer
- – intermolecular 19
- – intramolecular 161–165
- – electron magnetic interaction 27–31
- – nuclear magnetic interaction 37–48, 135
- – releasing effect 216, 264, 265, 271, 275, 298, 331, 336, 338, 341, 358, 360, 365
- – withdrawing effect 216, 292, 298, 302, 317, 325, 333, 336, 338, 339, 341
- – *Zeeman* (*see there*)
- ENDOR (electron-nuclear double resonance) 40, 83–95
- accessories 99
- enhancement 87, 90, 94
- frequency 90–92
- number of lines 87, 88, 109
- physical fundamentals 84–87
- sensitivity 87
- spectra 87–94, 129–132
- spectral resolution 87
- technique 84, 115, 116, 129–132
- of triplet molecules 94
- Enone radical anions 309, 311
- Ensemble of electron spins 6

- EPR (electron paramagnetic resonance) 10
 Equivalent nuclei 43, 109
 ESR (electron spin resonance)
 – absorption 6
 – – of randomly oriented triplet-state molecules 30
 – ESR-spectra
 – – analysis 97–165
 – – central and outermost lines 109, 112, 121
 – – simulation 92, 115–117
 – – superposition 120
 – – total extent 44, 45, 109, 113
 – nomenclature
 – – for protons 54
 – – for ^{13}C nuclei 67
 – physical fundamentals 3–9
 – spectrometer 97–99
 Ethane radical cation 376, 377
 1,6:8,13-Ethanediyliene[14]annulene radical cation 118–120, 271–274
 – ESR spectrum of 119
 2,2'-Ethanediyliene(1,3-dithiole) radical cation 351, 353, 354
 Ethene radical cation 189, 190
 – alkyl derivatives of 189–193
 Ethyl radical 14, 54, 55, 220, 378
 – conformation of methyl group 55
 – g_e anisotropy 102
 – spin delocalization 55
 1-Ethyl-4-carboxypyridinyl radical 17, 292, 294
 Even
 – alternant radical ions 229–254
 – nonalternant
 – – radical ions 254–261
 – – radical trianions 254, 256, 260
 Exchange
 – integral J 28, 386–388
 – of β -proton coupling constants 155–158
- F**
 Fermi-contact term 41–45, 135
 Ferrite isolator 98
 Fine splitting 28
 Flow system 15, 23
 Fluoren-9-ylidene triplet 394–396
 Fluoreniminoxyl radical 206, 207
 Fluorenone radical anion 148, 311, 312, 410
 Fluorenyl radical and radical dianion 225, 226
 Fluorescence 31, 32
 Fluoro-substituted radical anions 335–339
 1-Fluorofluoren-1-iminoxyl radical 206, 207
 Fluoronitrobenzene radical anions 337, 338
 1-(2-Fluorophenyl)ethaniminoxyl radical 206, 207
 Formyl radical 18, 75, 77, 182–185
 Four-jump process 159, 363
 Free rotation of methyl group 55
 Frémy salt as reference for g_e factor 101
 Freons (halocarbons) matrices (*see also* generation of radical cations) 26, 73, 92, 104
 Frequency of electromagnetic radiation 6, 97, 98, 100
 Fullerenes
 – in photoexcited triplet state 32, 393
 – radical addition to 16, 220
 – radical trianions 21
 Fulvalene
 – radical anion 255
 – radical ions, related to 255, 256
 Fulvene
 – π system 210
 radical ions, related to 255
 Furan radical cations 347, 348
- G**
 Galvinoxyl (4-[2',6'-di-*tert*-butyl-1'-oxocyclohexa-2'5'-diene-4'-diyliene)methyl]-2,6-di-*tert*-butylphenoxy) radical 18, 36, 294, 388, 389
 Gaussian
 – curve 9, 115
 – functions for MO calculations 82
 g_e (= g Factor of electron) 5, 41, 43, 99–102
 – anisotropy 101, 102, 137–139, 405
 – – of benzene radical anion 101
 – – of coronene radical anion 101
 – – direct measurement 101
 – – free-electron value 4, 100, 101
 – – of hydrocarbon π radicals 100, 101
 – – of nitro-radical anions 101, 203, 335
 – – of phenalenyl 101
 – – of phoshaarene-radical anions 101, 308
 – – of radicals, in general (*see* individual radicals and/or classes of radicals)
 – – of σ radicals 101, 185, 370, 379
 – – of semidione, semiquinone and ketyl anions 101, 313, 324
 – – tensors 101, 102, 139
 General-TRIPLE resonance 92, 95, 96, 117, 133, 134
 Generation
 – of neutral radicals (*see also* individual neutral radicals and/or classes of neutral radicals) 13–19
 – of paramagnetic species 10–36

- of radical anions (*see also* reduction as well as individual radical anions and/or classes of radical anions) 19–22
- of radical cations (*see also* oxidation as well as individual radical cations and/or classes of radical cations) 19, 20, 22–27
- triplet state molecules *see also* individual triplet state molecules 29–36
- Glassy solutions for randomly oriented triplet-state molecules 30, 392, 393
- Glyoxal (ethane-1,2-dione) radical anion 313, 314
- g_n (= g Factor of nucleus) 37, 38, 41, 43, 129
- Gyromagnetic ratio
 - of electron 6, 86
 - of nucleus 39, 88
- H**
- H/D replacement 45, 132, 135
- Half-field transition in triplet state 29–32, 79
- Heavy atoms 8, 99, 103
- Heisenberg exchange 8, 96, 103
- Heptafulvalene
 - radical anion 256, 408
 - radical cation 256
- Heptalene radical ions, related to 256
- Heptatrienyl radical 223, 224
- Heteroatom-containing conjugated radicals 290–374
 - with special structure 366–372
- Heterocycles
 - radical anions of 303–308
 - radical cations of 347–358
- Hexa-1,3,5-triene π system 210
- 1,2,2a,4a,6a,8a,10a,12a-Hexaaza-1,2,2a,3,4,4a,5,6,6a,7,8,8a,9,10,10a,11,12,12a-octadecahydrocoronene
 - dication triplet 35, 403
 - radical cation 358, 360
 - radical trication 24, 358, 360
- Hexachlorobenzene dication triplet 36, 403, 404
- Hexafluorobenzene radical anion 336, 338
- 1,1,1,3,3,3-Hexafluoropropan-2-ol as solvent 23
- 1,2,3,6,7,8-Hexahydropyrene radical ions 158
- Hexamethyl[3]radialene radical anion 68, 288
- 7,8,9,10,11,12-Hexamethyl[6]radialene radical anion 68, 121, 122, 288, 358
 - ESR spectrum of 121
- Hexamethyldiphosphine radical cation 209
- N,N,N,N',N',N' -Hexamethylphosphoric triamide (HMPT) as solvent 20, 104, 162–165
- n -Hexyl radical 170, 171
- High-energy irradiation 26
- HOMO (highest occupied MO) 211–213, 237, 242, 254, 260, 269, 274, 287
- Homoazulene (1,5-methano[10]annulene) radical anion 272, 273
- Homoconjugation 270, 271, 274, 275
- Host molecule, single crystals studies 30, 390, 391
- Housane(s) (bicyclo[1.1.0]pentane) radical cations 381–383
- Hückel
 - -MO model 80, 81, 128, 211–213
 - rule 215, 242, 271, 276, 312, 358, 402
- Hund rule 51, 400
- Hydrazine radical cations 25, 193–196, 365, 367
 - phenyl-substituted 365, 367
- Hydrazyl radicals 193, 194, 295, 296
- Hydrocarbon radical
 - cations, saturated 375–385
 - conjugated 210–289
- 6-Hydrodipyrido[1,2-*c*;2',1'-*e*]imidazole radical cation 119, 120, 350
- Hydrogen atom 49, 50, 57
- Hydroquinone (1,4-dihydroxybenzene) radical cation 317, 362
- Hydroxyalkyl radicals 169, 171, 181, 182
- Hydroxyl radical 15, 177
- 4-Hydroxyphenoxyl radical 293, 294, 317
- Hydroxy-substituted radical cations 360–365
- Hyperconjugation 55, 61, 63, 68, 275
 - across double bond 183, 184
- Hyperfine
 - anisotropy 73–75, 137, 309, 405
 - – ^{14}N -hyperfine anisotropy 137, 138
 - – in ENDOR 92–94
 - – of σ radicals 78
 - – tensor (dipolar) 40, 41, 47, 53, 54, 73–75, 139
 - data for
 - – biradicals (*see* bisnitroxyl biradicals)
 - – ground-state triplets (*see* cycloalkane-diyls, trimethylenemethane, and perinaphtha-1,3-diyl)
 - – photoexcited triplet states (*see* naphthalene photoexcited triplet state)
 - – radicals (*see* individual radicals and/or classes of radicals)

- Hyperfine (cont.)
 – lines
 – – distribution of intensities 43
 – – integrated intensities 122
 – – number 43–45, 87
 – pattern 109–127
 – – anomalous 153
 – – asymmetric 99
 – – complex 115–118
 – – simple 109–115
 – splitting of ESR signal 39–48
 – – ^{133}Cs -hyperfine splitting 144, 145, 147, 407–412
 – – ^{39}K -hyperfine splitting 143–146, 407–413
 – – ^7Li -hyperfine splitting 143, 144, 408, 410, 412
 – – ^{23}Na -hyperfine splitting 143, 145, 407, 408, 410–413
 – – for one nucleus with $I = 1/2$ and $I = 1$ 42
 – – ^{85}Rb , ^{87}Rb -hyperfine splitting 143, 145, 147, 407, 408, 410–412
 – – in triplet state molecules 48, 94, 399, 400
 – – for two equivalent nuclei with $I = 1/2$ and $I = 1$ 44
 – tensors 47, 53, 54, 56, 73–75
 – – ^{13}C -hyperfine tensor 53
 – – ^1H -hyperfine tensor 53, 54, 73–75
 – – ^{31}P -hyperfine tensor 73
 – time-scale 151, 153
 Hyperfine-coupling constant (*see* coupling to and coupling constant) derivation 42, 43
 Hypericin radical anion 322, 324
 – of conjugate base (radical dianion) 322, 324
- I**
 1,6-Imino[10]annulene radical anion 344, 345
 Iminoxyl radicals 19, 75, 204–208
 Iminyl radicals 182–185
 INDO method 82, 129
 Inductive effect 216, 262, 264, 265, 269, 271, 275
 Inert-gas matrices 26
 Inner shell AOs 51, 52, 65
 Instrumentation 97–99
 Interconversion of two forms of radical 153–155
 Internal conversion 31, 32
 Intersystem crossing 31, 32
 Ion
 – pairing 21, 44, 136, 141–153, 409–413
 – – spin redistribution 146–152
 – pairs
 – – loose 142–146, 151, 283
 – – solvent-separated 142, 145
 – – tight 142–146, 151, 279, 283
 Ionization energy (IE) (ionization potential) 19, 26, 143, 245
 Irradiation with (*see also* individual radicals and/or classes of radicals)
 2.8-MeV electrons 14
 – γ -rays 26
 – X-rays 16
 Isomerization, *cis-trans* 245, 307, 308, 363
 Isophthalonitrile (1,3-dicyanobenzene) radical anion 325, 326
 Isopropyl radical 171, 378
 2-Isopropylidencyclopentane-1-diyl triplet 33, 34, 400, 401
 Isotopes 37, 38
 – natural abundance 38, 120, 123, 125
 Isotopic replacement 45, 129–132
- J**
 Jablonski diagram 31, 32, 389
 Jahn-Teller
 – distortion in alkane radical cations 375, 376, 378
 – effect
 – – dynamic 90, 161, 217, 372, 375, 377, 379
 – – static 161
 – species 161, 217
 – theorem 161, 217
- K**
 Ketone radical anions 19, 169, 180–182, 309, 311, 312, 313
 Ketyl anions (*see* aldehyde and ketone radical anions)
 Klystron 97, 98
- L**
 LCAO (linear combination of atomic orbitals) 52, 58
 – coefficients 59, 63, 81, 128, 211, 212, 260, 262, 265, 269–271, 275, 276
 Lifetime of spin state 8
 Line-broadening
 – by anisotropy 137–141
 – by Jahn-Teller effect 161
 – homogenous and inhomogeneous 153
 Line-form 8, 9
 Line-width 8, 9, 87, 103, 108, 122, 123, 153
 – alternating 160, 161, 363
 – at the half-height 9
 – of satellites 122, 124
 – time-dependent effects on 153–155

- Liquid crystals 141
- Long-range coupling 64, 65, 173, 192, 315
- Lorentzian curve 9, 115
- LUMO (lowest unoccupied MO) 211–213, 237, 242, 254, 260, 265, 268–271, 274–276, 278, 279, 287, 305, 307, 325, 340, 341, 344, 347, 348
- M**
- Magnetic
- field 3–7, 28, 29, 39, 40, 42, 47
 - strength 5, 6, 28, 39, 99
 - moment of
 - electron 4, 5, 11, 28, 37, 40, 41
 - nucleus 37, 39–41
 - spin quantum number of
 - electron 3, 5, 10–12, 29–31, 40–44, 85, 86
 - nucleus 37–44, 46, 48, 86, 154, 155
- Magnetization 6, 7, 35
- Manxine (1-azabicyclo[3.3.3]undecane) radical cation 176, 177, 179
- McCormell equation 57, 67, 128, 260, 265, 341
- McLachlan procedure 80, 81, 128, 211, 233, 260, 262
- Menadione (vitamine K₃) radical anion 320, 324
- Metallic mirror 20, 105
- Metalloporphyrane radical anions 373, 374
- Metalloporphyrin radical ions 372, 373
- [2.2]Metaparacyclophane radical anion 116–118, 129–134, 279, 282, 408
- ESR spectrum of 117
 - ENDOR spectrum of 131
 - general-TRIPLE resonance spectrum of 134
 - radical anions of deuterio derivatives 130–132
 - ENDOR spectra of 131
- Methane radical cation 375
- Methaniminyl radical 182, 183, 185
- 1,6-Methano[10]annulene radical anion 76, 272, 273, 408
- 1,6-Methano[11]annuleny radical and radical dianion 270, 271, 413
- N,N'-Methano-1,6:8,13-diimino[14]annulene radical cation 368, 369
- Methine and methylene groups bridging two π centers 63, 64
- Methoxyl radical 177, 178
- Methoxy-substituted radical cations 360, 362–365
- Methyl radical(s) 14, 15, 50–54, 169–171
- parameters for substituents 170
 - phenyl substituted 217–220
 - spin polarization in 49, 51, 52, 57–60
 - spin trapped 406
- Methyl-like distorted radical 221, 222
- 2-Methyl-1,6-methano[10]annulene radical anion 76
- 1-Methylbicyclo[1.1.0]butane (1-methylcyclobutane-1,3-diyl) radical cation 381, 382
- Methylcarboxypyridinyl radicals 292, 294
- Methylcyclohexane radical cation 377, 379
- 2-Methylcyclopentane-1,3-diyl radical cations (from 5-methylhousanes) 381–383
- Methylene (simplest carbene) singlet and triplet 33, 393, 396
- 4,5-Methylenephenathrene radical dianion 226, 228
- 1-Methylnaphthalene radical anion 76
- Methylsulfinyl and methylsulfonyl radicals 208
- 2-Methyltetrahydrofuran (MTHF) as solvent 20, 31, 104, 162, 164, 165
- Methylthio-substituted radical cations 360, 363–365
- Methylthiyl radical 189
- Microwaves (MW) 6, 86, 97, 98
- MO (molecular orbital) *see also* HOMO, LUMO, NBMO, NHOMO, NLUMO and SOMO) 47
- Modulation 98
- amplitude 108
 - frequency 108
- Modulator 98
- Multi-redox systems, radical ions of 372–374
- Multiresonance 83–96
- N**
- Naphthalene
- as electron accepting π moiety 163–165
 - in photoexcited triplet state 30, 32, 79, 390, 392
 - perdeuterated in photoexcited triplet state 392
 - π system 210, 212, 213
 - radical anion 19, 76, 129, 130, 143, 234, 407
 - as electron-donating π moiety 163–165
 - ESR spectrum 130
 - 1,4,5,8-tetradeuterated radical anion 129, 130
 - ESR spectrum of 130
 - radical cation 73–75, 234
 - dimeric radical cation 234, 238
 - radical ions, alkyl-substituted 240–242

- [2.2](1,4)Naphthalenophane radical anions 151, 284
- [2.2](2,7)Naphthalenophane-1,11-diene radical anion 283, 285, 287
- Naphthazarin (1,4,5,8-tetrahydroxynaphthalene) radical cation 158, 159, 363, 364
- 1,8-Naphthoquinodimethane (naphtho-1,8-quinodimethane) triplet 33, 34, 400, 401
- Naphtho[1,8-*c,d*][2,6]thiadiazine radical cation 354, 356, 357
- 2,3-Naphthotropy radical dianion 227, 413
- Naphthyl radicals 186
- Naphthylmethaniminoxyl radical 206, 207
- Naphthylmethylene triplets 396, 397
- NBMO (nonbonding π MO) 211, 393, 394, 400, 402
- of alternant system 212, 219, 344, 354, 397
- Negative spin density 49, 50
- Negative spin population (*see also* individual radicals and/or classes of radicals) 50, 52, 60
- NHOMO (Next highest occupied MO) 212, 213
- NLUMO (Next lowest unoccupied MO) 212, 213, 325
- Nitrene
- (simplest) singlet and triplet 394, 397, 398
- triplets, in general 32, 393, 397, 398
- Nitro-substituted radical anions 203, 204, 331–335
- Nitroalkane radical anions 203, 204
- 4-Nitroaniline (*p*-nitroaniline) radical cation 358, 359
- Nitrobenzene radical anion 148, 331, 332, 335, 339, 412
- Nitrogen (nitric) oxide 200, 201
- Nitromethane as solvent 23
- Nitrotoluene radical anions 332, 339
- Nitronyl-nitroxyl radicals 136, 409
- p*-Nitrophenol radical anion 332, 333
- 4-Nitrophenylnitroxyl (*p*-nitrophenylnitroxyl) radical 298, 299
- 4-Nitropyridine radical anion 333, 412
- 2-Nitroso-2-methylpropane radical anion 203
- Nitrosoalkane radical anions 203
- Nitrosobenzene
- radical anion 331, 332, 366
- radical cation 27, 331, 332, 367
- Nitroso-*tert*-butane as spin trap 406
- Nitroxyl radicals 17, 73, 200–203, 298–301
- as spin labels 138, 405
- as spin adducts 16, 405, 406, 409
- NMR (nuclear magnetic resonance) 39, 40
- activation barriers 160
- of radicals 135–137
- transitions 83, 85–87, 94
- Nonbenzenoid alternant radical ions 242–244
- Non-bond resonance 307
- Non-*Kekulé* hydrocarbons 33, 211, 400–404
- Norbornadiene radical cation 231, 232, 379
- Norbornane radical cation 377, 379
- Norbornyl radicals 173, 174
- Normalization condition 212
- Nuclear
- magnetism 37–39
- magneton 37
- – spin relaxation 90
- – *Zeeman* levels 42, 85, 86
- Nucleus
- composition of protons and neutrons 37, 38
- magnetic moment of 37, 40, 41, 46
- spin vector 37, 39, 40
- O**
- Octafluorocyclooctatetraene radical anion 336, 338
- 1,1,2,2,9,9,10,10-Octafluoro[2.2]paracyclophane radical anion 339, 340
- Octamethyl- and octaphenyl[4]radialene radical ions 287, 288
- 4,5,7,8,12,13,15,16-Octamethyl[2.2]paracyclophane radical anion 280, 283
- 2,2,4,4,6,6,8,8-Octamethyl-2,4,6,8-tetrasilobicyclo[3.3.0]oct-1(5)ene radical cation 123, 124, 366
- ESR spectrum of 123
- Odd
- alternant radicals 217–224
- nonalternant radicals and radical dianions 224–229
- radical diions 210
- Open-shell configuration 397, 402
- Optimal conditions for ESR spectra 102–109
- Orbital
- angular momentum 3, 10
- *n*-Orbitals (lone-pair MOs) nonbonding 37, 196, 389
- π -Orbitals (MOs) 37, 196, 211, 389
- σ -Orbitals (MOs) 50, 75, 196
- Organic
- metals 24, 325
- radicals centered on one, two, or three atoms 169–208

- Oxidation (*see also* individual radicals and/or classes of radicals)
- with conc. sulfuric acid 23
 - electrolytic 24
 - with Lewis acids 23
 - with peroxides 17
 - by γ -rays 26
 - with transition-metal ions 17, 23
 - in trifluoroacetic acid (TFA) 23
 - with tris(4-bromophenyl)- or tris(2,4-dibromophenyl)-ammoniumyl hexachloroantimonate (“magic blue” and “magic green”, resp.) 23
- 1,6-Oxido[10]annulene radical anion 344, 345
- Oxiranyl radical 172, 173
- 9-Oxo-9,10-dihydroacridinyl radical 291, 292
- N-Oxyaza-2-adamantane radical 136, 137
- Oxyl radicals 177, 178, 290, 293–295
- P**
- Pagodane radical cations 383–385
- Pairing properties of MOs in alternant π system 81, 211, 215, 237, 242, 269, 274, 276, 369
- [2.2]Paracyclophane
- in photoexcited triplet state 32, 393
 - radical anion 150, 151, 162, 279, 280, 408
 - ESR spectra of 150
- [2.2]Paracyclophane-1,9-diene radical anion 159, 160, 279, 280
- [2.2]Paracyclophane-4-yl-*tert*-butylnitroxyl radical 136, 137
- Paramagnetic
- impurities 105
 - molecules (species) 1, 10–36, 49
- Paramagnetism 10
- Peak-to-peak-distance of derivative curve 9
- Pentachlorocyclopentadienyl dication triplet 36, 402, 403
- Pentadienyl radicals 223, 224
- Pentalene
- radical anion 255
 - radical ions, related to 255, 256
- Pentaphenylcyclopentadienyl triplet dication 35, 36, 402, 403
- n*-Pentyl 170, 171
- Perchlorotriphenylmethyl radical 16, 36, 228
- Perdeuteriobiphenyl radical anion 135, 136
- Perdeuteriopyrene in photoexcited triplet state 32, 390
- Perfluoroalkane radical anions 338
- peri*-Positions 306
- Perinaphtha-1,3-diyl triplet 34, 400, 401
- π -Perimeters (monocyclic π systems) 213–217
- degenerate MOs (*see there*)
 - 5-membered 214, 215, 262, 264, 292
 - 6-membered 214, 215, 265, 268, 305, 325, 341, 347, 402
 - 7-membered 262–265
 - 8-membered 267, 269
 - 10-membered 271, 273, 344, 346
 - 11-membered 269–271
 - 12-membered 344, 346, 354
 - 14-membered 271, 274–276, 344, 369
 - 18–26-membered 276–278
 - perturbed 216, 217, 261–278
- Persistent (persistence of) radicals 14, 176, 185, 193, 197, 198, 200, 202, 290, 294, 301
- Perylene
- radical cation
 - as reference for g_e factor 101
 - dimeric radical cation 235
 - radical ions 235, 237, 238
 - ESR spectra of 238
- Phane radical ions 278–287
- Phenalenyl radical 16, 17, 67, 80, 83, 94–96, 101, 110, 111, 141, 224, 225, 354, 357
- derivatives of 224, 225
 - ENDOR and TRIPLE-resonance spectra of 95
 - ESR spectrum of 95, 111
- Phenanthroline 306
- Phenanthrene
- in photoexcited triplet state 32, 390, 392
 - radical anion 235, 407
- 1,10-Phenanthroline radical anion 306, 410
- Phenathrylene-4,5-ketone radical anion 312
- Phenazine radical anion 305, 356
- 10-Phenoxazinyl radical 291, 292
- Phenothiazine radical cation 356–358
- 10-Phenothiazinyl radical 291, 292
- Phenoxazine radical cation 356–358
- Phenoxy radical 290, 293
- related to 16, 292, 293–295
- Phenyl radical 18, 75, 77, 78, 185, 186
- derivatives of 19, 185, 186
 - spin trapped 406
- Phenylaminyl radical 290, 291
- related to 292, 295, 296
- 1-(Phenyl)ethaniminoxyl radical 206, 207
- p*-Phenylenebisgalvinoxyl biradical 36, 388
- p*-Phenylenediamine radical cation 24, 358, 359
- Phenyl-group protons, coupling constants 220
- Phenyliminyl radical 183, 184

Phenylnitrene triplet 33, 398
 Phenylnitroxyl radical 298, 299, 331
 – radicals, related to 299
 Phenyl-*tert*-butylnitrene as spin trap 406
 Phoshabenzene radical anion 69, 307
 – derivatives of 307
 Phosphinyl and phosphonyl radicals, phenyl substituted 301, 302
 Phosphoranyl radicals 301, 302
 Phosphorescence 31
 Photoexcited molecules in triplet state
 – in single crystals 30–32, 389–391
 – in glasses 30–32, 389, 391–393
 Photolysis of
 – iodides and diacylperoxides 14
 – *tert*-butylperester and di-*tert*-butylperoxide 15
 Phthalonitrile (1,2-dicyanobenzene) radical anion 326, 411
 Phytonodione (vitamin K₁) radical anion 320, 324
 Pleiadene radical ions, related to 259, 260
 Polar losses 103
 Polarity of solvent 104, 142
 Polyaryl radical ions 244, 246–249
 Polyene radical ions
 – acyclic 230, 232, 233
 – cyclic 231–233
 Population of Zeeman levels 6
 – excess of 6, 85, 103, 135
 Porphycene radical anion 373, 374
 Porphyrin radical ions 372, 373
 Precession of spin vector about the magnetic field 4, 12
 Principal values of tensors 53, 54, 56, 73
 1,6:8,14-Propane-1,3-diylidene[15]annulenyl radical 270, 271
 – radical dianion 270, 271, 413
n-Propyl radical 56, 171, 378
 Protic impurities 105
 Pumping of ENDOR transition 95, 96
 Pyracene
 – radical anion 151, 152, 240, 241, 407
 – radical cation 118, 138, 152, 153, 239–241
 – – dimeric radical cation 240, 241
 Pyramidalization 77, 170, 176, 177, 180, 331
 Pyrazine radical anion 303, 305, 351, 410
 Pyrazine-di-*N*-oxide radical anion 303, 305
 Pyrene
 – radical anion 235, 406
 – radical cation 235, 239
 – – ESR spectrum of 239
 – – dimeric radical cation 235, 238–240
 – – – ESR spectrum of 239

Pyridazine radical anion 303, 365
 Pyridine radical anion 69, 303, 305, 325
 Pyridine-*N*-oxide radical anion 303, 305
 Pyrimidine radical anion 303, 305, 325
 Pyrrole radical cations 347, 348
 Pyrrolidinyl radical 175, 176
 1-Pyrrolyl radical 291, 292

Q

Q-band klystron 98
 Q-parameter of *McConnell* equation
 – charge dependence 58
 – dependence on CCC bond angles 260
 Quadricyclane radical cation 377, 379
 Quinoline in photoexcited triplet state 32, 392
 Quinolylmethylene triplets 395, 396
 Quinone radical anions 19, 83, 315, 317–325
 Quinoxaline in photoexcited triplet state 32, 390
 Quinuclidine dimeric radical cation 197

R

Radialene radical ions 287–289
 Radical(s)
 – anions (*see also* pertinent individual radical anions and/or classes of radical anions) 20–22
 – cations (*see also* pertinent individual radical cations and/or classes of radical cations) 22–27
 – definition 13
 – dianions 22, 212, 224, 225–227, 269–271, 413
 – dications 24, 212, 360, 361, 403
 – C-centered radicals 169–175, 182–188
 – CC-centered radicals 189–193
 – definition 75
 – N-centered radicals 175–177
 – NN-centered radicals 193–199
 – NO-centered radicals 200–203
 – NO₂-centered radical anions 203, 204
 – O-centered radicals 177–185
 – σ -Radicals 14, 18, 75–78, 182, 204–208, 338, 366–372, 375–379
 – P-centered radicals 186, 188, 189
 – pentacations 24, 351, 352
 – π -Radicals 14–18, 56–75, 100, 101
 – – theoretical introduction 210–217
 – – transition from π 76
 – PO-centered radicals 208
 – PP-centered radicals 208, 209
 – S-centered radicals 188, 189
 – Si-centered radicals 186, 188, 189
 – SO-centered radicals 208

- SO₂-centered radicals 208
- SS-centered radicals 209
- trianions 21, 247, 276, 277, 325, 329
- trications 24, 351, 352
- Radio
 - frequency (RF) 83, 86
 - waves 39
- Rare-gas matrices 108
- Recorder 98
- Reduction (*see also* individual radicals and/or classes of radicals)
 - with alkali metal 20, 21, 24, 104
 - electrolytic 15, 22
 - with glucose 22
 - with mercury metal 22
 - with sodium dithionite 22
 - with solvated electrons 20
 - with zinc powder 15, 22, 24
- ¹⁴N/¹⁵N replacement 45, 132
- Resonance condition 4–6, 42, 98, 99, 101
- Resonant cavity 97, 98, 103
 - cylindrical 97
 - rectangular 97
- Ring
 - flipping, conformational 279
 - inversion 158, 172
- Rubrene (1,5,11,12-tetraphenyl-naphthacene) radical anion 244, 249

S

- S-Donors 351, 352
- Sample cell 97, 98
- Satellite lines 120–127
 - ¹³C satellites 120–123
 - ¹⁵N satellites 132
 - ¹⁷O-satellites 124, 125, 128
 - ³³S-satellites 124–126
 - ²⁹Si satellites 123, 124
- Saturation 7, 86, 103, 161
 - term 7, 103
- Schlenk's hydrocarbon (7,7,8,8-tetraphenyl-*m*-benzoquinodimethane) triplet 33, 34, 400–402
- Second-order splitting 45–47, 118, 119
 - by ENDOR 119
 - for 1–4 equivalent nuclei with $I = 1/2$ 46, 47
- Selection rules
 - for ESR transitions 5, 29, 86, 389
 - for NMR transitions 39, 86
 - Semidione anions (*see* dione radical anions) 290, 313
 - Semiquinone anions (*see* quinone radical anions) 83, 109, 152, 290, 313, 317
- Sesquiterpene radical cations 25, 192
- Short-lived (transient) radicals 14, 16, 108
 - spin trapped 406
- Signal-to-noise-ratio 102, 108
- Silyl radicals 188
 - phenyl substituted 301, 302
- Singlet-spin function 10
- Singly occupied orbitals 10, 28, 49, 51, 210–217
- Slater orbitals 82
- Solvent, choice for ESR spectrum 103
 - for radical anions 20
 - for radical cations 22–27
- SOMO (singly occupied MO) 58, 60, 61, 63, 75, 77, 79, 80, 119, 128, 145, 211, 216, 225, 261, 262, 264, 265, 269, 275, 276, 296, 301, 325, 338, 341, 344, 347, 353, 368, 389
- Spacer separating two π moieties 161, 162, 165, 404
- Special-TRIPLE-resonance 92, 94, 95
- Spin/Spins
 - adducts 16, 73, 405, 406, 409
 - arrangements of formally paired electrons in C–H σ bond of methyl radical 52
 - delocalization 50, 61–64
 - density 41, 43, 50
 - – definition 49
 - of electrons
 - – paired 10, 28, 51, 52, 59
 - – unpaired 10, 11, 28, 39–41, 49–52, 56, 58, 59
 - down (spin β) 3–6, 8, 10, 11, 85
 - functions 3, 10
 - inversion 5
 - labels (labeling) 138, 405
 - localization 149–151, 164, 165, 279–281, 283–286, 315, 325
 - orbital (space) function 11
 - multiplicity 10–13, 389
 - π - σ - and π , π -spin polarization in π -radicals 56–64
 - polarization 49–52, 57–60, 62, 63, 65, 66, 68, 71
 - population (*see also* pertinent individual radicals and/or classes of radicals) 49–52, 55–61, 65–72, 77, 79–82, 124, 128, 139, 141, 143, 144, 157
 - – calculations 80–82
 - – definition 50
 - traps (trapping) 16, 405, 406, 409
 - up (spin α) 3–6, 8, 10, 11, 85
 - vector
 - – of electron 3, 11, 12, 28, 39, 40
 - – of nucleus 37, 39, 40

- Spin-lattice relaxation (SLR) 6–8, 90, 103, 104, 135, 153
 – time 7, 8, 90, 103, 104, 135
 Spin-orbit coupling 7, 10, 31, 100, 254
 Spin quantum numbers of
 – electron 3, 10, 115
 – nucleus 37, 38, 43–47
 Spin-spin relaxation (SSR) 8
 – time 8, 9, 103, 153
 Spirobifluorene (bis(*o,o'*-biphenylene)-methane)
 – radical anion 149, 150
 – triplet dianion 150, 404
 Spiro[5.5]undeca-1,4,6,9-tetraene-3,8-dione radical anion 315
 – ESR spectra of 149
 Stick diagrams 111, 112, 115
 Stilbene radical anion
 – *trans* 133, 245, 250
 – *cis* 245, 250
 Strong-field approximation 40
 Subsets for equivalent nuclei 46
 Succinimidyl radical, spin trapped 406
 Sulfonyl radicals, phenyl substituted 301, 302
 Sulfur hexafluoride as matrix 26
 Supporting salt 104
sym-Tetrazine radical anion 303, 305
 π -Systems
 – alternant and nonalternant 79, 210–213
 – linked by a spacer 210, 212, 213
 – – radical anions 163–165
 – – triplet dianions 165–404
 – monocyclic 213–217
- T**
 Temperature, effect on ESR spectrum 103–105
 Terephthaldehyde (1,4-diformylbenzene) radical anion 158, 159, 316
 Terephthalonitrile (1,4-dicyanobenzene) radical anion 326, 411
o-Terphenyl radical ion 244, 246
 1,4,5,8-Tetraazanaphthalene radical anion 44, 45, 109–112, 140, 410
 – ESR spectrum of 112
 2,4,5,6-Tetrachloro- $\alpha,\alpha,\alpha',\alpha'$ -tetrakis-(pentachlorophenyl)-*m*-xylylene 36
 7,7,8,8-Tetracyano-2,3,5,6-tetrafluorobenzo-1,4-quinodimethane radical anion 337
 Tetracyanoarenoquinodimethanes
 – radical anions 325, 327–331
 – radical trianions 325, 327, 328, 330, 331
 7,7,8,8-Tetracyanobenzo-1,4-quinodimethane (TCNQ) 22
 – in donor acceptor complex, ESR spectrum of 354
 – radical anion 325, 327, 330, 354
 Tetracyanoethene (TCNE) 22, 141, 326
 11,11,12,12-Tetracyanopyreno-2,7-quinodimethane:
 – radical anion 325, 330
 – radical anion and radical trianion, ESR spectra of 330
 – radical trianion 21, 325, 327–330
 Tetradehydro[*n*]annulene(s)
 – radical anions 276–278, 408
 – radical cations and radical trianions 276–378
 5,6,11,12-Tetradehydro-7,8,9,10-tetrahydro-dibenzo[*a,c*]cyclodecene radical anion 252, 253, 254
 5,9,11,12-Tetradehydrodibenzo[*a,e*]cyclooctene radical ions 242, 243
 1,2,4,5-Tetrafluorobenzene radical anion 336, 338, 339
 Tetrafluorobenzo-1,4-quinone (tetrafluoro-*p*-benzoquinone) radical anion 337, 338
 Tetrafluoroethene radical anion 336, 338, 339
 Tetrahydrofuran (THF) as solvent 20, 104, 162
 4,5,9,10-Tetrahydropyrene radical ions 158
 1,4,5,8-Tetrahydro-1,4,5,8-tetrathiafulvalene (TTF) 24, 25, 124, 125, 140,
 – radical cation 124, 125, 140, 325, 351, 352
 – – ESR spectrum of 125
 1,2,4,5-Tetrahydroxybenzene radical cation 363, 364
 Tetrakis(dimethylamino)ethene 24, 25
 – radical cation 359
 1,4,5,8-Tetrakis(dimethylamino)naphthalene radical cation 360, 361
 1,2,4,5-Tetrakis(methylthio)benzene radical cation 363, 364
 4,4',5,5'-Tetrakis(methylthio)-2,2'-ethanediylidene-(1,3-dithiole) radical cation 351, 354
 – in donor acceptor complex, ESR spectrum of 354
 Tetrakis(perfluorocycloalka)cyclooctatetraene radical anions 339, 340
N,N,N',N'-Tetrakis(trimethylsilyl)-*p*-phenylenediamine radical anion 341, 343
 Tetraalkylhydrazine radical cations 194, 195

- 1,2,4,5-Tetramethoxybenzene 24, 25
 – radical cation 363
- 2,2,6,6-Tetramethyl-2,2,6,6-bipiperidone-4-azine-1,1'-dioxyl biradical 36, 387
- 9,9,10,10-Tetramethyl[2.2](2,7)-naphthalenophane-1,11-diene radical ions 285, 287
- 2,2,6,6-Tetramethyl-4-oxopiperidinyl-1-oxyl (TEMPO) radical 18, 36, 136, 202, 387
- 3,3,5,5-Tetramethyl-1-pyrazoline 198, 410
- Tetramethylcyclobutadiene radical cation 242, 243
- 1,1,2,2-Tetramethylcyclopropane radical cation
 – ring-closed form 378
 – ring-opened form 380
- Tetramethyldisulfide radical cation 209
- N,N'*-Tetramethylene-1,6:8,13-diimino[14]annulene radical cation 25, 26, 368, 369
- Tetramethyleneethane (TME)
 – radical anion 230, 232
 – radical cation 193, 230, 232
 – triplet 33, 400, 401
- 1,2,3,4-Tetramethylnaphthalene radical ions and dimeric radical cation 240, 241
- 2,2,6,6-Tetramethylpiperidinyl-1-oxyl radical 202, 387
- 1,4,5,8-Tetranitronaphthalene radical anion 334, 335
- Tetraoxaporphycene
 – five redox stages 373
 – radical anion 144, 373, 374, 412
 – radical cation 374
- Tetraoxaporphyrin
 – five redox stages 373
 – radical ions 373, 374
- 1,1,3,3-Tetraphenylallyl radical 221, 228
- 4',4'',5',5''-Tetraphenyl-1,2:9,10-dibenzo[2.2]paracyclophane-1,9-diene
 – radical anion 281, 283
 – radical trianion 21, 281, 283
 – triplet dianion 404
- Tetraphenylene radical ions 244, 247
- Tetraphenylethene radical ions 251, 260, 371
- Tetra-*tert*-butyl-tetrahydro[*n*]annulenes, *n* = 14, 18, 22, 26
 – radical anions 276, 277, 408, 409
 – radical cations and radical trianions 276, 277
- Tetrathia-radical cations 351, 356
- Tetrazolanyl radicals 296–298
- Thiaheterocycle radical cations
 – related to TTF 351–354
 – not related to TTF 354–356
- Thianthrene radical cation 83, 351, 352
- 6a-Thiathiophthene radical anion 307, 308
 – derivatives of 158, 307, 308
- Thioether radical cations 189
- Thiophene radical cation 347, 348
- Thiyl radicals 189
 – phenyl substituted 301, 302
- Three-electron N–N π bond 25, 193, 196, 295
- Three-electron N–N σ bond 25, 27, 75, 196, 368, 369
 – length 197, 369
- Through-bond interaction 64, 196
- Through-space interaction 65, 197
- α -Tocopherol (vitamin E) radical anion 319, 324
- Tolane (diphenylacetylene)
 – in photoexcited triplet state 32, 390
 – radical anion 252, 253
- Toluene
 – in photexcited triplet state 32
 – radical ions 266
- Transition probability 7
- Trialkylamine radical cations 176–178
- Trialkylsilyl radical 15, 188
- Trialkylstannyl 15
- N*,7,7-Tricyanobenzo-1,4-quinomethanimine radical anion 328–331
- Tricyclopropylamine radical cation 176–178
- Trifluoromethyl radical 77, 170, 171
- Trifluoromethyl-substituted radical anions 339–341
- p*-Trifluoromethylnitrobenzene radical anion 332, 333
- 1,2,3-Trihydropyrenyl radical 155–158, 224, 225
 – ESR spectra of 156
- Triisopropylamine radical cation 25, 178
- N,N'*-Trimethylene-1,6:8,13-diimino[14]-annulene
 – radical anion 345
 – radical cation 25, 26, 119, 120, 368
- Trimethylene radical cation 380
- Trimethylenemethane (TMM) triplet 33, 79, 80, 400, 401
 – ESR spectrum of 80
- Trimethylsilyl-substituted radical anions 72, 341, 342
- Trimethylsilylmethyl-substituted radical cations 365, 366
- 1,3,5-Trinitrobenzene radical anion 333, 335

- Triphenylamine radical cation 361
 1,3,5-Triphenylbenzene
 – dianion triplet 403
 – in photoexcited triplet state 32, 392
 – radical anion 247
 Triphenylene
 – dianion triplet 35, 403
 – in photoexcited triplet state 32, 392
 – radical anion 235, 407
 Triphenylmethyl (trityl) 13, 14, 80, 83, 101, 217–220
 2,4,6-Triphenylphenoxy radical 293, 294
 2,4,6-Triphenylphosphabenzene
 – radical anion 307
 – radical trianion 21, 307
 Triphenylsilyl radical 301, 302
 1,3,5-Triphenylverdazyl radical 17, 297
 Triple bonds, effect on π perimeters 262, 276–278
 TRIPLE resonance (*see also* special and general TRIPLE resonance) 83, 94–96
 – accessories 99
 Triplet-spin
 – function 11, 28
 – spin state 27–31, 79
 Triplet-state
 – dianions of molecules with two π moieties and a spacer 404
 – in ground state 32–36, 79, 165, 393–404
 – ions and diions of axial molecules 35, 402–404
 – molecules 27–36, 386–404
 – molecule, ESR spectrum of 30
 – photoexcited 31, 32, 79, 389–393
 – spin population 79
 – thermally accessible 32–36, 393–394
 Tris(dimethylamino)cyclopropenium radical dication 24, 358, 361
 2,4,6-Tri-*tert*-butylphenoxy radical 18, 293, 294
 2,4,6-Tri-*tert*-butylphenyl radical 19, 185, 186
 2,4,6-Tri-*tert*-butylphosphabenzene radical anion 73, 74, 140, 307
 – ESR spectra of 74
 Tropone 313
 – radical anion 122, 123, 139, 312
 – – ESR spectrum of 122
 Twisting out of coplanarity 333, 335
 Two-jump process 159
- U**
 Ubiquinone radical anion 319, 324
 Uncertainty relation (principle) 8, 153
- V**
 Varian Associates 84, 98
 Vector joining the magnetic moments or spin vectors of two unpaired electrons 28
 Verdazyl radicals 296–298, 388
 Vibronic mixing of MOs 217
 Vinyl radicals 18, 75, 159, 182, 183–185
 Vinylcyclopentadienyl π system 210
 Vinylnitroxyl radicals 300, 301
 Viscosity of medium 73, 104, 137–139
- W**
 W-plane arrangement 64, 173, 184, 315
 Water radical cation 177, 180
 Waveguide 97, 98
 “Whiffen effect” 63, 68, 119, 224, 232, 275, 350, 382, 399
 Wurster’s blue (*N,N,N',N'*-tetramethyl-*p*-phenylene diamine radical cation) 19, 24, 83, 105, 106, 358, 359
 – effect of dioxygen 105, 106
 – ESR spectra (central part) of 106
- X**
 X-band 6
 – klystron 97
o-Xylene radical anion 267, 407
p-Xylene radical anion 267, 338, 407
m-Xylylene (*m*-benzoquinodimethane) triplet 33, 34, 400, 401
- Y**
 Yang’s biradical 388, 389
- Z**
 Zeeman
 – effect 3
 – level 6, 54, 85, 86, 135
 – – for nuclei 85, 86
 – – -population 6, 85, 86, 103, 135
 – splitting for radicals 4–6
 – – for triplet states 29
 Zero-field splitting (ZFS) 28, 29,
 – parameters 28, 152, 165, 386, 404
 – tensor 28
 Zigzag line arrangement 64, 77